2009

Beach morphodynamics behind a series of detached breakwaters in a mesotidal environment

Fairley, Iain Alastair

Beach morphodynamics behind a series of detached breakwaters in a mesotidal environment

By Iain Fairley

A thesis submitted to the University of Plymouth in partial fulfilment for the degree of

Doctor of Philosophy

School of Marine Science and Engineering
Faculty of Science and Technology

December 2009

Beach morphodynamics behind a series of detached breakwaters in a mesotidal environment, by Iain Alastair Fairley.

Morphodynamics of beaches protected by detached breakwaters have been investigated in this thesis at timescales ranging from days to years. A site consisting of nine breakwaters on a coast open to energetic wave conditions in a meso-tidal environment is studied. Two phases of breakwaters were built at the site: phase one comprising of four fully emergent, 200m long structures, which have caused the formation of tidal tombolos; and phase two, five 160m long breakwaters, submerged at high tide, behind which salients have formed. The site allows for comparison of response at beaches protected by different breakwater designs under similar wave and tidal forcing.

Three analysis strands are presented: video derived intertidal changes; differential global positioning system (DGPS) surveys; and numerical modelling of the breakwater scheme. Together, the three strands allow for determination of important changes to beach morphology and their relation to forcing. A dataset of weekly mean sea level contours and a set of pre- and post- storm inter-tidal surveys were extracted from the video data. DGPS surveys were conducted of the beach and the inshore bathymetry at monthly intervals; these allowed definition of supra- and sub-tidal changes not achievable from the video data. A 'state of the art' numerical model, MIKE21, was used to model waves, hydrodynamics and sediment transport about the scheme for prevailing boundary conditions. The numerical modelling gave insight into the sediment transport pathways and the relative importance of waves and tides as driving forces for morphological change.

The beaches protected by the breakwaters were found to be eroding at an average rate of 0.5m yr^{-1} (vertical elevation change), a rate comparable to unprotected beaches. Thus it seems the detached breakwater scheme is failing to substantially reduce the local erosion problem. The dynamic nature of the beaches, especially the tombolos and salients, means that an equilibrium shoreline cannot be established. The breakwater protected beaches were less variable than the unprotected beaches, displaying 65-75% of the standard deviation of vertical change. However, morphological changes were still considerable: range in cross-shore movement of the mean sea level contour was between 6m in the bay centres and 80m on the tombolo horns.

Empirical orthogonal function analysis of the DGPS and mean sea level contour datasets allowed for determination of three main modes of change which were similar for both phases. The changes were: a general erosion and accretion (46-75% of the dataset variance), a longshore movement of the salients and tombolos (6-27% of the dataset variance), and cross-shore profile changes (~10% of the dataset variance). Correlation analysis and consideration of the numerical modelling results and storm induced morphological change provided relation of the observed changes to wave and tidal forcing. Differences in morphological response were noted for the different breakwater designs. Patterns of response behind the larger breakwaters were better defined due to higher gradients in wave energy between sheltered and unsheltered regions. Cross-shore changes displayed additional three-dimensionality for the smaller breakwaters which led to an increase and decrease in the amplitude of salient sinuosity. An additional mode of change, sub-tidal erosion and accretion of the bay floors, was observed for the larger breakwaters.

Temporal signals showed more seasonality for the phase two breakwaters. In summer the beaches protected by the smaller breakwaters were wider, higher and salient amplitudes were greater. The changes behind the phase one breakwaters exhibited greater dependence on specific wave and surge events. The general erosion and accretion showed an eroding trend with erosion exacerbated by higher water levels for beaches protected by both sizes of breakwater. The longshore movement of the tombolos and salients was forced by obliquely incident waves. For the tombolos, numerical modelling also demonstrated the importance of tidally induced movement. Magnitude of longshore movement (typically ~25m) depended strongly on the antecedent morphological conditions. Cross-shore profile changes were storm induced for the beaches protected by the larger structures: storms reducing profile gradients rapidly and subsequent post-storm recovery. For the beaches protected by the smaller structures, storm induced gradient changes were also important but an additional correlation with wave period was noted. The sub-tidal changes to the phase one bay floors were forced by storm and surge conditions.

Table of contents

List of Figures

Chapter 4

List of Tables

List of symbols

a – semi-major axis of ellipse
a_k – kth normalising factor from EOF de-composition.
a – semi-minor axis of ellipse
c_k – kth temporal component from EOF de-composition.
d_{50} – Median grain size
ds – Depth of water at breakwter
e_k – kth spatial eigenfunction from EOF de-composition.
G_b – Breakwater gap length
G_B^* - Dimensionless gap length
g – gravity
HT – High tide level
H_s – Significant wave height
h – water depth
I_s – Beach response index
k_s – Bed roughness length
k_1, k_2 – Distortion co-efficients
L – Wavelength
L_b – Breakwater length
L_i – geometrical co-efficient of camera calibration where i=1:11.
L_B^* - Dimensionless breakwater length
M – Manning number
n_t – Number of temporal samples
n_x – Number of spatial samples
Q_l – Rate of longshore sediment transport (directional)
Q_{abs} – Non directional longshore sediment transport
RTR – Relative tidal range
R – Pearson's product moment correlation co-efficient
S_{xx} – X component of radiation stress
S_{yy} – Y component of radiation stress
t – Time
TR – Tidal range
T – wave period
T_m – Mean wave period
T_p – Peak wave period
U – Image co-ordinate
u – current velocity in x-direction
V – Image co-ordinate
v – current velocity in y-direction
x – Real world co-ordinate system x-component
X_b – Distance from shoreline to breakwater
X_c – Computed value
X_m – Measured value
ΔX_m – Measurement error
X_s – Sailent length
X_s^* - Dimensionless salient length
y – Real world y co-ordinate

z – Real world z (elevation) co-ordinate
α_b – wave angle at breaking.
η – Wave set-up
ρ- Water density
δ_{nm} – Kronecker delta
λ_k – Eigenvalue of the k^{th} eigenfunction

Acknowledgments

This thesis has been completed via a studentship provided by the U.K. Engineering and physical sciences research council as part of the LeaCoastII project.

Foremost, a huge amount of thanks to Dr. Mark Davidson, my primary supervisor for endless advice and encouragement. Thanks also to Dr. Ken Kingston, my second supervisor, particularly for advice on all matters Argus.

I am indebted to all participants in the LeaCoastII project, the coastal processes team at University of East Anglia in particular. Of this group, Dr. Tony Dolphin must be singled out for his support, advice and encouragement.

Irv Eshoff and Robin Morrelison, of Deltares, were particularly helpful in the initialisation of the Sea Palling argus system and the implementation of the new generation of Argus code. Peter Ganderton's help was also invaluable in the initialisation of the Argus system.

I would like to thank Sarah, my parents, office mates, and friends for ongoing support during the course of my PhD studies.

AUTHOR'S DECLARATION

At no time during the registration for the degree of Doctor of Philosophy has the author been registered for any other University award without prior agreement of the Graduate Committee.

This study was financed with the aid of a studentship from the Engineering and Physical Sciences Research Council.

Relevant scientific seminars and conferences were regularly attended at which work was often presented; external institutions were visited for consultation purposes and several papers prepared for publication.

Publications:

Fairley, I., Davidson, M., Kingston, K., Dolphin, T., Phillips, R., 2009, Empirical Orthogonal Function Analysis of Shoreline Changes Behind Two Different Designs of Detached Breakwaters. Coastal Engineering, 56(11-12): 1097-1108.

Fairley, I., Davidson, M., Kingston, K., 2009. The morpho-dynamics of a beach protected by detached breakwaters in a high energy tidal environment. Journal of Coastal Research, S.I. 56 (Proceedings of 10th International Coastal Symposium): 607-611.

Fairley, I., Davidson, M., Kingston, K., 2009. Video monitoring of overtopping of detached breakwaters in a mesotidal environment, Proceedings, 5th Coastal Structures International Conference, World Scientific, Venice. 1923-1932

Fairley, I., Davidson, M., Kingston, K., 2009. A Video Based Investigation into the Morphological Impacts of Storms Behind a Series of Detached Breakwaters, In: R. Lehfeldt and H. Schuttrumpf (Editors), Poster Proceedings of 31st International Conference on Coastal Engineering. Druckservice Zillekens, Hamburg, pp. 80-91.

Presentations, Courses and Conferences Attended:

Coastal and Estuarine Morpho-dynamics Summer School, Skallingen, Denmark, 2007.
Coastal morphodynamics short course at ICCE08, Hamburg
Young Coastal Scientists and Engineers Conference 2007, Plymouth, UK, Poster presentation.
Coastal Structures '07, Venice, Italy, Oral presentation,
Coastal Engineering 2008, Hamburg, Germany, Poster presentation,
International Coastal Symposium 2009, Lisbon, Portugal, Oral presentation,
Various internal seminars at University of Plymouth.

External Contacts:

Coastal Processes Research Group, University of East Anglia.

Word count of main body of thesis:55,980

Signed Ian Fairley

Date 1/06/2010

xxx

Figure 1.1: A photograph showing three rubble mound detached breakwaters used to protect a vulnerable village. The accumulation of sediment behind the breakwaters, in the form of tombolos, can clearly be seen. Also observable is the formation of an embayed beach between the two structures.

1. Introduction

1.1 Motivation for research

The coastal zone experiences substantial pressure due to the conflict between increasing coastal development and the threat of coastal erosion. Over 70% of the world's population live in the coastal zone (Charfas, 1990) and coastal areas are popular and lucrative tourism destinations (Coombes *et al.*, 2009). Both these factors lead to large investment in coastal infrastructure. Equally, the threat of rising sea levels and increased storminess exacerbate problems of coastal erosion (IPCC, 2007). Clearly, to protect both lives and investment, measures must be taken to protect and stabilise vulnerable coastlines. Despite, recent promotion of 'soft' defence, whereby receding coastlines are left to erode, societal pressures on policy makers (Myatt *et al.*, 2003) mean that this approach is rarely taken in populated areas. Instead, a 'hold the line' approach utilising hard structures, such as groynes, sea walls and breakwaters, to maintain current coastline positions is often taken. This means that beaches are often artificially formed and maintained by human intervention.

One coastal protection strategy, that has become prevalent world wide, is deployment of a detached breakwater scheme (Figure 1.1). These can be built as a single structure or in series and with varying crest levels from fully emergent to completely submerged. The sheltering effects of the breakwaters lead to accumulation of sediment in their lee, producing wider beach widths and greater protection of the hinterland. This accumulation can take the form of tombolos, where the accreted material reaches the breakwater, or salients, where the shoreline becomes sinuous but does not reach the structure. Where detached breakwaters are deployed in series, the beaches take the form of embayments similar to natural embayed, or pocket, beaches. A wide variety of research into coastal protection structures is required to inform coastal engineers and managers so that the correct structures can be implemented given specific coastal management aims.

There is a large body of work on detached breakwaters, the focus of this effort has been on their effect on hydrodynamics (Loveless *et al.*, 1998; Drei and Lamberti, 1999; Loveless and Macleod, 1999; Van der Meer *et al.*, 2000; Van Der Meer *et al.*, 2004; Caceres *et al.*, 2005; Ruol *et al.*, 2005; Van der Meer *et al.*, 2005; Caceres *et al.*, 2008), equilibrium conditions and design criteria for predicting the plan-forms they produce (Pope and Dean, 1986; Suh and Dalrymple, 1987; Ahrens and Cox, 1990; McCormick, 1993), or comparison of case studies with design predictions (Thomalla and Vincent, 2004). Much of this research has been conducted in low energy, low tidal range environments and thus further research is required in tidal environments (Pilarczyk and Zeidler, 1996) and under UK conditions (Ilic *et al.*, 2005b). Little attention has been paid to man made beach morphodynamics on short to medium timescales (Ojeda and Guillen, 2008). This is the case for artificial beaches created by detached breakwater systems. As more and more beaches become artificially maintained to some extent, research is required into the short to medium term morphodynamics of artificially created / maintained beaches. This research is required

both to give further insight into breakwater protected beaches for coastal managers and to determine similarities in morphodynamic response between artificial and natural beaches.

1.2 The LeaCoastII project

The work presented in this thesis was undertaken as part of the EPSRC funded LeaCoastII project. The aim of this research project was to develop understanding of the morphodynamics of beaches protected by detached breakwaters in meso-tidal UK conditions over long spatial and temporal scales, hence rectifying the knowledge gap identified by Pilarczyk and Zeidler (1996). The project built on a previous grant, LeaCoast, which focussed on morphological changes induced by storms (Bacon *et al.*, 2003; Zhu *et al.*, 2004; Bacon *et al.*, 2005; Dolphin *et al.*, 2005; Bacon *et al.*, 2007). Partners from the University of Plymouth (UOP), University of East Anglia (UEA), Proudman Oceanographic Laboratory (POL) and BODC utilised various numerical modelling methodologies, in-situ process experiments and routine data collection via a video system, radar and beach and bathymetric surveys were used to investigate changes at the site. The project focussed on the detached breakwater scheme at Sea Palling on the East coast of England (described in detail in Chapter 3). The beaches at this site are protected by 9 breakwaters of two designs behind which both tombolos and salients have formed. The great advantage of using this site is the ability to study the similarities and differences in morphological response for beaches protected by the two different designs undergoing near identical hydrodynamic forcing conditions. The coastal processes team at UEA, lead by Professor Chris Vincent and Dr. Tony Dolphin, collected routine monthly GPS beach and bathymetric surveys and deployed some in situ instruments. The team from POL deployed in situ meausurment instruments (Prof. Peter Thorn and Dr. Judith Wolf) and conducted radar based remote sensing (Dr. Paul Bell). The coastal engineering department at UOP

conducted two types on numerical modelling: A team lead by Prof. Dominic Reeve looked at 1- and n-line morphological modelling of the breakwater system whilst a team led by Prof. Shunqi Pan investigated 3-d numerical modelling of the site. The results from this research project were fed to commercial partners from HR Wallingford and Halcrow with the aim of incorporating them into new design guidelines for detached breakwaters in the U.K.

The specific role of the PhD within the LeaCoast2 project was to utilise the Argus video system to analyse morphological changes at the site. The video system allows a higher temporal sampling resolution than global positioning system surveys. This means that shorter temporal scale changes can be identified and hopefully better links to wave and tidal forcing developed. To aid and enhance understanding of the changes observed in the video the UEA collected DGPS data was analysed and a 2DH numerical model of the scheme was set up using MIKE21. MIKE21 is a commercially available coastal area model produced by the Danish Hydraulic Institute. The 2DH model was run to test characteristic wave and tidal conditions. The use differed from the previously mentioned numerical modelling exercises because generic rather than actual events were modelled.

1.3 Thesis objectives

The work presented here aims to investigate the morphodynamics of breakwater protected beaches on timescales ranging from days to years, hence filling a gap in research on short to medium term morphodynamic response of artificial beaches identified by Ojeda and Guillen (2008) and extending detached breakwater research to provide greater understanding of breakwater effects in tidal conditions (Pilarczyk and Zeidler, 1996) and in UK environments (Ilic *et al.*, 2005a).

The specific aims of this thesis are:

1) To extend previous research at the site, which focussed on the larger breakwaters, to the second phase of breakwaters,
2) To quantify the morphological variability of the scheme,
3) To determine types of morphological changes at the Sea Palling breakwater protected beaches,
4) To establish forcing mechanisms and timescales of morphological change,
5) To utilise a numerical model of the site to gain understanding of the site hydrodynamics and sediment dynamics, and the balance between wave driven and tidally driven forcing,
6) To compare the morphodynamic response of the two different designs of breakwaters.

A secondary outcome will be to establish the evolution of the scheme over the time period analysed, which will establish whether the scheme is successfully performing a coastal protection role.

1.4 Thesis content and structure

In this thesis, data from an Argus video system (Holman and Stanley, 2007) and differential global positioning system (DGPS) surveys are used to determine types and timescales of morphological change at the Sea Palling study site. Statistical techniques are used to form links between wave and tidal forcing and morphological change. A numerical modelling system (DHI's MIKE21) will be used to provide insight into the causal mechanisms of the morphological changes by establishing current and sediment transport pathways around the scheme under different conditions. A review of the current literature on these topics will be presented in Chapter two and the study site described in detail in Chapter 3.

Two datasets were collected from the Argus video cameras (Chapter 4): A set of pre and post storm surveys and a time series of the mean sea level contour. Patterns of erosion and accretion over storms were determined from the pre- and post- storm surveys and these related to the forcing conditions. The mean sea level contour dataset was analysed using an empirical orthogonal function (EOF) analysis which allowed determination of modes of change and correlation of that change with forcing conditions.

Video derived morphology is restricted to the intertidal region and so the DGPS surveys were used to extend the analysis into the sub- and supra- tidal regions (Chapter 5). The DGPS surveys were analysed using both simple techniques and via an EOF analysis similar to that used on the MSL dataset but extended to 2 spatial dimensions. This section allowed determination of cross-shore changes as well as isolation of additional sub-tidal changes in the bay regions of the larger breakwaters.

The numerical model was used to examine the current patterns and sediment transport pathways caused by characteristic wave and tidal conditions (Chapter 6), which could be related to the morphological changes observed in the video (Chapter 4) and DPGS surveys (Chapter 5).

The synthesis of the three analysis strands allows for development of understanding of the different modes of response (Chapter 7). These changes can then be considered in terms of other breakwater protected beaches and natural beaches and the implications of the research discussed.

2. Literature review

2.1 Foreword

Detached breakwaters are used worldwide as a method of shore protection promoting the formation of tombolos or salients in their lee and increasing beach widths. Little research has been conducted at detached breakwater schemes in high energy tidal environments, nor has there been substantial investigation into short to medium timescale morphodynamics of breakwater protected beaches. This study addresses the deficit in research by investigating responses of a detached breakwater protected beach to wave and tidal forcing using analysis of video derived data, DGPS surveys and numerical modelling using MIKE21. The literature review will follow broadly that form: describing current knowledge about detached breakwater hydrodynamics and morphodynamics; video analysis techniques; numerical modelling, and the statistical techniques used. Work specifically relating to Sea Palling (the study site) will be presented in Chapter 3 which provides background information on the site.

2.2. Detached Breakwaters

2.2.1. Introduction

The first detached breakwater was built in 1905 in Santa Monica, USA (Ilic *et al.*, 2005) and the first investigations into the effect of detached structures on beach morphology were undertaken around the same time (Vedel, 1905). Detached breakwaters solely designed for shore protection were built by the 1930's but it was not until the 1970's that their usage became prevalent (Komar, 1998). Detached breakwaters can be built in isolation to protect a particularly vulnerable area, or in series (known as a segmented breakwater system) in order to protect a length of coastline. The first detached breakwater in the U.K. was built in

1982 at Leasowe bay on the Wirral and consisted of two breakwaters. Further small schemes were built at Monks bay, Isle of Wight, King's Parade, Wirral and Sidmouth, Devon. A larger scheme consisting of eight breakwaters was built at Elmer in West Sussex (King *et al.*, 2000) and another scheme of nine breakwaters was built at Sea Palling, Norfolk (Hamer 1998).

Detached breakwaters can be either submerged or emergent and their interaction with the near shore hydrodynamics and sediment transport patterns vary considerably depending on this distinction (Martinelli *et al.*, 2006). Sediment deposits build up behind the breakwater due to the forced current patterns and the breakwater preventing offshore transport of sand. Differing morphological forms can be produced: Tombolos, where a spit is formed that joins to the breakwater; salients, where a sinuous shoreline is formed that protrudes towards the breakwater without reaching it; or no shoreline change (Komar, 1998). These distinctions are clearly continuous and formations at a breakwater system may vary over time depending on forcing conditions. In tidal conditions distinctions are less clear cut with the possibility of salients at high tide and tombolos at lower tides, hereafter referred to as a tidal tombolo (King *et al.*, 2000; Bacon *et al.*, 2005), or equally salients at low water and no appreciable change at high water. The effect of detached breakwaters on hydrodynamics and beach morphology is still poorly understood (Pilarczyk and Zeidler, 1996).

2.2.2 Moderation of coastal hydrodynamics by detached breakwaters.

Detached breakwaters create a variety of morphological features depending on a delicate balance of hydrodynamic processes. Emergent detached breakwaters shelter the area directly behind the breakwater from the full force of the incident wave energy although a certain proportion of the wave energy is transmitted through the breakwater. Wave energy

is translated into the protected area via diffraction and refraction. This causes a longshore variation of wave height that causes a longshore variation in set-up height which drives currents towards the sheltered area. Diffraction also alters the angle of wave incidence which changes longshore current patterns, although sediment formations reduce this effect once a scheme is in equilibrium. Currents are deflected by the breakwaters and the morphological features to produce complex circulation patterns (Gourlay, 1974).

Submerged breakwaters produce different circulation patterns based on the amount of wave transmission and overtopping (Pilarczyk and Zeidler, 1996; Ranasinghe and Turner, 2006). A schematic of the different standard predicted current patterns is shown in Figure 2.1.

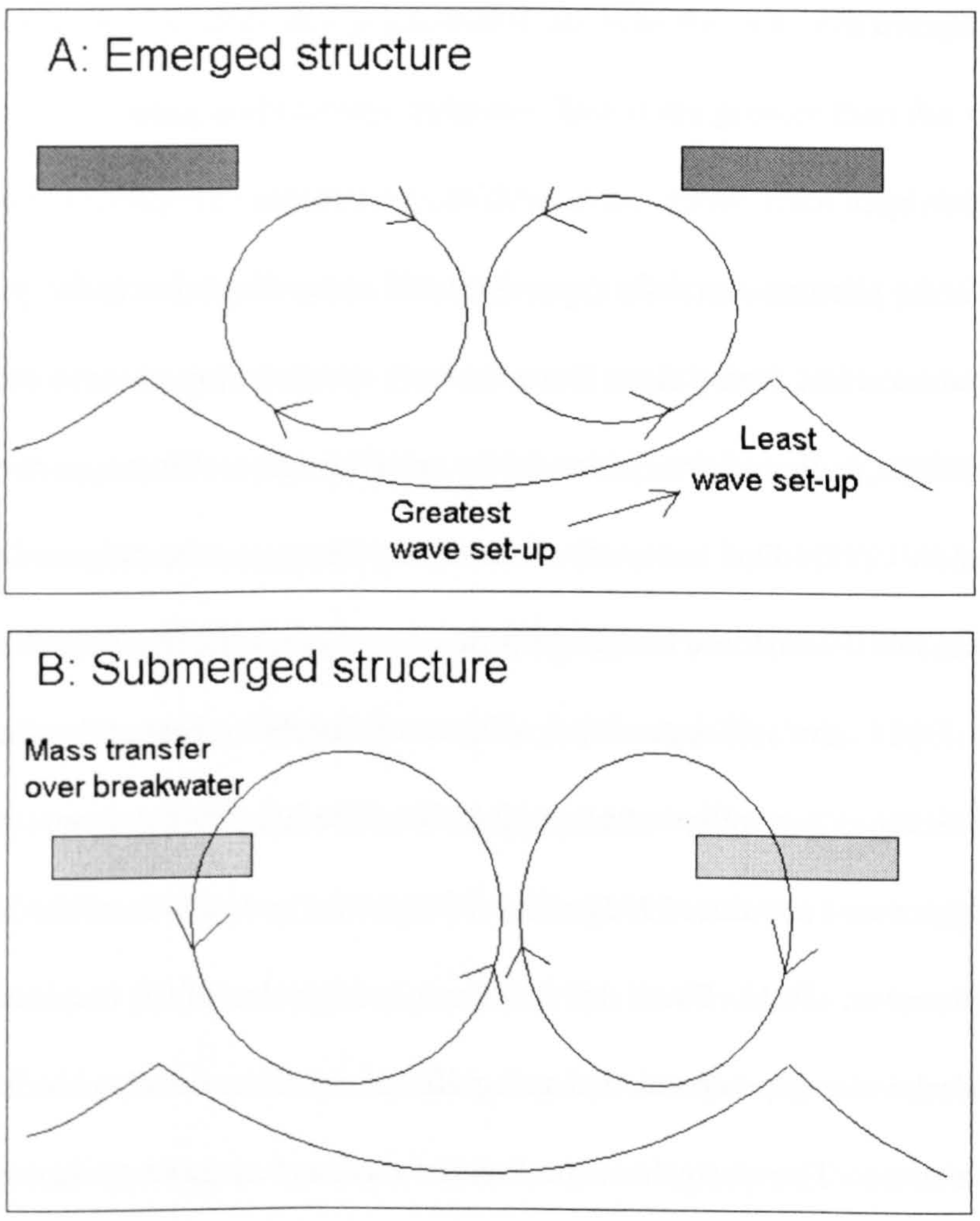

Figure 2.1 Current patterns for A: an emerged structure and B: a submerged structure

2.2.3 Wave Diffraction

Diffraction is the phenomenon whereby energy is transmitted along the wave crest. Diffraction was first scientifically observed in light waves by Francesco Maria Grimaldi whose results were published in 1665. It was he who coined the term 'diffraction.' In coastal oceanography, it is most noticeable in circumstances such as breakwater systems where there is wave shadowing. Diffraction causes energy leakage into the shadow zone so that some wave energy penetrates the breakwater protected area (Komar, 1998). Diffraction causes bending of the wave rays which mean that, until a breakwater system is in equilibrium, longshore currents are generated towards the centres of the breakwaters (Komar, 1998).

2.2.4 Wave set-up.

Wave setup is the phenomenon of a super-elevated water-level due to the presence of waves. Radiation stress theory describes a force in the direction of wave propagation (S_{xx}) and a force at right angles (S_{yy}) to it due to the orbital motion of water particles in the waves, (Komar, 1998). Due to Newton's laws this force must be balanced by an equal and opposite force. For the onshore momentum flux S_{xx}, this results in a pressure gradient formed by a slope in the still water level, with water levels highest at the shoreline.

Wave setup is generally between 10-20% of the height of waves at breaking (Longuet-Higgins and Stewart, 1963) and is often estimated at 17% of the wave height (Guza and Thornton, 1981). Since the wave height in the lee of the breakwaters is smaller than in the breakwater gaps due to sheltering effects and directional spreading, the set up levels are lower too. The alongshore gradient in wave set-up generates currents at the shoreline flowing from the region of greatest setup, the bay centres, to the region of the lowest setup, the centre of the sheltered region (Gourlay, 1974).

2.2.5 Overtopping/wave transmission

As described in the previous section, detached breakwaters cause currents to be driven towards their centres by variations in wave set-up caused by wave sheltering and by obliquely incident waves caused by diffraction. However, when breakwaters are submerged or have a low freeboard, wave transmission and overtopping can reduce or even reverse this process. Overtopping and transmitted waves can generate a wave field behind the structure where ordinarily, or in the case of an impermeable structure, one might not expect one (Van Der Meer *et al.*, 2004).

Several 2-D physical model studies have shown that water levels can be significantly higher behind detached breakwaters because the volumes transmitted landwards (via overtopping and through structure flows) are greater than the volumes returning offshore through the structure (Loveless *et al.*, 1998; Ruol *et al.*, 2005). Such a process is commonly termed piling up, although some authors' term the phenomenon breakwater controlled setup. Piling up depends upon crest height and offshore wave height, with maximum piling up observed with zero freeboard (Loveless *et al.*, 1998) and increasing wave height increasing piling up levels (Drei and Lamberti, 1999).

In the 3-D case the observed levels of piling up are much smaller because water can return offshore though gaps in the breakwater (Loveless and Macleod, 1999). Since the volume of overtopped water is the same, this necessarily results in strong offshore flows (Ruol *et al.*, 2005; Martinelli *et al.*, 2006). The effect on beach evolution of these currents is not well understood (Loveless and Macleod, 1999). However it is deemed possible that these currents could act to erode any tombolos deposited at lower water levels or wave heights. Numerical simulations have shown that when overtopping occurs there is an increase in return flows through breakwater gaps of between 19-100% (depending on overtopping formulation used) and an increase in currents along the leeside of the

breakwater of 10-15% (Caceres *et al.*, 2005). This demonstrates the importance of currents generated by overtopping waves. The same study considers the effect of overtopping on a single breakwater and finds the circulation field behind the breakwater is significantly altered with the direction of the cross-shore current reversed.

Factors that influence the amount of wave transmission include the angle of wave attack, whether the waves are long or short crested and the design and construction material of the breakwater. Lab based experiments done by Van Der Meer (2004) suggest that there is very little difference between long and short crested waves (~1% difference). Angle of incidence had very little effect on the transmission co-efficient for low crested structures, for higher crested structures the transmission co-efficient reduces slightly although it is not thought significant. When waves approach a rubble mound structure obliquely it is found that the angle of the transmitted waves is about 80% of the angle of incident waves. It is postulated that this to do with the pattern of wave energy dissipation (Van Der Meer *et al.*, 2004). Information about obliquely incidence waves is of importance at Sea Palling where the wave climate is highly variable in direction. Wave steepness is also a factor with greater wave steepness leading to reduced transmission as more energy is dissipated by the wave breaking process, (Ruol *et al.*, 2005).

As well as only a proportion of the wave energy being transmitted, spectral changes can be observed with higher frequencies being dissipated more by the breakwater and so a higher proportion of the transmitted energy is low frequency (Van Der Meer *et al.*, 2004).

Most of the work done on breakwater overtopping is done using modelling (either physical or numerical) studies. A certain amount of work has been done to investigate full scale over-topping of breakwaters but very little of this relates to the sloping rubble mound design (the Sea Palling type). This normally is achieved through tanks on the lee side of breakwaters which are instrumented to measure overtopping volumes, (Troch *et al.*, 2004;

Briganti *et al.*, 2005). The breakwaters used in these studies are significantly larger than those found at Sea Palling, incorporating roads along their crests. Some conclusions from these full-scale tests are still likely to be relevant to the Sea Palling scheme. An onshore wind increases the rate of overtopping with a factor of two wind increase leading to a factor of five increase in overtopping (Briganti *et al.*, 2005). Large wave events are normally accompanied by strong onshore winds at Sea Palling which would favour such increases in overtopping.

2.2.6 Morphodynamic responses to detached breakwaters.

The concept behind detached breakwaters is that they should produce an equilibrium bay where wave crests are normally incident at all points due to diffraction. However, other responses have been observed: a breakwater system in Louisiana, USA, exhibited a novel sediment formation termed reverse salients whereby sediment built up from the lee of the breakwater towards the shore. It was explained that such a formation was due to dominant cross-shore, rather than long shore, sediment transport patterns with the offshore component of this being trapped by the breakwater (Stone *et al.*, 1999). In some cases erosion rather than accretion has been observed, especially for submerged breakwaters (Dean *et al.*, 1997)

Angle of wave approach can effect the shape of the features formed (Thomalla and Vincent, 2003), with the shape of the equilibrium bay skewed in regions of predominantly oblique wave approach. The longshore dimension of an equilibrium bay is fixed by the breakwater layout whereas the cross-shore dimension depends upon the amount of wave transmission (Ilic *et al.*, 2001). Martinelli *et al.* (2006) report that, based on physical and model simulations, beach steepening occurs in the swash zone behind a breakwater scheme.

Due to the tidal regime present in the UK, relatively few detached breakwater schemes have been built. One scheme that has received considerable attention is the scheme at Elmer, West Sussex because it, along with Sea Palling, is the only large breakwater scheme in the UK. The beach at the scheme consists of a shingle upper beach and sand lower beach and has a mean spring tidal range of 5.3m. Eight inter-tidal rock island break waters were constructed with a terminal groyne at the down drift end (King *et al.*, 2000). The scheme differs significantly from Sea Palling in that the breakwaters are in the intertidal zone, the beach sediment is considerably different and the tidal range much larger. At Elmer sandy tidal tombolos were formed with shingle salients on top of these. These size of the shingle salients were much larger than expected in the design guidelines (King *et al.*, 2000).

Much of the work done on the effect of breakwaters on beach morphology has taken the form of design guidelines (see next section). These are based on the geometry of the scheme. It has been reported, based on numerical modelling work, that the effect of differing wave climate and sediment characteristics on morphological changes behind a certain type of breakwater design are minimal (Zyserman and Johnson, 2002). The only stipulation for this to hold is that there is enough sediment available for the scheme to reach equilibrium.

Larger scale morphological effects also occur due to detached breakwaters influence on the longshore sediment transport. If tombolos form they can effectively block longshore sediment transport through a scheme. This often leads to significant erosion down drift of a scheme if a scheme is situated in a region with a predominant direction of longshore transport (King *et al.*, 2000; Bowman and Pranzini, 2003). Equally sand can be stored up-drift of a scheme widening beaches in this region (Thomalla and Vincent, 2003). The direction of longshore sediment transport can also have an effect on the morphology behind

a series of breakwaters with differing amount of sediment being available to the different embayments and causing differing morphological features. In severe cases this can cause erosion and no salient/tombolo formation behind the furthest down drift breakwaters (Bowman and Pranzini, 2003).

Short term morphodynamics have received less attention. Sedrati *et al.* (2009) investigated the behaviour of a swash bar on a micro-tidal beach protected by a low crested structure and found behaviour very similar to natural beaches. Axe and Chadwick investigated profile variability behind the detached breakwater system at Elmer using a gridded empirical orthogonal function analysis (Axe and Chadwick, 1997). They discovered that profile variability was reduced within the breakwater scheme compared to up and down drift regions. Two seasonal beach states were observed: in winter sediment was stored on elevated bay floors; in summer sediment was stored in an accretionary berm. A submerged breakwater at Lido de Dante, Italy, has been subject to substantial research effort (Archetti and Lamberti, 2006; Archetti and Lamberti, 2008; Archetti, 2009). A beach rotation was observed under storm conditions, although this is possible more due to groynes than the submerged structure, it was found that sediment was eroded from the up-drift side of the embayments and deposited against the down drift groyne

2.2.7 Design Guidelines

In order to design reliable offshore breakwaters various methods are used, both physical and numerical modelling can be used to predict shoreline response once a scheme's parameters are known. In order to effectively design these parameters various empirical guidelines have been produced based on quantities such as breakwater lengths, gap widths and distances offshore. Many different guidelines have been proposed, giving either salient

lengths, shoreline curves or descriptive classifications. The most commonly cited are described in the following paragraphs.

Pope and Dean (1986) looked at seven different breakwater systems in the USA and created a descriptive classification based on two parameters: the ratio of segment length to gap length (which represents the transmission of incident wave energy) and the ratio of structure to shore distance and water depth (which represents the structure capability to affect wave transformations). This classification scheme is shown in Figure 2.2. However all the schemes studied were situated in relatively low energy wave environments with short period waves meaning the guidelines have limited applicability.

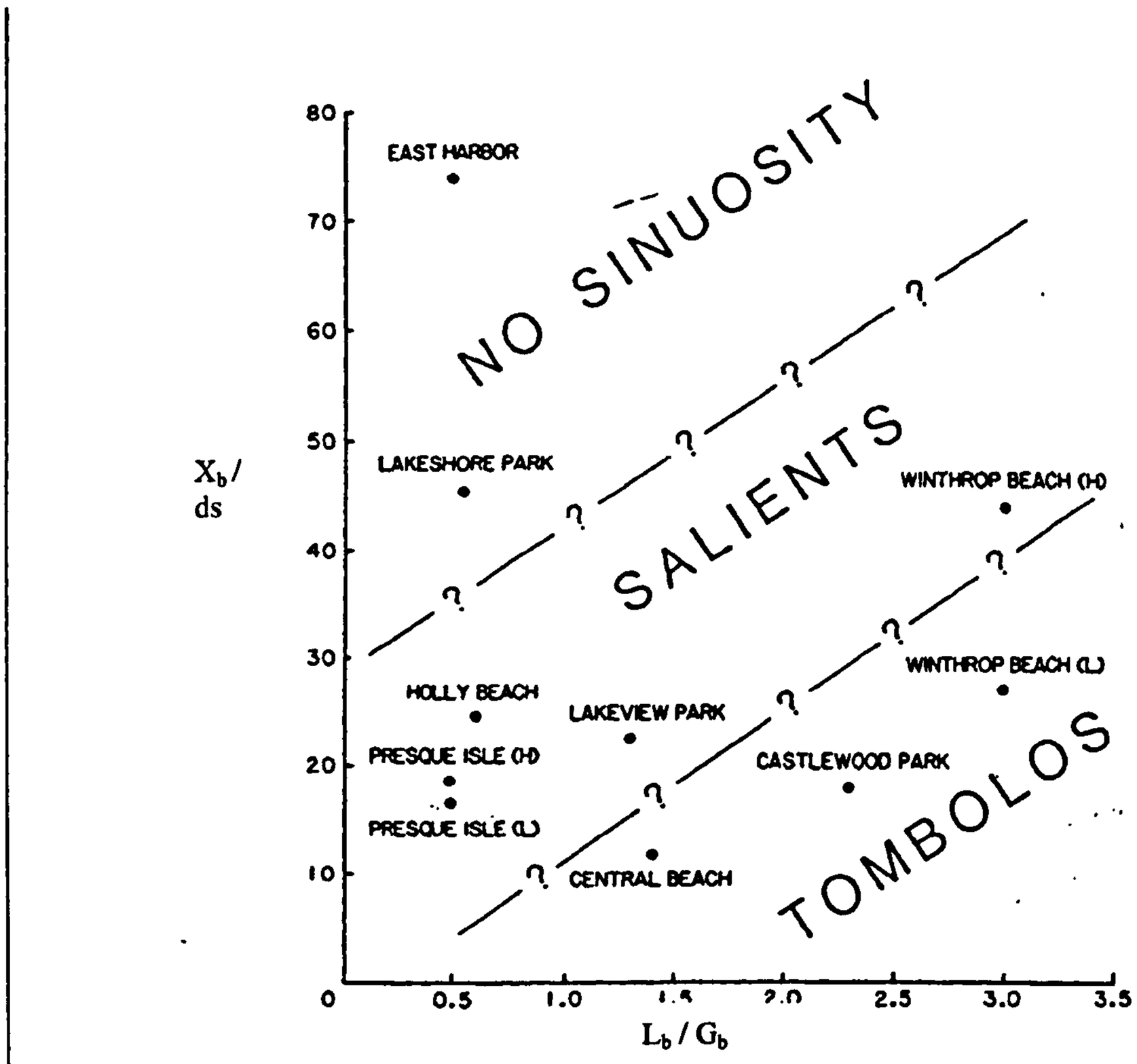

Figure 2.2: A diagram describing the beach response depending on breakwater parameters (Pope and Dean, 1986). L_b is the breakwater length, G_b is the breakwater gap width, X_b is the distance from shoreline to breakwater and *ds* is the local water depth at the breakwater

A beach response index (I_s) was suggested to fit the Pope and Dean (1986) categories (Ahrens and Cox, 1990). This ranges between 1-5, with 1 being permanent tombolos, and 5 being no sinuosity. Ahrens and Cox (1990) used regression analysis to fit an equation for their beach response index based on the Pope and Dean (1986) data. The equation was:

$$I_s = \exp\left[1.72 - 0.41\left(\frac{L_b}{X_b}\right)\right] \tag{2.1}$$

Where L_b=breakwater length, X_b=effective distance offshore.

Suh and Dalrymple (1987) used small scale model tests in a radial wave basin to determine the morphological changes due to both a single offshore breakwater, and breakwaters in series. For a single breakwater, differing morphological features were formed depending on the dimensionless breakwater length, the ratio of breakwater length to distance of breakwater offshore (L_b/X_b). Generally a double tipped salient was formed which turned into a single tipped salient over time due to the offshore current. In cases where the breakwaters were further offshore no morphological changes were observed even in cases when L_b/X_b was the same as inshore breakwaters that produced morphological change. For the case of multiple breakwaters, the only parameter varied was the gap spacing. With a gap spacing of twice the incident wavelength the breakwaters behaved independently, for smaller gaps elliptic erosive patterns occurred in the gaps and salients evolved behind the structures. One anomaly was the presence of a tombolo behind the furthest breakwater down-drift. This is contrary to popular belief that since sediment supply lessens down-drift, through a scheme the up-drift breakwater should have the largest morphological features.

By fitting a curve to this data and data collated from other sources Suh and Dalrymple (1987) found an equation for the dimensionless salient length, X_s^* (the salient length divided by the breakwater length). This equation is:

$$X_s^* = 14.8\left(\frac{G_B^*}{L_B^{*2}}\right)\exp\left[-2.83\left(\frac{G_B^*}{L_B^{*2}}\right)^{1/2}\right] \tag{2.2}$$

where G_B^* is the dimensionless gap width (gap width divided by distance of breakwater offshore) and L_B^* dimensionless breakwater length previously mentioned.

McCormick (McCormick, 1993) built on the work of Hsu and Silvester (1990) to produce an equation for the equilibrium shoreline behind both single and multiple detached breakwaters. For wave incidence normal to the shoreline (α_0) the equation is:

$$\frac{(y \mp h)^2}{a^2} + \frac{x^2}{b^2} = 1 \tag{2.3}$$

Where the notation is described on the below diagram (Figure 2.3), h is the distance from the breakwater centre to the centre of the ellipse, a is the ellipse's semi-major axis and b the semi-minor axis. These all depend on the beach slope, the deep water wave steepness, the breakwater length and the distance from the original shoreline to the breakwater. The positive and negative components refer to the up-drift and down-drift shorelines.

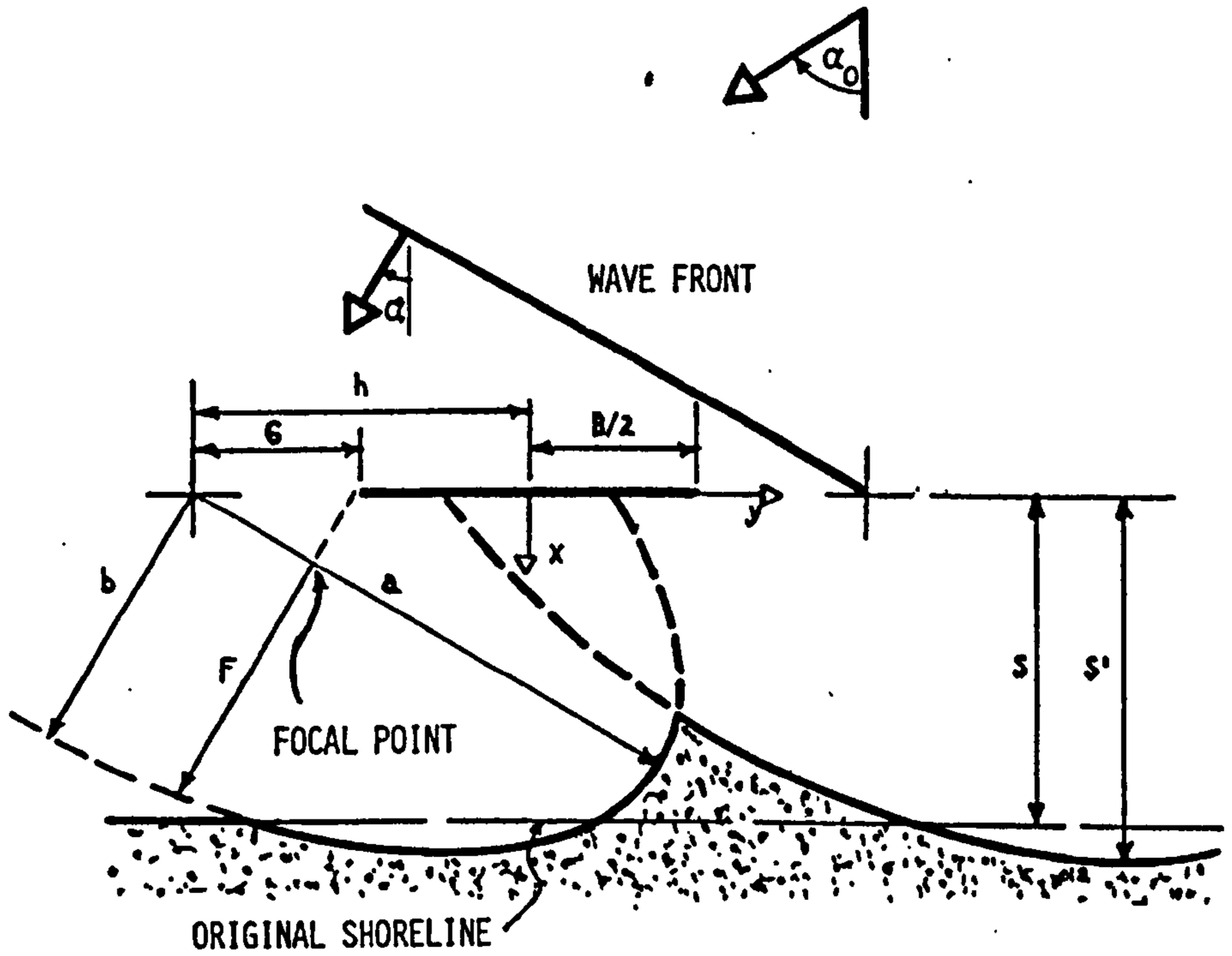

Figure 2.3: A diagram showing the shoreline response behind a breakwater and its notation (McCormick, 1993)

Equation 2.3 is generalised to the situation of oblique approach:

$$\frac{[Y \mp h\cos(\alpha)]^2}{a_\alpha^2} + \frac{[X \pm h\sin(\alpha)]^2}{b_\alpha^2} = 1 \qquad (2.4)$$

Where $X=x\ cos(\alpha)-y\ sin(\alpha)$ and $Y=x\ sin(\alpha)+y\ cos(\alpha)$. Different equations are given for a_α and b_α depending on whether a single breakwater or segmented system is being considered. The equation was tested against data from an 11 breakwater system on Chesapeake bay and was found to fit the surveyed data well.

All these guidelines have been designed for low energy environments and without consideration of tidal effects. Their accuracy in predicting the morphology at Sea Palling

was described by Thomalla and Vincent (2004). In general, the design guidelines failed to accurately replicate the observed shorelines (further discussion in Chapter 3).

2.3. Image analysis and Argus Video Systems

2.3.1 An introduction to Argus Video Systems, their history, uses and benefits.

The Argus network (Holman and Stanley, 2007) originated at Oregon State university where Rob Holman first used time lapse video of wave run-up to study infragravity edge waves (Holman and Guza, 1984) motivated by the difficulty of deploying in-situ instrumentation in the high energy nearshore environment of the United States Pacific north west. It has subsequently grown into an international collaboration of coastal scientists with many camera stations around the world.

Initial work on the extraction of beach profiles from video images was done in order to aid the extraction of swash parameters from video as well as for the study of beach erosion (Lippmann and Holman, 1991). A line was marked on the beach using a hose in order to constrain the alongshore position. Standard photogrammetric principles could then be applied to extract cross-shore distance and vertical elevation information from the images. Tests showed that this technique was accurate to ±5cm. Whilst the tests were conducted on a line marked by a hose, a similar line could be marked using a shadow cast by a pole or by a beam of light at night. This technique gives a low cost accurate technique which enables long term records to be built up easily. However spatial coverage is limited to a few profiles within 100m of the camera.

Quickly other uses for video imaging of the coast became apparent. Time averaged (timex) images allowed the positions of sand bars and rip currents to be determined based on the intensity patters of wave breaking (Lippmann and Holman, 1989). A proxy for shoreline position was found in the intensity maximum due to the shore break in a timex

image (Plant and Holman, 1997). Advantages of video imaging over traditional beach survey techniques include: the high temporal coverage possible which allows capturing of morphological changes that traditional techniques might miss (Elko *et al.*, 2005); large length scales of high resolution coverage; and low time and monetary expenditure.

More recently, utilising the intensities of selected pixel arrays has enabled the collection of hydrodynamic data such as wave celerity, wave period, wave direction and surface currents. Utilisation of the wave celerity have allowed estimation of the sub tidal bathymetry (Stockdon and Holman, 2000). Further shoreline extraction techniques have been developed such as using the differences in Hue Saturation Values between wet and dry pixels, and this combined with knowledge of tidal height and wave conditions allows for intertidal beach profiling (Aarninkhof *et al.*, 2003b).

Argus camera systems are increasingly being used in coastal zone management (Davidson *et al.*, 2004; Turner *et al.*, 2004). The concept of coastal state indicators have been developed which allows quantitative methods to determine when intervention is required in the coastal zone.

2.3.2 Photogrammetric principles and Argus image rectification

Transformations must be made between image (U, V,) co-ordinates and the real world (x, y, z) co-ordinates they represent before useful information can be extracted from images. In order to go from image to real world co-ordinate systems two steps must be taken: firstly the distortion due to the camera lens must be removed; secondly transformation equations between the undistorted (U, V,) co-ordinates and the (x, y, z) co-ordinates must be applied. To go from (x, y, z) to (U, V,) co-ordinates the reverse processes is applied, firstly transforming between co-ordinate systems and secondly applying the distortion (Aarninkhof *et al.*, 2006).

Only the radial distortion is considered. The distortion co-efficients, k_1 and k_2 are obtained by calculating the differences between observed and predicted points on an image of a square grid of circular dots taken in a controlled setting (Holland *et al.*, 1997).

U and V can be calculated from the following co-linearity equations:

$$U = \frac{L_1x + L_2y + L_3z + L_4}{L_9x + L_{10}y + L_{11}z + 1}; V = \frac{L_5x + L_6y + L_7z + L_8}{L_9x + L_{10}y + L_{11}z + 1}; \tag{2.5}$$

Where the co-efficients $L_{1\text{-}11}$ can be calculated from the (x, y, z) co-ordinates of the camera and ground control points with known (x, y, z) and $(U, V,)$ co-ordinates.

If one of the (x, y, z) co-ordinates is known $(U, V,)$ co-ordinates can be rectified using the following inverse relations (Holland *et al.*, 1997):

$$\begin{bmatrix} [L_1 - L_9U] & [L_2 - L_{10}U] & [L_3 - L_{11}U] \\ [L_5 - L_9V] & [L_6 - L_{10}V] & [L_6 - L_{11}V] \end{bmatrix} \bullet \begin{bmatrix} x \\ y \\ z \end{bmatrix} = \begin{bmatrix} U - L_4 \\ V - L_8 \end{bmatrix} \tag{2.6}$$

Conventionally in the rectification of Argus images it is the z value that is constrained with the tidal height at the time of interest being used (Aarninkhof *et al.*, 2003b). Errors in these techniques are of pixel magnitude and are largely due to random calibration errors (Aarninkhof, 2003).

2.3.3 Extraction of information from Argus images

Three main morphological parameters can be extracted from video images: Intertidal beach profiles commonly built up utilising shoreline positions over a tidal cycle; sub-tidal bar locations and surf zone bathymetry based on wave dissipation (Aarninkhof *et al.*, 2003a); and sub-tidal bathymetry based on wave celerity (Stockdon and Holman, 2000) or wave dissipation patterns. This first method will be discussed in detail below as it is the approach taken to measure beach morphology in this thesis.

The rapid sampling of selected pixels allows certain nearshore hydrodynamic parameters to be calculated. Longshore currents (Chickadel *et al.*, 2003), swash processes (Stockdon *et al.*, 2006), and wave celerity and angle (Lippmann and Holman, 1991) have all been computed. Calculation of longshore currents requires a wide surf zone with distinct foam traces. This only occurs at Sea Palling under storm conditions when wind induced tower movement made the calculation of these currents inaccurate, hence further detail of pixel based analysis will not be included in this literature review. A breakwater specific parameter, overtopping, has been derived from video (Archetti, 2009; Fairley *et al.*, 2009). This is useful in determining the onset of overtopping and the percentage of waves that overtop a structure in give conditions. Waves transmitted through the structure can also be observed. Unfortunately the key engineering parameter for overtopping, volume, cannot be extracted. The methodology did allow for determination of spectral changes in wave field over the breakwater (Fairley *et al.*, 2009). Various non-oceanographic parameters have also been extracted from images, for example, beach goer numbers and distribution (Jimenez *et al.*, 2007)

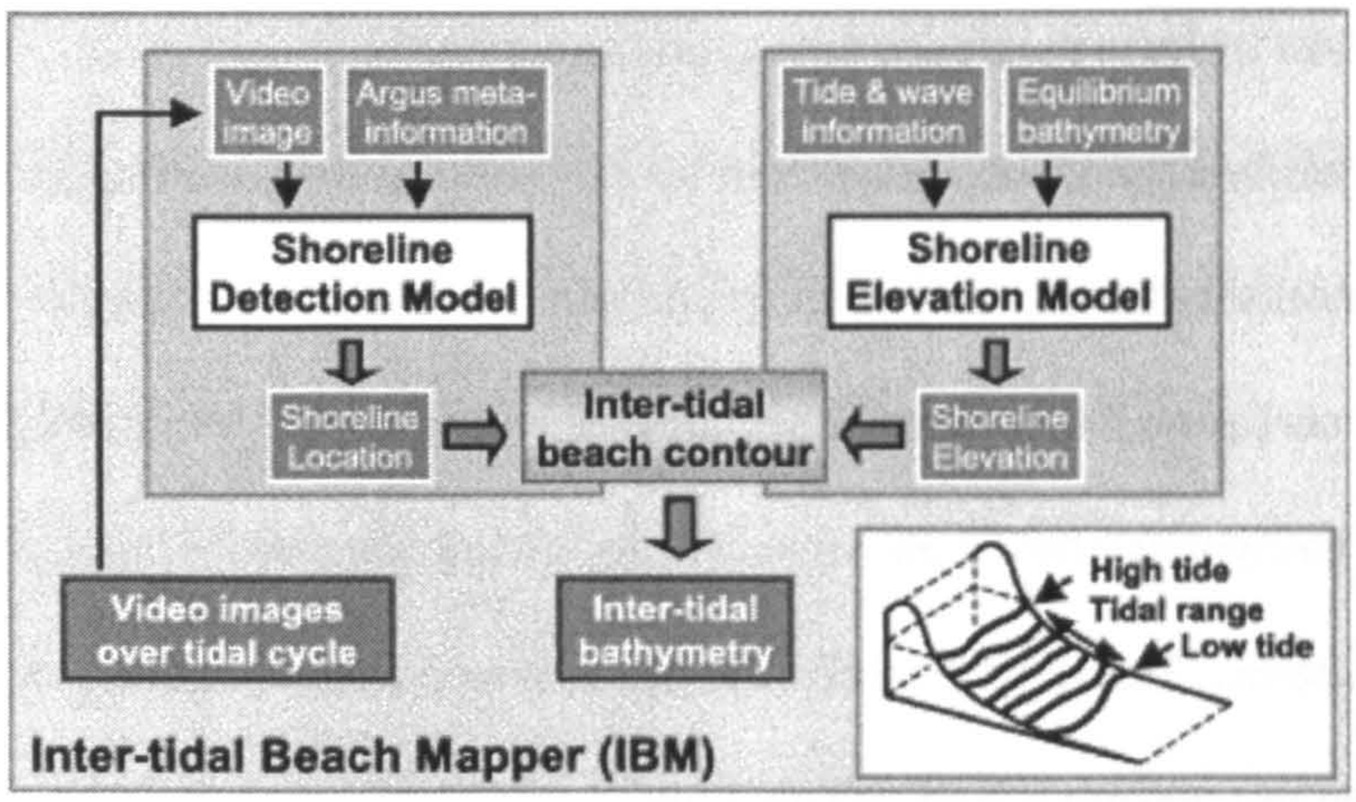

Figure 2.4: A schematic diagram of the intertidal beach mapper (Aarninkhof *et al.*, 2003b).

2.3.4 Extraction of shoreline information.

The analysis of intertidal profiles from Argus image data is achieved from two stages. A water level elevation based on tide and wave setup is determined and this is coupled with a waterline derived from the images. Images are captured every hour or half hour, so over a tidal cycle an intertidal profile can be built up. (Figure 2.4)

The question of what constitutes the shoreline is a non-trivial question (Boak and Turner, 2005). Argus image analysis of shorelines is normally restricted to timex images which remove the instantaneous changes of shoreline position due to swash motions. The exact location of the shoreline extracted from images depends on the technique involved. Often an artificial shoreline proxy such as the intensity maximum due to the shore-break is extracted. Whilst this cannot be considered a 'real' shoreline consideration of the behaviour of the swash-zone still allows useful information to be extracted (Plant and Holman, 1997).

The presence of a shoreline intensity maximum (SLIM) in greyscale time exposure images was first noticed by Lippman and Holman (1989). Cross-shore positions of shoreline intensity maxima were plotted against survey-based shoreline positions (calculated from the

intersection of the still water level with the surveyed profile). r^2 values were found to be very good but the gradient was found to be slightly greater than unity, probably due to swash zone processes. The intercept is negative due to the SLIM being offshore of the actual shoreline.

Plant and Holman (1997) considered the relationship between the SLIM and actual bathymetry. The SLIM was obtained by selecting a cross-shore intensity profile, selecting a sub-section of that around the expected shoreline, normalising the intensity and fitting a quadratic to it. The maximum of this polynomial was then taken to be the SLIM. The position of the SLIM depends on bathymetry, wave characteristics and swash processes. An equation relating the true bed level z_{bed} to the SLIM is:

$$z_{bed}(x_0, y_0, t_0) = z_{tide}(t_0) + \bar{\eta}(x_0, y_0, t_0) + d_{s\lim}(x_0, y_0, t_0) \qquad (2.7)$$

Where z_{tide} is the tidal elevation, $\bar{\eta}$ the total set-up at the SLIM location and d_{slim} the depth at the SLIM location. The only measured parameter is likely to be tidal elevation, so unless the effects of setup and SLIM depth can be ignored (e.g. reflective beach under low wave conditions) they must be estimated in some way before useful information can be extracted. Two approaches are available: modelling these parameters from a fluid dynamical point of view and modelling them empirically. The first requires many parameters which may not be available but does allow the derivation of unknown parameters based on physical concepts. The second approach requires fewer parameters but is likely to require site-specific calibration.

Comparing DGPS surveys with SLIM shoreline estimates based only on tidal elevation gives an r^2 value of 0.88. As is to be expected, the SLIM shoreline estimate lay further offshore and had an elevation offset compared to the surveyed shoreline position.

Errors were observed to increase as wave height increased up to a critical value of 1m (which was assumed to equate to the height at which waves started breaking on the offshore bar). Over this critical height, errors started to reduce with increasing wave height (Plant and Holman, 1997).

Beach cusps cause problems for the SLIM technique since the hydrodynamic effects of the beach cusps cause a seaward movement of the SLIM in the centre of the cusp, the reverse of the actual morphology. Other errors occurred where alongshore variations in nearshore bathymetry altered the properties of the SLIM. These factors mean that short scale alongshore bathymetric variations are not well resolved (Plant and Holman, 1997). Problems with the SLIM technique, especially on dissipative beaches led to the development of other techniques. Aarninkhof *et al.* (2003) obtained the shoreline based on visual differences between sand and water in full colour images. Hue-Saturation-Value (HSV) colour space information is used to discriminate between wet and dry pixels. HSV space was chosen rather than RGB because it is deemed to better represent the way humans experience colour (Aarninkhof, 2003). Hue and saturation are used in colour-based discrimination; an alternative discrimination based on luminance uses the value quantity. The data is sampled across both beach and water, normalised and filtered to produce a smooth histogram with two separate peaks for wet and dry pixels. A line l separating the two peaks is defined:

$$I_y = p_1 I_x + p_2 \tag{2.8}$$

where I_x = hue, I_y = saturation, for colour discrimination.

A discriminator function is then defined such that:

$$\Psi=0; \quad \Psi(I_x,I_y)=p_1I_x + p_2 - I_y. \tag{2.9}$$

This equation is applied to all pixels in the region of interest to produce a map of Ψ and the Ψ=0 contour taken to be the shoreline. This shoreline position is at some point in the swash zone. The water elevation corresponding to the shoreline is then the sum of the tidal elevation, the wave induced set-up and some factor based on the vertical component of swash excursion.

Testing of the model against GPS surveyed datasets from Egmond showed a mean vertical deviation of under 15cm. Far field results were less accurate due to the lower pixel resolution in the far field leading to a near-field bias in colour intensity characteristics. This symptom will be present in any similar pixel property based analysis (Aarninkhof *et al.*, 2003b)

Another pixel property based technique utilises RGB properties of the colour images to determine the shoreline. Sea surfaces often look blue under a variety of lighting conditions. Based on this the divergence of the RGB colour channels is used to identify the shoreline. An edge detection method is used to pick the cross-shore point at which the channels diverge and this is repeated at all points in an alongshore direction producing a shoreline (Turner *et al.*, 2000).

An artificial neural network approach has also been applied to shoreline detection (Kingston, 2003). Artificial neural networks (ANN's) are non linear models that aim to mimic the human brains capacity to reason. An ANN consists of a number of interconnected neurons arranged in a series of layers, an input layer, an output layer and a number of hidden layers. The neurons are connected to each other with each connection given a different weighting. All neurons in the hidden layers contain activation functions which govern the output signal.

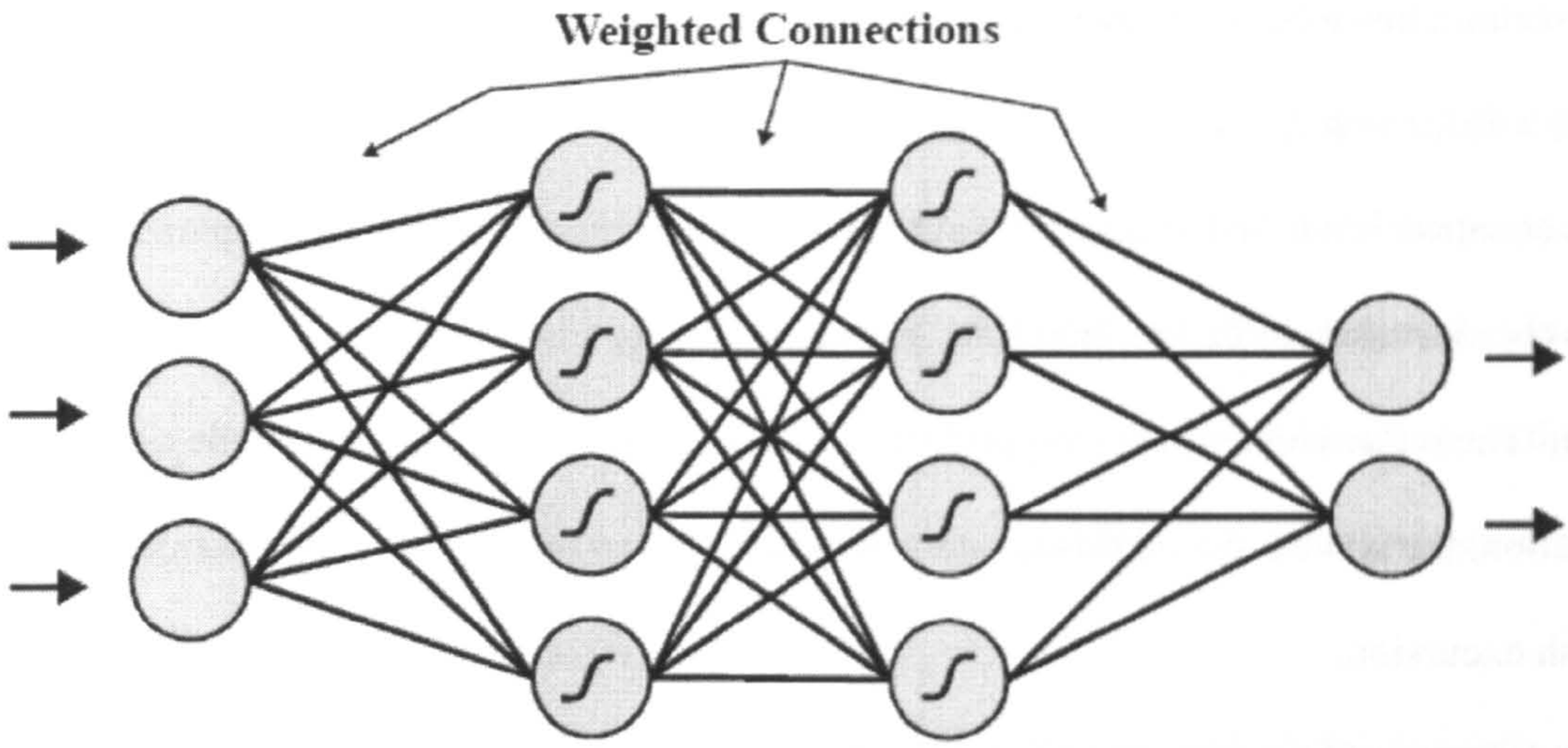

Figure 2.5: A diagram of a feed forward neural network(Kingston, 2003)

One of the most commonly used neural networks is the feed-forward neural network, its architecture is shown in Figure 2.5. The network is trained on a test input-output set so that the weights and activation functions are optimised in order that the desired output is matched.

ANN's have been used in coastal engineering and hydrodynamic applications such as wave forecasting, satellite data analysis and breakwater stability estimation. Lesser use has been made of ANN's in morphodynamic applications (Kingston, 2003). Kingston *et al.* (2000) used an ANN method to correct remotely sensed sandbar location due to the effects of tidal elevation and wave characteristics on wave breaking.

Kingston (2003), also developed a technique to determine the shoreline location based on ANN methods. Colour information in RGB space from Argus timex images was used as the input and a binary value for beach and water given as the output to train the network. A two layer feed-forward network with 15 nodes in the hidden layer was used to discriminate between beach and water using the inputted RGB values. Different ANN

models are trained for each camera using inputs of pixel values that are known beach and water over a range of lighting conditions. When the network is used to simulate the whole profile the output is no longer binary but has values close to 1 for beach and close to 0 for water with a continuous variation across the shoreline region. An output value is determined for all pixels in a region of interest and a classification surface built up. A threshold value for the shoreline and confidence intervals are determined from a probability density function of the output values. The vertical level of the shoreline is, as in previous shoreline extraction techniques based on the still water level and a wave information derived value for run-up and swash (Kingston, 2003).

2.4. Numerical modelling

Numerical modelling is becoming increasingly used in coastal science and engineering as computational power and modelling capabilities increase. These models range from one dimensional longshore shoreline models (Hanson, 1989) and cross-shore profile models (Nairn and Southgate, 1993; Southgate and Nairn, 1993; Reiners *et al.*, 1995), through 2-dimensional models such as MIKE21, to fully 3 dimensional models such as Delft 3D (Roelvink and Vanbanning, 1994; Lesser *et al.*, 2004).

2.4.1 Mike 21

The model used in this thesis, MIKE21 FM (DHI, 2008a; DHI, 2008b; DHI, 2008c), is a state of the art 2DH flexible mesh coastal area model which can simulate waves, hydrodynamics and sediment transport in a fully coupled fashion.

Different types of grid are available for numerical models, both in terms of grid shape (triangular, square, quadrilateral) and in terms of layout. Grids are normally of constant size or nested. Meshes with grids of constant size are simplest to implement but

mean computational power is wasted on areas of little interest. Previously, nested grid models have been used to allow fine resolution in areas of interest while not wasting computational power on areas where less detail is required. However, nested models typically only allow a one way transfer of information at boundaries between grids. In order to resolve this problem, and to further reduce computational power, an unstructured flexible triangular mesh is used in MIKE21 FM (Sorenson *et al.*, 2004b). A cell centred finite volume approach is taken for both the wave and hydro-dynamic modules (Sorenson *et al.*, 2004a).

Finite volume approaches have recently attracted much attention for their advantages over finite difference and finite element approaches (Daoud *et al.*, 2008). Finite difference models substitute differences for derivatives; these are normally forward differences in the time domain. Finite elements cover the mode domain in faces that are small enough such that the variables only vary a little over element face. Pure finite elements can only be applied to very simple problems (Dyke, 1996). Finite volume approaches express governing equations in terms of conservation of mass, energy and momentum in a unit volume. A finite volume expression combines the computational efficiency of a finite difference approach with the geometric flexibility of a finite element approach (Chen *et al.*, 2003).

The coupled flexible mesh version MIKE21 is a relatively recent alternative to prior iterations such as MIKE21 CAMS, nonetheless the wave and current modules have been well tested and found accurate. The wave model was tested against both analytic solutions and real scenarios for storm conditions in the North Sea and in a Baltic sea bay (Sorenson *et al.*, 2004b). Under both scenarios the comparison of model results and measured data found excellent agreement. Subsequently the wave model has been extended to include diffraction, after Holthusijen *et al.* (2002), which will increase the models performance in

areas such as detached breakwater fields where diffraction is important. Test of the coupled wave and flow model allowed modelling of wave current interaction in the Bristol Channel and the Gradyb tidal inlet (Sorenson *et al.*, 2004a). Again, good agreement was found with measured data and it was shown that using a quasi stationary formulation of the wave model could reduce computational time without reducing the quality of results significantly.

2.4.2 Model validation

Numerical models are powerful tools that can provide excellent results for both research and coastal engineering. However, in order for the model results to be meaningful some calibration and verification must be undertaken (van Rijn *et al.*, 2003). Often an inadequate qualitative approach is taken, whereby model comparison is ranked as 'good' or 'reasonable' with no rationale for the ranking (van Rijn *et al.*, 2003). Sutherland and Soulsby (2004a) drawn on work from the meteorological field and distinguish between bias, accuracy and skill. Bias is whether a model constantly over or under predicts, this can be measured by comparison of means of the modelled and measured data. Accuracy is a measure of how well model outputs fit measured data in terms of differences between the two datasets. Skill indicates a models capability to predict future outcomes. Skill scores (Murphy and Epstein, 1988), such as the brier skill score (van Rijn *et al.*, 2003; Sutherland *et al.*, 2004a) compare a predicted outcome with a measured outcome at the end of the simulation time. Since data is not available for such a comparison in this thesis, skill scores will not be discussed further and attention concentrated on measures of accuracy.

Accuracy can be measured by the mean squared error (MSE), root mean squared error (RMSE) or the mean absolute error (MAE). The RMSE is more commonly used than the MSE to preserve units of measurement. As a statistic, the MAE is less susceptible to

mathematical manipulation and it is particularly suitable for comparison of hydrodynamic data (Sutherland *et al.*, 2004b). One problem with this statistic is that it assumes that the measured data is completely accurate which is unlikely to be the case (Sutherland *et al.*, 2004a). Van Rijn *et al* (2003) avoid this by utilising the relative mean absolute error (RMAE) which incorporates the measurement error and can be calculated using:

$$\frac{\langle |X_c - X_m| - \Delta X_m \rangle}{\langle X_m \rangle} \tag{2.10}$$

where X_c is the computed value, X_m the measured value, ΔX_m the measurement error and <..> indicates the averaging over the time series of data.

Van Rijn *et al* (2003) provide a table of qualification for the RMAE so that different model results can be compared on the same scale. This table is replicated in Table 2.1. This approach is used in the validation of the MIKE21 model used in Chapter 6. As well as considering accuracy it is useful is consider how well correlated modelled and measured data are (Sutherland *et al.*, 2004a). Correlation is discussed in section 2.5.2.

Table 2.1: Qualification of RMAE values (from van Rijn *et al* (2003))

Qualification	Wave height RMAE	Current velocity RMAE
Excellent	<0.05	<0.1
Good	0.05 – 0.1	0.1 – 0.3
Reasonable	0.1 – 0.2	0.3 – 0.5
Poor	0.2 – 0.3	0.5 – 0.7
Bad	>0.3	>0.7

2.5. Data analysis techniques

In this section the two statistical techniques used in this thesis will be outlined. Firstly empirical orthogonal function analysis will be discussed and then basic correlation analysis will be explained.

2.5.1 Empirical orthogonal function analysis

Empirical orthogonal function (EOF) analysis is a statistical form of data reduction whereby a complex set of data through time is decomposed into orthogonal spatial modes and temporal components. The technique (also called principle component analysis) was first developed in the early part of last century independently by both Pearson (1901) and Hotteling-Williams (1933). While EOF analysis was developed as a method of data reduction, the technique allows for the determination of beach changes and their temporal relation to forcing (Larson *et al.*, 1999).

Empirical orthogonal functions can only describe standing modes of change, to describe propagating modes of change complex empirical orthogonal functions must be used (Emery and Thomson, 1997). However, use of complex EOFs requires the assumption of cross-shore and longshore independence (Ruessink *et al.*, 2000) which cannot be assumed at the Sea Palling site due to high three dimensionality in the morphology and forcing. For embayed beaches, whether artificial or natural, standing modes, such as beach rotation, are the prevalent response and so standard EOF methods are quite sufficient.

The first use of empirical orthogonal function analysis in the geophysical sciences was the use of EOF's as a statistical method of weather prediction by Lorenz (1956) who first used the term empirical orthogonal function analysis. Early coastal uses of the technique include work on beach profiles (Winant *et al.*, 1975; Aubrey, 1979). This work

allowed isolation of different modes of cross-shore change including the bar / berm profile and related them to seasonal sediment movement. Application of the technique to longshore shoreline changes are less common (Miller and Dean, 2007) but are becoming more frequent. Miller and Dean (2007) used EOF analysis to investigate and characterise longshore shoreline variability at several sites, motivated by the requirement to determine longshore uniformity when using cross-shore profile models. The technique has also been used to investigate the response of a beach after nourishment (Munoz-Perez *et al.*, 2001), to investigate the behaviour of sandwaves (Medellin *et al.*, 2008) and to investigate changes at a detached breakwater system (Rihouey *et al.*, 2009).

The EOF technique has been extended to two spatial dimensions. While there are some statistically involved way of doing this (Uda and Hashimoto, 1982), the simplest method is to re-sample a bathymetric matrix into a vector than can be analysed in the exact way as a beach profile or shoreline vector (Reeve *et al.*, 2001b). Two-dimensional EOF analysis has been applied to off-shore sandbanks (Reeve *et al.*, 2001a; Reeve *et al.*, 2001b; Reeve *et al.*, 2008), estuarine morphology (Karunarathna *et al.*, 2008), bathymetric datasets (Rihouey and Maron, 2003) and beach re-nourishment (Larson *et al.*, 1999).

EOF methodology

In this section the procedure and mathematics of empirical eigenfunction analysis is explained, the mathematical explanation is based on Miller and Dean (2007) and Emery and Thomson (1997). The EOF procedure requires data through time at specific spatial points. Often the analysis is conducted upon the raw dataset whereupon the mean comes out in the first mode of change, often called the 'mean beach function.' Munoz-Perez *et al* (2001), advocate de-meaning the dataset which allows better definition of changes about the mean.

Matrix properties are utilised to identify standing modes in the dataset and separate the dataset into n combinations of orthogonal functions in space and time. The size of n must be smaller than the number to spatial measurement points and smaller than the number of temporal samples:

$$y(xt) = \sum_{k=1}^{n} a_k c_k(t) e_k(x) \tag{2.11}$$

Where $y(x,t)$ is the original dataset; $e_k(x)$ is the spatial eigenfunction; $c_k(t)$ the temporal component and a_k is the normalising factor, which is sometimes incorporated into $c_k(t)$. The normalising factor is given by:

$$a_k = \sqrt{\lambda_k n_x n_t} \tag{2.12}$$

where n_x is the number of spatial samples, n_t is the number of temporal samples and λ_k is the eigenvalue of the *kth* eigenfunction.

So that the different modes are statistically independent, the orthogonality condition requires:

$$\sum_x e_n(x) e_m(x) = \delta_{nm} \tag{2.13}$$

Where the summation is over all spatial measurement points, n and m indicate different modes of change and δ_{nm} is the Kronecker delta:

$$\delta_{nm} = \begin{cases} 1, n = m \\ 0, n \neq m \end{cases} \tag{2.14}$$

The data itself is used to determine the forms of the constituent functions. A least squares method is utilised such that the first mode of change presents the largest amount of

variability and higher modes sequentially less. Mathematically this can be expressed with the Lagrange multiplier:

$$Ae_k(x)=\lambda_k e_k(x); \qquad or\ AE=\Lambda E \tag{2.15}$$

Where E is the matrix of spatial eigenfunctions and Λ is a diagonal matrix containing the eigenvalues λ_k. A can be computed in various ways and indicates the spatial co-variability of the data.

The temporal co-efficients can then be calculated either following a similar method to the spatial eigenfunctions or directly using the equation:

$$c_k(t) = \frac{1}{a_k}\sum_{i=1}^{n_x} Y(x_i,t)e_k(x_i) \tag{2.15}$$

The dataset is now decomposed into a set of functions which can either be considered individually or, given that the bulk of the variance is described by the first few modes, used as a form of data reduction whereby the dataset is re-composed just using the first few eigenfunctions.

2.5.2 Correlation analysis

Correlation is a measure of the linear relationship between two variables. The product correlation co-efficient r is a numerical measure of this relationship based on the difference of points from the mean. For two sets of data, x and y, the product moment correlation co-efficient can be calculated by:

$$r = \frac{\sum_{i=1}^{n}(x_i-\bar{x})(y_i-\bar{y})}{\sqrt{\left[\sum_{i=1}^{n}(x_i-\bar{x})\right]\left[\sum_{i=1}^{n}(y_i-\bar{y})\right]}} \tag{2.16}$$

The value of r ranges between -1 and 1, with 0 indicating no correlation and ±1 indicating perfect correlation (the two variables form a straight line $y=mx+c$). A negative value indicates that as one variable increases the other decreases, a positive value gives the reverse effect. Commonly r^2 is used rather than r, this represents the percentage of the total variance which can be explain by a linear regression of y on x *(Emery and Thomson, 1997).*

Whilst values of 0 and ±1 are easy to interpret, intermediate values need to be tested for significance. Assuming that x and y are both jointly normally distributed the probability that the correlation is significant can be tested using a two tailed significance test.

The value of t is calculated using the follow equation:

$$t = r\sqrt{\frac{n-2}{1-r^2}} \tag{2.17}$$

Where r is the correlation co-efficient and n is the number of sample pairs. A look up table can then be used to determine what significance can be assigned to that t-value for n-2 degrees of freedom (Clarke and Cooke, 1998).

2.6. Summary

In this chapter, previous relevant research on detached breakwaters, coastal imaging and numerical modelling has been presented. From the research presented, disparity between work on breakwater induced hydrodynamics and breakwater induced morphodynamics can clearly be seen. Key aspects of theory behind empirical orthogonal function analysis and correlation analysis have been described. This background provides a foundation for the research contained in this thesis.

3. The Sea Palling Site

The site studied in this work is at Sea Palling on the Norfolk coast of the United Kingdom (Figure 3.1a). This area suffers one of the fastest shoreline retreat rates in the UK and the low lying hinterland is historically prone to flooding. In order to protect the Sea Palling village, nine breakwaters were built (Figure 3.1b) utilising two different designs. The two breakwater designs implemented next to each other, and hence undergoing similar forcing, makes the Sea Palling site an attractive area to study the effect of detached breakwaters on beach morphology since it allows comparison between the two designs. In this chapter the study site will be described and previous academic research on the site discussed.

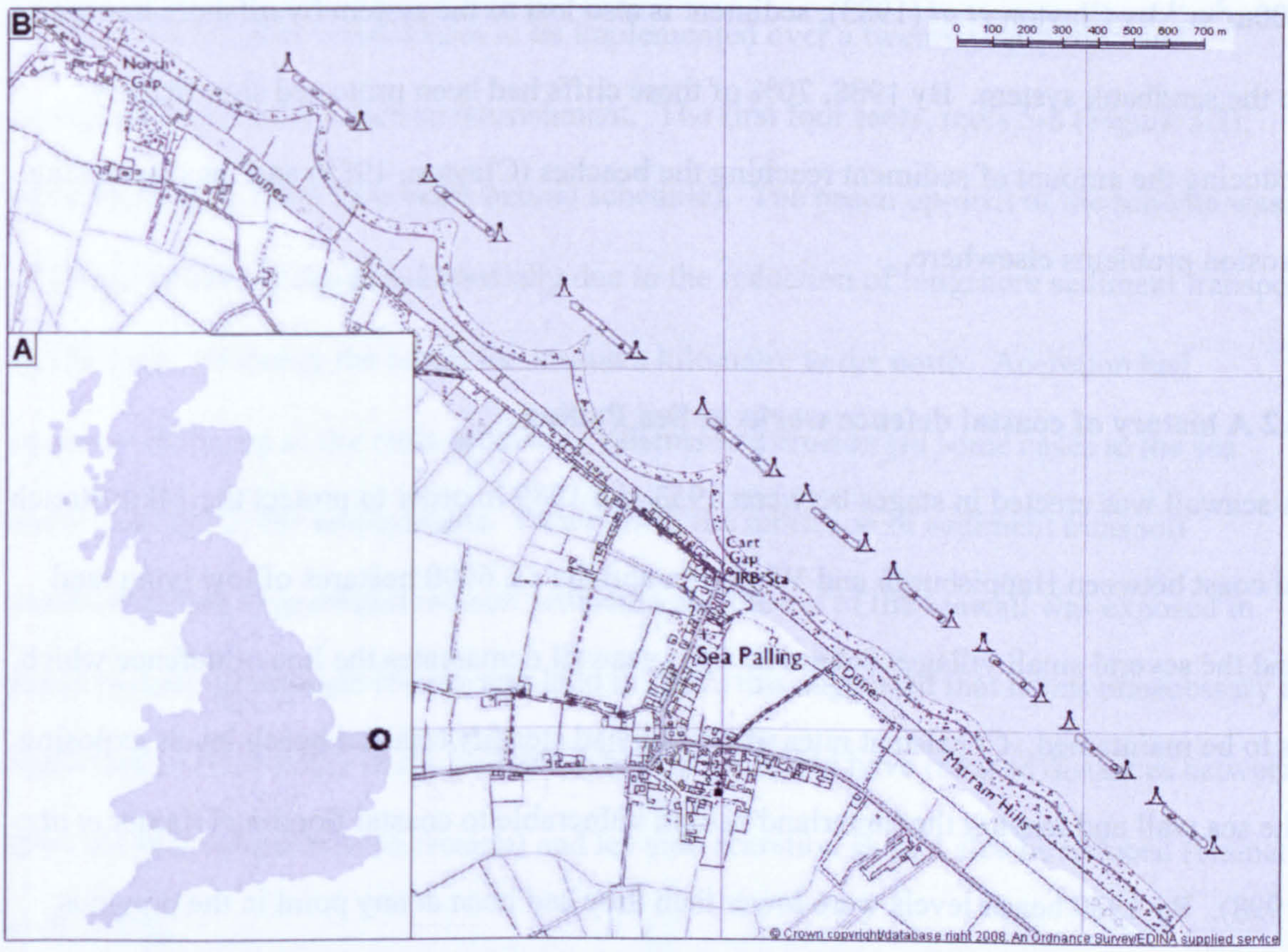

Figure 3.1: a) A map of the UK with the location of Sea Palling marked; b) A map of Sea Palling showing the village and the lay out of the nine breakwaters.

3.1 A background to the Norfolk coast

The East Anglian coastline has lengths of poorly consolidated Quaternary cliffs and sandy beaches backed by dunes. Extensive sandbanks lie several kilometres offshore along much of the Norfolk coastline. There are three main sections of cliffs, the North Norfolk Cliffs between Sheringham and Overstrand to the North and two shorter sections of cliffs, the Dunwich Cliffs and the Covehithe and Easton Cliff further South past Lowestoft. Erosion of these cliffs provides a source of sediment for the beaches and dunes which protect the low lying hinterland (Thomalla and Vincent, 2003). Sediment transport pathways are largely from the north to south. The rate of littoral drift was estimated to be of the order of $100m^3yr^{-1}$ by Clayton *et al* (1983), sediment is also lost to the system by offshore transport to the sandbank system. By 1988, 70% of these cliffs had been protected significantly reducing the amount of sediment reaching the beaches (Clayton, 1989) and thus increasing erosion problems elsewhere.

3.2 A history of coastal defence works at Sea Palling.

A seawall was erected in stages between 1953 and 1989 in order to protect the 14km stretch of coast between Happisburgh and Winterton and the ca. 6000 hectares of low lying land and the several small villages behind it. This seawall demarcates the line of defence which is to be maintained. Consistent rates of erosion had steadily reduced beach levels exposing the sea wall and leaving the hinterland behind vulnerable to coastal flooding (Hamer *et al.* 1998). By 1989 beach levels were lower than they had been at any point in the previous 5000 years (Clayton, 1989).

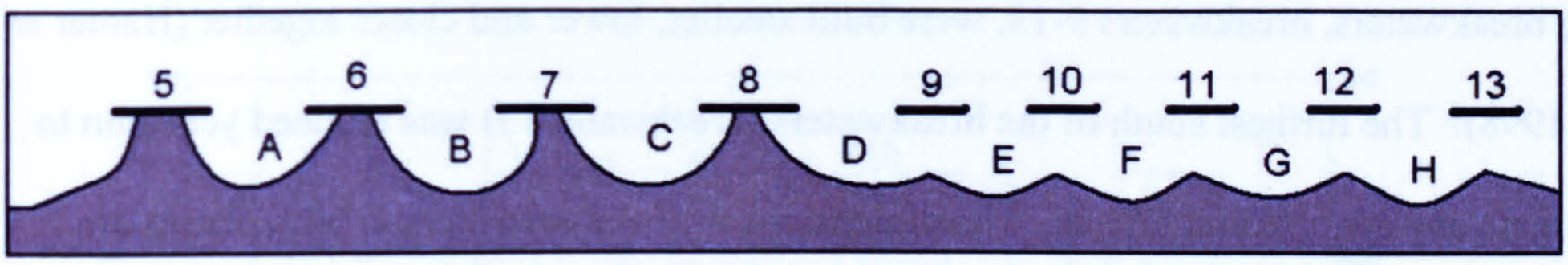

Figure 3.2: A schematic of the site with the breakwater and embayment naming convention which will be used through the thesis displayed. Phase one consists of breakwaters 5-8 and phase two of breakwaters 9-13.

British Maritime Technology, commissioned in 1987 by the National Rivers Authority, produced a shore protection strategy based on fishtail groynes, however subsequent numerical modelling by Halcrow suggested that an offshore reef scheme would be more effective. In 1991, Halcrow proposed a new sea defence strategy based on this, the strategy involved 16 offshore breakwaters to be implemented over a twenty year period and incorporated periodic beach re-nourishment. The first four reefs, reefs 5-8 (Figure 3.2), were finished in 1994 (two years behind schedule). The beach up-drift of the scheme was observed to have accreted substantially due to the reduction of longshore sediment transport by the reefs, widening the beach for around a kilometre to the north. Accretion had occurred in the lee of the reefs producing salients and erosion (in some cases to the sea wall) occurred in the embayments. Down-drift, the reduction of sediment transport southwards had exacerbated erosion problems and the toe of the seawall was exposed in many places. A strategic review was held in 1995, this suggested that it was unnecessary to build further reefs to the north, and that future reefs should have reduced distances between them (to reduce embayment erosion) and lee side accretion should also be reduced (Hamer *et al*, 1998).

A new plan was devised whereby the scheme size was reduced with only a further five breakwaters to be built to the south of the phase one breakwaters, with a possibility of further construction at Horsey. In order to fulfil the strategic recommendations, the phase

two breakwaters, breakwaters 9-13, were built smaller, lower and closer together (Hamer *et al,* 1998). The furthest south of the breakwaters (breakwater 13) was reduced yet again to mitigate any adverse end effects. The dimensions of the breakwaters in both phases are given in Table 3.1.

3.3 Hydrodynamic conditions at Sea Palling

The tidal regime at Sea Palling is typical of the Southern North Sea, being dominated by the M2 component (Bacon *et al.*, 2003) and approximating a progressive wave with a spring tidal range of around 3.0 metres. Peak currents occur at high and low water and, offshore, reach a maximum shore parallel value of $1.5ms^{-1}$. At the breakwaters peak currents associated with spring tides reach $0.8ms^{-1}$.

The tide is asymmetric with a shorter ebb period. This asymmetry leads to a net tidal current towards the south east (Bacon *et al.*, 2005). Figure 3.3 shows a section of data measured at Horsey (~2km from Sea Palling) which shows tidal elevation, current velocity and direction. The data was measured using an AWAC by Gardline Environmental for the UK Environment Agency. To aid clarity, the current data was smoothed using a block moving average filter with a window size of eight samples. The plot clearly shows the progressive nature of the tidal wave (peak currents at high and low water) and the asymmetry in the currents with currents being visibly larger at high tide than at low tide.

Table 3.1: Dimensions of the breakwaters at Sea Palling

	Breakwater Length (m)	Gap width (m)	Distance offshore (m)	Crest elevation ODN (m)
Phase One (Reefs 5-8)	200	300	275	3
Phase Two (Reefs 9-11)	160	160	275	1.3

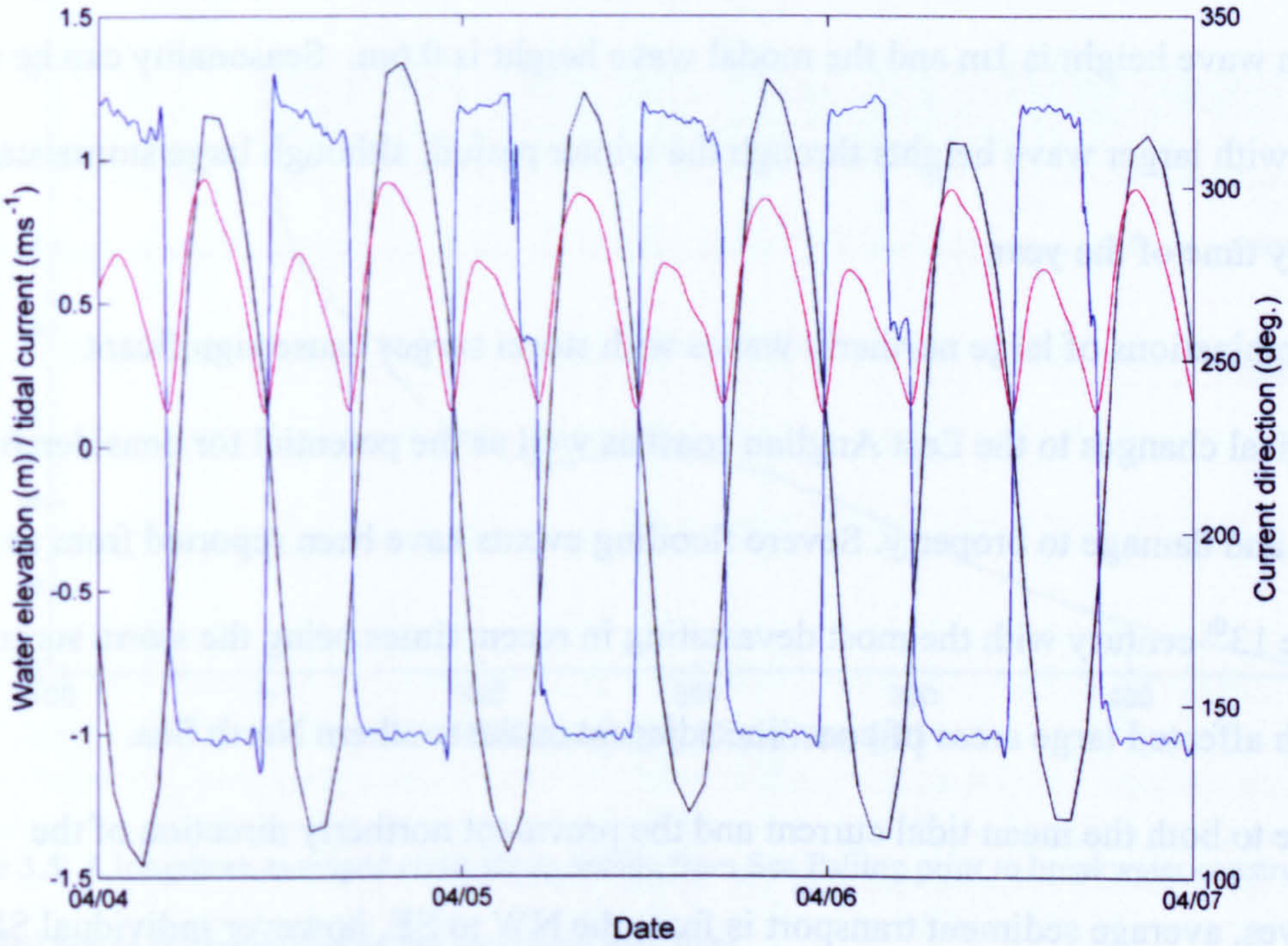

Figure 3.3: Tidal elevation from ODN (black), current speed (red) and current direction (blue). This data was measured at Horsey in ~6m water depth.

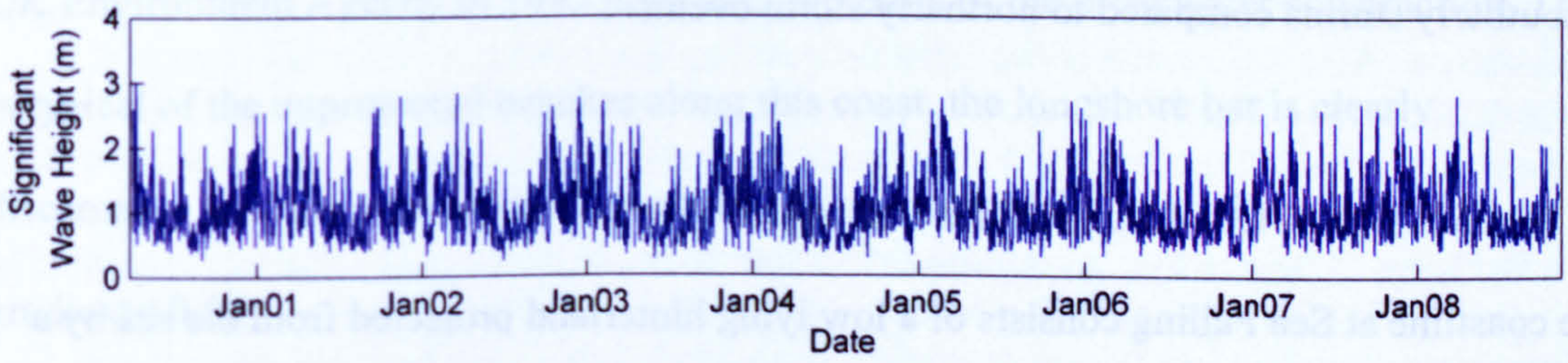

Figure 3.4: Wave heights from a UK met office hind-cast output point showing the slight seasonality to the data.

Current direction varies between north westward (low tide) and south eastward (high tide). The site at Sea Palling has little shelter and so large waves can approach from directions between north west and south east (Thomalla and Vincent, 2003). The largest waves approach from the north and are fetch unlimited. Figure 3.4 shows seven years of hind-cast wave height data from a met office wave model output point approximately 2km from Sea

Palling in 16m water depth. Minimum wave height at this depth is 0.18m, maximum is 3.3m, mean wave height is 1m and the modal wave height is 0.6m. Seasonality can be seen in the data with larger wave heights through the winter period, although large storms can occur at any time of the year.

Combinations of large northerly waves with storm surges cause significant morphological changes to the East Anglian coast as well as the potential for considerable loss of life and damage to property. Severe flooding events have been reported from as early as the 13th century with the most devastating in recent times being the storm surge of 1953 which affected large areas of coastline adjacent to the southern North Sea.

Due to both the mean tidal current and the prevalent northerly direction of the largest waves, average sediment transport is from the NW to SE, however individual SE storm events can reverse this direction over shorter periods of time. In some years the yearly sediment transport has been reversed (Thomalla *et al.*, 2001) due to a large number of southerly storms compared to northerly storm events.

3.4 Morphological Conditions at Sea Palling

The coastline at Sea Palling consists of a low lying hinterland protected from the sea by a single dune ridge fronted by a largely sandy beach. The beaches are highly dynamic, single storms have been reported to erode over 1,000,000m^3 from the beach face along the 14km stretch of coast from Happisburgh to Winterton (Dolphin *et al.*, 2005).

The sediment is medium to coarse sand having a d_{50} of 430μm (Bacon et al 2004). Beneath the sand are layers of erosion resistant peat deposits and wind rows that occasionally get exposed at very low beach levels. Before the reefs were constructed the Sea Palling beach was steep and narrow with a sub-tidal longshore bar located between 170-270m from the sea wall (Thomalla *et al.*, 2001).

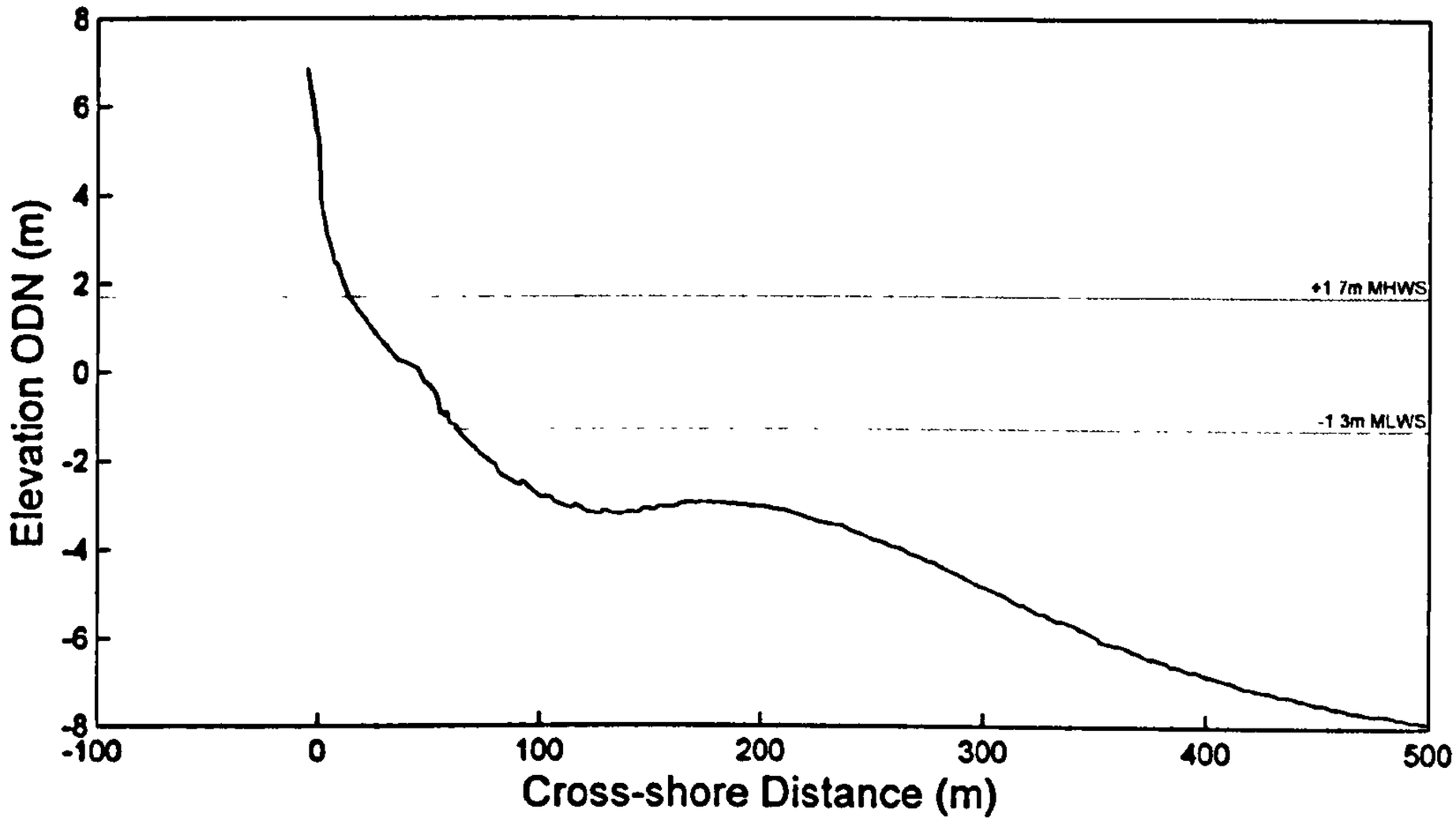

Figure 3.5: A longshore averaged cross-shore profile from Sea Palling prior to breakwater construction. The intertidal region is demarcated by the horizontal grey lines.

Figure 3.5 shows a longshore averaged cross-shore profile based on profiles taken by the UK Environment Agency in 1993 prior to completion of the breakwater construction. This is typical of the unprotected beaches along this coast, the longshore bar is clearly discernable as is the narrow steep intertidal region (intertidal width= 49m; intertidal gradient= 0.06).

The breakwater scheme has been in place for over a decade (phase one completed in 1995 and phase two in 1997) and the morphology has changed dramatically with the destruction of the longshore bar and trough and creation of tidal tombolos through phase one and sinuous salients through phase two. Figure 3.6 presents a time averaged morphological map based on DGPS beach and bathymetric surveys conducted by the Coastal Processes Research Group at the University of East Anglia. Nine surveys taken between 26/04/2006 and 20/02/2007 have been averaged in this plot to give an annually representative morphological map showing the general morphology of the scheme.

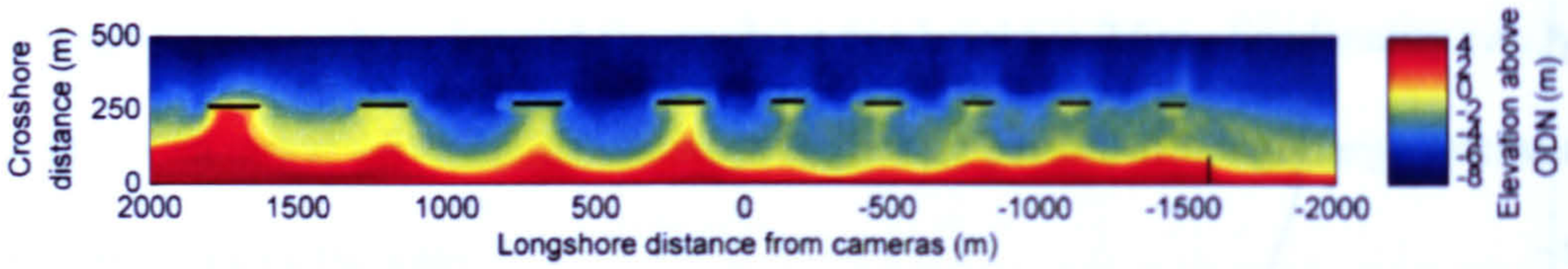

Figure 3.6: A bathymetric map of the Sea Palling site. Data taken over a year has been averaged to display the average morphology of the site. Black lines indicate the breakwaters and terminal groyne, grey lines indicate the limits of sufficiently accurate camera resolution.

The map is displayed in a site specific co-ordinate system based on the location of the Argus camera station: The *y* axis gives offshore distance and the *x* longshore distance (positive to the North West and negative the South East).

The breakwater locations and position of a terminal down drift groyne are displayed. One can notice the difference in response between phase one and phase two: phase one producing tidal tombolos and phase two producing salients in the lee of the breakwaters. Also noticeable is the difference in bay floor levels. Sediment transport is predominantly from the north-west and the northernmost bay is significantly shallower than the other bays. There is also a gradient in the size of the tidal tombolos due to the northerly sediment supply, although the southernmost tombolo is larger due to the bi-directional sediment supply. Some sediment transport occurs from a southerly direction and the southern bays in phase two are wider than the more northern bays. This means that the narrowest beaches are in the centre of the scheme. Resumption of the sub-tidal bar can be seen down drift of phase two. The limits of sufficiently accurate Argus video camera resolution are shown as vertical grey lines. The cameras capture the more central embayments in both phases and miss the end embayments and areas outside the breakwater scheme.

3.5 Previous research at the Sea Palling site.

Numerous field campaigns and modelling exercises have focussed on the Sea Palling site since there are few other UK breakwater schemes in high energy meso-tidal settings. Work by Thomalla and Vincent (2003) describes the changes to beach morphology that occurred when the breakwater scheme was implemented based on the Environment agency monitoring and additional surveys. As previously mentioned, prior to the breakwaters' construction the beach at Sea Palling was characterised by a steep, narrow beach and a shallow trough with a longshore bar. Analysis showed that local changes between significant erosion and significant accretion occurred commonly, highlighting the volatility of the beach. Whilst the reefs were being constructed significant erosion occurred between the reefs and accretion behind the structures. The beach width behind the northernmost breakwater increased by 30m, with accretion observable up to 400m offshore. After the reef construction, salients developed, however steep beach faces between the reefs allowed large waves to propagate close inshore leading to beach lowering in places. Hence between 1996-7 a beach re-nourishment of 1,300,000m^3 was undertaken (Dolphin *et al.*, *Submitted*) after which tidal tombolos formed behind the reefs. Seasonal beach changes were noticed; average winter morphologies consisted of large volumes of material stored on the bay floors and on the up-drift embayment slopes, summer morphologies showed a berm had been re-built, largely on the up-drift side of the salients/tombolos and down drift side of the embayment.

Thomalla and Vincent (2004) compared the various design guidelines to the morphological features produced by the phase one reefs at Sea Palling. The Pope and Dean (1986) method failed to predict any shoreline development at any water levels for phase one at Sea Palling (Thomalla and Vincent, 2004) where tidal tombolos are formed. It has been suggested that the Pope and Dean (1986) prediction does not work well in regimes

with a considerable amount of longshore transport (Axe *et al.*, 1996). All sites analysed by Pope and Dean (1986) were in areas of low wave energy and minimal tidal range which may well restrain their classification to use in those areas (Pilarczyk and Zeidler, 1996). The equation given by Ahrens and Cox (1990) suggested subdued salients for Sea Palling. Although this is a reasonable prediction for the high tide line, the same response is given for lower water levels where salients/tombolos are formed. It is postulated by Thomalla and Vincent (2004) that wave transmission could play a key role in this difference since the Ahrens and Cox formula is only supposed to give a beach response description.

The equation for salient length produced by Suh and Dalrymple (1987) gives good results for lower water levels, however it over-predicts salient lengths for the higher water levels(Thomalla and Vincent, 2004). This equation's propensity for over predicting salient lengths has previously been noted by Pilarcyzk and Zeidler (1996). The problem at Sea Palling arises from the difficulty in determining the original shoreline which is needed to determine the distance between the breakwater and shoreline which is input into the equation. Rising water levels increase this distance whilst the gap length remains constant, this explains the failure of the equation at higher water levels (Thomalla and Vincent, 2004).

The McCormick model for shoreline change fits the Sea Palling salients well at the higher water levels but under predicts the salients at lower water levels. The model fits the shoreline in the bays less well, over-predicting the curvature at high tide and under-predicting it at low tide. Various tests were run with differing wave input parameters and significant differences were found in the predicted shoreline (Thomalla and Vincent, 2004). Thomalla and Vincent (2004) suggest that it may be impossible to predict an equilibrium shoreline at a site such as Sea Palling where the wave climate is highly variable with waves approaching from a wide range of directions.

The fate of sand that approaches the breakwaters from the north has not yet been ascertained, volumetric considerations suggest that the sand is not being stored on the beaches nor bypassing the breakwaters to arrive at the beaches immediately south. Numerical modelling has suggested the presence of jet-like currents that could carry sand out from the bays to be dispersed by tidal currents (Thomalla *et al.*, 2001). However, these jets have yet to be observed in the field and could be due to the monochromatic waves used in the modelling. The same modelling study suggests that when waves approach the structures from an angle of 45 degrees, radiation stresses forced by the sheltering effects of the breakwaters cause a current to be driven reverse to the expected direction due to longshore drift (Thomalla *et al.*, 2001). A similar result is shown in Chapter 6 for waves of easterly incidence.

Tidal currents play an important part in the morphological development of the Sea Palling beaches, both by forcing sediment transport themselves (Bacon *et al.*, 2003) and by affecting the sediment transport pathways of sediment entrained via wave action (Bacon *et al.*, 2005). Tidal currents of up to $0.8ms^{-1}$ occur at Sea Palling and are strong enough to entrain and transport sediment. Numerical modelling suggests that it is only over spring tides that tidal flows are fast enough to entrain sediment, although wave stirring can enhance the transport which then follows tidal current pathways. Sand transported via tidal currents largely remains in the breakwater system but a small amount (approximately $10000\text{-}12000m^3yr^{-1}$) is lost offshore, tidal asymmetry leads to a net transport direction towards the south east. Whilst the volume is small compared to wave driven sediment transport its continuous nature means it should not be neglected (Bacon *et al.*, 2005).

The predecessor of LeaCoastII, LeaCoast, focussed on phase one of the scheme. Work was done to assess the performance of phase one under storm conditions (Dolphin *et al.*, 2005), Beach and bathymetric surveys were taken before and after storm events and

compared with in-situ wave and tide measurements taken within one of the bays and from an offshore source. Two storms and a subsequent calm period were observed. It was found that beach faces and berms were the most volatile with lesser changes occurring on the sub-tidal bay floors and supra-tidal areas of the tombolos.

During the first storm it was found that the north western sides of the tombolos were severely eroded whilst accretion occurred on the south east sides. This translated to a tombolo displacement of 25-30m to the South East and the formation of asymmetric tidal tombolos. During high water levels large quantities of sand were eroded from the back beach but were largely deposited on the beach face. Hence no net erosion occurred. All zones suffered erosion during storm two, there was no alongshore accretion which suggests that sediment was lost offshore. The asymmetry of the tombolos increased further. The period of quieter waves allowed the beach to recover somewhat. The tombolos migrated back toward the North West, returning to a symmetrical shape. Whilst storms cause the largest morphological changes (more sand was lost during storm two than for a whole year of tidal erosion), tidal effects influence the sediment transport pathways. At low tides the emergent tombolos' prevent longshore transport (during the peak ebb current towards the North West), at high tide when the current is reversed the tombolos' are submerged and longshore transport possible. This asymmetry in the tidal currents causes an asymmetry in the movement of sediment suspended during storm events. It is believed that sediment redistribution around the embayments occurs during all storm events but it is only the largest northerly storms that cause sediment to be transported to the offshore region. Onshore migration of sediment occurs during the period of lower wave activity, returning the beach to its pre-storm state. It is believed that this return of sediment occurs due to bed-load transport under shoaling waves and sediment being pushed further up the beach-face via swash processes. The tombolos migrate towards the NW returning to their symmetric

pre-storm shape. Due to the asymmetry in the tidal component of longshore transport, Dolphin *et al.* (2005) believe that NW sediment transport is unlikely, instead infilling of the eroded north western flank is suggested. The same storms analysed by Dolphin *et al.* (2005), were modelled by Zhu *et al.* (2004). They highlighted the variation in current patterns around the site over a tidal cycle, specifically the blocking of currents at low tide and the ability of strong currents in the breakwater gaps to affect wave fields.

4. Video derived morphology

4.1 Introduction

The use of video data to derive morphological information about beaches is becoming increasingly common (see Section 3.2) but still remains a relatively new method of obtaining beach data. This chapter considers two separate datasets obtained from video data: intertidal morphological maps collected pre and post storm and a long term high frequency dataset of the mean sea level contour. Both datasets are well suited to collection via video methods. The continuous hourly data collection means that storm response can be isolated and that long term datasets can be built up at low cost. Storm-scale beach response is important at this site due to the energetic nature of the wave climate and because storm scale beach response is of great importance in assessing a coastal protection schemes performance. The medium term shoreline record allows for elucidation of the modes of morphological change and the evolution of the scheme.

Firstly, in this chapter, the methodology for extracting morphological data from video images will be explained and the acquisition of supplementary wave data used to explain forcing conditions described. Secondly, the results from the two different morphological datasets will be separately presented and discussed. Finally the results from both datasets will be drawn together and summarised.

4.2 Methodology for analysis of video data

4.2.1 The 'Argus Runtime Environment'- A framework for image analysis

The Argus Runtime Environment (ARE) is a set of Matlab based programmes, conventions and a database structure that facilitates the collection and analysis of coastal images.

Central to the system is the database that holds information about the cameras, camera sites, images and hydrodynamic metadata. MySql is used for the database because it efficiently stores information without extensive memory usage. Programmes interface between MySql and Matlab for the input and retrieval of data. A variety of programmes allow for the rectification of images, picking of shorelines and other standard tasks.

There are some conventions that are used with the Argus software: the most important of these is the Argus co-ordinate system. Image co-ordinates must be transformed to real-world co-ordinates, but rather than use a standard co-ordinate system (e.g OSGB36) a local co-ordinate system is adopted. The camera location is taken to be the origin and the *y*-axis shore-normal, increasing with distance offshore from the camera. The *x*-axis is then shore parallel, positive values indicating regions (in this case) to the north west and negative regions to the south east of the cameras. The motivation for this approach is to facilitate manipulation and analysis of the images. All video derived data, and most other results, are displayed in this co-ordinate system.

4.2.2 The Sea Palling Camera System.

Six digital video cameras were mounted 17m above sea level on a tower located on the dune between phase one and phase two. The camera type used was Point Grey Scorpion II which has an image size of 1392 x 1040. Three different lenses were used to provide optimum resolution across the scheme, two wide angle lenses covered the ground directly in front of the camera tower, two zoom lenses covered up and down the coast and two

standard lenses covered the intermediate area. Images from the six cameras are shown in Figure 4.2.1 and the design pixel footprint in figure 4.2.2. The footprint shown was created using software that is part of the Argus Runtime Environment (Section 4.2.1). Due to pixel footprint limitations analysis was restricted to ±1250m from the cameras which gives a maximum pixel footprint of 15m longshore and 4-8m cross-shore. This limitation means the end embayments of both phases are not included. The limits of camera coverage are shown in Figure 3.6 (p.46).

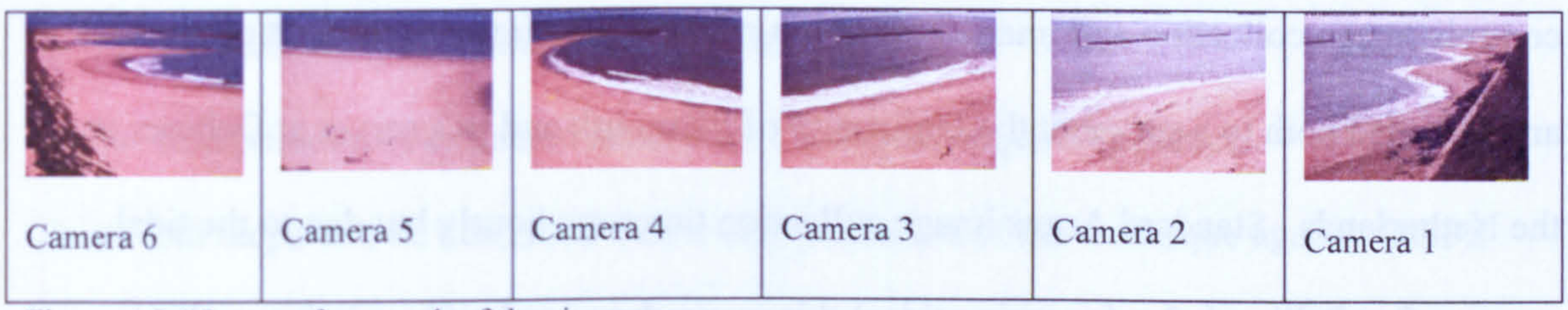

Figure 4.2.1 Images from each of the six cameras

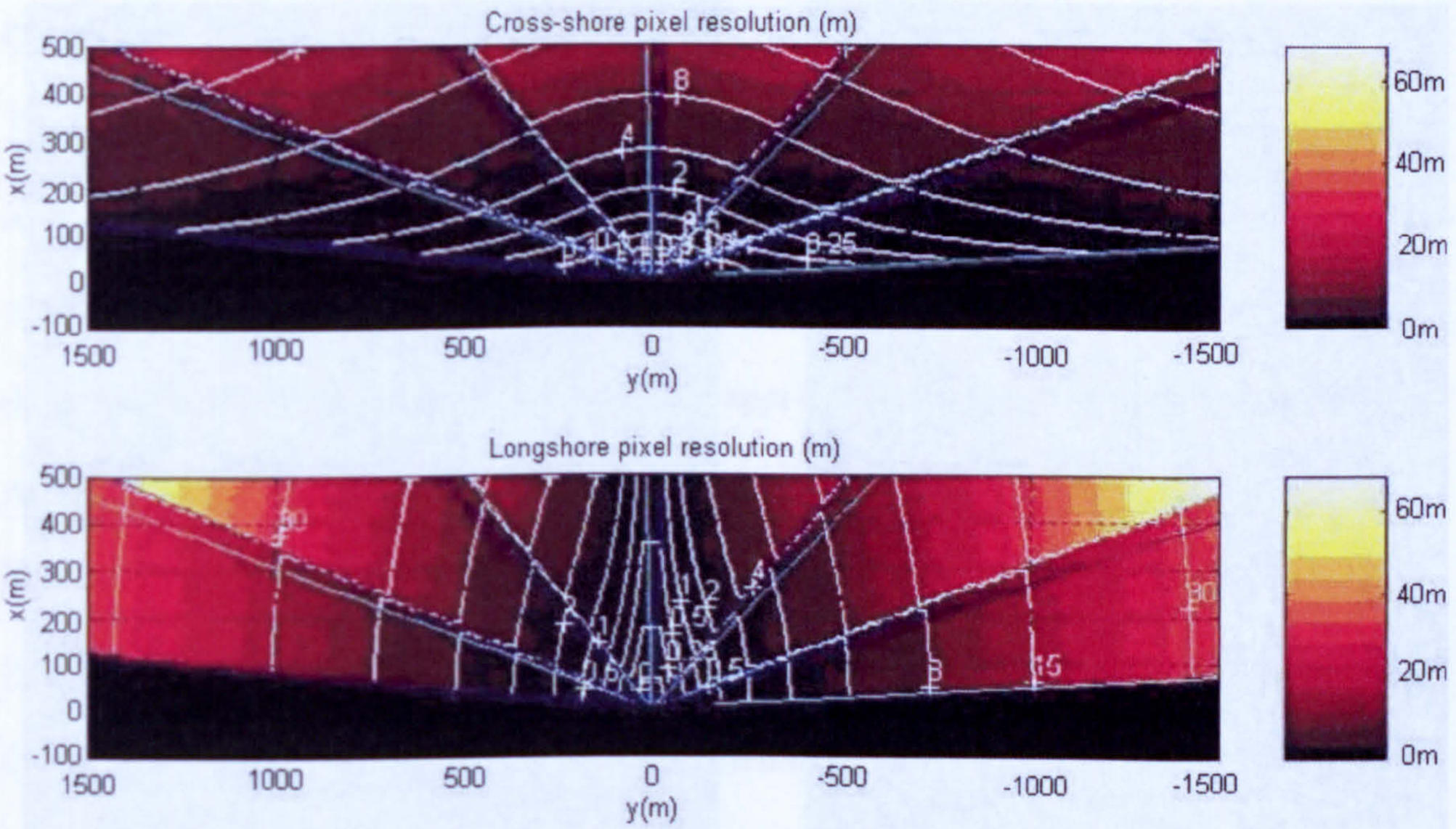

Figure 4.2.2 Maps of pixel resolution for the six cameras

The tower used for the video deployment was a triangular lattice radio mast made from galvanised steel. The tower was constructed such that the lower half had a width of 0.5m and the upper half 0.381m. To minimise tower movement imposed by wind stress, 6 stainless steel guys were attached to the tower. Two guys were attached to each corner, one half way up and the other close to the top, just below the camera location. The guys and tower are shown in Figure 4.2.3. The cameras were mounted in weatherproof housings attached to the tower by means of a steel plate and u-bolts (Figure 4.2.4). The tower was situated close to a small building which allowed for the location of a local computer which controls image collection and image upload via a broad band internet connection. Images are uploaded both to a server at the University of Plymouth and to a server at Deltares in the Netherlands. Standard Argus image collection times are hourly but due to the tidal range at Sea Palling (~3m for spring tides) this was reduced to half hourly intervals.

Figure 4.2.3: A photo of the Sea Palling camera tower with guys attached

Figure 4.2.4: A picture of the six cameras and attachments

4.2.3 Extraction of information from images

In this study morphological information was obtained from video images via extraction of shorelines at known water elevations. Intertidal morphological maps, contours at specific elevations and cross-shore profiles can all be obtained via this method. The technique can be considered to have four steps:

1) Determination of co-efficients to allow transformation between image and real world co-ordinate systems,
2) Acquisition of water level data,
3) Extraction of shorelines from images,
4) Interpolation of extracted shorelines to produce required product,

These four steps will be described below and validation of the technique against DGPS survey data presented.

Co-ordinate transformation

To translate from image to real world coordinates, the images must have the lens distortion removed and the undistorted images transformed from image *(U, V)* to real world *(x,y,z)* co-ordinates. The methodology used here is standard to Argus image processing and is based on work by Holland *et al.* (1997). A two step approach is taken whereby the intrinsic parameters (horizontal and vertical scaling factors relating to pixel shape, lens distortion co-efficients and co-ordinates of the idealised image plane centre) are calculated in the laboratory and the extrinsic parameters and effective focal length (an intrinsic parameter) are calculated in the field. The intrinsic parameters only need to be calculated once for each camera / lens set up, hence the possibility of laboratory calibration, whilst the extrinsic parameters must be calculated every time the camera is moved. Laboratory calibration allows for constraint of several free parameters and hence the intrinsic parameters can be

calculated based on differences from known positions of a rectangular array of dots and images of the dot array. The extrinsic parameters are calculated based on relationships between known *x,y,z* co-ordinates (termed ground control points or GCPs) and their position *(U, V)* in the image. Assuming the camera location is known, only two GCPs' are required to produce a geometry solution. Production of the geometry solutions is achieved via selection of known points in the image using the FG tool in the ARE suite. This graphical user interface allows mouse selection of known points in an image and computation of the geometrical co-efficients. Ideally one would assume that the cameras were static and hence the geometrical co-efficients would remain constant through time. Unfortunately, for the Sea Palling site the tower location, nature of the tower and large area of the camera housings exposed to wind stress meant that this was not the case and hence new geometrical solutions had to be found for every image analysed.

In order to obtain unknown *(x,y,z)* locations from *(U, V)* points, one of the three unknowns must be determined. Since it is the shoreline location that is of interest the *z* co-ordinate can be specified since water surface elevation can be obtained. This leads to distortion at other elevations in the image but for this study (where only the shoreline location is required) the inaccuracies are not relevant.

Method for obtaining water elevation

Accurate extraction of morphology from video images relies heavily on accurate water levels, both for correct association of water level with shoreline and for the shoreline rectification procedure. Whilst direct water measurements were taken at the Sea Palling site using a Nortek Aquadopp, data gaps and sensor drift errors meant that the record was not suitable for use as a long term tidal record. However, sections of the locally measured water level were suitable for verification of other water level records. The approach taken to

obtain water level at Sea Palling was to use a linear extrapolation between two UK National Tide and Sea Level Facility (NTSLF) gauges at Cromer and Lowestoft (Figure 4.2.5). The Sea Palling water level was considered to be a weighted average of the two water level records, with the weighting based on distance from Sea Palling. The extrapolation used Ordinance Datum Newlyn (ODN), and took the form:

$$SP_{ODN} = \left(\frac{5547}{8080}\right) Cro_{ODN} + \left(\frac{2633}{8080}\right) Lowe_{ODN}$$

Where SP=Sea Palling water level, Cro=Cromer recorded water level and Lowe= Lowestoft recorded water level.

Figure 4.2.6 shows a plot of a section of the Aquadopp time series with the long term drift removed against the tidal series interpolated from Cromer and Lowestoft. The two series are highly correlated (r^2=0.97). The mean absolute difference between the two series is 0.07m with the largest errors occurring at low water. The instrument used to measure water levels at Sea Palling was situated on a marker pile close to the northern most breakwater and suffered from tidal flow induced water set up/down at high and low waters: it is the authors belief that this explains the larger differences at low water.

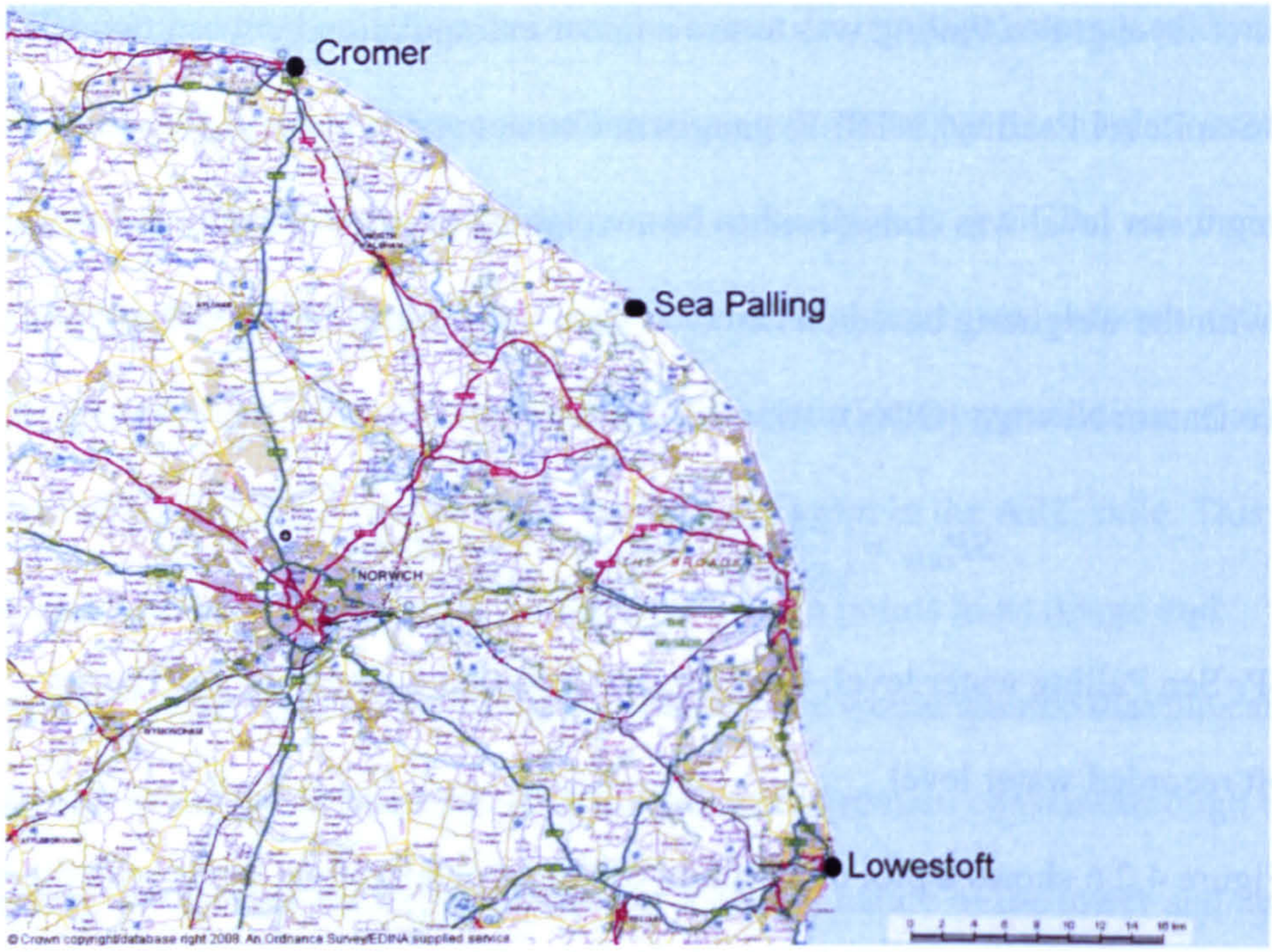

Figure 4.2.5: The location of the two NTSLF gauges in relation to Sea Palling

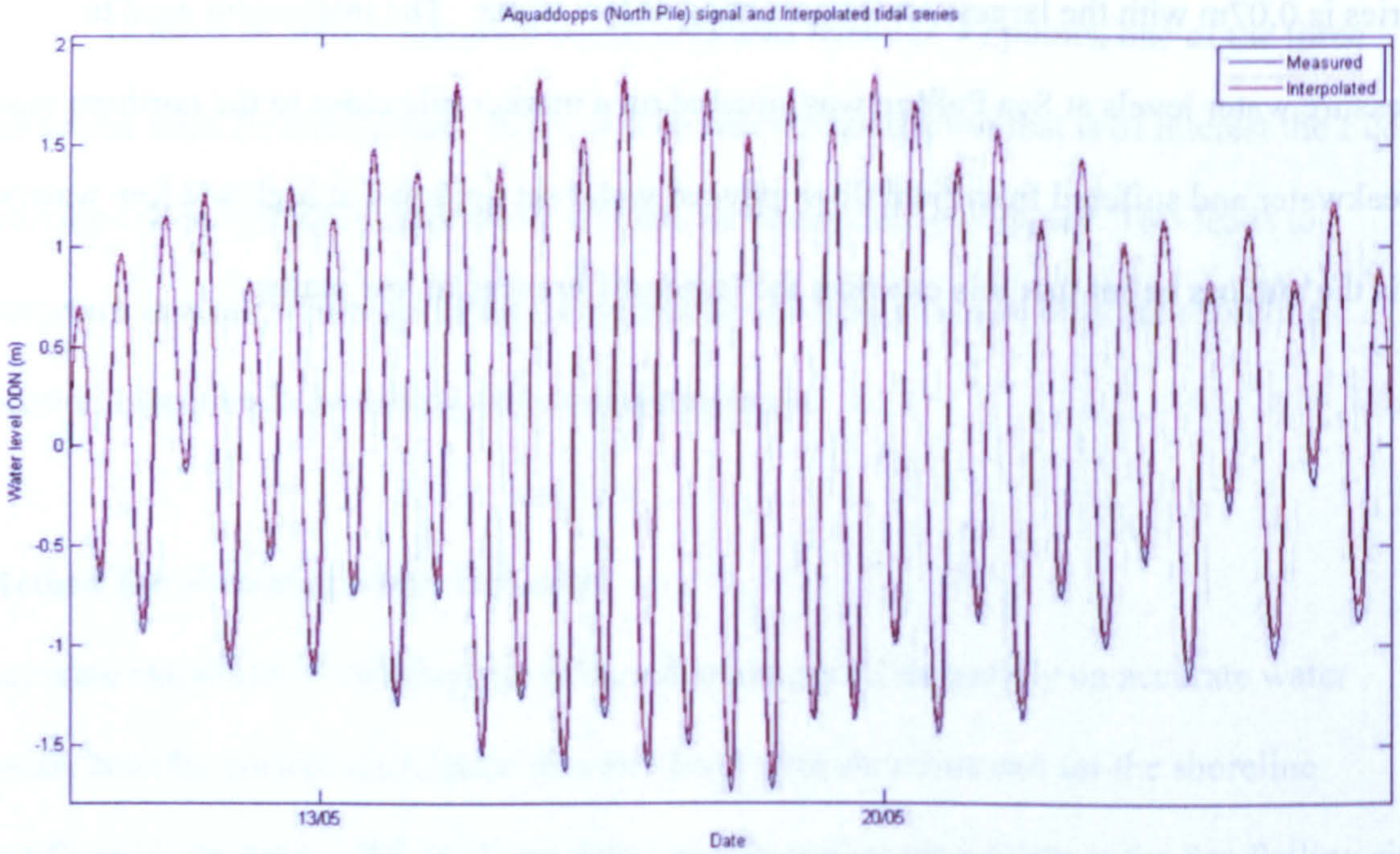

Figure 4.2.6: A section of the Aquadopp measured tidal record and the interpolated series showing the good comparison between records.

Shoreline extraction

Shorelines can either be selected in the oblique images and the shoreline co-ordinates transformed to real world space or images transformed to a plan view at the water elevation level and shorelines picked in these. In this analysis, the former approach as adopted for two reasons: firstly, merging and rectifying images results in some loss of pixel resolution and associated accuracy, and secondly, shorelines picked in *u,v* space are more robust against errors in ancillary data. That is, the *u,v* shorelines will always remain the same, and therefore calculated *x,y,z* shorelines can always be corrected should errors in geometrical co-efficients or water levels be detected.

This study followed the standard Argus approach (Plant and Holman, 1997; Aarninkhof *et al.*, 2003; Plant *et al.*, 2007) of using timex images for the shoreline extraction. Timex images are 10 minute time averaged images. The motivation for using timex images is that individual swash and wave group induced set up motions of the shoreline are removed, producing a more robust statistic for analysis. Shorelines were only extracted on days with high image clarity: rain-drops, wind induced vibration and fog can all render an image unsuitable for analysis. Shorelines were extracted on days with low wave height (H_s<0.2m) to reduce differences between measured water level and shoreline water level due to wave set-up.

Whilst changes to shoreline elevation due to wave set-up can be computed, the presence of the breakwaters at Sea Palling means the wave height and hence set-up at shoreline varies considerably around the embayments and determination of the varying set-up induced component of elevation is prohibitively difficult. Maximum errors induced by wave set up are of the order of 0.04m since wave set up can be estimated at 17% of the wave height (Guza and Thornton, 1981). Use of days with low wave heights also reduces uncertainty in the shoreline position due to a wide swash zone.

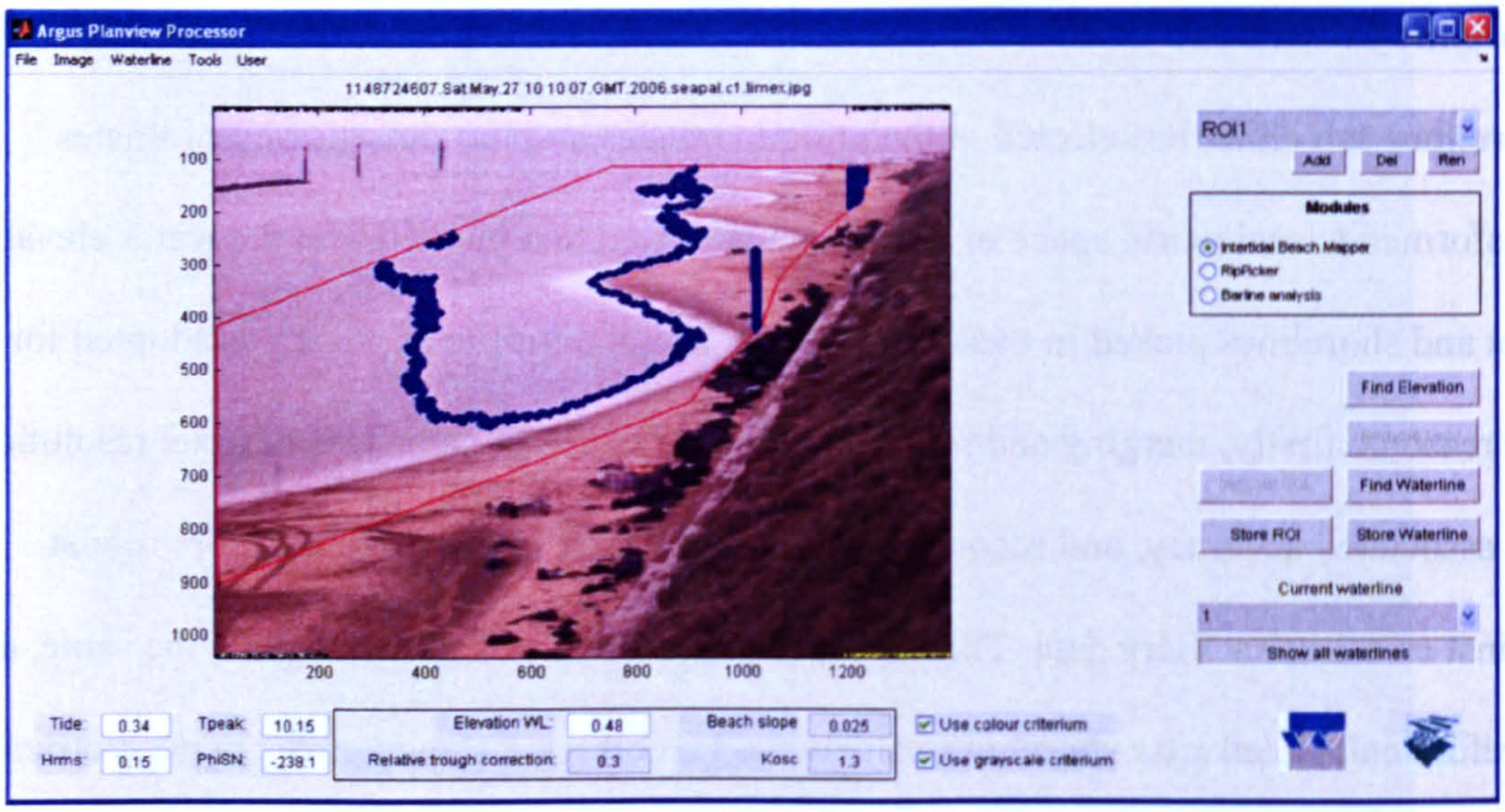

Figure 4.2.7 An example screen from the intertidal beach mapper showing the failure to accurately pick shorelines.

As has been described in the literature review, there are several methods for computing the location of a shoreline in the image. None of the standard methods performed consistently well at Sea Palling, an example of this failure is displayed in Figure 4.2.7. There are several reasons for these failures: the high sediment concentration in the water means that colour discrimination between water, wetted beach and dry beach (Aarninkhof *et al.*, 2003) is often impossible; the shoreline intensity maximum (SLIM) method (Plant and Holman, 1997) fails due to low wave heights meaning there is no shore break to provide the shoreline maximum, or that there is a shore break in the bay centre but not around the tombolo horns. Beach cusps also provide automatic picking routines with difficulties, the cusps cause circular regions of greater shore break intensity which leads to the SLIM shoreline following the outside of the circle and giving a protrusion to the shoreline rather than an indent. Manual picking of shorelines was adopted since no automatic method was suitable, whilst this approach is time consuming and user intensive it was found to be the most accurate method of picking shorelines.

Methods for obtaining the two datasets

The dataset describing storm induced beach change consists of pre- and post-storm 3-D intertidal morphological maps. These intertidal maps are obtained by extracting shorelines from every image over a half tidal cycle (low - high or high – low). Collation of shorelines from all images and times gives contour lines at 12 vertical elevations. These contours are interpolated onto a regular mesh using the Matlab 'griddata' command to produce the intertidal map. Due to the narrow intertidal region and high degree of longshore curvature, linear interpolation between points was found to be the best interpolation method. Interpolation caused erroneous values for the bay floors and tombolo centres where there was no data. To remove these false values a mask was produced to retain grid points within the region of picked shorelines and to set all other grid points to NaN (Not a number). Shadowing of the beach by berms on the tombolo crest lead to loss of information from some areas of the intertidal region and these sections were also set to NaN.

The second dataset extracted was the mean sea level (MSL) shoreline which was defined as the shoreline at a tidal elevation of 0.18m Ordnance Datum Newlyn (the mean tidal level over the time period analysed). Images were not always available at MSL, due to automatic half hourly image collection routines, so the MSL contour was obtained by linear interpolation between image shorelines at vertical elevations above and below the MSL elevation. The picked shorelines (above and below MSL) were interpolated onto a regular 2m longshore spacing and then vertical interpolation between the two shorelines at each longshore point used to obtain the MSL contour. Figure 4.2.8 shows a schematic of this method. There is some deviation between real and interpolated MSL location but due to the linear nature of the Sea Palling intertidal region and the small vertical distance between the two measured waterlines (0.1-0.5m) this difference does not affect results.

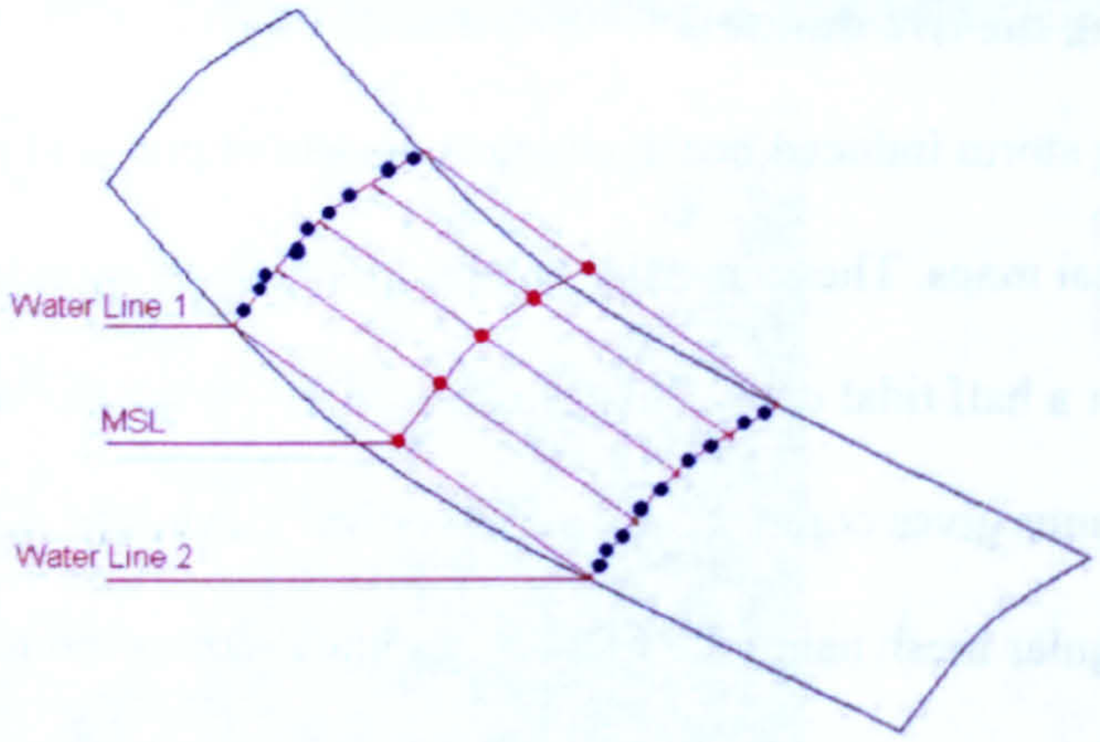

Figure 4.2.8: A schematic of the MSL extraction process. The black indicates a section of beach face, the blue picked shoreline locations and the red dots interpolated MSL shoreline points.

Comparison with survey data

Validation of the methods used to obtain shoreline information from the video was provided by comparison with RTK-GPS survey data taken by the coastal processes research group at the University of East Anglia. Two forms of comparison were undertaken to reflect the two datasets extracted from the images: comparison of the MSL shoreline and comparison of intertidal bathymetry. A plot showing the MSL contour from the DGPS data and the video is shown in figure 4.2.9. It can be seen that the two shorelines agree closely and the mean absolute cross-shore difference between the two is just 2.1m. The mean range in shoreline location is 30m which gives a good signal to noise ratio of $\frac{30}{2.1} = 14.2$.

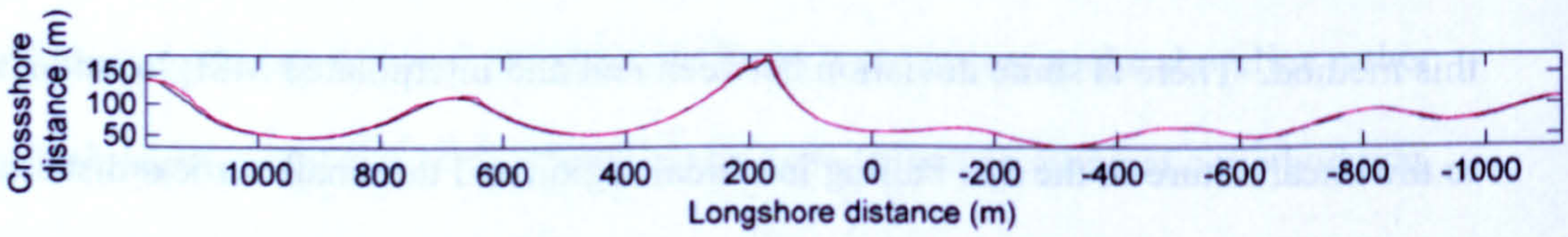

Figure 4.2.9 A plot of video derived (red) and DGPS measured (black) mean sea level contours

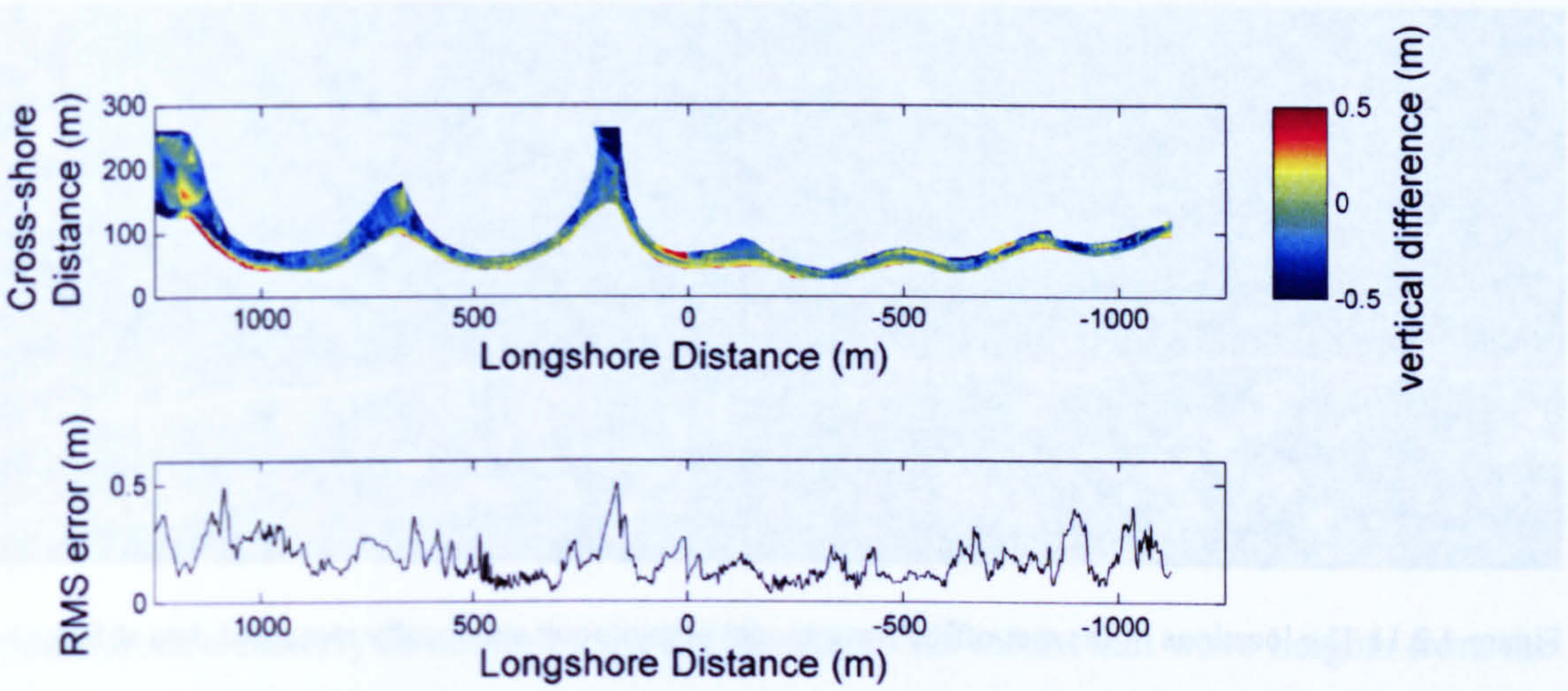

Figure 4.2.10 a) A map of vertical differences between DGPS and video derived profiles, and b) a plot of the cross-shore averaged RMS error.

Figure 4.2.10 shows a 2-d map of vertical differences between a video derived intertidal bathymetry and a DGPS intertidal survey (upper panel) and a plot of root mean square errors (lower panel). Largest errors are in the far field of the study area and in the regions sheltered by the tombolos and salients where the shoreline faces away from the cameras. Larger errors are also observable in the top and bottom of the intertidal regions, partially due to the larger errors in tidal estimation previously described and partially due to difficulties in interpolation and masking at the top and bottom of the video derived intertidal profile. The mean vertical RMS error is 0.17m which is comparable to accuracy of other methodologies of obtaining morphologies from video (Aarninkhof, 2003). More crucially, beach elevation changes over storms in phase one have been previously measured to be in excess of 1m (Dolphin *et al.*, 2005). This gives a favourable signal to noise ratio of $\geq \frac{1}{0.17} \approx 5.9$; which means that storm induced beach changes will be adequately captured.

Figure 4.2.11 The locations of the met office wave model output point and locally measured data at Sea Palling (Aquadopp), Walcot and Horsey (AWACs')

4.2.4 Supplementary wave data

In the following section the methodology for obtaining the supplementary wave data used in the analysis will be explained and a new parameterisation of hydrodynamic data described. Several sources of measured wave data were available for the Sea Palling site, however none were suitable for this study due to non directional data or significant data gaps. Instead, hind-cast model data from the UK Met Office was used and transformed inshore. The Met Office wave model (Bidlot and Holt, 1999; Bradbury *et al.*, 2004) is a second generation wave model that uses a global wave model and a nested U.K. waters grid. The global wave model is used to provide wave boundary conditions for the finer UK waters model. As well as being finer resolution, the UK waters model includes shallow water effects which the global model does not. An output point for the UK waters model was available close to Sea Palling (Figure 4.2.11). The output is partitioned into resultant, swell and wind wave components. The resultant wave output, giving single value wave height, period and direction representations of the sea state is utilised in this study.

Despite being unsuitable for long term analysis the locally measured wave data was used to validate the use of modelled data. Two potential wave data sources were available:

measured data from a Nortek Aquadopp at the northern end of the Sea Palling breakwater scheme (in ~5m water depth) and data measured by AWAC's at two locations, Walcott and Horsey either side of the scheme, both in ~6m water depth (Figure 4.2.11).

Comparison of the two measured datasets shows that the data from the AWACS at Walcott and Horsey is of better quality than the Aquadopp dataset. The data from the Aquadopp has periods of falsely measured wave height due to being sheltered from waves incident from a easterly direction by the breakwater. This meant that wave heights from the Aquadopp and the AWAC agree closely for northerly incident waves but that the Aquadopp under represents waves incident from the east(Figure 4.2.12). This figure displays wave height from both the Aquadopp and the AWAC in the upper panel and AWAC measured wave direction in the lower panel. The wave direction is in radians and the dotted line represents shore normal wave approach. Directions above the dotted line are incident from the south and directions below the dotted line incident form the north. It can be seen that for southerly incident waves such as the event at 10/15 the Aquadopp under represents wave height whereas for the northerly event between 10/29 and 11/05 both the AWAC and the Aquadopp are in close agreement. Thus the AWAC measured data was used for verification of the modelled data used.

Before comparison with the measured data, the met office dataset was cleaned of non-incident wave directions (present due to the output point being 2km offshore) and the remaining data transformed inshore using MIKE21. Only waves between 350 and 170 have been used with other directions removed. The data has been transformed further inshore from the output point using the MIKE21 spectral wave model (Sorenson *et al.*, 2004) coupled to the hydrodynamic model. The hydrodynamic model was used to implement tidal effect which was modelled as varying water levels at all boundaries with tidal currents neglected.

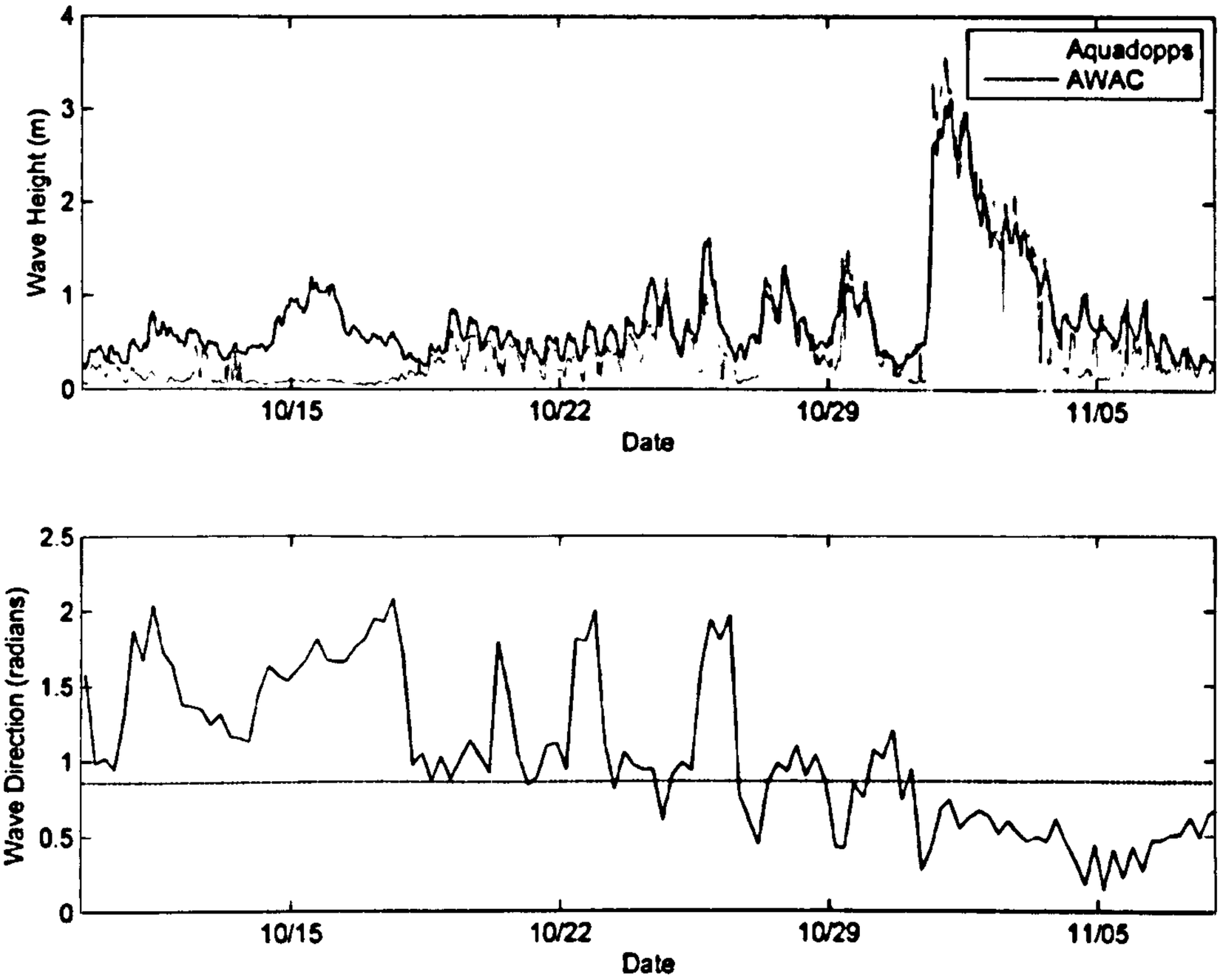

Figure 4.2.12: a) wave height measured with the AWAC and Aquadopps and b) Wave direction with the dotted line representing shore normal incidence

The spectral wave model was run using the Met Office resultant wave output for input significant wave height, wave period and direction. The final required input for the spectral wave model was the directional spreading. This is not output from the met office model and thus the wave transformation was run with three different values for the directional spreading parameter. The three values of directional standard deviation used were 32, 23 and 17 (maximum, default and minimum values specified by the MIKE21SW handbook).

To verify the validity of using the modelled data both the raw met office data and the transformed data was compared to the AWAC data from Walcott. Both correlations and RMAE's (van Rijn *et al.*, 2003) were used to determine the best of the four model versions

to use. Table 4.2.1 shows the correlation values against the Walcott data. It can be seen that the various parameters all have similar correlations. These correlations are all significant at the 99% level. A Hotelling-Williams test was used to determine whether the differences in correlation co-efficient were statistically significant but no statistical significance was found. However, visually the MIKE 21 SW run with the directional standard deviation of 32 best fitted the significant wave height data. Table 4.1.2 shows RMAE (van Rijn *et al.*, 2003) for the different model runs against the Walcot data. Against the Van Rijn scale (van Rijn *et al.*, 2003) these outputs all rank as 'bad' (>0.3), however it can be seen that the DSD 32 run performs the best. A visual comparison of the Walcott measured data and the MIKE21 transformed met office data is displayed in figure 4.2.13. The model generally over-estimates wave heights but the shape and timing of the different wave events looks reasonable (Pearson's product moment correlation co-efficient r=0.86). The model does not show the same variability in wave period as the measured data, but shows similar trends

Table 4.2.1: Pearson product moment correlation co-efficients' (r) for wave parameters from the different MIKE21 runs against the Walcott measured data.

	Significant wave height	Mean Wave Period	Mean wave dir.
Met office output	0.81	0.53	0.52
MIKE21 DSD 32	0.86	0.52	0.52
MIKE21 DSD 23	0.86	0.52	0.52
MIKE 21 DSD 17	0.85	0.52	0.52

Table 4.2.2: RMAE's of wave height for the met office wave output and the different model runs.

Met Office output	MIKE21 DSD 32	MIKE21 DSD 23	MIKE 21 DSD 17
0.69	0.33	0.36	0.37

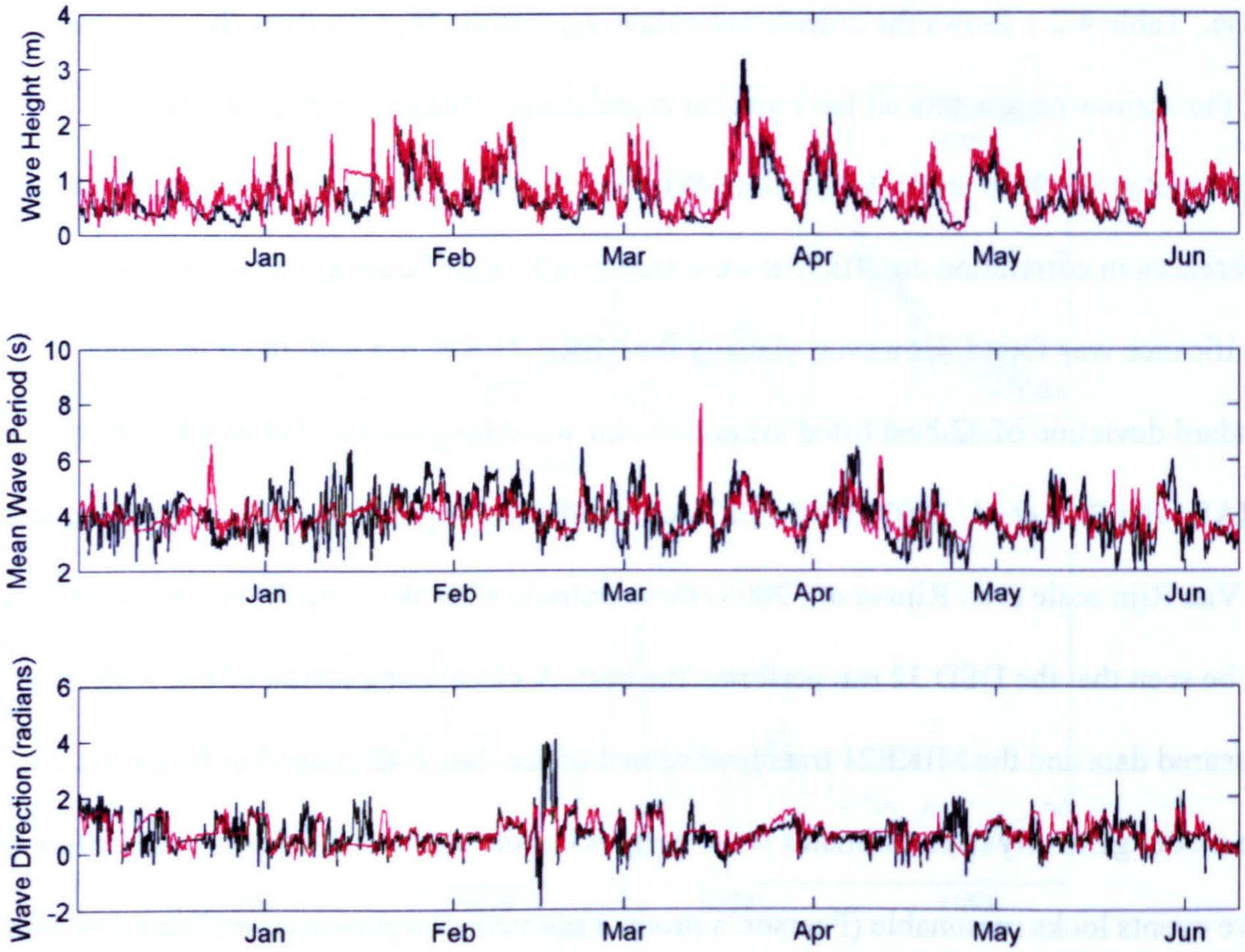

Figure 4.2.13: Comparison between modelled (red) and measured (black) wave parameters

Due to problems with the met office model there was one period of 29 days during November 2006 where there was no model output. This was a period in which several storms took place. In order to fill in this gap the Walcot AWAC data was used. This approach is justified because of the similarity between the Walcot data and the model data. The rationale being the belief that having some form of data is better than none and the importance of being able to account for the large morphological changes over that period.

Additional parameters and parameterisations used in correlation testing for the medium term shoreline dataset

As well as the standard hydrodynamic parameters (significant wave height, wave period, wave steepness, tidal range) several other quantities were utilised in correlation testing between the medium term shoreline dataset and forcing. These were relative tidal range, high tide elevation, a summation of high tide level and wave height and the longshore sediment transport for a straight undefended coastline. Relative tidal range is normally used in the classification of beach types (Masselink and Short, 1993) and is calculated with average parameters. In this study a time series based on daily parameters was used to indicate the relative importance of tides and waves to morphological change since it have been shown that tidal currents contribute significantly to the sediment transport at this site (Bacon *et al.*, 2005). It is calculated as:

$$RTR = \frac{TR}{H_s}$$

where RTR is the relative tidal range, TR is the tidal range and H_s is the significant wave height. Large values suggest tide dominance and small values wave dominance.

The time series of high tide elevation and the summation of high tide elevation and wave height were used to indicate the potential penetration of wave energy in the embayments. Higher water levels allow greater wave penetration as there is greater overtopping, lesser wave dissipation on the bay floors and the gaps between breakwaters are wider due to the sloped breakwater sides. Large spring high water levels and surges also allow the mobilisation of sediment from the supra-tidal beach and potentially open additional sediment transport pathways over the large northernmost tombolo that is normally dry throughout the tide.

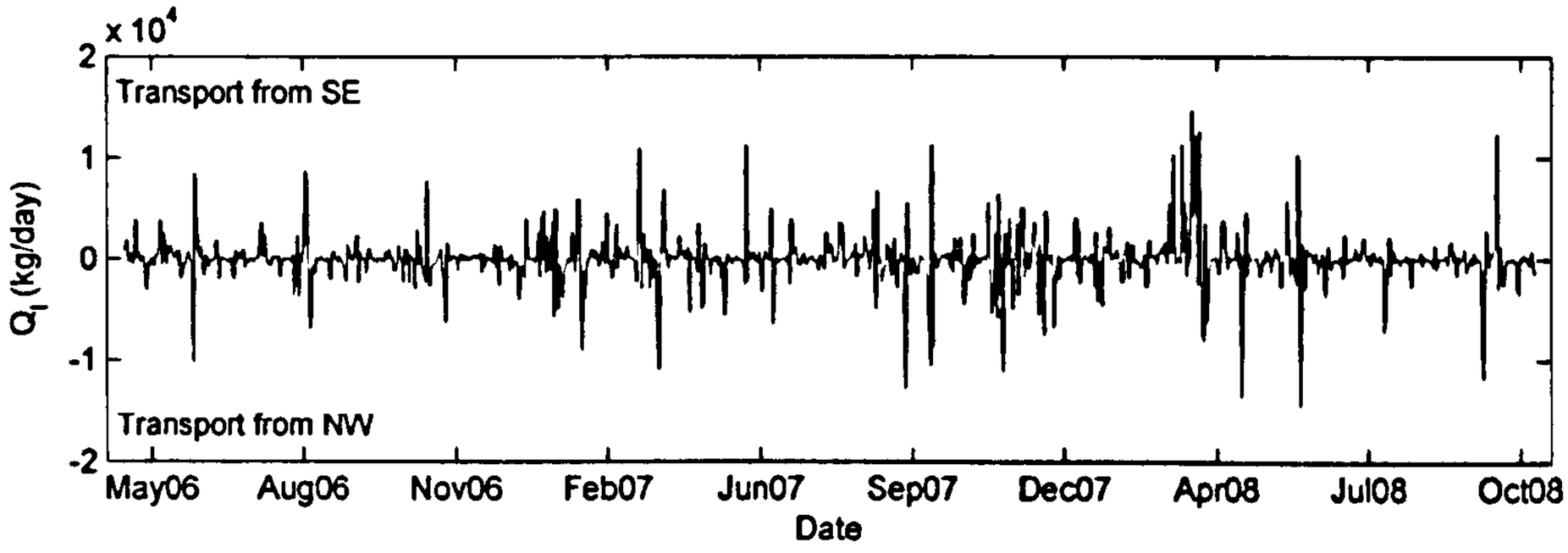

Figure 4.2.14: Estimate of the longshore sediment transport rate with sign indicating direction, negative values indicating transport from the north-west and positive from the south east.

An estimate of the volumetric longshore sediment rate (Q_l) assuming a long straight undefended coastline was also tested. This parameter was calculated based on the equation (Komar, 1998):

$$Q_l = 0.46\rho g^{3/2} H_s^{5/2} \sin\alpha_b \cos\alpha_b \quad (2)$$

where ρ is the density of water, g is gravity, H_s is significant wave height and α_b is the wave angle at breaking. The actual co-efficient (0.46) is unimportant as it is the shape rather than the magnitude of the function which is of importance here. Longshore sediment transport was given a positive sign for transport from the south-east and a negative sign for transport from the north-west, the bi-directional nature of the sediment transport is clearly visible in Figure 4.2.14. As well as the directional estimate, the modulus quantity of this was used to represent the amount of sediment available for trapping by the scheme without directional reference.

A new manifestation of the hydrodynamic parameters was introduced in this study: the cumulative integral of the de-meaned parameters. This was calculated via the following equation:

$$X_n = \int_{t_0}^{t_n} (x - \bar{x}) dt \qquad (3)$$

where X_n denotes the cumulative integral of a parameter at a time-step n, x the parameter, $\bar{x}$ the mean value of the parameter, t the time, t_0 the initial time and t_n the time at the final time-step for the integral. Motivation for the cumulative integral manifestation was twofold: Firstly, changes to beach morphology are dependant on the beaches initial condition which itself depends on prior forcing; secondly, hydrodynamic conditions often change far quicker than the beach morphology and thus linking morphological changes to hydrodynamic parameters can be difficult (Quartel *et al.*, 2008). A further rationale for the considering the cumulative integral was that beaches are often assumed to have an equilibrium state based on sediment properties and mean wave conditions, deviations from the equilibrium beach are caused by variations from the mean wave conditions. Removing the mean value thus shows deviations from equilibrium conditions. The cumulative integral was used since it encapsulates the cumulative effects of antecedent hydrodynamic conditions. Periods of lower than mean conditions produce negative gradient, mean conditions gradients of zero and periods of higher than mean conditions positive gradients. An example of this parameterization, the cumulative integral of de-meaned wave height, is shown in Figure 4.2.15. This figure shows the seasonal trend in wave heights with summers generally showing smaller then mean wave heights (negative gradients) and winters larger than mean wave heights (positive gradients). These general trends are shown by the thick grey lines in Figure 4.2.15. It can be seen that the winter of 2007-2008

exhibited longer periods of larger than mean wave heights than the previous winter. The effect of individual storms is also observable in the record in the form of sharp upwards shifts in the cumulative integral; for example, the steep upward shift at the start of November 2006 corresponds to a large storm at that time (indicated by an asterisk in Figure 4.2.15).

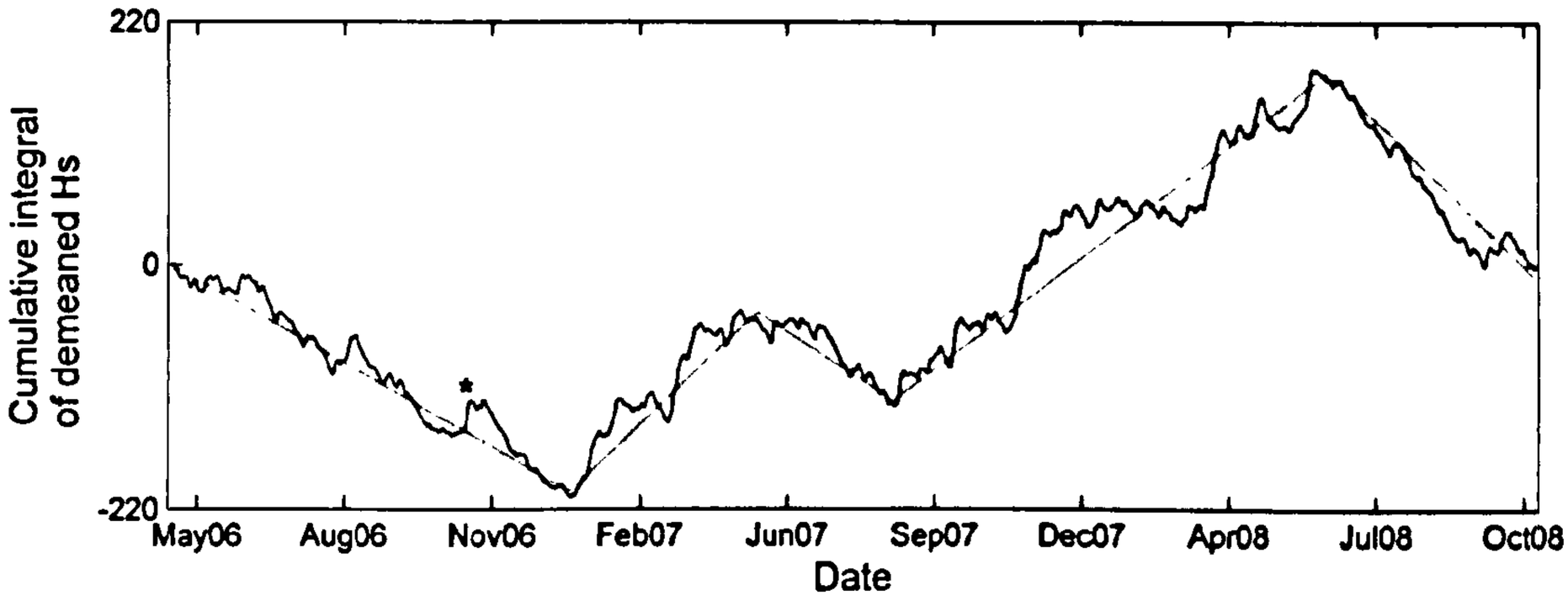

Figure 4.2.15: The cumulative integral of the de-meaned significant wave height; this shows deviation from the mean wave height and has proved useful in comparing hydrodynamic conditions with time series of morphological change. The asterisk indicates a storm induced positive shift in the cumulative integral. The grey lines show general trends in the cumulative integral and make the seasonality in the wave heights more obvious.

4.3 Storm induced morphological change

4.3.1 Introduction

Storm scale beach changes receive a considerable amount of research effort due to the magnitude of beach response and the potential capacity for loss of infrastructure and life. Current work on climate change suggests that as well as rising sea level increasing risks of coastal inundation, storms are likely to become more intense and storm tracks alter (IPCC, 2007) exacerbating pressure on the coast and hence amplifying the importance of research into storm scale beach morphodynamics.

There is an extra incentive in researching storm scale change on protected beaches: good performance (retention of sediment) of a coastal protection scheme under storm conditions is vital in assessing a coastal protection schemes performance.

In this section the results from a series of pre- and post- storm video derived intertidal surveys are presented in the form of erosion-accretion plots, comparison of cross-shore profiles and a detailed look at salient and tombolo changes.

4.3.2 Results

Storms with different angles of incidence, different durations and different surge levels were investigated. An annotated wave power time series for the period evaluated is displayed in Figure 4.3.1, and the basic storm parameters are described in Table 4.3.1. The directional convention used in the table is 0 being shore normal, positive wave angles represent waves incident from the north and negative angles from the east. Surge level is determined as the difference between the NTSLF gauge at Cromer (15miles from Sea Palling) and predicted tides at that point. It can be seen that the two storms incident from the east are not associated with surge events.

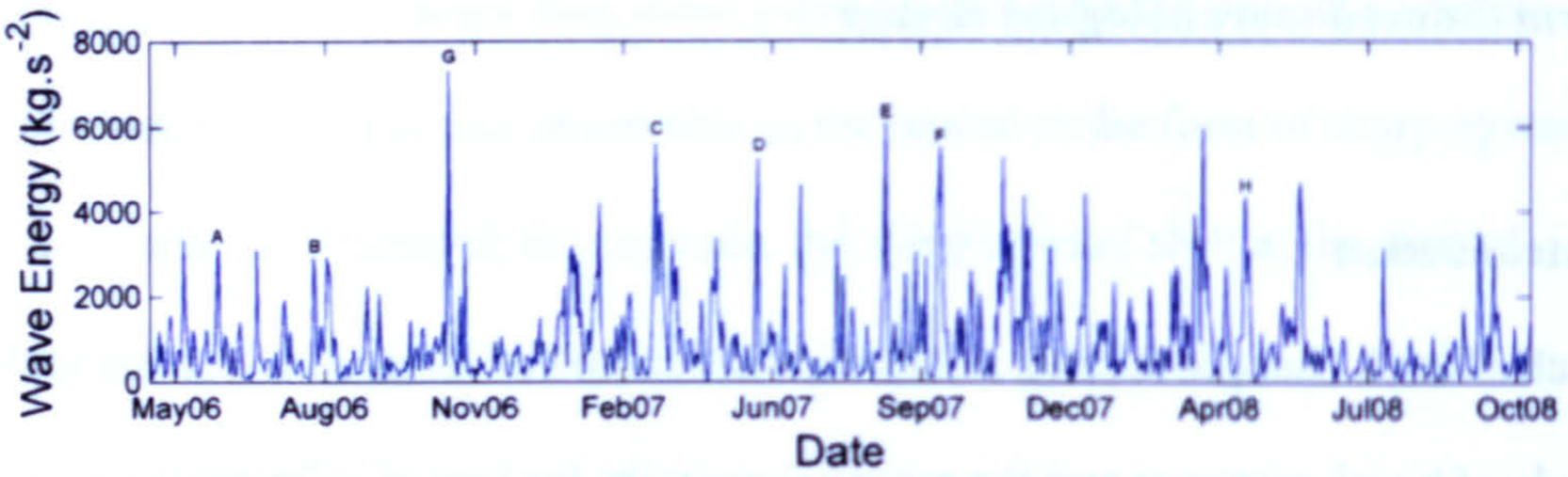

Figure 4.3.1: A wave energy time series with the evaluated storms labelled.

Table 4.3.1: Basic storm parameters for the storms analyzed.

Storm	Duration between video surveys	Max. H_s	Wave Direction	Surge level
A	2	2.6	40	0.5
B	2	2.4	30	0.5
C	6	3	30	1.3
D	1	2.5	-25	0.15
E	4	3	30	0.5
F	4	3	±10	0.4
G	17	3	40	1.0
H	10	2.1	-25	±0.1

Erosion-Accretion plots

Erosion accretion plots for the eight storms are shown in Figure 4.3.2. Negative *z* values indicate erosion and positive *z* values accretion. The longshore movement of the tombolos and salients is clearly displayed in storm A, with erosion on the up-drift and accretion on the down drift side of the tombolos. The salients show less defined displacement although still in the same direction. The same trend is evident, but to a lesser extent in storms B and C. Storms D and H, where waves are incident from the east rather than north, shows opposing direction of displacement of the salients and tombolos.

Storm F, with shore normal wave incidence shows the tombolos staying at the same longshore location, but flattening, with erosion on the upper horn and accretion either side.

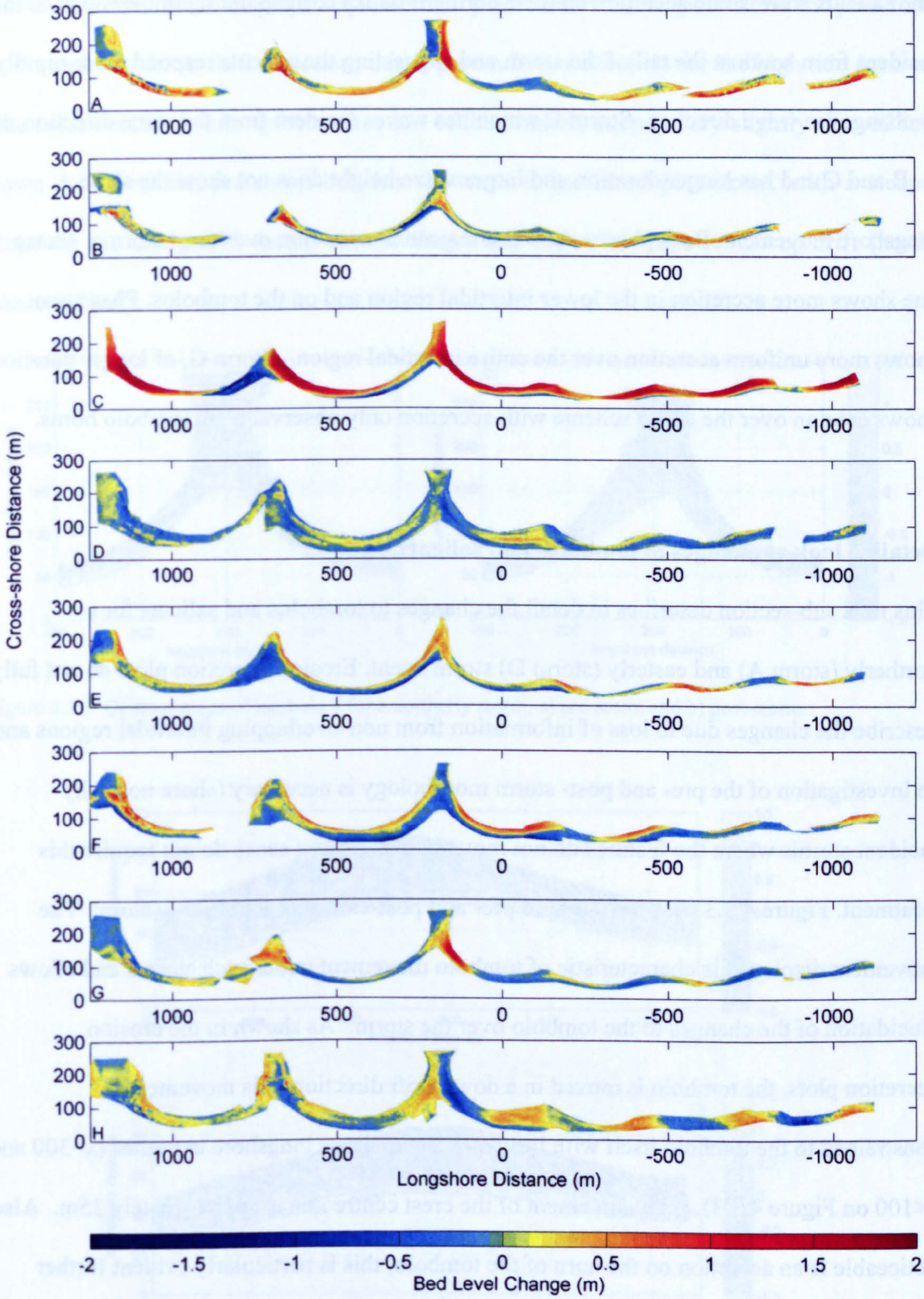

Figure 4.3.2: (a-h) Erosion-accretion plots for the eight storms analysed. Erosion is indicated with darker colours and accretion with lighter colours. Gaps in coverage are due to sheltering of certain regions by the tombolo crests.

The salients show some accretion on their northern flanks corresponding to the waves being incident from south at the tail of the storm and suggesting the salients respond more rapidly to changes in wave direction. Storm E which has waves incident from the same direction as A, B and C and has longer duration and larger wave height does not show the same longshore movement. Both phases show some general accretion over most storms. Phase one shows more accretion in the lower intertidal region and on the tombolos. Phase two shows more uniform accretion over the entire intertidal region. Storm G, of longer duration shows erosion over the entire scheme with accretion only observable on tombolo horns.

Detailed look at changes to tombolos and salients

This next sub-section describes in detail the changes to tombolos and salients for a northerly (storm A) and easterly (storm D) storm event. Erosion-accretion plots do not fully describe the changes due to loss of information from non-overlapping intertidal regions and so investigation of the pre- and post- storm morphology is necessary (shore normally incident storms where the features do not move in a longshore sense do not require this treatment. Figure 4.3.3 shows a tombolo pre- and post-storm for a northerly storm. The movement displayed is characteristic of tombolo movement under such storms and allows elucidation of the changes to the tombolo over the storm. As shown in the erosion accretion plots, the tombolo is moved in a down drift direction, this movement is constrained to the tombolo itself with little movement at the longshore extremes (x>300 and x<100 on Figure 4.3.3). The movement of the crest centre line is approximately 25m. Also noticeable is an accretion on the horn of the tombolo, this is particularly evident further seaward (200-275m cross-shore) where the salient crest accretes by ~0.5m. A skewness in the tombolo form is induced by the oblique waves.

Pre-storm the tombolo displays a symmetrical plan-form, whereas post-storm the plan-form is skewed in a down-drift direction; this is particularly noticeable for the high tide contour. The cross-section in a longshore direction of the tombolo horn is very slightly skewed in a down drift direction pre-storm but this skewness is increased post-storm, with a steeper slope on the down-drift (south-eastern flank) and a gentler slope to the up-drift (north-western flank).

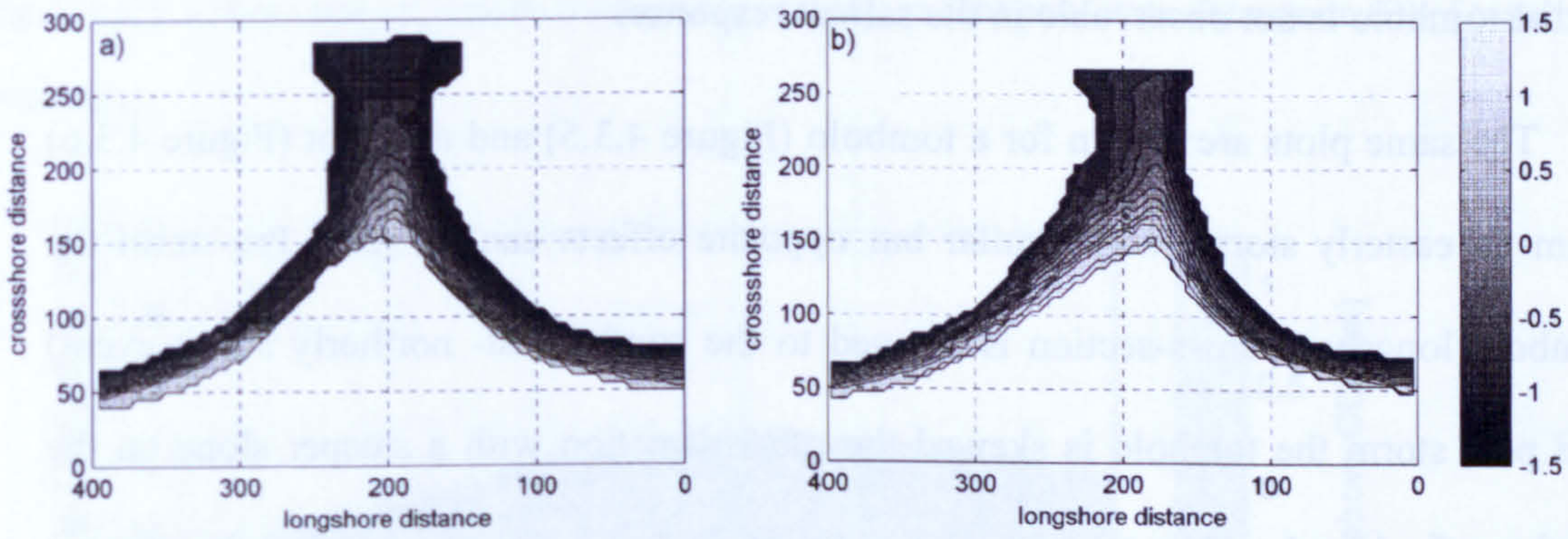

Figure 4.3.3: Contour maps of tombolo 8 for a northerly storm; a) pre-storm and b) post-storm.

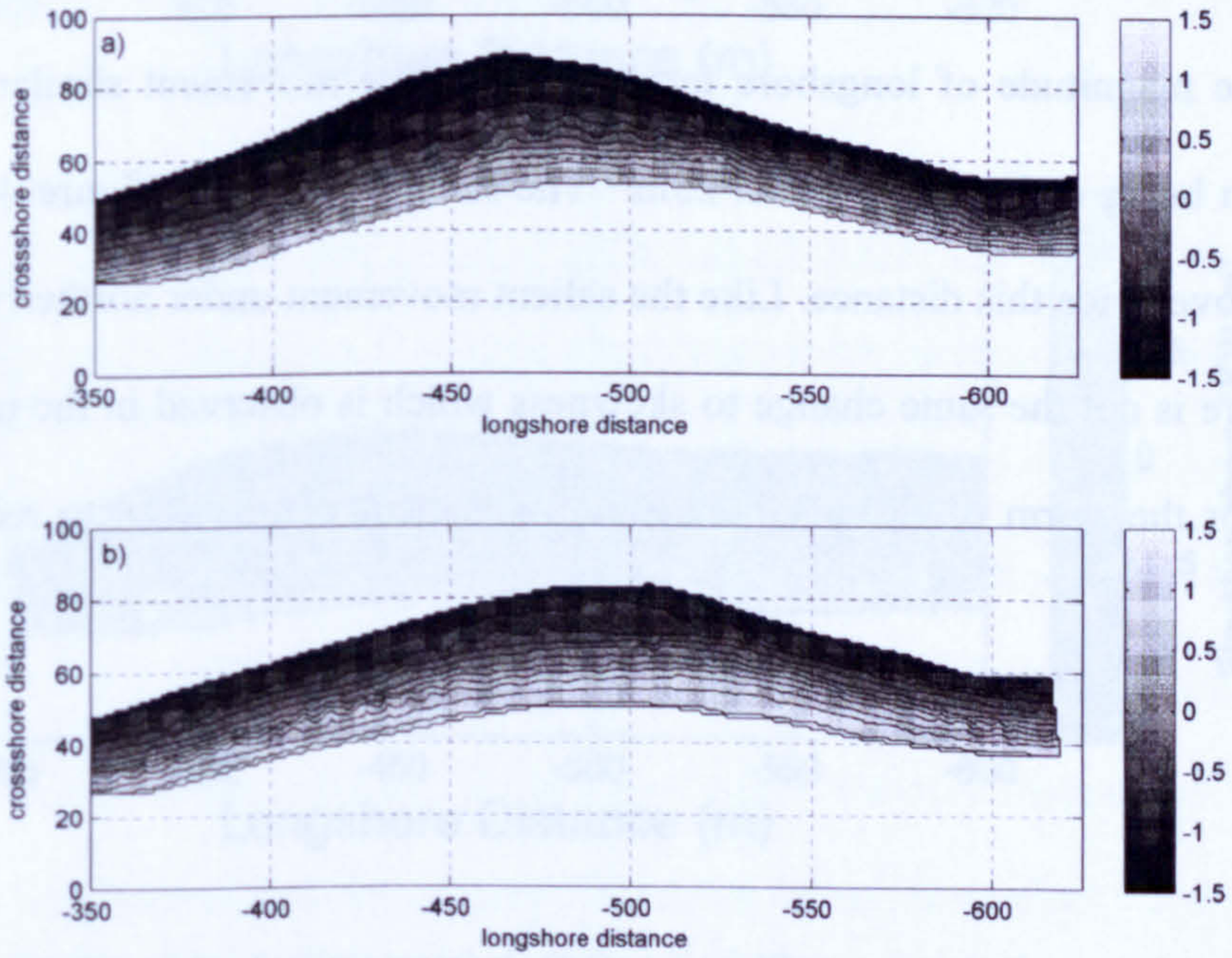

Figure 4.3.4: Contour plots of salient 10 a) before and b) after a northerly event (storm A).

Pre- and post-storm contour plots for a phase two salient from the same northerly storm as the previous plots of a tombolo are shown in Figure 4.3.4. It can be seen that there is a southward shift of the feature of similar longshore magnitude (~25m) to the tombolo (Figure 4.3.3) but the movement is much less defined in the salient. Similar to the tombolo, accretion occurs over the storm but the accretion is over the entire region rather than specifically on the horn of the tombolo. The increased skewness displayed by the tombolo is not observable in the salient response.

The same plots are shown for a tombolo (Figure 4.3.5) and a salient (Figure 4.3.6) from an easterly storm: very similar but opposite effects can be seen. Pre-storm the tombolo longshore cross-section is skewed to the south (post- northerly storm event) and post storm the tombolo is skewed the other direction with a steeper slope on the northern flank and gentler slope on the southern flank. The severity of this skewness is much less than for a northerly storm. Numerical modelling (Chapter 6) suggests that this is due to different sediment transport pathways forcing the different directions of movement. The magnitude of longshore tombolo centreline movement similar to the northerly storm being estimated at about 25m. The salient centreline (figure 4.3.6) is estimated to move twice this distance. Like the salient movement under northerly storm conditions, there is not the same change to skewness which is observed in the tombolo movement. For the storm of easterly incidence, the salient can be seen to reduce in sinuosity.

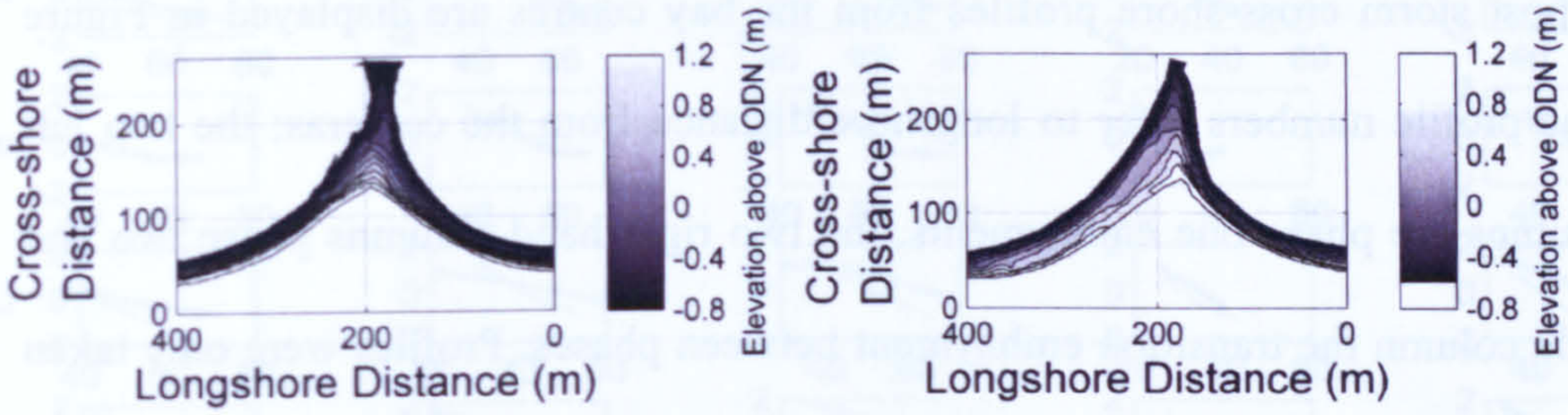

Figure 4.3.5: contour plots of tombolo 8 morphology (a) pre- and (b) post- storm for a storm (D) of easterly incidence.

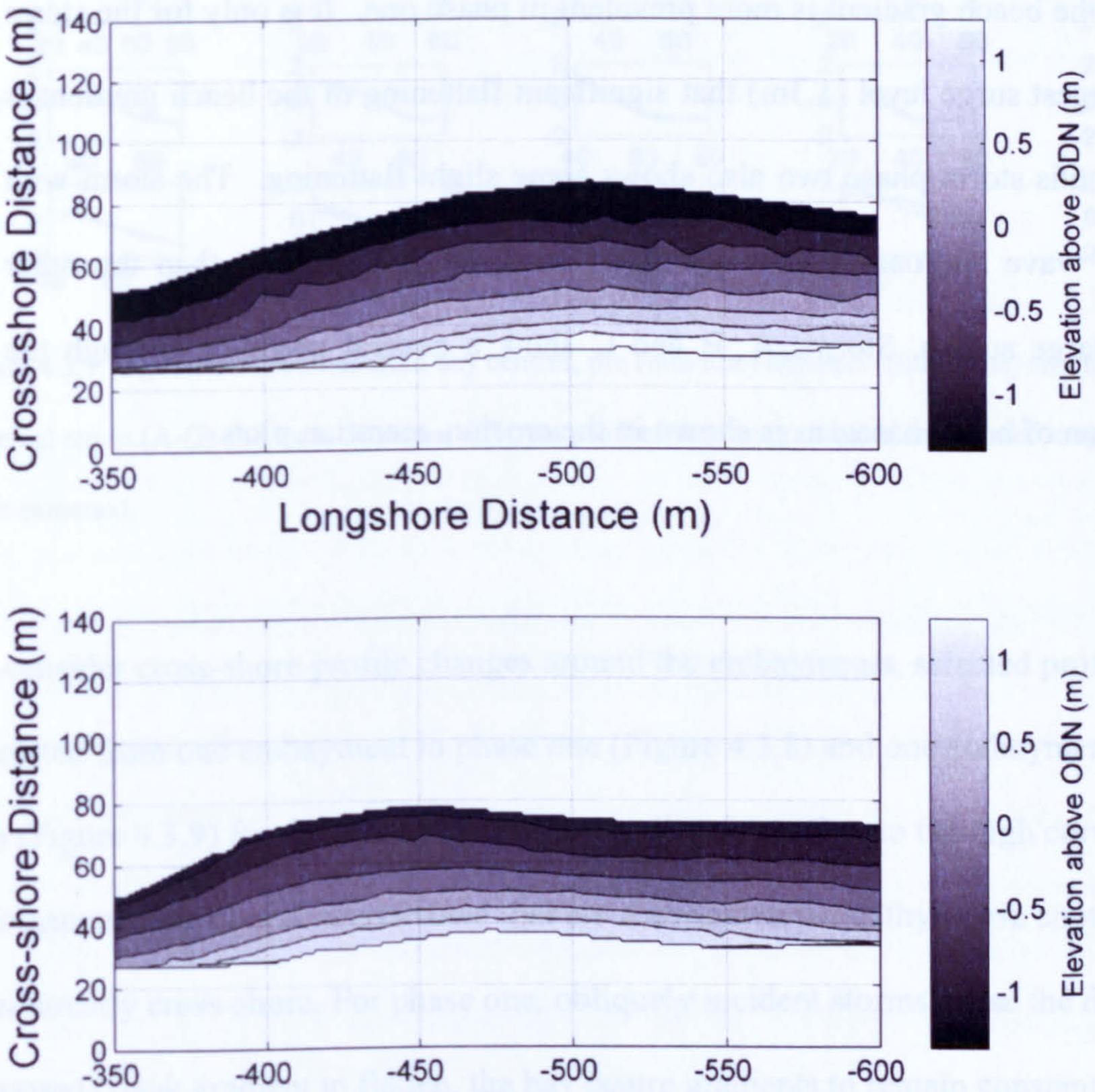

Figure 4.3.6: Contour plots of salient morphology for salient 10 over an easterly event (storm D); (a) pre- and (b) post- storm.

Cross-shore profile changes

Pre and post storm cross-shore profiles from the bay centres are displayed in Figure 4.3.7. The profile numbers refer to longshore distance from the cameras; the two left hand columns are phase one embayments, the two right hand columns phase two and the middle column the transition embayment between phases. Profiles were only taken in the bay centres to minimize the impact of the longshore movement of the salients and tombolos on the cross-shore profile changes. It can be seen that the cross-shore profile gradients in phase two remains similar regardless of wave height or storm duration. Flattening of the beach gradient is more prevalent in phase one. It is only for the storm C with the largest surge level (1.3m) that significant flattening of the beach gradient is observed, for this storm phase two also shows some slight flattening. The storm with shore normal wave approach (storm F) shows more beach flattening than the other storms with large surges. Storms A, B and C show a general accretion through the intertidal region of both phases, as is shown in the erosion-accretion plots.

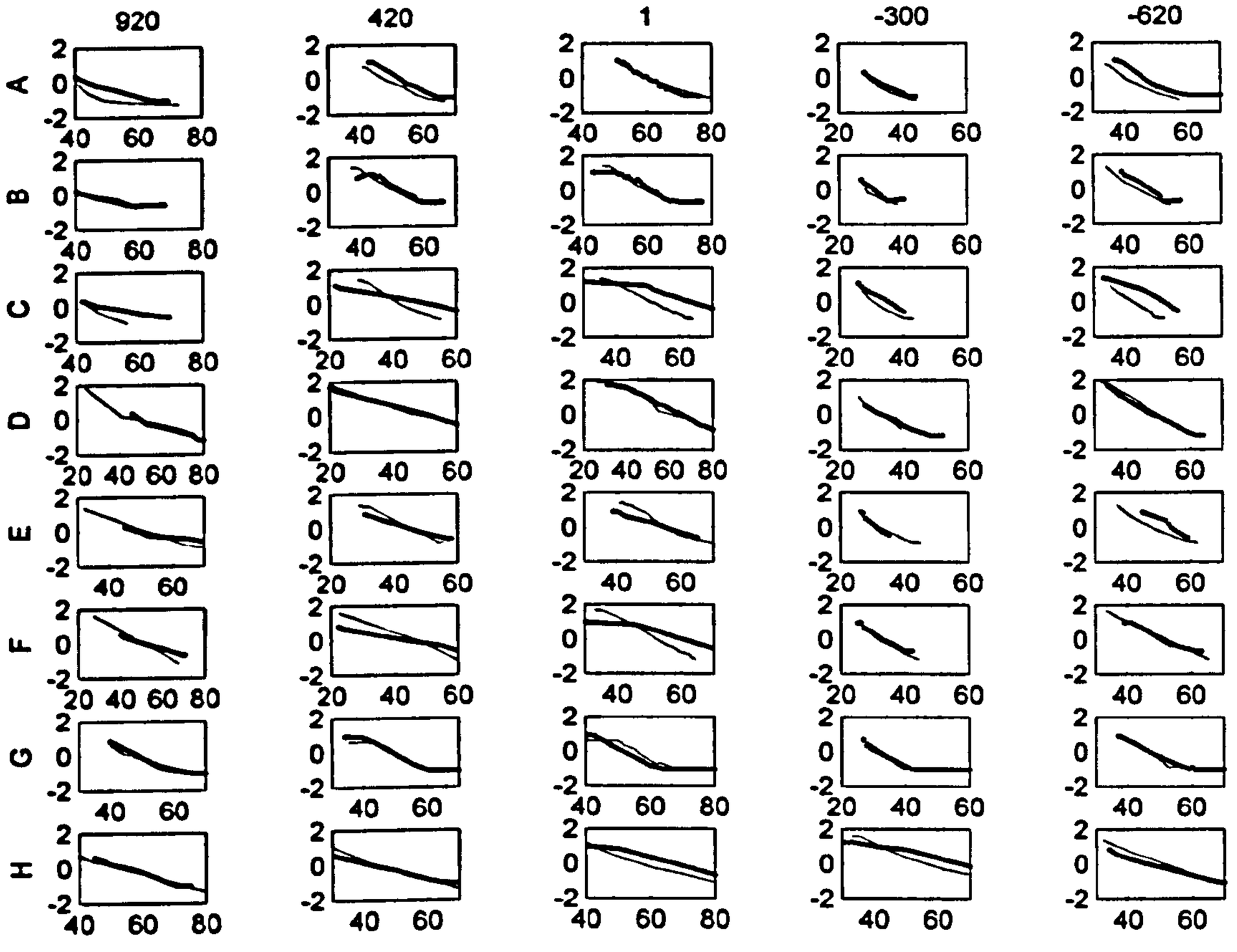

Figure 4.3.7: Cross-shore profiles from bay centres, pre (thin line) and post- (thick line) storm. Each row is a different storm (A-G) and each column a different profile location (numbered in terms of longshore distance from cameras).

To consider cross-shore profile changes around the embayments, selected profiles were extracted from one embayment in phase one (Figure 4.3.8) and one embayment in phase two (Figure 4.3.9) for the three different storm directions. Due to the high curvature of the embayments, profiles were extracted that were normal to the bathymetric contours rather than directly cross-shore. For phase one, obliquely incident storms cause the down drift (exposed) flank gradient to flatten, the bay centre gradients to remain constant and the up-drift (sheltered) flank to become steeper. The shore normally incident storm causes flattening of the bay centre profile with little change to the gradient of the flanks.

Conversely, for the phase two embayment the profiles maintain similar gradients around the embayment for all storm directions.

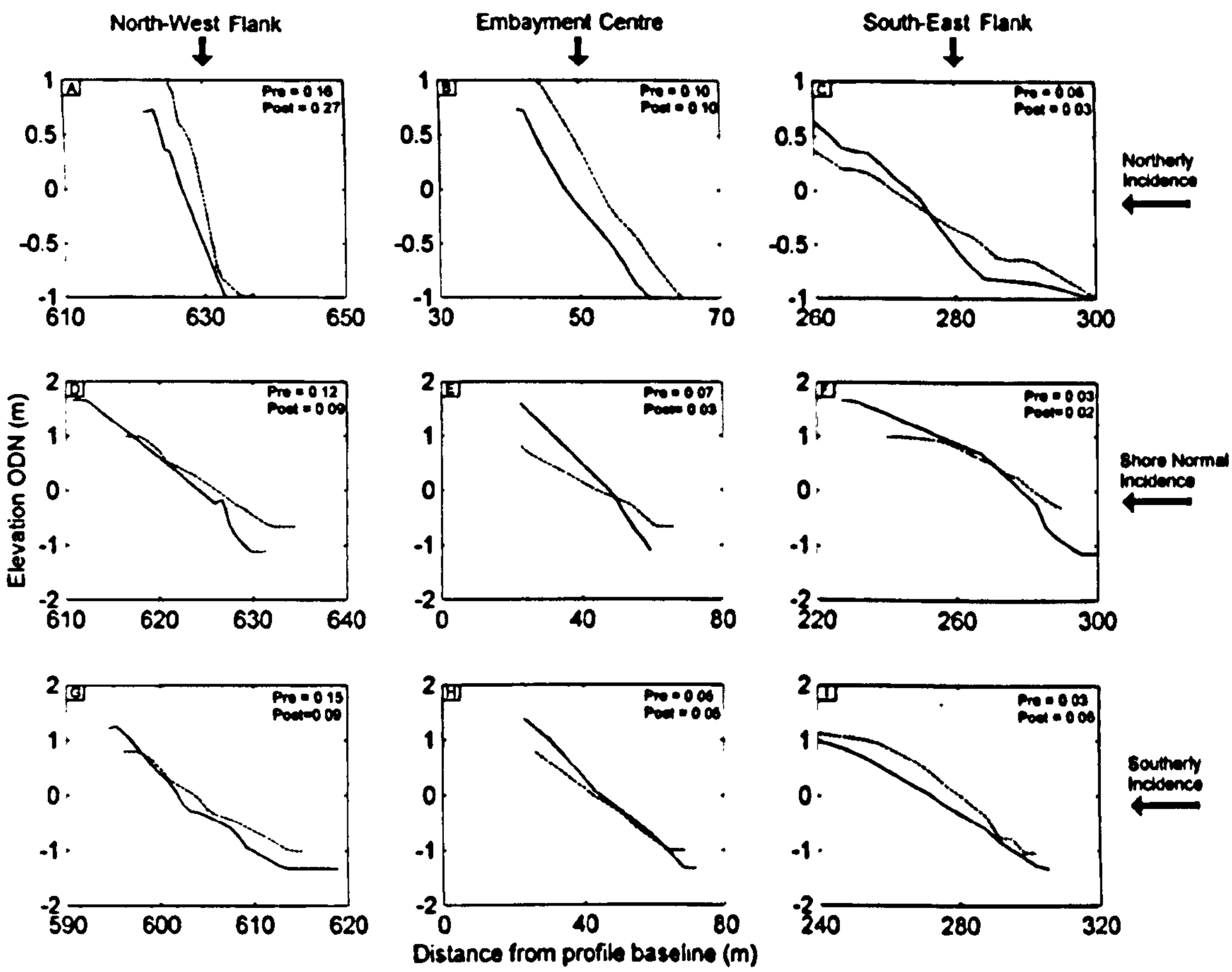

Figure 4.3.8: Storm scale profile changes from a phase one embayment for: (a-c) an northerly event; (d-f) a shore normal event; and (g-i) an easterly event. Solid lines indicate pre- and dotted lines indicate post- storm profiles. Profile gradients are displayed in the upper right corner of each panel. The left hand column (a, d, g) shows profiles from the north-western flank, the central column (b, e, h) shows profiles from the bay centre and the right hand column (c, f, i) shows profiles from the south-eastern flank.

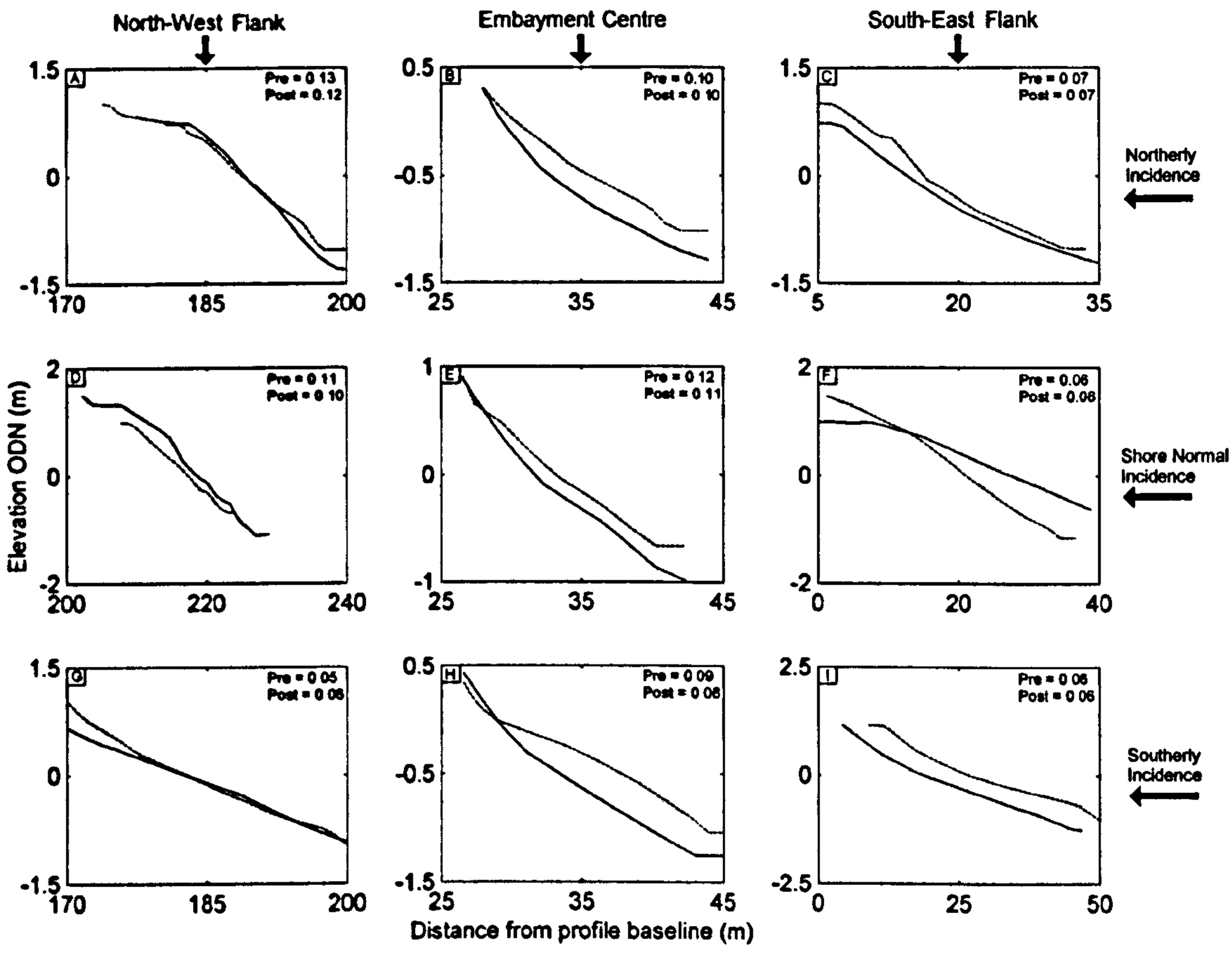

Figure 4.3.9: Storm scale profile changes from a phase two embayment for: (a-c) an northerly event; (d-f) a shore normal event; and (g-i) an easterly event. Solid lines indicate pre- and dotted lines indicate post- storm profiles. Profile gradients are displayed in the upper right corner of each panel. The left hand column (a, d, g) shows profiles from the north-western flank, the central column (b, e, h) shows profiles from the bay centre and the right hand column (c, f, i) shows profiles from the south-eastern flank.

4.3.3 Discussion of storm scale change

Analysis technique

Intertidal profiles were extracted as described in section 4.2.3. The concept is standard in derivation of beach morphology from video images and has been successfully used to isolate storm scale changes here. There are some shortfalls in the concept however. Firstly, only the intertidal region can be analysed, surges associated with storms often lead to changes in the supra-tidal beach and this change is not measurable with video techniques. This shortfall is partly alleviated via analysis of DGPS surveys (Chapter 5) although the temporal resolution does not allow total isolation of storm scale change. Secondly, since the intertidal footprint varies pre and post storm (due both to beach change and variation in tidal range) there is some loss of information when utilising erosion-accretion plots. This shortfall can be overcome to some extent by examining other products such as cross-shore profile lines. A site specific problem is that berms on the tombolo/salient crests, at times, obscure the far side beaches. The only way to rectify this would be to build a taller tower, raising the cameras and reducing the shadowing effect.

Cross-shore profiles are difficult to extract from coastlines with high curvature. Past studies have suggested fitting log-spiral curves to the coastline (Harley and Turner, 2008) and hence artificially straightening an embayed coastline to allow easier consideration of cross-shore change. However, the small scale, number and temporal variability of the embayments in this study means such an approach is not practical. Instead, profiles were taken in the bay centres (where embayment curvature is not relevant) for all storms and example profiles from other areas extracted from shore-normal lines that were manually selected. Such an approach is suitable for selected profiles over short time scales but the variability of the embayments meant selecting a line that is shore normal both

pre and post storm is difficult and hence only a few profiles can be extracted with confidence that pre- and post-storm comparison is valid.

Interpretation of results

The southward movement of the tombolos under a northerly storm has previously been reported by Dolphin et al (Dolphin *et al.*, 2005) who used GPS surveys to measure morphological changes under two storms in phase one. As expected, the video analysis corroborates these previous findings and shows that for waves from the opposite direction the reverse movement takes place. Whilst such reversal in tombolo movement might seem obvious, the asymmetry in the strong tidal current means such movement cannot be assumed a priori. Storms of shore normal approach do not lead to significant longshore movement of the tombolos or salients. Associated with the longshore movement of the tombolos is an increase in tombolo asymmetry over an oblique storm.

This work extends the investigation into phase two where the same direction of feature movement is displayed in the salients. The salient movement is more diffuse, this can be explained by the lesser difference between sheltered and unsheltered regions in phase two, caused both by the shorter breakwater lengths and the increased overtopping and wave transmission. The longer, emergent, phase one breakwaters lead to steeper gradients in wave exposure and hence the more defined response in the longshore movement of the features. The nature of features themselves exacerbates this: the tombolo horn positions are more firmly 'tied' to the structure locations. This concept can be used to explain the lack of longshore tombolo movement in storm E: if previous storms from one direction have displaced the tombolos to the limit of the sheltered region, further storms from that direction will produce no further longshore movement. Hence sensitivity to initial conditions will affect the amount of longshore tombolo movement. It appears that the phase

two salients respond more readily to changes in wave direction, this, it is believed, is due to the storm wave overtopping of the phase two structures reducing the amount of diffraction through the gaps and hence waves approach the shore more obliquely than for phase one.

Dolphin *et al* (2005) pose the question of storm recovery of tombolo position due to the dominance of northerly waves and the asymmetry in tidal transport giving a net south easterly transport, meaning that sediment transport to the north is not favoured. This work helps to address this: firstly, as expected, easterly events return the features northward; secondly, observed changes to the tombolo shape allow postulation of a return mechanism. The tombolo actually accretes over the storm period and becomes more asymmetric in cross section. This means that in order to return to the original position further accretion is not required, instead erosion of the tombolo crest and smoothing of the asymmetry could return the tombolo to its original form.

Inter-tidal cross-shore gradients in bay centres remain similar over the storm in phase two whereas phase one embayments show some beach flattening. Classically one would expect reduction in profile gradient under storm conditions however this is not always observable. A reduction in profile variability was observed at the Elmer breakwater scheme by Axe and Chadwick (1997). The difference in breakwater gap length explains the difference between phases: the gaps in phase one are almost twice as wide as the phase two gaps and so transmit more wave energy into the bay regions (Numerical modelling in chapter 6 shows this difference in wave penetration). Differences in sediment abundance and supra-tidal beach widths could also explain this difference. The beaches in phase two are narrower both due to the lesser sheltering of smaller breakwaters and since they are down drift of phase one and suffer from reduced sediment supply. High tide shorelines are constrained by the sea wall, which is reached most high tides, and hence further shoreline recession is impossible. The wider phase one beaches allow for upper- intertidal and supra-

tidal erosion and associated flattening of the beach gradient. Greater flattening is observed for the shore normally incident storm due to the angle of wave attack. Consideration of gradient changes about the embayments show that for phase one the obliquely incident waves lead to reduction of profile gradient on the down-drift flank and steeper gradients on the up-drift flank. This profile change is the same as the increased asymmetry of the tombolos over a storm. For phase two the gradients remain similar for all storm directions.

It is thought that the sediment deposited in the intertidal region over the storm could well be taken from the supra-tidal beach, the other likely source is increased longshore sediment transport under storm conditions. Supra tidal erosion after storms is observable after storms (Chapter 5). Since, as previously stated, there is little supra-tidal sediment in phase two (unless surge levels are high enough to allow erosion of the dune above the sea wall), the general intertidal accretion of phase two is believed to be due to increased longshore sediment supply. In phase one, larger storm waves intensify circulation patterns and lead to greater deposition on the tombolo horns where circulation diverges; overtopping of the phase two breakwaters reduces this effect which leads to lesser accretion behind the structures.

4.3.4 Conclusions of storm event analysis

Obliquely incident storm waves move the tombolos and salients in a down drift direction. Both designs of breakwater produce the same direction of longshore salient/tombolo movement under oblique waves. The larger phase one structures constrain this movement giving better defined regions of change compared to phase two. The amount of longshore movement is sensitive to the initial morphological conditions; specifically the tombolo position in relation to the breakwater. Associated with the longshore movement of the tombolos is an increased skewness to the tombolo shape which is not observable in the salient morphology. This skewness is also observed in beach profiles around the embayment: reduction in gradient on the exposed flank; increase in gradient on the sheltered flank. This suggests that the tombolo skewness is caused partially by the down drift feature movement and partially by cross-shore profile flattening under large waves.

Accretion is observed in the intertidal region over storm periods. In phase one this accretion is focussed on the tombolos whilst phase two exhibits a more general accretion over the intertidal area. The beaches protected by the smaller lower breakwaters show little changes to beach gradient over the storm, whereas the beaches protected by the large structures show beach flattening. It is believed that is more related to the presence of the sea wall and lack of sediment than the breakwater geometries.

4.4 Medium term behaviour of the mean sea level contour

4.4.1 Introduction

This dataset consists of mean sea level (0.18m ODN) shoreline contours extracted from the video images. Monitoring changes to shoreline position through time has long been used to inform coastal management and to aid coastal research and engineering. A single shoreline representation of beach morphology is an attractive proposition since it allows for a simpler description of changes over time than 3-dimensional morphological maps, often leading to identification of trends that can be difficult to extract from more complex datasets. Determination and definition of a viable shoreline is a non trivial question and a bad choice in this matter can affect validity of results (Boak and Turner, 2005). The actual shoreline, defined as the land/water intersection, is constantly changing due to tidal and wave (set-up and swash) processes; thus a shoreline proxy or representative shoreline (e.g mean high water shoreline) is normally used. Boak and Turner (2005) provide a review of the different shoreline proxies commonly in use today, typically these are shorelines at a certain water level or features such as cliff lines. One concept that provides a robust shoreline proxy is to determine an artificial shoreline position based on the volume of sediment in a measured profile. The momentary coastline, a statistic used successfully in the coastal management of the Netherlands, is calculated from the volume of sand in a meter wide profile between specified vertical levels divided between the vertical distance between these two levels and so encapsulates information about the entire beach in a simple "shoreline" (Van Koningsveld and Mulder, 2004). A video derived version of this proxy, the momentary intertidal coastline position (MICL) has also proved successful in the understanding and management of the Dutch coastline (Van Koningsveld and Mulder,

2004; Wijnberg *et al.*, 2005; Kroon *et al.*, 2007; Smit *et al.*, 2007). In the video derived proxy only the intertidal region is considered and vertical limits set appropriately. Whilst the MICL has proved a useful tool it has two disadvantages: firstly, unless the smallest neap tide range is utilised the MICL can only be realised on certain tides; secondly, the number of processed images needed to derive the MICL is large, leading to longer computation times. These disadvantages meant that a single shoreline representation was preferred: utilisation of a single water level shoreline has the advantage that it can reduce the data processing time (since fewer images need analysing) thus allowing an increase in the temporal resolution. In order to have the capability to extract shorelines from every tide, a level inside the neap tide limits is required. The mean sea level shoreline position (MSL) was believed to be the most useful shoreline definition. This shoreline has the advantage that it adequately captures the morphological features of the scheme; a shoreline at higher water levels would miss much of the variability in the shapes of the salients and tombolos. To verify the mean sea level shoreline was a reliable shoreline for analysis, it was compared with MICL's at Sea Palling (Figure 4.4.1). In this instance the MICL's utilised had vertical limits ±1m from mean water level. The two shorelines showed a very good correlation (r=0.997) suggesting that, given the documented success of the MICL, the MSL would be a suitable shoreline to analyse. It is believed that the similarity between the MICL and the MSL is due to the relatively linear shape of the cross-shore beach profile in the intertidal region at Sea Palling. A similar correlation between mean sea level contour and beach volume was found at Tairua Beach, New Zealand by Smith and Bryan (2007)

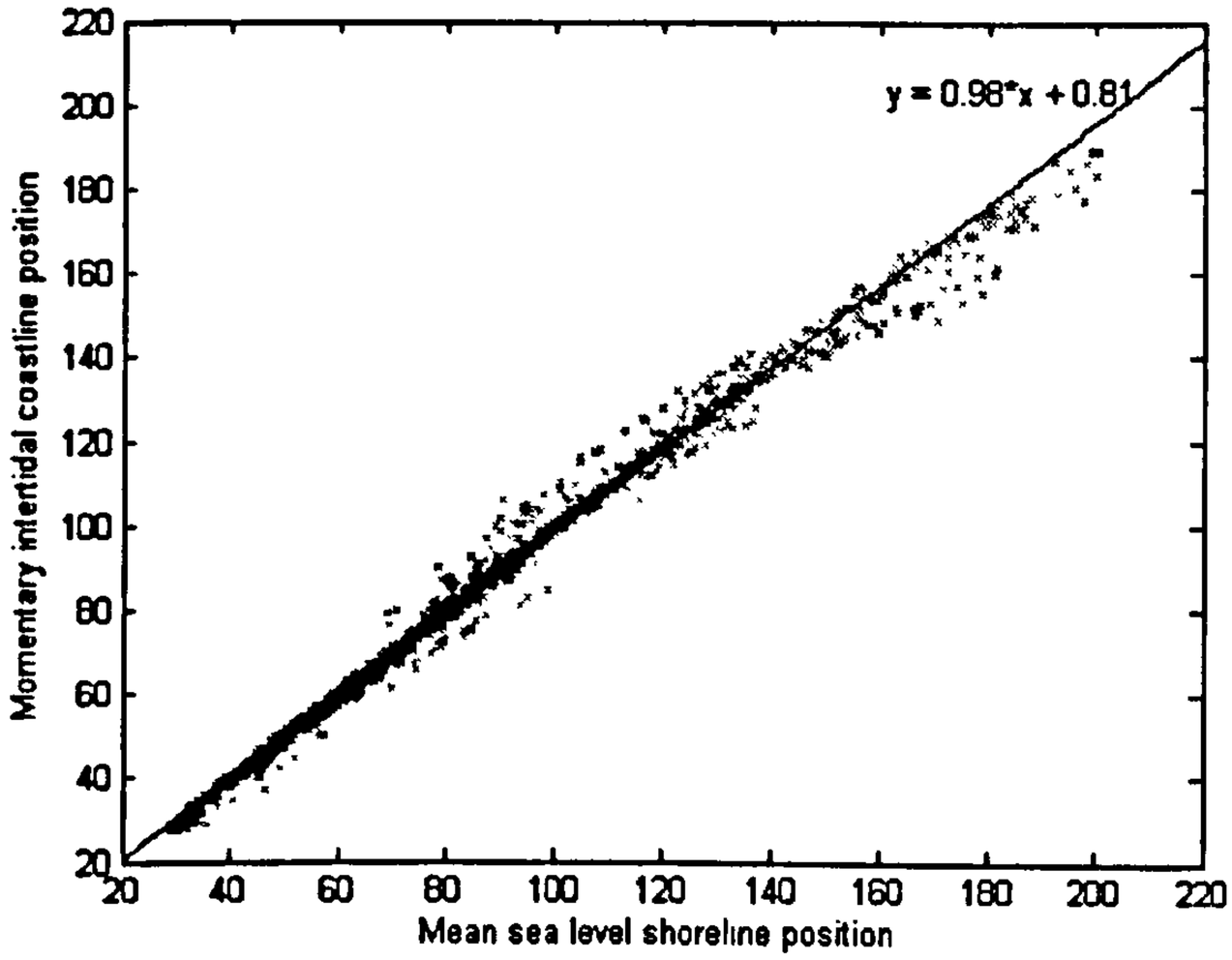

Figure 4.4.1: Scatter plot showing the high correlation between momentary intertidal coastline position and mean sea level shoreline position

The dataset, containing 127 shoreline realisations, spans from 02/05/2006 until 25/10/2008. A weekly temporal resolution was aimed for but shorelines were also picked pre and post storm to capture storm induced shoreline changes. Shorelines were only picked on days with good image clarity and low wave heights which meant that the temporal spacing was sometimes longer than weekly. The spacing of the shorelines along with the underlying wave height climate is shown in Figure 4.4.2.

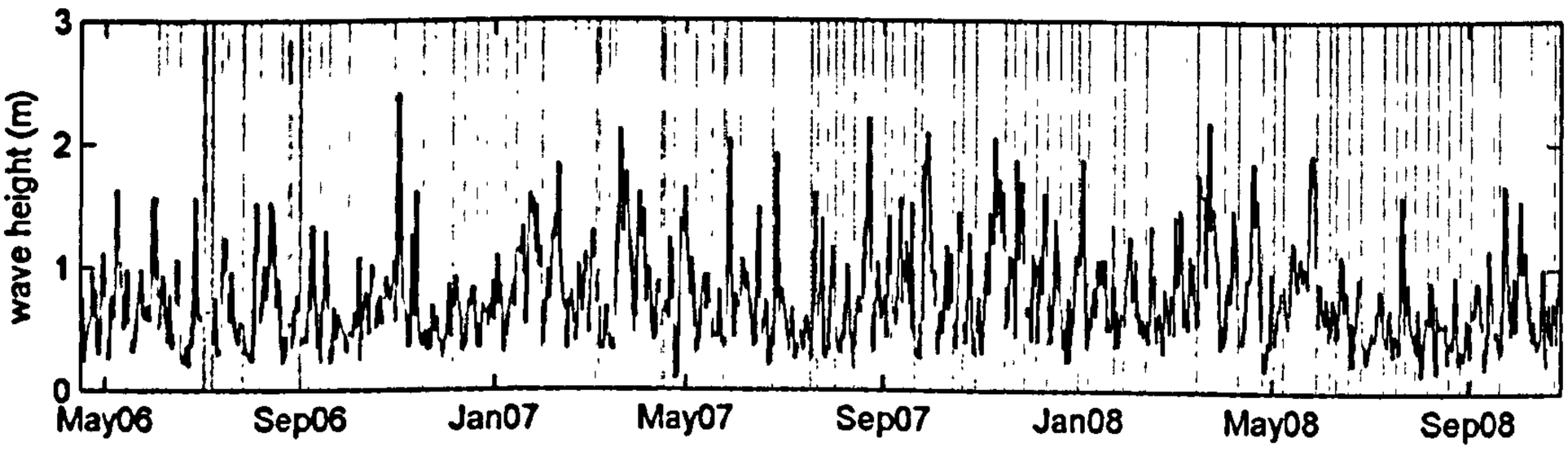

Figure 4.4.2: A plot of the incident wave height climate with vertical lines representing the dates that mean sea level shorelines were picked.

4.4.2 Results

A two dimensional surface plot of the dataset is show in Figure 4.4.3. The most observable changes are the growth and shrinking of the tombolos / salients and the longshore movement of these features. In this chapter, a range of simple analyses will be used to describe the dataset before EOF analysis is used to decompose the dataset into its constituent modes of change. Time series of morphological change were correlated with forcing conditions using Pearson's product moment correlation co-efficient.

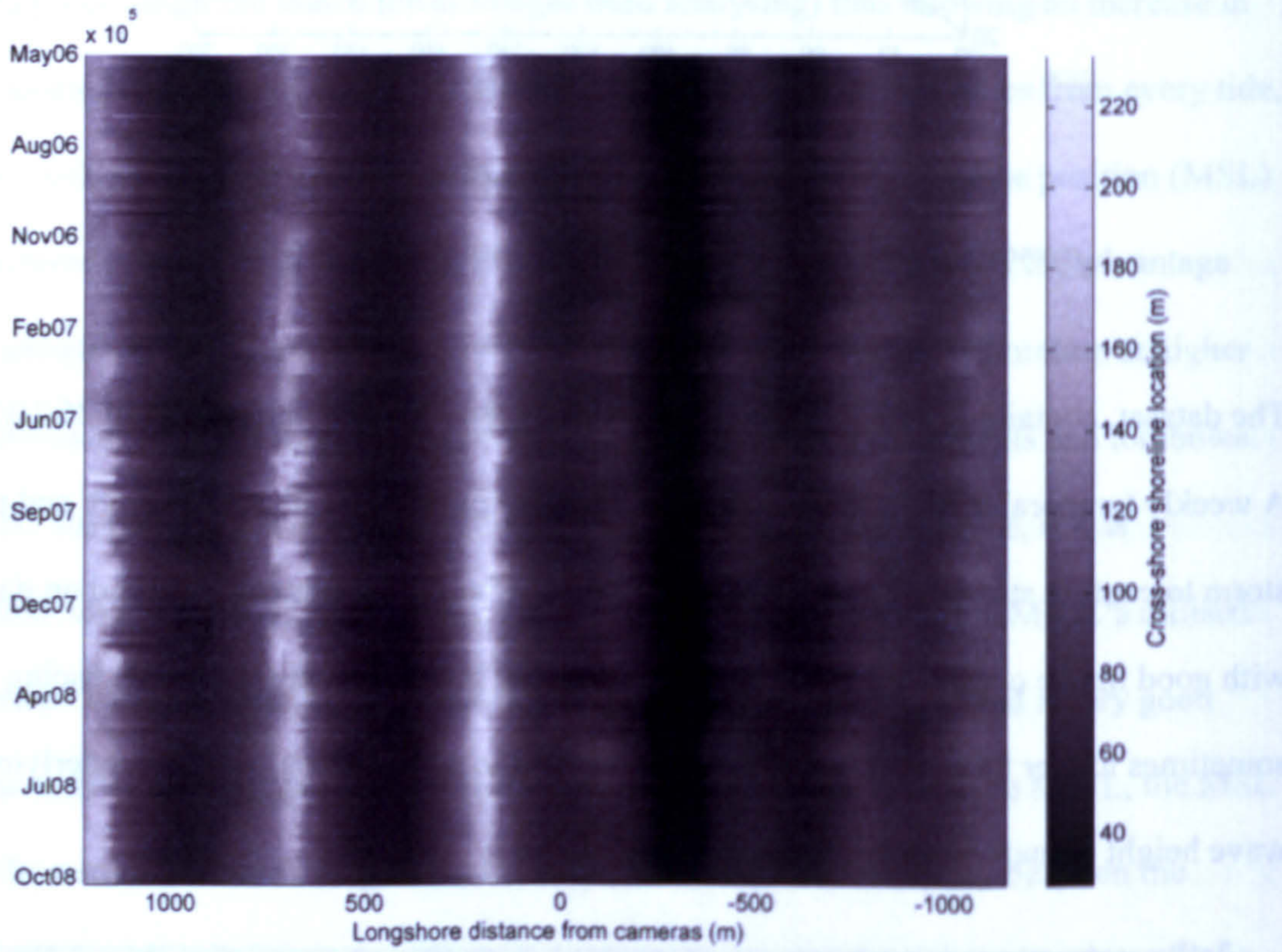

Figure 4.4.3: A surface plot showing the cross-shore location of the mean sea level shoreline through time

Shoreline variability

The simplest statistic considered is the variability in the dataset (both the range and the standard deviation). The cross-shore range in the MSL contour ranged from 6m to 88m. The variability in range was not randomly distributed through the scheme but strongly dependant on the longshore locations (Figure 4.4.4). The dataset shows greater shoreline variability in the salients and tombolos than in the bay centres. The change is of greater magnitude in phase one, corresponding to the larger size of the phase one accretionary features. The greatest variability is focused on the tips of the phase one features. In phase two there are two peaks either side of the salient tip. The standard deviation (Figure 4.4.5) shows a similar trend but the double peaks in phase two are not observed. There are secondary peaks in the standard deviation in the sheltered regions behind the tombolos indicative of lack of shoreline information for some times in these regions.

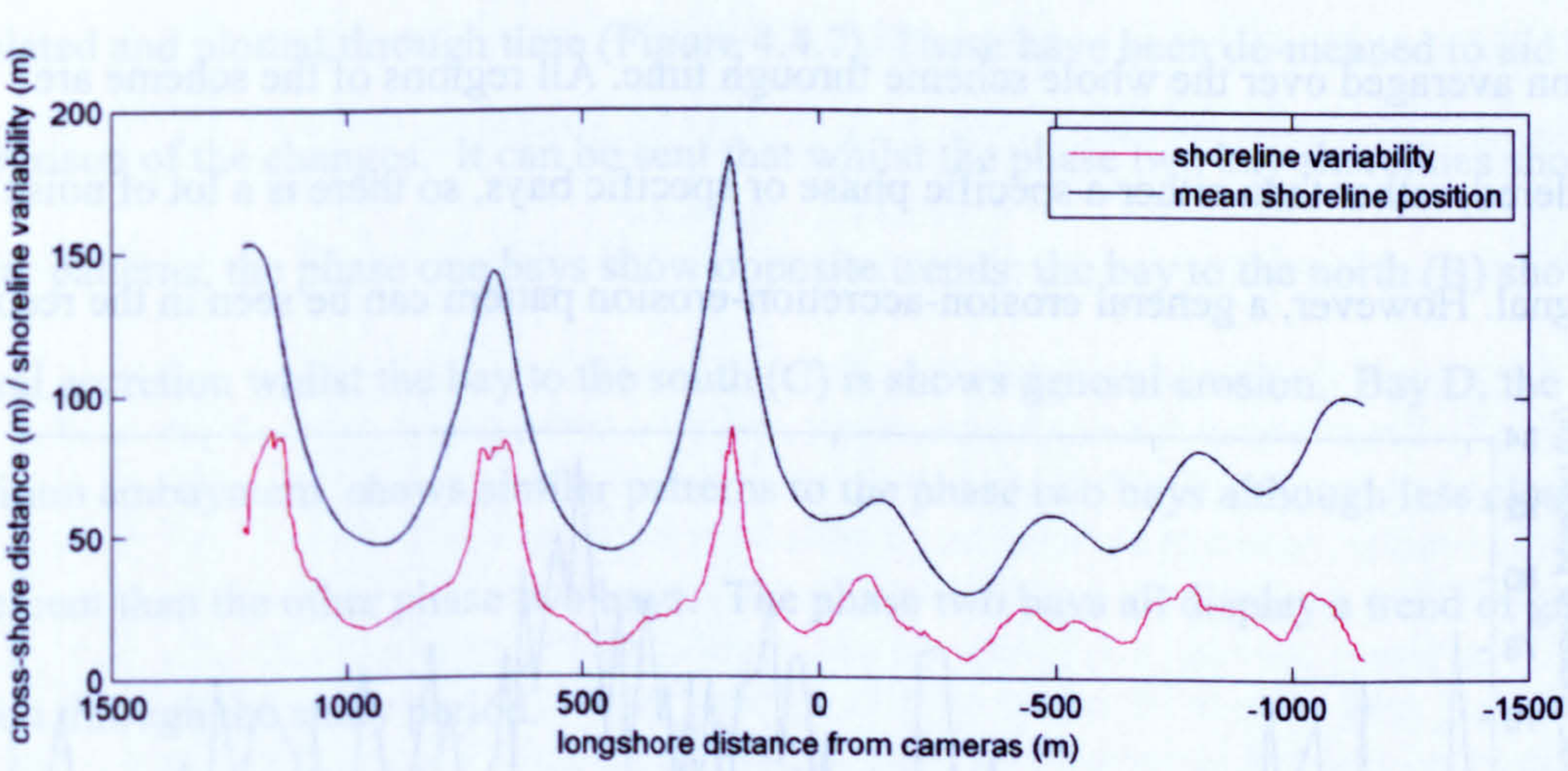

Figure 4.4.4: The mean shoreline position (black) and the range of shoreline variability (grey)

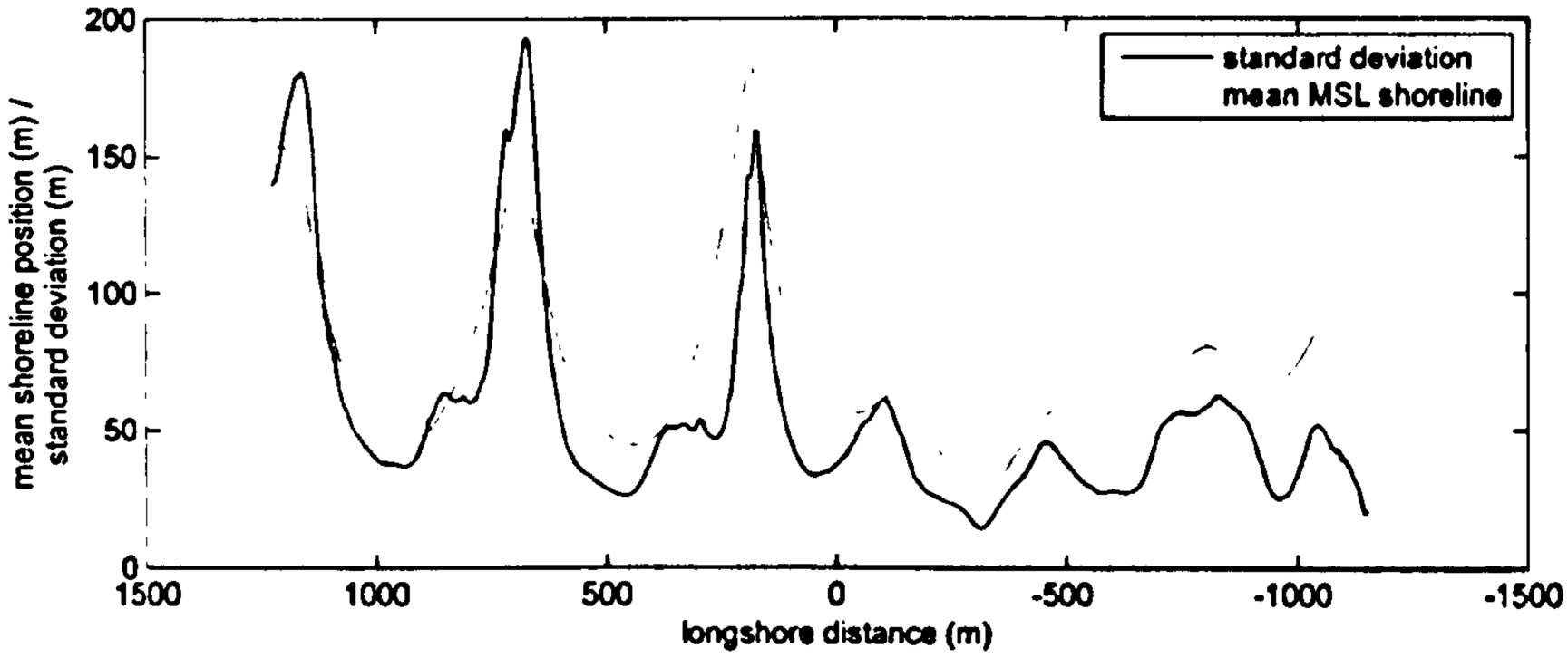

Figure 4.4.5: The standard deviation (multiplied by 10) of the shoreline location and the mean shoreline position.

Mean cross-shore shoreline location

The simplest temporally varying statistic, in a dataset such as this, is the cross-shore location of the shoreline averaged in a longshore direction. Figure 4.4.6 shows the shoreline location averaged over the whole scheme through time. All regions of the scheme are considered, rather than either a specific phase or specific bays, so there is a lot of noise in the signal. However, a general erosion-accretion-erosion pattern can be seen in the record.

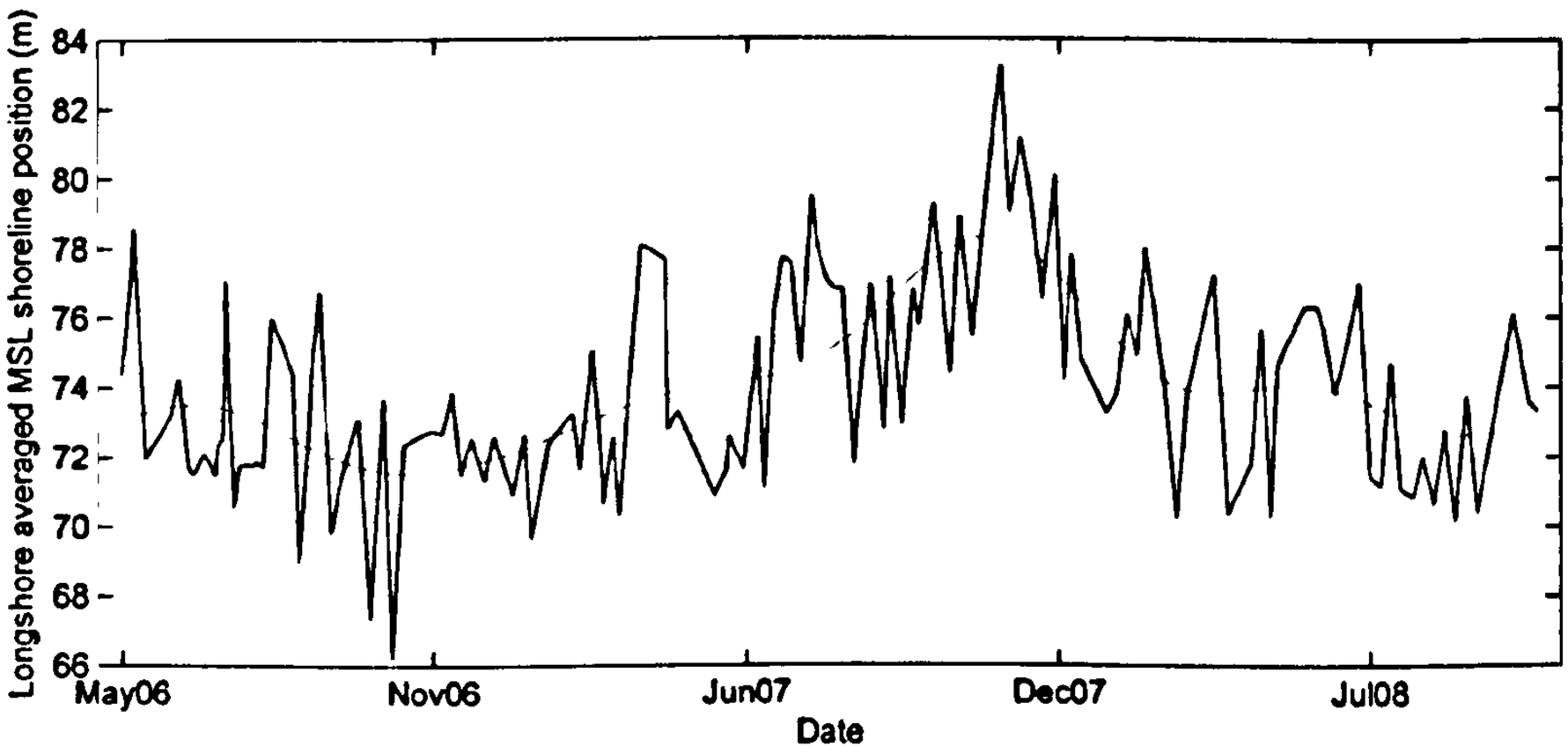

Figure 4.4.6: A plot showing the longshore averaged MSL shoreline position through time: measured shoreline (black) and low passed time series with a three month cut-off period (grey).

The shoreline position was correlated with the parameters described in section 4.2.4. The highest correlation was with the absolute value of longshore sediment transport (Q_{abs}) the Pearson's product moment correlation co-efficient (r) was 0.3886 which, although only 15% of the variance can be described by changes to Q_{abs}, is significant at the 99% level. Intertidal shoreline progradation is associated with high longshore sediment flux.

Bay shoreline positions

To reduce the noise, and to produce a more meaningful record to analyse the shorelines in the individual bay centres were investigated. Only the bays were considered since they are more stable than the tombolos (Figure 4.4.4) and better describe the general trends in erosion and accretion through the scheme. The mean of the central 20m of each bay was calculated and plotted through time (Figure 4.4.7). These have been de-meaned to aid better comparison of the changes. It can be sent that whilst the phase two bay shorelines show similar patterns, the phase one bays show opposite trends: the bay to the north (B) shows general accretion whilst the bay to the south (C) is shows general erosion. Bay D, the transition embayment, shows similar patterns to the phase two bays although less close agreement than the other phase two bays. The phase two bays all display a trend of gradual erosion through the study period.

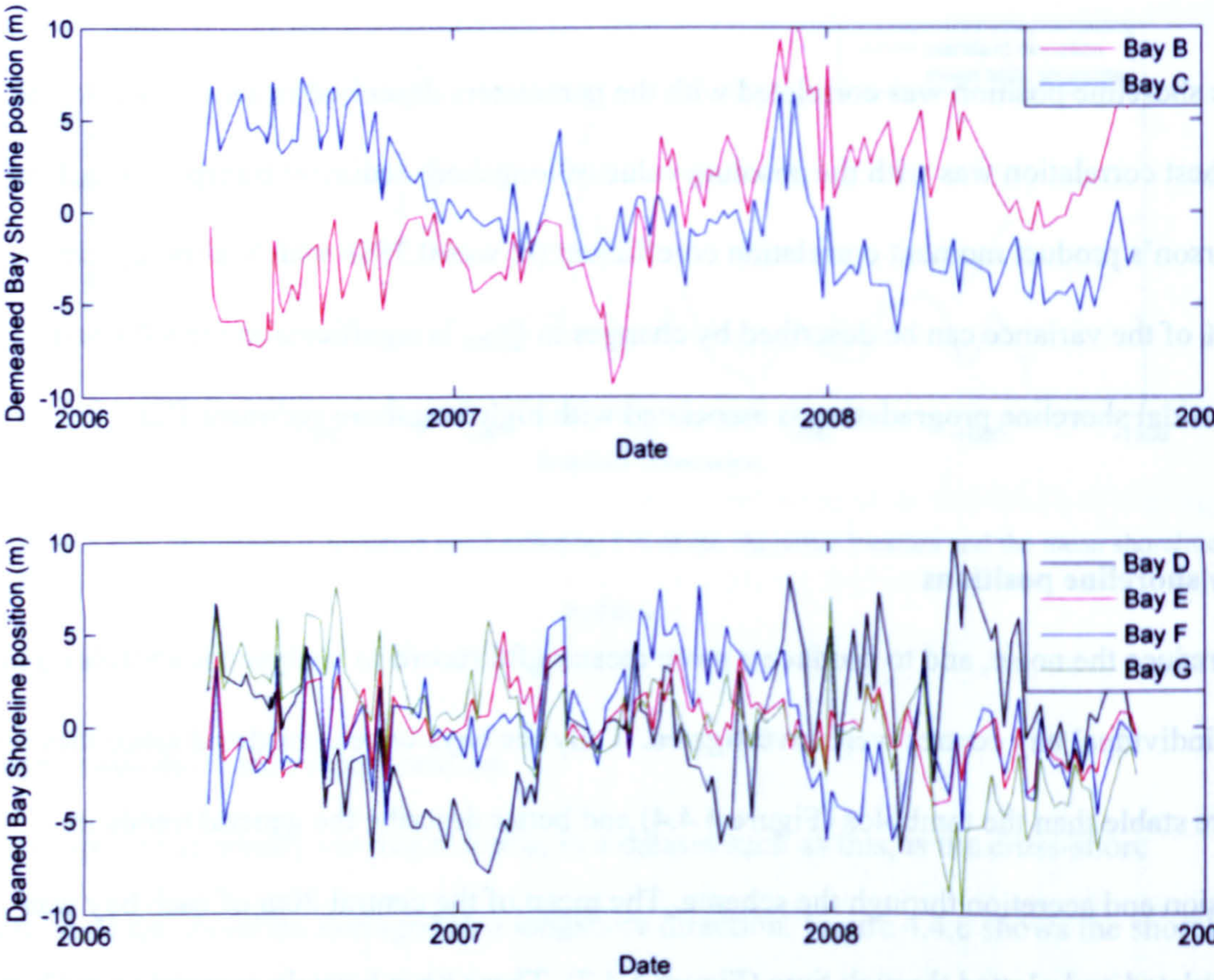

Figure 4.4.7: Plots of the demeaned bay shoreline positions for a) phase one and b) phase 2 including the transition embayment.

The visually described correlations are confirmed by a correlation matrix showing the Pearson's product moment correlation co-efficients between the different bays (Table 4.4.1). The phase one bay shorelines are not significantly correlated with each other but what correlation exists is negative backing up the visual observation of differences. All three phase two embayments are significantly positively correlated suggesting they are all behaving in similar manners. Bay C is also positively correlated with bays F and G, the two more southern bays captured by the video.

Table 4.4.1: Pearson's product moment correlation co-efficients for the different bay shorelines. Significant correlations are in bold type.

	B	C	D	E	F	G
B	1	-0.29	**0.33**	0.09	0.04	-0.26
C		1	0.06	0.22	**0.31**	**0.74**
D			1	-0.00	-0.00	-0.16
E				1	**0.66**	**0.47**
F					1	**0.39**
G						1

In order to examine the cause of these changes to bay shoreline positions the different bay shorelines were correlated against a variety of hydrodynamic parameters (Table 4.2). Correlations that are significant at the 99% confidence interval are shaded light grey in the table and the highest correlation shaded for each temporal component is in bold type. All the bays show better correlations with the cumulative integral of the de-meaned parameters, the only parameter which shows significant correlations for all bays in its raw form is the relative tidal range. Bays B and D are positively correlated with wave height, period and steepness which means larger or steeper waves are associated with shoreline progradation whereas the other bays are negatively correlated meaning larger/steeper waves cause shoreline recession. The different bays do not all have highest correlations with the same parameter which suggests that the bay shoreline changes depend on more than just the incident conditions. The relative position of each bay and the amount of sediment supply is equally instrumental.

Table 4.4.2: Pearson's product moment correlation co-efficients for the bay shoreline positions with the different hydrodynamic parameters. Significant correlations are shaded light grey and the most significant correlations for each bay are bold.

	Phase one		Transition	Phase Two		
	Bay B	Bay C	Bay D	Bay E	Bay F	Bay G
Wave height (H_s)	0.24	0.02	0.06	0.23	0.21	0.06
Wave Period (T)	**0.40**	-0.13	-0.14	0.23	0.08	0.01
Wave Steepness (H_s/L)	0.08	0.07	0.13	0.15	0.18	0.05
$\int_{t_0}^{t_n}(H_s - \overline{H}_s)dt$	0.44	-0.44	0.63	**-0.39**	-0.35	-0.54
$\int_{t_0}^{t_n}(T - \overline{T})dt$	0.42	-0.58	0.51	-0.31	**-0.35**	-0.60
$\int_{t_0}^{t_n}((H_s / L) - \overline{(H_s / L)})dt$	0.39	-0.32	**0.63**	-0.38	-0.29	-0.44
$\int_{t_0}^{t_n}(Q_l - \overline{Q}_l)dt$	-0.33	0.06	-0.08	-0.26	0.14	-0.21
$\int_{t_0}^{t_n}(\langle Q_l \rangle - \langle \overline{Q}_l \rangle)dt$	0.48	-0.44	0.62	-0.38	-0.35	-0.55
Relative tidal range (RTR)	0.30	-0.43	0.38	-0.36	-0.31	-0.54
$\int_{t_0}^{t_n}(RTR - \overline{RTR})dt$	-0.44	0.49	-0.61	0.33	0.29	0.57
$\int_{t_0}^{t_n}(TR - \overline{TR})dt$	0.45	**-0.83**	0.26	-0.17	-0.20	**-0.74**
$\int_{t_0}^{t_n}(HT - \overline{HT})dt$	**0.60**	-0.82	0.12	-0.01	-0.12	-0.66
Tide plus Wave	-0.21	0.40	-0.34	0.29	0.22	0.47
$\int_{t_0}^{t_n}((H_s + HT) - \overline{(H + HT)})dt$	0.56	-0.63	0.51	-0.27	-0.32	-0.64

Bay B shows highest correlation with the cumulative high tide level which describes 36% of the variance in the shoreline. This suggests the importance of high water levels in opening sediment transport pathways through bay A. Bay C and G both display highest correlation with the cumulative series of tidal range which explains 69% and 54% of the variance respectively. The other bays show highest correlations with the cumulative series of incident wave parameters: Bay D with the wave steepness (39% of variance explained); Bay E negatively with the wave height (15% of the variance) and Bay F negatively with the wave period (12% of the variance). Apart from Bay C, all of these correlations, whilst significant, are weak.

EOF analysis

A more sophisticated analysis used to investigate spatial and temporal changes in a dataset is empirical orthogonal function (EOF) analysis which is also know as principle component analysis. This technique decomposes a dataset into unrelated functions consisting of two components, spatial and temporal. A fuller discussion of the technique can be found in Chapter 2.5.1. In terms of the MSL contour data set discussed here, EOF analysis splits the dataset into the different modes of change. The spatial component describing how each mode of change varies through the scheme and the temporal component describes how this change varies through time. Most uses of EOF analysis in coastal science conduct the analysis on the raw dataset, the mean of the dataset then comes out as the first eigenfunction, often called the 'mean beach function' and describes the vast majority of the variance. In this study the mean of the dataset was removed. It is believed that in doing so variations from the mean are better displayed since if the mean is not removed the 'mean beach function' still varies through time. Such an approach is also advocated by Munoz-Perez *et al.* (2001). Before EOF analysis was conducted the dataset was split and the two

phases considered separately. They were separated in the middle of the transition embayment, at the 0 in the Argus co-ordinate system. The rationale for splitting the dataset into separate phases was two-fold. Firstly, the different breakwater designs interact differently with the incident hydrodynamics, producing different circulation patterns and different morphological features and so the supposition that both phases will respond in similar ways to the same forcing is not necessarily valid. Therefore, it is not logical to force the two phases to have the same modes of change by considering the dataset as a whole. Secondly, if both phases are considered in the same dataset, it is likely that the phase one changes will dominate since the variance is greater in phase one, which would lead to the phase one changes dominating the modes and potential false representation of phase two changes.

Phase one

The first five spatial eigenfunctions and associated temporal components for phase one are shown in Figure 4.4.8. The first mode describes the cross-shore translation of the shoreline whilst the lower modes all represent various components of the longshore movement of the tombolos. The first two modes represent 75% of the variance in the dataset (59% in the first mode and 16% in the second mode) and these will be discussed in detail. The lower modes, which each account for less than 4% of the variance will be not considered further since the small amount of change is hard to correlate with the incident hydrodynamics and does not add to understanding of the scheme morphodynamics. It can be seen from the spatial components that the lower modes all produce similar response to the second mode but to much lesser extents.

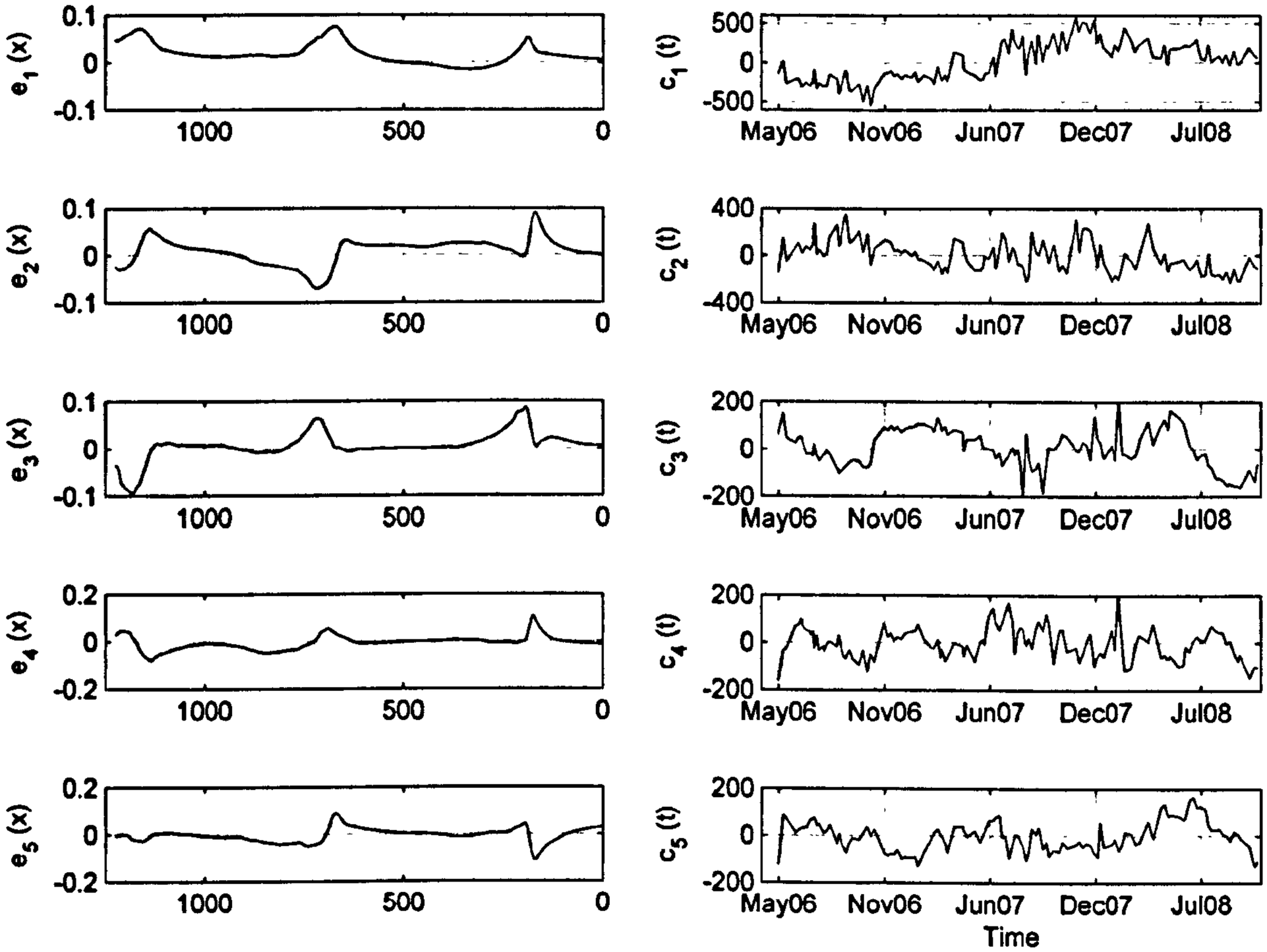

Figure 4.4.8: The spatial eigenfunctions and temporal components for the first five modes of change

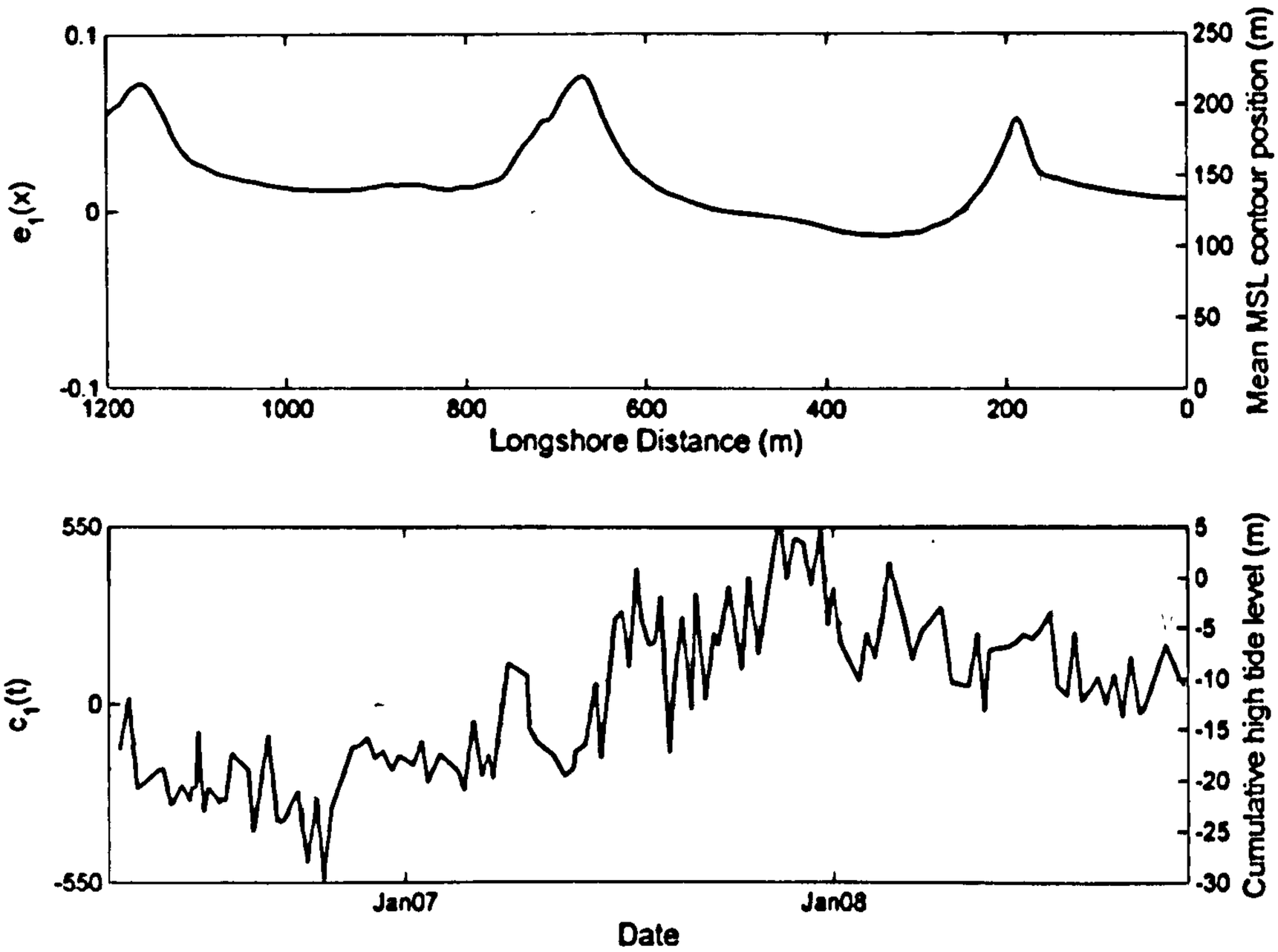

Figure 4.4.9: The first mode of change for phase one; a) The spatial eigenfunction (black) and the mean shoreline position (grey); b) The associated temporal component (black) and the cumulative integral of the high tide level (grey).

The first mode is presented in Figure 4.4.9, the upper panel shows the spatial eigenfunction in black and the mean shoreline position in grey, the lower panel shows the temporal co-efficient in black with the cumulative integral of the high tide level in grey. The cumulative integral of the high tide level is shown since it displays the highest correlation with the temporal component (Pearson's product moment correlation co-efficient r=0.67).

The spatial eigenfunction (Figure 4.4.9a) shows that the primary shoreline change is focussed on the tidal tombolos with lesser magnitude of displacement in the bay centres. The direction of change is opposite for the southern bay compared to the rest of the scheme. A positive temporal component leads to accretion of the majority of the phase (tombolos

and northern bay) and erosion of the southern bay and a negative temporal component gives the reverse effect. There is a slight positive trend through the first modes temporal component, meaning general accretion in the northern bay and tombolos and erosion of the southern bay throughout the period analysed. The correlations against hydrodynamic parameters for temporal components of the discussed modes in both phases are shown in Table 4.4.3. The temporal component for the first mode is significantly correlated with the mean wave period, the cumulative series for all wave parameters, three of the manifestations of longshore sediment transport, and all the time series including a tidal component. The highest correlations are with cumulative high-tide level (44% of variance explained), which is shown in Figure 4.4.9b and the cumulative time series of wave and tidal height (41% of the variance explained). This correlation implies that under spring high tide and surge levels the temporal component is positive and there is a shoreline progradation through phase one (except bay C which recedes due to lesser sediment availability).

The second mode accounts for 16% of the dataset variance and describes the longshore translation of the tidal tombolos, this is indicated by the change in sign at the tombolo centres (Figure 4.4.10a) which means that for a given temporal component one side of the tombolo accretes and the other erodes. A positive temporal component corresponds to a south-eastward shift of the tombolos (to the right in the figure) and a negative component corresponds to a shift to the northwest (to the left). The second temporal component (Figure 4.4.10b) regularly changes from positive to negative which means the tombolos are regularly shifting either side of their mean position

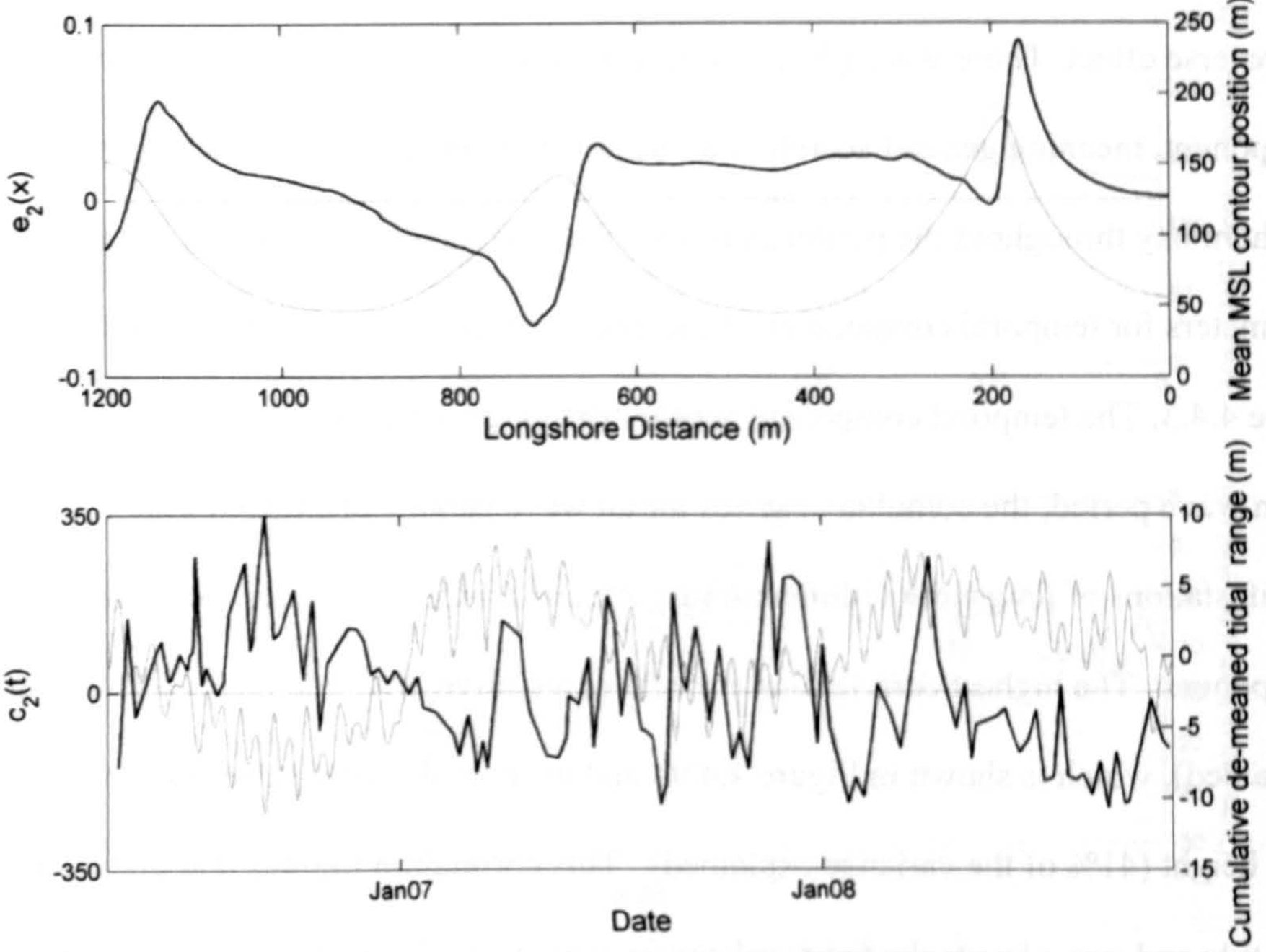

Figure 4.4.10: The second mode of change for phase one; a) The spatial eigenfunction (black) and the mean shoreline position (grey); b) The associated temporal component (black) and the cumulative integral of the de-meaned tidal range (grey).

The highest correlation is with the cumulative tidal range which explains 32% of the variance. The negative correlation means that smaller than mean tidal ranges are linked to movement to the south east and larger than mean tidal ranges are linked to north westward transport. The temporal component is also negatively correlated with the cumulative series of period (T) meaning that lower than average values of T lead to a movement to the South East and higher than average values of T a movement to the northwest.

Table 4.4.3. Pearson's product moment correlation co-efficients (r) for the temporal components against hydrodynamic parameters. Correlations significant at the 99% level are shaded grey, maximum correlations for each temporal component are in bold type. All symbols in cumulative integrals are as referred to in table text. Additionally, L stands for wavelength; HT stands for high tide and TR for tidal range.

	Phase One		Phase Two		
	$c_1(t)$	$c_2(t)$	$c_1(t)$	$c_2(t)$	$c_3(t)$
Significant wave height (H_s)	0.29	0.21	0.06	-0.13	0.24
Mean wave period (T)	0.34	0.06	-0.16	0.04	**0.42**
Wave steepness (H_s/L)	0.16	0.19	0.14	-0.17	0.06
$\int_{t_0}^{t_n}(H_s - \overline{H}_s)dt$	0.52	-0.26	-0.39	-0.75	-0.21
$\int_{t_0}^{t_n}(T - \overline{T})dt$	0.51	-0.38	-0.45	-0.64	-0.14
$\int_{t_0}^{t_n}((H_s / L) - \overline{(H_s / L)})dt$	0.47	-0.16	-0.30	-0.74	-0.22
Longshore sediment transport (Q_l)	0	0.02	-0.13	0.12	0.04
Absolute value of Q_l ($\langle Q_l \rangle$)	0.32	0.28	0.10	-0.14	0.27
$\int_{t_0}^{t_n}(Q_l - \overline{Q}_l)dt$	-0.38	-0.01	0	-0.06	-0.12
$\int_{t_0}^{t_n}(\langle Q_l \rangle - \langle \overline{Q}_l \rangle)dt$	0.54	-0.23	-0.42	-0.76	-0.18
Relative tidal range (RTR)	0.31	-0.34	-0.37	0.61	-0.14
$\int_{t_0}^{t_n}(RTR - \overline{RTR})dt$	-0.56	0.27	-0.37	**-0.77**	0.14
$\int_{t_0}^{t_n}(TR - \overline{TR})dt$	0.62	**-0.57**	-0.49	0.58	0.22
$\int_{t_0}^{t_n}(HT - \overline{HT})dt$	**0.67**	0.51	**-0.51**	0.50	0.40
$\int_{t_0}^{t_n}((H_s + HT) - \overline{(H_s + HT)})dt$	0.64	-0.37	-0.47	0.73	-0.01

Phase Two

The first five spatial eigenfunctions and their associated temporal components are shown in Figure 4.4.11. The first three modes represent 82% of the variance with the variance more evenly spread through the modes than phase one. The first mode represents 46% of the variance, the second mode 27% and the third mode 9%. Like phase one the higher modes each represent just a few percent of the variance. The fourth and fifth modes both show forms of beach rotation. The first three modes will be considered in greater detail.

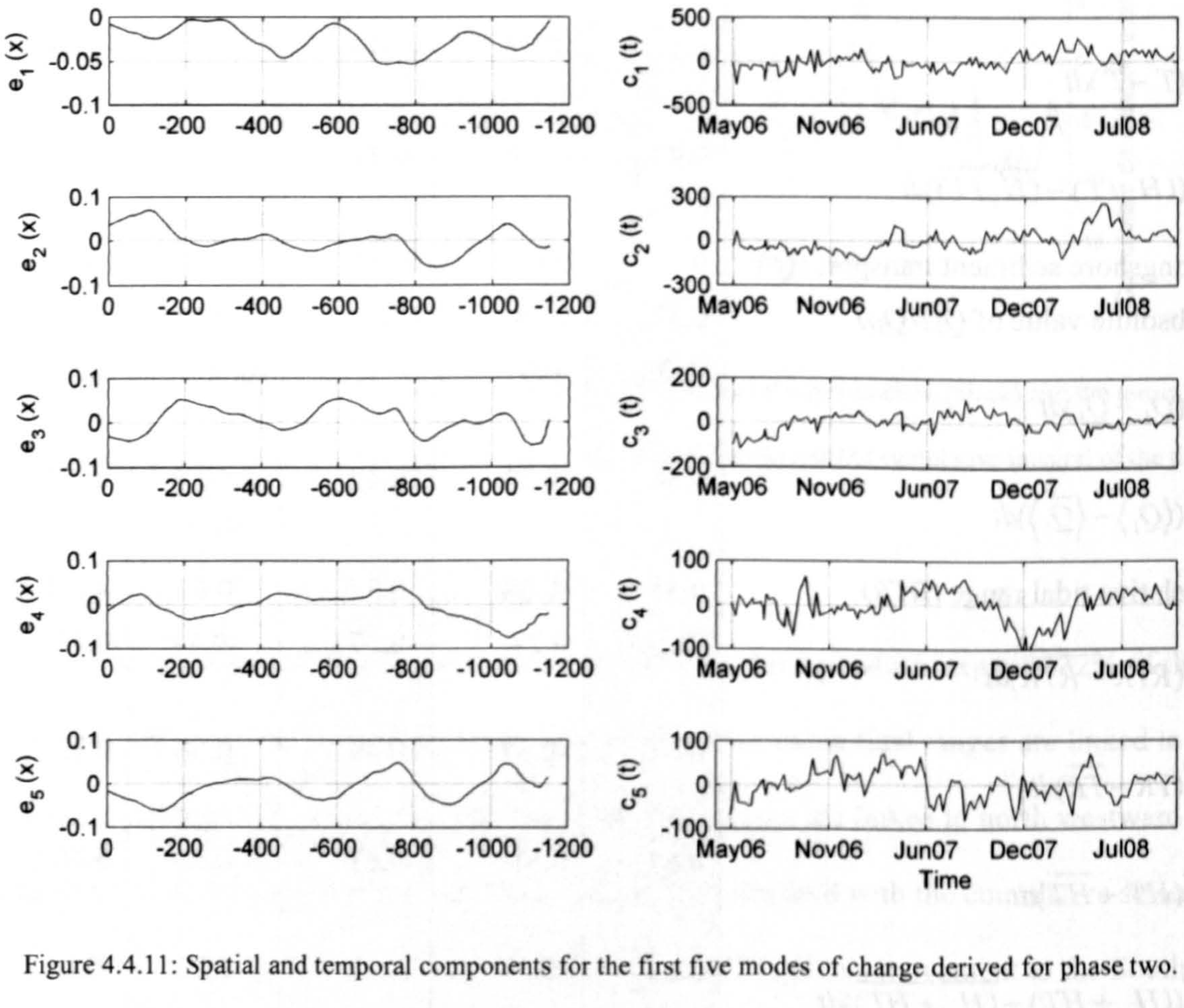

Figure 4.4.11: Spatial and temporal components for the first five modes of change derived for phase two.

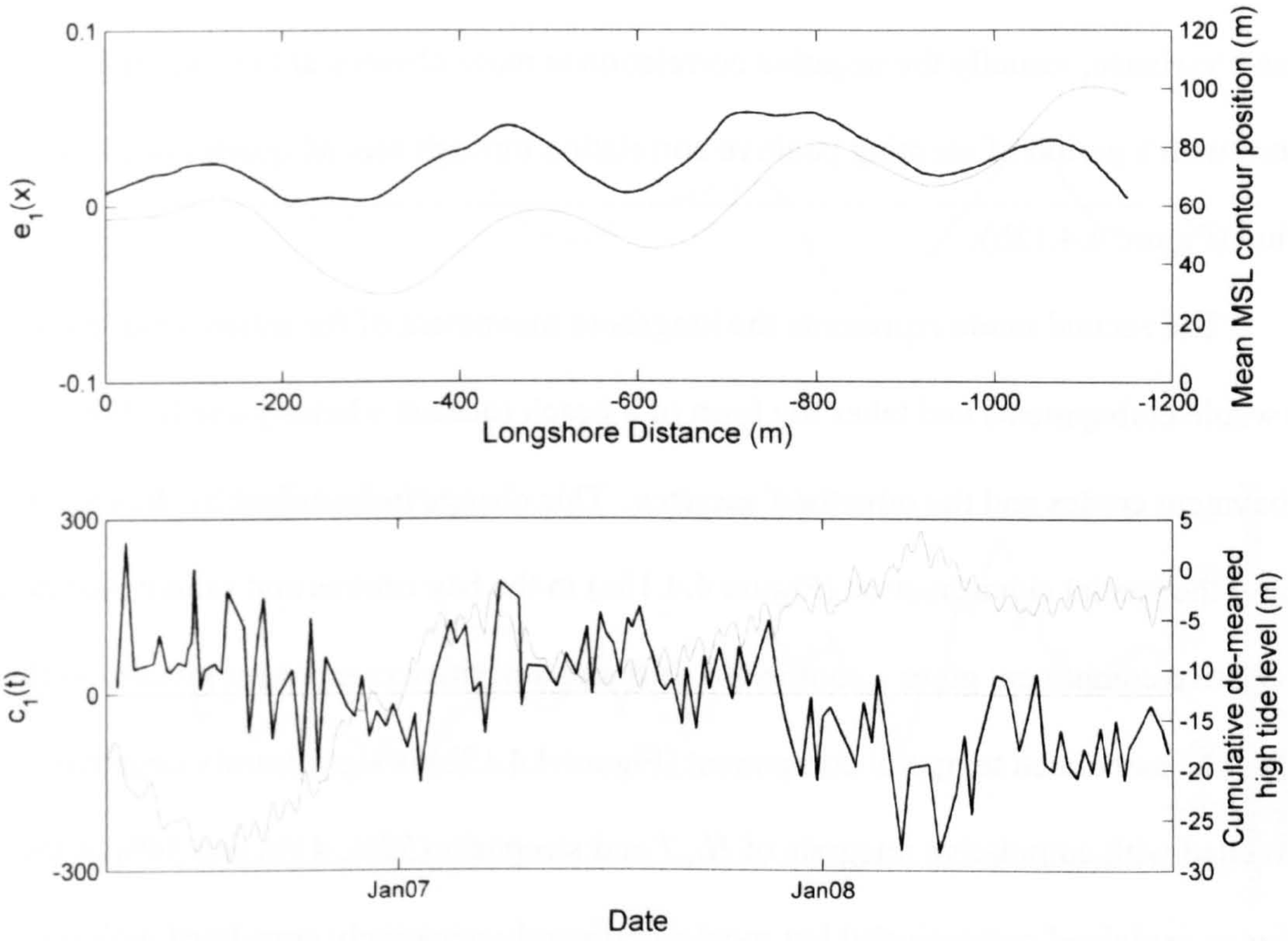

Figure 4.4.12: The first mode of change for phase two; a) The spatial eigenfunction (black) and the mean shoreline position (grey); b) The associated temporal component (black) and the cumulative integral of the de-meaned high tide level (grey).

The first mode describes shoreline progradation and recession. The whole scheme shows the same direction of change for a given temporal component with greater changes over the salients (Figure 4.4.12a). The temporal component (Figure 4.4.12b), whilst noisy, shows some seasonality, being largely positive in summer (shoreline progradation) and negative in winter (shoreline recession), although the final summer, whilst increasing from the previous winter is still negative. There is a negative linear trend through the temporal component suggesting an overall shoreline recession through the measurement period. The temporal component is significantly negatively correlated with the cumulative integrals of the wave parameters (9-19% of the variance described) but most correlated with the cumulative

integral of the high tide level. This correlation is negative and represents 26% of the dataset variance, visually the negative correlation is more obvious at the start and end of the record with a period of seeming positive correlation through second quarter of the study period (Figure 4.4.12b).

The second mode represents the longshore movement of the salients but involves the whole embayments and takes the form of a beach rotation whereby one half of the embayment erodes and the other half accretes. This change is described by the change in sign of the spatial eigenfunction (Figure 4.4.13a) in the bay centres and salient mid-points. A negative component gives a southward shift and a positive component gives a northward shift. The associated temporal component (Figure 4.4.13b) is significantly negatively correlated with cumulative integrals of H_s, T and steepness (55%, 41% and 54% of the variance explained respectively) but most significantly negatively correlated with the cumulative integral of demeaned relative tidal range which explains 60% of the variance (Table 4.4.3). Negative correlation in both general trends and in short term shifts can be seen in the time series plotted in Figure 11b. The negative correlation means large values of *RTR* are linked with the salients being north of mean and small values of *RTR* are linked with the salients being south of mean.

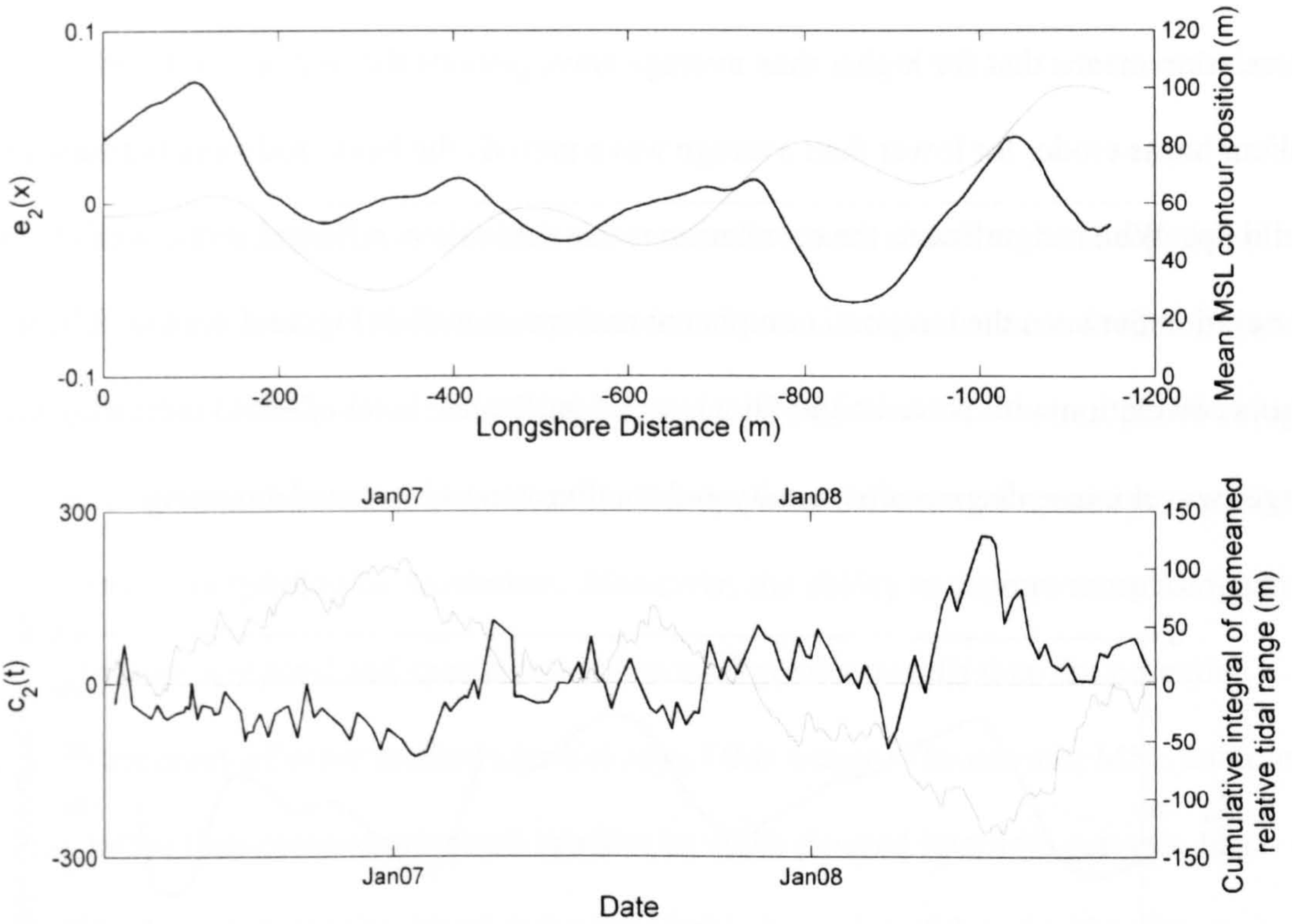

Figure 4.4.13: The second mode of change for scheme two; a) The spatial eigenfunction (black) and the mean shoreline position (grey); b) The associated temporal component (black) and cumulative integral of the relative tidal range (grey).

The third mode of change involves an increase or decrease in the sinuosity of the shoreline (Figure 4.4.14a). The cross-shore salient lengths are either enhanced or subdued depending on the sign of the temporal component and at the same time the embayments eroded or in-filled. A positive temporal component leads to a reduction in amplitude of shoreline sinuosity and a negative temporal component effects an amplitude of the shoreline sinuosity. The temporal component for the third mode of change (Figure 4.4.14b) increases through the winters and reduces through the summers indicating seasonal behaviour with enhanced salients and eroded bays through the summer periods and reduced salients and in-filled bays in the winter periods. The highest correlation is with the wave period which

explains 18% of the variance in the temporal component (Table 4.4.3). The positive correlation means that for higher than average wave periods the bays are in-filled and salient horns erode, for lower than average wave periods the bays erode and the salients build up. Whilst significant, the correlation is low and this is reflected in the weak visual correlation between the temporal component and wave period (Figure 4.4.14b). There is also a correlation with wave height (at a lower significance level of 90%) indicating that larger waves cause decreased sinuosity and smaller waves increased sinuosity.

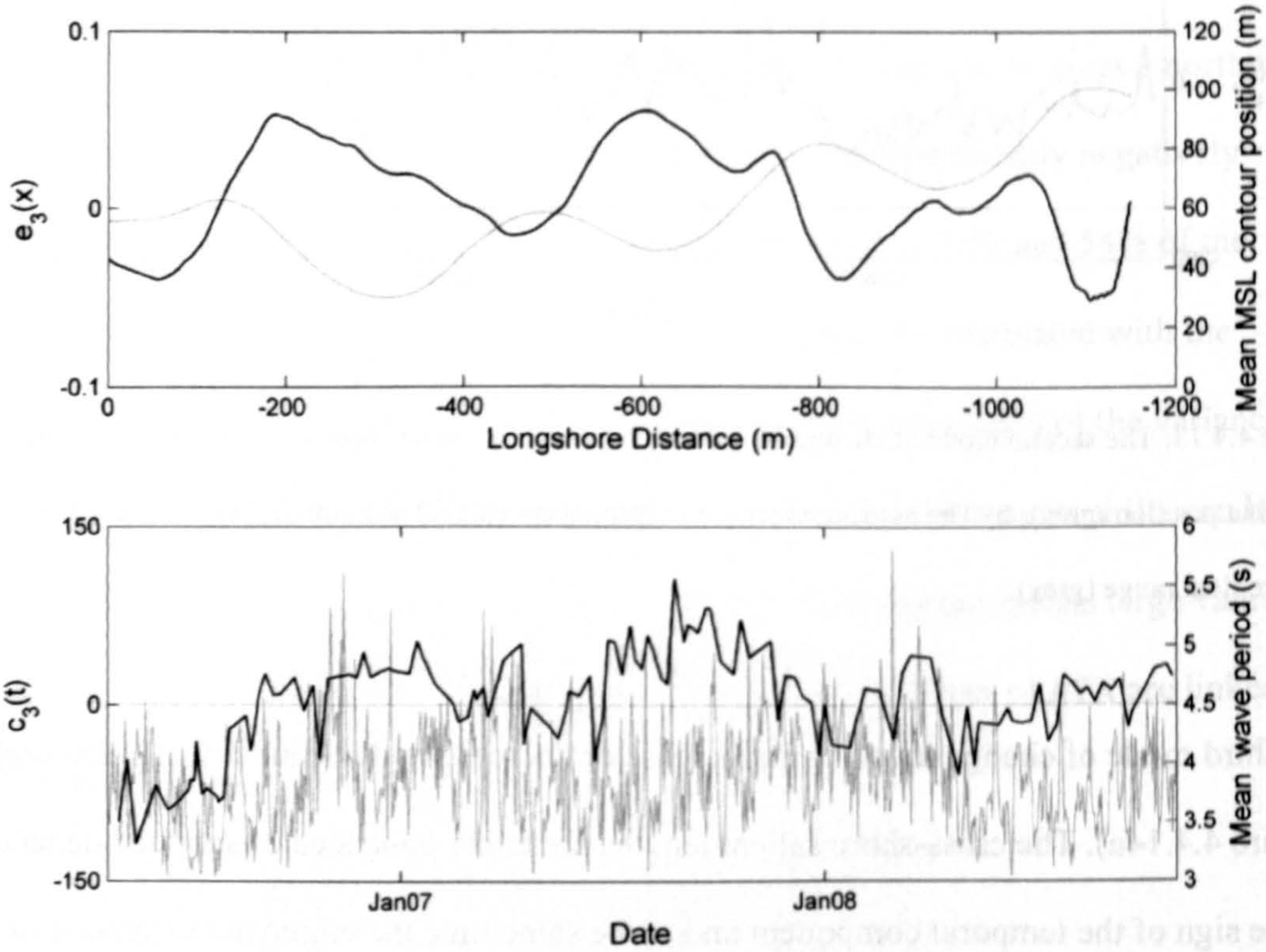

Figure 4.4.14: The third mode of change for phase two; a) the spatial eigenfunction (black) and the mean shoreline position (grey); b) the associated temporal component (black) and the mean wave period (grey).

4.4.3 Discussion of the mean sea level contour dataset

Analysis technique

The method for extracting the mean sea level contour has been shown to be acceptably accurate when compared to DGPS data (section 4.2.3). Whist there is some deviation (mean difference in cross-shore position of 1.2m), the variability of the MSL contour position (up to 80m) is far greater than the error in the shoreline position, allowing for reliable identification of morphological evolution. Moreover, the ability to capture morphological changes at a high temporal and spatial resolution is of greater benefit than the potential increase in accuracy of other methods for a study of this nature. The use of a MSL contour shoreline, rather than cross-shore beach profiles or video derived intertidal surveys, has proved valuable in determining beach behaviour behind a series of detached breakwaters. Cross-shore beach profiles are not applicable to this study for two main reasons: firstly, prohibitively many profile lines would be needed to adequately capture the longshore variability; secondly, definition of stationary shore normal lines on a coastline of high and varying curvature is impossible over a long time scale. 2-dimensional intertidal profiles, whilst useful for short term storm scale comparisons (Section 4.3), are less useful for longer term monitoring of these beaches where the intertidal region is narrow and the (x, y)-position of the intertidal region varies temporally making comparison difficult. Use of a single shoreline representation does have some shortfalls however, primary being the difficulty of distinguishing between long- and cross-shore drivers of morphological change.

An EOF analysis was successfully used to decompose the shoreline dataset into constituent modes of change. The analysis is a statistical technique which isolates orthogonal modes of change. These modes of change do not necessarily have a physical significance and interpretation must be undertaken with care (Dommenget and Latif, 2002).

In this case confidence that all computed modes of change are real is gained by previous observation of the described changes: the progradation and recession of the shoreline is visible in the images; previous work has described the longshore movement of the tombolos and salients (Section 4.3, Dolphin *et al.*, 2005) and post storm reduction in salient sinuosity is described in Section 4.3. The EOF analysis gives definition to this change and aids understanding of the nature of the temporal variation of the individual modes

Interpretation of results

The basic analysis shows that the tombolos and salients are more variable than the bay centres. These features are forced by the breakwaters and are inherently unstable to changes in wave direction. Numerical modelling (Chapter 6) shows that the tombolos are the most dynamic region of the scheme. The bay centres, despite being exposed to wave action, are more stable since the tombolos/salients block longshore sediment transport.

Consideration of bay shoreline positions demonstrates the gradient in longshore supply through the scheme caused by the hindrance of longshore transport by the tombolos. The predominant direction of transport is from the north to south. Bay B is shows an accretionary trend throughout the record whereas bay C, and the phase two bays, show an erosive trend. Bay A (outside of this analysis) is much shallower than the other bays. It is believed that bay A has reached its capacity to store sediment and that there is a progressive accumulation of sediment in the system from the north. The capability of bay B to trap sediment is starving bay C leading to erosion. It is believed that at some future time bay B may reach capacity like bay A and bay C will start to prograde. However, at present, DGPS analysis (Chapter 5) shows that the accretion only occurs in the intertidal region with erosion in the sub-tidal region. The phase two bays all behave in similar fashion because the phase two salients do not trap sediment so effectively or constrain sediment

transport as extensively as the phase one tombolos and thus the shoreline erodes and accretes as a whole.

The EOF analysis shows that for all modes of change, the dominant spatial length scales are dictated by the length of the embayments. The first two modes of response are similar in action for the two phases though the temporal components differ. For both phases, the first mode of response is the cross-shore translation of the shoreline, however, the variance ascribed to this mode and the details of the changes are different. 67% of the shoreline variance is described by the first mode in phase one whilst only 46% of the phase two variance is described by the first mode. There is a greater abundance of sediment in the phase one region and supra-tidal beach widths seaward of the sea wall are generally greater which allows for freer shoreline movement. Whilst the change is focused on the salients/tombolos for both phases, this focussing is greater for phase one. It is thought that this is due both to the larger size of the tombolos and also due to the greater difference between sheltered and unsheltered regions for the larger breakwaters leading to larger gradients in forcing. For phase two, the change is all in the same direction for a given temporal component whereas in phase one the more northern bay shoreline progrades whilst the other bay shoreline recedes. The positive trend to the phase one temporal component shows that the northern bay is generally prograding and the southern bay receding throughout the record. This is the same trend that was described by the bay shoreline positions. There is a negative trend through the first temporal component for phase two which means there is general erosion through phase two over the duration of the record, again, this is also shown in the bay centre shoreline record. This erosion suggests that phase one is starving phase two (down drift under predominant wave conditions) of sediment. There is seasonality in the phase two temporal component which is not present in the phase one component. This seasonality results in shoreline progradation in summer and

recession in winter. The temporal components for both phases both show maximal correlation with the cumulative integral of high tide level. However for phase one this correlation is positive (progradation under larger high tide elevations) and for phase two this is negative (recession under larger high tide elevations). This difference is due to breakwater design and sediment abundance. Higher tide elevations allow greater wave penetration into the embayments, greater mobilisation of sediment and access to the supra tidal beach. The phase one breakwaters and the larger tombolos better trap the mobilised sediment whilst the smaller phase two structures do not and hence the shoreline recedes and sediment is lost from the system. The ability of the phase one breakwaters to trap sediment means that the down drift phase two does not receive sufficient sediment to maintain a healthy beach. There is a larger back beach to phase one which allows for erosion of the supra-tidal region which is deposited in the intertidal region. The high-tide line in phase two is approximately level with the concrete sea wall and thus there is little supra-tidal material available for erosion. Additionally, under surge conditions the most northern tombolo (outside the limits of this analysis) is submerged which opens another sediment transport pathway injecting extra sediment into phase one.

The second mode of response for both phases is also similar, representing the longshore movement of the salients and tombolos. A greater amount of variance is attributed to this mode for phase two than for phase one, probably because the smaller, lower breakwaters allow for greater wave exposure and hence greater longshore movement. The change is focussed on the tombolos for phase one whilst the longshore movement of the salients involves the whole embayment. This difference was also observed in post storm changes (section 4.3). It is believed that this difference is due to the large difference between sheltered and unsheltered regions in phase one causing more intense and better defined circulation patterns which constrain the longshore changes to the tombolos. The

smaller breakwaters in phase two, which are readily overtopped, provide less variation in shelter and less intense circulation patterns, this means that the salient response is less defined than the tombolo response. The temporal components for both phases oscillate between positive and negative (tombolos south and north of mean). Curiously, despite section 4.3 demonstrating down-drift movement of the salients and tombolos over storm events, neither temporal component demonstrated significant correlation with the directional estimate of longshore sediment transport. This suggests that there are additional, more complex, mechanisms forcing the longshore movement of the features than just the down drift movement of sediment under oblique waves. The breakwater length considerably controls the extent of longshore movement, especially for phase one, and thus the starting position of the tombolo is of critical importance; if previous forcing has moved the tombolo to the furthest extent of the possible movement continued movement in that direction is impossible. This suggests that the initial morphological conditions exert an important control on subsequent shoreline change. Numerical modelling (Chapter 6) verify these premises and emphasises the non-linear forcing of salient and tombolo movement. The temporal component for phase one is best correlated with the cumulative integral of tidal range, smaller than mean tidal ranges lead to south-eastward movement and larger than mean tides lead to north westward movement. The correlation is weak, only describing 32% of the variance. Tidal currents alone are sufficient to entrain sediment over the tombolos (Bacon *et al.*, 2005) and the tidal asymmetry varies over the spring-neap cycle (Bacon *et al.*, 2007). However, the correlation here is counter intuitive since the asymmetry leads to stronger southward currents and thus one might expect larger ranges (stronger currents) to be correlated with feature locations being south of mean. This suggests that either the correlation is not physically important or a more complex mechanism than residual currents is important. The temporal component also shows significant correlation

with the cumulative integral of wave period. Lower than mean wave periods lead to a south-eastward movement and higher than mean periods lead to a north-westward movement of the tombolos. Wave period dictates the way in which the wave rays are turned via refraction and diffraction as they penetrate the embayments, with shorter period waves undergoing lesser turning than longer period waves. Thus short period waves approaching obliquely form the north (the predominant direction for oblique waves) would only act on the southern flank of the embayment whilst longer period waves would refract and diffract to a greater extent thus acting on a greater portion of the embayment.

The temporal component of the second mode for phase two shows higher correlations with the tested parameters, possibly due to the lesser breakwater induced constraints on movement. The highest correlation, which accounts for 60% of the variance, is with the cumulative integral of relative tidal range. This parameter suggests that the interplay between wave-driven and tide-driven currents is vital. The negative correlation means that large values of RTR (large tide ranges, small wave heights) are linked with the salients being north of mean and small values of RTR (small tidal ranges, large wave heights) are linked with the salients being south of mean. If a unit wave height is considered (RTR = tidal range) the direction of salient movement is the same as tombolo movement. If constant tidal range is considered, the correlation suggests larger waves (most predominantly incident from the north) lead to southward movement of the salients. One problem with use of the relative tidal range is that a 1m tidal range and 1m wave height has the same RTR as a 4m tidal range and 4m wave height, when clearly the morphological response would be very different. This temporal component is also significantly negatively correlated with cumulative integrals of H_s, T and steepness (55%, 41% and 54% of the variance explained respectively). The phase two breakwaters provide less modification of

the incident wave field reaching the beach which explains the added importance of the wave parameters compared to the second mode of change for phase one.

The phase one dataset only displayed two important modes of change, the higher modes describing very little of the variance individually and the spatial eigenfunctions of the higher modes all closely replicating the second spatial eigenfunction. Phase two exhibited a third mode of change which accounted for 9% of the dataset variance. The third mode of change represented an intensification and reduction of the sinuosity of the shoreline. EOF analysis of DGPS surveys (Chapter 5) has shown that the change described here is forced by three-dimensionality in cross-shore profile changes, cross-shore changes also occur in phase one but are two- dimensional and so are not observable the MSL contour dataset. The temporal component indicates seasonality in this change with intensified sinuosity in summer and reduced sinuosity in winter. The temporal component is most strongly positively correlated with the wave period, however this correlation is weak with only 18% of variance explained. For higher than average wave periods the bays are in-filled and the salient horns erode, for lower than average wave periods the bays erode and the salients are built up. Previous work (Fairley *et al.*, 2009) has shown that longer period waves are better transmitted through the phase two breakwaters and this might explain the salient erosion under these conditions.

4.4.4 Conclusions from MSL contour analysis

The shoreline dataset has provided several important insights into the intertidal beach behaviour at Sea Palling. It was noted that the MSL contour was highly correlated with the intertidal beach volume and thus changes to this contour relate to changes to the whole intertidal region.

The magnitude of shoreline variability (range and standard deviation of shoreline position) is dependant on the longshore location: greater variability is shown over the tidal tombolos and salients than in the bay centres. In general the changes to the shoreline were related to the cumulative integral of de-meaned parameters. This shows that the intertidal morphology at Sea Palling varies at a slower rate than the incident conditions, with periods of higher or lower than mean conditions forcing changes to the MSL contour. However, visual matching of changes to individual storms shows that storm scale changes can cause significant changes, especially for phase one. Investigation of the average cross-shore location of the MSL contour through time shows the scheme as a whole retains sediment in the intertidal region under larger than normal values of Q and looses sediment under lower than normal values.

Consideration of the bay centre shoreline locations through time gives indication of the evolution of the scheme through time: it seems that bay B is gradually infilling whilst bay C and phase two are gradually eroding due to the predominant longshore sediment transport from the north and the tombolos ability to trap longshore sediment transport.

EOF analysis shows that two modes of response describe the majority of changes to phase one and three modes describe the majority of changes to phase two. This analysis shows that the cross-shore movement of the shoreline is the most dominant mode for both phases catering for 59% of the phase one variance and 46% of the phase two variance.

The change is focussed on the salients and tombolos but the difference between bay and salient is far less for phase two than for phase one. The phase one first mode shows the opposite direction of change in the bay section of Embayment C compared with the rest of the phase which agrees with the bay shoreline position analysis. Correlation of the temporal components with forcing show that both phases are best correlated with the cumulative integral of high water level.

The second mode of response for both phases was the longshore movement of the salients and tombolos. This mode described 16% of the phase one variance and 27% of the phase two variance. The spatial eigenfunctions show that for both phase one and phase two the salients/tombolos move in the same direction. The phase one temporal component also showed correlation with the cumulative integral of tidal range as well as the cumulative integral of period. The phase two temporal component showed similar maximal correlation with the relative tidal range and also showed correlation with the cumulative integral of the wave parameters.

Whilst the remainder of the phase one modes described just a few percent of the variance each, the third mode in phase two described 9% of the variance and showed a enhancement/reduction of the salients and associated bay erosion (linked with enhancement) and infilling (linked with salient reduction). The temporal component is best correlated with the wave period such that longer period waves erode the salients and infill the bays.

4.5. Synopsis of video derived behaviour

In this section a synopsis of the morphological changes determined from the video analysis of both datasets will be presented. The medium term dataset showed the same two primary modes of shoreline change behind both phases of the breakwater scheme, with an additional mode of change observable on the beaches protected by phase two. The most dominant mode of change was the cross-shore translation of the MSL contour. The phase one shoreline change was focused on the tombolos whereas for phase two the change was spread more evenly across the phase. In phase one, the northern bay showed the opposite direction of change than the rest of that phase. For both phases this change was best correlated by the cumulative high tide level, however the correlation was positive for phase one (progradation under higher water levels) and negative for phase two (recession under higher water levels). Higher water levels allow for greater wave overtopping, wave penetration into the embayments and mobilistation of supra tidal sediment. This mode of change was observable in the storm scale changes with accretion in the intertidal region over a storm event; like the EOF derived mode, accretion was focussed on the tombolos.

The second mode of change obtained from the EOF analysis was the longshore movement of the tombolo/salients; in phase one this was strongly concentrated on the tombolos whereas for phase two the change involved the whole embayment. Similar patterns of change were observed over storms of oblique incidence. The storms moved the tombolos/salients in a down drift direction, but a correlation of the temporal components with oblique waves was not observed, highlighting the multiple factors involved in longshore salient movement. Tidal range (phase one) and relative tidal range (phase two) showed the highest correlation with the temporal components, it is believed that this is indicative of the importance tidal currents around the scheme and the balance between tidal and wave driven currents. Larger ranges (stronger currents) were associated with the

tombolos/salients being north of the mean position. Additionally, the storm scale tombolo movement is associated with an increase in skewness of tombolo shape, with flattening of the exposed flank, an increase in gradient for the sheltered flank and change in plan view shape from symmetrical to asymmetric (skewed towards the down drift direction). The variation in profile gradient can be seen around the phase one embayments with flatter exposed sections and steeper sheltered sections post storm.

The third mode of change is only observable in phase two and produces and increase and decrease of sinuosity of the shoreline. The temporal correlation is highest with wave period (longer periods producing a less sinuous shoreline) and there is also a correlation with wave height (higher waves correlated with a less sinuous shoreline).

Consideration of cross-shore profile changes over storm events shows that the phase two does not exhibit much flattening of beach profile under any storm accept one associated with a large surge event. There is some reduction in profile gradient in phase one, particularly for the areas of maximum wave exposure for each storm event and this flattening is exacerbated by the combination of a storm with a large surge.

The medium term shoreline dataset also sheds some light on the continuing evolution of the scheme: through the study period bay B shows a general accretionary trend whereas bay C and phase two show a general erosive trend. Since the net sediment transport is from north to south it is believed that bay B is trapping the majority of sediment from this direction and starving the rest of the scheme.

5. Morphological changes observed in global positioning system surveys

5.1 Introduction

In this chapter, results from analysis of a set of three dimensional real-time kinematic global positioning system (RTK-GPS) surveys from the Sea Palling site will be presented. GPS survey techniques (Baptista *et al.*, 2008) are one of the most prevalent methodologies used to obtain beach morphology data in current coastal research (e.g Quartel *et al.*, 2008; Capo *et al.*, 2009) and have the advantage of very high (centimetre) accuracy. This dataset, collected by the Coastal Processes Research Group at University of East Anglia as part of the LeaCoastII project, incorporates both beach and bathymetric surveys allowing determination of sub aqueous changes.

The aim of this work is threefold: firstly to understand the behaviour of the sub- and supra-tidal areas of the scheme; secondly to determine the relation of intertidal change to changes through the whole scheme; and thirdly to help qualify whether the changes observed in the video derived MSL contour are long- or cross- shore driven processes. Neither sub- or supra-tidal regions can be measured using the video system at this site (Chapter 4) and thus the use of RTK-GPS data is complementary to the video work and helps extend the previous analysis. The extension into the sub-tidal is also useful for comparison with numerical modelling (Chapter 6).

Sub-tidal changes are effected by wave shoaling, surf zone processes under energetic conditions and tidal sediment transport. Sub-tidal morphology can influence intertidal beach change by affecting wave transformation / dissipation and due to onshore sediment transport from the sub-tidal to intertidal regions. Understanding of sub-tidal change is important in order to understand sediment transport between embayments. The

most striking supra-tidal changes occur under storm and surge conditions and typically involve the removal of material from the supra-tidal to the inter- and sub-tidal regions, this is balanced by a slower accretionary period. Dune erosion and sea wall failure can occur during significant supra-tidal changes.

Low temporal sampling resolution means that some higher frequency changes can be lost via temporal aliasing and this can lead to mis-identification of the dominant processes. However, EOF analysis of the MSL contour extracted from RTK-GPS data shows that the same modes of change are identified and suggests that the lower frequency RTK-GPS data can be used to help explain the modes of change observed in the video data.

Data reduction is required when investigating 3-d morphological surveys due to the large quantity of information captured in the survey: many different length and temporal scale processes occur on beaches and separation of these is vital if useful knowledge is to be derived from the dataset. The highly complex four dimensional (x, y, z, t) change was reduced using EOF analysis to produce maps of statistically unrelated vertical change in (x, y) and components of their temporal variation. The extension of EOF analysis from (x, t) to (x ,y, t) has previously been used to examine datasets such as beach morphology (Rihouey and Maron, 2003), offshore sandbanks,(Reeve *et al.*, 2001; Reeve *et al.*, 2008), and estuaries. Such an approach is useful on a highly 3 dimensional coast where traditional data reduction techniques, such as longshore averaged cross-shore profiles, fail to correctly resolve changes due to highly varying shoreline curvature.

5.2 Methodology

This morphological dataset was collected using a differential global positioning system technique. Differential GPS systems allow for greater accuracy than conventional GPS systems via the use of a base station located over a known benchmark position to calculate differences between the two GPS units. This gives a positional accuracy of O1cm. Two different types of survey were conducted: a beach survey utilising a quad bike mounted real time kinematic (RTK) GPS system and a bathymetric survey utilising a small rigid inflatable boat (RIB) with an echo-sounder attached to a RTK GPS unit.

The beach surveys followed a break of slope methodology whereby lines of change of gradient were followed. The bathymetric survey was conducted in longshore lines in the offshore and phase two regions, whilst for phase one concentric circles were traced in the embayments. The shallow draught of the RIB boat meant that there was no loss of information between beach and bathymetric surveys. The data was post processed by the UEA team to remove erroneous data. To facilitate better comparison with the video derived data, the raw data was transformed into the Argus co-ordinate system before being interpolated onto a regular grid of 1m cross-shore and 4m longshore spacing. Figure 5.2.1 shows an example survey track for the beach and bathymetry in the Argus co-ordinate system and figure 5.2.2 shows an example interpolated elevation surface.

The 2-D EOF procedure is identical to that used on the shoreline dataset (Chapter 4) with the exception being that the 2-D matrix of beach elevation is re-shaped into a vector prior to analysis and then the resulting EOFs also re-shaped using the same indexing. This simple approach is advocated by Reeve *et al* (2001) over more statistically sophisticated methods since it requires no assumptions of longshore and cross-shore independence, as other methods such as Uda and Hashimoto (1982) do, and because the results are easier to interpret.

The region considered in this analysis extends in a cross-shore sense from the supra-tidal to the inshore side of the breakwater. The hydrodynamic conditions outside of the breakwater field are significantly different and hence this area is not included in the analysis. The longshore extent of the 2-D EOF analysis has been confined to the region covered by the video analysis. The motivation for this approach is twofold: firstly, to allow better comparison with the video data and secondly because it is believed that end effects may skew results if the last embayments are considered. The northern most bay is much shallower and so may have a different dynamic and, in phase two, the most southern breakwater is substantially lower and so causes a different hydrodynamic regime due to greater overtopping (Chapter 6). Like the analysis in Chapter 4.2, the data has been split into phase one and phase two. The motivation for this is that the beaches protected by the two different breakwater designs cannot be assumed to be responding to forcing in the same manner.

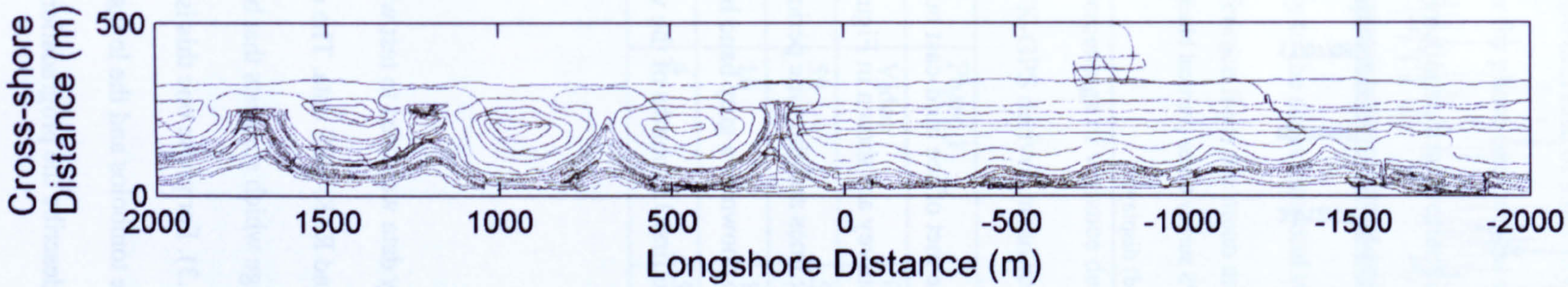

Figure 5.2.1: An example survey track for the combined beach and bathymetric surveys

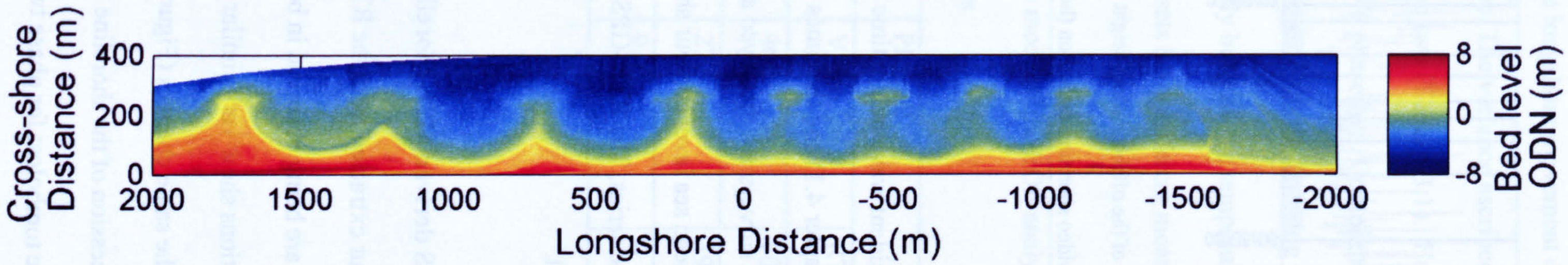

Figure 5.2.2: An example surface produced by interpolation of the survey data onto a regular grid

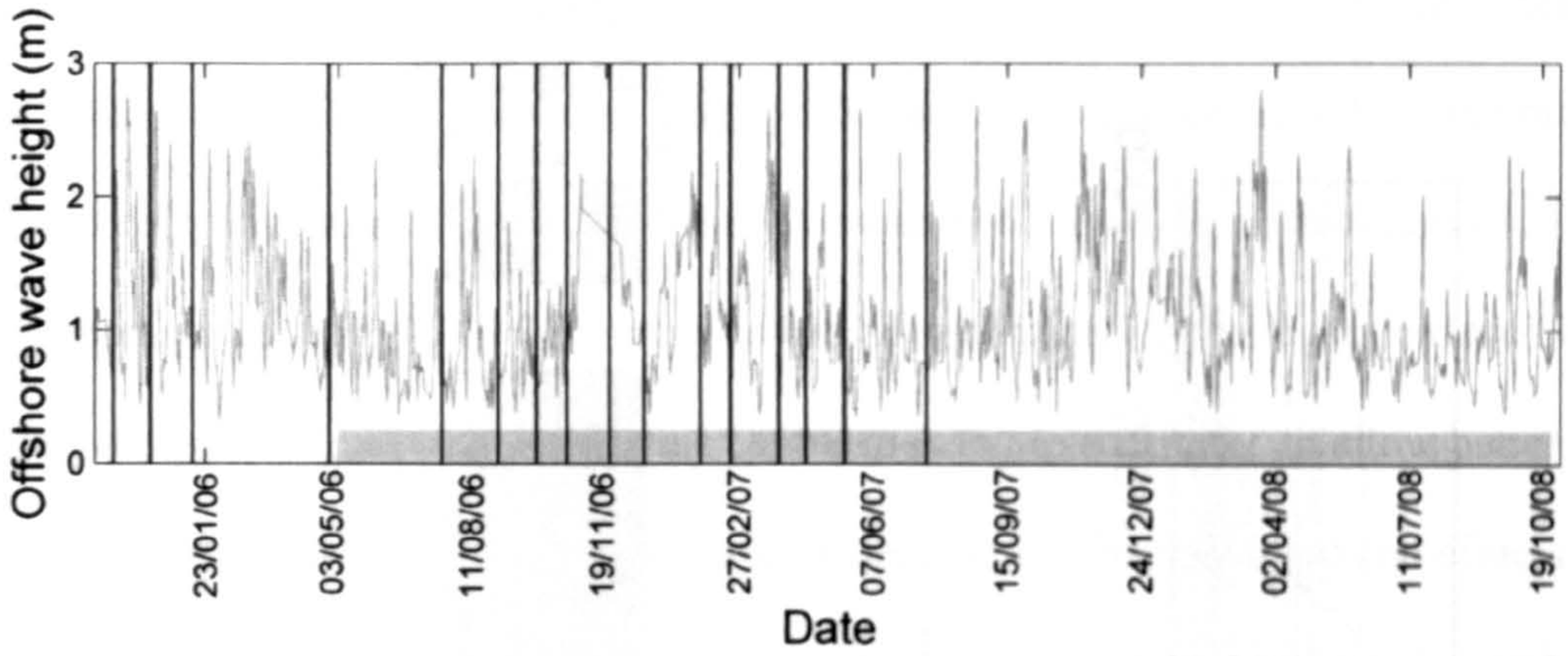

Figure 5.3.1 A plot of the offshore wave height with the RTK-GPS survey times (vertical black lines) and the time period of the video shoreline extraction (horizontal grey band) displayed.

5.3 Results.

A plot of the incident wave height time series (from the met office hind-cast output point described in Chapter 4.1) and the times of RTK-GPS survey are shown in Figure 5.3.1. The dates of the surveys are displayed as vertical black lines and the time period of the video derived mean sea level contour shorelines is also shown as a grey band below the wave height time series. The RTK-GPS data covers the first 13 months of the video derived shoreline dataset.

5.3.1. RTK-GPS derived MSL shoreline

The MSL contour extracted from the RTK-GPS survey data was used to test whether similar changes are being observed in both the video and RTK-GPS data. The empirical orthogonal functions show very similar modes of change which suggests that both datasets are identifying the same changes (Figure 5.3.2 and 5.3.3). For phase one this is the progradation/recession of the shoreline focussed on the tombolos and the longshore movement of the tombolos; for phase two, the modes describe the progradation/recession of

the shoreline with some focussing on the salients; the longshore movement of the salients and the increase/decrease of sinuosity of the shoreline. The variance ascribed to each mode is very similar for phase one but less similar for phase two (Table 5.3.1). However, the spatial eigenfunctions show greater visual similarity in phase two. Comparison of the temporal components (not shown) is less fruitful, due partly to the differing sampling interval, partly to the short temporal overlap and partly because the temporal component describes difference from the mean and the two datasets have different mean MSL contours

Table 5.3.1 Percentage of variance described to each mode of the EOF analysis for the video and RTK-GPS derived mean sea level contours

	Phase 1		Phase 2	
	Video	RTK-GPS	Video	RTK-GPS
Mode 1	59	55	46	60
Mode 2	16	19	27	19
Mode 3	4	5	9	9

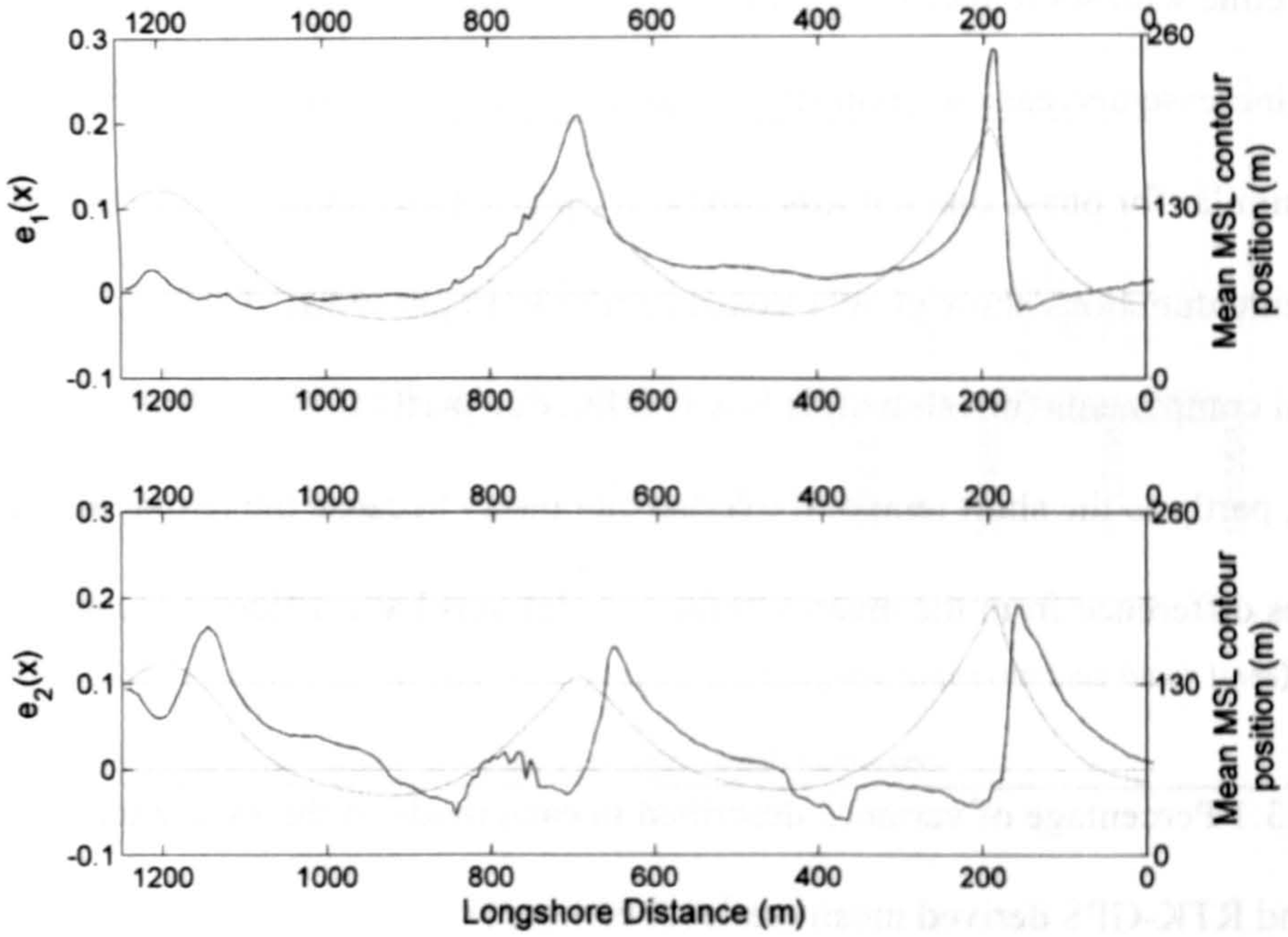

Figure 5.3.2 Spatial eigenfunctions for phase one (black) and mean MSL contour (grey)

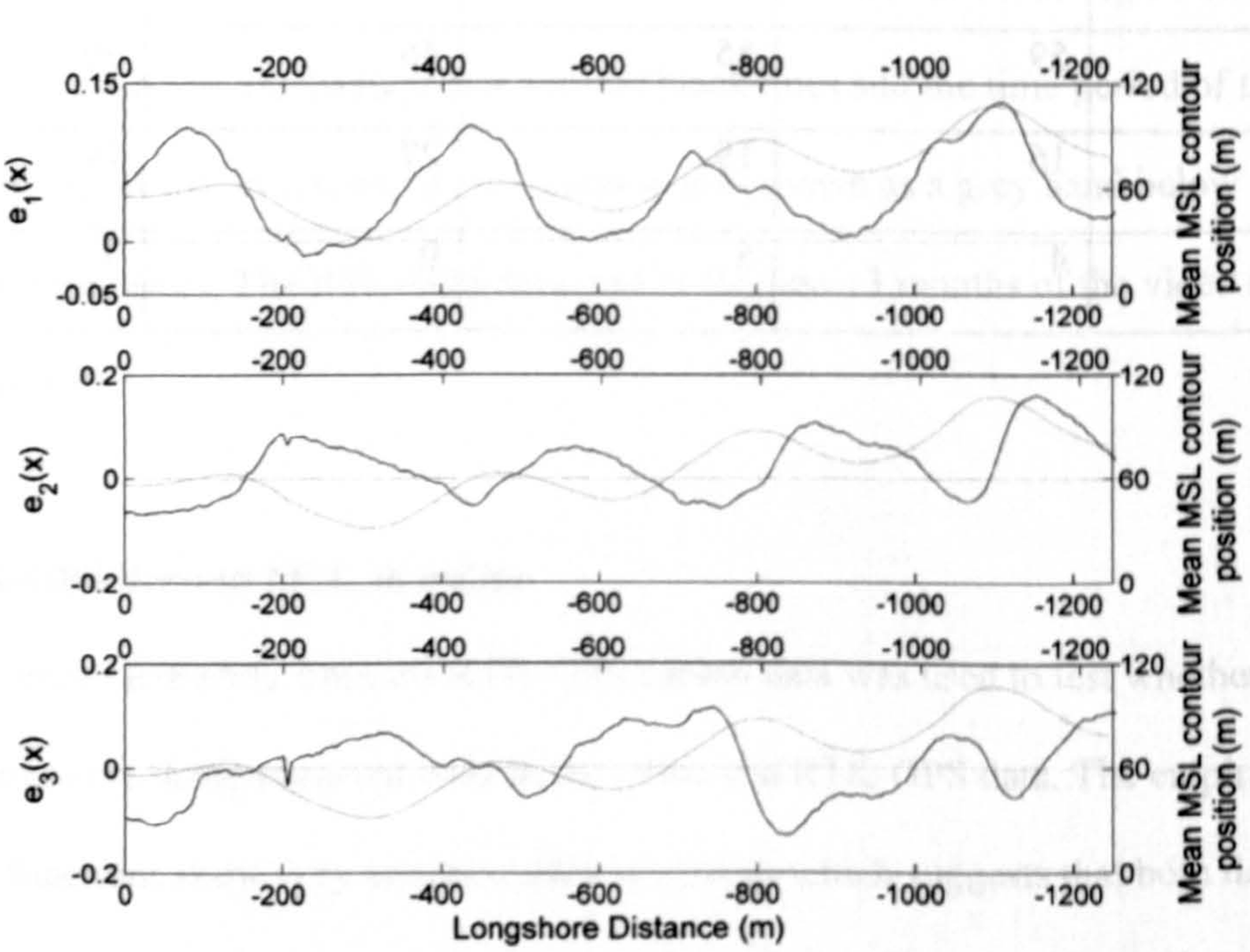

Figure 5.3.3 The spatial eigenfunctions for phase two (black) and the mean MSL shoreline contour (grey).

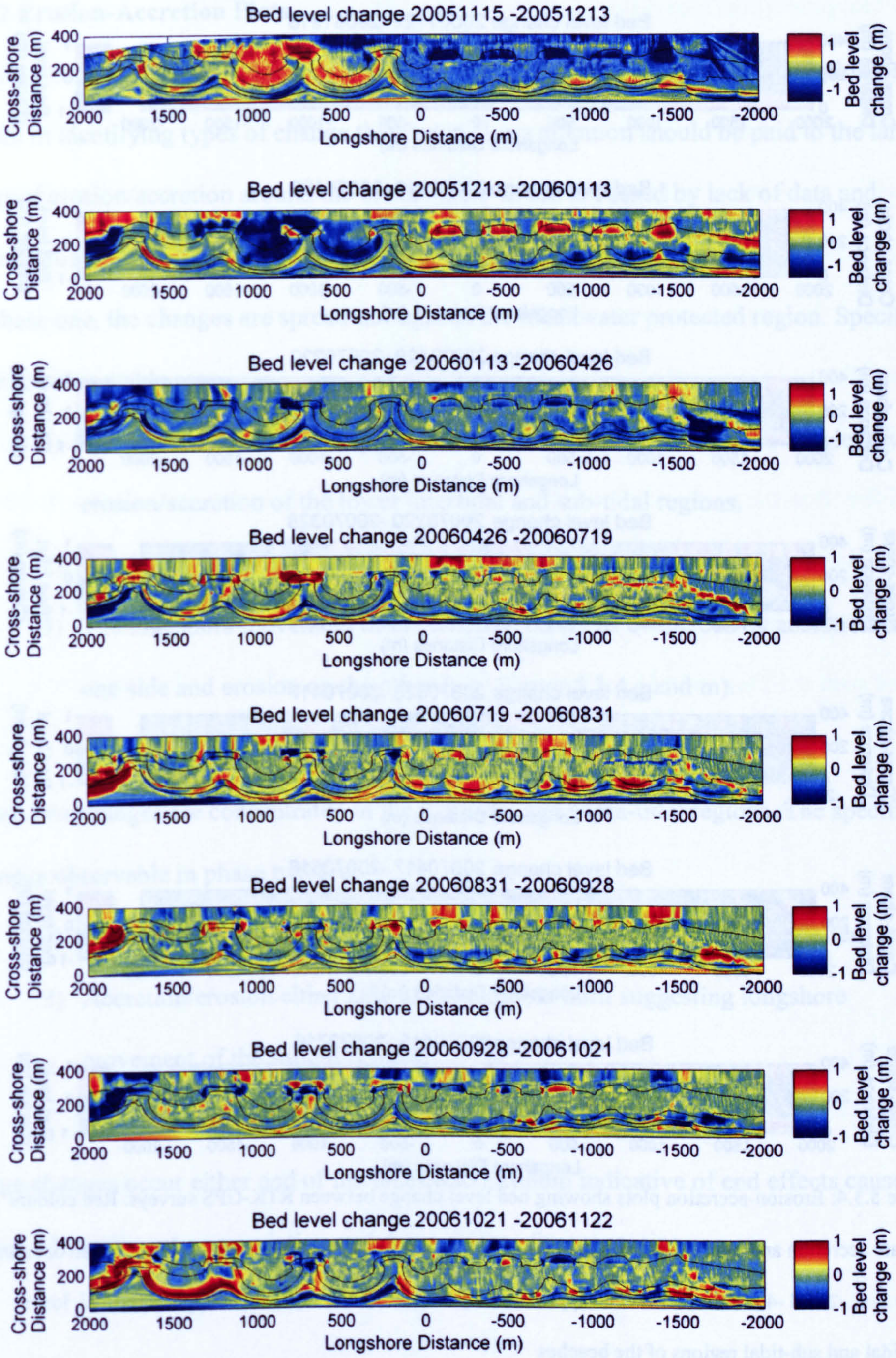
Bed level change 20051115 -20051213
Bed level change 20051213 -20060113
Bed level change 20060113 -20060426
Bed level change 20060426 -20060719
Bed level change 20060719 -20060831
Bed level change 20060831 -20060928
Bed level change 20060928 -20061021
Bed level change 20061021 -20061122
Cross-shore Distance (m)
400
200
0
2000
1500
1000
500
0
-500
-1000
-1500
-2000
Longshore Distance (m)
1
0
-1
Bed level change (m)

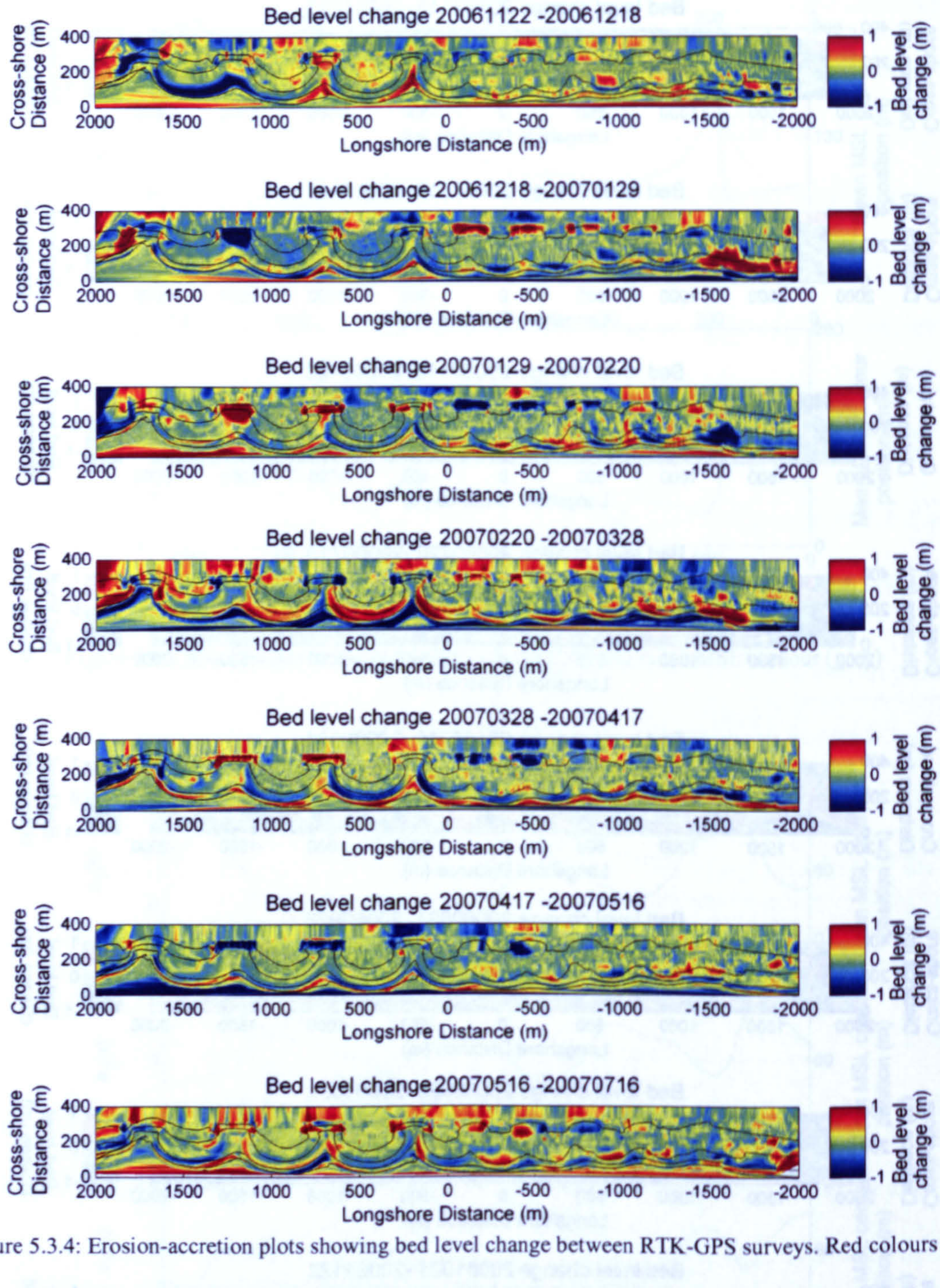

Figure 5.3.4: Erosion-accretion plots showing bed level change between RTK-GPS surveys. Red colours indicate accretion and blue colours indicate erosion. The black lines indicate contours of the mean bathymetry at the 2, 0, -2 and -4 m ODN levels and approximately demarcate the supra-tidal, upper intertidal, lower intertidal and sub-tidal regions of the beaches

5.3.2 Erosion-Accretion Plots

Figure 5.3.4 shows the bed level changes between each RTK-GPS survey, these plots are useful in identifying types of change that occur. Less attention should be paid to the large areas of erosion/accretion around the breakwaters which is caused by lack of data and interpolation through these regions.

In phase one, the changes are spread throughout the breakwater protected region. Specific changes observable are:

1) Accretion/erosion of the upper intertidal and supra-tidal areas, co-incident with erosion/accretion of the lower intertidal and sub-tidal regions.
2) Erosion/accretion of the sub tidal bay floors.
3) The longshore movement of the tombolo centre as evidenced by accretion on one side and erosion on the other (e.g. Figure 5.3.4 g and m).

Phase two changes are concentrated in the intertidal and supra-tidal regions. The specific changes observable in phase two are:

1) Accretion/erosion of the lower intertidal and sub tidal between the salient horns.
2) Accretion/erosion either side of the tombolo horn suggesting longshore movement of the salient centres.

Large changes occur either end of the breakwater system indicative of end effects caused by up drift sediment accumulation and down drift sediment erosion.

5.3.3 Morphological variability

To examine the spatial change in morphological variability about the scheme, the standard deviation of the RTK-GPS surveys were plotted (Figure 5.3.5). It can be seen that the variability is, in general, greater for phase one than for phase two. The mean value for the standard deviation over the whole scheme is 0.34m; standard deviation for phase one is 0.36m and 0.31m for phase two. In phase one, the variability is greatest on the north-western flanks of the tombolos. The upper intertidal and sub tidal regions show greater variability than the lower intertidal regions. The phase two intertidal regions show greater variability than the phase two sub tidal regions. Greater variability again is shown in the supra tidal region. There is a noticeable increase in variability for the last embayment in phase two where the breakwater is lower than the rest of the phase. Large variability can also be seen at either end of the scheme indicative of the end effects of the breakwater scheme.

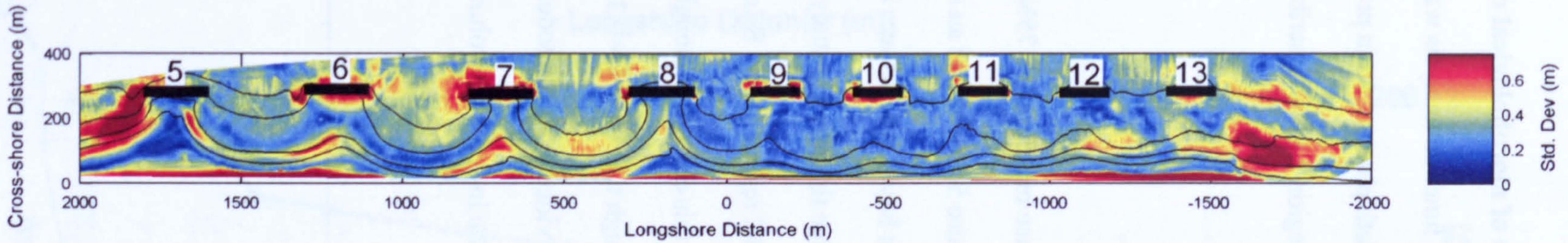

Figure 5. 3.5: The standard deviation of RTK-GPS surveyed beach elevation. The thick black lines indicate the breakwater positions (numbered above) and the thin contours are mean beach contours at -4, -2, 0 2 m elevations.

5.3.4. Two dimensional EOF analysis of morphological change.

Two dimensional empirical orthogonal function analysis was utilised to investigate the patterns of morphological change for both phases. As in previous analyses (Chapter 4.3.2) the first three eigenfunctions for each region will be described since these describe the majority of the variance.

Phase One

The first three modes of change for phase one describe 75% of the dataset variance (49, 15, 11 %) The first mode of response (Figure 5.3.6) shows an overall accretion throughout the phase apart from the intertidal region in bay B where there is erosion. The temporal component for this mode shows a decline through the study period meaning that bays B and C are slowly deepening and the intertidal region of bay B is slowly accreting. There is no significant correlation with forcing for this change, although the highest correlation is with the cumulative integral of de-meaned high tide level (r=0.35). This is the same parameter as was shown to be correlated with the video derived mode. Consideration of embayment volumes show the same gradual decrease in sediment volume through the study period (Figure 5.3.7)

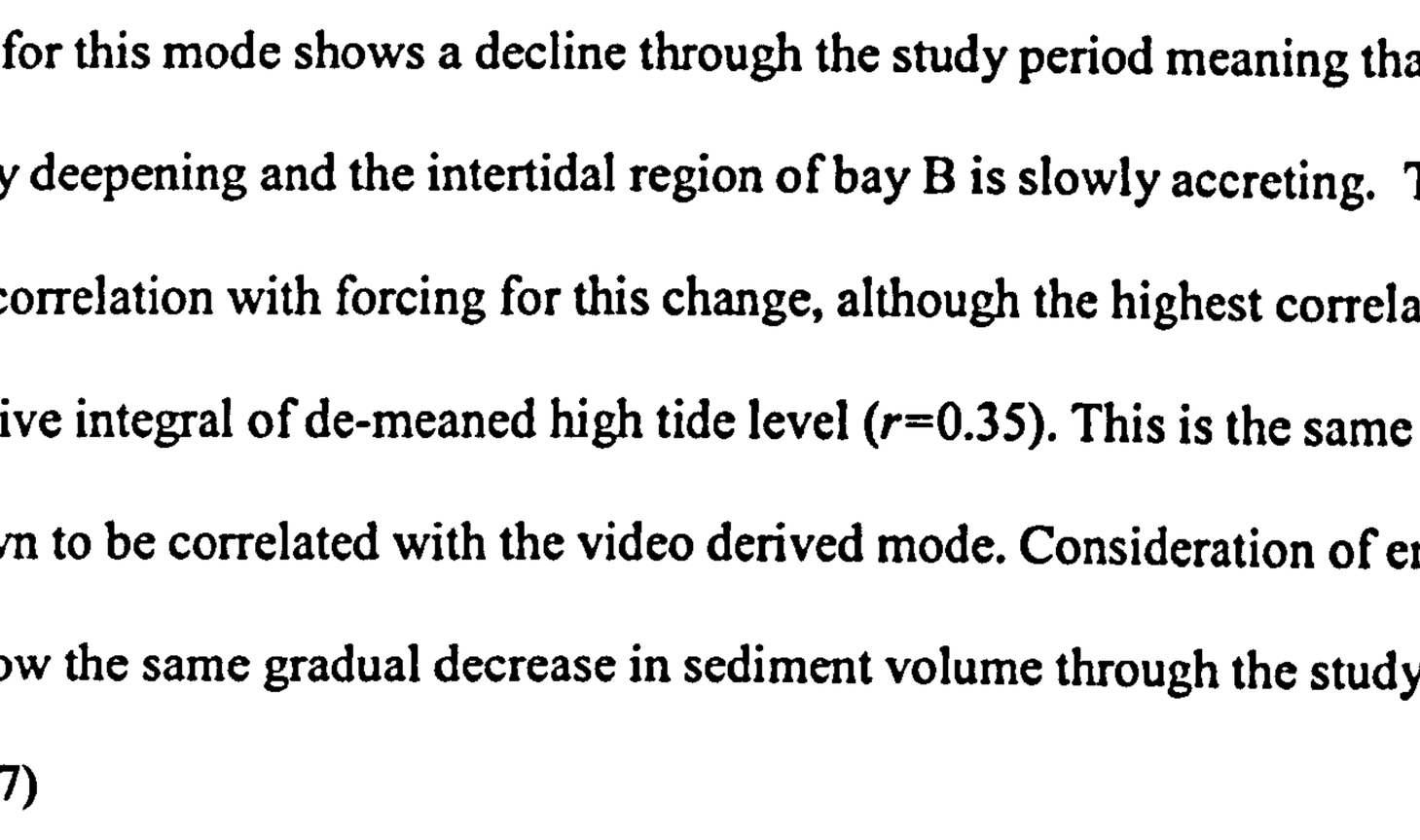

Figure 5.3.7: Embayment volumes through time for embayments B and C.

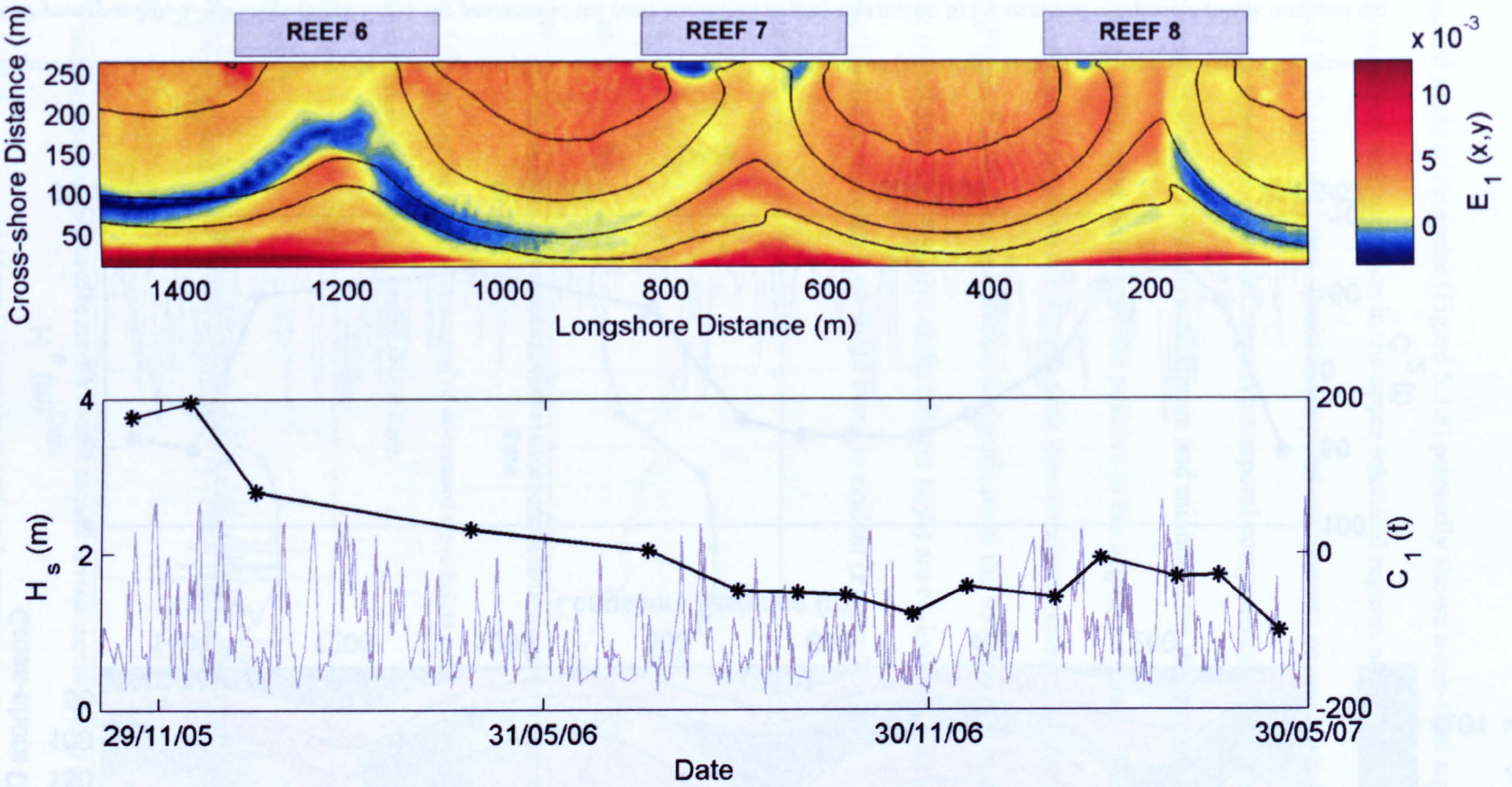

Figure 5.3.6: A plot of the first mode of change for phase one;. a) The spatial eigenfunction (coloured shading) and contour lines of the mean bathymetry at 2,0,-2,-4m ODN (black lines), the positions of the reefs are shown as grey rectangles; b) the temporal component (black line) and the incident wave height time series (grey line).

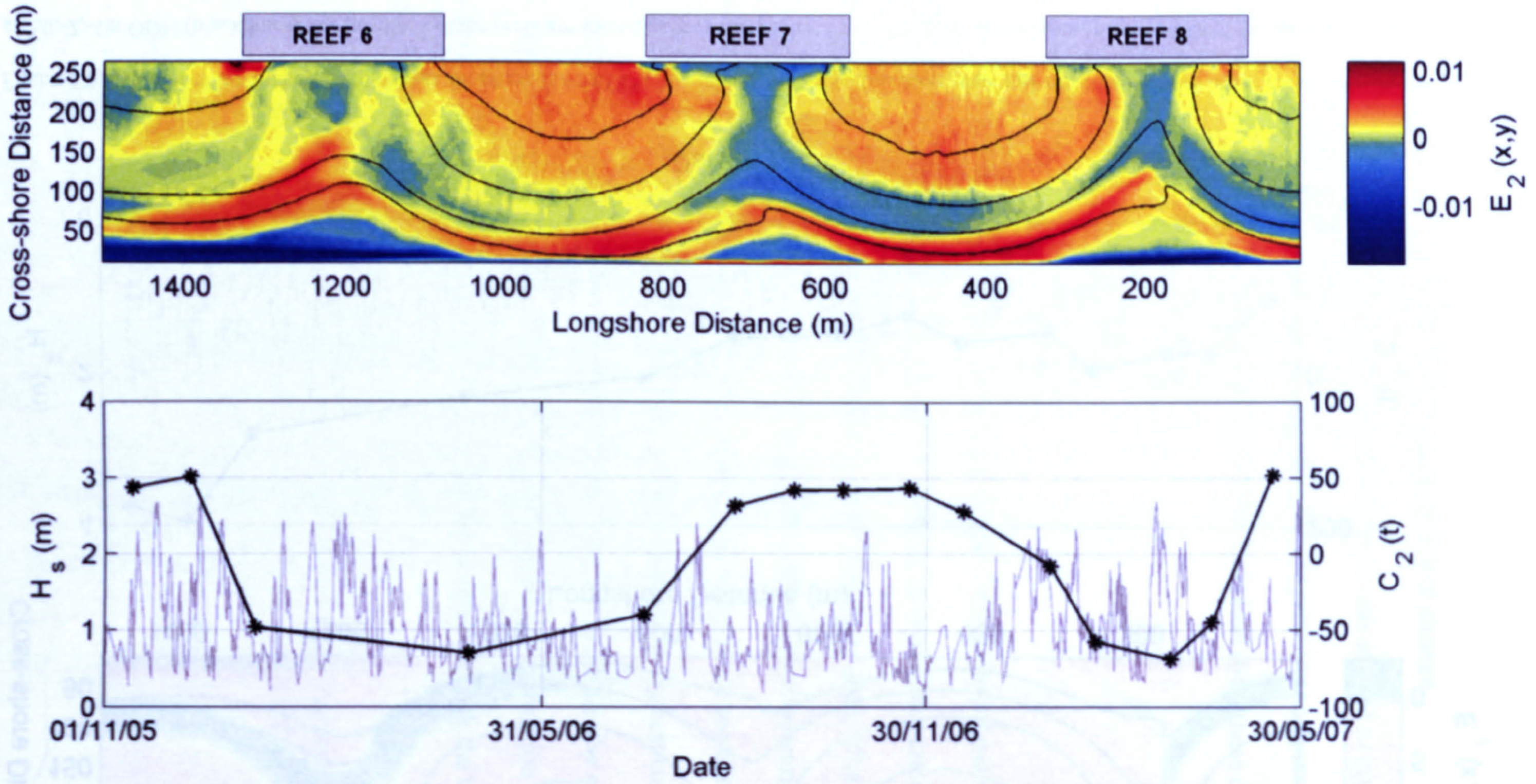

Figure 5.3.8: A plot of the second mode of change for phase one;. a) The spatial eigenfunction (coloured shading) and contour lines of the mean bathymetry at 2,0,-2,-4m ODN (black lines), the positions of the reefs are shown as grey rectangles; b) the temporal component (black line) and the incident wave height time series (grey line).

The second mode of response (Figure 5.3.8) primarily shows a sub-tidal accretion of the bay floors paired with accretion in the upper intertidal regions and erosion of the areas protected by the breakwaters. Positive temporal components equate to shallower bays and accretion on the upper intertidal, negative temporal components produce the reverse effect. There is an oscillation between a maximum and minimum for the temporal component of this change, with rapid shifts from the positive to the negative extents. The temporal component shows negative correlation with the cumulative integral of demeaned wave height (Figure 5.3.9). This correlation is significant at the 95% interval but the correlation is weak (r =-0.55). The negative shifts (deeper bays) are co-incident with surge events whereas for the positive shift no surge event is evident (Figure 5.3.10).

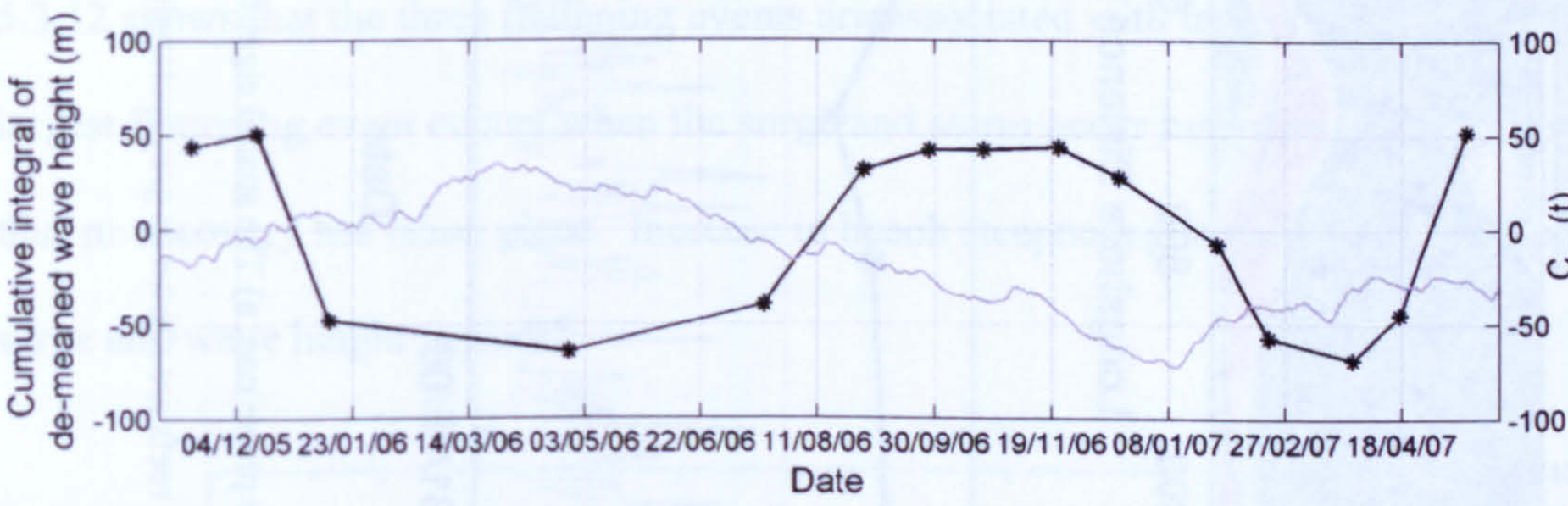

Figure 5.3.9: A plot of the cumulative integral of de-meaned wave height (grey line) and the temporal component for the second mode of change (black line).

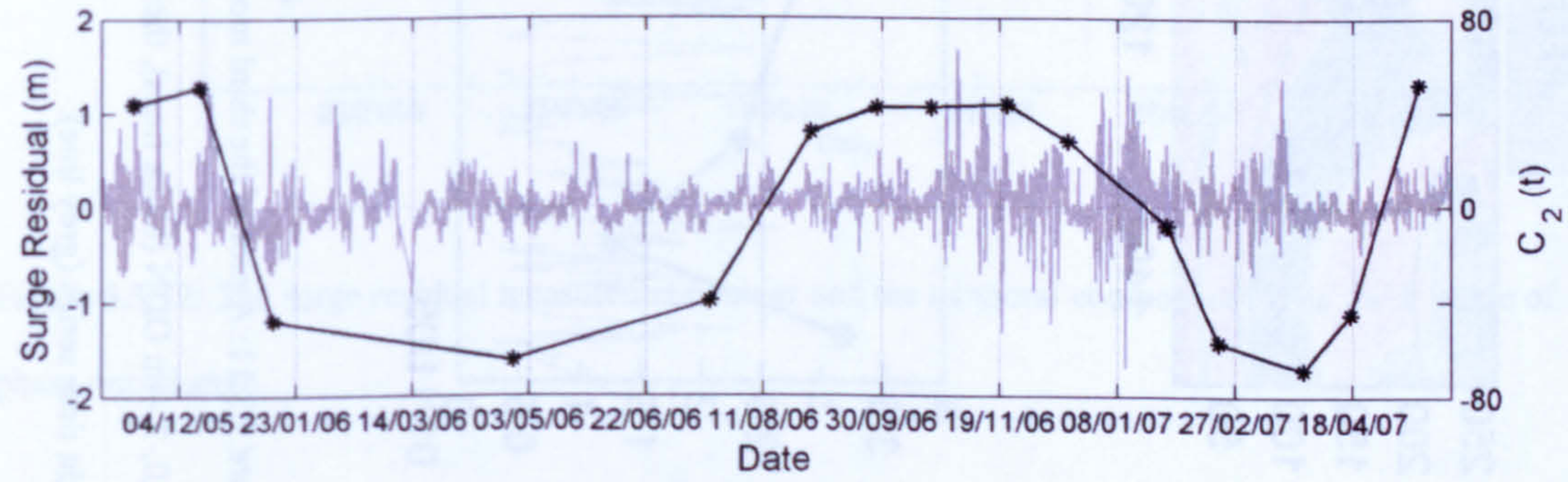

Figure 5.3.10: The surge residual (grey line) and the second mode temporal component (black line).

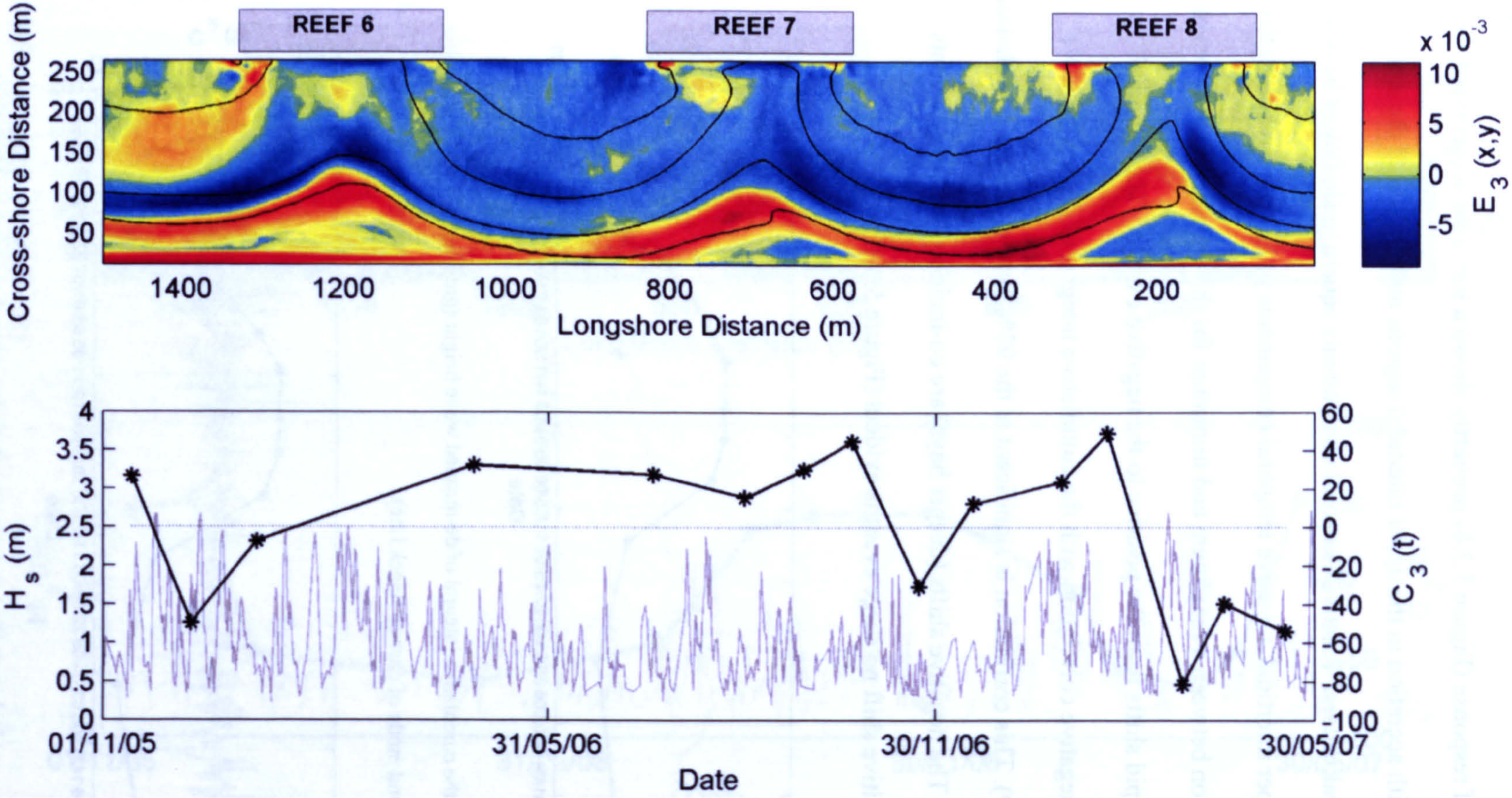

Figure 5.3.11: A plot of the third mode of change for phase one; a) The spatial eigenfunction (coloured shading) and contour lines of the mean bathymetry at 2,0,-2,-4m ODN (black lines), the positions of the reefs are shown as grey rectangles; b) the temporal component (black line) and the incident wave height time series (grey line).

The third mode of change is focussed on the intertidal region and describes a uniform beach profile gradient increase or decrease represented by accretion in the upper intertidal and erosion in the lower intertidal (Figure 5.3.11a). Positive values of the temporal component produce a steeper than mean beach gradient and negative values a flatter than mean gradient. The temporal component (Figure 5.3.11b) shows a generally increasing trend (increasing gradient) with three significant beach gradient reduction events. These beach gradient reduction events occur over storms and are all subsequently followed by a faster than normal increase in beach steepness indicative of post storm re-adjustment. Not all storms produce a flattening event, this is possibly due the antecedent conditions: a previously flattened beach will already be in equilibrium with the storm profile. Figure 5.3.12 shows that the three flattening events are associated with large surge events. The largest flattening event occurs when the surge and storm occur just prior to the survey and thus no recovery has taken place. Increase in beach steepness generally occurs under low surge and wave height periods.

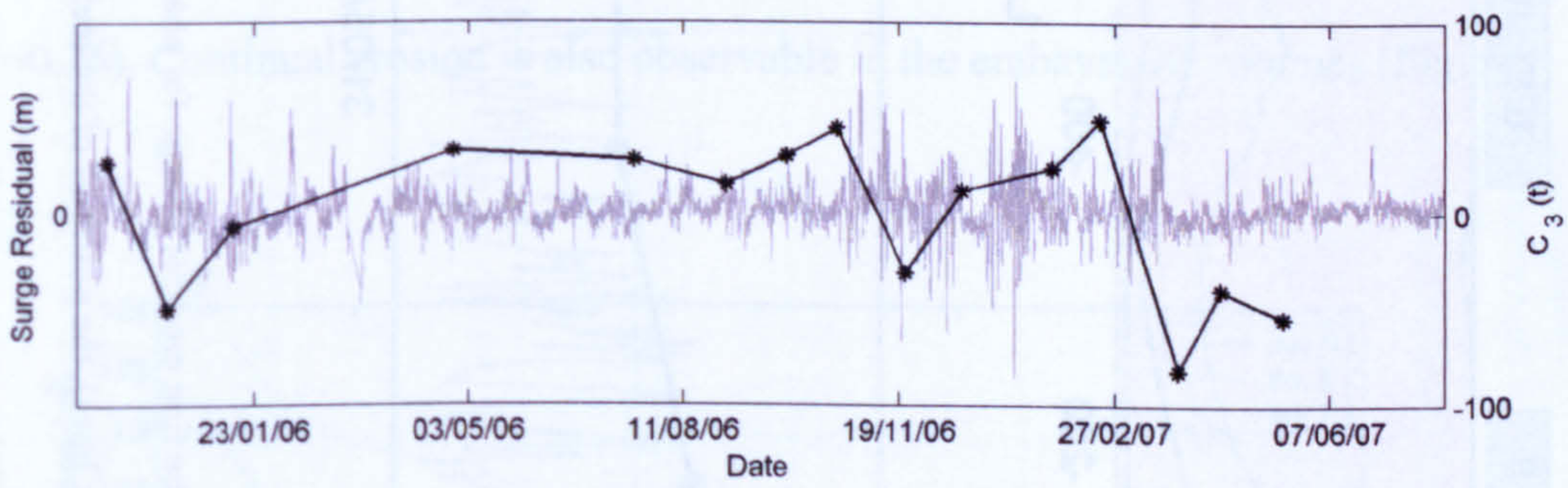

Figure 5.3.12: The surge residual measured at Cromer and the temporal component of the third mode of phase one change.

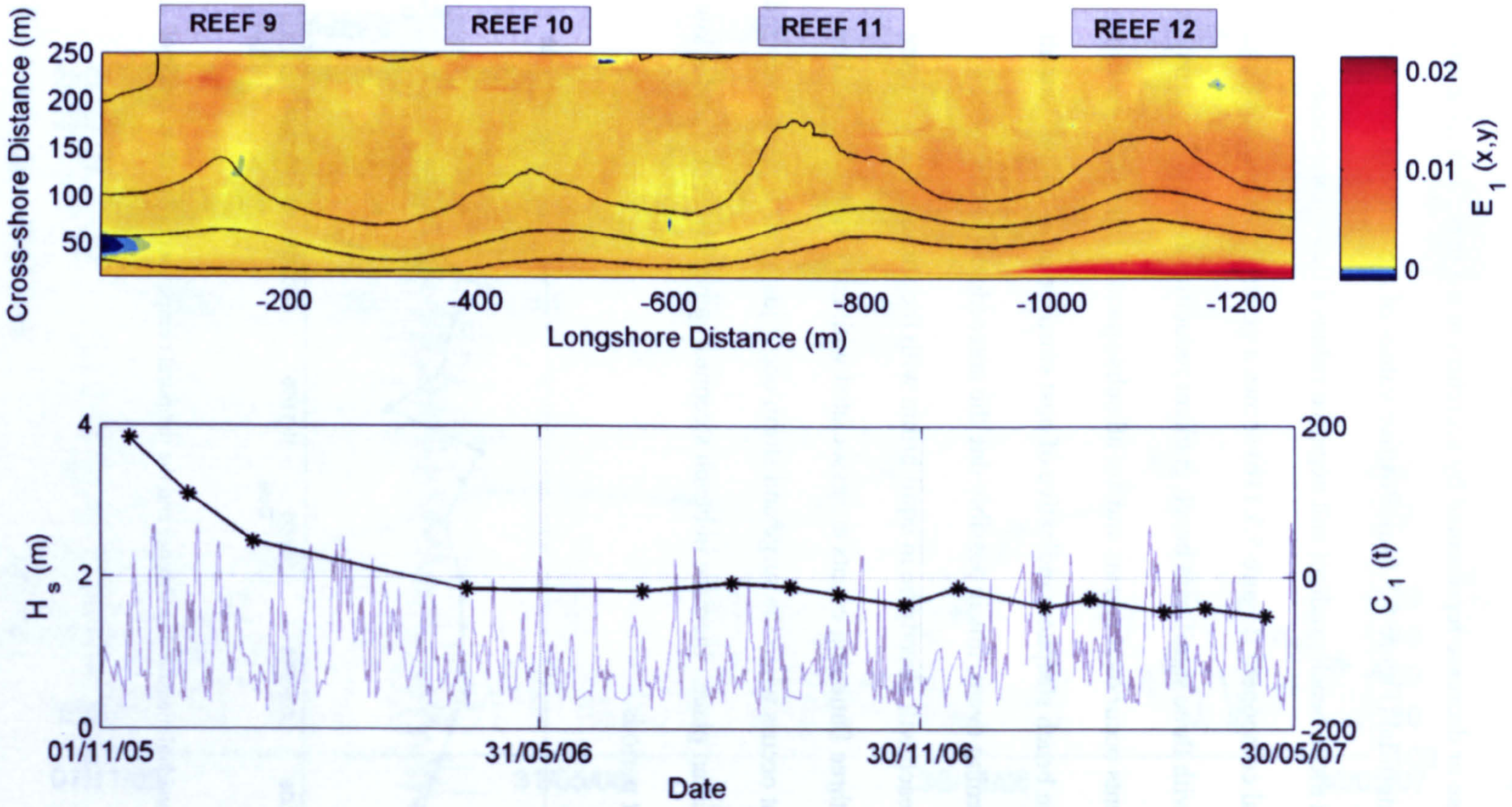

Figure 5.3.13: A plot of the first mode of change for phase two; a) The spatial eigenfunction (coloured shading) and contour lines of the mean bathymetry at 2,0,-2,-4m ODN (black lines), the positions of the reefs are shown as grey rectangles; b) the temporal component (black line) and the incident wave height time series (grey line).

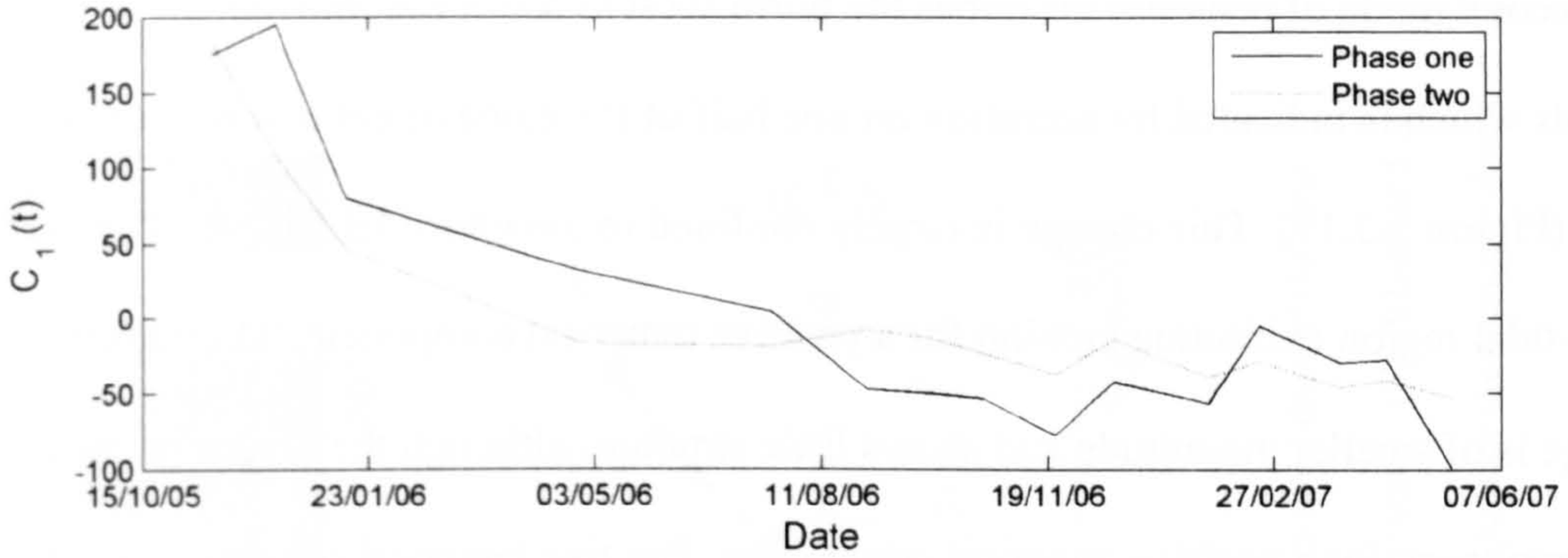

Figure 5.3.14: Comparison between the first mode's temporal component for both phases.

Phase two

The first three modes of change represent 77% of the dataset variance (58, 11, 10 %). The first mode of change (Figure 5.3.13) describes a phase wide accretion (for a positive temporal component). The temporal component declines through the study period meaning there is erosion over the time period. The temporal component is very similar to the temporal component for the first mode of phase one (Figure 5.3.14), and also shows highest, but insignificant, correlation with the cumulative integral of demeaned high tide level (r=0.26). Continual erosion is also observable in the embayment volumes (Figure 5.3.15).

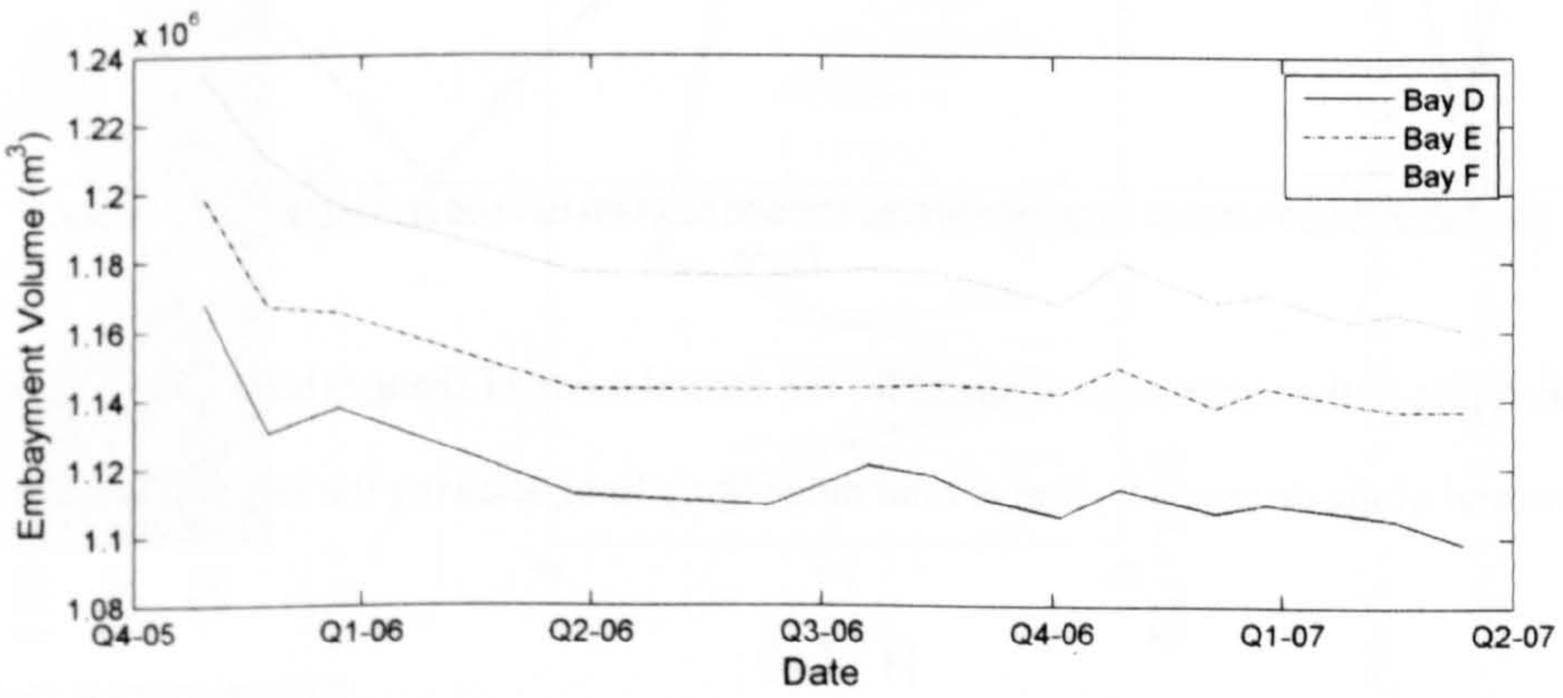

Figure 5.3.15: Embayment volumes for phase two.

The second mode of response describes the north-west to south-east movement of the salients which is indicated by accretion on one half of the embayment and erosion on the other (Figure 5.3.17). This change is largely confined to the intertidal regions with the supra-tidal region exhibiting erosion for a positive temporal component. The sub-tidal change is of smaller magnitude and shows little structure although the predominant change is accretionary for a positive temporal component. Positive temporal components lead to a north-westward shift of the salient centre and negative temporal components to a south-eastward shift. The temporal component is negative in winter and positive in the summer. The temporal component shows a negative correlation with the cumulative integral of the relative tidal range (Figure 5.3.16) with a Pearson's product moment correlation co-efficient of r=-0.68 (significant at the 99% confidence interval), meaning that large values of RTR are associated with the salients being north-west of mean and small values with the salients being south-east of mean.

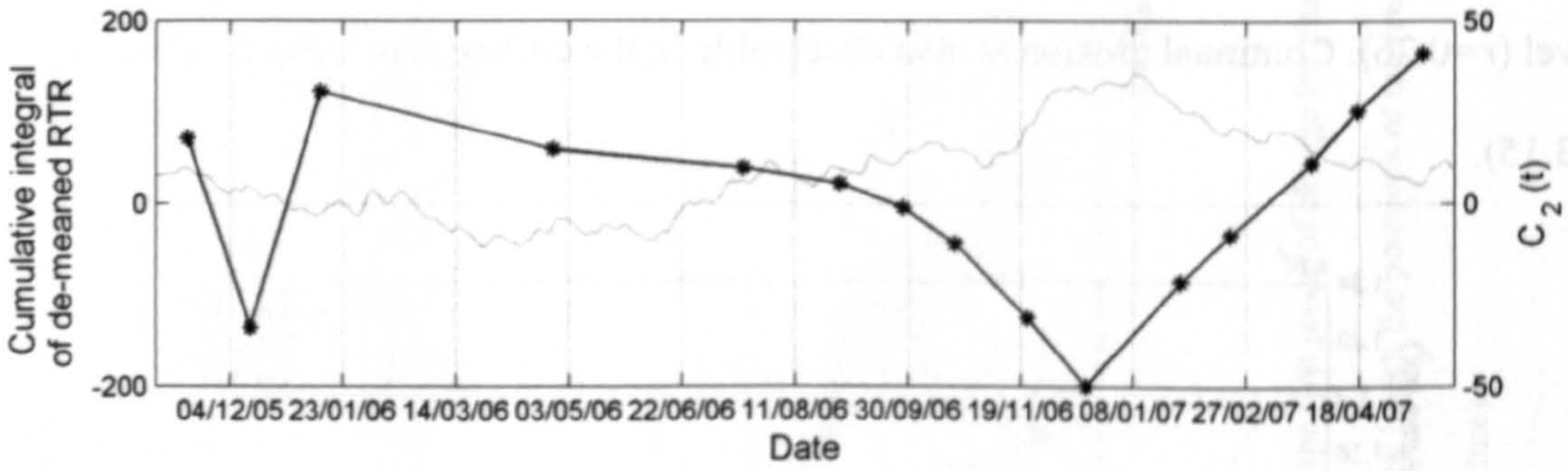

Figure 5.3.16: A plot of the temporal component for the second mode of change (black line) and the cumulative integral of the de-meaned relative tidal range (grey line), showing the negative correlation.

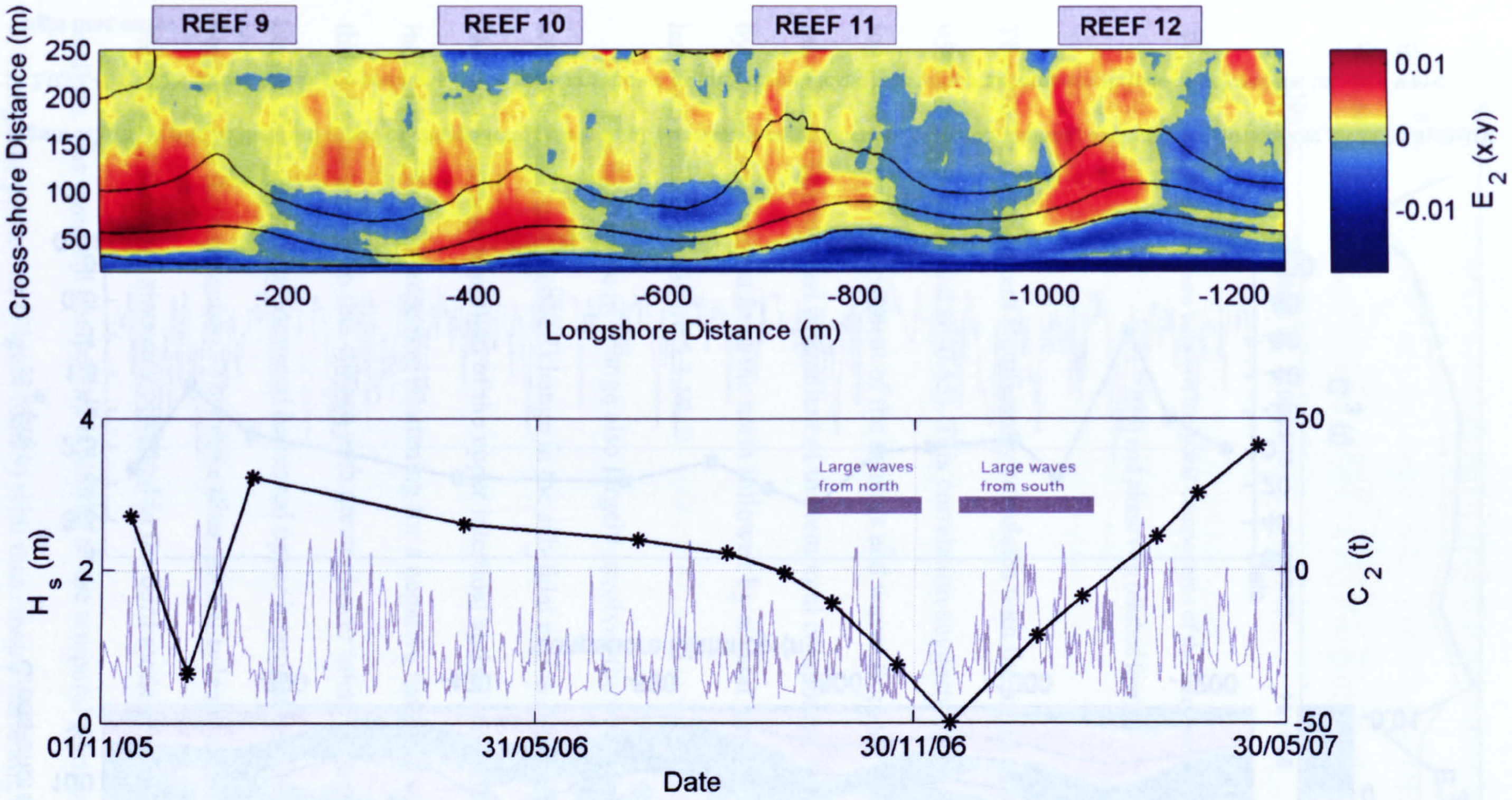

Figure 5.3.17: A plot of the second mode of change for phase two; a) The spatial eigenfunction (coloured shading) and contour lines of the mean bathymetry at 2,0,-2,-4m ODN (black lines)), the positions of the reefs are shown as grey rectangles b) the temporal component (black line) and the incident wave height time series (grey line). Two periods of waves from opposing directions have also been marked to illustrate the change in direction of salient movement,

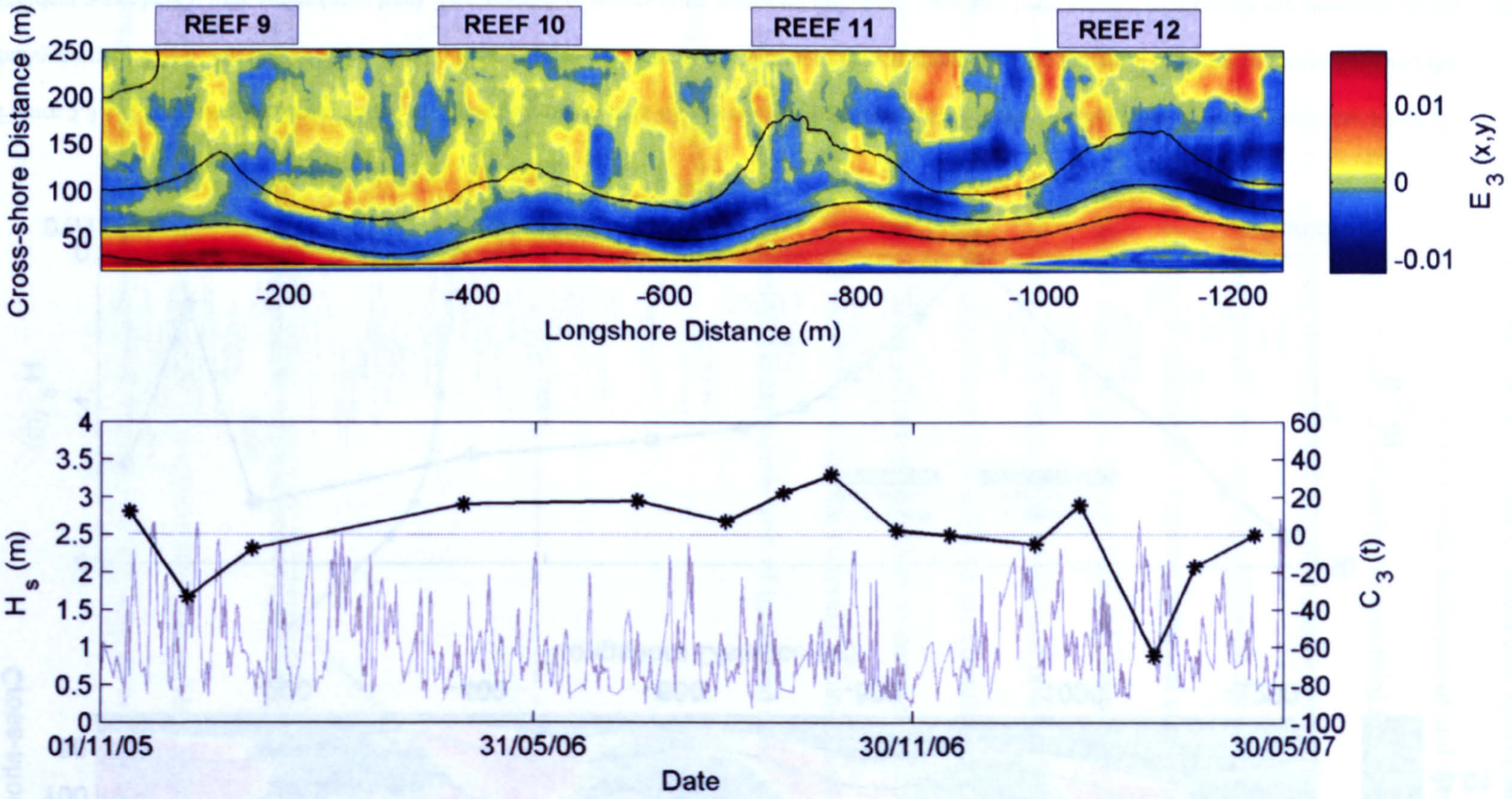

Figure 5.3.18: A plot of the third mode of change for phase two. a) The spatial eigenfunction (coloured shading) and contour lines of the mean bathymetry at 2,0,-2,-4m ODN (black lines), the positions of the reefs are shown as grey rectangles; b) the temporal component (black line) and the incident wave height time series (grey line).

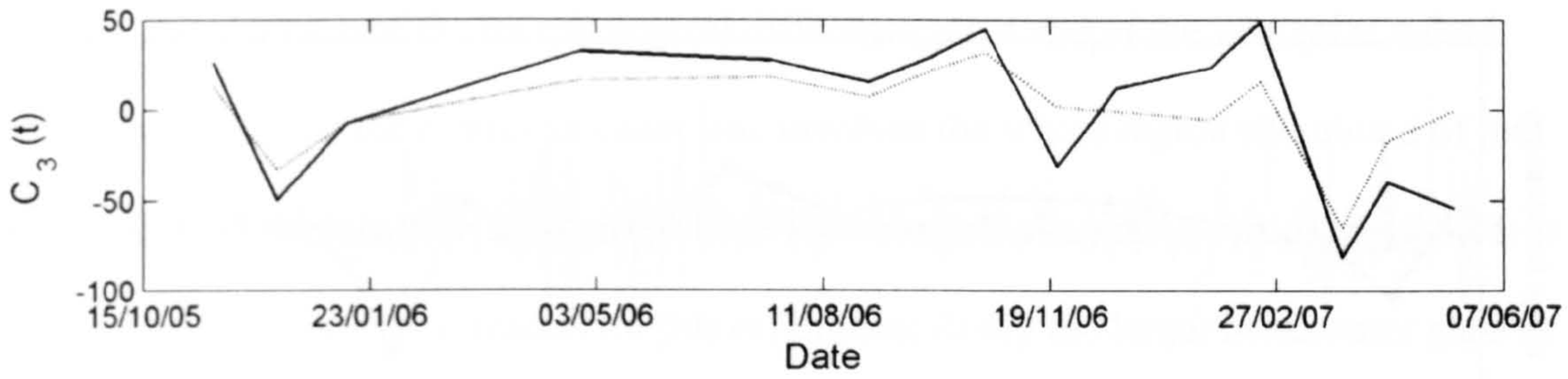

Figure 5.3.19: A comparison between temporal components of the third mode of change for phase one (solid line) and phase two (dashed line).

The temporal component significantly correlates with the angle of wave incidence at the 95% confidence interval (r=0.55). This correlation suggests that waves from the south lead to north-westward movement of the salients and waves from the north to south-eastward movement. The reversal in gradient of the temporal component in December 2006 is caused by several large storms from the north followed by several large storms from the east. This has been marked on Figure 5.3.17.

The third mode of change also largely involves the intertidal and supra-tidal regions with lesser and unstructured change in the sub-tidal region (Figure 5.3.18). The intertidal change involves an accretion of the upper intertidal and an erosion of the lower intertidal indicative of beach steepening (flattening for a negative temporal component). There is a three dimensionality to this change with greater lower intertidal erosion in the embayment centres than the salient horns and increased upper intertidal accretion on the salient horns compared to the bay centres. This three dimensionality leads to the enhancement and reduction in shoreline sinuosity observed in the third mode of the MSL contour EOF analysis. The temporal component is similar to the temporal component for the third mode of change for phase one (Figure 5.3.19) with three major flattening events (negative shifts in the temporal components). The relative magnitude of the flattening is less for phase two than for phase one.

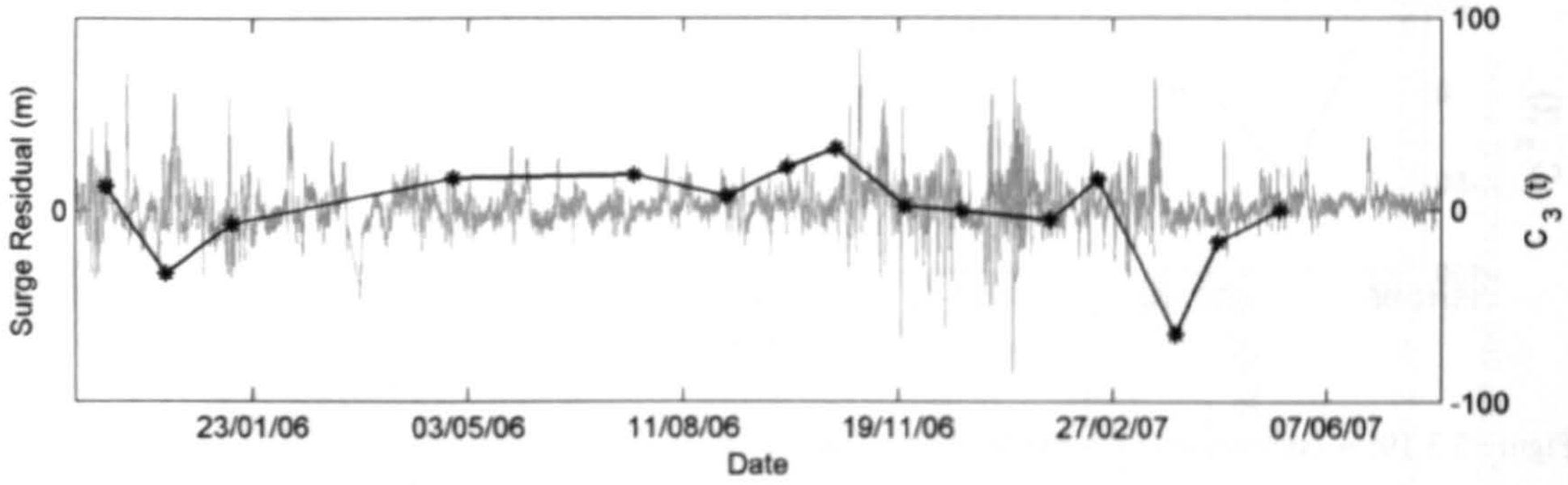

Figure 5.3.20: A plot of the temporal component for mode 3 (black line) and the surge residual (grey line).

These flattening events are co-incident with large storms (Figure 5.3.18b) and surge events (Figure 5.3.20). Beach steepening (indicated by a positive gradient to the temporal component) is co-incident with calmer periods of wave activity (Figure 5.3.18b) and non-surge conditions (Figure 5.3.20).

5.4 Discussion

The MSL contour extracted from the RTK-GPS dataset displayed similar modes of change to the video derived data. This means that the same spatial changes are being resolved in both datasets and thus it is reasonable to use the RTK-GPS data to support and inform findings based on the video data. For the spatial eigenfunctions the difference between weekly and monthly surveys is small. However, statistical correlation of the temporal components with forcing was only possible for the second mode of change for both phases and only at a lower confidence limit than for the video derived data. This has implications for the scheduling of surveys: monthly surveys seem adequate to resolve modes of change but in order to allow meaningful correlation with forcing, surveys should be planned more frequently.

Consideration of the morphological difference plots and of the vertical standard deviation shows that the change in phase one involves the whole region shoreward of the breakwaters whereas in phase two the change is concentrated on the intertidal regions. It is believed that there are two reasons for this difference; firstly the larger breakwater gaps in phase one allow greater penetration into the embayments (Chapter 6) and secondly the tombolos mean that sediment exchange between embayments is prohibited thus enhancing individual embayment changes. In phase two the salients allow exchange of sediment between embayments and hence any sediment input/loss for the sub-tidal region in phase two is readily distributed about the whole phase meaning that changes are of lesser magnitude. For phase one particularly the greatest variance is on the southern intertidal flanks of the embayments, which are most exposed to the predominant wave direction. Similar trends were shown in beach volatility maps for the site by Dolphin *et al.* (2005).

The 2-D EOF analysis backed up the observation that the phase two change was largely constrained to the intertidal region whereas the phase one change showed structure in the sub tidal regions too. The phase one RTK-GPS dataset changes showed significant differences from the MSL contour dataset whereas for phase two the changes over the whole region were similar to the MSL contour dataset. This difference is due to the nature of EOF analysis which produces orthogonal modes which are given preference by the amount of variance they contain. For phase one the intertidal variance is not dominant compared to the variance over the whole region and thus the changes described by the EOF analysis are not identical to the MSL contour analysis. Phase two conversely, since the majority of change is focussed on the intertidal region, shows the same modes of change in the MSL dataset and the 3d survey EOF analysis. This means that for phase two the RTK-GPS survey data can be used to better explain the changes observed in the MSL contour dataset.

The first and third modes of change derived from the 3-d surveys are similar for both phases whilst the second mode of change is different for the two different phases.

The first mode of change for phase one describes overall erosion through the study period apart from the bay B intertidal region which showed an overall accretion. While the MSL contour dataset does pick up this change (accretion in bay B, erosion in bay C), the MSL contour dataset also describes accretion focussed on the tombolos. This suggests that the accretionary trend observed in the first mode of video derived mean sea level contour change for phase one (Chapter 4) is not representative of the phase one change as a whole. There is no significant correlation with forcing for this mode of change, although the highest correlation is with the cumulative integral for the de-meaned high tide level which is the same as for the video derived MSL contour analysis. The first mode of change for phase two displays a similar behaviour. For phase two the first mode is also a general erosion / accretion. Unlike phase one, the change is in the same direction for the whole phase and the change shows the same trend for the 3-d survey data and the MSL data. This means that the erosion / accretion observable in the MSL contour is representative of the whole phase two change and indicates real erosion and accretion rather than being caused by redistribution of sediment around the profile from regions not covered by the video system (non-intertidal regions). For both phase one and phase two the first mode of change is comparable to the change in beach volume, a similarity which has previously been reported by Rihuoey et al (2009) for breakwater protected beaches in the Mediterranean.

The lack of correlation with forcing for both phases could well be due to the low sampling frequency, the video derived MSL contour dataset showed correlation with the high tide level for both phases. Both phases are undergoing erosion through the study period. One possibility is that the northernmost tombolo, which is constantly emerged, is reducing sediment input to the scheme from the north-west (the predominant direction of longshore

sediment transport), whilst sediment is still leaving the scheme to the south (due to oblique waves and tidal asymmetry) and thus the scheme is slowly losing sediment.

The second mode of change for phase one and phase two are different: in phase one the second mode largely describes and erosion/accretion of the sub-tidal regions coupled with a steepening/flattening of the intertidal region whereas the second mode for phase two describes a longshore movement of the salients.

For phase one the change involves the entire breakwater protected region. The predominant change is the erosion and accretion of the sub-tidal bays. The temporal component for this trend shows an oscillatory component and is negatively correlated with the wave height such that smaller waves lead to shallower bays and larger waves to deeper bays. It is believed that this change is related to sediment exchange with the offshore region through the breakwater gaps. Under larger waves offshore transport dominates both due to undertow and due to rip currents through the structure gaps induced by the large volume of overtopped water (Martinelli *et al.*, 2006). Large negative shifts (bay deepening) are co-incident with surge events: surge events increase

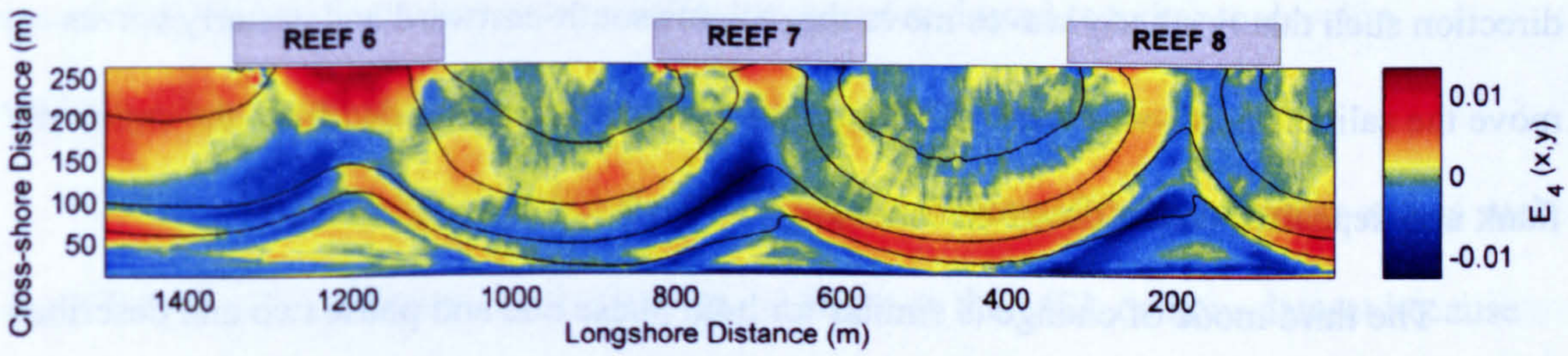

Figure 5.4.1: The spatial eigenfunction for the fourth mode of phase one change showing the longshore tombolo movement as evidenced by erosion on the left side of the tombolo centre-lines and accretion on the right side.

overtopping leading to piling up of water behind the structure, strengthening the offshore directed currents and exacerbating the erosion of the sub tidal areas. Under calm conditions sediment is transported onshore through the gaps via tidal transport (Chapter 6) and wave shoaling processes.

The lack of tombolo movement in the 2nd mode for phase one, despite being present in the MSL contour dataset is due to the small amount of variance taken up by the tombolo movement due to the small area involved. Longshore movement of the tombolo is observable in the fourth mode (Figure 5.4.1) but only represents 6% of the dataset variance and so is not considered in this analysis.

The second mode of change for phase two derived from the RTK-GPS dataset describes the longshore movement of the salients. There is little structure to this change outside of the intertidal region and the intertidal structure suggests that this change is caused by longshore movement of sediment. This change is the same as for the second mode of response in the MSL contour dataset. The same correlation of the temporal component with the cumulative integral of relative tidal range is observed as for the MSL dataset (discussed in Chapter 4). The change is also significantly correlated with wave direction such that northerly waves move the salients south-eastward and easterly waves move the salients north-westward. This suggests that material is eroded from the exposed flank and deposited on the down-drift flank.

The third mode of change is similar for both phase one and phase two and describes an intertidal cross-shore change between the upper and lower intertidal regions leading to an intertidal steepening or flattening. For phase two, this change shows an added 3-dimensionality with the lower intertidal changes greatest in the bay centres and the upper intertidal changes greatest on the salient horns. This produces the increase/decreases in shoreline sinuosity observable in the MSL dataset and suggests that the third mode of phase

two change for the MSL contour dataset is driven by cross-shore processes. For phase one, the nodal point is close to the MSL contour line and so this change is not picked up by the MSL dataset. Temporal components are similar for both phases and show that large profile flattening events are linked to storms accompanied by surges over 1.3m. This linkage is backed up both by the video measured storm changes which showed significant flattening of the profile gradient only occurred for storms associated with a large surge event (Chapter 4.2) and the correlation of the temporal component of the third mode of MSL contour change for phase two with the cumulative integral of the de-meaned high tide level. Post storm, the rate of increase in beach gradient is faster than in other periods indicative of a swift intial recovery period as the beach seeks to return to an equilibrium condition.

5.5 Conclusions

Consideration of the mean sea level contour extracted from the RTK-GPS data shows that the same modes of change are observable in the RTK-GPS data as in the video derived MSL contour. Correlation of RTK-GPS described change with forcing proves less successful due to the temporal sparseness of the data. The similarity in modes of response means that the two datasets can be readily compared and used together to develop understanding of beach changes behind the breakwater system.

Changes in phase one affect the whole region inshore of the breakwater and as such the 2-D EOFs do not show exactly the same changes as the MSL contour dataset because the level of variance ascribed to the intertidal changes is less than the amount of variance ascribed to changes over the whole region. Changes to the phase one intertidal cannot be considered as a proxy for changes to the whole phase one breakwater protected area. The first mode of change observed in the RTK-GPS dataset for phase one shows that the general trend is opposite to the intertidal change. The second mode of change shows a

largely sub-tidal change involving bay floor erosion and accretion. Under large waves the bay floor is eroded and under smaller waves accretion is evident. Surge conditions exacerbate this erosion and lead to a shift from shallow to deep bays. The third mode of change for phase one shows a flattening or steepening of the beach profile. This change is largely intertidal but the nodal point is close to the MSL contour which means that the change is not observable in the MSL contour dataset. Large reductions in beach gradient are co-incident with large storm and surge events.

For phase two, morphological changes are largely constrained to the intertidal region and so intertidal changes represented by the MSL contour dataset are representative of changes to the scheme as a whole. The RTK-GPS dataset provides qualification of the phase two changes observed in the MSL contour dataset. The first mode of change is a real, phase wide, erosion / accretion. The longshore movement of salients is driven by longshore sediment movement and the temporal component of the RTK-GPS dataset shows the same correlation with the relative tidal range as the video derived MSL contour dataset. The third mode of change shows a similar profile steepening and flattening as the phase one change, and the temporal component shows the same link of storm and surge events with gradient reduction. The cross-shore exchange of sediment shows some three dimensionality: change is focussed on the upper intertidal salient horns and lower intertidal salient bays. This leads to the increase and decrease in sinuosity observed in the third mode of change for the MSL contour dataset.

It is believed that the difference in areas of variability between phase one and phase two (phase one displays variability over the whole region, phase two shows intertidal variability only) is caused in part by greater wave penetration through the larger breakwater gaps and in part by the tombolos restraining trans-embayment sediment transport and leading to greater changes to individual bays.

6. Numerical Modelling

A commercially available 'state of the art' numerical model, the Danish Hydraulic Institute's MIKE21, was used to model the scheme of breakwaters at Sea Palling. Numerical models are a useful tool for predicting the hydrodynamic conditions causing morphological change over wide spatial scales, especially in cases where high three dimensionality in hydro- morphodynamics mean findings from in-situ point measurements cannot be used to make generalisations about the greater area.

Rather than investigate specific events, it was deemed more useful to investigate characteristic modes of response under different wave and tide conditions. The rationale for this approach was threefold: firstly, the timescale of both the video derived dataset (30 months at weekly resolution) and the DGPS dataset (monthly resolution) prohibited modelling of the whole study period due to computational time restrictions; secondly, suitable data for use as tidal boundary conditions were not available for the whole study period and thirdly other participants in LeaCoast2 were concentrating on modelling of specific events at the breakwater scheme (Pan *et al.*, 2009) which would lead to duplication of research effort. However, for model validation a real world scenario over part of a LeaCoast2 process experiment was modelled, which demonstrated the capability of the model system to accurately model the breakwater scheme.

The aim of this modelling section was to develop an understanding of the hydrodynamic current circulation patterns; the wave action and the sediment transport pathways that force the observed modes of morphological change obtained from the video data (Chapter 4) and DGPS surveys (Chapter 5). Specific questions that require answering are:

1) The relative importance of tides and waves around the scheme, especially for storm conditions,

2) The balance of forcing mechanisms and potential range of salient and tombolo movement.

Three sections of modelling work were undertaken: Firstly, wave only conditions were investigated, looking at the effects of varying water level, wave height, period and direction on the current speeds and circulation patterns produced. Secondly, tidal conditions were investigated for neap, mean and spring tidal cycles. Thirdly, combined wave and tidal conditions were modelled. Tidal currents have previously been shown to be important to the sediment transport pathways at the site (Bacon *et al.*, 2003; Bacon *et al.*, 2005; Bacon *et al.*, 2007) and hence tides and waves were tested separately before being combined to facilitate definition of the relative contribution of both types of forcing to the morphological change. Particular attention was paid to storm events due to the dramatic morphological changes forced these conditions.

6.1 The model used: MIKE21 FM.

In this study the Danish Hydraulic Institute's MIKE21 FM model (Jones *et al.*, 2007) was used. This is a coastal area model with three fully coupled components: a hydrodynamic module (DHI, 2008a); a spectral wave module (Sorenson *et al.*, 2004b; DHI, 2008c) and a sand transport module (DHI, 2008b). The coupling is shown in Figure 6.1.1. The model allows for a flexible mesh which means finer resolution can be obtained for the areas of interest, in this case for the shallower regions inshore of the breakwaters. The model is a depth averaged 2DH model. The hydrodynamic module solves the 2 dimensional incompressible Reynolds averaged Navier-Stokes equations for continuity and momentum to provide surface elevations and current velocities about the breakwater scheme. The spectral wave module simulates wave transformation over the model domain based on the wave action conservation equation. The sediment transport is calculated as total load using a quasi 3-D approach to generate look-up tables of sediment transport. The model domain and the set-up of the three modules will be presented in the following sections.

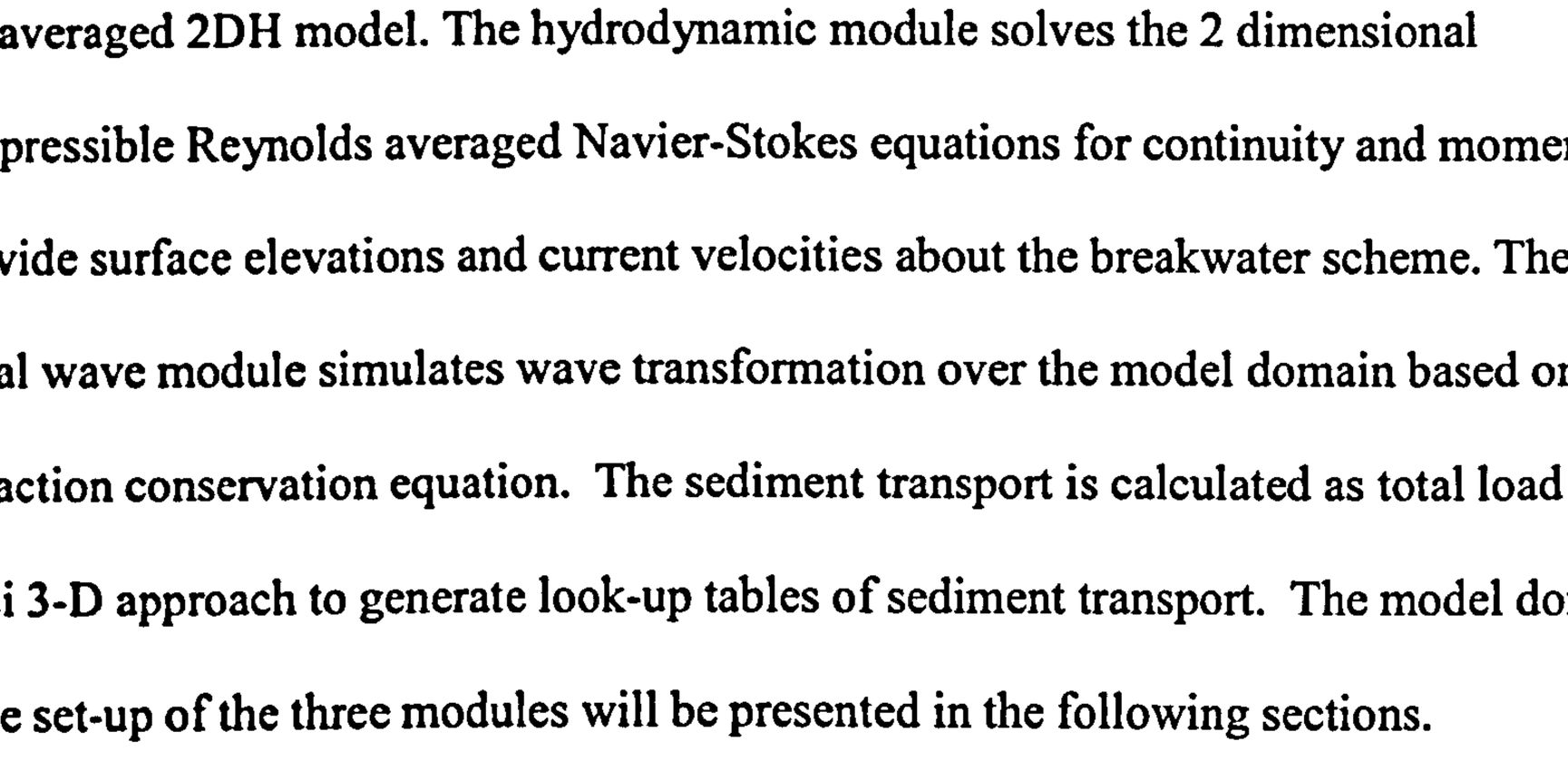

Figure 6.1.1: A diagram showing the dynamic coupling of the three modules used.

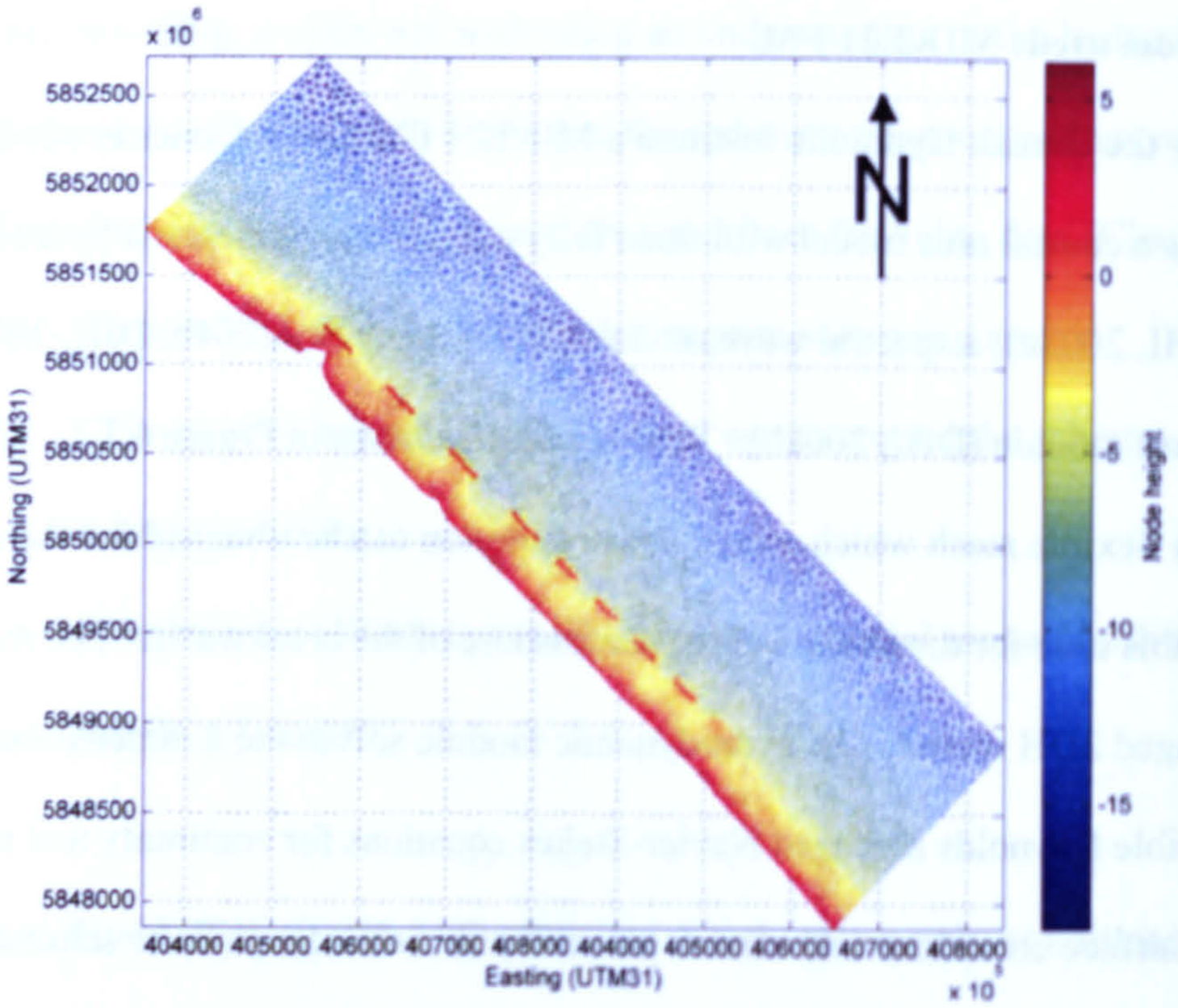

Figure 6.2.1: The model domain

6.2. Model Set Up

6.2.1 Model domain.

The model domain is shown in Figure 6.2.1. The domain was made wide enough to ensure that any boundary effects dissipated prior to the region of interest. DGPS survey data collected by the University of East Anglia (UEA) on 26/04/2006 was used for the bathymetry. The mesh was refined so that the shallower regions around the breakwater had finer resolution. Maximum element area was 2500m^2 and the finest was 300m^2. The elements are triangular which gives node separation length scales of approximately 25–70 m.

The breakwaters were incorporated as bathymetry and internal boundaries used to preserve the breakwater shape in the flexible mesh. An additional layer specifying the depth of the erodible surface was used to prevent erosion of the breakwaters. The erodible

depth was set to 0m for the breakwaters 10m for all other areas. There is no potential to include wave transmission or overtopping in MIKE21 FM and so waves are only transmitted when the breakwaters are submerged. The bed roughness (hydrodynamic module) is also increased over the breakwater to cater for the large size of the boulders.

6.2.2 Hydrodynamic module

In this section the model set-up and boundary conditions for the hydrodynamic module will be described. Two options are available for the solution technique: lower and higher order schemes. The lower order scheme was selected because, whilst less accurate, it was faster and made running the model on a standard desktop PC a more viable proposition. Flooding and drying is included in the model to enable water level changes over the tidal cycle. Density is set to be barotropic (no influence of temperature or salinity) due to the lack of freshwater inputs or the importance of temperature changes over the timescales being modelled. Eddy viscosity is set to a constant value of $0.004 m^2 s^{-1}$. This was the default value, sensitivity testing with other values showed no appreciable difference in results. Bed resistance is based on the Manning number M which can be estimated via:

$$M = \frac{25.4}{k_s^{1/6}} \tag{6.1}$$

Where k_s is the bed roughness length. The bed roughness length depends upon current speed, grain size and bed form characteristics but can be estimated solely on type of material. Soulsby (1997b) suggests values of k_s in the range 0.4-6mm, which gives Manning numbers between 18-32. Tests were run with various Manning number and it was found that the lower manning numbers produced inaccurately slow current speeds and thus a value M=32 was used in the model. In order to smooth out instabilities at the boundary a

thin (two element thick) strip of large bed roughness (M=5) was implemented, after the recommendation in the MIKE21 manual.

The hydrodynamic module is forced by waves, water level and currents. Wave radiation stress is input directly from the SW module. Boundary conditions are forced with tidal current and water level. Three different types of tests were run: fixed water level, varying water level and varying water level plus tidal currents. Water level and tidal current data was obtained from Environment Agency / Gardline Environmental AWACs deployed at Walcott and Horsey (Figure 6.2.2).

The measured data consisted of water levels, u and v velocities which were linearly interpolated through space to obtain values at boundaries A and C. This approach is justified by the similarity in the measured data at Horsey and Walcott, the linearity of the coast and the short distance between the measurements and the boundary locations.

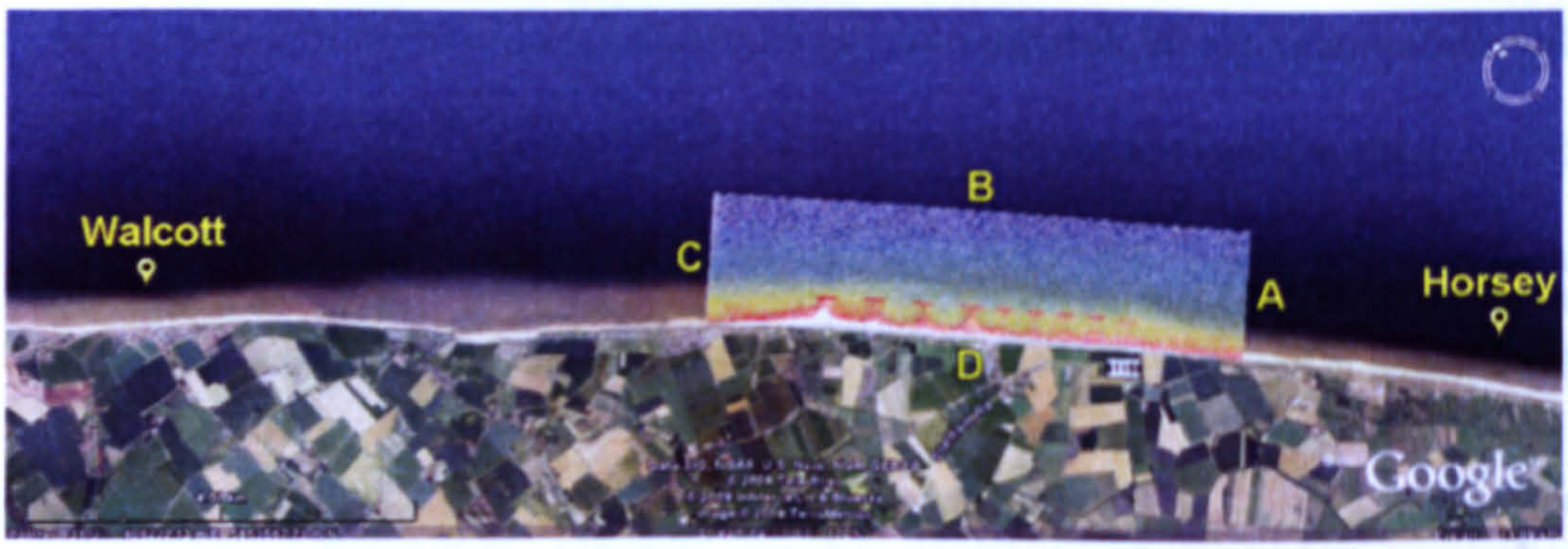

Figure 6.2.2: The model domain with locations of the two AWAC measurement devices and the boundary nomenclature.

The data was used to synthesize a mean tidal cycle to allow modelling of characteristic tidal conditions. This was achieved via 4 steps:

1) Data at boundaries A and C split into low water to low water tidal cycles.
2) Tidal cycles with associated large wave heights (indicative of surge events) or clearly erroneous data removed
3) Mean tidal cycle length determined and data interpolated to that temporal scale
4) Ensemble averaged values of water level and *u,v* velocities obtained.

Figure 6.2.3 shows the synthesized tidal cycle for boundaries A and C. The progressive nature of the tidal wave is clearly observable. In order to correctly force the progressive tidal wave, boundary A was forced with velocity and boundary D with water level (Bacon *et al*, 2005). The offshore boundary (B) was forced with velocity and the inshore boundary (D) set as 'land'. For the tests with constant water level the desired water level was set at all wet boundaries. For the varying water level with no tidal current tests the water level from boundary C was used for all wet boundaries.

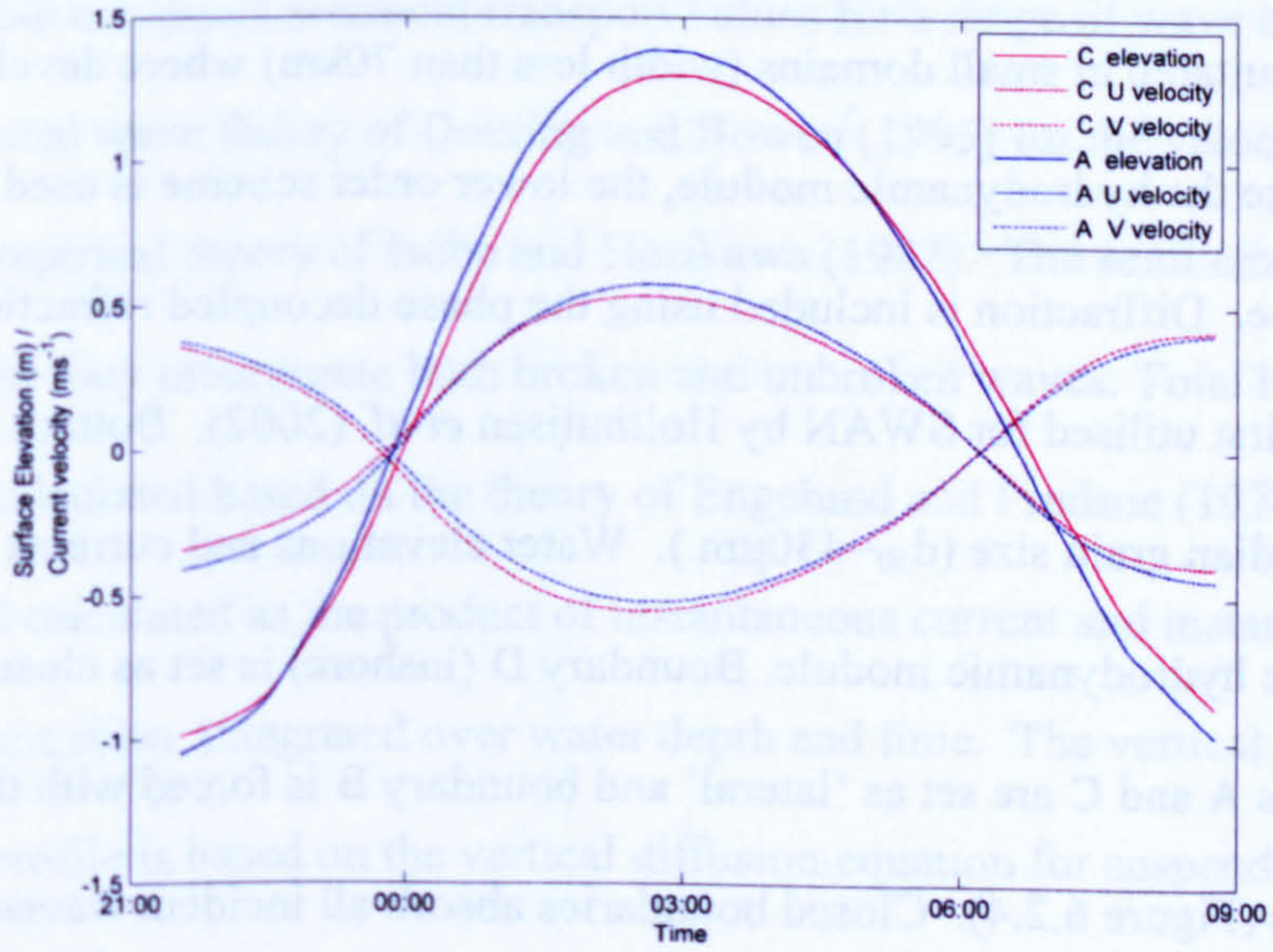

Figure 6.2.3: Tidal cycle elevation and *u,v* velocities for boundary C and boundary A.

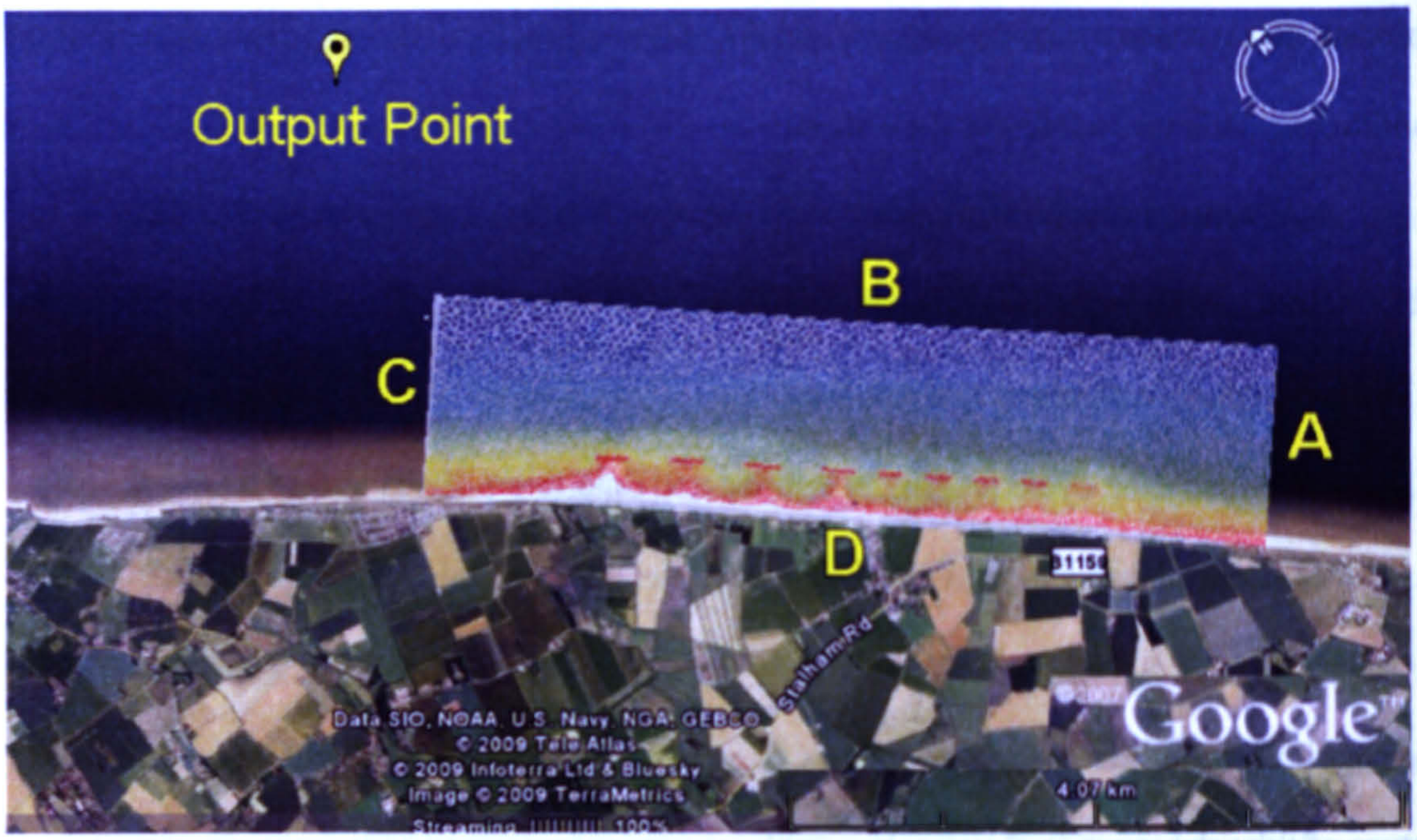

Figure 6.2.4: The model domain, boundary nomenclature and the met office wave model output point.

6.2.3 Spectral wave module

The spectral wave module is run using a directionally de-coupled parametric formulation based on the parameterisation of the wave action conservation equation in the frequency domain after Holthuijsen *et al.* (1989). This parameterisation is more computationally efficient and is suitable in small domains (width less than 70km) where developed seas are dominating. Like the hydrodynamic module, the lower order scheme is used to reduce computation time. Diffraction is included using the phase decoupled refraction-diffraction approximation first utilised for SWAN by Holthuijsen *et al.* (2002). Bottom friction is based on the median grain size (d_{50}=430μm). Water elevations and currents are forced directly from the hydrodynamic module. Boundary D (inshore) is set as closed, the cross-shore boundaries A and C are set as 'lateral' and boundary B is forced with the incident wave conditions (Figure 6.2.4). Closed boundaries absorb all incident waves, however, due to the nature of the domain this boundary is never utilised as there are dry cells prior to the

boundary at all tidal stages. Lateral boundaries solve the basic one dimensional wave equation along the boundary, taking the incident waves (boundary C) as input at the offshore end of the boundary and 0 at the inshore end. Utilisation of this boundary prevents wave shadows caused by the offshore boundary being forced by obliquely incident waves. Data for the offshore boundary was taken from the UK met office output point located close to the breakwater scheme (Figure 6.2.4). Seven years of hind-cast data was available from this output point and allowed for the determination of characteristic wave conditions. Mean wave conditions and mean storm conditions were tested as were a variety of test cases with different wave heights, periods, and directions.

6.2.4 Sand transport module

The sand transport module is forced by wave and current inputs from the spectral wave and hydrodynamic modules. Boundary conditions are set to zero sediment flux gradient and the sediment data to a constant median grain size of $d_{50} = 430\mu m$. At each time-step sediment transport is calculated based on a pre-computed quasi-3D sediment transport look up table. The look up table computes sediment transport values for a range of wave conditions using the semi-empirical wave theory of Doering and Bowen (1995) for the velocity skewness and the semi-empirical theory of Isobe and Horikawa (1982). The semi empirical theories are used because they incorporate both broken and unbroken waves. Total load is computed with bed load calculated based on the theory of Engelund and Fredsoe (1976) and suspended load calculated as the product of instantaneous current and instantaneous sediment concentration, integrated over water depth and time. The vertical sediment concentration profile is based on the vertical diffusion equation for suspended sediment of Fredsoe *et al.* (1985).

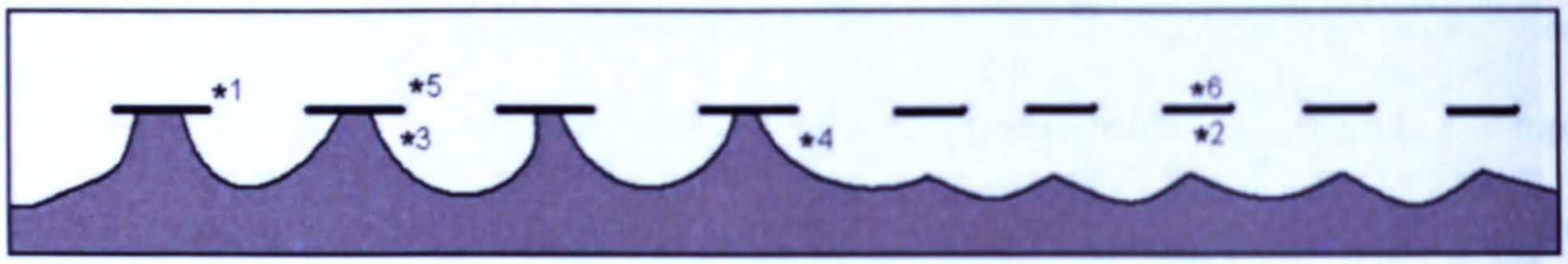

Figure 6.3.1: A schematic map of the breakwater system with the locations of the measurement frames

6.3 Model validation.

In order to validate the model setup was producing accurate results the model was run over the same time period as a process experiment conducted primarily by Proudman Oceanographic Laboratory (POL) and UEA, where measurements of tidal currents, tidal elevation and wave statistics were obtained form various frame locations about the scheme (Figure 6.3.1). The model was forced with the met office wave model hind-cast data on the offshore boundary and the tidal elevation and currents measured at Horsey and Walcott interpolated to the cross shore boundaries. Three tests were undertaken to examine the performance of the model: firstly a visual inspection of the data was conducted to verify that the right trends were being modelled; secondly the r^2 value was calculated to numerically test the similarity between the modelled and measured data and thirdly the root mean absolute error (RMAE) (van Rijn *et al.*, 2003) was calculated to test whether the model results were suitable accurate. Van Rijn (2003) produced a performance scale for model outputs based on the RMAE and this scale was used to determine the suitability of the calibration results.

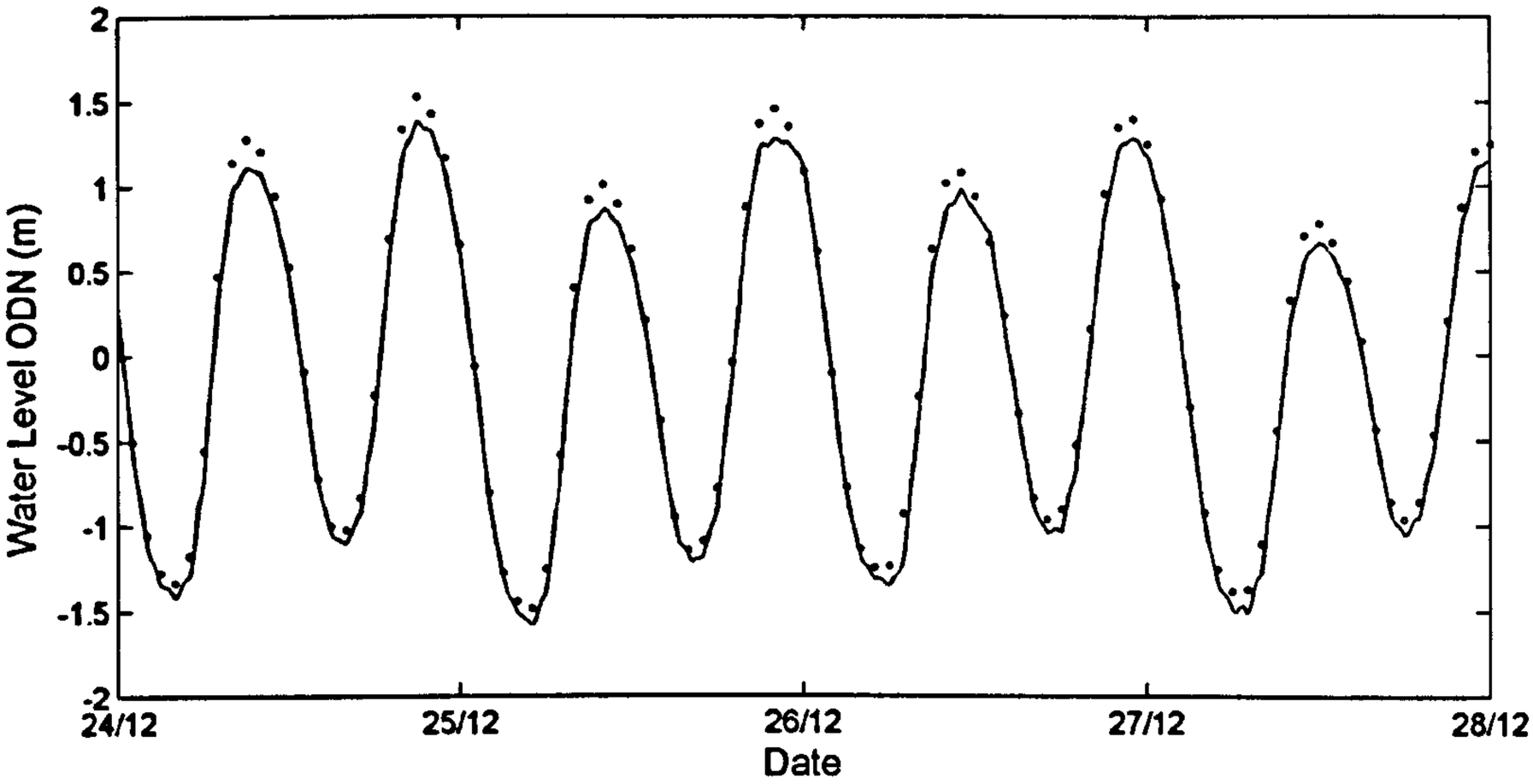

Figure 6.3.2: A section of the validation test showing measured (circles) and modelled (line) water levels for frame one

6.3.1 Water level

Only one water level point was available for comparison (Frame 1). The modelled water level showed good comparison with measured data: $r^2 = 0.996$ and RMAE =0.1. Whilst van Rijn (2003) does not provide qualification of the RMAE values for tidal elevation, if one takes tidal elevation to be analogous to wave height the model produces good results. The van Rijn (2003) scale is replicated in Table 2.1. Visually, it can be seen that there is a slight underestimation of the high and low tide elevations (Figure 6.3.2).

6.3.2 Current speeds

Comparison was made between measured and modelled *u* and *v* velocities at four locations about the scheme. Figure 6.3.3 shows comparison of *u* and *v* velocities for the four stations and Table 6.3.1 give correlation co-efficients and RMAE values for the *u*, *v* velocities for the different frames. The RMAE values rank as between good and reasonable based on the Van Rijn scale apart from the frame 4 *u* velocity which is poorly represented. The correlation co-efficients are all statistically significant at the 99.9% level. Frame 4, adjacent to the southern most tombolo, performs least well with under representation of the *u* velocity for the flood (south-eastward directed) current. This could partially be due to the model output being a depth averaged current and the measured value being a point value 1m above the seabed. The correct shape of the current signal is still well represented (as indicated by the significant correlation) Frame one, for which the comparison is best, is the only frame where a depth averaged velocity was obtained from ADCP measurements of current through the water column. The asymmetry of the flow at this frame is still correctly modelled, despite the magnitude of the flood peak being lower than measured.

In general, all current measurements are accurately represented by the model in terms of shape and magnitude. For all frames it can be seen that there is a slight phase shift between the modelled data compared to the measured data, it is thought that this is likely to be induced by the linear spatial interpolation of tidal measurements at Walcott and Horsey to the boundary locations. The phase shift is small and similar for all frames and it is the author's belief that it is not important since the magnitude is correct and modelling will be undertaken using a characteristic tidal cycle rather than real conditions.

Table 6.3.1: Correlation co-efficients (r^2) and RMAE's for *u, v*, velocities from the four frames

Frame No.	Velocity Compt.	r^2	RMAE	Van Rijn Ranking
1	*u*	0.88	0.28	Good
	v	0.88	0.24	Good
2	*u*	0.77	0.26	Good
	v	0.79	0.46	Reasonable
4	*u*	0.69	0.66	Poor
	v	0.72	0.47	Reasonable
5	*u*	0.67	0.49	Reasonable
	v	0.69	0.46	Reasonable

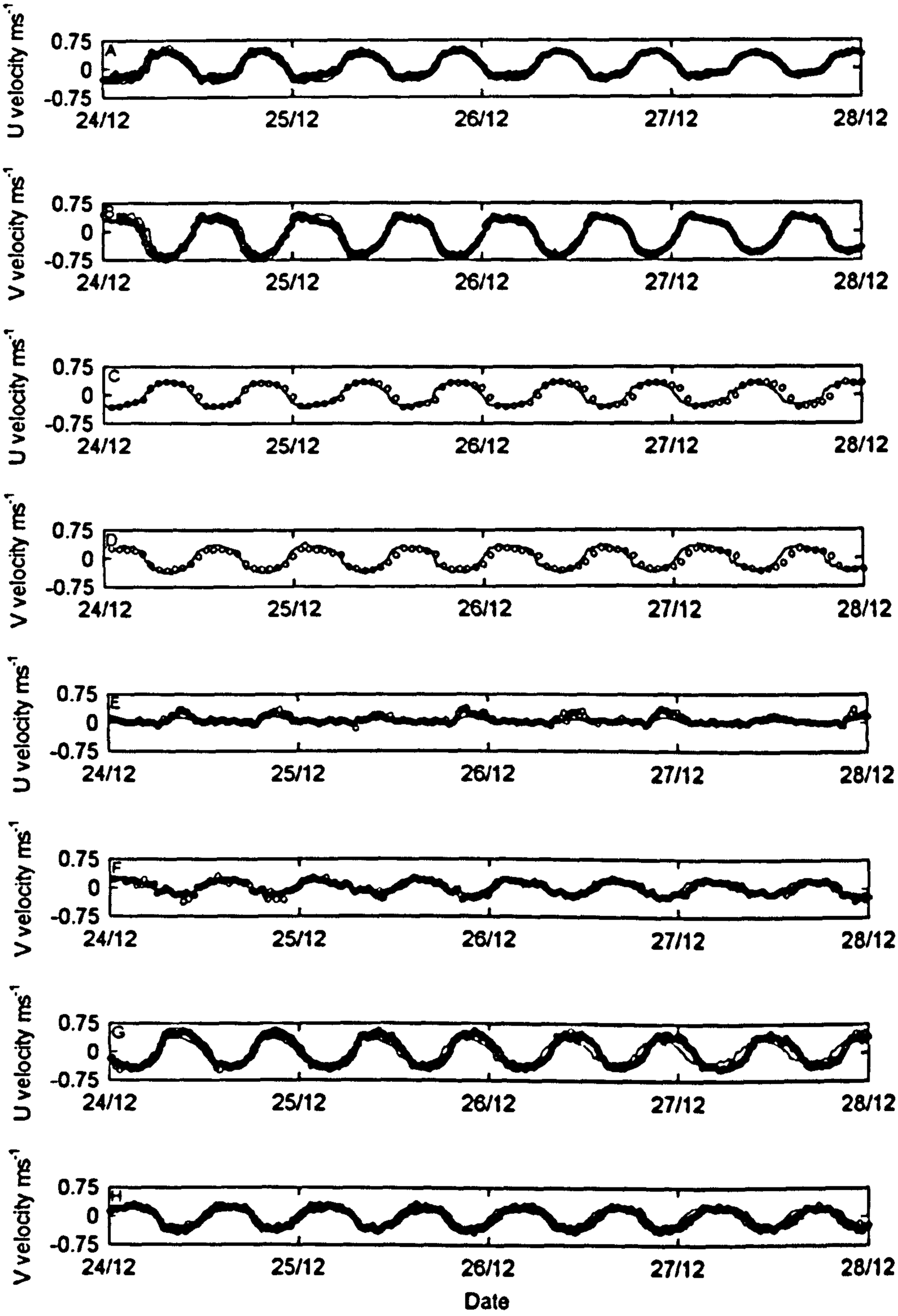

Figure 6.3.3: Measured (o) and modelled (-) *u,v* velocities for frame 1 (a-b), frame 2 (c-d), frame 4 (e-f) and frame 5 (g-h).

6.3.3 Wave statistics.

Wave height (H_s), period (T_p) and direction were measured at Frame 1 (Figure 6.3.4) and Wave height (H_s),and period (T_p) measured at frame 4 (Figure 6.3.5). The magnitude and general patterns of the wave heights is similar for both frames. For frame one the period is generally of the right order but there are periods of longer period waves that are not modelled, whilst for frame 4 the modelled period is approximately half the measured period. The wave direction (only measured at frame one) follows the measured direction well, although there are some measurement outliers these are thought to be erroneous measurements. The correlation co-efficients and RMAE's along with the RMAE ranking based on Van Rijn's categorisation are displayed in table 6.3.2. Van Rijn's categorisation does not cater for wave period or direction and so the wave height categorisation (stricter than the current velocity categorisation) was used to describe the performance based on the RMAE. Despite being low the correlations with wave height and direction are significant at the 99% confidence interval. Neither frame shows any correlation with wave period. The model results rank as poor-bad on the van Rijn categorisation. The wave parameters are less well modelled than the tidal currents and elevation.

Two points, however, should be considered. Firstly, the wave boundary conditions are obtained from another model (UK Met Office). The reason for the lesser agreement over the calibration period is likely to be the use of modelled wave heights as boundary forcing. Since characteristic wave conditions will be considered in this investigation the lesser agreement between modelled and measured wave heights is not considered to be prohibitively bad. The met office wave model has been shown to be suitably accurate over a long time period and hence characteristic conditions derived from 7 years of hind cast data will be representative of conditions at the site. Secondly, the key driver for wave induced morphological change is the relative spatial variation of the wave field about the

breakwater system. With only two wave measurement locations available for this time period, an accurate assessment of the spatial variation is impossible

Table 6.3.2: Correlation co-efficients and RMAE values for wave statistics from frame 1 and 4.

Frame No.	Wave statistic	r^2	RMAE	Van Rijn ranking
1	H_s	0.53	0.46	Bad
	T_p	0.06	0.23	Poor
	Dir	0.55	0.22	Poor
4	H_s	0.4	0.39	Bad
	T_p	0.03	0.51	Bad

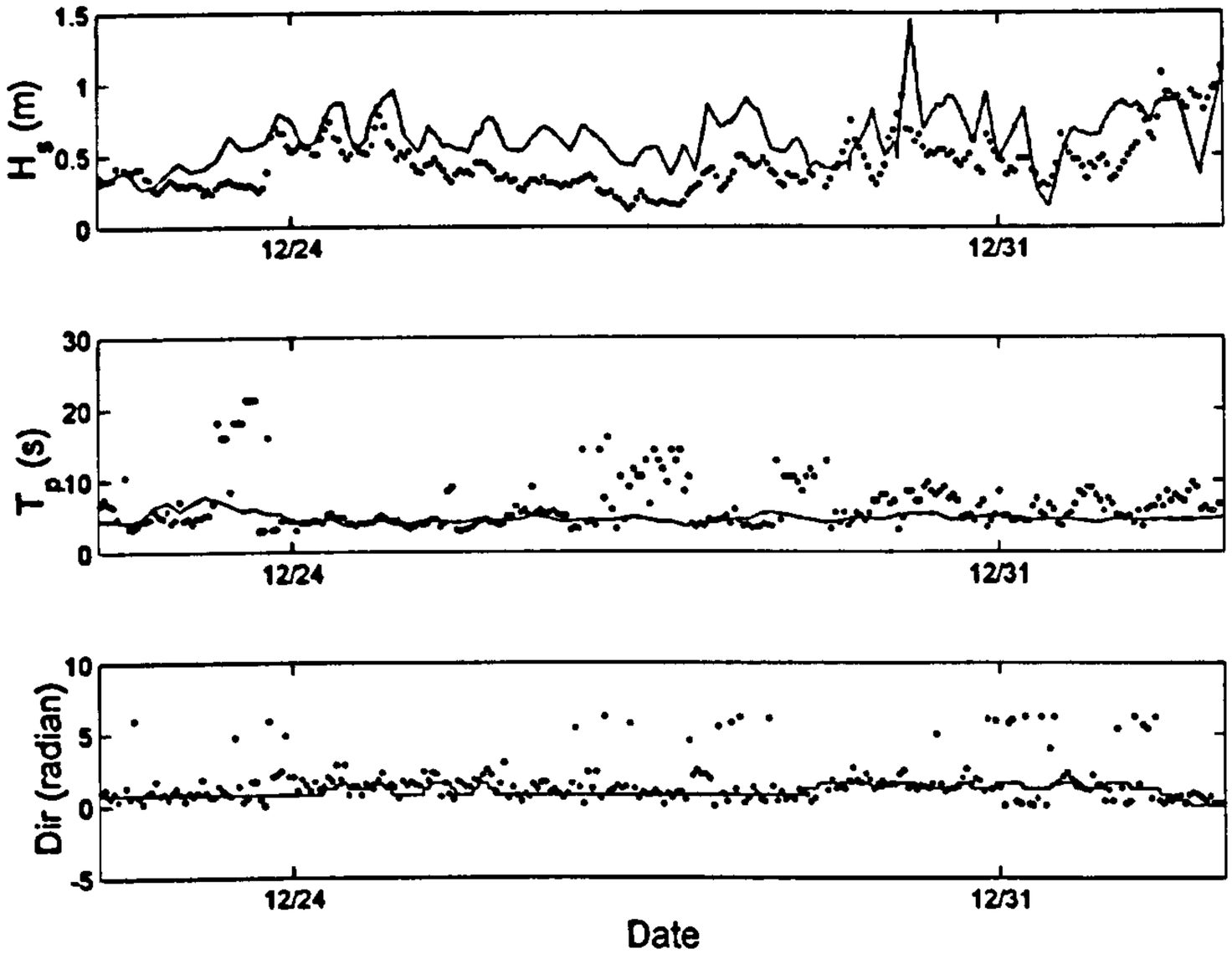

Figure 6.3.4: Comparison between a) wave height, b) wave period and c) wave direction for modelled (-) and measured (o) data from frame one

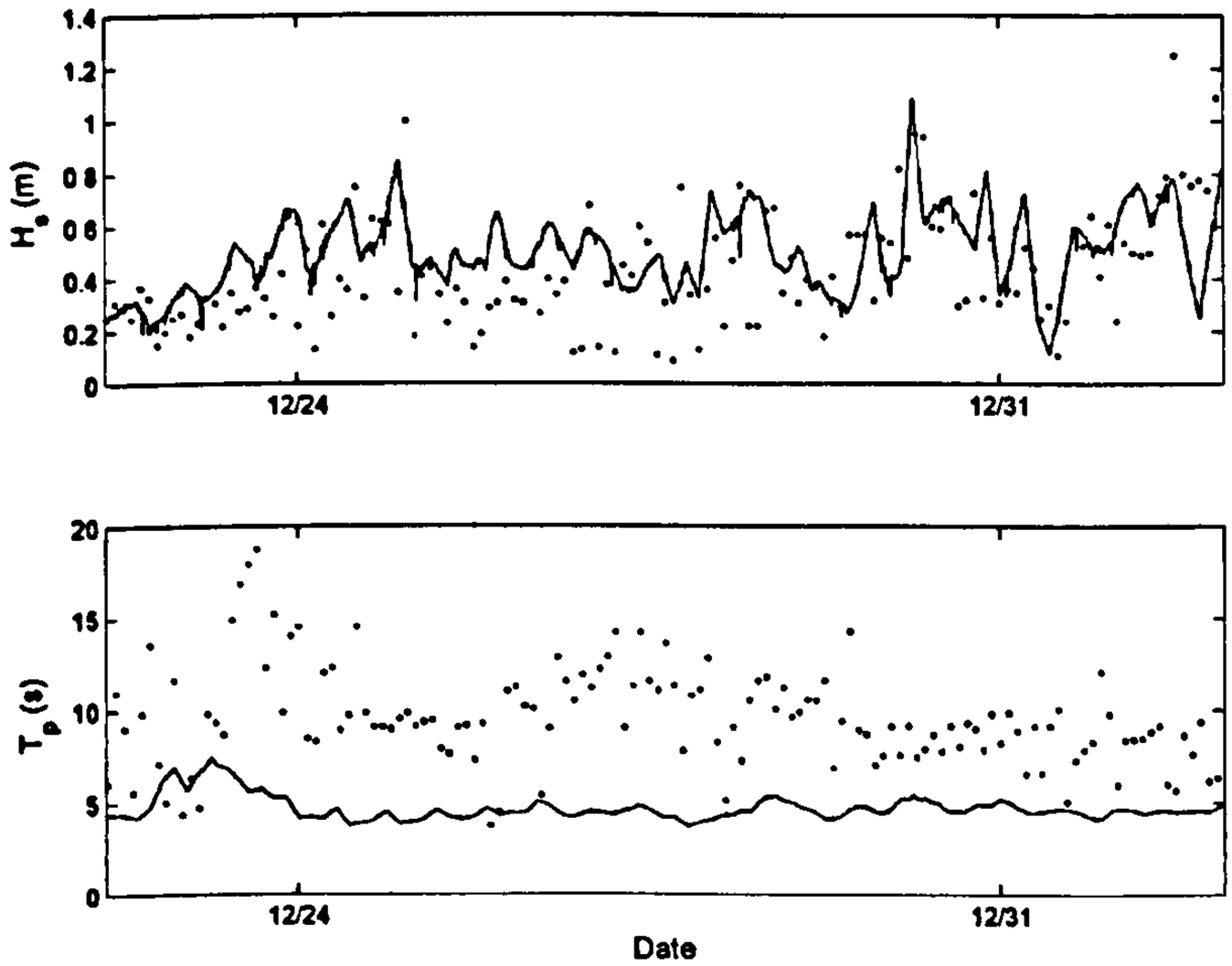

Figure 6.3.5: Comparison between modelled (o) and measured (-) wave heights and period for frame 4.

6.3.4 Morphological change

The model's capability to predict morphological change was tested by comparing modelled and measured data over two storm events. Storm event were used for two reasons: firstly morphological changes under low wave energy conditions are small and so comparison of response is harder and secondly because of computational time restrictions. Computational restraints meant modelling over long time periods wasn't feasible which meant the monthly GPS surveys were not suitable for model verification. Instead video derived pre- and post-storm intertidal surveys (Chapter 4.3.1) were used to compare model results against.

Two storms analysed in Chapter 4.3 were used for this test: storms A and E. To test the model against storm events, the bathymetry for the model grid was taken from the DGPS surveys prior to each storm. Since surveys were not conducted exactly before each storm the bathymetries used in the model are not exactly the same as the real world bathymetries measured by video. For both storms the lag time is about three weeks. Tidal boundary conditions were taken from the AWAC measured data at Horsey and Walcot. Wave data was taken from the Met Office model output point.

Both video derived and modelled bathymetric changes show similar patterns. The modelled change is slightly less than the measured change for storm A. The movement of the three tombolos is reasonably modelled for storm A, especially the south-easternmost tombolo. Changes in the bay areas of phase one are less well modelled, with the video suggesting general accretion and the model suggesting upper intertidal erosion and lower intertidal accretion. The modelled phase two change shows less defined patterns and so comparison with the video data is difficult, however the greater erosion in the transition embayment and accretion in the other embayments is modelled. The video and model data are more similar for storm E than storm A. There is little difference in magnitude and the patterns of change better represented. The overall upper intertidal erosion and lower

intertidal accretion is represented, as is the longshore definition in change over the phase two salients. The patterns of change over tombolos 6 and 7 are correctly predicted. The change over tombolo 8 is incorrectly predicted with the video showing accretion over the tombolo crest and the model predicting accretion.

It is not possible in this case to determine whether the difference between model and video are due to model architecture or difference in initial bathymetry. However, overall the predicted and modelled changes show similar patterns and magnitudes.

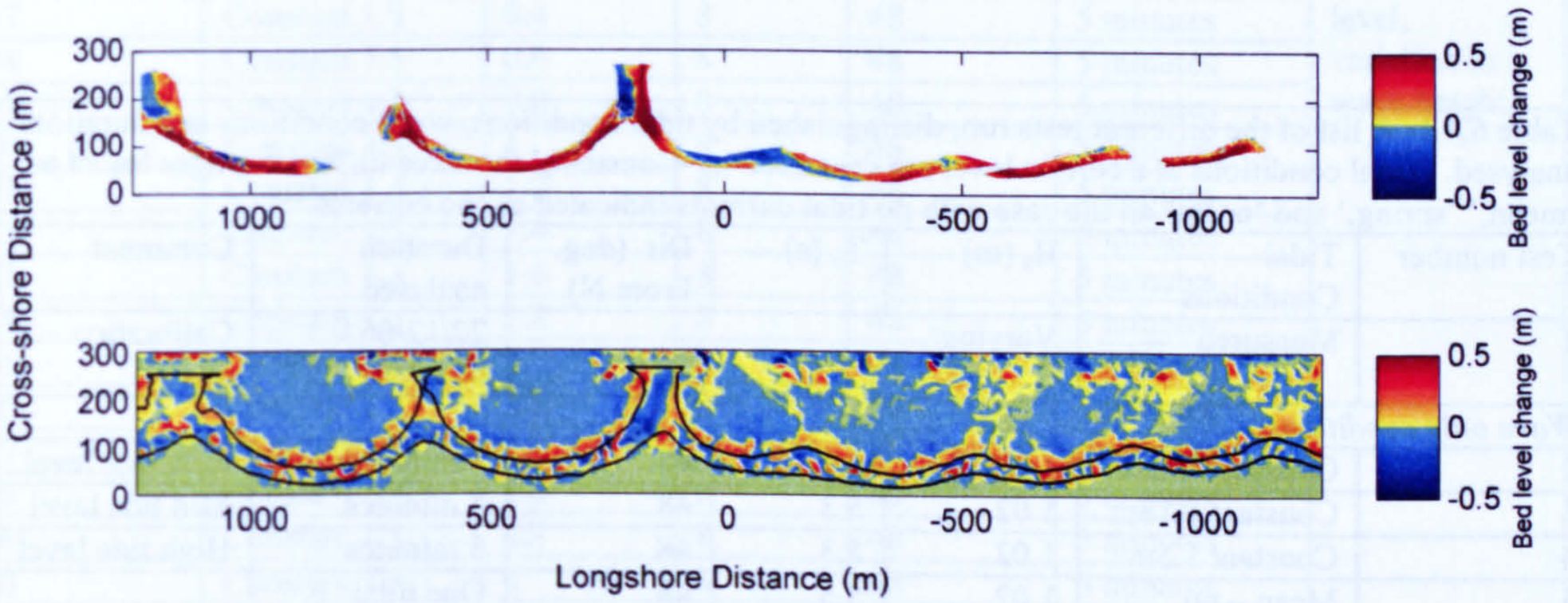

Figure 6.3.4: A comparison between a) video measured and b) model predicted changes over storm A. Black lines on the model results indicate the intertidal region.

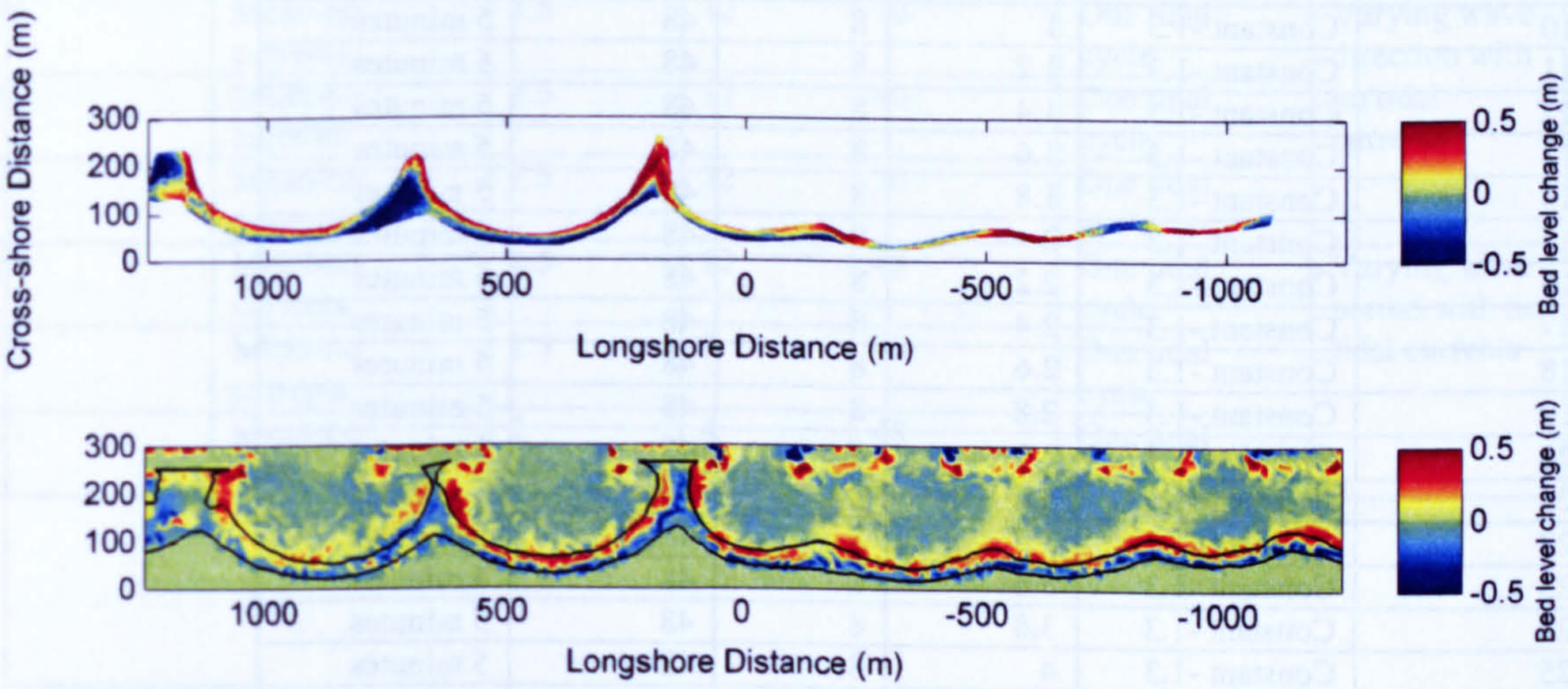

Figure 6.3.5: A comparison between a) video measured and b) model predicted changes over storm E. Black lines on the model results indicate the intertidal region.

6.4 Results

A variety of tests were run to elucidate wave and tidal forcing and the changes they effect, they are listed in Table 6.4.1. The tests can be split into three categories: waves, tidal currents and wave and tidal currents combined conditions. Only the most relevant results will be included in this chapter, plots for tests not included but still referred to will be included in Appendix A. Due to the number and complexity of results presented some discussion will accompany individual results where appropriate.

Table 6.4.1: A list of the different tests run, distinguished by tidal conditions, wave conditions and duration analysed. Tidal conditions at a certain level are described as 'Constant;' the three different ranges tested as 'mean,' 'spring,' and 'neap;' an the case with no tidal currents indicated as 'no currents.'

Test number	Tidal Conditions	H_s (m)	T_p (s)	Dir. (deg. From N)	Duration analysed	Comment
1	Measured	Varying			22/12/06 – 02/01/07	Calibration test
Wave only conditions						
2	Constant -1.3m	1.02	5.3	48	5 minutes	Low tide level
3	Constant 0.18m	1.02	5.3	48	5 minutes	Mid tide level
4	Constant 1.5m	1.02	5.3	48	5 minutes	High tide level
5	Mean – no currents	1.02	5.3	48	One tidal cycle	
6	Constant -1.3	0.2	8	48	5 minutes	Low tide level, variation in wave height
7	Constant -1.3	0.4	8	48	5 minutes	
8	Constant -1.3	0.6	8	48	5 minutes	
9	Constant -1.3	0.8	8	48	5 minutes	
10	Constant -1.3	1	8	48	5 minutes	
11	Constant -1.3	1.2	8	48	5 minutes	
12	Constant -1.3	1.4	8	48	5 minutes	
13	Constant -1.3	1.6	8	48	5 minutes	
14	Constant -1.3	1.8	8	48	5 minutes	
15	Constant -1.3	2	8	48	5 minutes	
16	Constant -1.3	2.2	8	48	5 minutes	
17	Constant -1.3	2.4	8	48	5 minutes	
18	Constant -1.3	2.6	8	48	5 minutes	
19	Constant -1.3	2.8	8	48	5 minutes	
20	Constant -1.3	3	8	48	5 minutes	
21	Constant -1.3	3.2	8	48	5 minutes	
22	Constant -1.3	3.4	8	48	5 minutes	
23	Constant -1.3	3.6	8	48	5 minutes	
24	Constant -1.3	3.8	8	48	5 minutes	
25	Constant -1.3	4	8	48	5 minutes	
26	Constant 0.18	0.2	8	48	5 minutes	Mid tide level, variation in wave height
27	Constant 0.18	0.4	8	48	5 minutes	
28	Constant 0.18	0.6	8	48	5 minutes	
29	Constant 0.18	0.8	8	48	5 minutes	
30	Constant 0.18	1	8	48	5 minutes	

31	Constant 0.18	1.2	8	48	5 minutes	Mid tide level, variation in wave height
32	Constant 0.18	1.4	8	48	5 minutes	
33	Constant 0.18	1.6	8	48	5 minutes	
34	Constant 0.18	1.8	8	48	5 minutes	
35	Constant 0.18	2	8	48	5 minutes	
36	Constant 0.18	2.2	8	48	5 minutes	
37	Constant 0.18	2.4	8	48	5 minutes	
38	Constant 0.18	2.6	8	48	5 minutes	
39	Constant 0.18	2.8	8	48	5 minutes	
40	Constant 0.18	3	8	48	5 minutes	
41	Constant 0.18	3.2	8	48	5 minutes	
42	Constant 0.18	3.4	8	48	5 minutes	
43	Constant 0.18	3.6	8	48	5 minutes	
44	Constant 0.18	3.8	8	48	5 minutes	
45	Constant 0.18	4	8	48	5 minutes	
46	Constant 1.5	0.2	8	48	5 minutes	High tide level, variation in wave height.
47	Constant 1.5	0.4	8	48	5 minutes	
48	Constant 1.5	0.6	8	48	5 minutes	
49	Constant 1.5	0.8	8	48	5 minutes	
50	Constant 1.5	1	8	48	5 minutes	
51	Constant 1.5	1.2	8	48	5 minutes	
52	Constant 1.5	1.4	8	48	5 minutes	
53	Constant 1.5	1.6	8	48	5 minutes	
54	Constant 1.5	1.8	8	48	5 minutes	
55	Constant 1.5	2	8	48	5 minutes	
56	Constant 1.5	2.2	8	48	5 minutes	
57	Constant 1.5	2.4	8	48	5 minutes	
58	Constant 1.5	2.6	8	48	5 minutes	
59	Constant 1.5	2.8	8	48	5 minutes	
60	Constant 1.5	3	8	48	5 minutes	
61	Constant 1.5	3.2	8	48	5 minutes	
62	Constant 1.5	3.4	8	48	5 minutes	
63	Constant 1.5	3.6	8	48	5 minutes	
64	Constant 1.5	3.8	8	48	5 minutes	
65	Constant 1.5	4	8	48	5 minutes	
66	Mean-no currents	1.5	12	10	One tidal cycle	Varying wave direction with no tidal currents
67	Mean-no currents	1.5	12	40	One tidal cycle	
68	Mean-no currents	1.5	12	70	One tidal cycle	
69	Mean-no currents	1.5	12	48	One tidal cycle	Varying wave period with no tidal currents
70	Mean-no currents	1.5	3	48	One tidal cycle	
71	Mean-no currents	2	4	48	One tidal cycle	

Tide Only Conditions						
72	Neap	0.1	6	48	One tidal cycle	Tidal range variation with wave stirring
73	Mean	0.1	6	48	One tidal cycle	
74	Spring	0.1	6	48	One tidal cycle	
Waves and tides combined						
75	Neap	1.02	5.3	48	One tidal cycle	Mean wave conditions for different tidal ranges
76	Mean	1.02	5.3	48	One tidal cycle	
77	Spring	1.02	5.3	48	One tidal cycle	
78	Neap	2	5.3	48	One tidal cycle	RTR=0.5 test
79	Mean	2.3	6	345	One tidal cycle	NNW storm
80	Mean	2.46	6	10	One tidal cycle	NNE storm
81	Mean	2.45	6	49	One tidal cycle	NE storm
82	Mean	2.44	6	75	One tidal cycle	ENE storm
83	Mean	2.2	6.5	115	One tidal cycle	ESE storm
84	Surge	2.46	6	10	One tidal cycle	Surge and N storm
85	Mean	2.46	6	10	7 tidal cycles	Long duration storms from N & S.
86	Mean	2.44	6	75	7 tidal cycles	
87	Mean	0.1	6	48	One tidal cycle	Post long N storm starting bathymetry
88	Mean	1.03	5.3	48	One tidal cycle	

6.4.1 Wave only conditions

The effect of water level

Mean wave conditions (calculated from 7yrs of met office hind-cast data) were run at fixed water levels to investigate water elevation forced variation of wave induced current patterns (Figure 6.4.1). Water levels of -1.3m, 0.18m and 1.5m ODN were tested. Mean wave conditions at the offshore boundary were H_s=1.02m, T_p=5.3s and wave direction =48° (approx shore normal). For all tidal elevations the maximum current speed is ~0.4ms^{-1} and the average value is less than 0.1ms^{-1}. The most striking observation is the effect of high tide water levels on phase two where wave transmission over the submerged breakwaters causes flow reversal and flow intensification. Second, is the lack of the typically expected double gyre system in many of the embayments and third is the non-similarity between same phase embayments caused by interaction between embayments and differing bathymetric conditions in the different embayments.

Figure 6.4.1 shows current speed (shading) and direction (arrows) for the scheme at different tidal levels. At high tide (Figure 6.4.1A), phase two shows similar patterns for all embayments. Overtopping of the submerged breakwaters leads to mass transport of water over the breakwater crest and the current circulation forms a double gyre in each embayment directed onshore over the breakwater and offshore through the gap. In phase one, bay A shows a double gyre, of reverse direction to phase two, while the other embayments show undefined circulation.

At mid tide, bay A displays a double gyre system, although the dominant current is from north to south and into embayment B. The bay B circulation pattern is a single gyre with the current at the shore directed from north to south. The other embayments show weak circulation patterns apart from bay H where the lower crest level of breakwater 13

leads to mass transport of water over the breakwater and a single gyre with return flow through the gap.

At low tide (Figure 6.4.1C), all the bays show different circulation patterns. In bay A there is a single gyre, flowing north to south at the shoreline. The recirculation (S-N) is weaker and occurs outside the embayment. Bay B shows a similar pattern but the recirculation is inside the embayment. Bay C shows a less defined circulation. The transition embayment (bay D) and bay E display double gyre circulations. Bay F shows a single gyre in the northern two thirds of the embayment with the southward flow passing into bay G rather than forming another gyre. This flow continues from north to south and then offshore through the breakwater gap in the offshore portion of the embayment. Inshore there is a small weak double gyre circulation. The bay H circulation is from south to north.

The difference in circulation patterns at different tidal levels is important in the consideration of storm induced change. If the peak of the storm occurs at high or low tide the morphological response in phase two is likely to be different. The circulation patterns in phase one are more similar throughout the tide, although overtopping of the emergent breakwaters is not included in the model which would have an effect at high tide, similar to the reversed circulation at high tide in phase two. The difference in circulation patterns is due partly to the initial bathymetry which varies between embayments and partly due to interaction of currents across the sheltered regions. Often it is assumed that for a long array of breakwaters each embayment has the same circulation. This is not the case at Sea Palling and helps explain the small differences in embayment responses for embayments of the same phase. Since this test considers shore normal waves without tidal currents (a very simple scenario), it is relevant to generalise beyond Sea Palling and suggest that this would occur for all systems of detached breakwaters where the breakwaters are sufficiently short to prevent currents reaching zero in the breakwater lee.

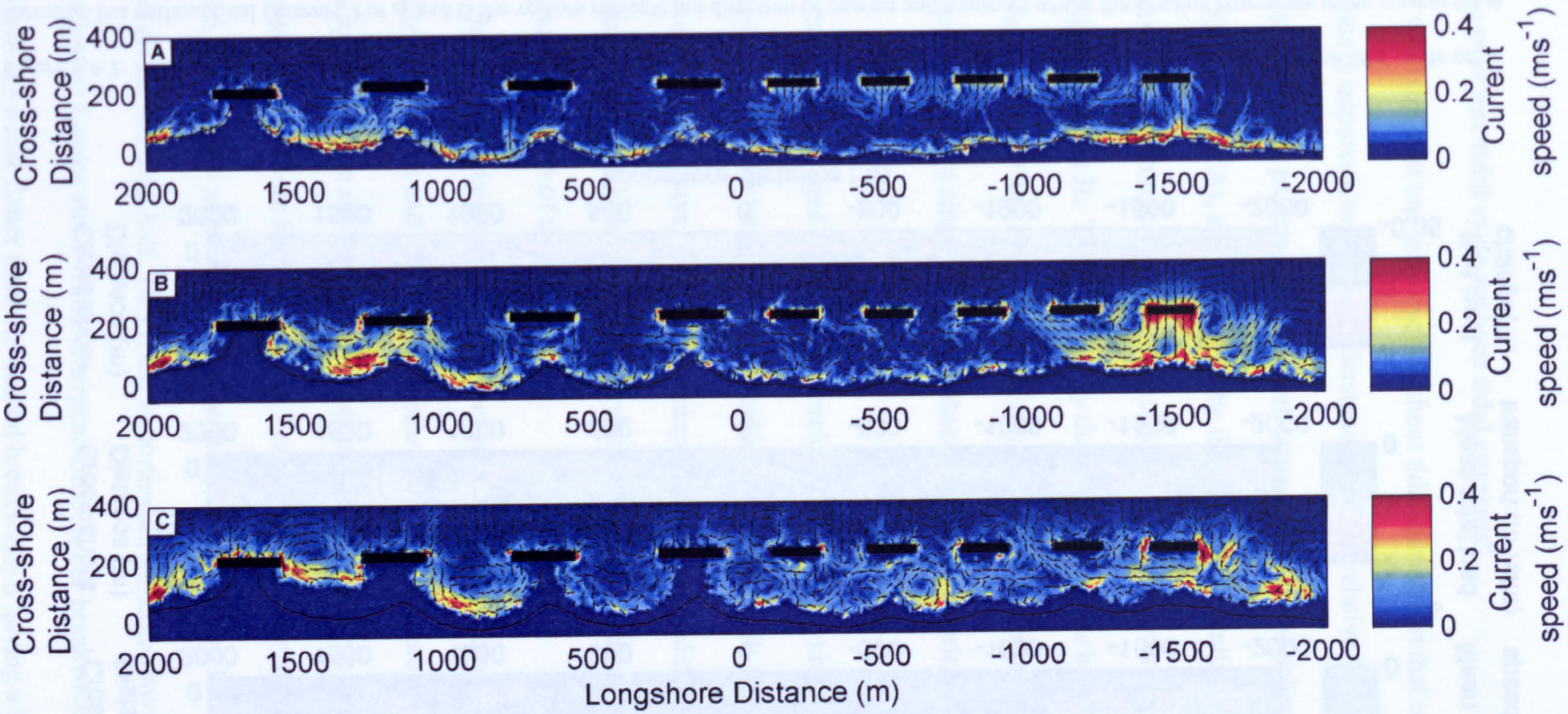

Figure 6.4.1: Wave induced current patterns for A) high tide, B) mid tide and C) low tide, with mean wave conditions.

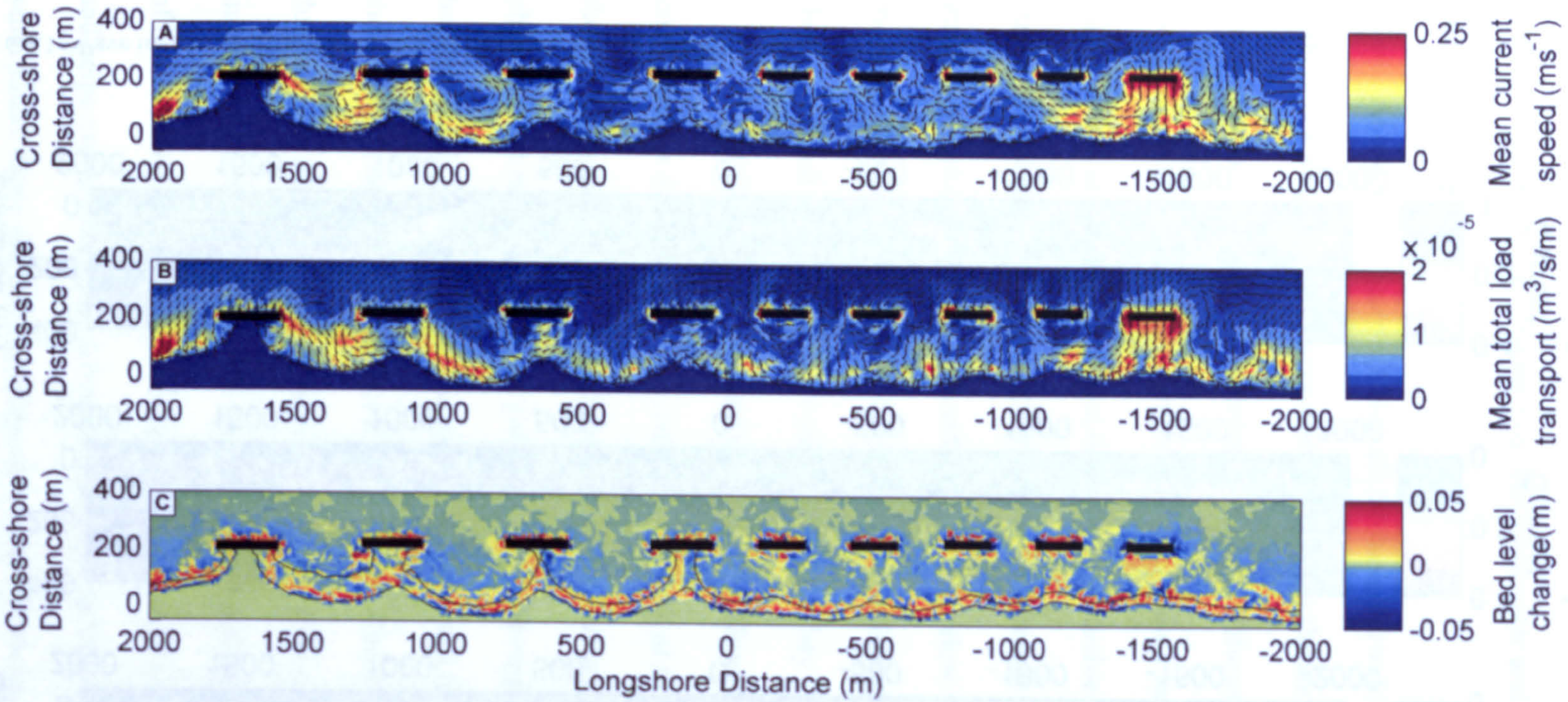

Figure 6.4.2: Plots of A) mean current speed, B) mean total load transport and C) bed level change for mean wave conditions run over one tidal cycle of elevation but without tidal currents. For A and B the vectors indicate net direction of current and transport whilst the shading represents mean current /total load transport values. The plot in C shows total change over the tidal cycle. The two contours in C indicate high and low tide contours. Only the high tide contour is displayed in A and B

Mean wave conditions over one tidal cycle without tidal currents

Mean wave conditions were run over one tidal cycle without tidal currents so that only elevation varied. This test is important to further understanding of the relative importance between tides and waves on current patterns and sediment transport about the scheme.

Mean current patterns (Figure 6.4.2 A), averaged over the tidal cycle, are similar to the mid tide case in the previous section. Strongest currents occur in bays A and B near the shoreline and in the end embayment H. This is probably due to greater wave breaking in the shallower bays A and B and, for bay H, due to mass transport over the lower crest level of breakwater 13. Phase one displays single gyres and phase two shows a variety of circulation patterns.

The total load transport averaged over the tidal cycle (Figure 6.4.2 B) is generally onshore directed. In bays A and B the transport is directed southward as well, due to the strong north-south currents in these bays. Total load transport converges and decreases in strength behind the centre of the breakwaters. For breakwaters 7 and 8 the region of convergence is to the north of centre of the breakwaters.

Net bed level changes over the tidal cycle show erosion on the bay floors, accretion through most of the intertidal region and some erosion near the high tide contour (Figure 6.4.2 C). Material is deposited in the sheltered regions behind the tombolos; in phase two there is little structure to this accretion; for breakwaters 7 and 8 in phase one there is more structure. For these two breakwaters accretion is concentrated on the northern half of the tombolos with erosion on the southern half. This leads to northward tombolo movement. This pattern is not evident on breakwater 5 (fully emergent tombolo) or breakwater 6. It is thought that this is due to the wider flatter tombolo behind breakwater 6 having a less defined tombolo crest.

The effect of wave height

To determine the effect of wave height on wave driven circulation, a test was run at constant water levels corresponding to mean sea level, low tide and high tide with shore normally incident wave with a period of 8 seconds and wave height varying between 0.2m and 4m in increments of 0.2m. Mean current speeds over all embayments in the breakwater protected areas were calculated for each wave height to give representation of the potential of wave driven currents to transport sediment. Current speed increases with wave height linearly until a certain point for each tidal level where the current speed tends towards a maximum value (Figure 6.4.3). The maximum value is approximately 0.17ms^{-1} at low, 0.28ms^{-1} at mid and 0.3ms^{-1} at high tide. The point at which wave height and current speed stop scaling linearly is the point at which significant dissipation of wave energy (wave height reduction) occurs outside the breakwater zone.

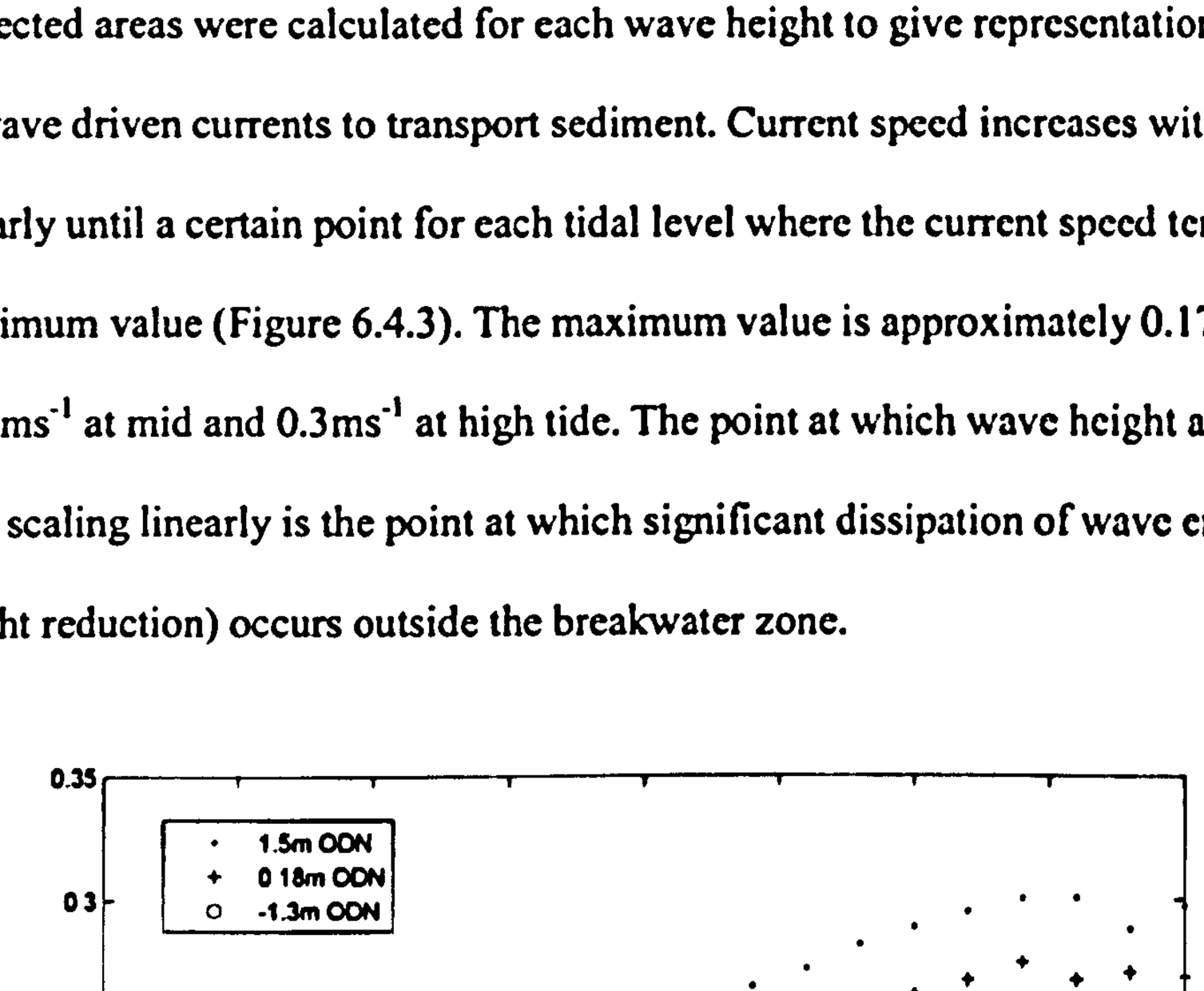

Figure 6.4.3: Mean current speed inside the embayments against wave height. Three tidal levels are displayed: 1.3m ODN (low tide), 0.18m ODN (mid tide), 1.5m ODN (high tide).

The low tide test shows the current speed levelling off lower than for the mid and high tide tests, this is because there is greater wave dissipation outside the embayments due to the shallower water depths. For all tests, current speeds have approached their maximum by a wave height of H_s=2.5m. A similar pattern is shown in the particle velocities at the bed (see Appendix A, Figure A1). The bed particle velocities are responsible for the entrainment of sediment and hence the capacity for sediment entrainment and transport reaches a maximum at an offshore wave height of 2.5m.

Circulation patterns vary depending on wave height. A description of the different current patterns for the mid tide test are listed in Table 6.4.2. Each embayment and wave height is described. The description 'double' describes a circulation whereby there is the expected double gyre circulation- onshore in the embayment centre, divergent at the shoreline and offshore in the sheltered region. 'Single' refers to a single gyre with the direction of flow at the shoreline noted in brackets (e.g. N-S refers to southward flow). 'Undefined' denotes a weak and undefined flow structure. 'Multiple' means that there are several small gyres present around the embayment shorelines. For the more central embayments (C-E) as wave height increases the flow pattern goes from undefined to multiple gyres to a double gyre system. Bays A and B start with double gyres with the southern gyre dominating and become single gyres as the wave height increases. For Bay A this becomes a North to South flow when H_s=1.2m. Bay H consistently has a single gyre (onshore over structure, offshore in gap) forced by the lower breakwater crest. Not all of the onshore flow returns through the gap and there is an additional northward flow into bay F that increases speed with increasing wave height. Circulation patterns remain similar for H_s>2m. Since current patterns remain similar for all wave heights over 2m and velocities similar for all wave heights over 2.5m, it is postulated that for all storm wave heights over 2.5m, unless surge conditions occur, there will be little difference in morphological change.

Table 6.4.2: A description of circulation patterns for each embayment as significant wave height increases.

H_s	A	B	C	D	E	F	G	H
0.2	Double (south bigger)	Double (south bigger)	undefined	Undefined	Undefined	undefined	undefined	Single (S-N)
0.4	Double (south bigger)	Double (south bigger)	undefined	Undefined	undefined	undefined	Weak double	Single (S-N)
0.6	Double (south much bigger)	Single(N-S) plus v. small (S-N)	multiple	Multiple	Multiple	multiple	Double(plus offshore N flow)	Single (S-N)
0.8	Single(N-S) plus v. small (S-N)	Single(N-S) plus v. small (S-N)	multiple	Multiple	Double	double	Double(plus offshore N flow)	Single (S-N) plus S-N flow
1	Single(N-S) plus v. small (S-N)	Single(N-S) plus v. small (S-N)	multiple	double	Double	Single northern half undefined southern half	Offshore N flow	Single (S-N) plus strong S-N flow
1.2	N-S flow plus v. small single (S-N)	Single(N-S) plus v. small (S-N)	multiple	double	Double	Undefined S-N flow	S-N flow plus small gyre at shoreline	Single (S-N) plus strong S-N flow
1.4	N-S flow plus v. small single (S-N)	Single(N-S) plus v. small (S-N)	multiple	double	Double	Undefined S-N flow	S-N flow plus gyre at shoreline	Single (S-N) plus strong S-N flow
1.6	N-S flow plus v. small single (S-N)	Single(N-S) plus v. small (S-N)	Double (south larger)	double	Double (south much larger)	S-N flow plus gyre at shoreline	S-N flow plus gyre at shoreline	Single (S-N) plus strong S-N flow
1.8	N-S flow plus v. small single (S-N)	Single(N-S) plus v. small (S-N)	Double (south larger)	double	Double	double	S-N flow plus gyres at shoreline	Single (S-N) plus strong S-N flow
2	N-S flow plus v. small single (S-N)	Single(N-S) plus v. small (S-N)	double	double	Double	double	S-N flow plus gyres at shoreline	Single (S-N) plus strong S-N flow
2.2	N-S flow plus v. small single (S-N)	Single(N-S) plus v. small (S-N)	double	double	Double	double	S-N flow plus gyres at shoreline	Single (S-N) plus strong S-N flow

Table 6.4.2(continued): A description of circulation patterns for each embayment as significant wave height increases.								
2.4	N-S flow plus v. small single (S-N)	Single(N-S) plus v. small (S-N)	double	double	Double	double	S-N flow plus gyres at shoreline	Single (S-N) plus strong S-N flow
2.6	N-S flow plus v. small single (S-N)	Single(N-S) plus v. small (S-N)	double	double	Double	double	S-N flow plus gyres at shoreline	Single (S-N) plus strong S-N flow
2.8	N-S flow plus v. small single (S-N)	Single(N-S) plus v. small (S-N)	double	double	Double	double	S-N flow plus gyres at shoreline	Single (S-N) plus strong S-N flow
3	N-S flow plus v. small single (S-N)	Single(N-S) plus v. small (S-N)	double	double	Double	double	S-N flow plus gyres at shoreline	Single (S-N) plus strong S-N flow
3.2	N-S flow plus v. small single (S-N)	Single(N-S) plus v. small (S-N)	double	double	Double	double	S-N flow plus gyres at shoreline	Single (S-N) plus strong S-N flow
3.4	N-S flow plus v. small single (S-N)	Single(N-S) plus v. small (S-N)	double	double	Double	double	S-N flow plus gyres at shoreline	Single (S-N) plus strong S-N flow
3.6	N-S flow plus v. small single (S-N)	Single(N-S) plus v. small (S-N)	double	double	Double	double	S-N flow plus gyres at shoreline	Single (S-N) plus strong S-N flow
3.8	N-S flow plus v. small single (S-N)	Single(N-S) plus v. small (S-N)	double	double	Double	double	S-N flow plus gyres at shoreline	Single (S-N) plus strong S-N flow
4	N-S flow plus v. small single (S-N)	Single(N-S) plus v. small (S-N)	double	double	Double	double	S-N flow plus gyres at shoreline	Single (S-N) plus strong S-N flow

Wave direction

To test the effect of wave direction, tests were run with wave heights of H_s = 1.5m and periods of T_m=12 seconds for three wave directions: North (10°); North East (40°) and East (70°). Angles of incidence were determined from the most prevalent wave direction for each compass sector. Tests were run over one tidal cycle keeping tidal currents as zero so that only water level variation was considered.

Figure 6.4.4 shows the patterns of wave incidence for the different directions. The obliquely incident waves move the area of maximum wave penetration from the embayment centres to the down drift embayment flanks. Less wave energy penetrates the embayments for the obliquely incident waves due to the smaller effective gap lengths. The effective gap length is the distance between breakwaters perpendicular to the wave crests, as the waves become more oblique this length reduces. Also observable is the spreading of wave energy into the sheltered regions caused by diffraction and refraction, the difference between sheltered and unsheltered regions is greater for phase one than for phase two. For all three directions there is less wave energy transmitted into the phase two bays than the phase one bays. Differing angles of wave approach cause differing circulation patterns and bed level changes.

Current patterns (Figure 6.4.5) and patterns of total load transport (Figure 6.4.6) are similar although the total load transport patterns are directed in a more onshore direction over the bay floors (onshore transport via wave shoaling) and offshore in the upper intertidal. For waves incident from the north both current and total load transport is directed in a north to south direction through the scheme. Flow intensification over the tombolo and salient crests leads to greater sediment transport in a north-south direction over these features. For waves incident from the south, the phase two current and total load transport patterns are similarly linear but opposite in direction to the pattern for waves

incident from the north. The linearity of the flow is greater for waves incident from the south due to current generation caused by mass transport of water over the lower end breakwater. Phase one displays non-similar patterns of both current and total load transport. Rather than a through flow of current/total load transport, each embayment displays a single gyre with current/total load direction from north to south near the shoreline. This is most evident in bays A and B. There is also current flow and sediment transport in a south-north direction over the tombolos. Since the angle from shore normal is equal for the oblique waves from different sides, this non-similarity must be induced by bathymetric controls. The mean embayment morphology is slightly asymmetric due to the prevalence of waves from the north and it is this difference which forces the difference between linear flow and gyres. The shore normally incident waves produce current patterns as described in Table 6.4.1. The sediment transport patterns largely follow the current patterns apart from the northern portion of phase two where the sediment transport follows a better defined double gyre system than is shown in the current patterns

Bed level changes for the three wave directions are shown in figure 6.4.7. Similar magnitudes of change are observed for all wave directions: maximum changes over one tidal cycle approach 0.2m All directions cause erosion of the upper intertidal and accretion in the lower intertidal. Material is eroded from the bay floors and there is accretion in the sheltered regions behind the breakwaters. The distribution of the deposited material depends upon the wave direction, which alters the area of wave sheltering. Northerly incident waves lead to accretion on the south-eastern side of the breakwaters and easterly incident waves lead to accretion on the north-western side. Waves incident from shore normal lead to accretion directly behind the breakwaters and some erosion of the crests of the phase one tombolos. Similar patterns of response have been observed in the video derived storm surveys (Chapter 4.2.).

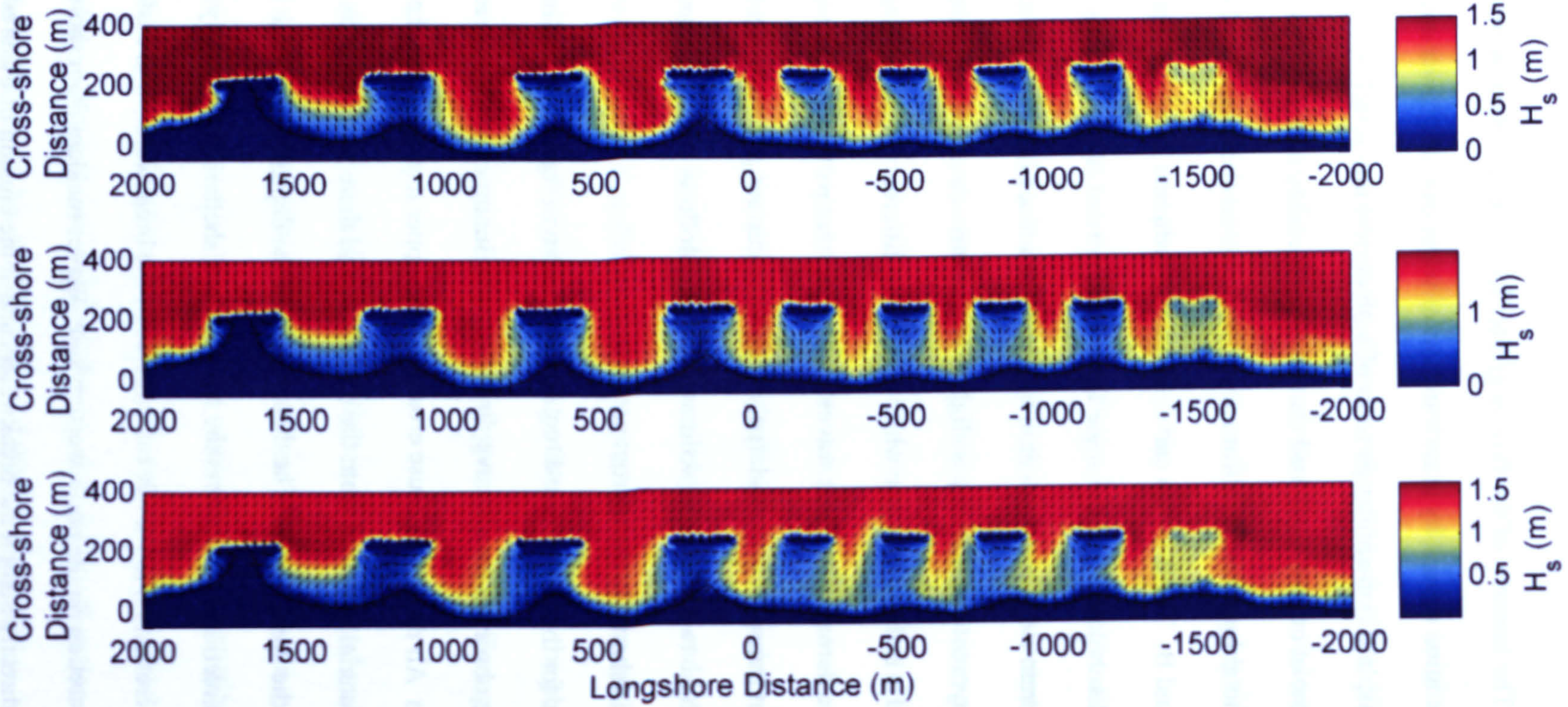

Figure 6.4.4: Patterns of wave incidence for the three different wave directions. a) Northerly incident waves; b) shore normally incident and c) easterly incident waves

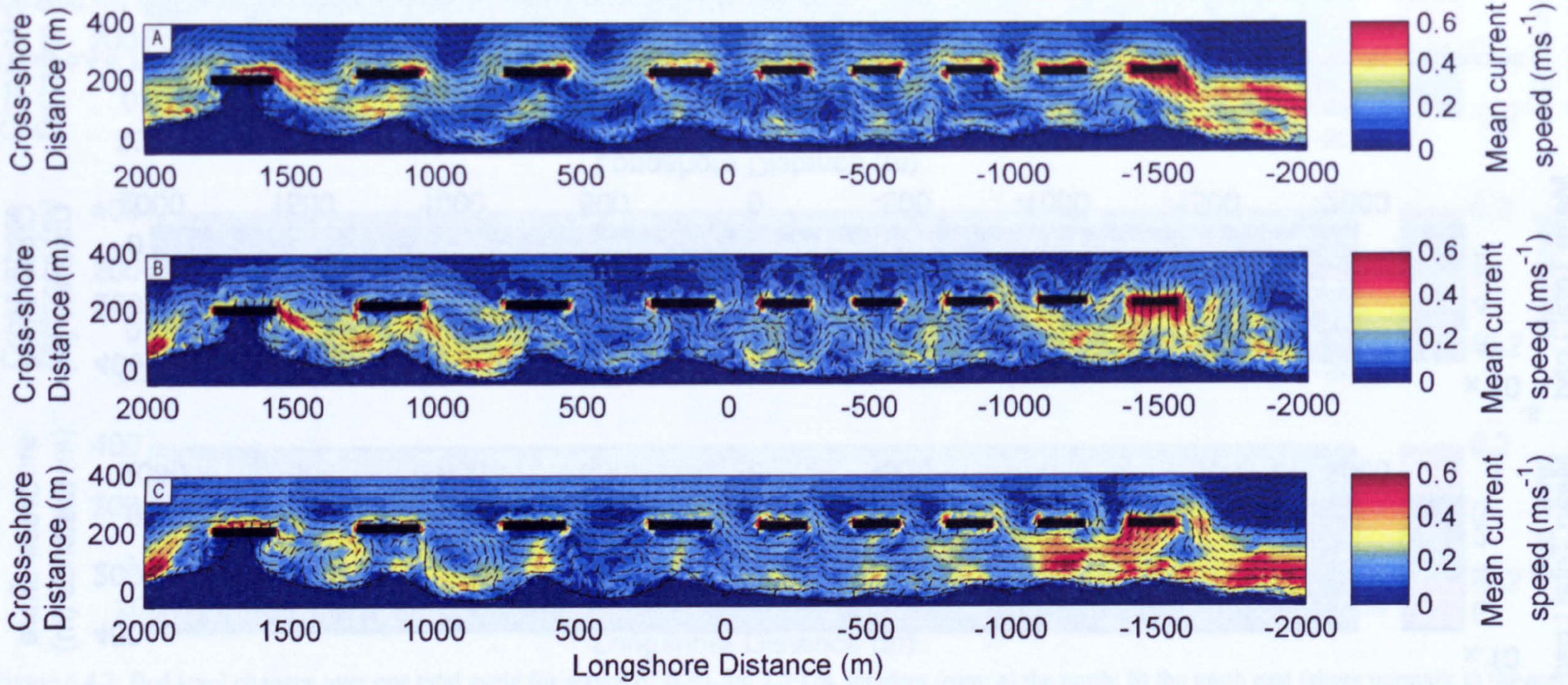

Figure 6.4.5: Current patterns for waves incident from a) the north, b) the north east and c) the east over one tidal cycle (without tidally induced currents).

The black arrows indicate mean current direction and the shading indicates mean current speed.

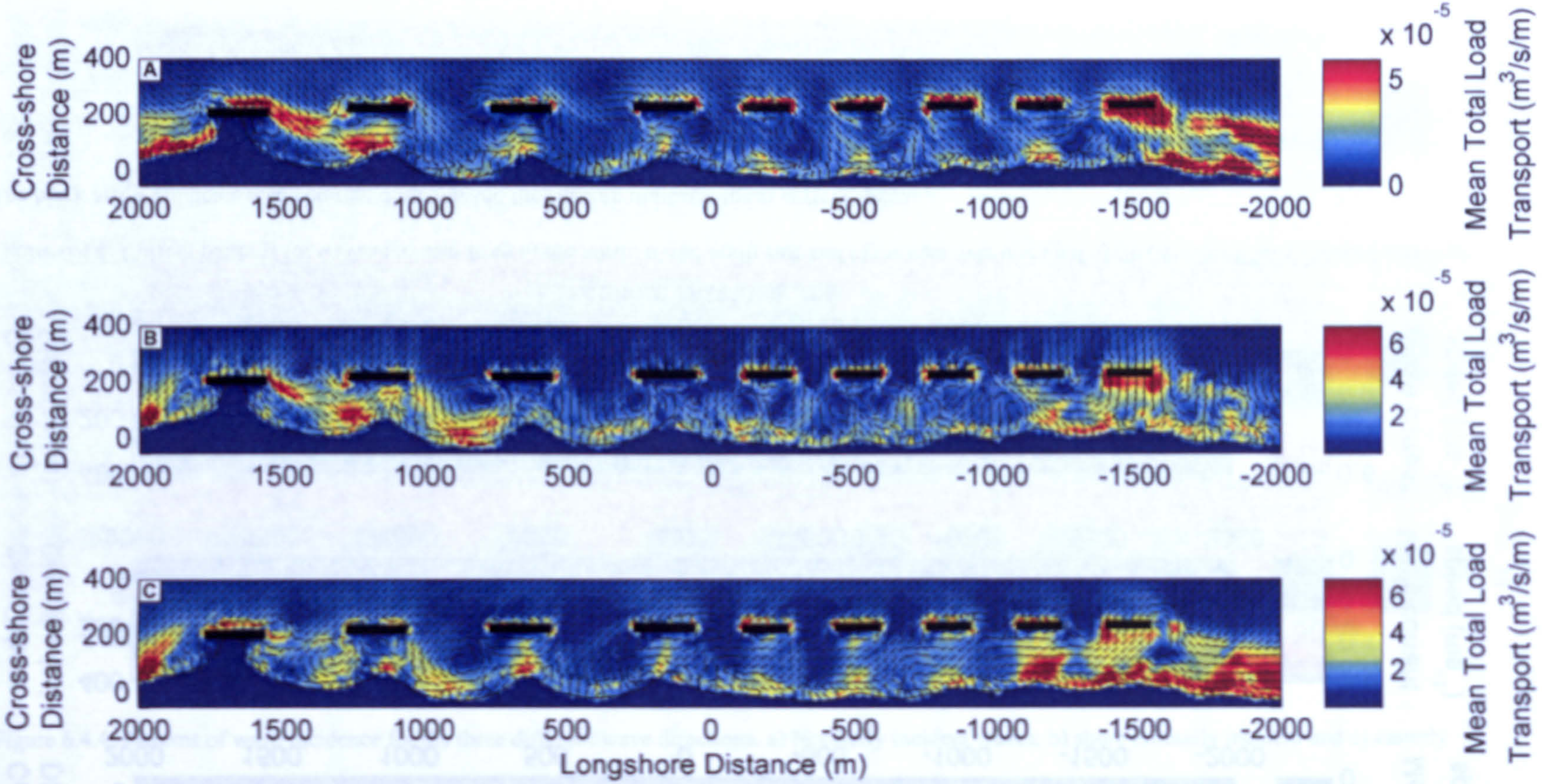

Figure 6.4.6: Patterns of total load transport for waves incident from A) the north; B) the north east; and C) the East. Vectors indicate the net direction of transport and shading the magnitude of mean transport over the tidal elevation cycle.

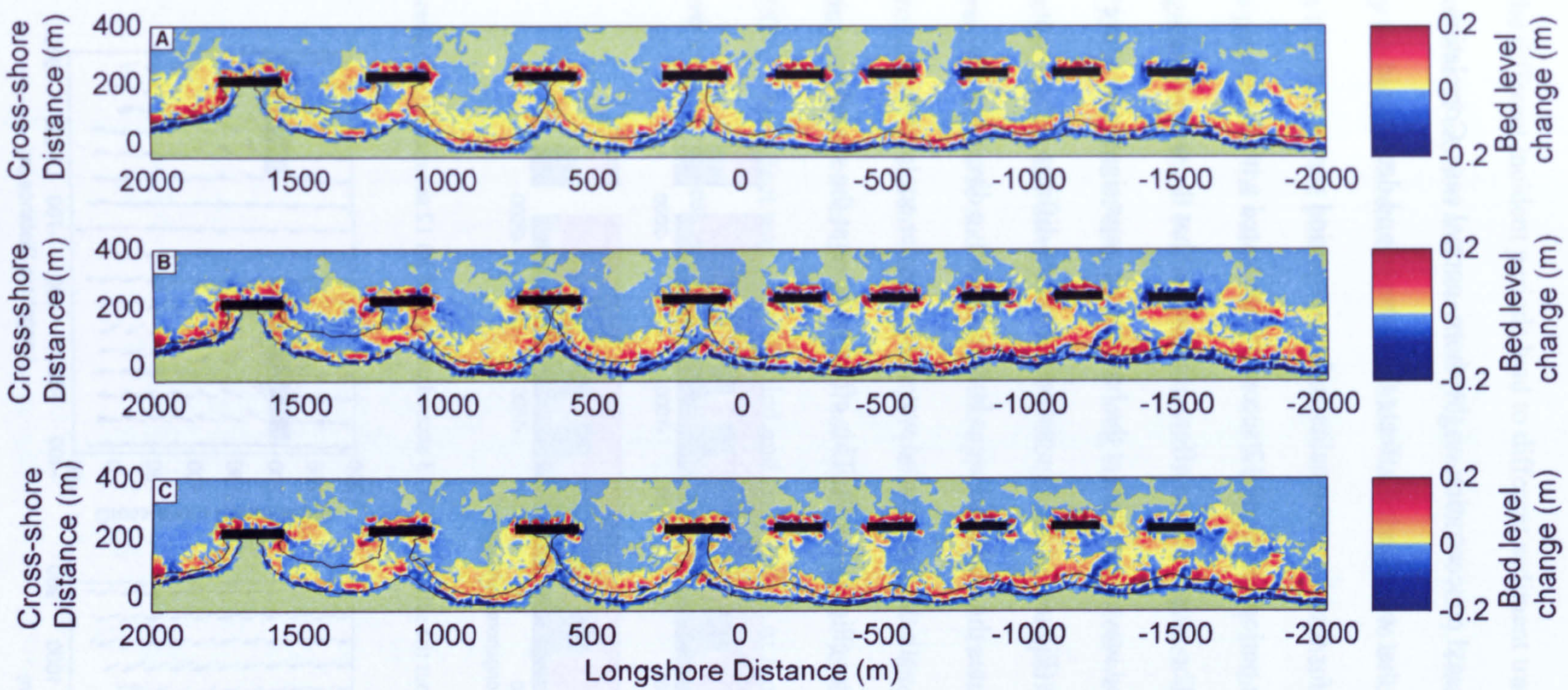

Figure 6.4.7: Bed level changes over one tidal cycle for waves of H_s=1.5m T_p=12s, incident from: a) the north; b) the north east (shore normal); c) the east.

Wave Period

The effect of period was investigated concentrating on the shore- normal case. Correlation analysis (Chapter 4.4) suggested that wave period affects the increase and decrease in amplitude of shoreline sinuosity for the phase two salients. Longer period waves were shown to reduce sinuosity. Wave periods of 3 and 12 seconds were tested with a wave height at the boundary of 1.5m. The most obvious effect of period is that the wave height decays rapidly for the short period waves and thus at the breakwater gaps significant wave height is 0.6m compared to 1.5m (Figure 6.4.8). Longer period waves diffract and refract more and so wave energy penetrates the sheltered areas better. The wave directions are different in the sheltered regions with the long period waves at a greater angle to shore normal than the short period waves (Figure 6.4.9). This effect reduces at the shoreline.

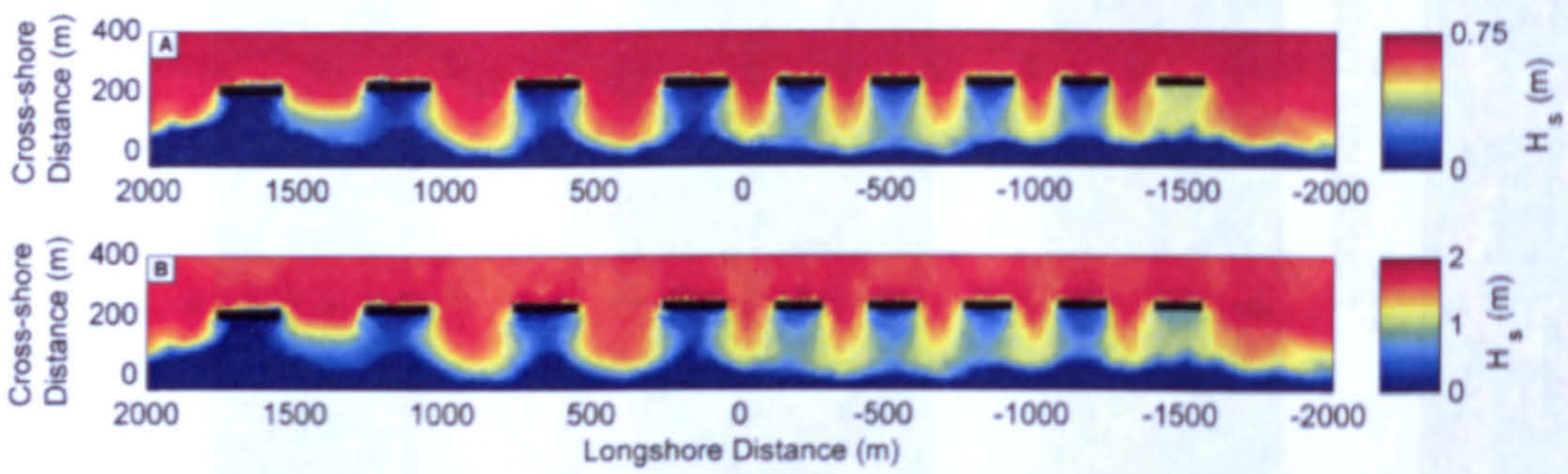

Figure 6.4.8: Wave height variation about the scheme for A) 3 second period and B) 12 second period waves.

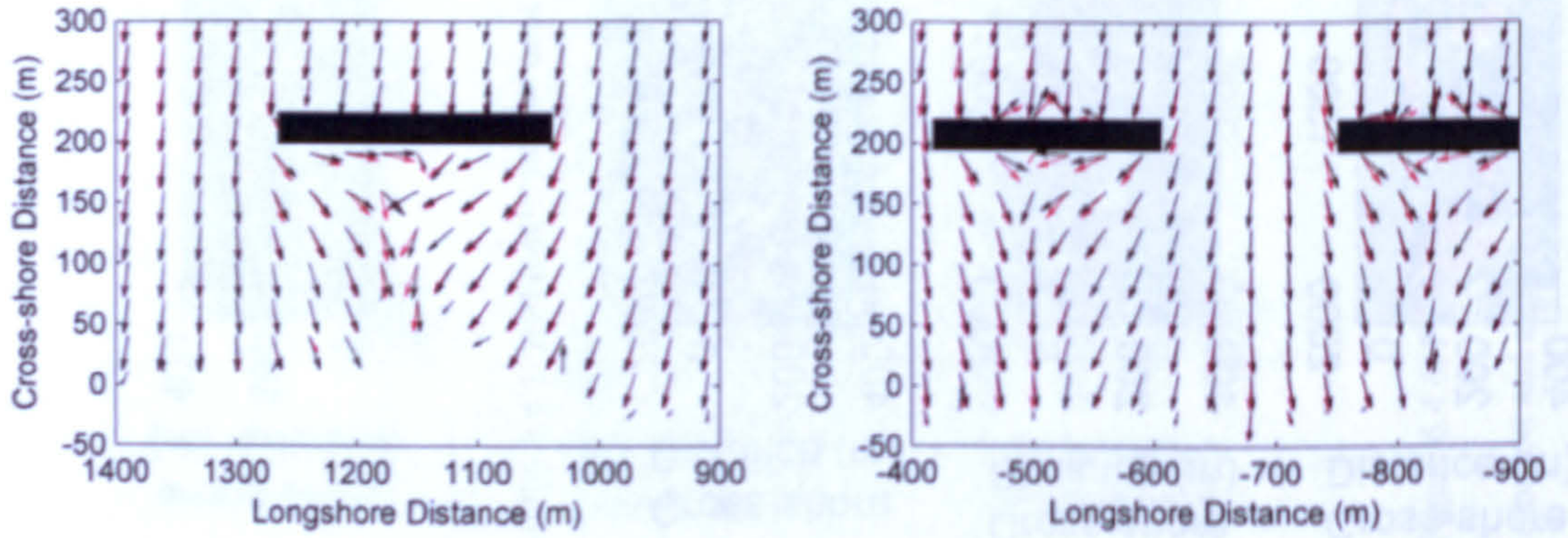

Figure 6.4.9 : Wave direction vectors around breakwaters in phase one (a) and phase two (b), for the 3s period (red) and the 12s period (black). Note the increased refraction/diffraction for longer period waves

The different incident periods lead to different sediment transport pathways and different patterns of erosion and accretion (Figure 6.4.10A &B). These differences are forced largely by the local differences in the shoaled wave height. No evidence of the increase or decrease in sinuosity of the phase two salients is observed. Another test was run with H_s=2 and T_p=4 to produce similar values for H_s at the breakwater gap to the longer period test, however again there was no evidence for the increase and decrease in salient sinuosity (Figure 6.4.10 C). The patterns of change for the long and short period waves of similar wave height behind the breakwaters were alike although the shorter period waves produces change of greater magnitude and erosion of the upper intertidal. It was postulated (Chapter 4) that the erosion of the salient horns by longer period waves was due to the greater transmission of longer period waves through the breakwater compared to short period waves (Fairley *et al.*, 2009). This effect was not modelled and so its effect or the effects of any other overtopping processes were not taken into account in these model tests.

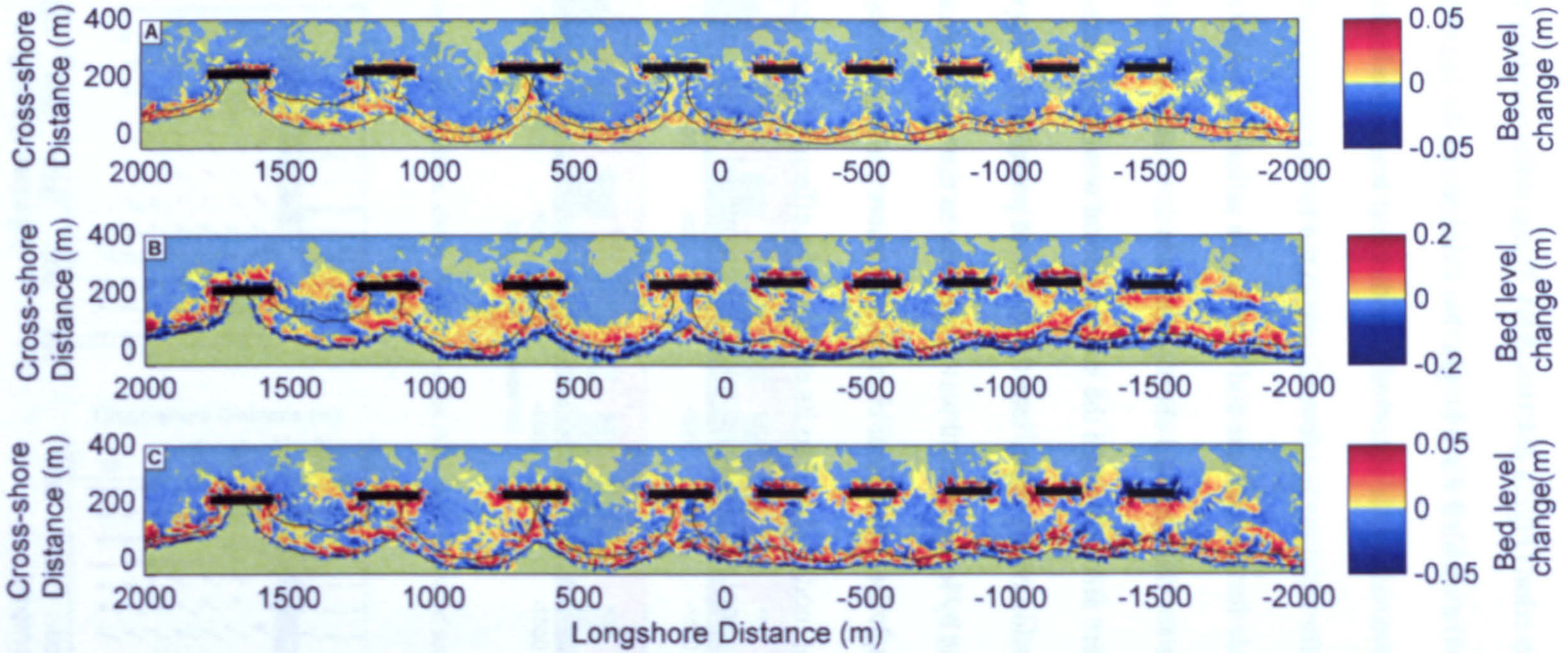

Figure 6.4.10: Patterns of bed level change for A) H_s=1.5, T_p=12; B) H_s=1.5, T_p=3; C) H_s=2m, T_p=4. Shading indicates magnitude of change with blue colours indicative of erosion and red colours accretion. The two contours demarcate the intertidal region.

6.4.2 Tidal currents

In the next section the effect of tidal currents with minimal wave stirring will be investigated. Wave stirring is included for two reasons: firstly assuming absolutely no waves is not realistic; secondly ,a pure current simulation in MIKE21 uses a different approach to sediment transport modelling and hence makes comparison of results difficult.

The wave forcing used in these experiments was H_s=0.1m; T_p=6; *dir*=40°. From Section 6.2.1 it can be seen that waves of this magnitude would generate mean currents of under 0.02ms^{-1} and little circulation patterns in most of the embayments thus tidal currents will dominate sediment transport processes. Three tests were run using a characteristic mean, spring and neap tide. Current speed increases linearly with tidal range can be seen in the measured data from Horsey (Figure 6.4.11).

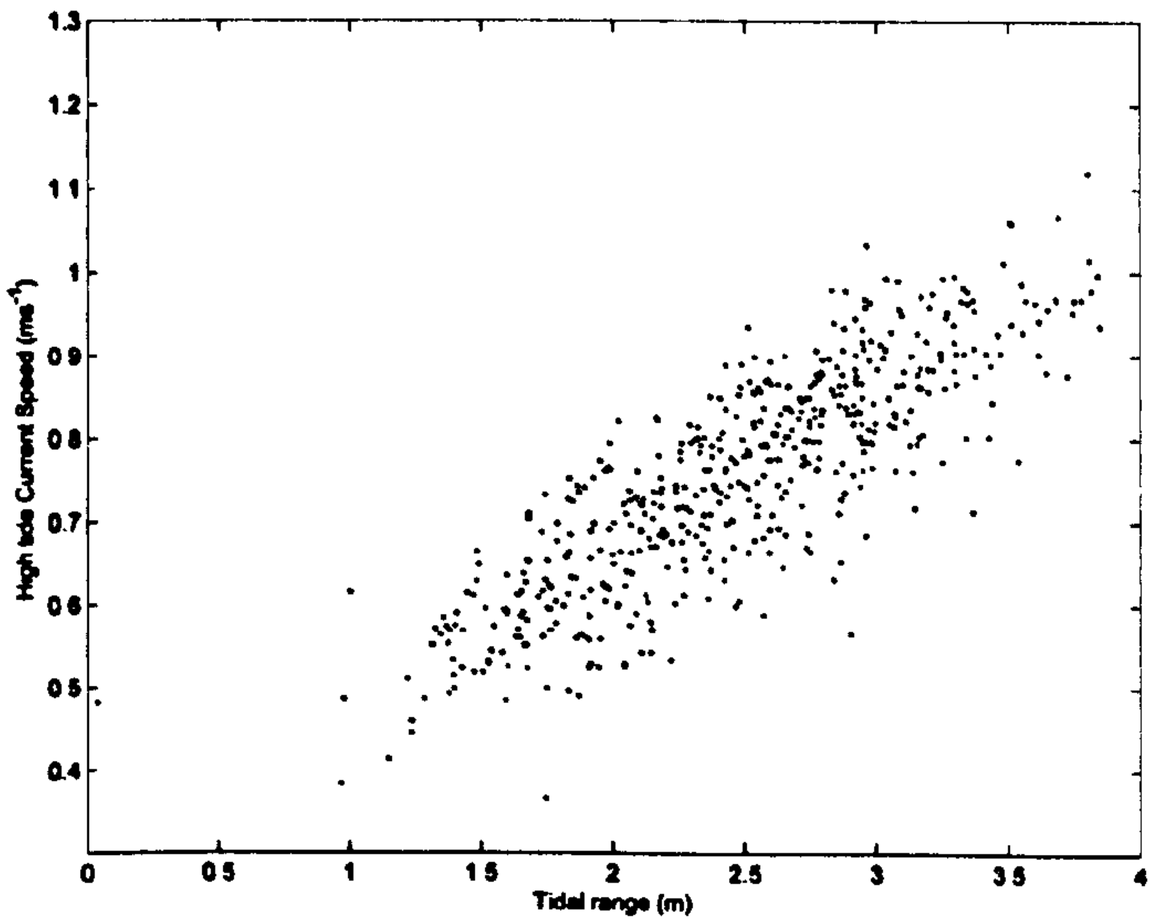

Figure 6.4.11: Current speed at high tide against tidal range measured at Horsey. The linear scaling of current speed with tidal range can clearly be observed.

Mean tide.

Figure 6.4.12 shows current speed and direction for 4 stages of the tide: high, mid tide falling, low and mid tide rising. Current direction is given by the black arrows and current speed by the underlying shading. Strongest tidal currents occur offshore of the breakwater scheme with strongest currents inside the breakwater scheme occurring behind the breakwaters caused by flow compression in both a horizontal and vertical direction. This flow intensification is strongest at high tide. The current speed is greatest over tombolo 8 reaching 0.75ms^{-1}. At all tidal stages in phase two the tidally induced flow is unidirectional through the scheme and is directed north to south at high tide and at mid tide on the rising tide and south-east to north west at low and mid tide dropping. The tidal tombolos in phase one cause tidally induced gyres at high and low water. These are more defined at low water due to the emerged tombolos and lead to a north west to south east current at the shoreline. At high water the reverse eddy direction occurs and the eddy is smaller only occurring in the nearshore region. The lower current speeds at mid tide (due to the progressive tidal wave) mean the eddies do not develop.

The asymmetry in the tidal flow means that there is a net current over the tidal cycle (Figure 6.4.13). This current is directed from north west to south east through the majority of the scheme but there is a residual eddy in bay A and re-circulation close to the shoreline in bays B and C. The transition embayment between phase one and two shows no obvious net current pattern. The cumulative current speed is greatest over the tombolo crests behind breakwaters 6 and 8.

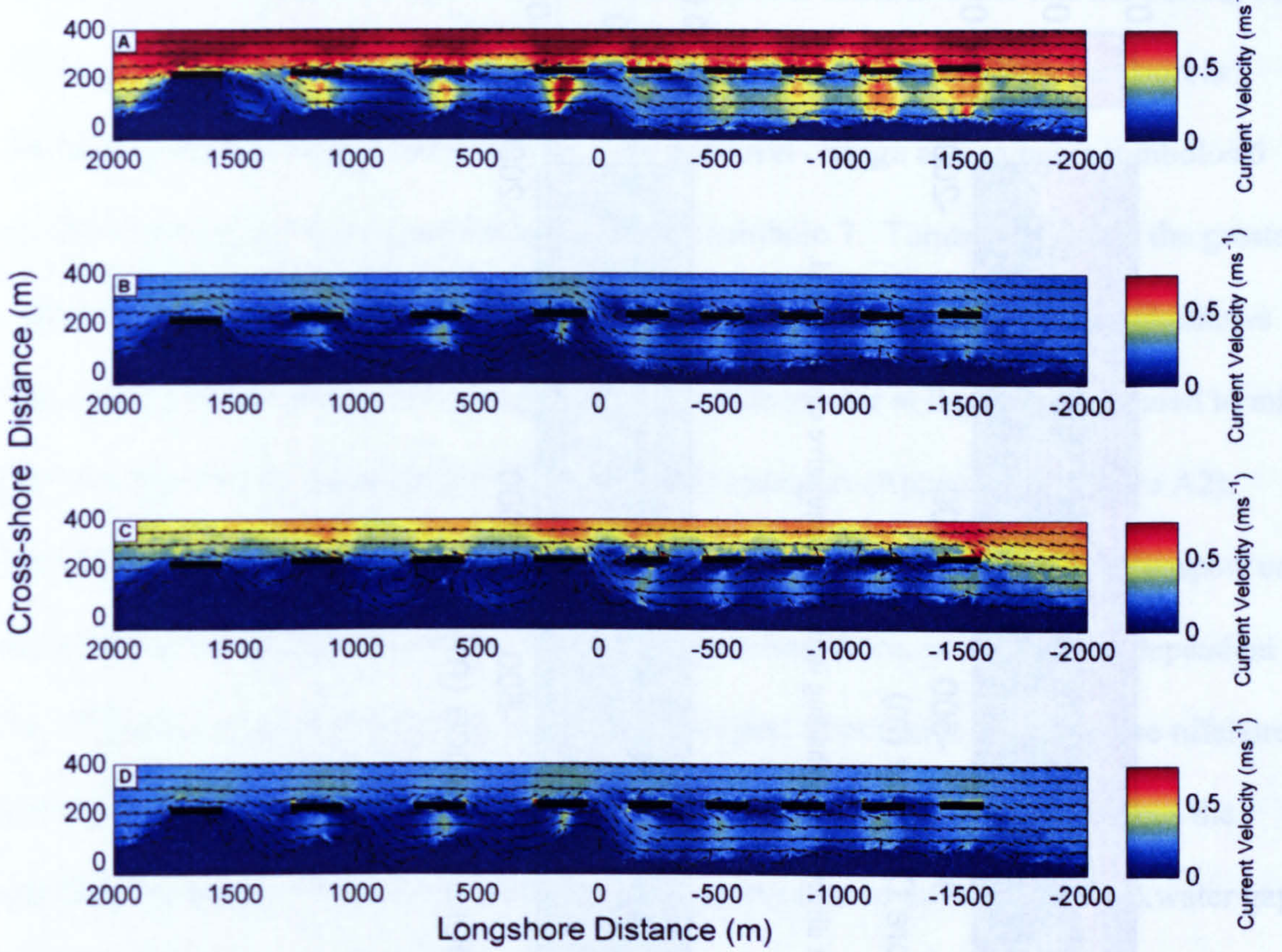

Figure 6.4.12: Tidal currents at different stages of tide: a) high tide, b)mid tide dropping, c) low tide and d) mid tide rising. Vectors indicate current direction and shading indicates current speed.

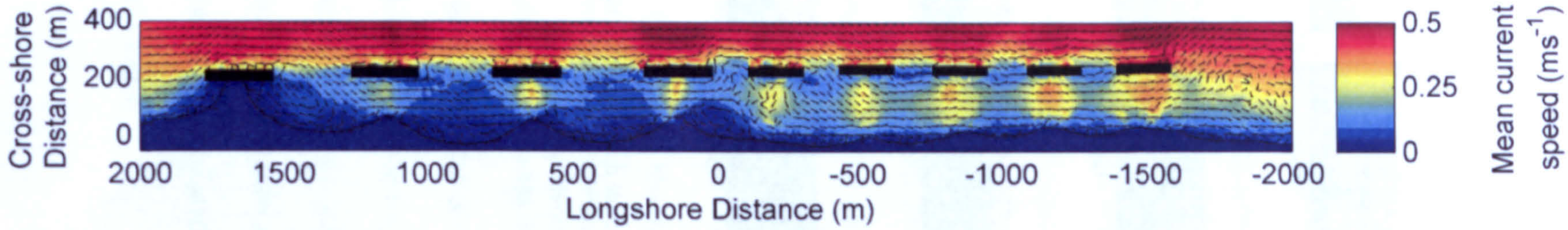

Figure 6.4.13: Net current over one tidal cycle. Vectors indicate current direction and shading indicates cumulative current speed.

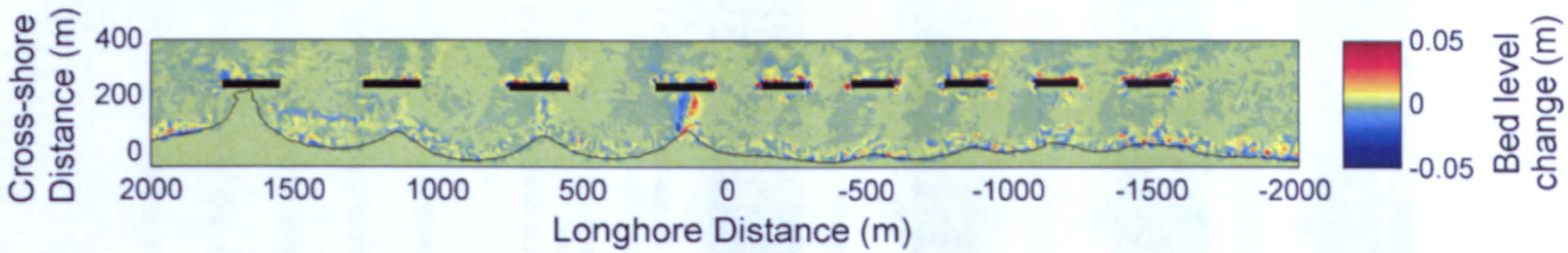

Figure 6.4.14: Net bed level change over a mean tidal cycle

Some sediment transport (Figure 6.4.14) occurs over the scheme under this net current but the magnitude is small (maximum bed level change ~5cm). The sediment transport is confined to the beach face and tombolos. The bed level change acts to move tombolos 6 and 8 in a south eastward direction and to flatten tombolo 7. Tombolo 8 shows the greatest change. Qualitative visual examination of the sediment transport through the tide shows that tidally induced transport is an order of magnitude greater at high tide compared to mid tide and the low tide transport is half the high tide transport (Appendix A, Figure A2). Transport only occurs through the phase two bays at high tide, at other stages transport only occurs in the lee of the breakwaters. The transport is longshore, with direction dependant on the offshore current direction. For phase one, transport direction is forced by the offshore current direction apart from the low tide scenario where an eddy circulation forces the sediment transport. There is some sediment transport onshore through the breakwater gaps at all tidal stages

Spring and Neap tides.

Spring tides (Appendix A, Figure A3) produce very similar residual current patterns to the mean tide but the magnitude of the current speed varies. The bed level change is likewise similar but the response is greater, over 5cm on tombolo 8 (Appendix A, Figure A4). Neap tides produce much weaker currents and the flow patterns are different, showing greater variability and eddy formations (Figure 6.4.15). However, due to the weaker tidal currents neap tides do not produce different patterns of tidally driven bed level change. Apart from changes to the beach face caused by the action of the low incident waves there is very little change at all; the only other modelled change is a small (~2cm) change over tombolo 8 which acts in the same direction as for the mean and spring tides (Figure 6.4.16). Sediment transport over the tombolo crests is of interest due both to the longshore

movement of the tombolos and due to the capacity for sediment transport between embayments. Total load transport was calculated at a specific point (figure 6.4.17) over tombolo 8 for mean, spring (Figure 6.4.18) and neap tides (Figure 6.4.19). Negative values indicate transport to the south and positive values indicate transport to the north. The spring tide shows southward transport at high tide, decreasing as the tide drops (current speeds reduce), as the current direction reverses there is some northward transport but this is cut off by the drying of the tombolo. When the tombolo re-submerges, sediment transport recommences but the current is already directed to the south and so southward transport continues. This leads to a net southward transport over the tidal cycle. Mean tides produce very similar total load to spring tides but of smaller magnitude (Appendix A, Figure A5). For the neap tide scenario the tested point on the tombolo does not dry and so the northward directed ebb tide transport can continue over low tide. The weaker currents meant that the magnitude of the transport is much lower and that around mid-tide (weakest currents) there is no sediment transport. The asymmetry in the tidal flow (stronger currents at high tide) mean that there is more southward directed transport and the same asymmetry in net total load transport as spring tides is shown.

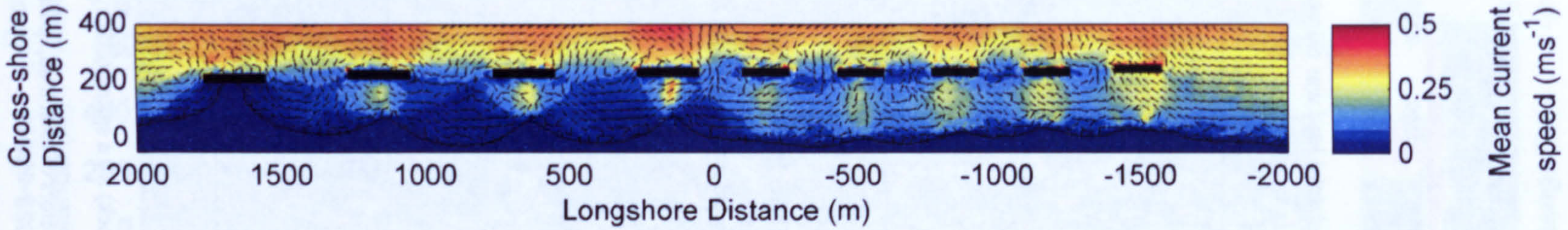

Figure 6.4.15: Mean current speeds over a neap tidal cycle with wave stirring. Mean current speed is represented by shading and direction by the vectors.

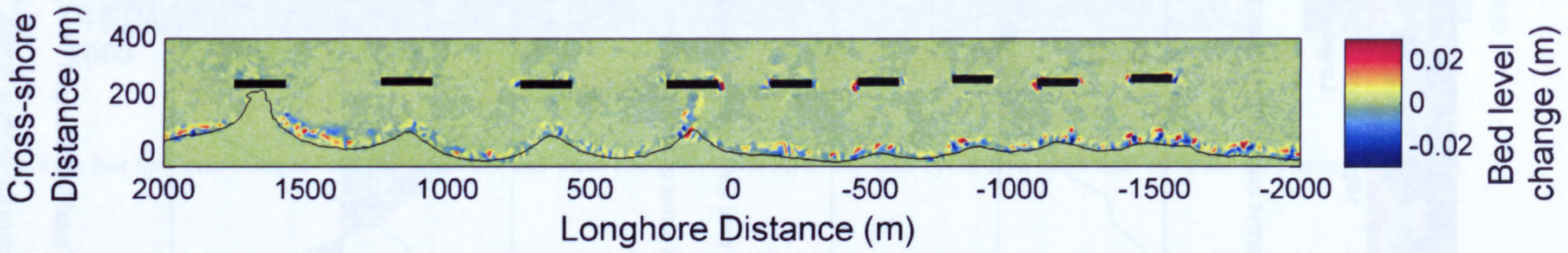

Figure 6.4.16: Net bed level change over a neap tidal cycle with wave stirring.

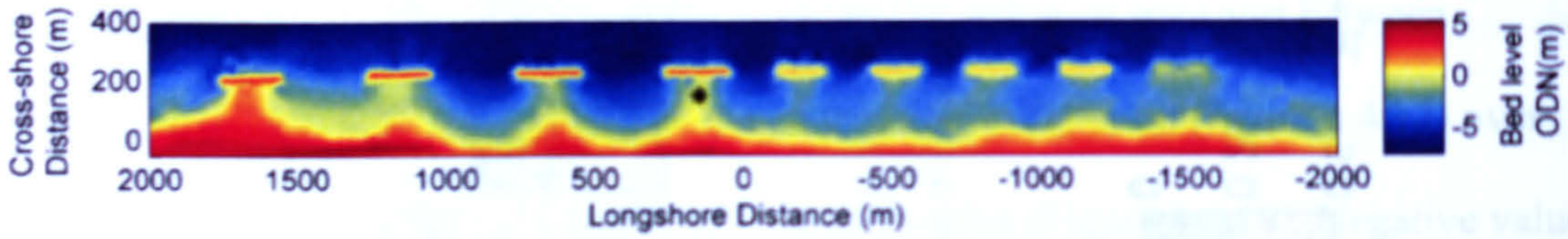

Figure 6.4.17: A bathymetric map of the scheme with the point at which total load was extracted displayed.

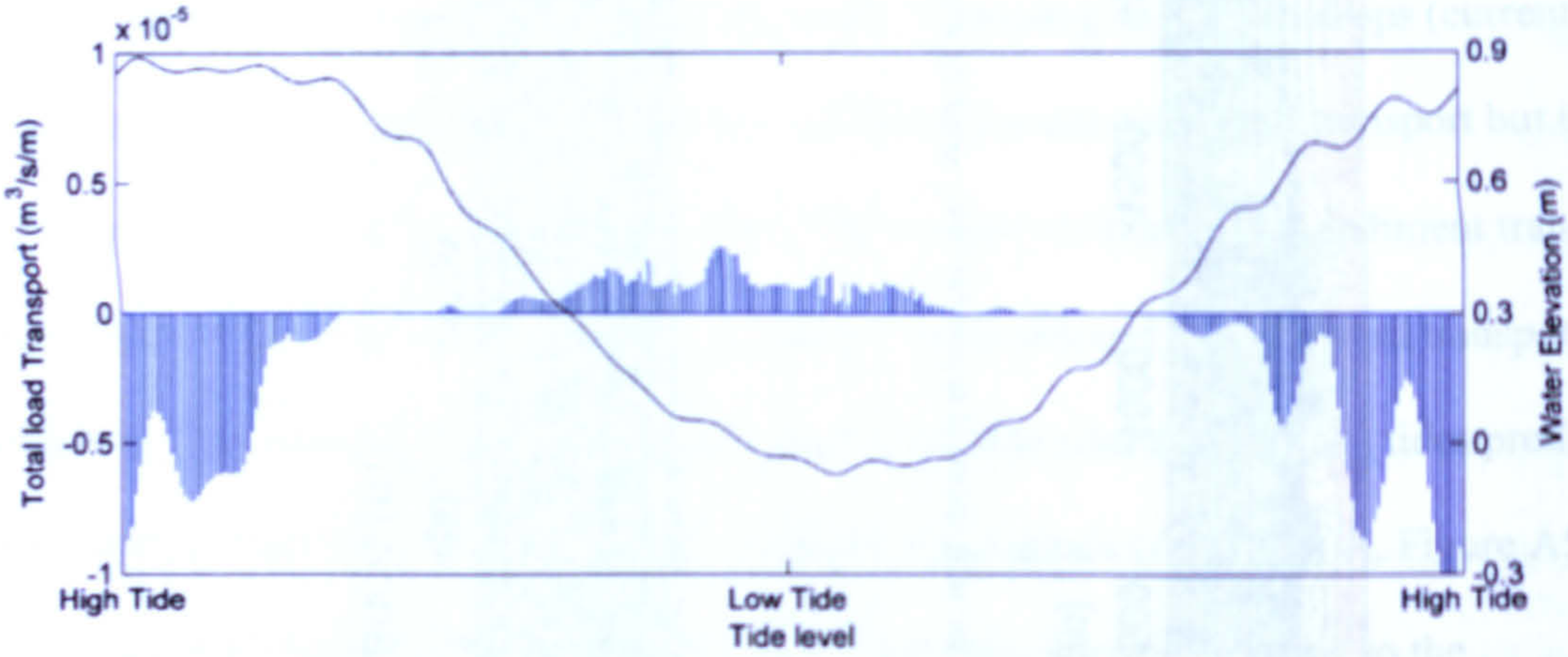

Figure 6.4.18: A plot of total load transport (blue) and tidal elevation (black) through a tidal cycle for a neap tide. The blue lines are vectors of total load, positive values for northward transport, negative values for southward transport.

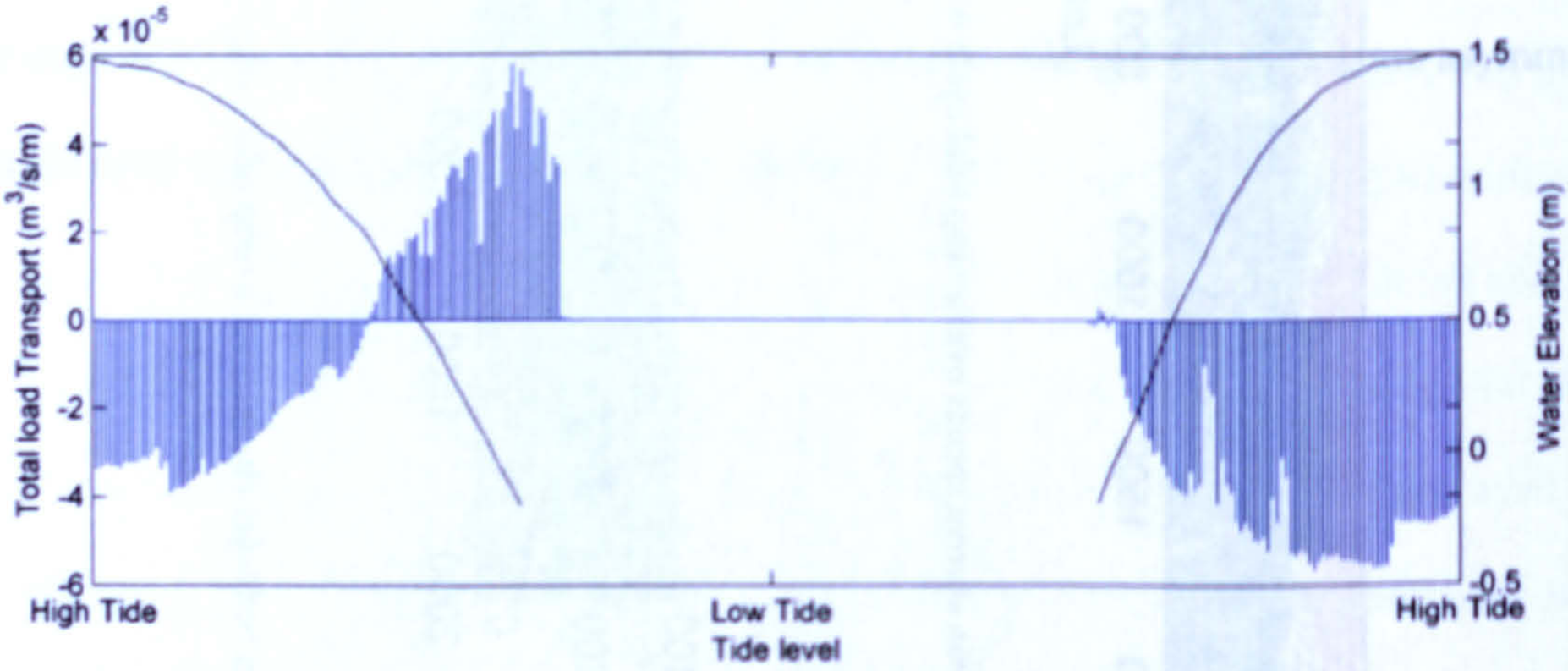

Figure 6.4.19: A plot of total load transport (blue) and water level (black) for a spring tidal cycle. The area of no water elevation indicates the tombolo drying. The blue lines are vectors of total load, positive values for northward transport, negative values for southward transport.

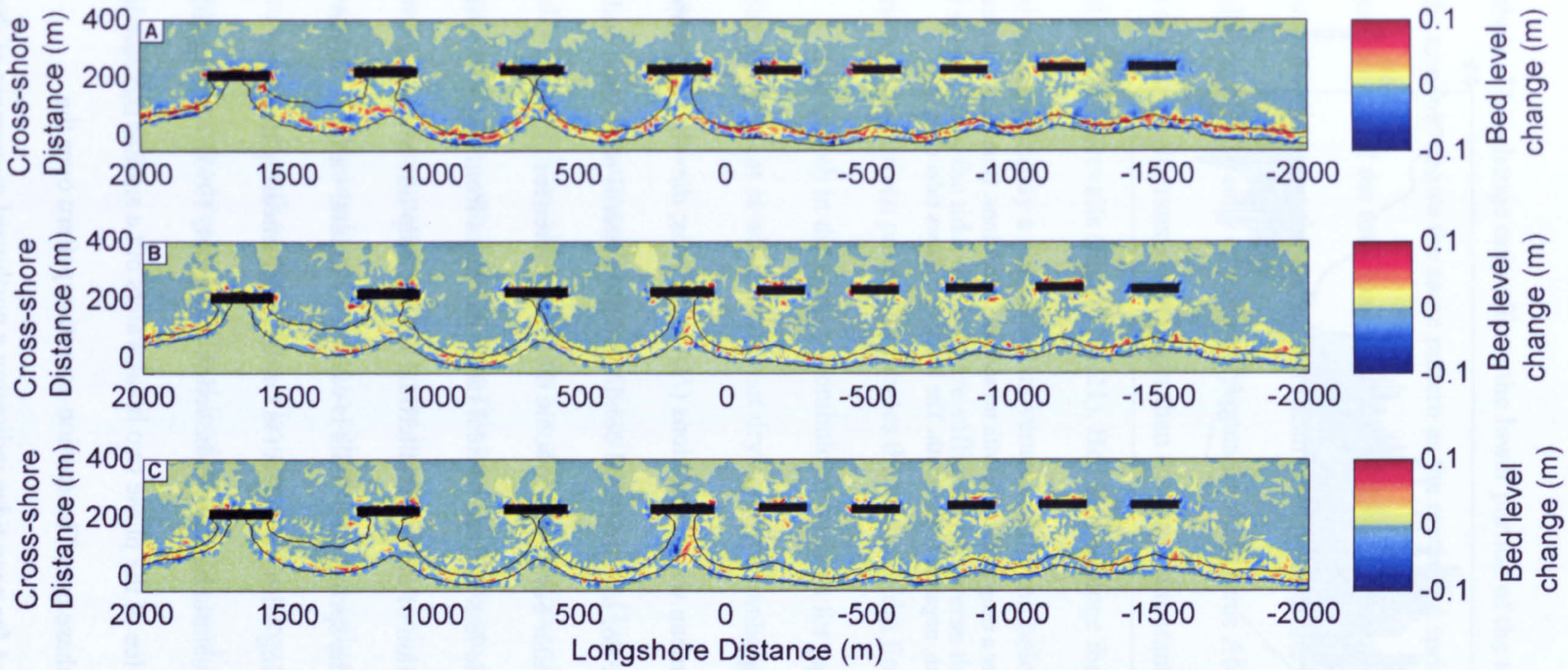

Figure 6.4.20: Net bed level changes for a combined tide and wave conditions over A) a neap tidal cycle; B) a mean tidal cycle and C) a spring tidal cycle.

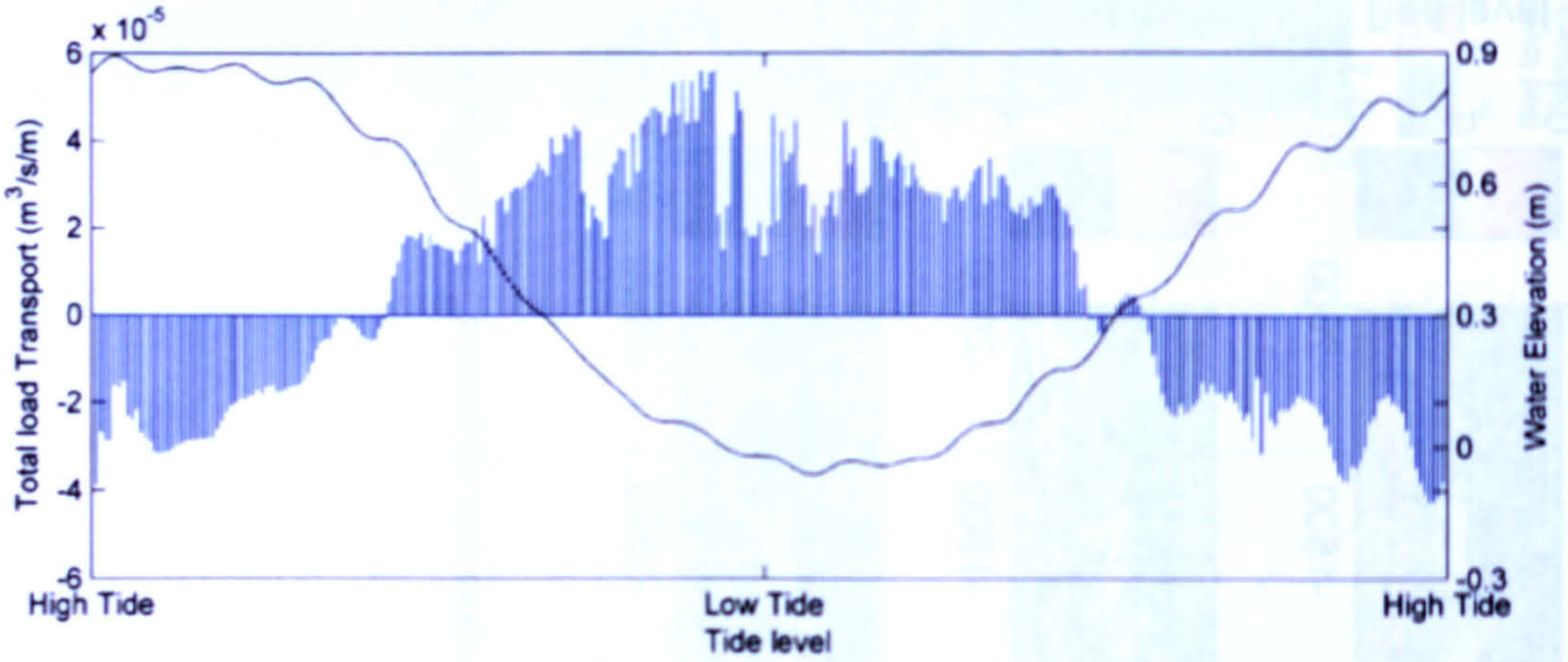

Figure 6.4.21: Total load transport over a neap tidal cycle with mean wave conditions. Blue vectors indicate total load transport; positive to the north, negative to the south. The black line shows tidal elevation

6.4.3 Tides and waves combined

Tides and mean wave conditions

A set of tests were run utilising mean wave conditions (H_s=1m; T_p=6s; *dir*=48°) for neap, mean and spring tide conditions. For all three tidal conditions the patterns of erosion and accretion (Figure 6.4.20) are similar but there are some distinct differences. In the intertidal region, changes become less defined as tidal range increases from distinct erosion of the upper intertidal and accretion of the lower intertidal for the neap tide to a more general but lesser accretion for the spring tide. This is caused by greater variation in the area of wave action over the spring tides, this effect is termed tidal smearing and has previously been documented in natural beaches (Masselink and Short, 1993). Spring tides lead to greater deposition in the lee of the phase two breakwaters but a similar increase in deposition is not observable in phase one. The erosion-accretion pattern over the southernmost tombolo is reversed for neap tides indicating a northward movement of the

tombolo. This change only affects the lower portion of the tombolo, whilst the upper region of the tombolo shows the same pattern as the mean and spring tidal cycles.

Consideration of the total load transport over the tidal cycle at the same point as for the tide only cases show that the spring and mean tides patterns are similar. These patterns are similar to the tide only conditions (Appendix A, Figures A6 & A7). For the neap tide the ebb tide northerly transport is larger than the flood tide transport and so a net northerly total load transport prevails (Figure 6.4.21). Bed level change for mean wave conditions without tidal currents display a northward movement of the tombolos, it is thought that for mean and spring tides the tidal currents are sufficient to reverse this pattern whereas for neap tides the wave driven pattern dominates the weaker tidal flows.

The switch in direction of tombolo movement for the neap tide case probably indicates the point at which sufficient drying of the tombolo occurs to retard the northward transport.

Current patterns for the mean and spring tides (Figure 6.4.22) are similar to the tidally induced flows although there are stronger southward directed currents near the shoreline in phase one. For the neap tide case, currents are not similar to the tidal current alone case. Current patterns form gyres in phase one similar to the wave only case. The phase two circulation is not similar to either the wave only or tide only case. In phase two there is a linear south to north flow. The speed of this flow intensifies in the sheltered regions behind the breakwater. Total load transport is predominantly onshore directed for the neap tide case.

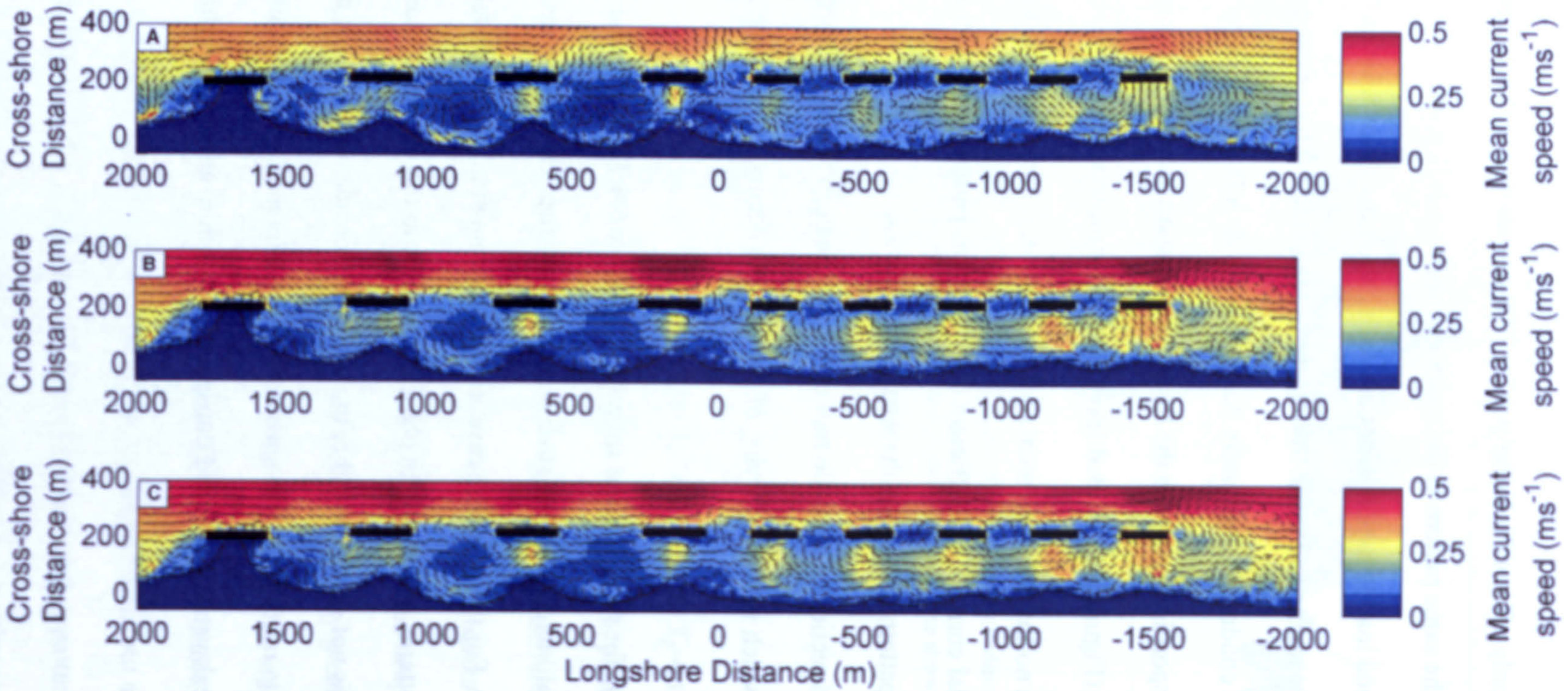

Figure 6.4.22: Mean current velocities over a tidal cycle with mean wave conditions for A) a neap tidal cycle; B) a mean tidal cycle; and C) a spring tidal cycle

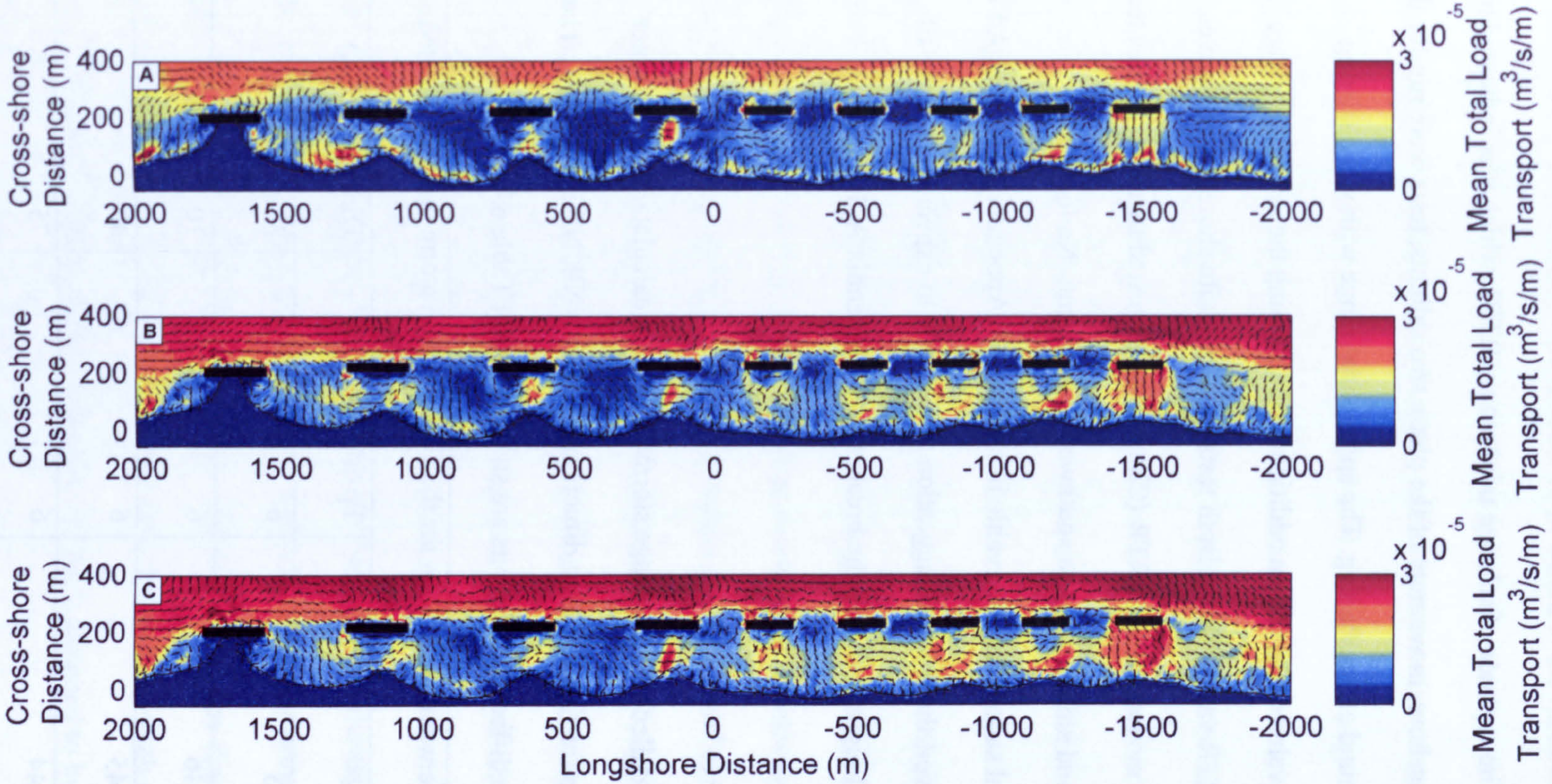

Figure 6.4.23: Patterns of total load transport over one tidal cycle for combined tides and mean wave conditions; A) neap tide scenario; B) mean tide scenario; and C) spring tide scenario.

Relative tidal range.

In order to determine the importance of relative tidal range (RTR), which was indicated to be correlated with the longshore movement of the phase two salients, tests were run for the extreme values of RTR found at Sea Palling. The spring tidal range with wave stirring (Hs=0.1m) gave an RTR value of 30 and an additional test utilising the neap tidal range with 2m waves gave an RTR value of 0.5. Both tests were run with shore normal waves. The correlation of salient movement with RTR (Chapter 4) suggested that large values lead to northward movement and small values to southward movement. No longshore movement of the intertidal salients is observable in either case (Appendix A, Figures A4 & A8). Interestingly, however, there is the suggestion of opposite to expected direction of movement in the sub tidal regions behind the breakwaters (Appendix A, Figure A8).

Storm conditions

Storm condition were modelled using average storm conditions calculated from the met office hind cast wave data for five different directions (NNW, NNE, NE ENE ESE). The mean conditions for these different directions are summarised in Table 6.4.3.

Table 6.4.3: Characteristic wave conditions for the five different storm directions tested

Storm name	Hs	Tp	Direction (deg.)
NNW	2.3	6	345
NNE	2.46	6	10
NE	2.45	6	49
ENE	2.44	6	75
ESE	2.2	6.5	115

Average storm wave heights are around 2.5m which is the threshold at which increasing wave height does not increase mean current speeds near bed particle velocities and so average storm wave heights can be taken to be representative of severe storm events as well. Patterns of wave incidence averaged over a tidal cycle (Appendix A, Figure A9), are similar for the obliquely incident waves in Section 6.4.1. Increasing wave obliqueness leads to a decrease in the amount of wave energy reaching the breakwater lee as the effective gap length shortens further. As previously demonstrated for oblique waves without tidal currents (Figure 6.4.5), the tombolos are moved in a down drift direction (Figure 6.4.24). The salients are also moved in a down drift direction but the pattern of this movement is less defined. For the more oblique waves, the extent of the tombolo/salient movement is less (Figures 6.4.24A & E), and the general magnitude of bed level change is also lower. This is likely due to the lesser wave energy reaching the breakwater's lee for the waves of greater obliqueness. This also provides a reason for the lack of correlation with a direction estimate of longshore sediment transport (Chapter 4.3). The longshore sediment transport was calculated for an idealised long straight coast where increasing wave obliqueness increases magnitude of longshore sediment transport. The sheltering effect of the breakwaters negates this as increasing obliqueness leads to a narrower effective gap length and less wave action in the sheltered regions. For the shore-normal storm event (Figure 6.4.24C), the erosion-accretion pattern is similar to the shore-normal wave event without tidal currents (Figure 6.4.5B), material is eroded from the bay floors and the is accretion behind the breakwaters. The main difference is the north to south movement of tombolo 8. which is not observable in the no tide case and so is assumed to be induced by tidal current effects.

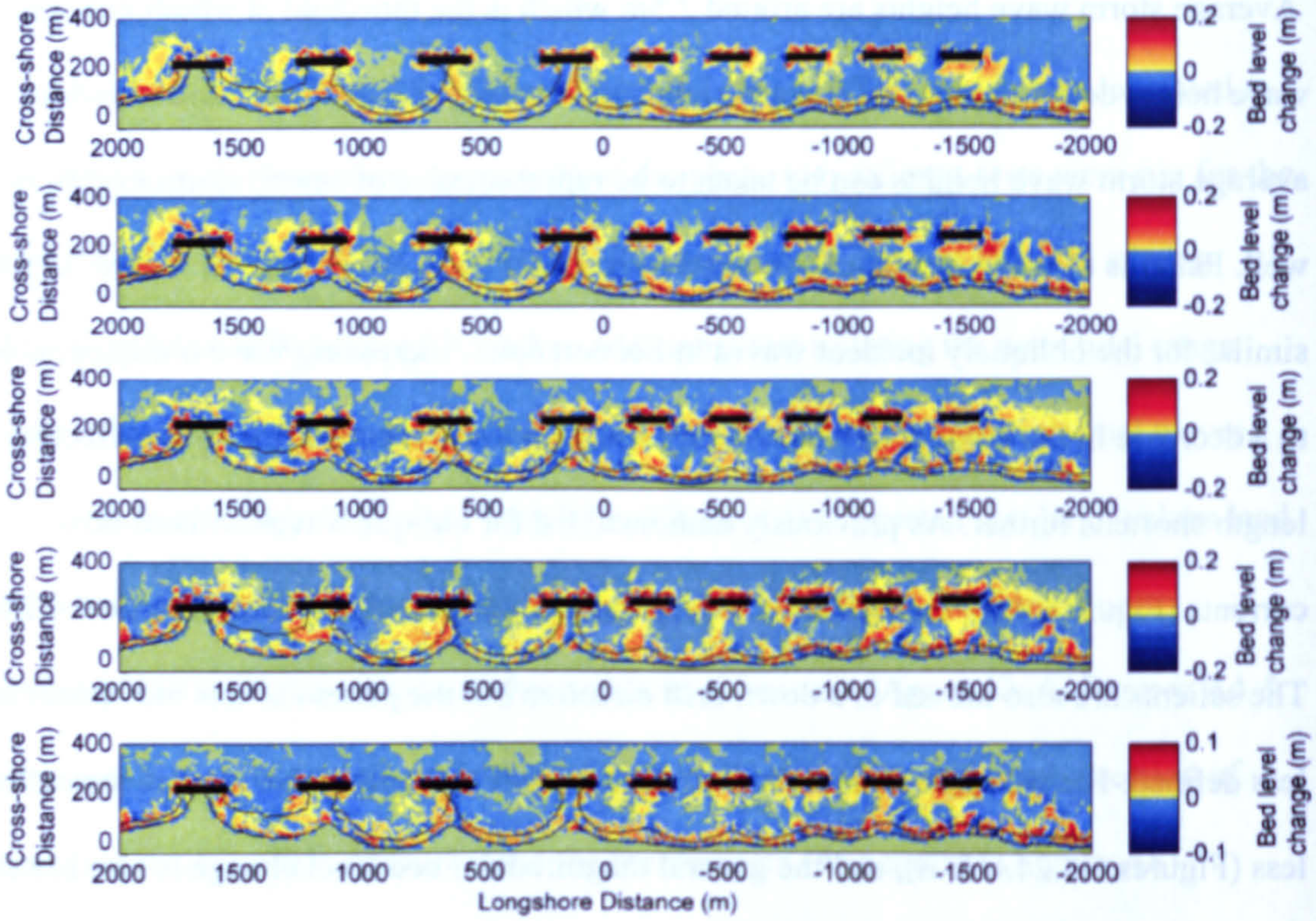

Figure 6.4.24: Net bed level changes over one tidal cycle for the 5 different storm directions tested: A) NNW; B) NNE; C) NE; D) ENE; E).ESE.

Patterns of current velocity and total load transport for the oblique waves (Appendix A. Figures A10 &A11), are similar to those in the non-tidal case (Figure 6.4.6 and Figure 6.4.7). Increasing wave obliqueness does not change the current or sediment transport patterns although the magnitude reduces. The shore normal case (Appendix A, Figures A10 & A11) is similar to the no current cases (Figure 6.4.6 and Figure 6.4.7) apart from the southward directed current and sediment transport pathways over tombolo 8. These results suggest that for storm wave conditions, wave driven circulation dominates and tidal currents do not significantly alter current or sediment transport pathways except for the shore normal case where they influence the southward movement of tombolo 8.

Storm and surge conditions

A test was conducted using the northerly storm wave conditions and water level and current conditions from a large surge event where the high tide level reached 2.2m. Northerly storm wave conditions were used because the majority of surge events are associated with northerly wave events. Storm surges cause important morphological changes at this site as the elevated water levels allow for greater wave penetration into the embayments and mobilisation of the supra tidal sediment. The elevated water level means that the northernmost tombolo is submerged. Current patterns and sediment transport pathways (Figure 6.4.25B & C) were similar to the northerly storm event without surge. The main difference is that the current pattern is a more unidirectional north to south flow for the surge case. Bed level changes (Figure 6.4.24D) are of greater magnitude for the surge case compared to the non surge case: the elevated high tide level means that the supra tidal region suffers greater erosion and there is deposition in the lower intertidal. The greater magnitude of change means that there is greater reduction in profile gradient for the surge conditions (greater erosion of upper intertidal and supra tidal and greater accretion in the lower intertidal). As previously stated however, there is no overtopping of emergent breakwaters or wave transmission through the structures incorporated in this model. It is under surge conditions that overtopping becomes most important as the lower breakwater freeboards facilitate the process. The pattern of wave incidence clearly shows the distinct sheltered regions for phase one (Figure 6.4.24D). in reality this would be less distinct due to overtopping and wave transmission and thus some processes associated with surge events are undoubtedly missing. It is likely that this leads to lesser erosion being modelled than is realistic since overtopping increases offshore directed currents (Martinelli *et al.*, 2006) and also increases the amount of wave action at the shoreline.

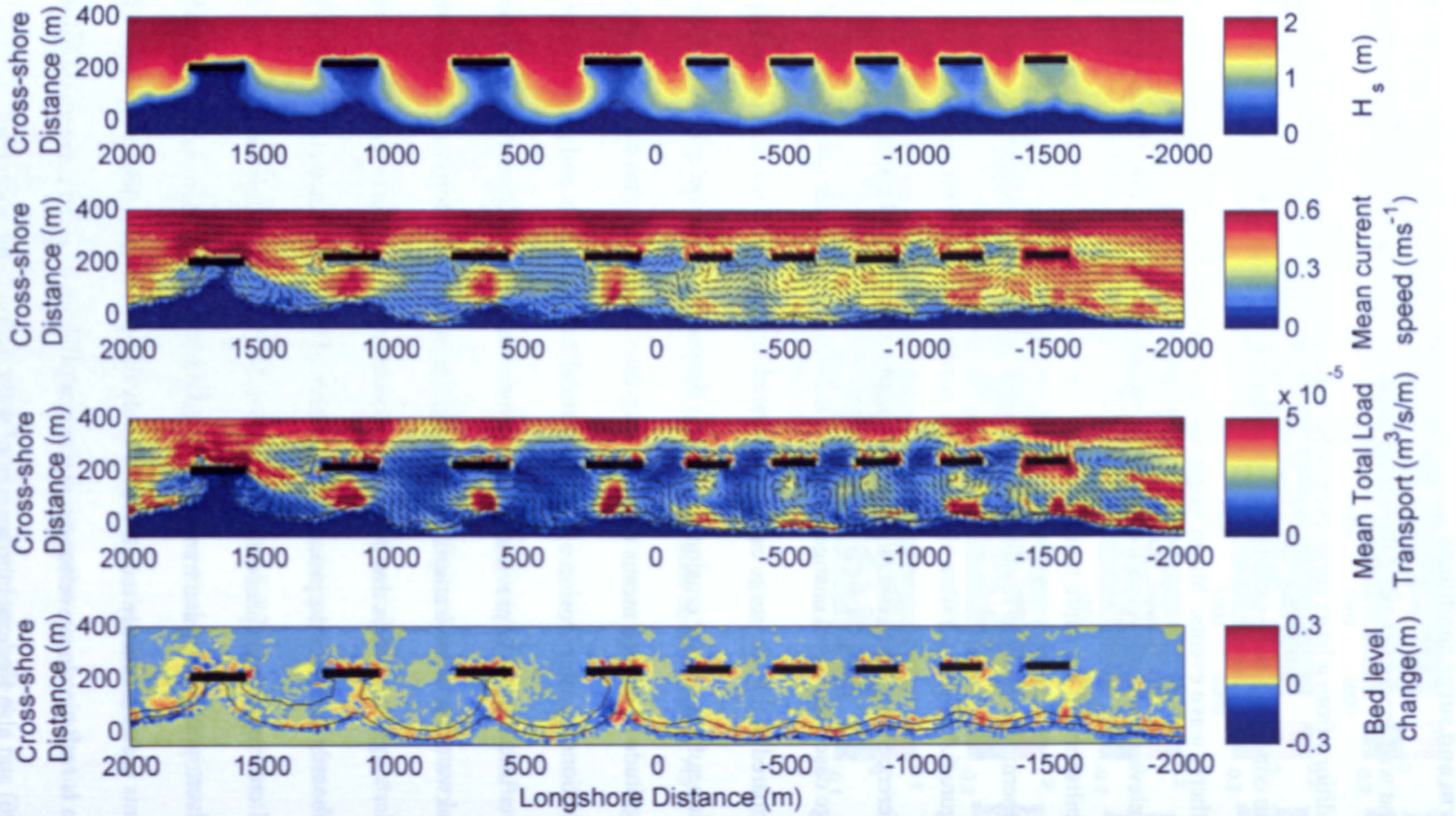

Figure 6.4.25: A) Wave incidence patterns; B) mean current velocities; C) mean total load transport and D) net bed level change over one tidal cycle with surge and *northerly wave conditions.*

Tombolo and salient movement under storms of long duration

It has been hypothesised that the breakwaters constrain the potential movement of tombolos and salients: the rate of movement will ultimately reduce under waves from the same angle of incidence. Figure 6.4.26 shows a longshore vertical cross-section of tombolo 8, which is similar to the other tombolos, over seven tidal cycles of northerly waves. The tombolo lowers and moves south (right in Figure 6.4.26). After the 4th low tide, southward movement stops, the crest continues to lower and the cross-section asymmetry increases as material gets eroded from the northern side and material is deposited on the southern side.

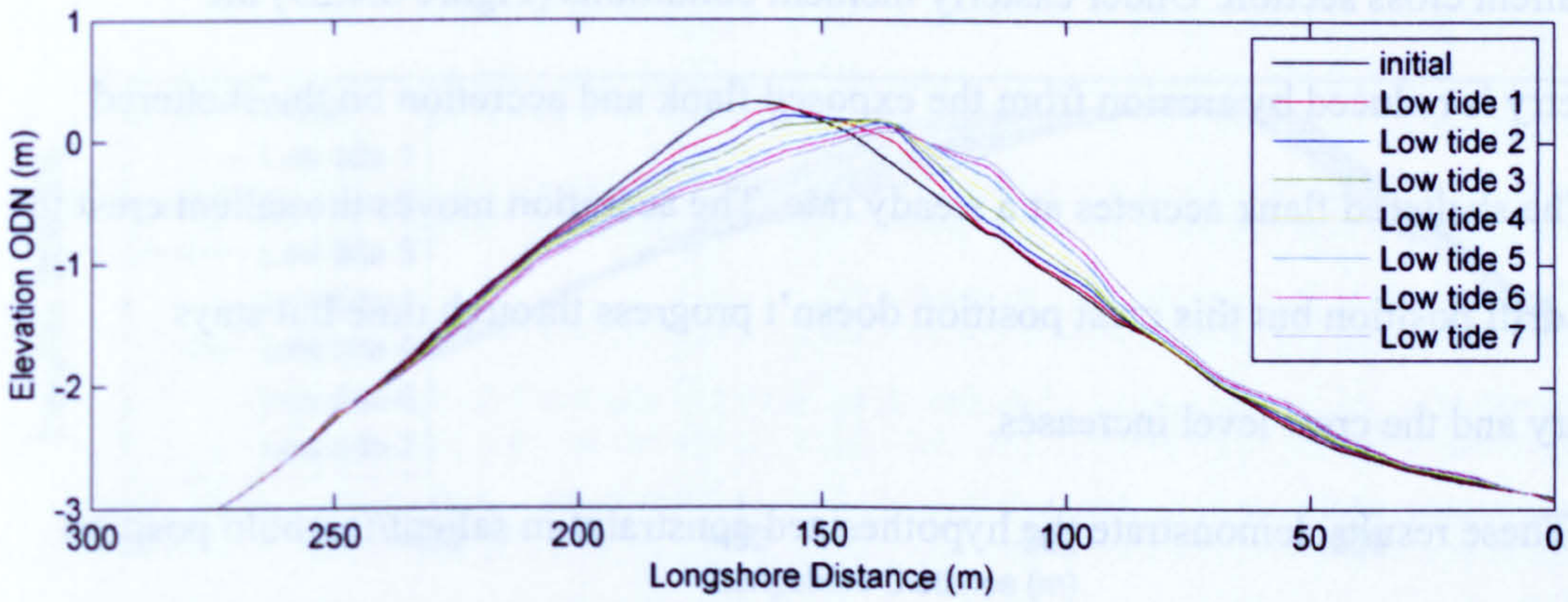

Figure 6.4.26: A vertical longshore cross-section of tombolo 8 showing tombolo movement under persistent storm conditions incident from the north.

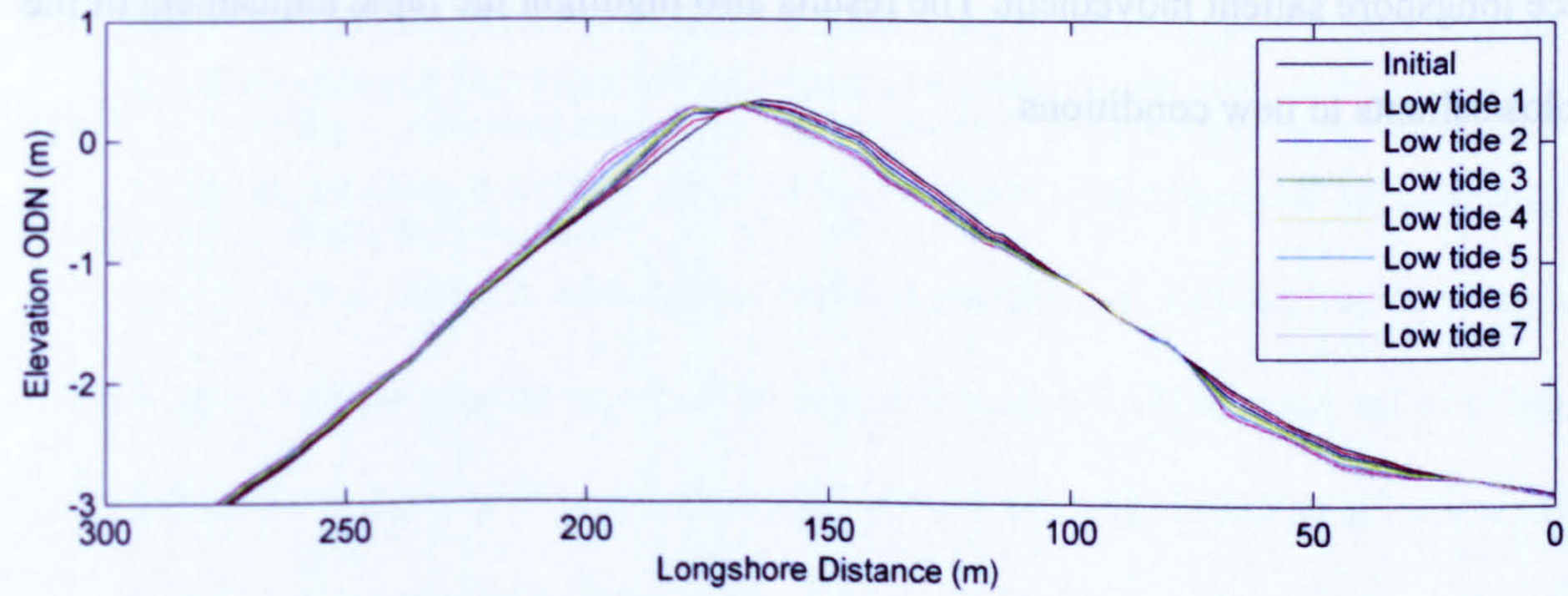

Figure 6.4.27: A vertical longshore cross section of tombolo 8 showing the tombolo movement under persistent storm conditions incident from the east

Likewise, under an easterly storm (Figure 6.4.27) the crest moves in a down drift direction to the north. Within two tidal cycles the crest has moved to its northern position, the crest then accretes, which is opposite to the erosion under the northerly storm conditions.

Salient movement under the northerly incident conditions (Figure 6.4.28) shows little erosion of the exposed side and steady accumulation of sediment on the down-drift side. Accumulation is constrained to the down-drift flank with little longshore progression of the salient crest after the first tidal cycle. The accretion serves to increase the asymmetry in the salient cross section. Under easterly incident conditions (Figure 6.4.29) the asymmetry is reduced by erosion from the exposed flank and accretion on the sheltered flank. The sheltered flank accretes at a steady rate. The accretion moves the salient crest to a down drift position but this crest position doesn't progress through time but stays stationary and the crest level increases.

These results demonstrate the hypothesized constraint in salient/tombolo position mentioned in Chapter 4. Continuing wave conditions from one direction do not move the salients and tombolos continually down-drift. This means that if the tombolos are already in their extreme position for one oblique wave direction, waves of that direction will not produce longshore salient movement. The results also highlight the rapid adjustment of the tombolos/salients to new conditions.

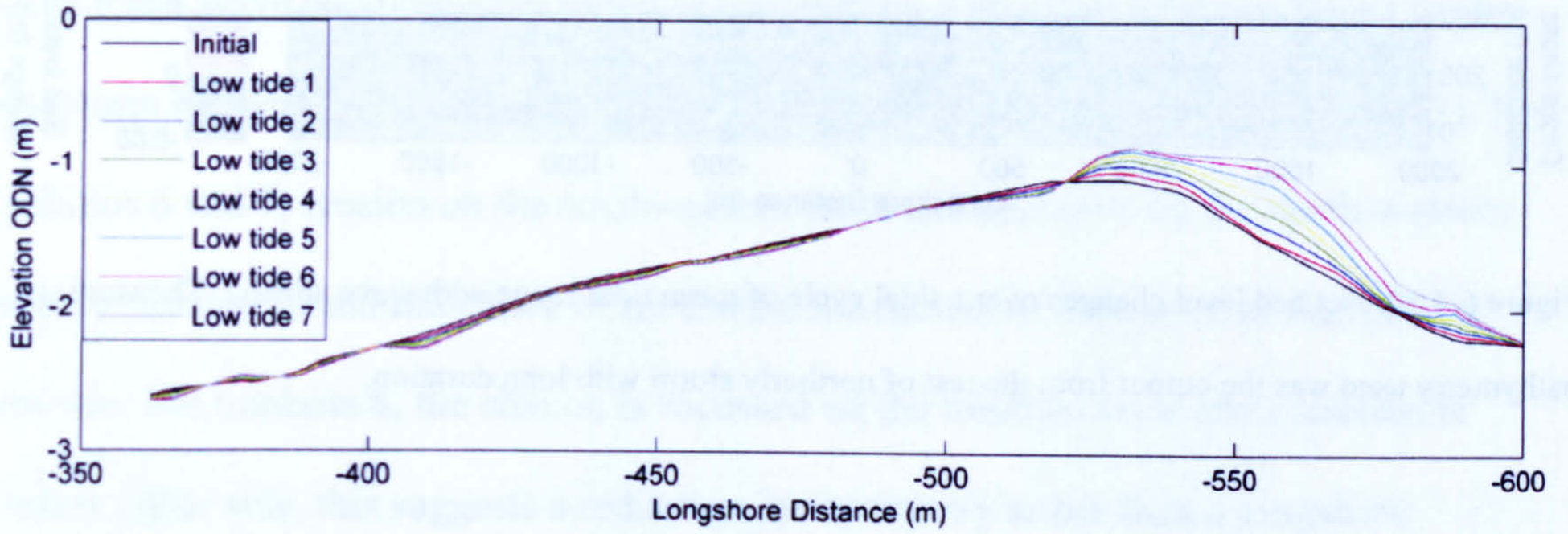

Figure 6.4.28: A vertical longshore cross-section of salient 10 showing the salient movement under persistent storm conditions from the north.

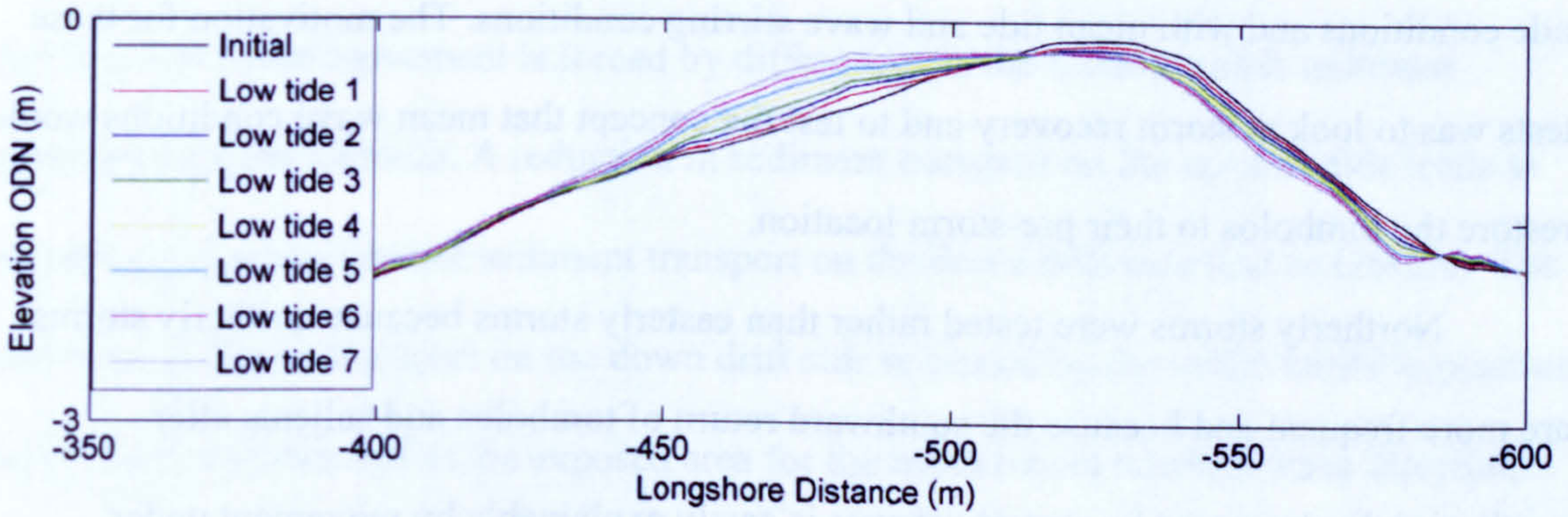

Figure 6.4.29: A vertical longshore cross-section of salient 10 showing the salient movement under persistent storm conditions from the east.

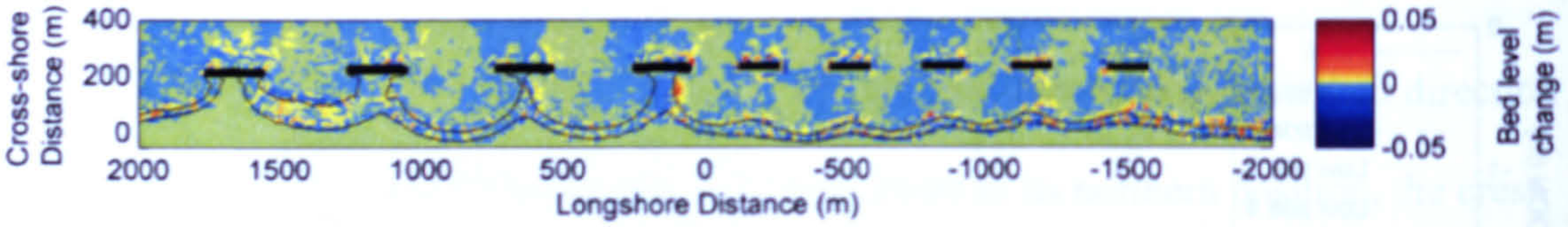

Figure 6.4.30: Net bed level changes over a tidal cycle of mean tidal range with wave stirring. The starting bathymetry used was the output from the test of northerly storm with long duration.

Storm recovery

The bathymetry from the final time-step of the model run over several tidal cycles of northerly storms was utilised as a starting bathymetry for model runs with mean wave and tide conditions and with mean tide and wave stirring conditions. The motivation for these tests was to look at storm recovery and to test the concept that mean wave conditions would restore the tombolos to their pre-storm location.

Northerly storms were tested rather than easterly storms because northerly storms are more frequent and because the southward return of tombolos and salients after northward displacement by easterly storms is easily explainable by movement under normal mean tide and wave conditions (Fig. 6.4.20B). Bed level changes for the tide and wave stirring case (Figure 6.4.30) displayed similar changes to the previously tested morphology (Figure 6.4.14). The slight reduction in magnitude and difference in erosion and accretion patterns over the tombolo 8 is forced by the increased asymmetry of the tombolo producing less rapid flow compression over the shallower gradient up-drift flank. Current patterns and patterns of sediment transport (Appendix A, Figures A11 & A12) are very similar to the patterns for the mean tide case with the previously tested morphology. This result is to be expected since the mainly longshore linear flow over the tombolos and salients will be similar whatever the longshore location of the tombolos and salients.

When mean wave conditions are tested in conjunction with mean tidal conditions for the post storm bathymetry, recovery in the tombolo positions can be seen (Figure 6.4.31). For tombolos 6 and 7, erosion on the south-eastern flank and accretion on the north-western flank is observable and indicative of northward movement of the centre of mass of the tombolo. For tombolo 8, the erosion is focussed on the tombolo crest and accretion is evident either side, this suggests a reduction in asymmetry rather than a longshore translation. There is also erosion on the southern side and accretion on the northern side of the sub tidal regions behind the breakwaters in phase two. The current patterns and total load sediment transport patterns averaged over a tidal cycle (Figures 6.4.32 & 6.4.33) show that this northward movement is forced by differences in the north to south sediment transport over the tombolo. A reduction in sediment transport on the up-drift side leads to accretion and an increase of sediment transport on the down drift side lead to erosion. The increased sediment transport on the down drift side is caused by the initial tombolo position being south of mean and in the exposed area for the mean (shore normal) wave direction.

These tests have shown that a northward migration of the displaced tombolo occurs under mean wave conditions and thus waves incident from the south are not required to move the tombolo northward after northerly storm events but rather waves from a non-north direction. Tides alone do not facilitate northward movement in this depth averaged model. The results further emphasize the importance of initial bathymetric conditions on morphological changes at the site.

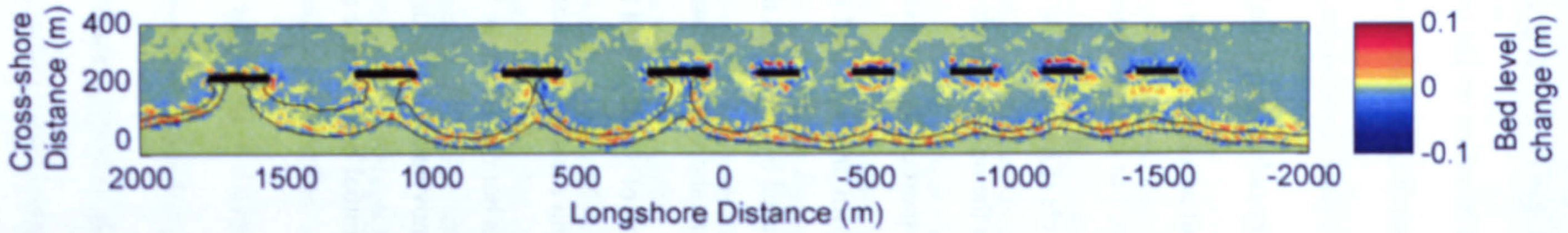

Figure 6.4.31: Net bed level changes over a tidal cycle of mean tidal range with wave mean wave conditions.

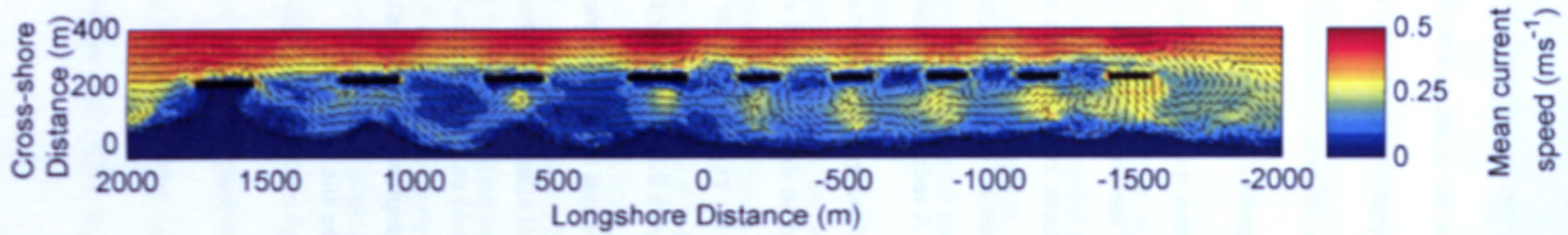

Figure 6.4.32: Current speeds averaged over a tidal cycle. Shading indicates speed and vectors indicate direction.

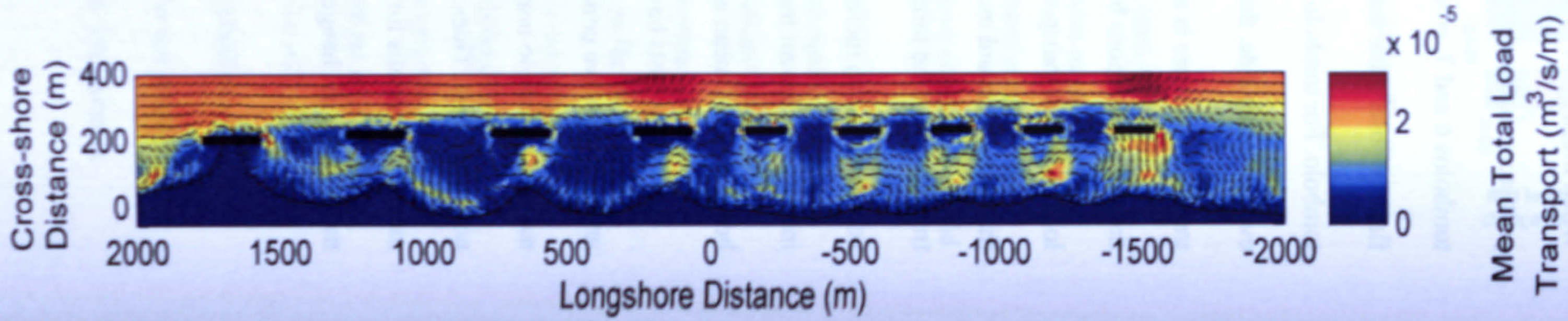

Figure 6.4.33: Total load sediment transport averaged over a tidal cycle.

6.5. Discussion and Conclusions

6.5.1 The numerical model

The numerical model, MIKE21, is a well known commercial model that has been shown to perform well in a variety of situations (Sorenson *et al.*, 2004a; Sorenson *et al.*, 2004b; Jones *et al.*, 2007). While, as far as the author is aware, the flexible mesh coupled suite has not been applied to detached breakwater systems, previous iterations of MIKE21 have been successfully used to model breakwater protected beaches (Zyserman and Johnson, 2002; Johnson *et al.*, 2005).

Calibration with measured data shows that the breakwater scheme is well modelled using the MIKE21 FM coupled numerical modelling suite. Comparison of modelled and measured tidal currents and water elevations gave rankings of reasonable to good agreement based on the van Rijn (2003) RMAE scale. The wave height output at two locations showed the right patterns and magnitude of wave heights were being represented (statistically significant at the 99% level). While consideration of the van Rijn scale showed that the wave module was performing less well; this can be partially explained by the use of model data for the boundary conditions and partially due to wave period measurement errors. More important for wave driven change is the spatial gradients in wave energy. Qualitatively the wave incidence patterns predicted by the model looked realistic. The only shortfall of the flexible mesh system is the inability to model wave overtopping and wave transmission through the emergent breakwaters. This will alter results in some conditions, particularly under storm conditions and for the lower phase two structures.

Predicting sediment transport and associated changes to morphology is an inexact science which additionally may display chaotic behaviour, hence for coastal modelling studies accuracy of better than a factor of 5 is unlikely in 70% of cases (Souslby, 1997a).

However, in this study the important factor is the relative variation of change in time and space rather than the absolute magnitude of change. Errors can be caused by relevant processes not being included in the model, poor representation of included processes or inaccurate input parameters. Previous discussion of hydrodynamic and wave model validation gives confidence in the input parameters. Since the model is depth averaged and does not include breakwater overtopping some processes will not be included. To test the performance of the sediment transport model, two storm events were modelled and morphological changes were compared to video measured intertidal changes (Section 6.3.4). The magnitude of change was similar and patterns of change were similar form much of the measured area. This result, in conjunction with other visual correlation of modelled and measured changes, gives confidence in the sediment transport model.

Rather than model real events, characteristic tidal conditions were calculated from data measured close to the site, and characteristic wave conditions calculated from 7 years of hind-cast model output using the met office inshore waters model. This approach has proved successful in isolating differences between the different forcing conditions experienced by the breakwater system. The use of characteristic conditions allows for easier generalisation which is vital when considering long time series of measured morphological data.

6.5.2. Interpretation of results

A variety of model tests were conducted and these help to elucidate forcing for changes observed in both video and DGPS surveys. A synthesis of the three data sources (video, DGPS and model) will be presented in the next chapter (Chapter 7) and so these conclusions will focus on the model results alone rather than comparison with other results.

The two goals posed at the start of this chapter were to investigate the relative importance of waves and tides and to look further at the range and forcing of the longshore movement of the tombolos and salients.

The results show that there is a delicate balance between wave and tides, with waves being dominant in some cases and tides in others. Circulation patterns are tide dominated for the mean wave conditions with mean and spring tidal ranges. Under neap tide conditions (lower tidal current speeds), wave conditions dominate circulation. Under storm conditions, larger wave heights mean that wave forcing dominates the circulation patterns. Tides alone (with small wave stirring) only force change over the tombolos and salients. As wave heights increase the amount of sediment mobilised increases and thus the region of morphological change extends to the whole breakwater scheme. Initially the sediment transport pathways are forced by the tidal circulation but as wave heights increase (over the mean wave height for mean tidal conditions) the wave forcing starts to dictate circulation and sediment transport pathways.

The movement of the tombolos is particularly influenced by the balance between waves and tides: the area sheltered from wave action is the area of the breakwater scheme most affected by tidal currents. Initial morphology is also of utmost importance in determining the extent of tombolo movement. Whilst obliquely incident waves do force a down drift movement of the tombolos and salients, this forcing is non-linear, depending on the prior tombolo location and on the angle of incidence. Increasing angle of incidence does not increase the amount of down drift movement due to the reduction of wave energy in the lee of the breakwaters.

Analysis of the simple wave only conditions lead to some important findings. The wave induced double gyre circulation that is often assumed behind detached breakwaters is not present in all embayments. In phase one, prevalent circulation is either single gyres or

asymmetric double gyres with one gyre much larger than the other. Phase two shows more variable circulation. This deviation from the expected double gyre circulation is caused by the short breakwaters allowing hydrodynamic interaction between embayments. Interactions between embayments mean that embayments in the same phase are not forced by identical hydrodynamics although there are similarities, this leads to small differences in morphological response, especially for the sheltered regions . This is compounded by differences in the bathymetry of same phase embayments, especially for phase one This is likely to be the case for all breakwater schemes and is an important consideration when designing coastal protection schemes consisting of a detached breakwater array. As wave heights increase circulation patterns vary and become more developed. These tend towards the double gyre circulation for the more central embayments not influenced by end effects.

Increasing wave height was shown to increase current velocities and near bed particle velocities (averaged across the breakwater protected zone) linearly until a certain height at which velocities level off due to saturation of the surf zone region tested. This wave height was lower for the low tide case, probably due to increased wave dissipation outside of the breakwater zone. Velocities approached a maximum at H_s= 2.5m. This wave height is the average storm wave height which suggests that, for Sea Palling, the protection afforded by the breakwaters means that extreme storms should produce no greater morphological change than storms of average size, neglecting the effect of additional overtopping and surge effects which often accompany large storms. Circulation patterns become similar for all wave heights over 2m.

Mean wave conditions were modelled over a tidal cycle of elevation with tidal currents removed. Mean currents and sediment transport over this cycle were investigated. A largely onshore sediment transport was displayed with deposition in the sheltered regions behind the breakwaters.

Obliquely incident waves move the centre of maximum wave action from the centre to the down drift flank of the embayments. This leads to a down drift movement of the salients and tombolos. This change is forced by different mechanisms for obliquely incident waves from the N and E. Waves incident from the north cause a longshore flow throw the scheme, which intensifies in the sheltered regions and causes down drift tombolo and salient movement. Waves incident from the east force a gyre in the phase one bays and sediment is moved in an up drift direction into the sheltered region. The phase two current patterns for the easterly incident waves are similar but opposite to the northerly incident waves. This difference is forced by the bathymetry which is not symmetric through the embayments.

Modelling of tidal currents (with wave stirring) showed that the flood dominated tidal asymmetry leads to a net sediment transport through the scheme. Changes were concentrated on the tombolos, with a southward movement of the tombolos, especially for tombolo 8. Increasing tidal range led to increasing current speeds and thus produced greater magnitude of morphological change. This change ranged from a maximum vertical change of 2cm for a neap tide to over 5cm for a spring tide. Mean and spring tide current patterns are similar whereas the neap tide current patterns are less defined. The bed level change for all three cases is similar because the neap tide currents are not strong enough to produce any change except over tombolo 8. The transport asymmetry over the tombolos 8 is caused by the drying of the tombolos for the spring and mean tides during the northward ebb flow and due to the ebb currents being insufficient to move sediment for the neap tidal range test.

Modelling of the effects of combined tide and mean wave conditions showed that for the mean and spring tide tests, the current circulation patterns were very similar to the tide only patterns, which implies tide dominance. For the neap tide case, currents were

similar to the wave only case for phase one and similar to neither wave only nor tide only conditions in phase two. This suggests that phase one is wave dominated over neap tides whereas phase two shows a balance between the two forcing mechanisms. Intertidal bed level change shows greatest definition for the neap tide case this becomes less defined as tidal range increases, a phenomenon termed 'tidal smearing' (Masselink and Short, 1993).

Tombolo movement is from north to south over mean and spring tidal cycles. Under neap tidal conditions the tombolo moves northward due to the greater influence of waves compared to tidal currents. Under tide and storm wave conditions, wave driven circulation patterns dominate. Oblique waves move the tombolos and salients in a down-drift direction, as the angle of incidence increases the amount of down drift movement reduces due to reduction in the effective gap length. Tests with persistent storm conditions show that there are limits to the tombolo and salient movement. Oblique waves initially rapidly move the salient/tombolo down drift but this movement slows over successive tidal cycles. Model tests utilising post storm bathymetry showed that tidal conditions produced similar current patterns, sediment transport and morphological change to the previous bathymetry tested. With combined mean wave and tide conditions the tombolos showed a return toward their pre-storm location These tests emphasizes the importance of initial morphological conditions to tombolo evolution under wave dominated conditions. For tidally driven movement the longshore location is unimportant.

7. Synthesis and Discussion

In this chapter, the results from the video analysis, RTK-GPS surveys and numerical modelling will be compared, synthesized and discussed. The thesis aims, all of which were achieved, will be used as a framework for this discussion. The aims and objectives stated in the introduction were:

1) To extend previous research at the site, which focussed on the larger breakwaters, to the second phase of breakwaters,
2) To quantify morphological variability about the scheme,
3) To determine types of morphological changes at the Sea Palling breakwater protected beaches,
4) To establish forcing mechanisms and timescales of morphological change,
5) To utilise a numerical model of the site to gain understanding of the site hydrodynamics and sediment dynamics, and the balance between wave driven and tidally driven forcing.
6) To compare the morphodynamic response of the two different designs of breakwaters.

The third, fourth and fifth objectives will be discussed together to provide a comprehensive understanding of the scheme morphodynamics. The motivation for combining these three aims was to facilitate the simplest explanation of the complex dynamics at the site. Independent discussion of morphological changes and relevant forcing leads to duplication of explanation and reduces clarity in description of the relevant processes.

After consideration of the thesis aims, the work will be compared to other similar research and the implications of the research to the wider community highlighted.

7.1. Extension of research into phase two

The first aim of this thesis, one of the main goals of the LeaCoast2 project, was to extend research into phase two. The predecessor to the LeaCoast2 research project, LeaCoast, investigated the larger phase one breakwaters. The outputs of the initial LeaCoast project included measurement of storm scale morphological changes (Dolphin *et al.*, 2005), modelling of storm events (Zhu *et al.*, 2004), and investigation of tidal currents (Bacon *et al.*, 2003; Bacon *et al.*, 2005; Bacon *et al.*, 2007) for phase one. Extension of this research into phase two (aim one) was easily achievable via RTK-GPS survey strategy, selection of regions in interest in the video data and use of a suitable model domain. The video data allowed isolation of storm induced change and the numerical model was used to investigate both tide and wave driven processes. Both phases were subjected to the same analysis which facilitated the 6th objective (comparison of the two phases) which was conducted via qualitative comparison of the modes of change.

7.2 Morphological variability

In this section the outcome of objective two is discussed. Quantification of the variability of the breakwater protected beaches will be described and, additionally, the secondary outcome, longer term evolution of the scheme, will be considered based on volumetric consideration.

This work has shown that the breakwater protected beaches are less variable than those outside the system: vertical beach elevation changes display between 65-75% of the standard deviation of the up- and down- drift beaches. The standard deviation of the vertical change was 0.34m in the breakwater protected region compared to 0.54m and 0.43m in the up and down drift sections respectively (Appendix B). Standard deviation of the vertical change showed spatial variation throughout the phase one protected region,

whereas change was of similar magnitude for the whole phase two region, with slight concentration in the intertidal region. In phase one, change was greater on the tombolos, especially the northern flank, and on the sub-tidal bay floors. Standard deviation of the mean sea level contour showed that the variability increased on the tombolos and salients. The range in cross-shore location of the mean sea level contour varied from 6m, in the bay centres, to 80m, on the tombolo tips. The large range on the tombolo tips is, in part, due to the longshore movement of these features. A simple analysis of bay shoreline positions through time linked the largest changes to large (>2m) storm events.

Volumetric consideration shows that the scheme is losing sediment over the 1.5 year RTK-GPS survey coverage. The average vertical erosion rate, based on the RTK-GPS surveys, is around 0.5m per year throughout the scheme (Appendix B, Figure B5), although the rate of this loss seems to be reducing through time. Comparison with up- and down-drift beaches (Appendix B, Figure B5) shows that rate of erosion is similar inside and outside the scheme which suggests that the detached breakwater scheme is failing to ameliorate the local erosion problem. However, the up and down drift beaches tested were in close proximity to the breakwater scheme which means the beach behaviour may not be representative of the natural erosion rate. Interestingly, post analysis time period, a large sand replenishment scheme was instigated for phase two, where the high tide line had regressed to the sea wall, which backs up the observation that the structures are failing to retain sediment. Long term analysis of shorelines derived from aerial photographs have also shown similar trends of erosion for all embayments apart from A and H (the end embayments, excluded from this analysis). Maximum rates of shoreline retreat were found for bay E which reached 6.03m yr^{-1} (Dolphin *et al.*, *Submitted*).

7.3 Morphodynamics of the breakwater protected beaches

The third, fourth and fifth aims will be combined in this section to provide a description of the important morphodynamics of the breakwater protected beaches. All three objectives were successfully accomplished.

The third objective, determining types of morphological change, was achieved by investigation of storm induced change and through empirical orthogonal function (EOF) analysis. EOF analysis of the medium term video derived shoreline dataset (Chapter 4.4) and the monthly RTK-GPS surveys (Chapter 5) allowed definition of three modes of change for both phases and an additional mode of change for phase one (Objective 3). The two datasets were complimentary: the video providing a high temporal resolution and the RTK-GPS providing coverage of the entire scheme.

Objective four, to establish times scales and forcing mechanisms for the different observed changes was accomplished via correlation of the temporal component derived from EOF analysis with a variety of forcing parameters. This objective was also achieved by considering the results of the numerical modelling (Chapter 6) and the pre- and post-storm surveys (Chapter 4.3). Numerical results provided explanation of forcing and also reasons for the lack of correlation against some seemingly instrumental parameters. By utilising the video data, changes forced by storms can be isolated from other events due to the high temporal resolution.

The fifth objective, to utilise a numerical model to describe the scheme was achieved using the Danish Hydraulic Institute's MIKE21 FM and aided understanding of the important forcing mechanisms at the site.

Four different modes of change were established via the EOF analysis. These modes of change will be considered separately and the outcome of objectives three, four and five described to build understanding of the site morphodynamics.

Erosion and accretion

The primary mode of change derived from EOF analysis is the general erosion and accretion which manifests itself as a shoreline progradation and recession in the video dataset and an increase/decrease in elevation in the RTK-GPS dataset. For both datasets and phases the general trend is erosive. This mode accounts for 59% of the video derived variance and 75% of the RTK-GPS derived variance for phase one. In phase two 46% (video derived change) and 58% (RTK-GPS derived change) is described by this mode of change. The greater amount of variance attributed to this by the RTK-GPS dataset shows that the erosion and accretion is overwhelmingly dominant when considering all regions of the scheme but that in the intertidal region other changes have increased importance. This implies greater complexity to the intertidal change compared to the sub tidal. The phase one change described by the video and the RTK-GPS datasets are corroborative but the intertidal region is not representative of the change in the whole phase one protected area. Both the video and RTK-GPS datasets show that there is intertidal accretion in bay B and erosion in bay C. However, the sub-tidal (RTK-GPS derived) change shows that the overall trend is one of erosion. The storm change analysis (Chapter 4.3) showed accretion in the intertidal regions post-storm where classically one might expect erosion. This intertidal accretion might help explain the difference between intertidal and other regions: storm (and surge) conditions lead to erosion of the supra-tidal and accretion in the lower intertidal. The numerical model also shows this intertidal accretion over storm events (Figure 6.4.24 & Figure 6.4.25D).

The erosion and accretion in phase two shows a trend of erosion for both datasets. The intertidal and sub-tidal regions behave in the same fashion. This erosive trend in both phases is also shown in a simple bay volume analysis (Chapter 7.1). A previous beach re-nourishment led to the creation of a large, continually emergent tombolo behind breakwater

5 which blocks a substantial amount of the longshore sediment incident from the north from reaching the breakwater protected beaches, at the same time the predominant north to south movement of sediment is removing material from the scheme. The temporal component from the RTK-GPS analysis showed no significant correlation with forcing; however, this is not surprising given the temporal resolution and the steady long term trend in the data. For both phases, the temporal component for this mode from the video derived dataset showed highest correlation with the cumulative integral of high tide level (astronomical tide and surge effects). The cumulative integral emphasizes the importance of the antecedent conditions. The correlation for phase one suggested higher water levels lead to accretion in bay B and erosion in bay C. Relating this change to the RTK-GPS derived mode suggests that higher water levels lead to erosion. This is the same correlation with forcing as for phase two. Higher water levels equate to lower freeboards and allow greater wave penetration into the embayments. The temporal component for phase two, derived from video, also shows seasonality in response with accretion in the summer periods and erosion through winter periods. The numerical modelling of spring, mean and neap tidal cycles with mean wave conditions showed that spring tides (higher water levels) do lead to greater sub-tidal erosion than neap tidal cycles (Figure 6.4.20); equally storms with surge conditions lead to greater sub tidal erosion than storm without surges (Figure 6.4.24 & Figure 6.4.25). However, the intertidal patterns were not replicated with upper intertidal erosion and lower intertidal accretion for all cases. The neap tide case showed more spatially concentrated intertidal accretion than the spring tide case. Net total load sediment transport modelled over a tidal cycle for the neap tide case with mean wave conditions was directed onshore in all embayments (Figure 6.4.23A). For the spring tide case with mean wave conditions the total load sediment transport is directed onshore and southward in phase one and southward through the scheme in phase two (Figure 6.4.23C).

This difference is caused by the intensified tidal currents rather than the higher water levels. The numerical model is depth averaged which means that vertical current structure such as undertow is not captured. Additionally, higher water levels promote transmission through and overtopping of the structures. Wave transmission and overtopping of emergent structures is not incorporated into this model and so the expected increase in offshore directed rip currents (Martinelli *et al.*, 2006) is not observed, apart from at high tide for phase two. In reality wave overtopping of emergent breakwaters would occur at higher tides for both phases leading to even greater erosion under higher water levels than is currently modelled. Consideration of up and down drift sections (Appendix B) showed that down-drift of the breakwaters a very similar eroding trend is observable. Up-drift the trend was still erosive but there is greater variability and larger accretionary events, which indicates the blockage to natural longshore sediment transport caused by the breakwaters.

Longshore movement of tombolos and salients

The longshore movement of the salients and tombolos is the second mode of change derived from the video dataset for both phases. It is also the second mode of change for phase two derived from the RTK-GPS dataset. The longshore movement of the tombolos is the fourth mode of change in the RTK-GPS dataset. This means that compared to other changes the longshore movement of the tombolos is less important when the whole phase one breakwater protected region is considered. For phase two, the longshore salient movement describes 11% of the variance captured in the RTK-GPS dataset and 27% of the variance captured by the video. In phase one this is 16% for the video and 6% of the RTK-GPS data. The longshore movement of the tombolos and salients is also observed in both the pre and post storm video derived intertidal surveys (Figure 4.3.2) and in many results of the numerical model.

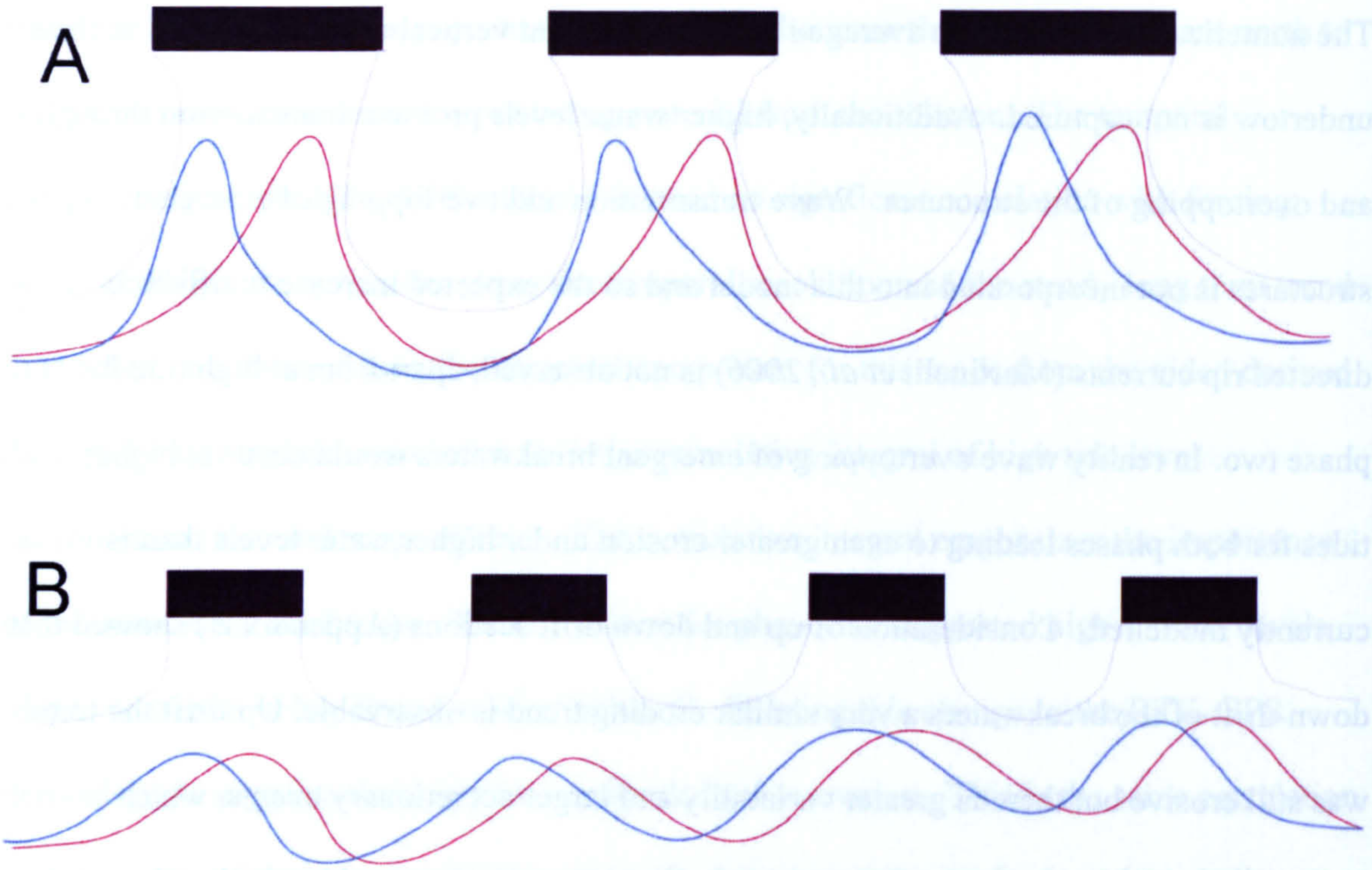

Figure 7.1: A schematic diagram of A) the tombolo movement and B) the salient movement. The blue lines indicate north-westward movement, the red lines south-eastward movement and the grey lines the regions of maximum wave energy (approximated from Figure 6.4.4).

In all cases the movement of the phase one tombolos is better defined than the movement of the phase two salients. This is due both to the greater difference in sheltered and unsheltered regions for phase one due to the larger, higher, breakwaters and due to the nature of the tombolos themselves. A schematic diagram of this is shown in Figure 7.1. The difference in sheltered regions and the effect on potential feature movement can be seen. The tombolos are larger features, creating a groyne-like effect and thus being more effective in trapping longshore mobile sediment, and are tied to their locations giving more defined changes. Storm induced longshore movement of these features is co-incident with beach rotation. In phase two the longshore movement of the salients is more diffuse and involves redistribution of sediment around the embayment which leads to a classic beach

rotation, in phase one this is observed in changes to the cross-shore profile gradient, oblique storm events cause flattening of the exposed (down-drift) tombolo flank and steepening of the sheltered (up-drift flank).

The numerical model results showed that the tombolos were particularly sensitive to forcing, exhibiting morphological change during all model tests. Wave only tests utilising the mean wave condition (shore normal) led to north-westward movement of the tombolos (Figure 6.4.2C). Tides with wave stirring tests showed that under all tidal conditions the tombolos exhibited south-eastward tombolo movement with erosion on the north-western flank and accretion on the south-eastern flank (Figure 6.4.14). Increasing tidal range increased the magnitude of this morphological change due to increased tidal current speeds. Magnitude of vertical change induced by tides alone ranged from 2cm to over 7cm for one tidal cycle. Tidal influence on the morphology of the breakwater protected area is concentrated on the tombolos and salients: whilst this region is the most sheltered from incident wave energy, flow compression in the horizontal (breakwater forced) and vertical (morphology forced) means that the tidally induced changes are greatest effect in the wave sheltered regions. Combining mean wave conditions with tidal conditions showed that neap tides with mean wave conditions lead to north-westward movement of the tombolos whilst mean and spring tidal ranges with mean wave conditions produced south-eastward movement. This result indicates the importance of tidal currents in directing morphological change and also provides a recovery mechanism for southward displaced tombolos. For all tests the southernmost tombolo, tombolo 8, was the most sensitive and showed the most defined regions of change. The model also replicated the increasing skewness in the tombolo for northerly storm events. This increase in skewness does not occur under easterly events due to the different sediment transport pathways: under wave action incident from the north the sediment transport pathway is linear from north to south, whereas for wave

action incident from the east, a gyre is formed (Appendix A, Figure 10). Tests run under persistent storm conditions from both oblique directions showed that both the tombolos and salients respond quickly over the first tidal cycle and then the rate of down-drift movement slows as the tombolo/salient crest reaches its limit of movement (Figure 6.4.26-29). This test proves two points that were postulated in Chapter 4: that there are limits to the longshore range of tombolo/salient movement and that antecedent morphological conditions are important to the wave driven tombolo/salient movement. The breakwater controlled limits on longshore movement of tombolos and salients mean that persistent wave conditions from one oblique direction will not move the tombolos/salients progressively further down-drift at a constant rate. Instead, the model predicts that under northerly storm conditions the tombolo crest level will lower (erosion) and under easterly storm conditions the tombolo crest will raise (accretion) without continued longshore movement. Antecedent morphological conditions are important to the extent of longshore movement because if for one survey the tombolos are in their southernmost position, at the next survey, if there have been continual northerly waves, there will be no longshore movement observed. Equally, the test for storm recovery under mean wave conditions (Figure 6.4.31) shows northward movement of the tombolos whereas the mean wave conditions for the standard bathymetry force a southward movement of the tombolos (Figure 6.4.20). These points mean that correlation of longshore movement with wave forcing becomes harder due to the non-linearity of response.

The timescale of the tombolo and salient response to changing wave conditions is rapid, of the order of days, translating 25m over single storm events (Figure 4.3.3). The numerical model results show tombolos reach their new longshore equilibrium position after 4 tidal cycles (Figures 6.4.26-27). Salients show similarly rapid response (Figure 4.3.4 & Figures 6.4.28-29). The rapidity of response is shown in the highly varying temporal

components for the relevant spatial eigenfunctions derived from EOF analysis (Figures 4.4.10 & 4.4.13). The temporal component for tombolo movement from the video derived dataset is best correlated with the cumulative integral of tidal range, this suggests that spring tides lead to north-westward movement and neap tides to south-eastward movement. Strangely, this is the reverse correlation as would be predicted by the numerical modelling, which showed that with mean wave conditions, neap tides lead to north-westward movement and spring tides to south-eastward movement especially for tombolo 8. However, closer inspection of this change for the neap tide case shows that the north-westward movement is concentrated on the lower intertidal and that for the upper intertidal the change is the same direction as for the spring tides. Hence the mean sea level contour would not be affected by the north-westward movement.

Both the DPGS and video derived temporal components for the second mode of change for phase two showed a significant correlation of the longshore salient movement with the relative tidal range parameter. This parameter (TR/H_s) is used to describe the balance of forcing between tides and waves The correlation between temporal components and relative tidal range suggested that large values of relative tidal range (large tidal range and small waves) were co-incident with the salients being north-west of the mean position and small values of relative tidal range (small tidal range and large waves) co-incident with the salients being south-east of mean. Numerical modelling did not show any difference in intertidal salient movement for differing values of RTR.

Despite down drift movement of the tombolos and salients forced by oblique waves being observed in the storm response and modelled under various wave conditions, none of the temporal components from video or RTK-GPS correlated with the estimate of longshore sediment transport. The lack of correlation is explained via the importance of antecedent conditions to the rate and direction of response. It was also determined from the

storm condition modelling that increasing wave incidence does not increase the extent of tombolo movement. The reverse occurs, as increasing wave obliqueness reduces the effective gap length and thus the amount of wave energy entering the protected area (Appendix A, Figure A9). This explains the lack of correlation with longshore sediment transport estimates as increasing wave obliqueness increases longshore sediment transport. The lack of correlation does not mean that obliquely incident waves are not important in the longshore movement of the salients and tombolos as it is clearly demonstrated to be important by the work on storm induced change (Chapter 4.3), the numerical modelling (Chapter 5) and previous work (Dolphin *et al.*, 2005).

Thus, to summarise the second mode of change, longshore movement of the salient and tombolos are forced by both waves and tides. Oblique waves, move the tombolos and salients in a down drift direction, but increasing obliqueness of angle of incidence does not increase the rate of down drift movement due to the reduction in wave energy entering the embayment. The antecedent morphology also influences the extent of longshore movement due to the breakwaters confining the range of feature movement. Mean wave conditions (shore normally incident) can act to move the tombolos in either direction, depending on the antecedent morphology and on the tidal range. The dependence of direction of movement under mean wave conditions on antecedent morphology can be considered a restorative action, moving the tombolo to the centre of the protected region. Tidal effects force a southward movement of the tombolos, especially tombolo 8, increasing tidal range increases the magnitude of this change. Lesser tidal effect is noticed for the salients. For smaller wave heights, wave action mobilises sediment but the transport pathways are dictated by the tidal currents. As wave height increases, or tidal range decreases, the effect of the wave driven circulation becomes more important. As wave and tidal conditions continually change the tombolos and salients are continually moving within the constraints

dictated by the sheltering effect of the breakwaters and the concept of an equilibrium tombolo/salient position is not viable in a wave climate with such varied angles of wave incidence. Response to changes in forcing is rapid because whilst the breakwaters shelter the tombolos and salients from shore normal waves, the features are exposed to obliquely incident waves and the size of the features are not large enough to resist down-drift movement.

Cross-shore changes

The third mode of change describes a cross-shore exchange of sediment and is observable in the RTK-GPS dataset and the phase two video derived dataset. This mode of change represents 11% of the phase one variance and 10% phase two of the variance in the RTK-GPS dataset. The change leads to an increase and decrease in beach profile gradient. The increase and decrease in cross-shore profile gradient is not observable in the phase one video derived dataset because the nodal point lies close to the mean sea level contour. Three dimensional patterns of change in the phase two cross-shore sediment exchange means that signatures of the cross-shore change are observable in the mean sea level contour dataset.

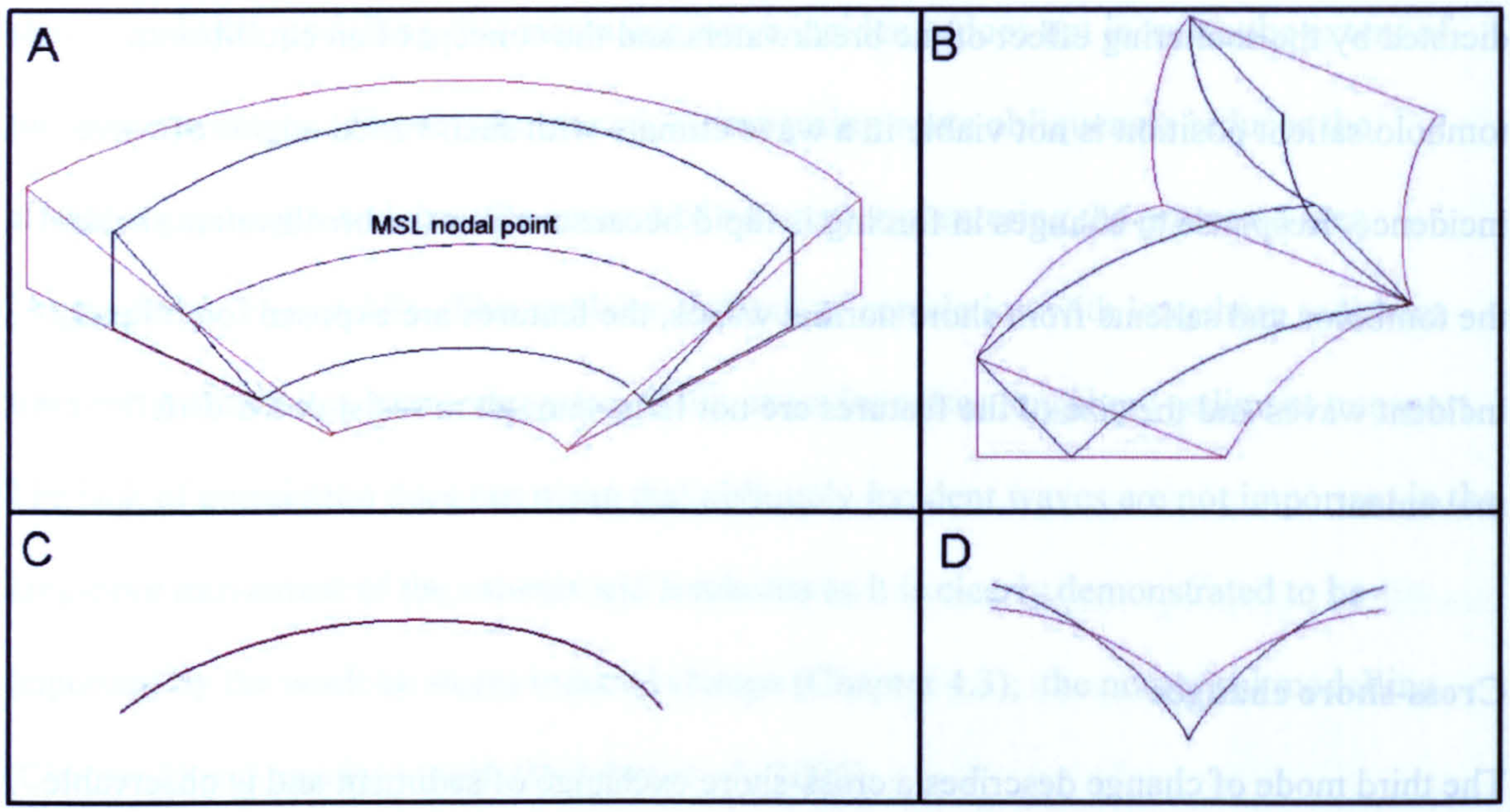

Figure 7.2: A schematic diagram of the cross-shore changes for (A) a section of phase one, (B) a section of phase two and the effect of the cross-shore change on the mean sea level contour for (C) phase one and (D) phase two. Flatter profiles are drawn in red and steeper profiles in black.

A schematic diagram of this change is shown in Figure 7.2. This diagram clearly shows how the cross-shore changes cannot be observed in the phase one mean sea level contour but how for phase two, due to the focuses of change on the lower intertidal bay areas and upper intertidal salient horns, the cross-shore change also effects the mean sea level contour sinuosity.

The phase one cross-shore sediment exchange is uniform about the embayments with accretion (erosion) in the upper-intertidal and erosion (accretion) in the lower intertidal. The nodal point is around the mean sea level contour.

In phase two this change shows an accretionary (erosive) focus on the upper intertidal salient horns and an erosive (accretionary) focus in the lower intertidal bay areas. This change produces the increase and decrease in shoreline sinuosity observed in mode three of the mean sea level contour dataset. The two temporal components for this change

from the RTK-GPS are similar and suggest that there is a slow steepening of the cross-shore profile (increasing phase two MSL contour sinuosity), interspersed with large flattening events (shore sinuosity reduced). Increases in beach steepness occur under low wave conditions whilst the flattening events are co-incident with large storm and surge conditions. Storms that are incident without surge conditions do not produce the same extent of profile gradient reduction (Figure 5.3.11 & Figure 5.3.12). Cross-shore profile changes measured over storms using the video cameras showed that large flattening only occurred under storm and surge conditions which corroborate this observation (Figure 4.2.7). Equally numerical modelling showed a greater beach flattening for surge conditions than for non surge storms (Figure 6.4.25), this is caused by the elevated water level allowing greater erosion of the supra-tidal and upper intertidal and correspondingly greater accretion lower down the beach profile. Post profile flattening events, the rate of profile steeping is greater than the background rate due to rapid initial beach recovery. The temporal component derived from the mean sea level contour showed seasonality with increased sinuosity in summer (smaller waves) and reduced sinuosity in winter (larger waves). The highest correlation for this mode of change was with wave period. Larger wave periods were correlated with reduction in shoreline sinuosity. It was suggested that longer wave periods, which refract and diffract into sheltered regions more and which are transmitted through the breakwater better would allow greater wave energy to act upon the sheltered salient horns, eroding them and depositing the eroded material in the embayments. The effect of wave transmission could not be tested using the numerical model because wave transmission through the breakwater was not included in the model architecture. A diagram of wave direction vectors computed from the numerical model (Figure 6.4.9) showed that the difference in refraction and diffraction for waves of different periods, whilst noticeable in the region close behind the breakwater, was insignificant

nearer the shore and so it is unlikely that the influence of wave period on refraction and diffraction would have much effect on the change in sinuosity. No difference in sinuosity was observed in the morphological change for model tests with differing period. Consideration of the up and down drift beaches (Appendix B) shows that steeper beaches are formed by a low tide terrace profile and flatter beaches by a long-shore bar and trough system (up-drift) or featureless profile (down-drift). The breakwater protected beaches do not display either a longshore bar and trough or a low tide terrace profile shape. This is due to the increased three-dimensionality and small embayment sizes meaning there is not enough space for the features to develop.

Sub-tidal changes in phase one

This mode of change involves the sub tidal embayment centres of phase one. Since the sub-tidal morphological change is only observable in the RTK-GPS dataset, no additional information can be obtained from consideration of the video data. This mode of change describes an erosion and accretion of the sub tidal bays which accounts for 15% of the variance in morphology for phase one. The temporal component for this change is oscillatory between two states corresponding to a shallow bay floor with steeper intertidal gradient and a deeper bay floor with shallower intertidal gradient. The magnitude of bay floor change is ~0.5m between deep and shallow states. The transition between states is rapid with lesser changes once the new state has been obtained. Three complete morphological periods are captured in the data and the residence time for one morphological period is 6, 6 and 2 months respectively. Transitions to a deeper bay state are co-incident with storms associated with surge events, transitions to a shallow bay state are also co-incident with energetic conditions but without surge conditions. Previous work (Martinelli *et al.*, 2006) have demonstrated offshore directed rip currents throught the

breakwater gaps for submerged and overtopped structures which would cause erosion of the sub tidal bays. While the numerical modelling of the Sea Palling breakwaters did not show this trend in phase one, it is believed that this is because the numerical model did not incorporate overtopping. Hence this mechanism is postulated as the reason for the sub-tidal erosion under surge conditions.

7.3 Comparison of phase one and phase two

The sixth thesis objective was to compare beach response behind the two different designs of breakwater. Volumetric analysis shows that both phases are eroding, showing similar rates of change and temporal signatures. The standard deviation of vertical morphological change is also similar (0.36m for phase one, 0.31m for phase 2). A comparison between modes of response for both phases is presented in Table 7.1. Both phases show the same order of relative importance for the common modes of change. The amount of variance attributed to the first mode is greater for phase one (59% video / 75% RTK-GPS) than for phase two (46% Video / 58% RTK-GPS), correspondingly, less variance is attributed to the second mode of change in phase one compared to phase two. Similar amounts of variance are attributed to the third mode of response.

Similarities in morphodynamics can be easily observed. For the first mode of response, the phase wide erosion and accretion, the main difference is the intertidal accretion of bay B in phase one. This accretion, whilst the rest of the phase erodes, is explained by the ability of the tombolos to act as groyne-like sediment traps. As the predominant longshore sediment transport direction is from north to south, the sediment is trapped in bay B and bay C continues to erode.

Table 7.1: A comparison between modes of change in phase one and phase two.

Mode of change	Aspect of change	Phase one	Phase two
1. General Erosion / Accretion	Variance Explained	Video: 59% RTK-GPS 75%	Video: 46% 58% RTK-GPS
	Detail of morphological response	Erosion/accretion except for bay B which accretes/erodes	Phase wide erosion/accretion
	Forcing	Higher water levels lead to enhanced erosion	Higher water levels lead to enhanced erosion
	Timescale	Dominant linear erosive trend	Dominant linear erosive trend, seasonal component (erosion in winter, accretion in summer)
2. Longshore movement of tombolos / salients	Variance Explained	Video: 16% RTK-GPS: 6%	Video: 27% RTK-GPS: 11%
	Detail of morphological response	Well defined change focused on tombolo horns	Less defined change incorporating most of intertidal embayment
	Forcing	Dominated by wave, some tidal influence	Dominated by wave, less tidal influence than phase one.
	Timescale	Rapid response to changes in wave forcing	Rapid response to changes in wave forcing
3. Cross-shore profile changes	Variance Explained	Video: N/A RTK-GPS: 11%	Video: 9% RTK-GPS: 10%
	Detail of morphological response	Beach gradient increase/decrease uniform around embayment	Three dimensionality in cross-shore change leading to increase and decrease in salient sinuosity amplitude
	Forcing	Storm events and recovery	Storm events and recovery, wave period.
	Timescale	Rapid storm induced flattening and subsequent slower recovery	Rapid storm induced flattening and subsequent slower recovery. Some seasonality also evident

The longer, higher, phase one breakwaters produce better defined regions of wave shelter which leads to better defined longshore movement of the tombolos compared to the salients (the second mode of response). This is compounded by the tombolo morphology which means both that the tombolos are tied to their location and that they undergo defined patterns of tidally induced bed level change. The shorter, lower phase two breakwaters lead to lesser gradients in wave action and so the salients move in a more diffuse fashion. The salient movement is linked to a beach rotation which is less obvious in the phase one

tombolo response. The more diffuse phase two response explains why there is a greater amount of variance attributed to this change in phase two compared to phase one.

The third common mode of change, the cross-shore sediment exchange, shows differences in morphological response. The change is uniform around the embayments in phase one whereas in phase two there is increased three-dimensionality. No evidence for explanation of this difference is available but the author postulates that it is due to the smaller embayment length scales and the greater exposure of the salient horns compared to the tombolo horns.

Forcing and timescales of response are similar although there is additional seasonality in the first and third mode observable in the phase two responses which is not seen in the phase one response. The larger fully emergent phase one breakwaters provide greater modification of the incident wave field and hence may reduce seasonal variations in wave incidence. For both phases, but more so for phase one, storm and surge events seem to play a dominant role in forcing. Higher water levels (surges) exacerbate the erosion described by the first mode of change; the longshore tombolo and salient movement is forced by oblique waves and increased wave energy increases the magnitude of response; cross-shore profile changes are forced by rapid storm response and slower recovery.

There is an additional mode of change in phase one which is not measured in phase two. This mode of change describes a sub-tidal infilling and erosion of the bay floors. The same change is not observable in phase two partly because the salients do not restrict and reduce the current patterns in the same way as the phase one tombolos (Figure 6.4.12), and partly because the drying tombolos allow for groyne like sediment accumulation. Sediment entering phase two is more likely to be transported through the system than deposited on the sub tidal bay floors. This change is forced by storm events, storms associated with

surges lead to bay floor erosion, energetic wave conditions without surges lead to bay floor accretion.

A final point of note in the comparison of the two phases is that despite identification of phase wide behaviour, individual embayments in each phase behaved in slightly different fashions. This was due both to the influence of currents from adjacent embayments and due to the slight differences in bathymetry for each embayment. These differences are heightened due to the strong longshore currents forced by both tides and oblique waves and by gradients in sediment supply. Hence it is postulated that in regions with large longshore components to flow, multi-breakwater systems should not be designed using simple design rules since each individual embayment will behave differently depending on its position within the scheme.

7.4 Comparison with previous work

The vast majority of work on detached breakwater morphology has focussed on the development of equilibrium bay shapes for use in design guidelines. Little research effort has previously focussed on short to medium term morphodynamics of beaches protected by detached breakwaters, however a certain amount of previous work has been conducted at the Sea Palling site. The work in this thesis corroborates previous research efforts at the Sea Palling site and extends that work both spatially (into phase two) and temporally (investigating longer time periods of change).

The importance of tidal currents to the sediment transport pathways observed by Bacon *et al* (2003) was also found in this numerical modelling and its importance to the longshore movement of the tombolos was noted.

The longshore movement of the phase one tombolos was previously observed under storm conditions (Dolphin *et al.*, 2005). The video based analysis and modelling have

shown that long-shore movement of the tombolos occurs also under non-storm conditions. Extension of research effort into phase two showed that the salients displayed similar longshore movement but lesser definition in terms of response due to the shorter lower breakwaters. Thomalla and Vincent (2004) previously suggested that prediction of an equilibrium shoreline at Sea Palling might be impossible due to the widely varying wave climate. The rapidity of response to the tombolos and salients modelled and measured in this work certainly corroborates this postulate.

Work at another system of detached breakwaters at Elmer in the UK (Axe and Chadwick, 1997) had demonstrated that profile variability reduced behind the breakwater system compared to up and down drift beaches. Consideration of the standard deviation (Appendix B) has shown the same occurs at Sea Palling, where standard deviation inside the breakwater scheme is 65-75% of the standard deviation outside the scheme. However, whilst variability of response reduces the complexity of response increases due to added three-dimensionality in initial morphology, wave forcing (due to the breakwaters) and resultant morphodynamic response. The same work (Axe and Chadwick, 1997), suggested that in winter sediment was stored on the bay floors whereas for phase one at Sea Palling the reverse seems to occur. This difference could be due to the Elmer breakwaters being positioned in the intertidal region.

The cresentic beaches formed by detached breakwaters are similar to natural embayed or pocket beaches. Natural embayed beaches have been shown to behave in similar ways. An EOF analysis of an embayed beach at Narrabeen (Australia), showed similar modes of response with the primary mode being an erosion/accretion mode (beach oscillation) and the second mode indicating beach rotation (Harley *et al.*, 2008). Both modes have slower temporal variance than for the Sea Palling beaches and this is probably related to the size for the beach and to differences in the local wave climate. Greater

dependence on incident wave height is shown for the oscillation mode, this highlights the effect the breakwaters have on altering the importance of hydrodynamic conditions. Beach rotation processes have been directly linked to varying directions of wave incidence, the temporal signal varying from days to years (Archetti and Lamberti, 2008). Short term beach rotation processes directly attributed to storm events have been observed in natural embayed beaches in Brazil (Klein *et al.*, 2002). The same work showed shorter beach lengths equated with shorter response times which corroborates the rapid response observable at Sea Palling. Beaches of higher curvature had more defined responses. This is similar to the better defined changes in phase one compared to phase two. A similar dependence on wave sheltering was postulated in Klein *et al.* (2002) as was described in this thesis to explain the differences between phase one and phase two.

7.5 Implications of this research

This work has investigated the morphodynamics of breakwater protected beaches at Sea Palling, UK. The breakwaters force morphology of high curvature and interaction of the breakwaters and resultant morphology with incident hydrodynamic conditions mean that the morphodynamics are different to the nearby unprotected beaches. The embayments formed by detached breakwaters are similar to embayed or pocket beaches and comparison with research into embayed beaches shows that there are similarities in morphodynamic response, especially in beach rotation to varying wave incidence. The difference is that the boundaries of the embayment move with the beach rotation and that the smaller embayment sizes lead to faster re-alignment. Classically one might expect seasonal beach rotation but at this site rotation occurs at a storm event timescale.

The continual erosion (mode of change 1) shows that the structures are failing to perform as coastal protection. The locality of the study site is on an eroding coastline and

the detached breakwater system is failing to ameliorate this erosive trend. Rates of erosion are similar inside the scheme to up- and down-drift beaches. The large tombolo to the north of the breakwater field blocks a significant amount of the longshore sediment transport and exacerbates the erosion problems down-drift. This suggests that at sites where there is significant longshore sediment transport, breakwaters that form salients rather than tombolos should be implemented.

A general observation of the work (especially via the numerical modelling) is the differences in hydro- and sediment dynamics and associated morphological response between embayments of the same phase. This is partially due to the morphological development of the scheme giving different bathymetric conditions in each embayment and partially due to current interactions between embayments. This difference in response should be expected for all sites where there is significant oblique wave incidence, significant longshore tidal currents and the breakwater lengths are not long enough such that wave induced currents reduce to zero in their lee.

Under tidal conditions, the effect of high water levels and the balance between tidal and wave driven currents are of utmost importance for the morphological evolution of the scheme. Two important points should be drawn from this: firstly tidal currents should be incorporated into models used for breakwater design in meso-tidal and macro-tidal areas; secondly, the importance of tidal height emphasizes the importance of breakwater crest level in design guidelines. The importance of storm surge conditions to morphological changes in this region is demonstrated both by the RTK-GPS and video data. The importance of this may well be site specific as the southern North Sea is well known to be particularly vulnerable to surge events.

Cross-shore drivers for longshore shoreline change (the increase and decrease in amplitude of salient sinuosity), suggests that simplistic one line models of shoreline change

may fail to fully represent changes at this site. Indeed, the complexity of response measured by the RTK-GPS and video was not fully modelled by a 2DH modelling system and hence a fully 3-dimensional model may be required to completely predict morphodynamics at sites such as Sea Palling. Overtopping of the emergent breakwaters, and transmission through the breakwaters, was not incorporated in the model used here. It is recommended that to increase accuracy of morphodynamic simulations these processes should be incorporated in future models.

The standard deviation of morphological response reduces behind detached breakwaters; however the complexity of the morphodynamics increases. This is largely due to increased three-dimensionality in response and the impediment to longshore sediment supply caused by the tombolos and salients. While this thesis goes some way to addressing this increased complexity via definition of modes of change, further research into the short to medium term morphodynamics of detached breakwater protected beaches would be fruitful. The LeaCoast2 project has made substantial in-roads into investigating breakwater protected beaches. An additional campaign of detailed instrumentation over a tombolo and salient would be interesting to help better elucidate the mechanisms of longshore feature movement. The high frequency video shoreline dataset proved invaluable in the determination of modes of change and their relation to forcing. Efforts to extend this dataset into the future can only further understanding of the system and allow determination of the scheme morphology's longer term evolution through time.

8. Final conclusions

Argus video data, differential global positioning surveys, and 2DH numerical modelling have been used to characterise and explain beach variability and beach morphodynamics behind a system of detached breakwaters built in two design phases. The breakwater system is failing to completely reduce the local erosion problem, with rates of erosion inside and out of the breakwater system being similar (vertical elevation changes per unit area of -0.5m yr^{-1}). However, the breakwater system, like other previously researched breakwater schemes (Axe and Chadwick, 1997), does reduce the variability of the protected beaches. Standard deviation of vertical change inside the scheme is 65-75% of the standard deviation of vertical change outside of the scheme. The change in the mean sea level contour is focussed on the tombolos and salients; the numerical model also shows that these are the most dynamic regions. Whilst the standard deviation of the change is less, the complexity of the change is greater due to three-dimensionality in forcing caused by both the breakwaters and the influence of the embayment morphology.

Morphodynamic responses of the breakwater protected beaches behind both designs of structure can be described with three main modes of change. These modes of change, in descending order of importance, are: a general erosion and accretion; a longshore movement of the tombolos and salients and cross-shore profile changes. Both the RTK-GPS surveys and the video derived mean sea level contour dataset show the same modes of change although the variance described to each mode of change is different. Differences in both details of the change and in temporal signals can be observed between the two phases. These differences are forced not only by the different breakwater geometries providing different wave field modification but also by the differing interactions of salients and tombolos with the wave and tidally forced currents.

The general erosion and accretion is spatially uniform through phase two, although the mean sea level contour analysis shows slight enhancement of change on the salient horns. The change in phase one displays greater spatial structure. The intertidal region in the middle of phase one bay (bay B) accretes whilst the rest of the phase erodes and, like phase two, the mean sea level contour analysis suggests focusing of change on the tombolo horns. The intertidal accretion in bay B when the rest of the phase is eroding was explained by the tombolos groyne-like effect. Numerical modelling has show that the tombolos and salients are the most dynamic regions which explains concentration of change in those areas.

The longshore movement of the phase one tombolos was better defined than for the phase two salients. The greater definition to response was caused by the greater gradients in wave energy between sheltered and unsheltered regions caused by the longer, higher phase one breakwaters and by the nature of the tombolo morphology. Associated with south-eastward movement of the tombolos is an increase in skewness in tombolo shape whereby the exposed flanks are flattened and the sheltered flank gradients become steeper. North-westward tombolo movement does not show the same increase in skewness due to the different sediment transport pathways forcing the change: the south-eastward movement is caused by a linear current whilst the north-westward movement is caused by a re-circulation gyre. The change in skewness is not observable for the salients and this is probably due to the lesser gradients in wave energy around the smaller structures.

The cross-shore profile changes have a nodal point around the mean sea level contour for both phases. In phase one the changes are uniform about the embayments. In phase two there is additional three-dimensionality to the cross-shore change with focussing of change on the upper intertidal salient horns and on the lower intertidal bay centres. This leads to an increase and decrease in the sinuosity amplitude of the mean sea level contour.

It is believed that the three dimensionality is caused partially by the greater exposure of the phase two salient horns and partially by the smaller embayment length scales in phase two.

The temporal signals are largely forced by individual storm and surge events for phase one. Phase two also shows a strong dependence on storm effects but clear seasonal dependence is also observable for the erosion/accretion of the beach and for the cross-shore profile changes. In winter, the phase two beaches are lower and narrower and the salients exhibit subdued sinuosity. In summer the phase two beaches are wider / higher and the salients are enhanced with more prominent horns and deeper bays. It is thought that the lack of seasonality to the changes in phase one is caused by the extent of wave field modification forced by the larger structures reducing differences in wave field between summer and winter. The smaller, lower, phase two structures provide lesser modification in the incident wave field and thus a seasonal component of change occurs.

For both phase one and phase two the temporal signal of the general erosion and accretion is dominated by the underlying erosive trend. Greater erosion occurs under higher water levels for both phases. Higher water levels (especially surges) enhance wave overtopping of the structures and promote erosion via increased wave action at the shoreline.

The longshore movement of the tombolos and salients is largely forced by oblique wave incidence and the temporal signal is one of rapid response to changes in wave direction, with largest changes forced by large wave events. The actual mechanism of change is different depending on the direction that the tombolos are moving: South-eastward movement is effected by linear flow over the tombolos whilst north-westward movement is caused by a gyre leading to deposition of material eroded from the exposed down drift flank on the up-drift sheltered flank. This difference in sediment transport pathway is forced by asymmetry in the embayment morphology. Movement of the salients

is caused by linear flow in both the north-westward and south-eastward directions. The wave forcing is non-linear with increasing obliqueness not increasing the rate of longshore movement. Increasing wave heights do increase the magnitude of change. The initial morphological conditions influence the extent and, in some cases, direction of the longshore movement. Continuous wave conditions from one direction will lead to rapid re-adjustment of the tombolo position, then the rate of longshore movement will slow and stop. The tombolo location is determined by the position of the region sheltered from wave action which is determined by the breakwater location and the incident wave direction. Tidal currents also affect the longshore movement of the tombolos, less tidal influence is observable on the salient movement. Tidal currents with wave stirring cause a slight north to south movement of the tombolos. Under mean wave conditions the tidal range determines the direction of tombolo movement: northerly movement under neap tidal ranges and southerly movement under spring and mean tidal ranges. These differences in tidally controlled transport are partially due to the tidal current speed (which increases with tidal range) and partially due to the extent of drying of the tombolos.

Cross-shore profile changes are forced by storm events in phase one, in phase two storm events are also important but a dependence on wave period is also observed.

A forth mode of change, the erosion and accretion of the sub-tidal bays, only occurs in phase one. In phase two, uninterrupted tidal currents smear sub-tidal changes and so such a mode of change is not observable. The morphology described by this mode of change oscillates between higher and lower bay floor elevations. Accretion on the bay floor is forced by energetic wave conditions bringing sediment into the embayments and erosion forced by storm and surge events where, it is postulated, offshore directed rip currents caused by overtopping lead to removal of material from the embayments.

The strength of the tidally induced currents mean that the scheme morphodynamics are controlled by a balance between wave driven currents and tidally driven currents. Both wave and tidal currents can produce gyres in phase one whilst in phase two tidal currents are linearly longshore directed and wave conditions produce gyres. Under storm conditions the circulation is wave dominated. For mean wave conditions, current patterns are close to the tipping point between wave and tide dominance: Spring tide conditions are tide dominated whereas neap tide conditions are wave dominated. Phase one shows greater tidal dominance than phase two because the tombolos are emerged at low tide which enhances tidal asymmetry and because when submerged, the tombolos are shallow leading to greater flow compression and increasing flow speeds over the tombolos.

9. References

Aargard, T., Kroon, A., Anderson, S., Sorensen, R., Quartel, S., Vinther, N., 2005. Intertidal beach change during storm conditions; Egmond, The Netherlands. Marine Geology, 218: 65-80.

Aarninkhof, S., 2003. Nearshore Bathymetry derived from Video Imagery. Doctoral Thesis Thesis, Delft University of Technology, Delft, 175 pp.

Aarninkhof, S., Morellisen, R., Cohen, A., 2006. The Argus Runtime Environment-Guidelines on Installation and Use. Delft Hydraulics pp. 48.

Aarninkhof, S., Ruessink, B.G., Roelvink, J.A., de Kruif, A.C., 2003a. Quantification of surf zone bathymetry from video observations of wave breaking, Coastal Sediments, Florida, USA.

Aarninkhof, S., Turner, I.L., Dronkers, T.D.T., Caljouw, M., Nipius, L., 2003b. A video-based techniqe for mapping intertidal beach bathymetry. Coastal Engineering, 49: 275-289.

Ahrens, J.P., Cox, J., 1990. Design and performance of Reef Breakwaters. Journal of Coastal research, 51(7): 61-75.

Alexander, P.S., Holman, R.A., 2004. Quantification of nearshore morphology based on video imaging. Marine Geology, 208: 101-111.

Archetti, R., 2009. Quantifying the Evolution of a Beach Protected by Low Crested Structures Using Video Monitoring. Journal of Coastal Research, 25(4): 884-899.

Archetti, R., Lamberti, A., 2006. Study of hydrodynamics induced by low crested structures through image processing. In: J. Mckee Smith (Editor), Proceedings of the 30th international conference on coastal engineering. World Scientific, San Diego, pp. 5021-5033.

Archetti, R, .Lamberti, A., 2008. Storm-driven shore changes of a beach protected by a low crested structure. In: J.M. Smith (Editor), Coastal Engineering 2008. World Scientific Publ Co Pte Ltd, Hamburg, Germany, pp. 1977-1989.

Aubrey, D.G., 1979. Seasonal patterns of onshore/offshore sediment movement. Journal of Geophysical Research, 84(C10): 6347-6354.

Axe, P., Chadwick, A., 1997. Beach variability behind detached breakwaters. In: E.B. Thornton (Editor), Coastal Dynamics '97. ASCE, Plymouth, U.K., pp. 744-753.

Axe, P., Ilic, S., Chadwick, A., 1996. Evaluation of beach modelling techniques behind detached breakwaters. In: B.L. Ledge (Editor), Coastal Engineering. ASCE, Orlando, Florida.

Bacon, J., Vincent, C., Dolphin, T., J., T., Pan, S., O'Connor, B., 2007. Shore-parallel breakwaters in meso-tidal conditions: tidal controls on sediment transport and their longer term, regional impacts at Sea Palling, UK. Journal of Coastal Research, S.I.50: 369-373.

Bacon, J.C., Vincent, C.E., Dolphin, T., Taylor, J., Pan, S.Q., O'Connor, B., 2005. The offshore breakwater scheme at Sea Palling, England; Sand transport generated by tidal currents. In: J.M. Smith (Editor), Coastal Engineering 2004, Vols 1-4, pp. 1896-1908.

Bacon, J.C., Vincent, C.E., Pan, S.-Q., O'Connor, B., 2003. Effects of tidal currents on sediment pathways around the shore-parallel breakwaters at Sea Palling, England., Coastal Sediments, Clearwater Beach, Florida, US.

Baptista, P., Bastos, L., Bernardes, C., Cunha, T., Dias, J., 2008. Monitoring sandy shores morphologies by DGPS - A practical tool to generate digital elevation models. Journal of Coastal Research, 24(6): 1516-1528.

Bertin, X., Oliveira, A., Fortunato, A.B., 2009. Simulating morphodynamics with unstructured grids: Description and validation of a modeling system for coastal applications. Ocean Modelling, 28(1-3): 75-87.

Bidlot, J.-R., Holt, M.W., 1999. Numerical wave modelling at operational weather centres. Coastal Engineering, 37: 409-429.

Boak, E.H., Turner, I.L., 2005. Shoreline definition and detection: A review. Journal of Coastal Research, 21(4): 688-703.

Bowman, D., Pranzini, E., 2003. Reversed responses within a segmented detached breakwater, the Tuscany coast, Italy - a case study. Coastal Engineering, 49: 263-274.

Bradbury, A., Mason, T., Holt, W., 2004. Comparison of the performance of the Met Office UK-waters wave model with a network of shallow water moored buoy data, 8th International Workshop on Wave Forecasting and Hindcasting, Hawaii, pp. G1.

Briganti, R., Bellotti, G., Franco, L., De Rouck, J., Geeraerts, J., 2005. Field measurements of wave overtopping at the rubble mound breakwater of Rome-Ostia yacht harbour. Coastal Engineering, 52(12): 1155-1174.

Caceres, I., Sanchez-Arcilla, A., Zanuttigh, B., Lamberti, A., Franco, L., 2005. Wave overtopping and induced currents at emergent low crested structures. Coastal Engineering, 52: 931-947.

Caceres, I., Stive, M.J.F., Sanchez-Arcilla, A., Trung, L.H., 2008. Quantification of changes in current intensities induced by wave overtopping around low-crested structures. Coastal Engineering, 55(2): 113-124.

Capo, S., Parisot, J.P., Bujan, S., Senechal, N., 2009. Short time morphodynamics response of the Truc Vert Beach to storm conditions. Coastal Education & Research Foundation, Lisbon, Portugal, pp. 1741-1745.

Charfas, C., 1990. The fringe of ocean - under siege from land. Science, 248(4952): 163-164.

Chen, C., Liu, H., Beardsley, R., 2003. An unstructured grid, finite-volume, three-dimensional, primitive equations oceans model: Application to coastal ocean and estuaries. Journal of atmospheric and oceanic technology, 20: 159-186.

Chickadel, C.C., Holman, R.A., Freilich, M.H., 2003. An optical technique for the measurement of longshore currents. Journal of Geophysical Research, 108(c11).

Clarke, G., Cooke, D., 1998. A basic course in statistics London. Arnold.

Clayton, K.M., 1989. Sediment Input from the Norfolk Cliffs, Eastern England- A century of Coast Protection and its Effect. Journal of Coastal Research, 5(3): 433-443.

Clayton, K.M., McCave, I.N., Vincent, C.E., 1983. The Establishment of a sand budget for the East Anglian coast and its implications for coastal stability Shoreline Protection. Thomas Telford, London, pp. 91-96.

Cohen, A., Aarninkhof, S., Chickadel, C., 2004. Video-derived observations of longshore currents, Coastal Engineering 2004, pp. 1468-1479.

Coombes, E.G., Jones, A.P., Sutherland, W.J., 2009. The Implications of Climate Change on Coastal Visitor Numbers: A Regional Analysis. Journal of Coastal Research, 25(4): 981-990.

Costas, S., Alejo, I., Vila-Concejo, A., Nombela, M.A., 2005. Persistence of storm-induced morphology on a modal low-energy beach: A case study from NW-Iberian Peninsula. Marine Geology, 224(1-4): 43-56.

Dally, W.R., Dean, R.G., Dalrymple, R.A., 1985. Wave height variation across beaches of arbitrary profile. Journal of Geophysical Research, 90: 11,917-11,927.

Daoud, A., Rakha, K., Abul-azm, A., 2008. A two dimensional finite volume hydrodynamic model for coastal areas: Model development and validation. Ocean Engineering, 35: 150-164.

Davidson, M., Van Koningsveld, M., de Kruif, A., Rawson, J., Holman, R., Lamberti, A., Medina, R., Kroon, A., Aarninkhof, S., 2007. The CoastView project: developing video-derived coastal state indicators in support of coastal zone management. Coastal Engineering, 54(6-7): 463-475.

Davidson, M.A., Aarninkhof, S.G.J., Van Koningsveld, M., Holman, R.A., 2004. Developing coastal video monitoring systems in support of coastal zone management. Journal of Coastal research, S.I. 39: 463-475.

Dean, R.G., Chen, R.J., Browder, A.E., 1997. Full scale monitoring study of a submerged breakwater, Palm Beach, Florida, USA. Coastal Engineering, 29(3-4): 291-315.

DHI, 2008a. MIKE 21 and MIKE 2 Flow Model FM, Hydrodynamic and Trnasport Module, Scientific Documentation, DHI Group, Horsholm.

DHI, 2008b. MIKE 21 and MIKE 3 FLOW MODEL FM, Sand Transport Module, Scientific Documentation, DHI Group, Horsholm.

DHI, 2008c. MIKE 21, Spectral Wave Module, Scientific Documentation, DHI Group, Horsholm.

Doering, J., Bowen, T., 1995. Parametisation of orbital velocities under shoaling and breaking waves using bispectral analysis. Coastal Engineering, 26: 15-33.

Dolphin, T., Taylor, J., Vincent, C., Bacon, J., Pan, S.Q., O'Conner, B., 2005. Storm-scale effects of shore-parallel breakwaters on beaches in a tidal setting (Leacoast). In: J.M. Smith (Editor), 29th International Conference on Coastal Engineering World Scientific, Lisbon, pp. 2849-2861.

Dolphin, T., Vincent, C., Bacon, J., Dumont, E., Terentjeva, A., *Submitted*. Medium-term impacts of a segmented shore-parrallel breakwater system Coastal Engineering.

Dommenget, D.Latif, M., 2002. A cautionary note on the interpretation of EOFs. Journal of Climate, 15: 216-225.

Drei, E., Lamberti, A., 1999. Wave pumping effect of a submerged barrier. In: Losada, M. (Editor), Coastal Sediments '99, pp. 667-673.

Dyke, P., 1996. Modelling Marine Processes. Prentice-Hall, 152 pp.

Elko, N.A., Holman, R.A., Gelfenbaum, G., 2005. Quantifying the rapid evolution of a nourishment project with video imaging. Journal of Coastal research, 21(4): 633-645.

Emery, W., Thomson, R., 1997. Data analysis methods in physical oceanography Elesvier Science. Gray publishing, Tunbridge Wells, 634 pp.

Engelund, F., Fredsoe, J., 1976. A sediment transport model for straight alluvial channels. Nordic Hydrology, 7: 296-306.

Fairley, I., Davidson, M., Kingston, K., 2009a. The morpho-dynamics of a beach protected by detached breakwaters in a high energy tidal environment. Journal of Coastal Research, S.I. 56: 607-611.

Fairley, I., Davidson, M., Kingston, K., 2009b. A video based investigation into the morphological impacts of storms behind a series of detached breakwaters. In: R. Lehfeldt and H. Schuttrumpf (Editors), Poster Proceedings of 31st International Conference on Coastal Engineering. Druckservice Zillekens, Hamburg, pp. 80-91.

Fairley, I., Davidson, M., Kingston, K., 2009c. Video monitoring of overtopping of detached breakwaters in a mesotidal environment. In: L. Franco, G. Tomasicchio and A. Lamberti (Editors), Coastal Structures '07. World Scientific, Venice, pp. 1923-1932.

Fairley, I., Davidson, M., Kingston, K., Dolphin, T., Phillips, R., 2009d. Empirical orthogonal function analysis of shoreline changes behind two different designs of detached breakwaters. Coastal Engineering, 56(11-12): 1097-1108.

Fairley, I., Davidson, M.A., 2008. A two-dimensional wave flume investigation into the effect of multiple vertical steps on the form of breaking waves. Journal of Coastal Research, 24(1): 51-58.

Farris, A.S., List, J.H., 2007. Shoreline change as a proxy for subaerial beach volume change. Journal of Coastal Research, 23(3): 740-748.

Fredsoe, J., Andersen, O.H., Silberg, S., 1985. Distribution of suspended sediment in large waves. Journal of waterway Port Coastal and Ocean Engineering, 3(6): 1041-1059.

Freitas, M.P., Menezes, J.T., Langui, M.P., Vintem, G., Klein, A., 2006. Morphological analysis of beach through global system position. Journal of Coastal Research, 2: 669-672.

Garcia, N., Lara, J.L., Losada, I.J., 2004. 2-D numerical analysis of near-field flow at low-crested permeable breakwaters. Coastal Engineering, 51(10): 991-1020.

Golding, B., 1893. A wave prediction system for real-time sea state forecasting. Quarterly journal of the Royal Meteorological Society, 109: 393-416.

Gonzalez, M., Medina, R., 1999. Equilibrium shoreline response behind a single offshore breakwater, Coastal Sediments '99. ASCE, New York, pp. 844-859.

Gourlay, M.R., 1974. Wave set-up and wave generated currents in the lee of a breakwater or headland, Proceedings, 14th Conference on Coastal Engineering. ASCE, Copenhagen, Denmark, pp. 1977-1995.

Guza, R.T., Thornton, E.B., 1981. Wave set-up on a natural beach. Journal of Geophysical Research, 86(C5): 4133-4137.

Hamer, B.A., Hayman, S.J., Elsdon, P.A., Fleming, C.A., 1998. Happisburgh to Winterton Sea Defenses: Stage Two, Coastlines, Structures and Breakwaters. Thomas Telford, London.

Hanson, H., 1989. Genesis - A Generalised Shoreline Change Numerical Model. Journal of Coastal Research, 5(1): 1-27.

Harley, M.D., Turner, I.L., 2008. A simple data transformation technique for pre-processing survey data at embayed beaches. Coastal Engineering, 55(1): 63-68.

Harley, M.D., Turner, I.L., Short, A.D., Ranasinghe, R., 2008. Rotation and ocsillation of an embayed beach. In: J.M. Smith (Editor). World Scientific, Hamburg, Germany, pp. 865-875.

Holland, K.T., Holman, R.A., Lippman, T.C., Stanley, J., Plant, N., 1997. Practical use of video imagery in nearshore oceanographic field studies. IEEE Journal of Oceanic Engineering, 22(1): 81-92.

Holman, R.A., 1981. Infragravity energy in the surf zone. Journal of Geophysical Research, 86(C7): 6442-6450.

Holman, R.A., Guza, R.T., 1984. Measuring run-up on a natural beach. Coastal Engineering, 8: 129-140.

Holman, R.A., Stanley, J., 2007. The history and technical capabilities of Argus. Coastal Engineering, 54(6-7): 477-491.

Holthusijsen, L.H., Booij, N., Herbers, T.H.C., 1989. A prediction model for stationary, short crested waves in shallow water with ambient currents. Coastal Engineering, 13: 23-54.

Holthusijsen, L.H., Herman, A., Booij, N., Cieslikiewicz, W., 2002. Diffraction in SWAN. In: J. Mckee Smith (Editor), International Conference Coastal Engineering., Cardiff, pp. 405-412.

Hotelling, H., 1933. Analysis of a complex of stastical variables into principle components. Journal of Educational Psychology, 24 (417-441): 498-520.

Hsu, T.-W., Jan, C.-D., Wen, C.-C., 2003. Modified McCormicks model for equilibrium shorelines behind a detached breakwater. Ocean Engineering, 30: 1887-1897.

Ilic, S., Chadwick, A., Fleming, C., 2005a. Investigation of detached breakwaters. Part 1 - hydrodynamics. Proceedings of the Institution of Civil Engineers-Maritime Engineering, 158(MA3): 91-102.

Ilic, S., Chadwick, A., Pan, S., Simmonds, D., O'Connor, B., 2001. The evolution of an equilibrium bay. In: H. Hanson, Larson, M., (Editor), Coastal Dynamics '01. ASCE, Lund, Sweden, pp. 16-25.

Ilic, S., Chadwick, A.J., Fleming, C., 2005b. Investigation of detached breakwaters. Part 2 - morphodynamics. Proceedings of the Institution of Civil Engineers-Maritime Engineering, 158(4): 163-172.

IPCC, 2007. Climate Change 2007, Cambridge.

Isobe, M., Horikawa, K., 1982. Study on water particle velocities of shoaling and breaking waves. Coastal Engineering in Japan, 25: 109-123.

Jimenez, J.A., Osorio, A., Marino-Tapia, I., Davidson, M., Medina, R., Kroon, A., Archetti, R., Ciavola, P., Aamikhof, S.G.J., 2007. Beach recreation planning using video-derived coastal state indicators. Coastal Engineering, 54(6-7): 507-521.

Johnson, H.K., 2005. Coastal area morphological modelling in the vicinity of groins. In: J.M. Smith (Editor). World Scientific Publ Co Pte Ltd, Lisbon, Portugal, pp. 2646-2658.

Johnson, H.K., 2006. Wave modelling in the vicinity of submerged breakwaters. Coastal Engineering, 53(1): 39-48.

Johnson, H.K., Karambas, T.V., Avgeris, I., Zanuttigh, B., Gonzalez-Marco, D., Caceres, I., 2005. Modelling of waves and currents around submerged breakwaters. Coastal Engineering, 52(10-11): 949-969.

Jones, O.P., Petersen, O.S., Kofoed-Hansen, H., 2007. Modelling of complex coastal environments: Some considerations for best practise. Coastal Engineering, 54(10): 717-733.

Karunarathna, H., Reeve, D., Spivack, M., 2008. Long-term morphodynamic evolution of estuaries: An inverse problem. Estuarine Coastal and Shelf Science, 77(3): 385-395.

Khang, K., Douglas, B., Leatherman, S., 2001. Beach erosion potential for severe nor'easters. Journal of Coastal Research, 17(2): 309-321.

King, D.M., Cooper, N.J., Morfett, J.C., Pope, D.J., 2000. Application of offshore breakwaters to the UK: A case study at Elmer Beach. Journal of Coastal Research, 16(1): 172-187.

Kingston, K., 2003. Applications of Complex Adaptive System Approaches to Coastal Systems. Ph.D. Thesis, University of Plymouth, Plymouth, 208 pp.

Kingston, K., Ruessink, B.G., van Enckevort, I.M.J., Davidson, M.A., 2000. Artificial neural network correction of remotely sensed sandbar location. Marine Geology, 169(1-2): 137-160.

Klein, A., Benedet, L., Schumacher, D.H., 2002. Short-term beach rotation processes in distinct headland bay beach systems. Journal of Coastal Research, 18(3): 442-458.

Komar, P.D., 1998. Beach Processes and Sedimentation. Prentice Hall, Upper Saddle River, New Jersey, 544 pp.

Kroon, A., Davidson, M.A., Aaminkhof, S.G.J., Archetti, R., Armaroli, C., Gonzalez, M., Medri, S., Osorio, A., Aagaard, T., Holman, R.A., Spanhoff, R., 2007. Application of remote sensing video systems to coastline management problems. Coastal Engineering, 54(6-7): 493-505.

Kroon, A., Larson, M., Moller, I., Yokoki, H., Rozynski, G., Cox, J., Larroude, P., Statistical analysis of coastal morphological data sets over seasonal to decadal time scales. Coastal Engineering, In Press, Corrected Proof.

Lamberti, A., Archetti, R., Kramer, M., Paphitis, D., Mosso, C., Di Risio, M., 2005. European experiance of low crested structures for coastal management. Coastal Engineering, 52: 841-866.

Larson, M., Hanson, H., Kraus, N., Newe, J., 1999. Short- and long-term responses of beach fills determined by EOF analysis. Journal of Waterway, Port, Coastal and Ocean Engineering, 126(6): 285-293.

Lesser, G.R., Roelvink, J.A., van Kester, J., Stelling, G.S., 2004. Development and validation of a three-dimensional morphological model. Coastal Engineering, 51(8-9): 883-915.

Lippmann, T.C., Holman, R.A., 1989. Quantification of sand bar morphology: A video technique based on wave dissipation. Journal of Geophysical Research, 94(C1): 995-1011.

Lippmann, T.C., Holman, R.A., 1991. Phase speed and angle of breaking waves measured with video techniques. In: N.C. Kraus (Editor), Coastal Sediments '91. ASCE, Seattle, Washington, USA, pp. 542-556.

Longuet-Higgins, M.S., Stewart, R.W., 1963. A note on wave set-up. Journal of Marine Research, 21(4): 4-10.

Loveless, J., Debski, D., Macleod, B., 1998. Sea level set-up behind detached breakwaters 26th International Conference on Coastal Engineering, Copenhagen, pp. 1665-1678.

Loveless, J., Macleod, B., 1999. The influence of set up currents on sediment movement behind detached breakwaters, Coastal Sediments '99, pp. 2026-2041.

Maron, P.P., Reeve, D.E., Rihouey, D., Dubranna, J., 2008. Transverse and longitudinal eigenfunction analysis of a navigation channel subject to regular dredgings: The Adour River mouth, France. Journal of Coastal Research, 24(1A): 206-215.

Martinelli, L., Zanuttigh, B., Lamberti, A., 2006. Hydrodynamic and morphodynamic response of isolated and multiple low crested structures: Experiments and simulations. Coastal Engineering, 53(4): 363-379.

Masselink, G., Short, A., 1993. The effect of tide range on beach morphodynamics and morphology: A conceptual beach model Journal of Coastal Research, 9(3): 785-800.

McCormick, M.E., 1993. Equilibrium shoreline response to breakwaters. Journal of Waterway, Port, Coastal and Ocean Engineering, 119(6): 657-670.

Medellin, G., Medina, R., Falques, A., Gonzalez, M., 2008. Coastline sand waves on a low-energy beach at "El Puntal" spit, Spain. Marine Geology, 250: 143-156.

Miller, J.K., Dean, R.G., 2007a. Shoreline variability via empirical orthogonal function analysis: Part 1 temporal and spatial characteristics. Coastal Engineering, 54(2): 111-131.

Miller, J.K., Dean, R.G., 2007b. Shoreline variability via empirical orthogonal function analysis: Part II relationship to nearshore conditions. Coastal Engineering, 54(2): 133-150.

Milligan, J., O'Riordan, T., 2005. Governance for sustainable coastal futures. Taylor & Francis Inc, London, ENGLAND, pp. 499-509.

Munoz-Perez, J.J., Medina, R., Tejedor, B., 2001. Evolution of longshore beach contour lines determined by the EOF method. Scienta Marina, 65(4): 393-402.

Murphy, A., Epstein, E., 1988. Skill scores and corelation c-efficients in model verification. Monthly waether review, 117: 572-581.

Myatt, L.B., Scrimshaw, M.D., Lester, J.N., 2003. Public perceptions and attitudes towards a current managed realignment scheme: Brancaster West Marsh, North Norfolk, U.K. Journal of Coastal Research, 19(2): 278-286.

Nairn, R.B., Southgate, H.N., 1993. Deterministic profile modeling of nearshore processes .2. Sediment transport and beach profile development. Coastal Engineering, 19(1-2): 57-96.

Ojeda, E., Guillen, J., 2008. Shoreline dynamics and beach rotation of artificial embayed beaches. Marine Geology, 253(1-2): 51-62.

Pan, S.Q., Wolf, J., Chen, Y., Bell, P., Du, Y., Fernando, P., Li, M., 2009. Modelling nearshore waves with presence of shore-parallel breakwaters. In: L. Franco, Tomasiccho, G., Lamberti, A., (Editor), Coastal Structures 2007. World Scientific, Venice, pp. 1125-1134.

Pearson, K., 1901. On lines and planes of closest best fit to systems of points in space. Philosophical Magazine, 6(2): 559-572.

Pilarczyk, K.W., Zeidler, R.B., 1996. Offshore breakwaters and shore evolution control. Balkema, Rotterdam.

Pinto, C.A., Taborda, R., Andrade, C., Teixeira, S.B., 2009. Seasonal and mesoscale variations at an embayed beach (Armacao De Pera, Portugal). Journal of Coastal Research(SI56 (Proccedings of the International Coastal Symposium 2009)): 118-122.

Plant, N.G., Aarninkhof, S.G.J., Turner, I.L., Kingston, K.S., 2007. The performance of shoreline detection models applied to video imagery. Journal of Coastal Research, 23(3): 658-670.

Plant, N.G., Holman, R.A., 1997. Intertidal beach profile estimation using video images. Marine Geology, 140: 1-24.

Pope, J., Dean, J., 1986. Development of design criteria for segmented breakwaters. In: B. Edge (Editor), Coastal Engineering. ASCE, Taipei, Taiwan, pp. 2144-2158.

Quartel, S., Kroon, A., Ruessink, B.G., 2008. Seasonal accretion and erosion patterns of a microtidal sandy beach. Marine Geology, 250: 19-33.

Ranasinghe, R., Symonds, G., Black, K., Holman, R., 2004. Morphodynamics of intermediate beaches: a video imaging and numerical modelling study. Coastal Engineering, 51(7): 629-655.

Ranasinghe, R., Turner, I., 2004. Processes governing shoreline response to submerged breakwaters: Multi-function structures a special case, Coastal Engineering 2004, pp. 1984-1996.

Ranasinghe, R., Turner, I.L., 2006. Shoreline response to submerged structures: A review. Coastal Engineering, 53(1): 65-79.

Ranasinghe, R.S., Sato, S., 2007. Beach morphology behind single impermeable submerged breakwater under obliquely incident waves. Coastal Engineering Journal, 49(1): 1-24.

Reeve, D., Li, B., Thurston, N., 2001a. Eigenfunction analysis of decadal fluctuations in sandbank morphology at Gt. Yarmouth. Journal of Coastal Research, 17(2): 371 382.

Reeve, D.E., Horrillo-Caraballo, J.M., Magar, V., 2008. Statistical analysis and forecasts of long-term sandbank evolution at Great Yarmouth, UK. Estuarine Coastal and Shelf Science, 79(3): 387-399.

Reeve, D.E., Li, B., Fleming, C.A., 2001b. Long-term morphological variations of a sandbank system. Proceedings of the Institution of Civil Engineers-Water Maritime and Energy, 148(1): 15-23.

Reiners, A., Roelvink, J., Walstra, D., 1995. Validation study of UNIBEST-TC model, Delft Hydraulics, Delft.

Rihouey, D., Dugor, J., Dailloux, D., Morichon, D., 2009. Application of remote sensing video systems to coastal defence monitoring. Coastal Education & Research Foundation, Lisbon, Portugal, pp. 1582-1586.

Rihouey, D., Maron, P., 2003. Empirical eigenfunction analysis of long-term bathymetric data along the beaches of Anglet. In: C.A. Brebbia, D. Almorza and F. LopezAguayo (Editors). Wit Press, Cadiz, Spain, pp. 495-504.

Roelvink, J.A., Vanbanning, G., 1994. Design and development of Delft-3D and application to coastal morphodynamics. In: A. Verwey, A.W. Minns, V. Babovic and C. Maksimovic (Editors), Delft, Netherlands, pp. 451-456.

Ruessink, B.G., Bell, P., van Enckevort, I.M.J., Aarninkhof, S., 2002. Nearshore bar crest location quantified from time averaged X-band radar images. Coastal Engineering, 45: 19-32.

Ruessink, B.G., van Enckevort, I.M.G., Kingston, K., Davidson, M.A., 2000. Analysis of observed two- and three-dimensional nearshore bar behaviour. Marine Geology, 169: 161-183.

Ruessink, B.G., Walstra, D.J.R., Southgate, H.N., 2003. Calibration and verification of a parametric wave model on barred beaches. Coastal Engineering, 48(3): 139-149.

Ruggiero, P., Kaminsky, G.M., Gelfenbaum, G., 2003. Linking proxy-based and datum-based shorelines on a high-energy coastline: Implications for shoreline change analyses. Journal of Coastal Research: 57-82.

Ruol, P., Faedo, A., Paris, A., 2005. Physical model study of water piling-up behind low-crested structures. In: J.M. Smith (Editor), Coastal Engineering 2004, Vols 1-4, pp. 4165-4177.

Sedrati, M., Ciavola, P., Reyns, J., Armaroli, C., Sipka, V., 2009. Morphodynamics of a Microtidal Protected Beach During Low Wave-energy Conditions. Journal of Coastal Research, S.I. 56: 198-202.

Siegle, E., Huntley, D.A., Davidson, M.A., 2004. Physical controls on the dynamics of inlet sandbar systems. Ocean Dynamics, 54(3-4): 360-373.

Siegle, E., Huntley, D.A., Davidson, M.A., 2006. Combining video imaging and numerical modelling for the extraction of intertidal morphology. Journal of Coastal Research, 1: 478-482.

Siegle, E., Huntley, D.A., Davidson, M.A., 2007. Coupling video imaging and numerical modelling for the study of inlet morphodynamics. Marine Geology, 236(3-4): 143-163.

Silva, P.A., Bertin, X., Fortunato, A.B., Oliveira, A., 2009. Intercomparison of sediment transport formulas in current and combined wave-current conditions. Coastal Education & Research Foundation, Lisbon, Portugal, pp. 559-563.

Smit, M.W.J., Aaminkhof, S.G.J., Wijnberg, K.M., Gonzalez, M., Kingston, K.S., Southgate, H.N., Ruessink, B.G., Holman, R.A., Siegle, E., Davidson, M., Medina, R., 2007. The role of video imagery in predicting daily to monthly coastal evolution. Coastal Engineering, 54(6-7): 539-553.

Smith, R.K., Bryan, K.R., 2007. Monitoring beach face volume with a combination of intermittent profiling and video imagery. Journal of Coastal Research, 23(4): 892-898.

Sorenson, O.R., Kofoed-Hansen, H., Jones, O., 2004a. Numerical modelling of wave-current interaction in tidal areas using an unstructured finite volume technique, Coastal Engineering 2004, Lisbon, pp. http://www.dhigroup.com/upload/icce2006_sw_paper_003.pdf.

Sorenson, O.R., Kofoed-Hansen, H., Rugbjerg, M., Sorenson, L.S., 2004b. A third-generation spectral wave model using an unstructured finite volume technique. In: J. Mckee Smith (Editor), Proceedings of the 29th International Conference on Coastal Engineering. World Scientific, Lisbon, pp. 894-906.

Soulsby, R., 1997. Dynamics of marine sands. Thomas Telford, London, 249 pp.

Southgate, H.N., Nairn, R.B., 1993. Deterministic profile modelling of nearshore processes.1. Waves and currents. Coastal Engineering, 19(1-2): 27-56.

Stauble, D.K., Tabar, J.R., 2003. The use of submerged narrow-crested breakwaters for shoreline erosion control. Journal of Coastal Research, 19(3): 684-722.

Stockdon, H.F., Holman, R.A., 2000. Estimation of wave phase speed and nearshore bathymetry from video imagery. Journal of Geophysical Research, 105(c9): 22,015-22,033.

Stockdon, H.F., Holman, R.A., Howd, P.A.Sallenger Jr., A.H., 2006. Empirical parameterization of setup, swash and run-up. Coastal Engineering, 53(7): 573- 588.

Stone, G.W., Wang, P., Armbruster, C.K., 1999. Unanticipated response to detached, segmented breakwaters along Racoon Island, Lousiana. In: N.C. Kraus, McDougal, W.G., (Editor), Coastal Sediments '99, New York, pp. 2057-2072.

Suh, K., Dalrymple, R., 1987. Offshore breakwaters in laboratory and field. Journal of Waterway, Port, Coastal and Ocean Engineering, 113(2): 105-121.

Sutherland, J., Peet, A., Soulsby, R., 2004a. Evaluating the performance of morphological models. Coastal Engineering, 51: 917-939.

Sutherland, J., Walstra, D., Chesher, T., Van Rijn, L., Southgate, H., 2004b. Evaluation of coastal area modelling systems at an estuary mouth. Coastal Engineering, 51: 119-142.

Thomalla, F., Vincent, C.E., 2003. Beach response to shore-parallel breakwaters at Sea Palling, Norfolk, UK. Estuarine Coastal and Shelf Science, 56: 203-212.

Thomalla, F., Vincent, C.E., 2004. Designing Offshore Breakwaters Using Empirical Relationships: A Case Study from Norfolk, United Kingdom. Journal of Coastal research, 20(4): 1224-1230.

Thomalla, F., Vincent, C.E., Black, K., 2001. The effect of the segmented shore parallel breakwaters at Sea Palling on the longshore transport of sand, Proceedings of the 36th Annual Conference of River and Coastal Engineers, Keele University, pp. 07.2.1-07.2.11.

Troch, P., Geeraerts, J., Van de Walle, B., De Rouck, J., Van Damme, L., Allsop, W., Franco, L., 2004. Full-scale wave overtopping measurements on the Zeebrugge rubble mound breakwater. Coastal Engineering, 51(7): 609-628.

Turner, I., V., L., Symonds, G., Mcgrath, J., Jackson, A., Jancar, T., Aarninkhof, S., Elshoff, I., 2000. Predicted and observed coastline changes at the Gold Coast artifical reef, Coastal Engineering. ASCE, New York, pp. 1836-1847.

Turner, I.L., 2006. Discriminating modes of shoreline response to offshore detached structures. Journal of Waterway, Port, Coastal and Ocean Engineering, 132(3): 180-191.

Turner, I.L., Aarninkhof, S.G.J., Holman, R.A., 2006. Coastal imaging applications and research in australia. Journal of Coastal Research, 22(1): 37-48.

Turner, I.L., Aarninkhof, S.G.J., McGrath, J., 2004. CZM applications of Argus coastal imaging at the Gold Coast, Australia. Journal of Coastal research, 20(3): 739-752.

Uda, T., Hashimoto, H., 1982. Description of beaches using an empirical model of beach profile changes, Proceedings 18th International Conference on Coastal Engineering. ACSE, Cape Town, pp. 1405 1418.

van Der Meer, J., Briganti, R., Wang, B., Zanuttigh, B., 2004. Wave transmission at low-crested structures, including oblique wave attack, Coastal Engineering 2004, pp. 4152-4164.

van der Meer, J., Briganti, R., Zanuttigh, B., Wang, B., 2005. Wave transmission and reflection at low crested structures: Design formulae, oblique wave attack and spectral change. Coastal Engineering, 52: 915-929.

van der Meer, J., Regeling, H.J., de Waal, J.P., 2000. Wave transmission: spectral changes and its effects on run up and overtopping. In: B. Edge (Editor), Proceedings of the 27th International Conference on Coastal Engineering. ASCE, pp. 2157-2168.

van der Werf, J.J., Magar, V., Malarkey, J., Guizien, K., O'Donoghue, T., 2008. 2DV modelling of sediment transport processes over full-scale ripples in regular asymmetric oscillatory flow. Continental Shelf Research, 28(8): 1040-1056.

van Koningsveld, M., Davidson, M., Huntley, D., Medina, R., Aaminkhof, S., Jimenez, J.A., Ridgewell, J., de Kruif, A., 2007. A critical review of the CoastView project: Recent and future developments in coastal management video systems. Coastal Engineering, 54(6-7): 567-576.

van Koningsveld, M., Davidson, M.A., Huntley, D.A., 2005. Matching science with coastal management needs: The search for appropriate coastal state indicators. Journal of Coastal Research, 21(3): 399-411.

van Koningsveld, M., Mulder, J.P.M., 2004. Sustainable coastal policy developments in The Netherlands. A systematic approach revealed. Journal of Coastal Research, 20(2): 375-385.

van Rijn, L.C., Walstra, D.J.R., Grasmeiger, B., Sutherland, J., Pan, S., Sierra, J.P., 2003. The predicatability of cross-shore bed evolution of sandy beaches at the time scale of storms and seasons using process-based profile models. Coastal Engineering, 47: 295 - 327.

van Vuren, S., Kok, M., Jorissen, R.E., 2004. Coastal defense and societal activities in the coastal zone: Compatible or conflicting interests? Journal of Coastal Research, 20(2): 550-561.

Vedel, P., 1905. Island harbours and the accumulation of material caused by detatched works. Transactions, ASCE.: 139-158.

von Storch, H., Hannostock, G., 1984. Comment on "Empirical orthogonal function analysis of wind vectors over the tropical Pacific region." Bulletin of the American Meteorological Society, 65: 162.

Walters, R.A., Hanert, E., Pietrzak, J., le Roux, D.Y., 2009. Comparison of unstructured, staggered grid methods for the shallow water equations. Ocean Modelling, 28(1-3): 106-117.

Wijnberg, K.M., Aarninkhof, S.G.J., Van Koningsveld, M., Ruessink, B.G., Stive, M.J.F., 2005. Video monitoring in support of coastal management. In: J.M. Smith (Editor), Coastal Engineering 2004, Vols 1-4, pp. 3136-3148.

Williams, E.J., 1959. The comparison of regression variables. Journal of the Royal Stastical Society, 21: 396-9.

Winant, C.D., Inman, D.L., Nordstrom, C.E., 1975. Description of seasonal beach changes using empirical eigenfunctions. Journal of Geophysical Research, 80(15): 1979-1986.

Wright, L., Short, A., 1984. Morphodynamic variability of surfzones and beaches: A synthesis. Marine Geology, 56: 93-118.

Zanuttigh, B., Lamberti, A., 2006. Experimental analysis and numerical simulations of waves and current flows around low-crested rubble-mound structures. Journal of Waterway Port Coastal and Ocean Engineering-Asce, 132(1): 10-27.

Zanuttigh, B., Martinelli, L., Lamberti, A., Moschella, P., Hawkins, S., Marzetti, S., Ceccherelli, V.U., 2005. Environmental design of coastal defence in Lido di Dante, Italy. Coastal Engineering, 52(10-11): 1089 -1125.

Zhu, Y., Pan, S., Fernando, P., Li, M., O'Connor, B., 2004. Modelling of coastal morphology under storm conditions around shore parallel breakwaters. In: Y. Yixin (Editor), 2nd Joint Sino-German Symposium on Coastal and Ocean Engineering, Nanjing, pp. 213-222.

Zyserman, J.A., Johnson, H.K., 2002. Modelling morphological processes in the vicinity of shore-parallel breakwaters. Coastal Engineering, 45: 261-284.

Zyserman, J.A., Johnson, H.K., Zanuttigh, B., Martinelli, L., 2005. Analysis of far-field erosion induced by low-crested rubble-mound structures. Coastal Engineering, 52(10-11): 977-994.

APPENDIX A

In this appendix, plots supplementary to Chapter 6 are presented.

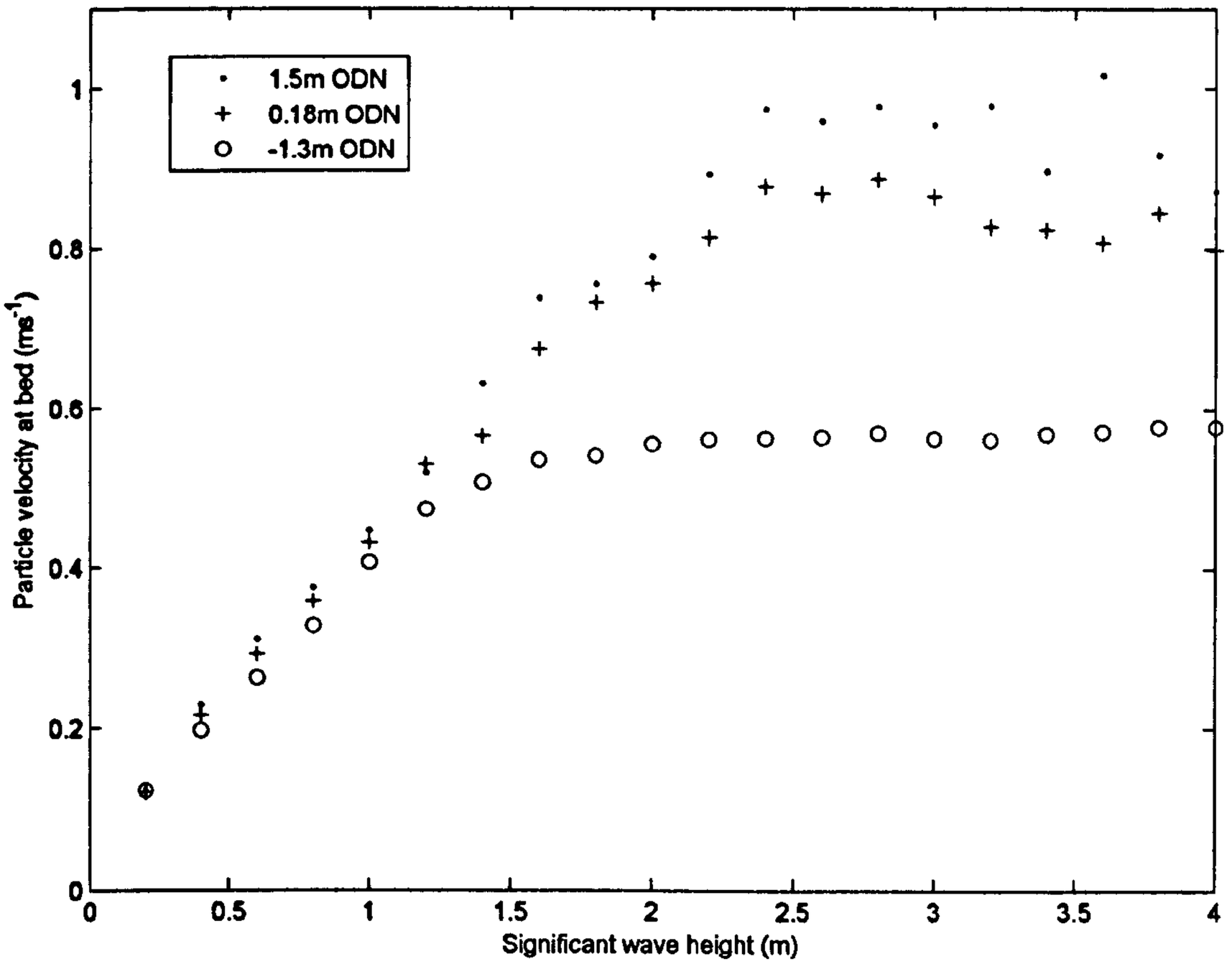

Figure A1: Mean near bed particle speeds against significant wave heights for the breakwater protected area at high (1.5m ODN), mean (0.18m ODN) and low (-1.3m ODN) water

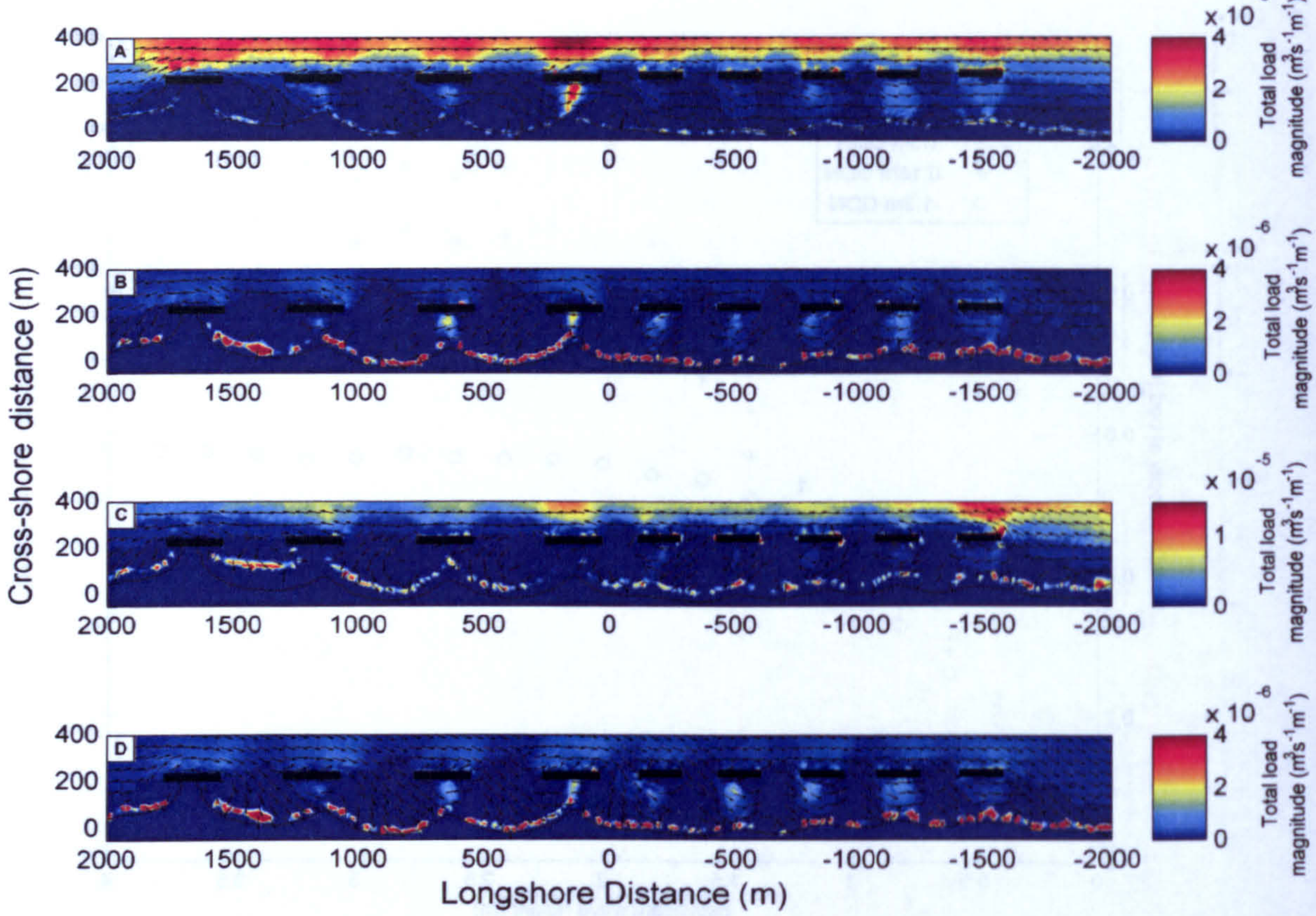

Figure A2: Total load sediment transport at different stages of tide: a) high tide, b)mid tide dropping, c) low tide and d) mid tide rising. Vectors indicate current direction and shading indicates current speed.

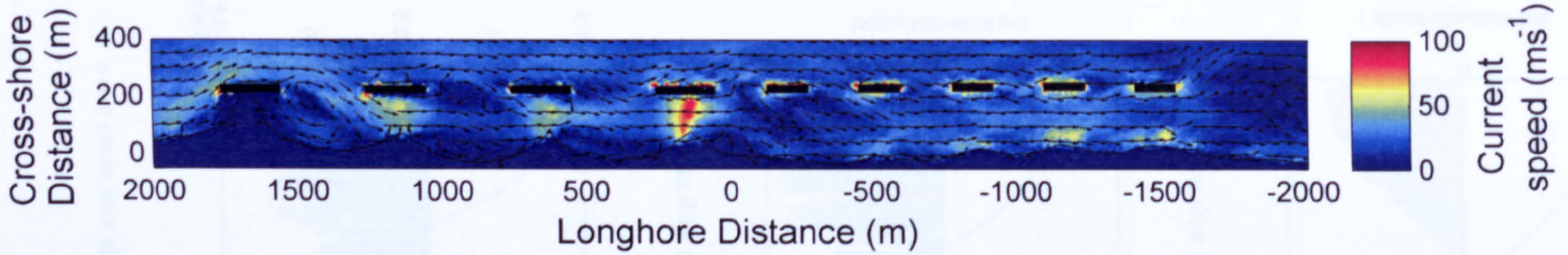

Figure A3: Cumulative current speeds over a spring tidal cycle with wave stirring

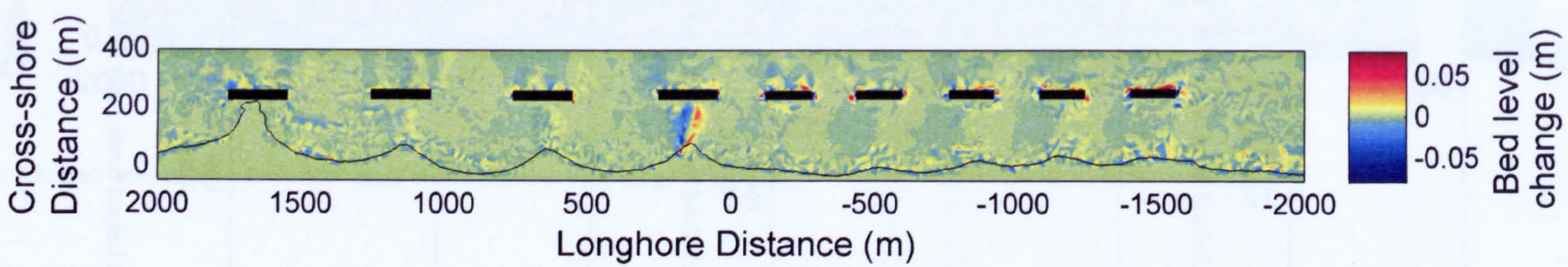

FigureA4: Bed level changes over a spring tidal cycle with wave stirring

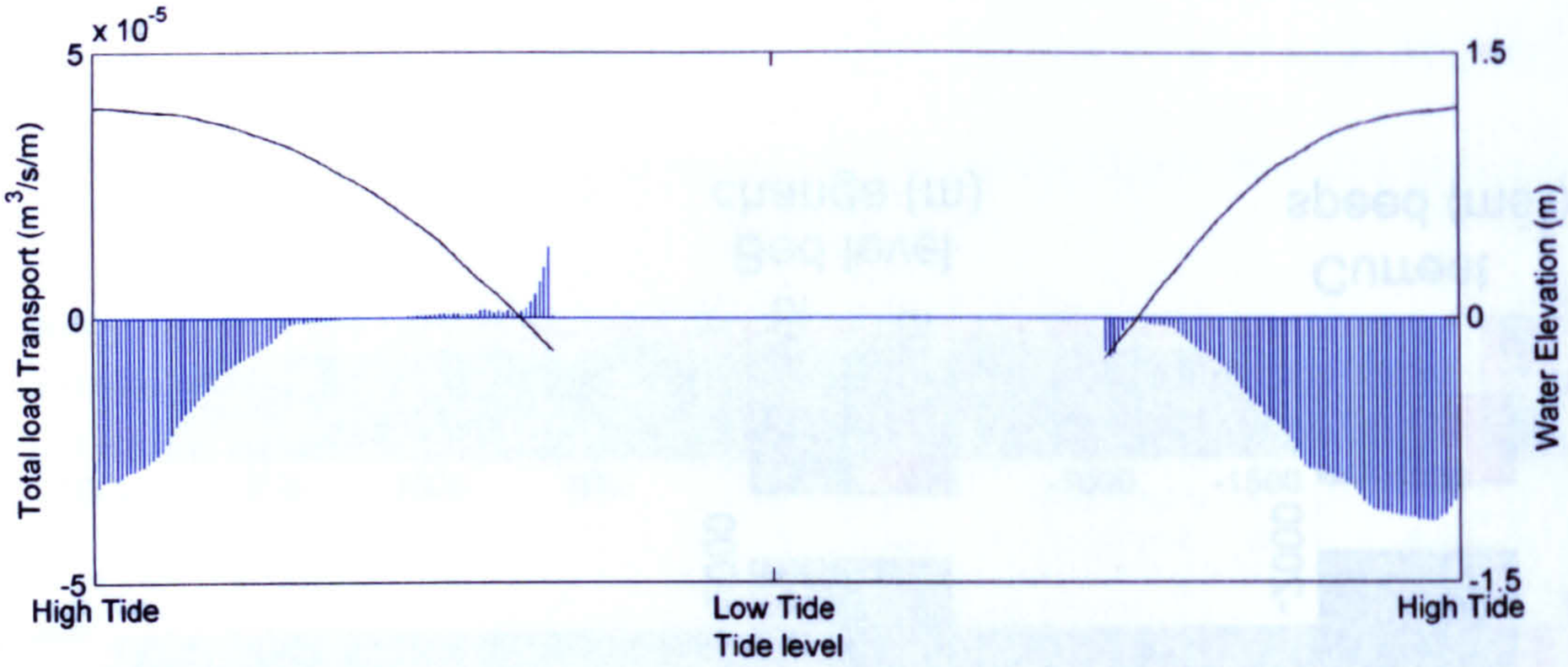

Figure A5: Total load transport at a point behind breakwater 8 for a mean tide with wave stirring.

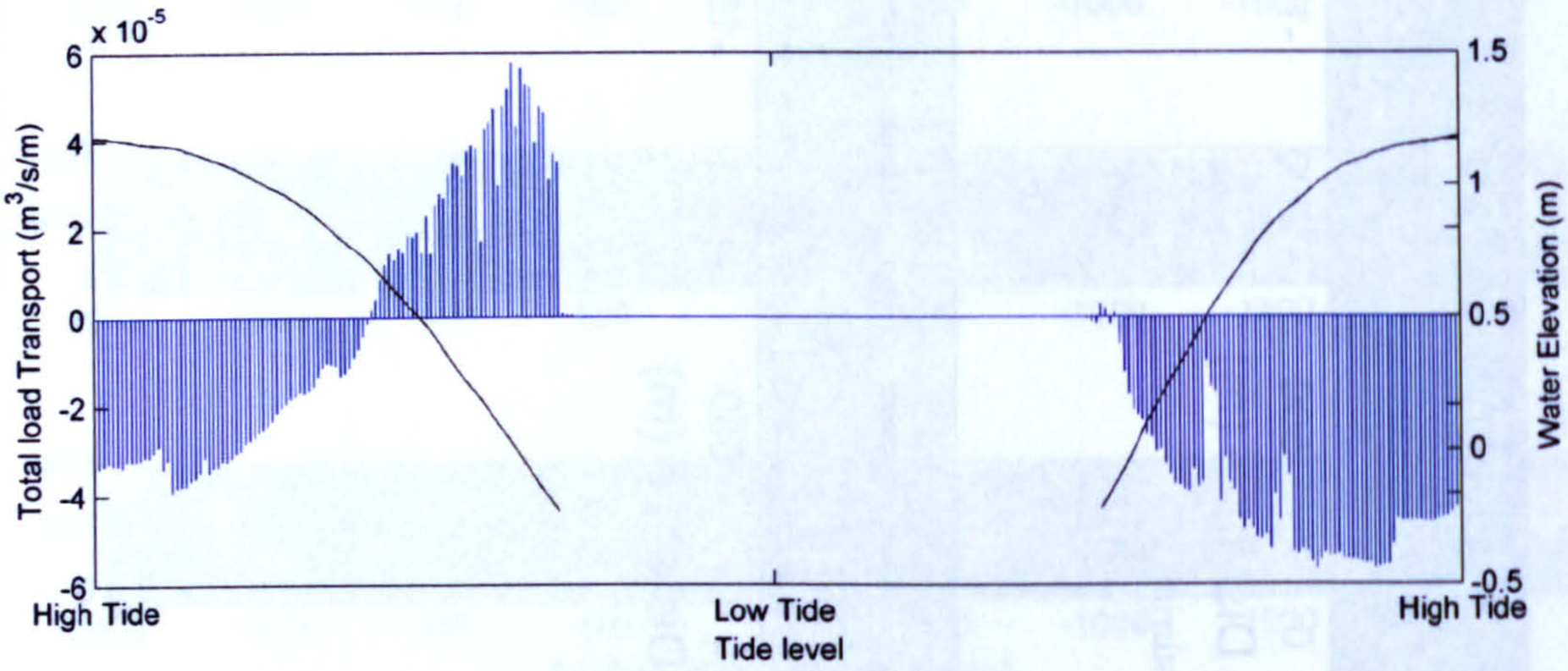

Figure A6: Total load transport at a point behind breakwater 8 for a mean tide with mean wave conditions.

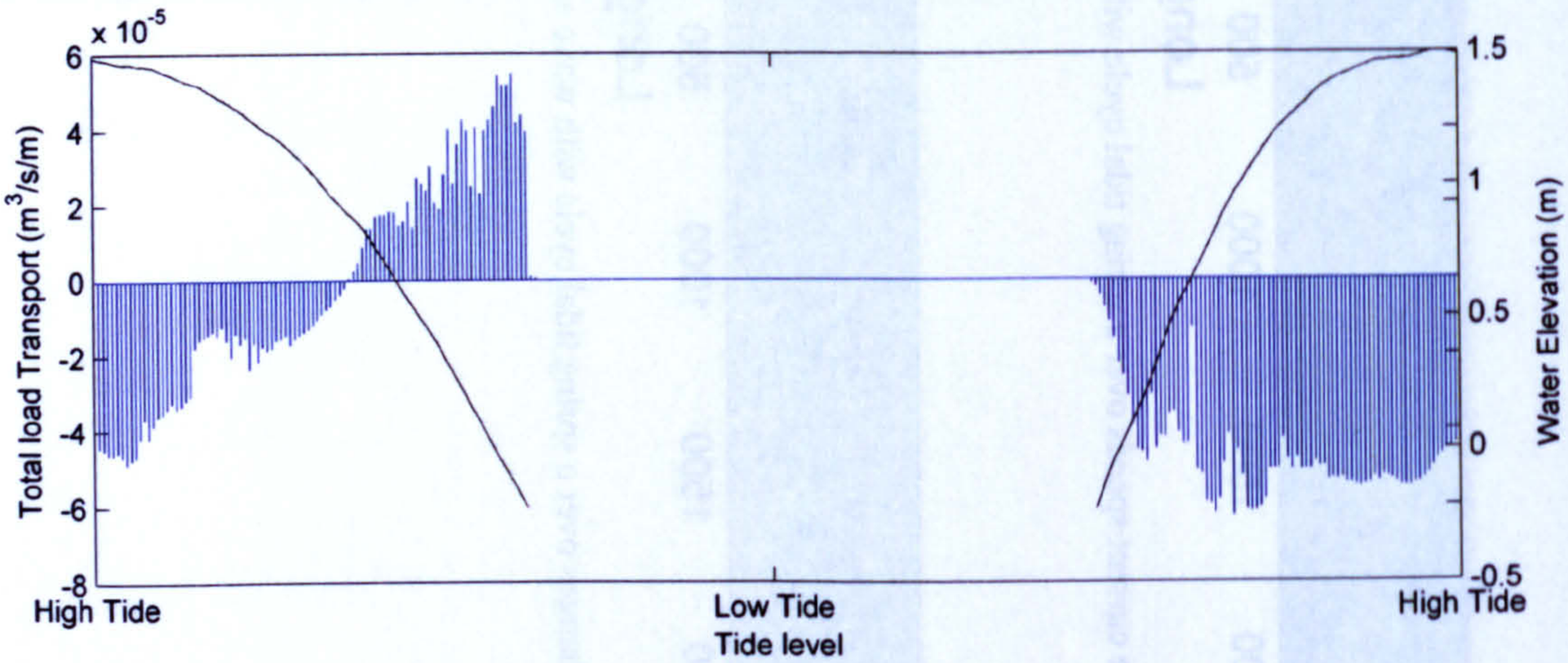

Figure A7: Total load transport at a point behind breakwater 8 for a spring tide with mean wave conditions.

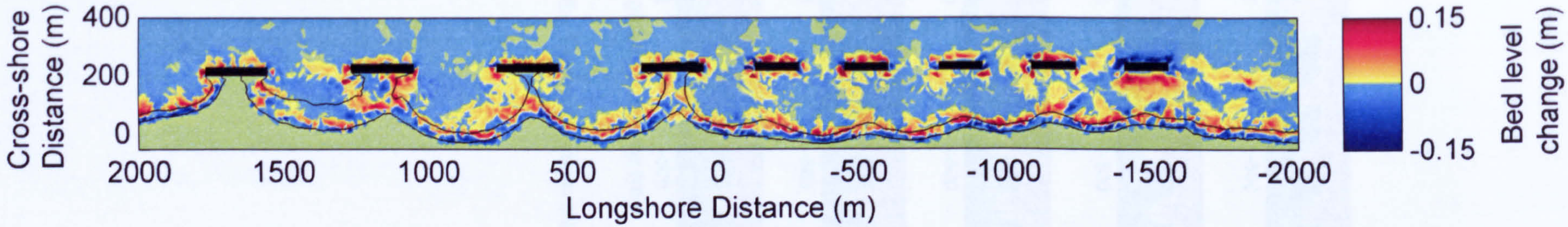

Figure A8: Bed level change for a tidal cycle with a relative tidal range of 0.5

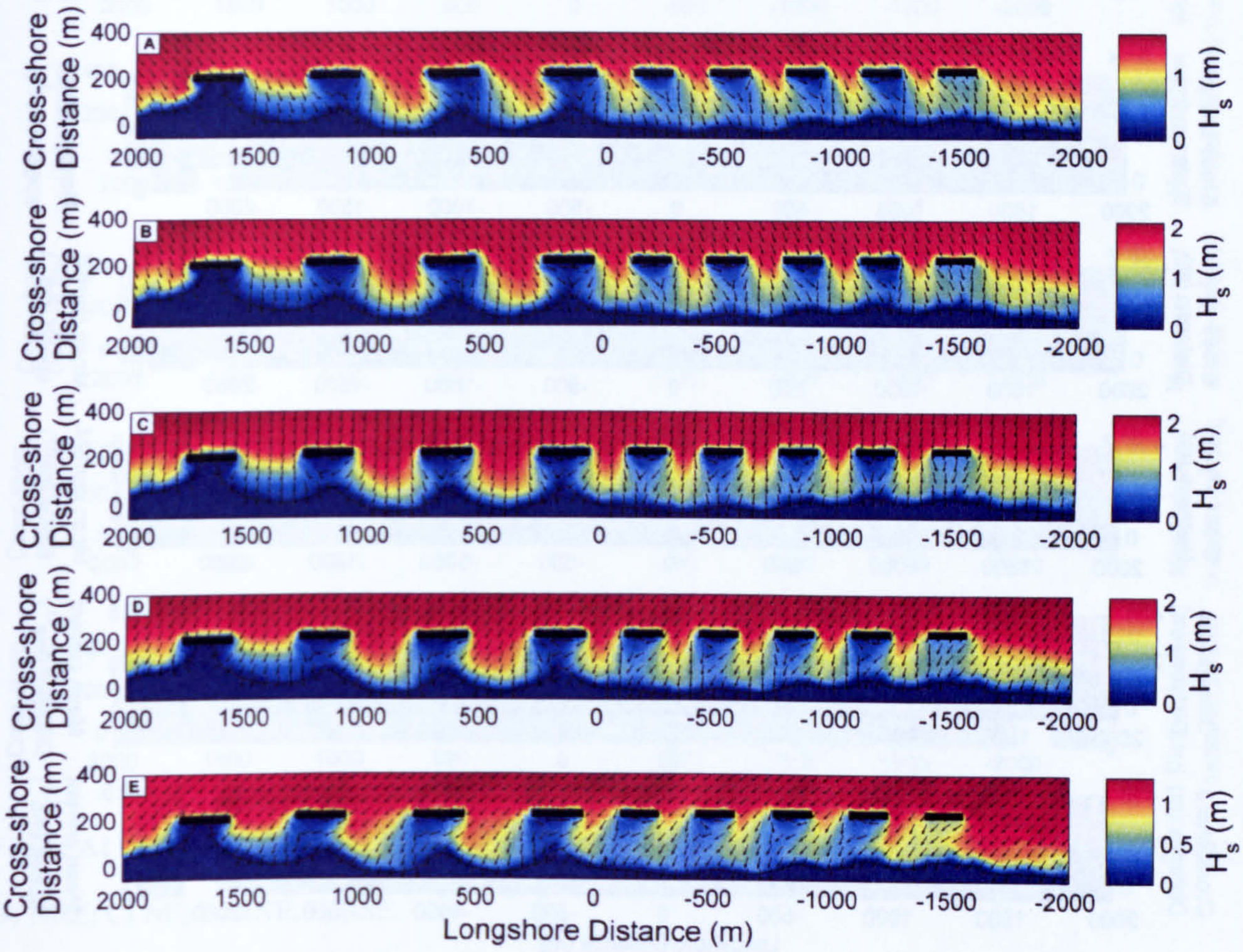

Figure A9. Patterns of wave incidence for the 5 storm directions tested: A) NNW; B) NNE; C) NE; D) ENE; E).ESE.

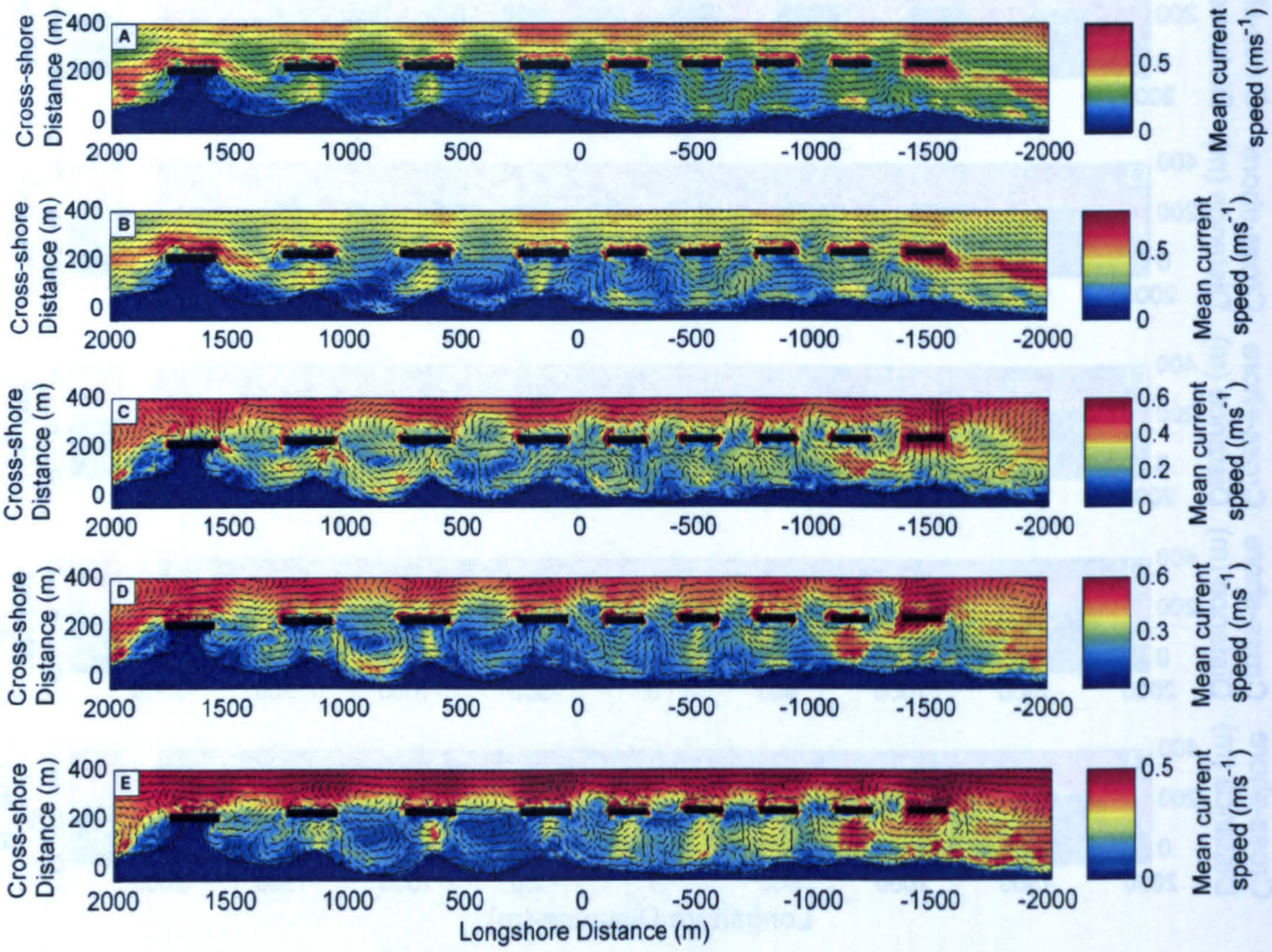

Figure A10: Mean current velocities over a mean tidal cycle for the 5 storm conditions tested: A) NNW; B) NNE; C) NE; D) ENE; E).ESE.

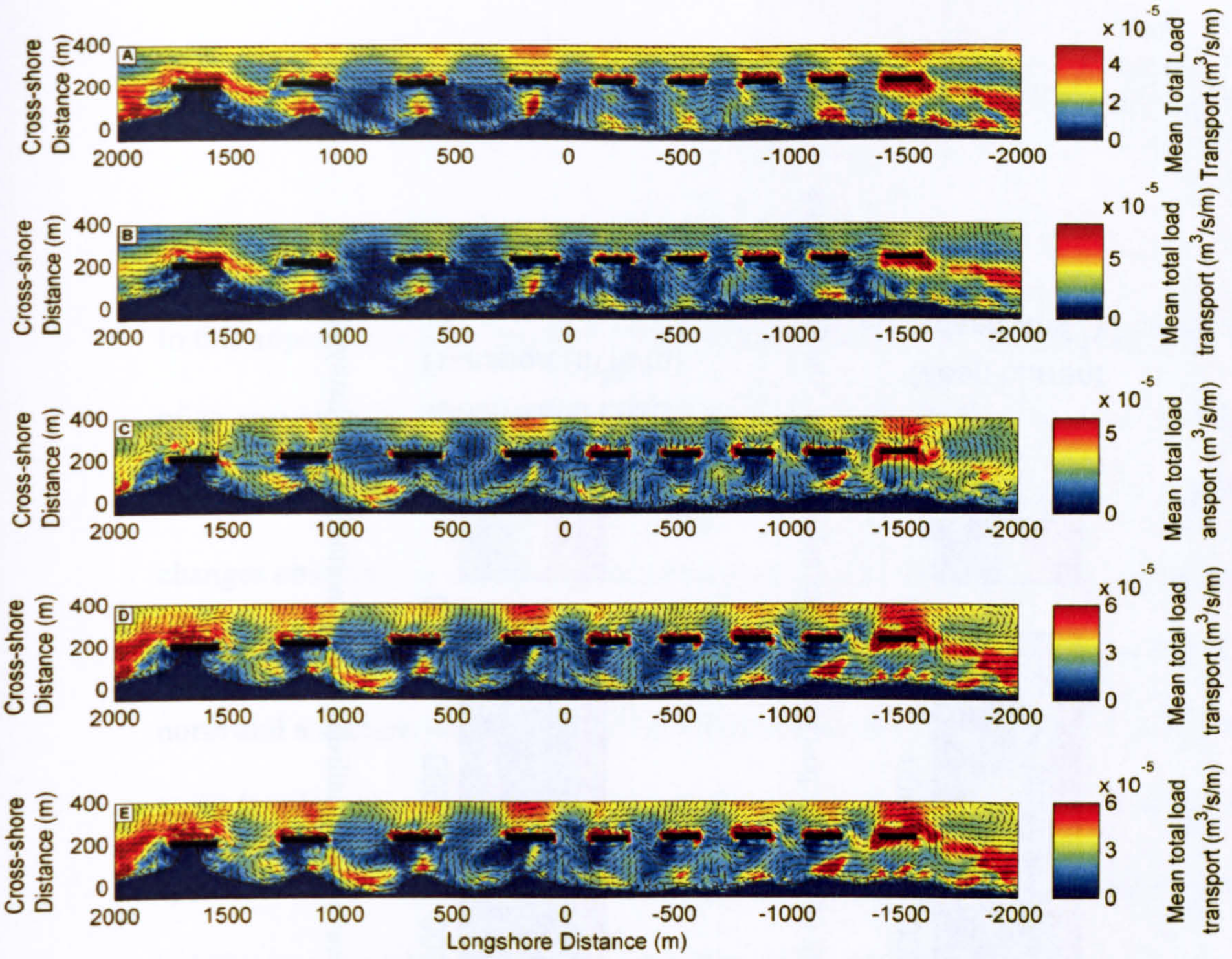

Figure A11: Mean total load transport over a mean tidal cycle for the 5 storm conditions tested: A) NNW; B) NNE; C) NE; D) ENE; E).ESE.

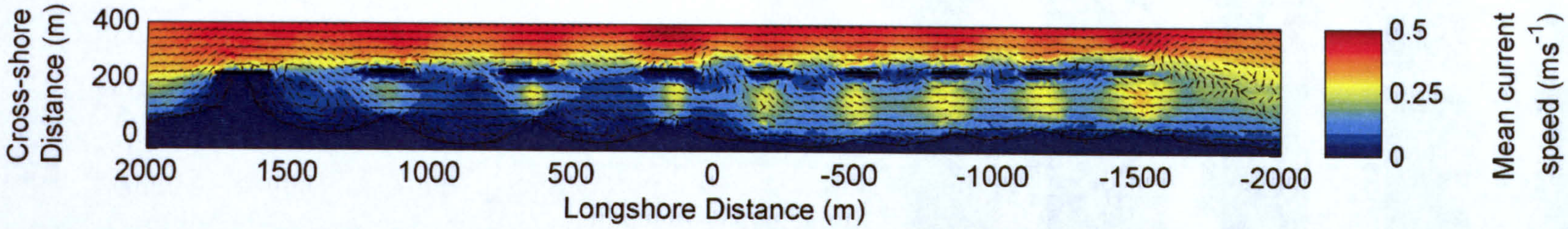

Figure A12: Current velocities averaged over a tidal cycle for a mean tidal range with wave stirring utilising the post northerly storm bathymetry. Shading indicates current speed and vectors indicate current direction.

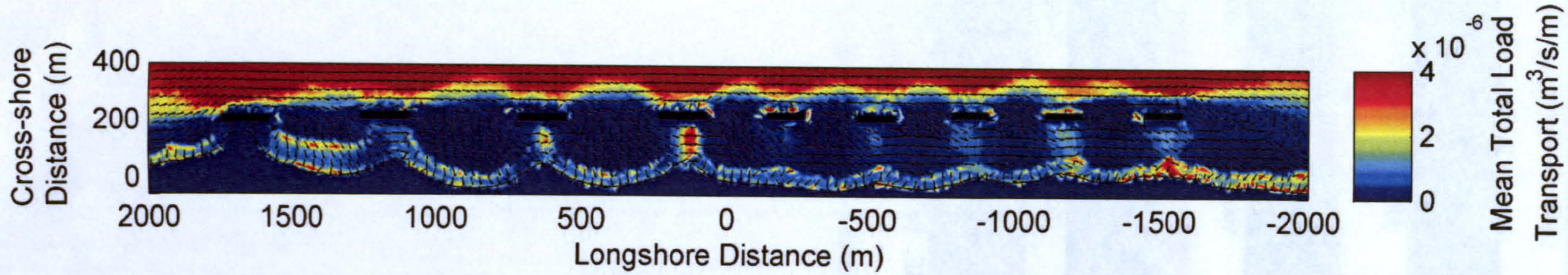

Figure A13:Total load sediment transport averaged over a tidal cycle for a mean tidal range with wave stirring utilising the post northerly storm bathymetry. Shading indicates magnitude and vectors indicate direction.

PAGE NUMBERING AS ORIGINAL

Appendix B: Morphological behaviour of nearby unprotected beaches

1. Introduction and Methodology

In this appendix, a brief investigation will be carried out into the morphological variability of an area close to, but outside of, the detached breakwater system. The aim is to quantify morphological trends of the nearby regions. This is necessary to aid qualification of the changes observed in the breakwater protected region. Due to limits in video resolution outside of the breakwater system, only the RTK-GPS dataset was utilised. A section to the north and a section to the south of the breakwater system was tested. The regions are close to the breakwater system and so are certainly influenced by end effects of the breakwater system. The down drift section is 1/2km to the SE of the end of the breakwater system and is 150m in a longshore direction and 308m in the cross-shore direction (Figure B1). The up-drift section is nearer the limits of the breakwater system, 1/4km away, and is 100m in the longshore direction and 308m in the cross-shore direction (Figure B2). The reason for the proximity to the breakwater system is due to the coverage of the RTK-GPS surveys.

The volume changes, and standard deviations of morphological change were calculated. The same EOF analysis as used in chapter 5 was used to determine modes of change.

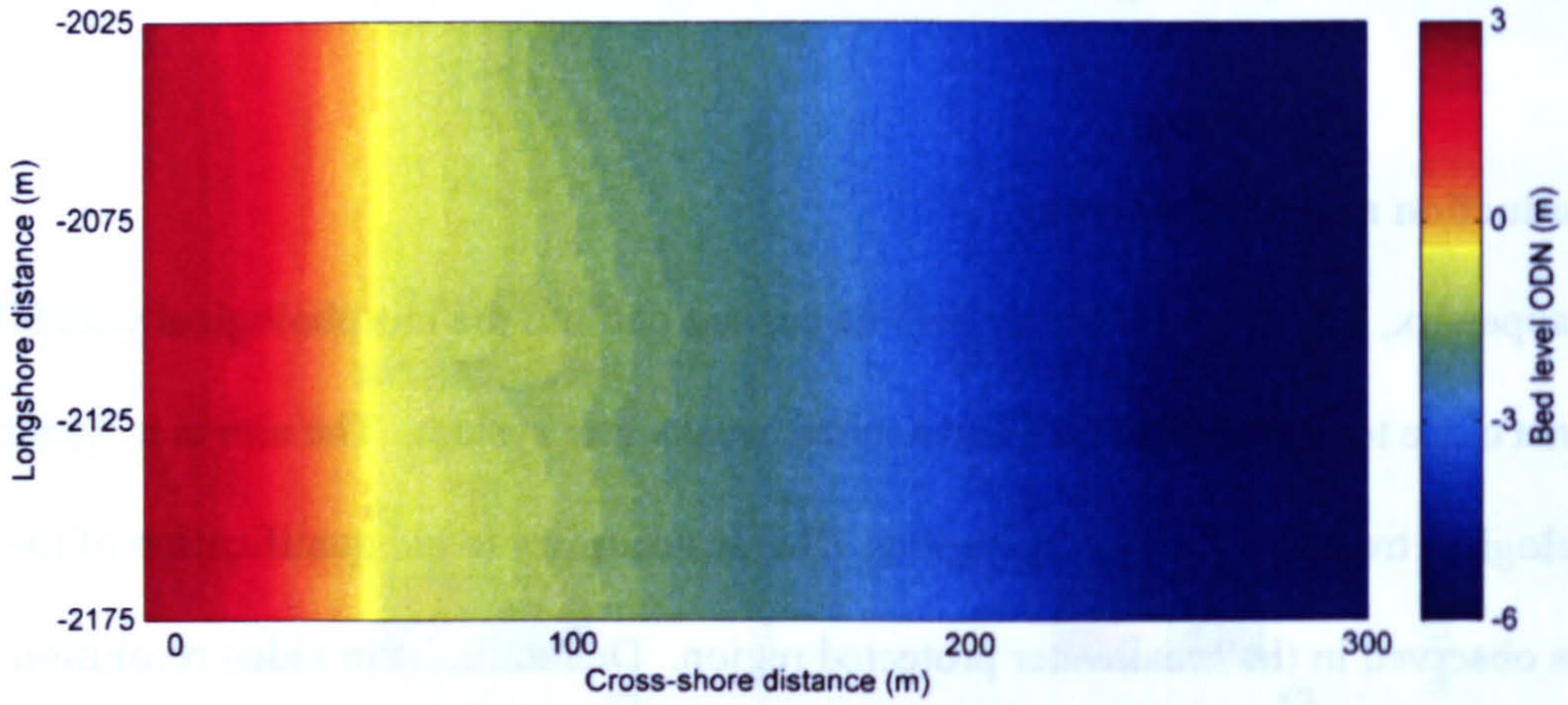

Figure B1: The mean bathymetry for the down-drift section tested

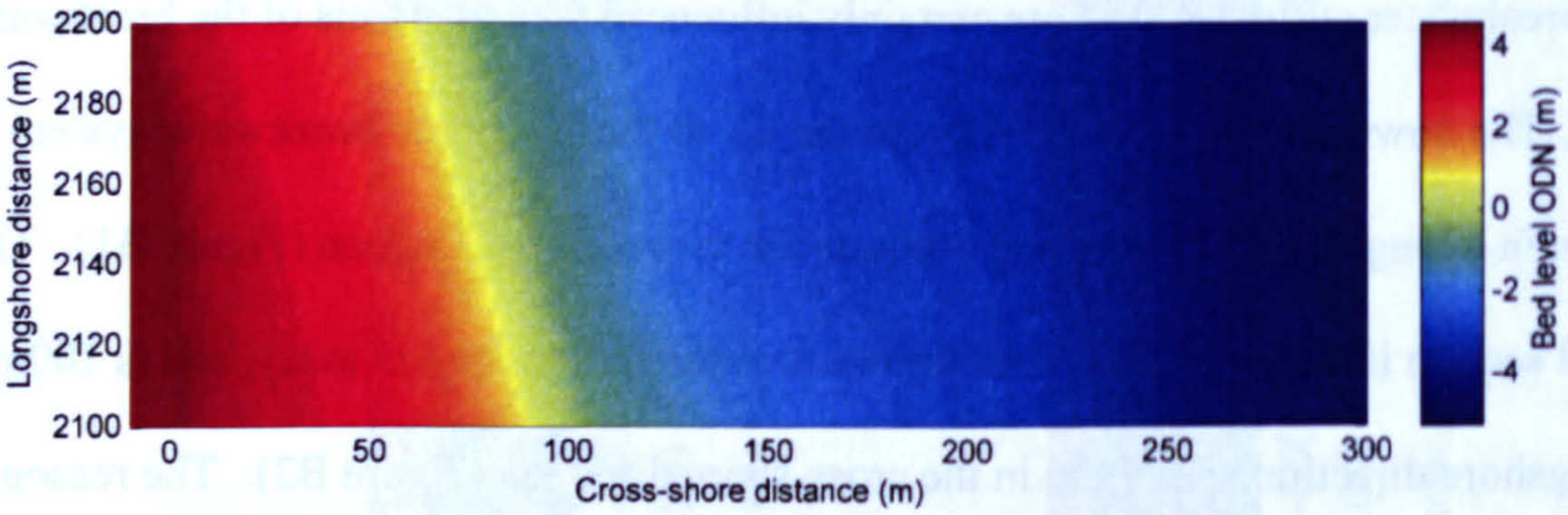

Figure B2: The mean bathymetry for the up-drift section tested.

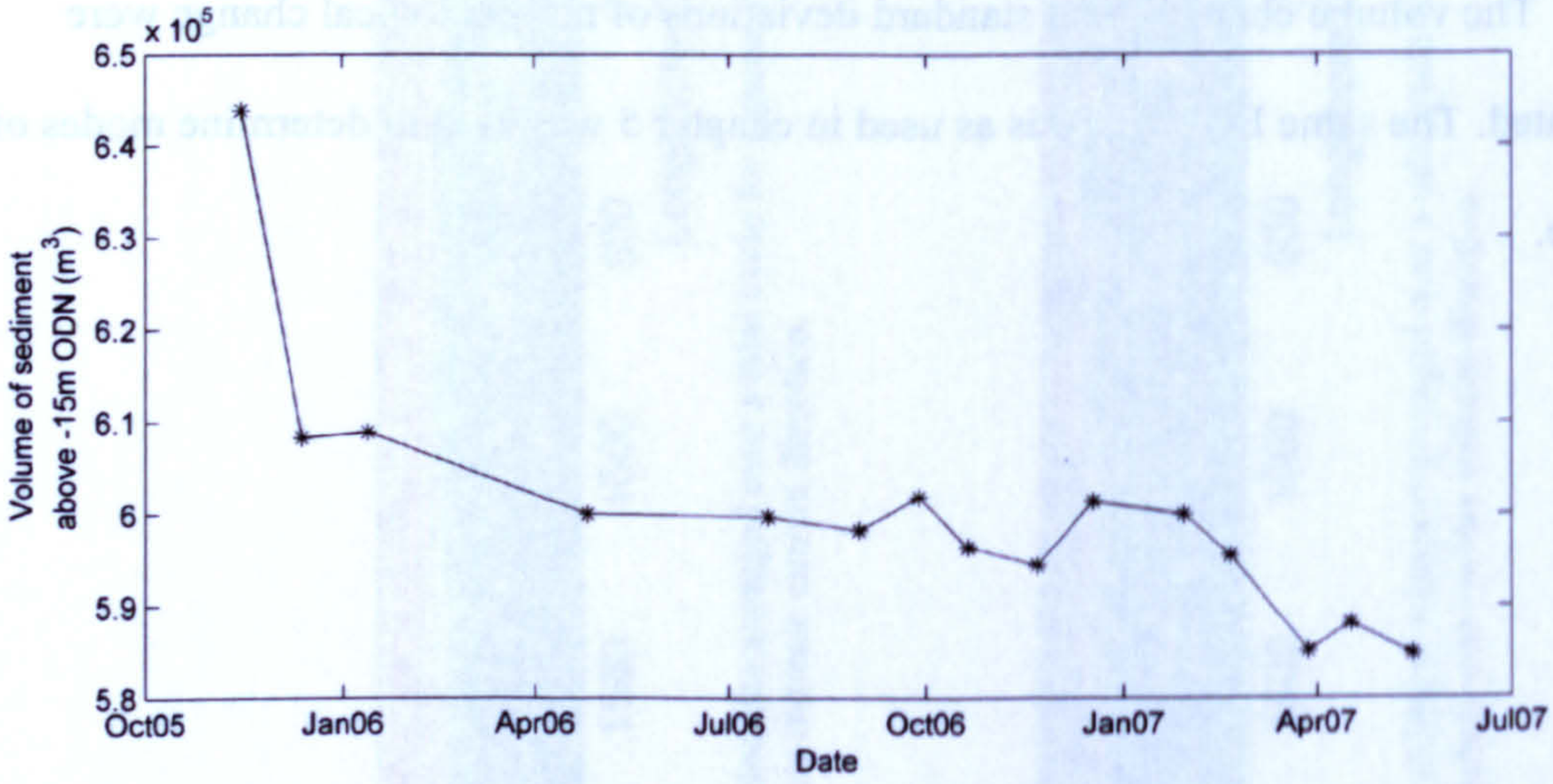

Figure B3: The volume of sediment in the down drift section above a level of -15m ODN through time.

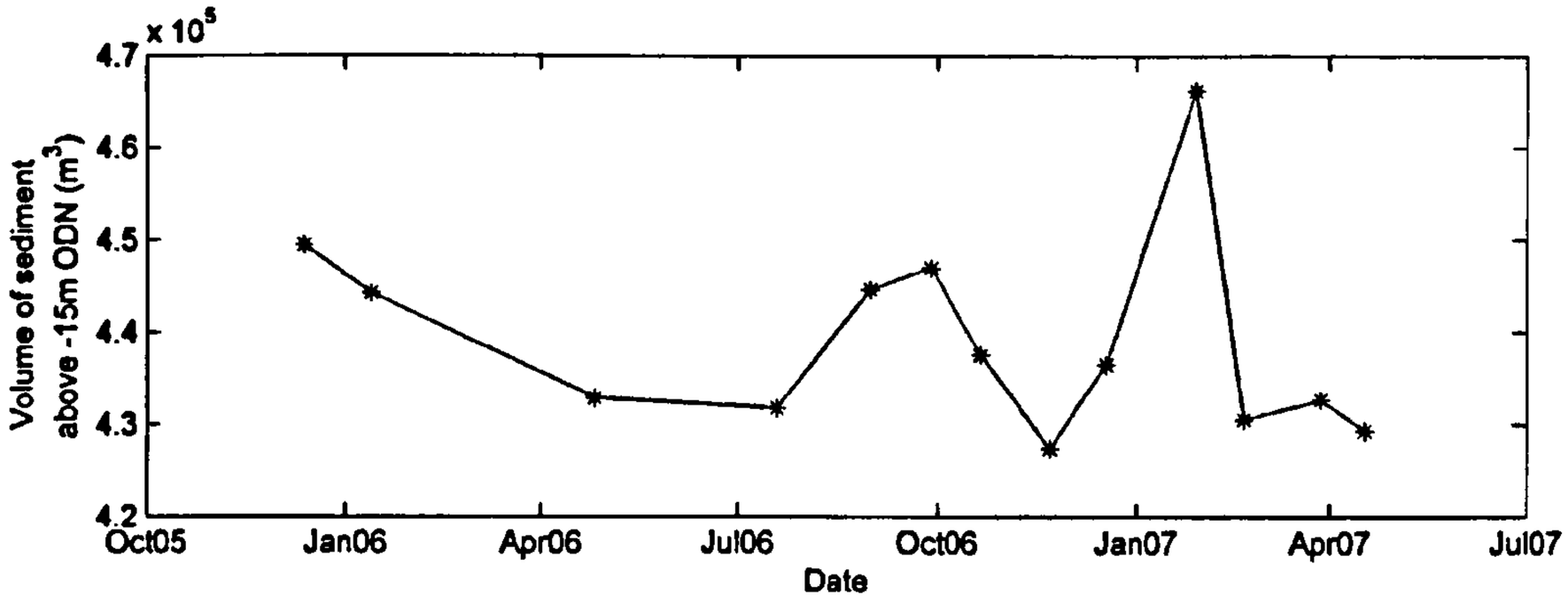

Figure B4: The volume of sediment in the up-drift section above a level of -15m ODN through time.

2. Results and discussion

Volume changes

The changes in volume are displayed in Figures B3&4. The down drift section shows similar volume changes to both phase one and two with a section of rapid erosion at the start and then a more gradual erosion with some accretionary periods. The up-drift section shows different patterns with greater accretionary events. Both the up-drift and down-drift sections are within the influence of the breakwater system, with the down drift section being starved of sediment and the up-drift section having the longshore movement of sediment impeded by the large tombolo at the northernmost breakwater. To compare up- and down-drift changes with changes inside the scheme, volumes were de-meaned and normalised by the area measured (Figure B5). The quantity displayed is representative of the average height change over time. Both up-drift, down-drift and within the breakwater system, the general trend is erosive, which is to be expected given the eroding nature of the East Anglian coast. For all areas the average gradient is of similar magnitude and the total loss over the 1.5 year study period is ~1m for all sections. This means that erosive trends inside and outside the scheme are similar. The up-drift section shows greater variability

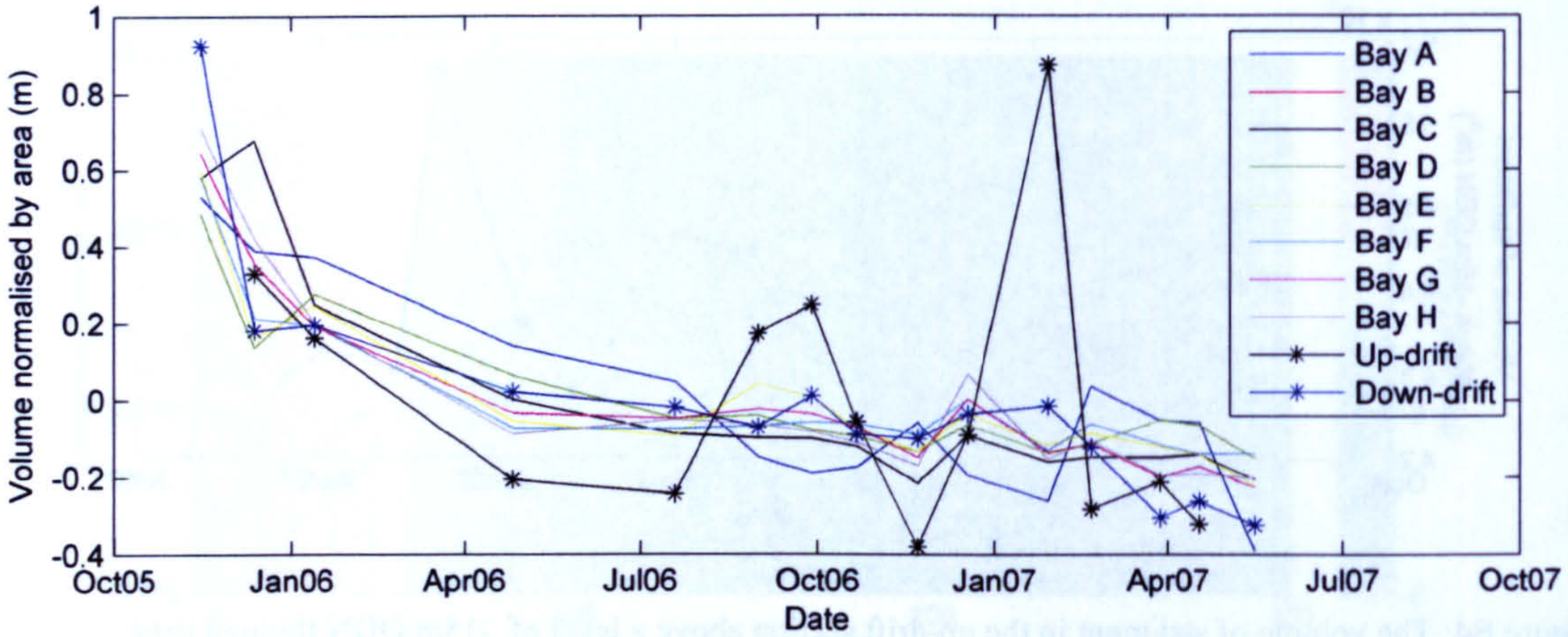

Figure B5: Volumes of the up-drift, down-drift and different bay sections which have been normalised by area.

with some large accretionary periods, which makes it harder to make judgement on the erosive gradient of this section. It is evident is that the block to longshore sediment transport caused by the breakwater system (and tombolo 5 in particular) causes different regimes up and down drift and that the large size of tombolo five (blocking sediment supply) is probably instrumental in the loss of sediment from down-drift and within the breakwater system.

Standard deviation.

The mean standard deviation for the up-drift section is 0.54m and the mean standard deviation for the down-drift section is 0.43m. This is greater than the standard deviation of change within the breakwater protected region (0.34m) and so suggests that, like the breakwaters at Elmer (Axe and Chadwick, 1997), morphological variability is reduced within the breakwater regions. The patterns of standard deviation are shown in Figures B6 & B7. The down drift section displayed greater variability in the offshore region below the -4m contour. The numerical model (Chapter 6) showed that there was significant

morphological change down-drift and at a similar offshore location to the breakwaters. This was forced by the lower breakwater 13 (more often submerged) leading to sediment transport southward and offshore out of the breakwater and by re-initiation of the offshore bar that was interrupted by the breakwater system. For the up-drift section the largest standard deviation is in the lower intertidal and just below the spring low tide level.

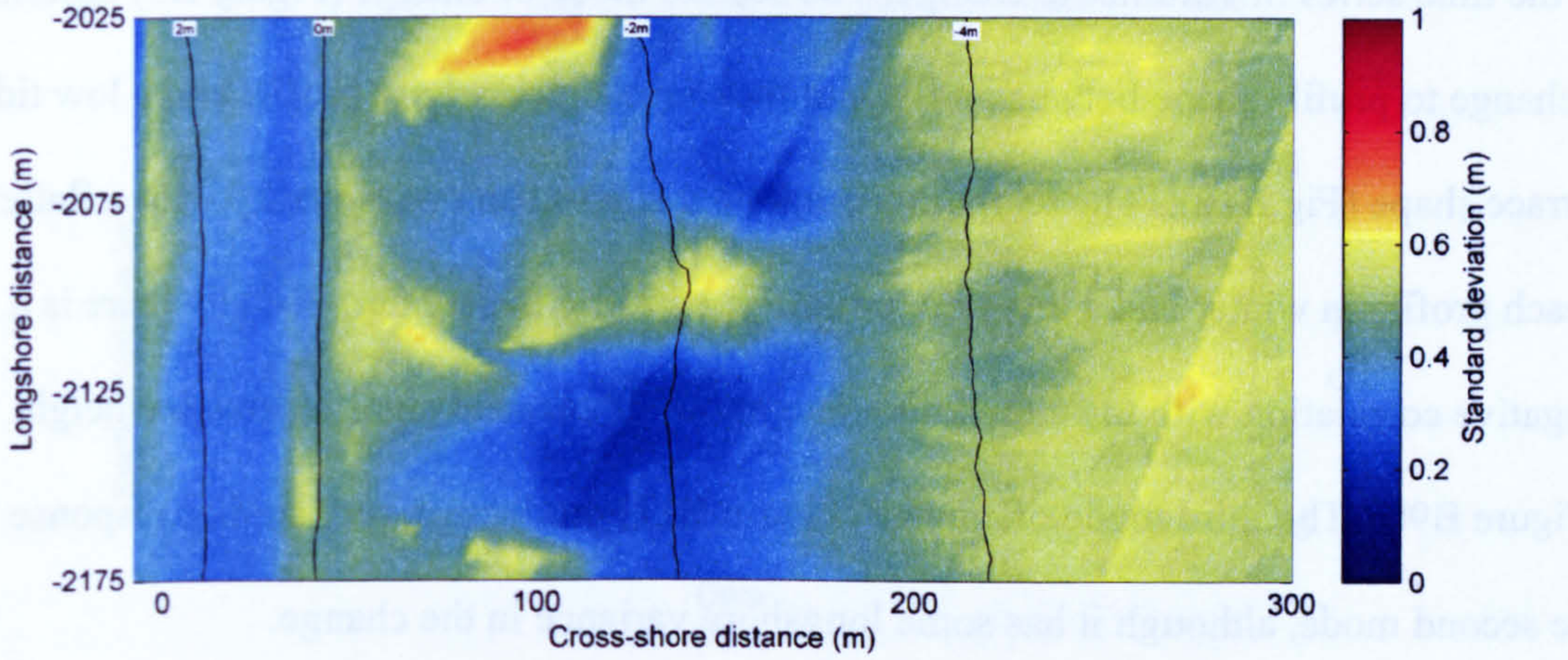

Figure B6: A map of the standard deviation for the down-drift section

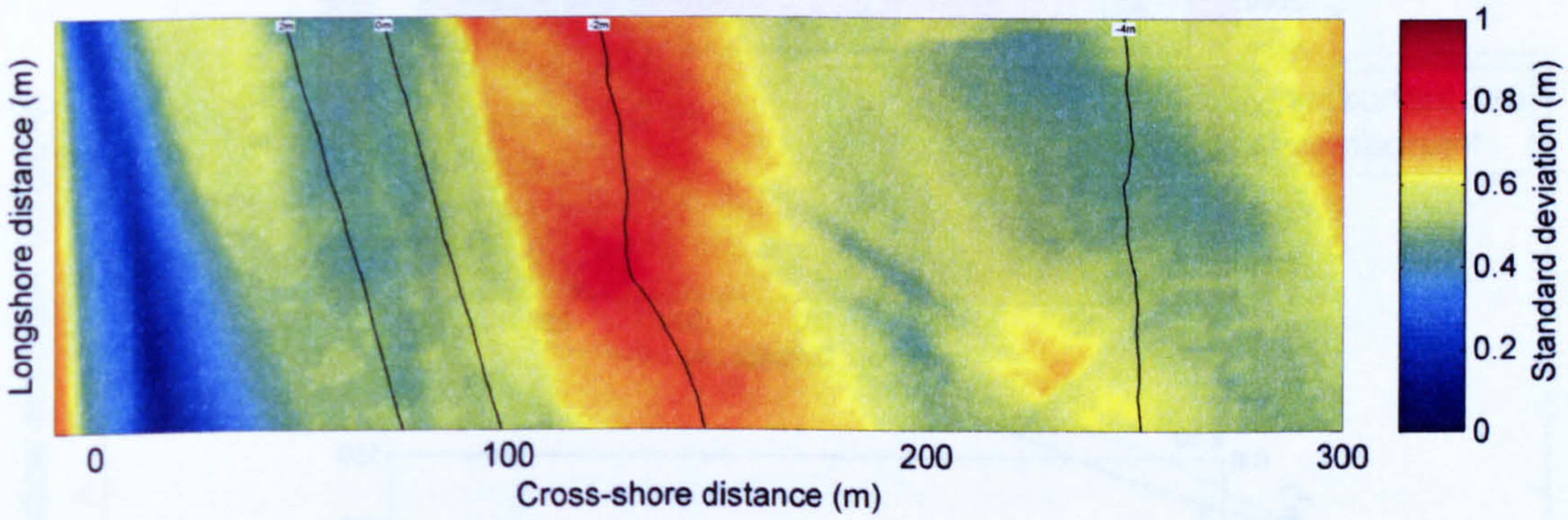

Figure B7: A map of standard deviation for the up-drift section.

Modes of beach change

The first three modes of change in the down drift section make up 87% of the variance in that section (64%, 15%, 8% respectively). The first mode of change (Figure B8) describes the volumetric change observed in the section volume analysis but shows that there is a section of accretion around the upper intertidal region. The temporal component is similar to the time series of volumetric change. The second mode of change (Figure B9) describes a change to profile shape between a flat and featureless cross-shore profile and a low tide terrace shape (Fig B10). The temporal component shows some seasonality with a flatter beach profile in winter and a low tide terrace type profile in summer, visually there is a negative correlation with the cumulative integral of de-meaned significant wave height (Figure B9b). The third mode of change (Figure B11) produces a very similar response to the second mode, although it has some longshore variance in the change.

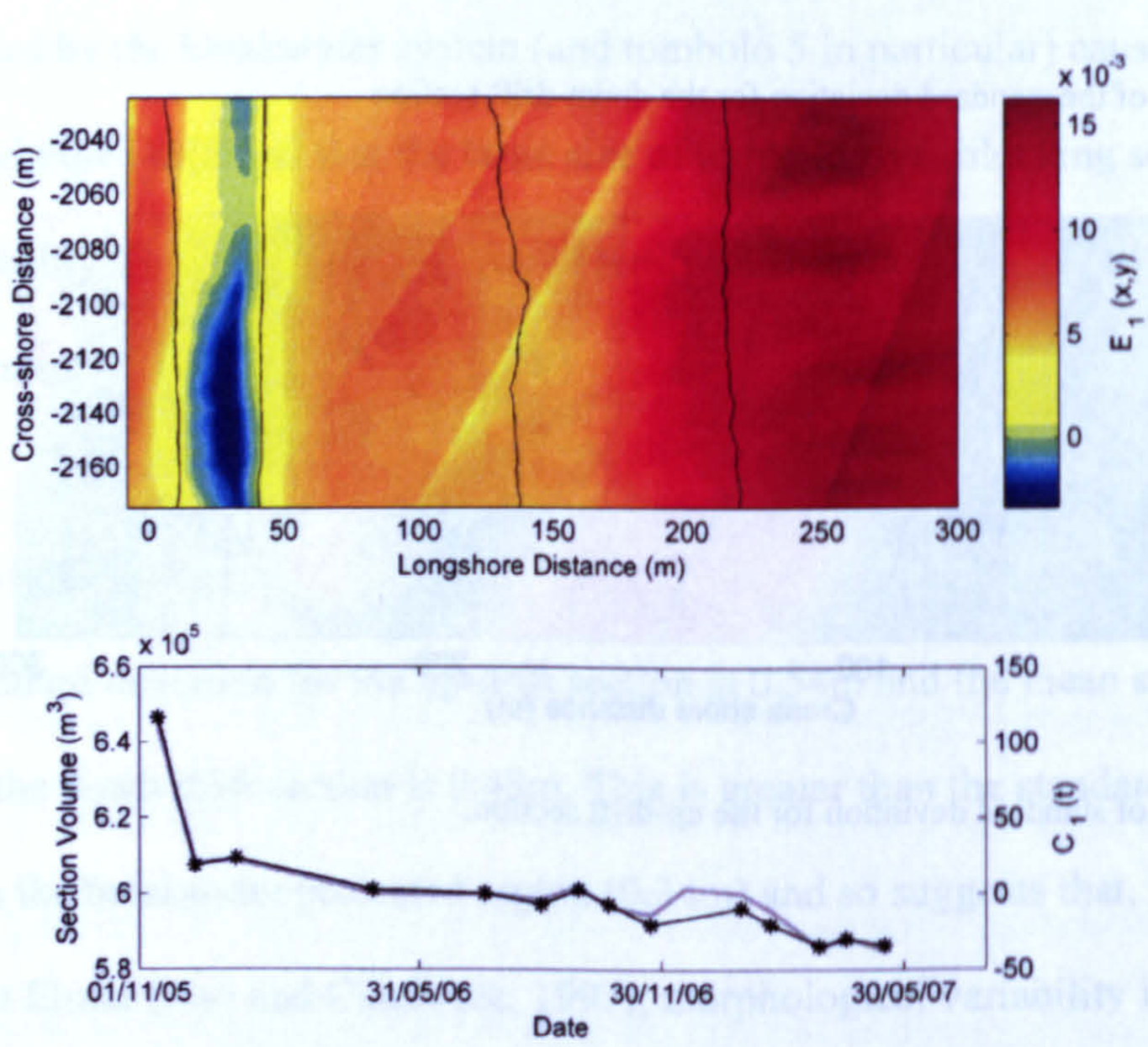

Figure B8: The first mode of change for the downdrift section a) the spatial eigen function and b) the temporal component (black line) and the total volumetric change (grey line).

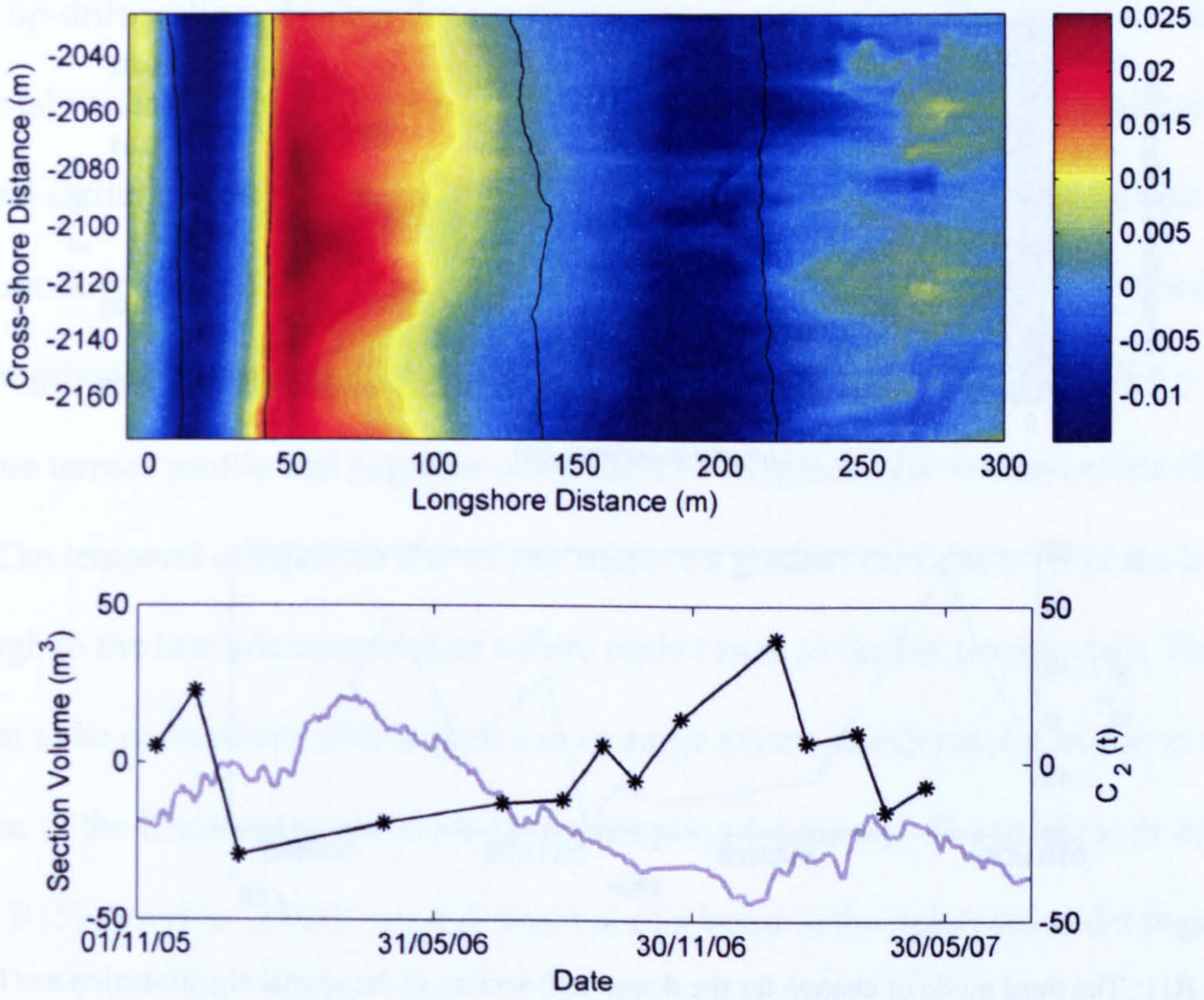

Figure B9: The second mode of change for the down-drift section a) the spatial eigenfunction and b) the temporal component (black starred line) and cumulative integral of de-meaned wave height (grey line)

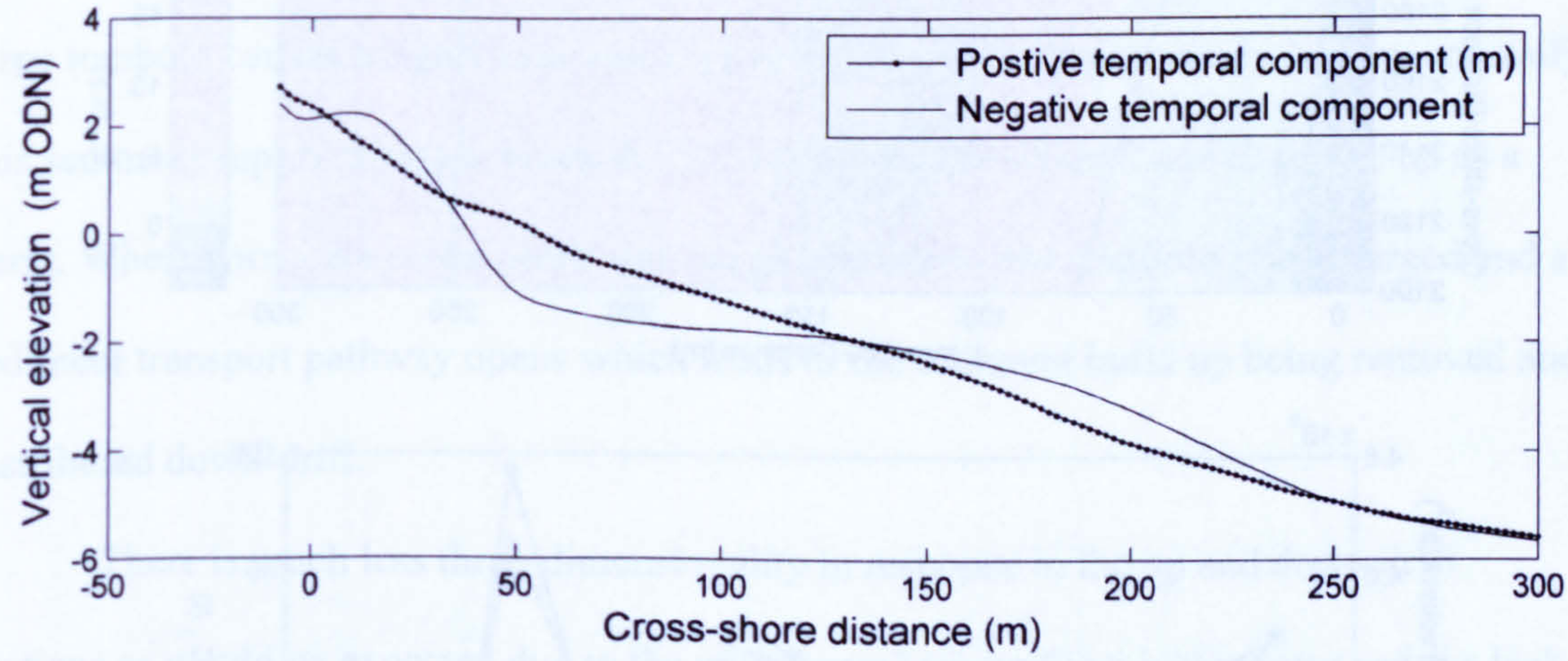

Figure B10: A longshore averaged depiction of the second mode of change showing the change between a flat and featureless profile (positive temporal component, predominantly in winter) and a low tide terrace profile (negative component predominantly in summer).

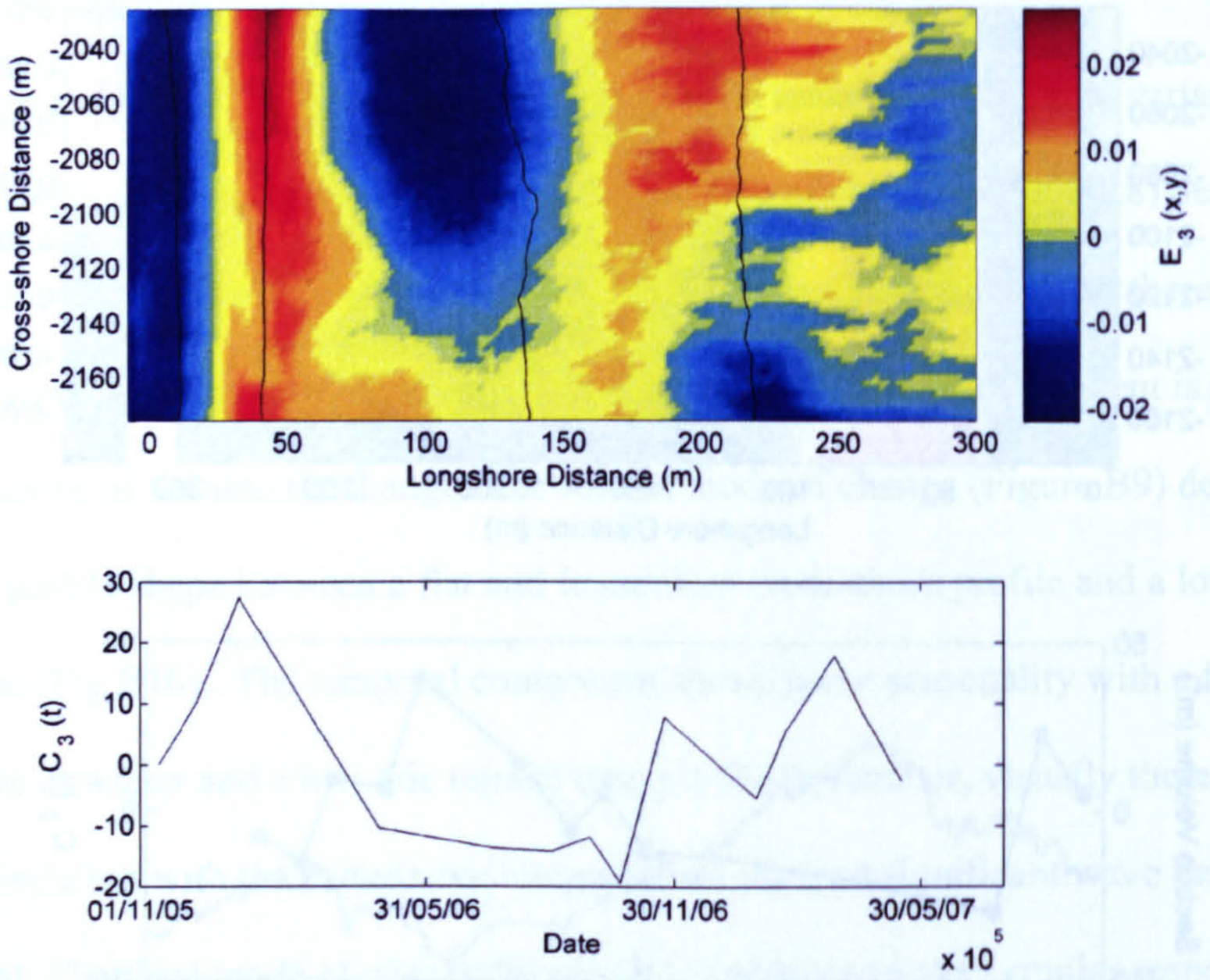

Figure B11: The third mode of change for the down-drift section a) the spatial eigenfunction and b) the temporal component.

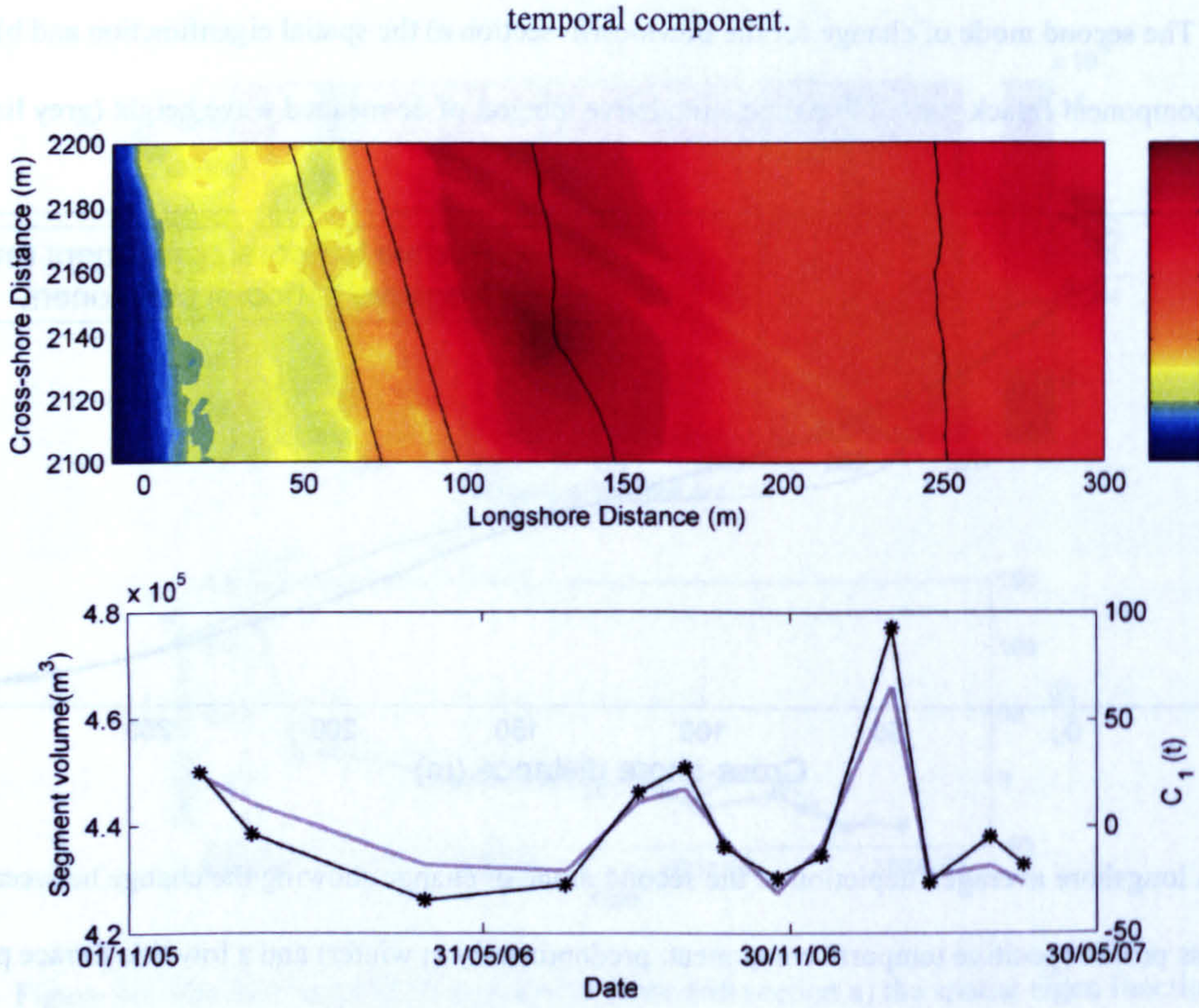

Figure B12: The first mode of change for the up-drift section a) the spatial eigenfunction and b) the temporal component

For the up-drift section, the first three modes of change make up 79% (48%, 18% and 13%) of the total variance. The first mode (Figure B12) described the volumetric change discussed earlier and shows the same temporal signal as the overall volume change. The second mode of change (B13) describes the change between a low tide terrace beach profile and a longshore bar-trough beach profile. Positive temporal components produce a longshore terrace profile and negative components a longshore bar trough profile (Figure B14). The temporal component shows that there is a gradual movement from the longshore bar trough to the low tide terrace state before rapid resets to the bar trough state. This does not seem to be co-incident with large storm or surge events which maybe to due to the influence of the breakwater system or to the sampling frequency. The third mode of change (Figure B15) describes a build up and removal of a berm in the upper intertidal region. However, whilst conventionally one considers berm formation to be related to low energy conditions, the temporal component shows that the berm is built up under storm conditions with no surge level and removed under storm conditions with an associated surge. The large tombolo causes a significant blockage to longshore sediment supply. Storms intensify this sediment supply which is blocked from continuing down-drift and so builds up as a berm. When storms are co-incident with surge conditions, the tombolo is submerged and a sediment transport pathway opens which leads to the sediment build up being removed and distributed down-drift.

There is much less three-dimensionality in response in the up and down drift sections as would be expected due to the more longshore uniform bathymetry and the lack of sheltered versus unsheltered regions. Like the breakwater protected regions, the dominant change is the overall increase and decrease in volume of the analysed sections. The EOF results give the same temporal signal as the basic volumetric considerations. Apart from the overall volumetric trends the dominant change is the cross-shore profile

changes. Down drift the beach profile is linear or in a low tide terrace state; up-drift the beach is either in a longshore bar trough state or a low tide terrace state. The breakwater protected regions show different cross-shore sediment patterns (chapters 4 & 5). Phase one displays a linear cross-shore profile that varies in steepness depending on incident conditions whilst in phase two the cross-shore exchange is 3-dimensional and leads to an increase and decrease in salient sinuosity.

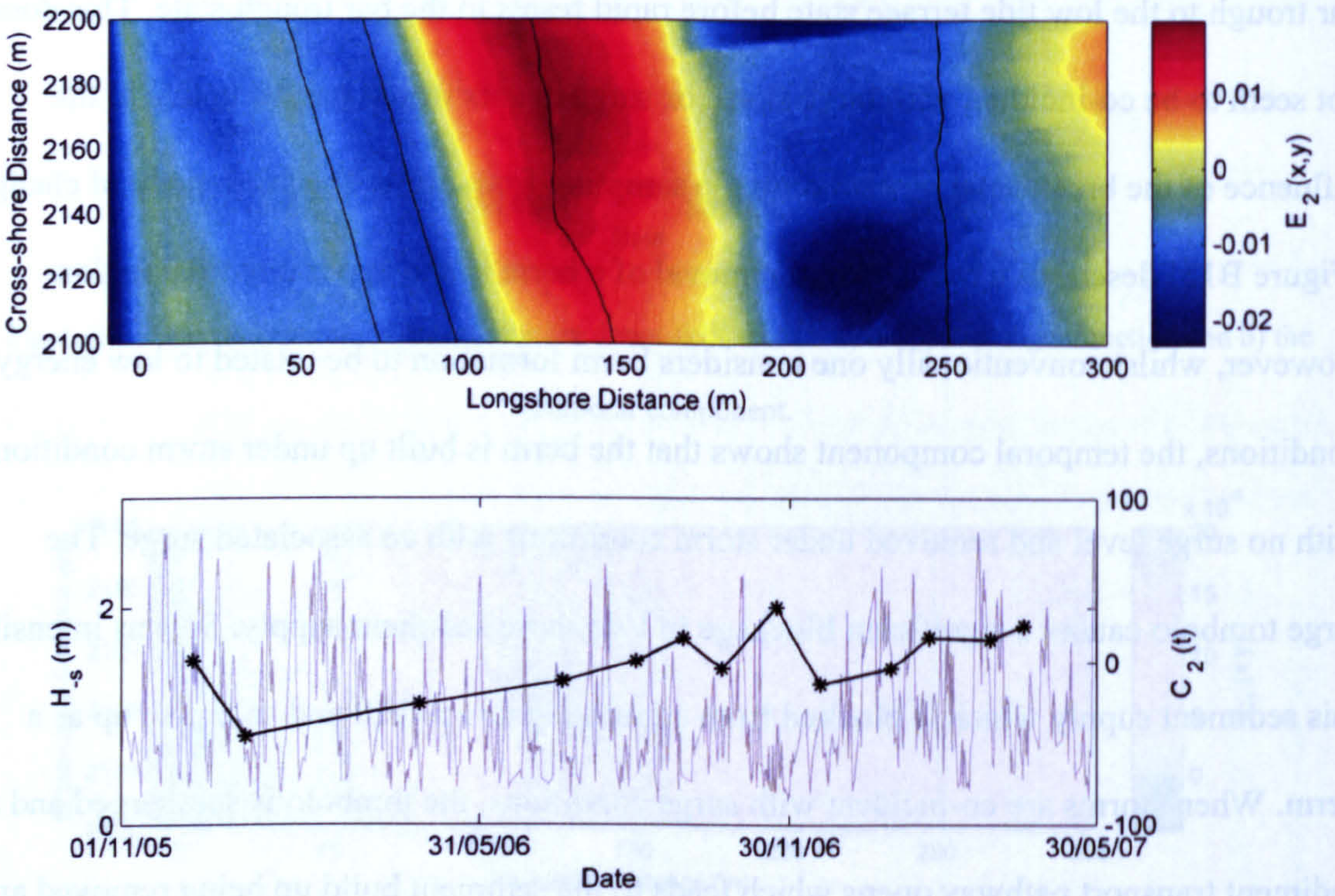

Figure B13: The second mode of response for the up-drift section; a) the spatial eigenfunction and b) the temporal component (black) and significant wave height (grey).

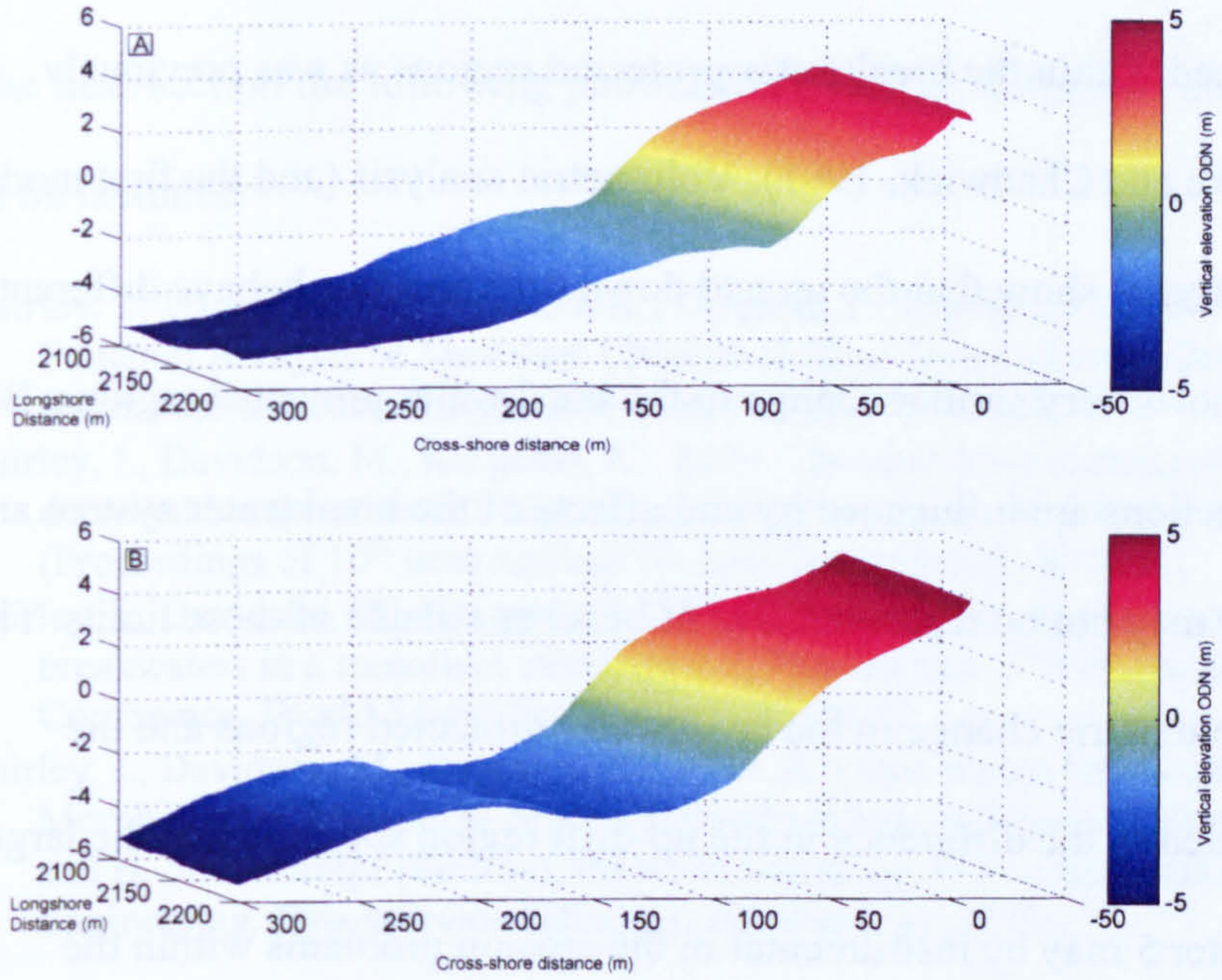

B14: A demonstration of the effect of the second mode of change with: a) a positive temporal component and b) a negative temporal component.

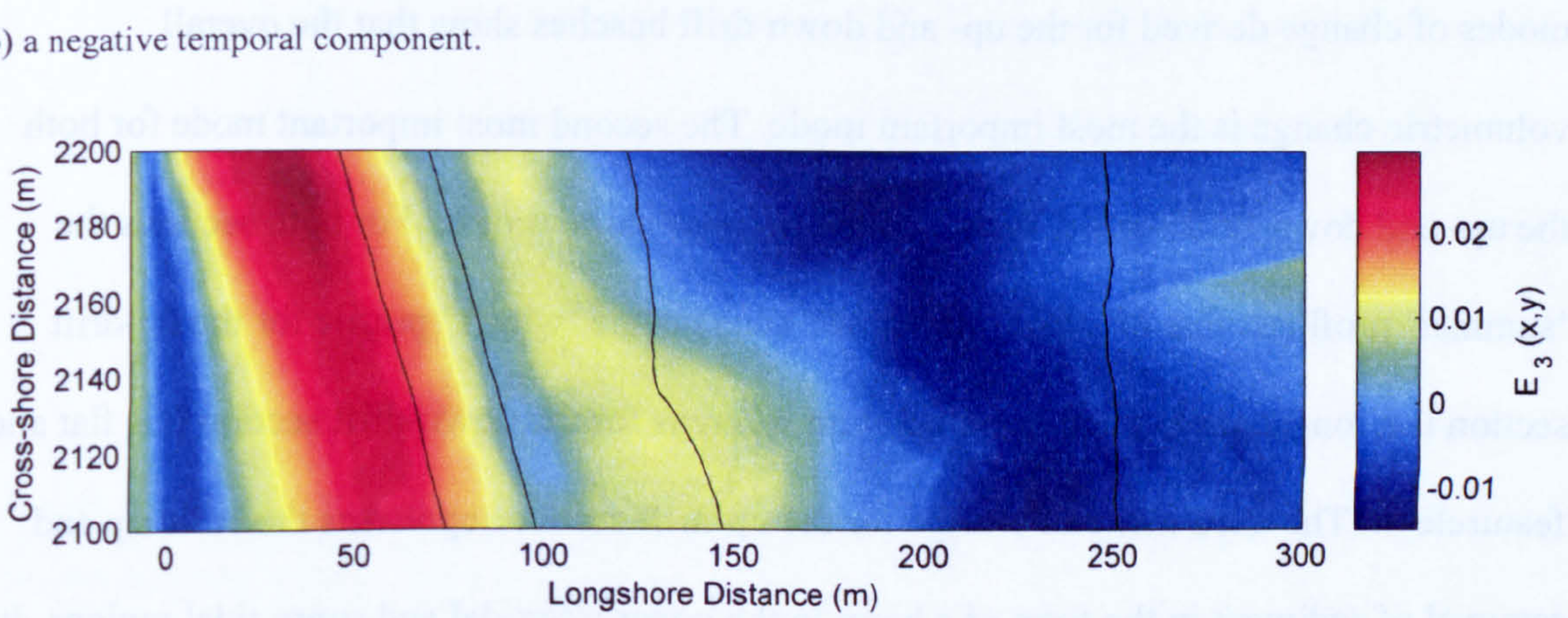

Figure B15: The third mode of change for the up-drift section a) the spatial eigenfunction and b) the temporal component (black) with the incident wave height (red) and surge residual (blue) also displayed.

3. Conclusions

Beach variability is reduced within the breakwater protected regions as was previously documented at Elmer (Axe and Chadwick, 1997). Volumetric analysis (and the first mode of change of the EOF analysis) show that the up and down drift sections behave differently. The down drift section shows very similar change to the breakwater protected regions. Both the up- and down-drift sections are influenced by end effects of the breakwater system and so the volumetric change may not be representative of beaches outside of these limits. The similarity between the volumetric change in the breakwater protected regions and the down-drift region compared to the difference in the up-drift region suggests that the large tombolo behind breakwater 5 may be instrumental in the erosion problems within the breakwater scheme due to the total block to longshore sediment transport it provides. The modes of change derived for the up- and down-drift beaches show that the overall volumetric change is the most important mode. The second most important mode for both the up- and down-drift section is the change in cross-shore profile. For both sections the 'summer' profile is that of a low tide terrace whereas the 'winter' profile for the up-drift section is a longshore bar and trough system whereas for the down-drift section it is flat and featureless. The third mode of change for the up-drift section represents the build up and removal of sediment in the form of a berm in the upper intertidal and supra-tidal regions. It is believed that this is due to the trapping of sediment by tombolo five. The third mode of change for the down-drift section is similar to the second mode. Whilst the unprotected (up- and down-drift) regions show greater magnitude of beach variability (greater standard deviations), the complexity of the change is less than for the breakwater protected regions due to the lesser three-dimensionality to the changes.

Axe, P.Chadwick, A., 1997. Beach Variability Behind Detached Breakwaters. In: E.B. Thornton (Editor), Coastal Dynamics '97. ASCE, Plymouth, U.K., pp. 744-753.

Publications

In the next section the following publications, written during the course of the PhD study, will be included:

Fairley, I., Davidson, M., Kingston, K., Dolphin, T., Phillips, R., 2009, Empirical Orthogonal Function Analysis of Shoreline Changes Behind Two Different Designs of Detached Breakwaters. Coastal Engineering, 56(11-12): 1097-1108.

Fairley, I., Davidson, M., Kingston, K., 2009. The morpho-dynamics of a beach protected by detached breakwaters in a high energy tidal environment. Journal of Coastal Research, S.I. 56 (Proceedings of 10th International Coastal Symposium): 607-611.

Fairley, I., Davidson, M., Kingston, K., 2009. Video monitoring of overtopping of detached breakwaters in a mesotidal environment, Proceedings, 5th Coastal Structures International Conference, World Scientific, Venice. 1923-1932

Fairley, I., Davidson, M., Kingston, K., 2009. A Video Based Investigation into the Morphological Impacts of Storms Behind a Series of Detached Breakwaters, In: R. Lehfeldt and H. Schuttrumpf (Editors), Poster Proceedings of 31st International Conference on Coastal Engineering. Druckservice Zillekens, Hamburg, pp. 80-91.

Coastal Engineering 56 (2009) 1097–1108

Contents lists available at ScienceDirect

Coastal Engineering

journal homepage: www.elsevier.com/locate/coastaleng

Empirical orthogonal function analysis of shoreline changes behind two different designs of detached breakwaters

I. Fairley [a,*], M. Davidson [a], K. Kingston [a], T. Dolphin [b], R. Phillips [b]

[a] Marine Institute, Coastal Processes Research Group, School of Earth Ocean and Environmental Sciences, University of Plymouth, Drake Circus, Plymouth, Devon, PL4 8AA, United Kingdom
[b] Coastal Processes Research Group, School of Environmental Sciences, University of East Anglia, Norwich, NR4 7TJ, United Kingdom

ARTICLE INFO

Article history:
Received 29 April 2008
Received in revised form 4 August 2009
Accepted 7 August 2009
Available online 4 September 2009

Keywords:
Video
Shorelines
Breakwaters
Morphodynamics
EOF analysis

ABSTRACT

This paper compares the shoreline responses immediately shoreward of two adjacent schemes of segmented shore parallel rubble mound breakwaters undergoing the same forcing by waves and tides. Scheme one consists of four longer, emergent breakwaters that have produced tidal tombolos in their lee. Scheme two consists of five shorter, lower breakwaters that are submerged at higher tides with salients in the breakwater's lee. Empirical orthogonal function analysis was used to decompose a video derived shoreline dataset into the dominant modes of shoreline change for both schemes. The two schemes showed similar modes of change. The primary mode of change for both schemes was the cross-shore growth and shrinking of the salients/tombolos. The secondary mode of change was the longshore movement of the salients/tombolos. For all modes of change, the dominant length scale was dictated by the breakwater dimensions and locations. A new manifestation of hydrodynamic parameters is introduced: the cumulative integral of the de-meaned parameters. This parameterisation allowed for meaningful correlation of the temporal EOF components with forcing parameters and identification of the important influence of the tide on observed morphodynamic change. Clear differences were observed between the shoreline responses measured in schemes one and two; including differences in bay erosion/accretion; and the longshore translation of salients/tombolos. The beaches in scheme two showed behavioural patterns similar to unprotected beaches which were not observable in scheme one. It is postulated that these differences are caused both by the different breakwater designs and by variation in longshore sediment supply.

1. Introduction

Detached breakwaters are used worldwide as a method of shoreline protection; their aim is to increase beach widths, providing a buffer zone against erosion and also increasing beach amenity value. Detached breakwaters create regions of wave sheltering and alter near-shore circulation patterns which normally result in accretionary features behind the structure. Two features are most commonly observed, either a salient extending from the beach in the lee of the structure or the extreme conclusion of this, a tombolo, where sediment accretes to such an extent that the salient reaches the breakwater. Features in tidal environments that are salients at high tide and tombolos at low tide are termed tidal tombolos. Many design guidelines have been produced that predict the type of response (Ahrens and Cox, 1990; McCormick, 1993; Pope and Dean, 1986; Suh and Dalrymple, 1987) but these focus on low energy, micro-tidal environments. Furthermore, it is known that poorly designed structures can cause erosion rather than accretion (Turner, 2006) and so care must be taken in the implementation of such structures. However, current knowledge does not accurately predict the beach response to detached breakwaters in tidal environments (Pilarczyk and Zeidler, 1996). Further understanding of the morphodynamic response of beaches to the presence of detached breakwaters in tidal environments is needed in order to inform future design guidelines. The LeaCoastII project aims to address this deficit in research by investigating the effects of detached breakwaters in a high energy, meso-tidal environment, the project is the first of its kind and involves partners utilising numerical modelling, process experiments and morphological surveys. The Sea Palling breakwater scheme is an ideal field site for the investigation of detached breakwaters since comparisons can be made between morphological changes behind two different breakwater designs undergoing the same hydrodynamic forcing.

This paper uses a system of 3rd generation Argus video cameras (Holman and Stanley, 2007) to derive shoreline time series over both schemes of the breakwater scheme for a period of 30 months with a temporal resolution varying from daily to fortnightly. The major benefit of coastal video systems over traditional beach survey techniques is the high spatial and temporal resolution that can be achieved at comparatively low financial and man hour costs. The high temporal resolution captures morphological changes that are missed in traditional monthly beach surveys. The temporal resolution, along

* Corresponding author. Tel.: +44 1752 584719; fax: +44 1752 584710.
E-mail address: iain.fairley@plymouth.ac.uk (I. Fairley).

0378-3839/$ – see front matter © 2009 Elsevier B.V. All rights reserved.
doi:10.1016/j.coastaleng.2009.08.001

with the nature of the site studied, makes this a unique dataset. Monitoring changes to shoreline position through time has long been used to inform coastal management and to aid coastal research and engineering. A single shoreline representation of beach morphology is an attractive method of data reduction since it allows for a simpler description of changes over time than 3-dimensional morphological maps, often leading to identification of trends that can be difficult to extract from more complex datasets. Determination and definition of a viable shoreline is a non-trivial question and a bad choice in this matter can affect validity of results (Boak and Turner, 2005). The actual shoreline, defined as the land/water intersection, is constantly changing due to tidal and wave (set-up and swash) processes; thus a shoreline proxy or representative shoreline (e.g. mean high water shoreline) is normally used. Boak and Turner (2005) provide a review of the different shoreline proxies commonly in use today, typically these are shorelines at a certain water level or features such as cliff lines. In order to have the capability to extract shorelines from every tide the mean sea level shoreline position (MSL) was used as the shoreline representation for this analysis. This water level has the advantage that it adequately captures the morphological features of the scheme; a shoreline at higher water levels would miss much of the variability in the shapes of the salients and tombolos. The MSL contour has been previously shown to have high correlation with the beach volume by Smith and Bryan (2007) for Tairua Beach, New Zealand.

The shoreline dataset is analysed using empirical orthogonal function (EOF) analysis allowing for identification of the different modes of shoreline change, their spatial characteristics and their temporal scales. The method has enabled the distinction of both similarities and differences in morphological changes between the two schemes given the same forcing. Empirical orthogonal functions have a history of use in coastal process and coastal engineering research, being used for the analysis of beach profile changes (Aubrey, 1979; Winant et al., 1975) and more recently longshore shoreline changes (Miller and Dean, 2007; Munoz-Perez et al., 2001). The technique has previously been applied to morphological changes behind detached breakwaters in the UK by Axe and Chadwick (1997) who showed that the profile variability was reduced behind breakwaters at Elmer, West Sussex.

2. The Sea Palling site

Sea Palling is on the North Norfolk coast of the UK (Fig. 1A). The Sea Palling site consists of a sandy beach backed by a single dune line and sea wall which is protected by nine detached rubble mound breakwaters (Fig. 1B) in two schemes. The breakwaters were built in two construction phases, named 'scheme one' and 'scheme two' in this paper: scheme one, completed in 1994, comprises of four larger emergent breakwaters and scheme two, completed in 1997, consists of five smaller breakwaters that are submerged at spring high tides (Hamer et al., 1998). The two schemes are adjacent to each other meaning independence in their responses cannot be assumed due to linked sediment supply and exchange between schemes. However,

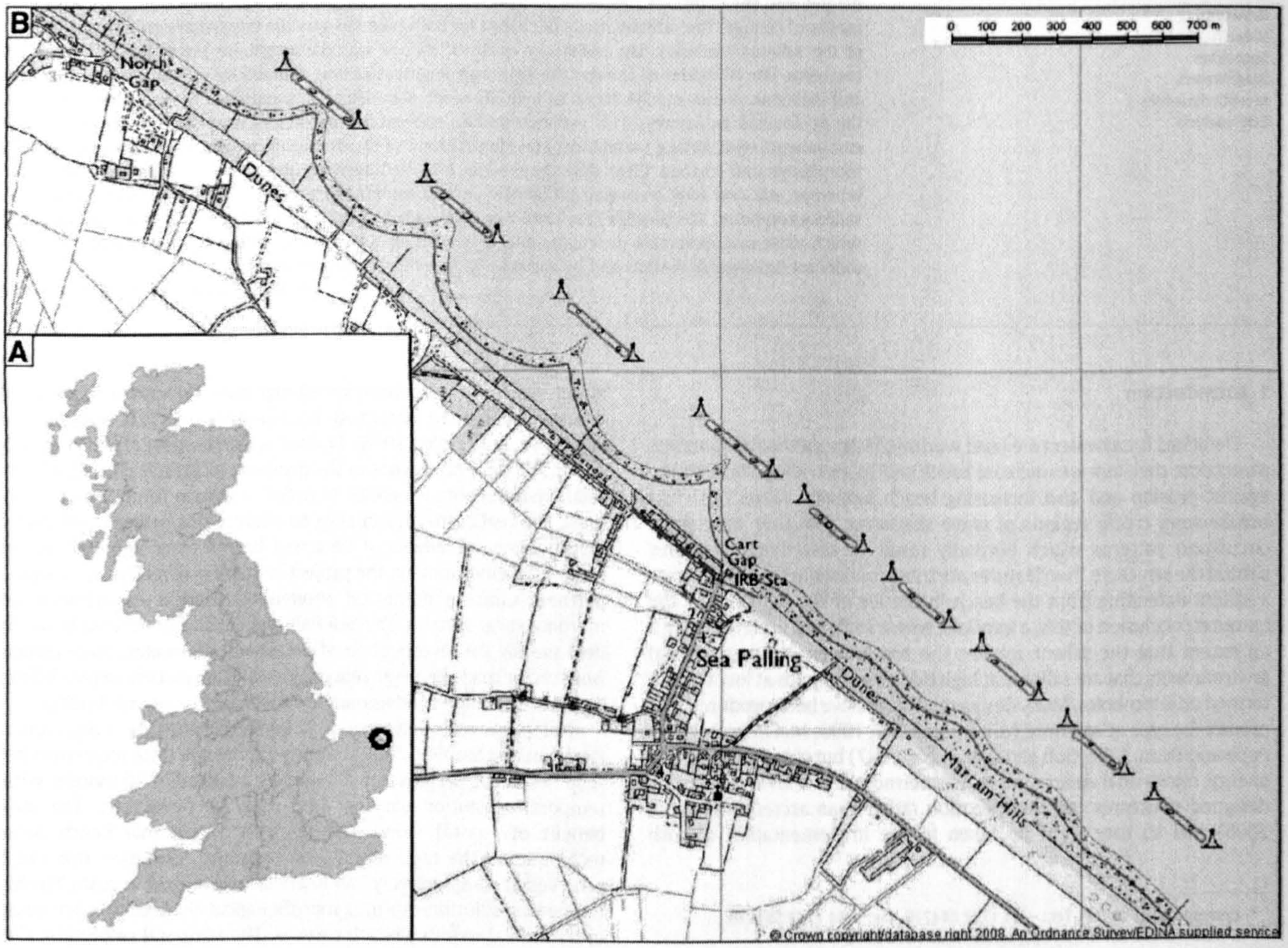

Fig. 1. A) A map of the United Kingdom with the location of Sea Palling marked with a black circle, and B) a map of Sea Palling showing the nine breakwaters, in the two schemes. The camera system is located between the two schemes at Cart Gap.

distinct differences in beach responses due to the different designs can be observed. The important breakwater dimensions are given in Table 1. The freeboard of the breakwaters at MHWS is 1.3 m for schemes one and −0.5 m for schemes two (submerged). The scheme two breakwaters are emergent at MHWN with a freeboard of 0.3 m.

The beach consists of medium to coarse sand with a d_{50} of 430 μm (Bacon et al., 2005) and prior to breakwater construction was steep and narrow with an offshore bar (Thomella et al., 2001). After construction, tidal tombolos (hereafter referred to as tombolos) were formed behind the scheme one breakwaters and subdued salients formed behind the scheme two structures.

The region's hydrodynamic conditions are characterised by a meso-tidal regime and energetic wave conditions. The tidal regime has a spring range of ~3.1 m and is a progressive tidal wave, typical of the southern North Sea. Peak tidal currents are at high (south-easterly current direction) and low water (north-westerly current direction). The tide is asymmetric: the flood tide has marginally longer duration (Bacon et al., 2005). This, along with partially blocked ebb flows due to the tidal tombolos, leads to a net tidally induced current through the schemes to the south-east.

Energetic wave conditions reach the site from all directions although the largest waves, reaching over 4 m, tend to approach from the fetch unlimited north. The net longshore transport is considerable with net volumes around 10^5 m^3 per year (Clayton et al., 1983) transported from north-west to south-east, although in some years a large number of southerly storms can reverse this direction (Thomella et al., 2001).

The wave record over the time analysed is presented in Fig. 2, the incident climate is plotted in black and a low passed series plotted in grey. A fast Fourier transform filter with a cut-off period of 90 days was used to obtain the low passed signal in order to test for seasonality in the incident conditions. The significant wave height H_s (Fig. 2A) shows a slight seasonality to the 'background' wave heights with higher wave heights through the winter months. Superimposed on the 'background' waves are storm events ($H_s > 1.5$ m) which have an average return period of 60 days, the minimum storm return period in this record is 3 days and the maximum 80 days. The majority of storm events are incident from the north. There is some seasonality to the mean wave period with slightly longer period waves through the winter months (Fig. 2B). No obvious seasonality is observed in the wave direction (Fig. 2C). An increase in surge events can be observed during the winter months in the tidal record (Fig. 2D). Surges are manifest as spikes (either positive or negative) in the tidal time series outside of the black band of spring neap variation. A greater number of surges can be seen between October and March in both winters.

3. Methodology

3.1. Shoreline extraction

Six cameras are situated between the two schemes at Cart Gap (Fig. 1B), 26 m above mean sea level on a guyed steel tower and are positioned such that the entire breakwater scheme is covered (Fig. 3). Longshore image resolution ranges from 0.1 m at close range to 30 m at ranges over 1.5 km; meaning that the ends of the scheme are excluded from this analysis due to reduction in accuracy of shoreline location. Analysis is confined to two embayments in scheme one, the transition embayment between the two schemes and three embayments in scheme two.

Table 1
A table displaying the breakwater dimensions for each scheme. (from Dolphin et al., 2005).

	Breakwater length (m)	Gap length (m)	Crest height (m)	Distance offshore (m)
Phase one	200	300	3	275
Phase two	160	160	1.2	275

The MSL shoreline was defined as the shoreline at a tidal elevation of 0.18 m Ordnance Datum Newlyn which was the mean tidal level over the time period analysed. Images were not necessarily collected at MSL, due to automatic half hourly image collection routines, so the MSL contour was obtained by linear interpolation between image shorelines at vertical elevations above and below the MSL elevation. The picked shorelines (above and below MSL) were interpolated onto a regular 2 m longshore spacing and then vertical interpolation between the two shorelines at each longshore point used to obtain the MSL contour. Tidal elevations were derived from UK National Tidal and Sea Level Facility gauges at Cromer and Lowestoft (15 and 23 miles away respectively), the interpolation was tested against several months of in-situ tide data and agreement found to be very good: largest differences were at high and low tide and were 0.07 m.

Various automated methods have been developed to pick shorelines from images (Plant et al., 2007), however these approaches tend to be site specific and none could be routinely applied to the Sea Palling images with comparable accuracy to manually picking the shoreline. Therefore, shorelines were picked manually from images using a point and click graphical user interface. Whilst this approach is user intensive, it affords the greatest accuracy in picked shoreline location and due to the reduction in number of images analysed to produce a shoreline, rather than an intertidal profile, it is not prohibitively time consuming. Ten minute time averaged images were used to extract the shoreline since time averaging removes discrepancies such as individual wave run-up events and gives a more robust shoreline estimate.

Shorelines were only picked from images with good clarity: images that were not obscured by fog, heavy rain or fuzziness caused by camera vibration in high winds. Typically, water levels for shorelines extracted from Argus images have a correction made for the elevation of the shoreline due to wave set-up. One of the characteristics of a system of detached breakwaters is that the wave set-up varies considerably around the embayments (and thus in an image) due to the sheltering of the breakwaters and wave diffraction through the gaps. Therefore no correction was made for wave set-up and instead shorelines were only picked from days when the significant wave height was below 0.2 m to reduce vertical errors in water elevation due to wave set-up which is approximately 17% of the wave height (Guza and Thornton, 1981), giving set-up values less than 3.4 cm. Wave heights were determined from a UK met office wave model (Bidliot and Holt, 1999; Golding, 1893) output 1 km from Sea Palling, that were transformed inshore using MIKE21SW (Sorenson et al., 2004). Fig. 4 shows an example comparison between the MSL contour extracted from video and the MSL contour extracted from a DGPS survey. The typical mean difference in cross-shore location between the DGPS and video derived shorelines is approximately ±1.2 m.

Shoreline extraction at a weekly temporal spacing was planned, with greater temporal resolution around storm events which were defined as events where the significant wave height reached over 1.5 m. However, due to bad image clarity or extended periods of moderate waves, weekly shorelines were not always realisable and thus the temporal spacing of shorelines varies from daily to fortnightly. A total of 127 shorelines were extracted between 03/05/2006 and 25/10/2008; the temporal spacing of the shoreline realisation and its relation to the wave time series is shown in Fig. 5. This figure shows the wave height record with the vertical lines indicating times at which MSLs' were realised. It can be seen that the majority of individual storm events are isolated; low image clarity or inopportune hydrodynamic conditions accounts for instances when storms are not independently captured.

The analysis presented in this contribution is conducted in an Argus co-ordinate system. The position of the camera tower is the

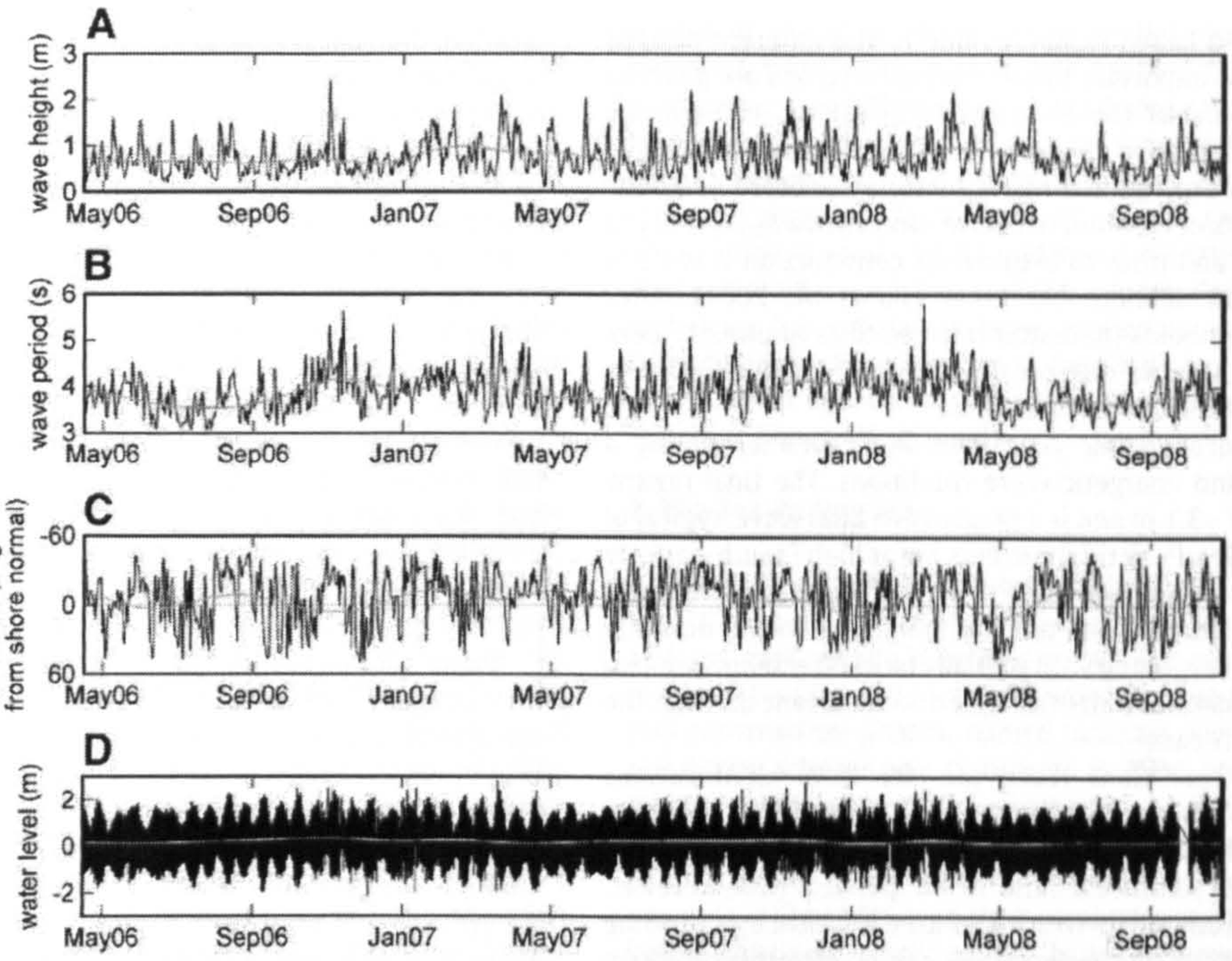

Fig. 2. Time series of hydrodynamic parameters (black) and low passed time series with a 90 day cut-off (grey) showing seasonal trends: A) significant wave height; B) mean wave period; C) mean wave direction from shore normal (negative values indicate waves incident from north of shore normal and positive values from the south of shore normal); D) tidal elevation.

origin, the *y*-axis increases with cross-shore distance offshore from the camera tower and the *x*-axis increases with longshore distance from the camera tower. The *x*-axis is positive in a northward-westerly direction (scheme one) and negative in a south-easterly direction (scheme two). The transformation between OSGB36 (the UK Ordnance Survey co-ordinate system) and the Argus co-ordinate system is affected using standard Argus routines (Aarninkhof et al., 2006) and facilitates easier manipulation and analysis of the images.

3.3. Empirical orthogonal function analysis

EOF analysis uses properties of matrix algebra to decompose a dataset into spatially orthogonal eigenfunctions, $e_k(x)$, and associated temporal co-efficients, $c_k(x)$. This allows for the isolation of unrelated modes of shoreline response in what can be a complex signal. The original dataset $y(x,t)$ can be represented as:

$$y(x,t) = \sum_{k=1}^{n} c_k(t)e_k(x). \quad (1)$$

Each combination $c_k(t)e_k(t)$ describes an orthogonal mode of change in the dataset and its variation through time. The 1st mode describes the most variance in the dataset and the variance described reduces with the higher EOFs. This paper uses an algorithm based on the most efficient algorithm proposed by von Storch and Hannostock (1984) to split the dataset into 10 spatial eigenfunctions and associated temporal co-efficients. Often the first EOF can describe the "mean shoreline" (Miller and Dean, 2007), however in this paper the data set is de-meaned prior to analysis which removes this feature. De-meaned

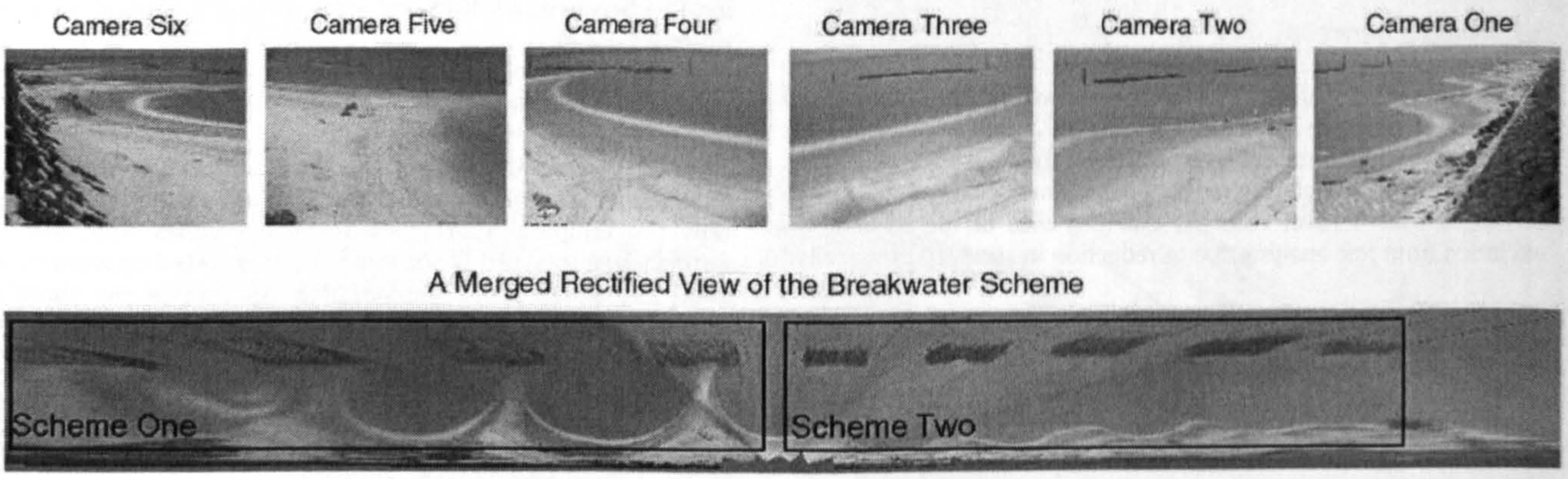

Fig. 3. Images from the six cameras and a merged, rectified plan view of the scheme from the six Argus cameras with the two schemes marked. Scheme one consists of 4 emergent breakwaters 200 m long and scheme two consists of 5 lower breakwaters 160 m long that are submerged at spring high tides.

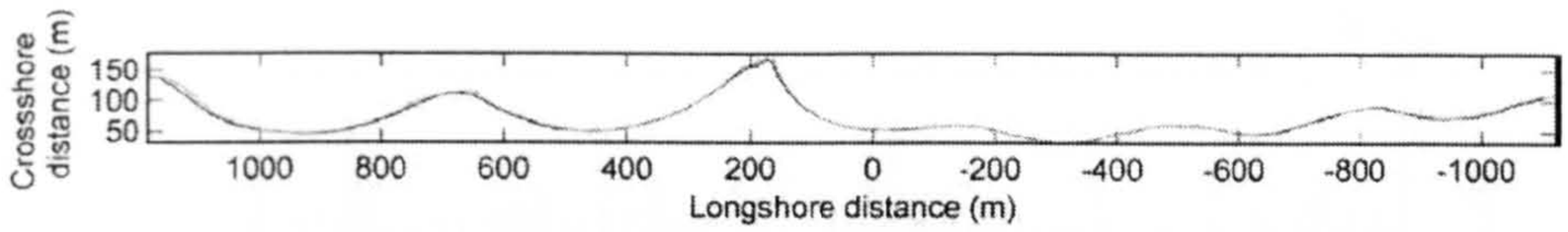

Fig. 4. Comparison between video derived MSL contour (grey) and DGPS surveyed MSL contour (black).

shoreline time series' allow for better identification of the changes taking place when the longshore variance in the mean is large (Munoz-Perez et al., 2001). In this dataset the tombolos/salients forced by the breakwaters cause this large longshore variability in mean shoreline position which can obscure observation of changes.

Before the EOF analysis was conducted the shoreline time series was split into two sections: scheme one and scheme two. The motivation for splitting the two schemes was twofold: firstly, since the two schemes of breakwaters are significantly different, it is not a valid assumption that they will have the same modes of change; secondly, the greater variance in scheme one is likely to obscure scheme two changes if the changes over both schemes are forced into one mode.

3.4. Comparison with hydrodynamic parameters

Pearson product moment correlation co-efficients (r) were calculated for the temporal components of the EOF analysis against various hydrodynamic parameters. These were tested for significance using the Student's T-test. Due to the large sample size (127) correlations were significant if the r value exceeded 0.29, meaning that even apparently weak correlations were significant. The amount of variance described by each correlated parameter is given by r^2. Standard parameters of wave height, period, steepness, tidal range and longshore sediment quantity were tested. Wave height was tested because wave-driven currents scale with wave height as does the amount of breakwater overtopping. Wave period was tested primarily because the period affects the wave diffraction patterns and hence the angle of wave incidence to the shoreline and the amount of energy transmitted to the sheltered region. Wave steepness indicates likelihood of erosion/accretion for a given wave height (steeper waves favoring erosion). The tidal range is used as a proxy for the tidal asymmetry which varies over the spring neap cycle and has previously been shown to be important at the site (Bacon et al, 2005). Also tested were the relative tidal range and a time series of high tide elevation. The rationale for utilization of these parameters follows: relative tidal range (TR/H_s) is normally used in the classification of beach types (Masselink and Short, 1993), however in this study it is used to indicate the relative importance of tides and waves. It has been shown that tidal currents contribute significantly to the sediment transport at this site (Bacon et al., 2005). As the magnitude of tidal currents scale with tidal range, the daily relative tidal range provides a parameter that encalpsulates the balance between tides and waves. The time series of high tide elevation was used to indicate the potential penetration of wave energy in the embayments. Higher water levels allow greater wave penetration as there is greater overtopping, lesser wave dissipation on the bay floors and the gaps between breakwaters are wider due to the sloped breakwater sides. Large spring high water levels and surges also allow the mobilisation of sediment from the supra-tidal beach and potentially open additional sediment transport pathways over the large northernmost tombolo that is normally dry throughout the tide. An estimate of the volumetric longshore sediment rate (Q_l) assuming a long straight coastline was also tested. This parameter was calculated based on the equation (Komar, 1998):

$$Q_l = 0.46\rho g^{3/2} H_s^{5/2} \sin\alpha_b b \cos\alpha_b \tag{2}$$

where ρ is the density of water, g is gravity, H_s is significant wave height and α_b is the wave angle at breaking. Longshore sediment transport was given a positive sign for transport from the south-east and a negative sign for transport from the north-west, the bi-directional nature of the sediment transport is clearly visible in Fig. 6. As well as the directional estimate, the modulus quantity of this was used to represent the amount of sediment available without directional reference.

Two manifestations of the hydrodynamic and sediment transport parameters were used: firstly, the average values of the parameters between shoreline realisations were used; secondly, the cumulative integral of the de-meaned parameters was tested which was calculated via the following equation:

$$X_n = \int_{t_0}^{t_n} (x - \bar{x}) dt \tag{3}$$

where X_n denotes the cumulative integral of a parameter at a time-step n, x the parameter, $\bar{x}$ the mean value of the parameter, t the time, t_0 the initial time and t_n the time at the final time-step for the integral. Motivation for the second manifestation was twofold: firstly, changes to beach morphology are dependent on the beach initial condition which itself depends on prior forcing; secondly, hydrodynamic conditions often change far quicker than the beach morphology and thus linking morphological changes to hydrodynamic parameters can be difficult. The rationale for the second parameter was that beaches are often assumed to have an equilibrium state based on sediment properties and mean wave conditions, deviations from the equilibrium beach are caused by variations from the mean wave conditions. Removing the mean value thus shows deviations from equilibrium conditions. The cumulative integral was used since it encapsulates the cumulative effects of antecedent hydrodynamic conditions. Periods of lower than mean conditions produce negative gradient, mean condition gradients of zero and periods of higher than mean conditions produce positive gradients. An example of this parameterization, the cumulative integral of de-meaned wave height, is shown in Fig. 7. This figure shows the

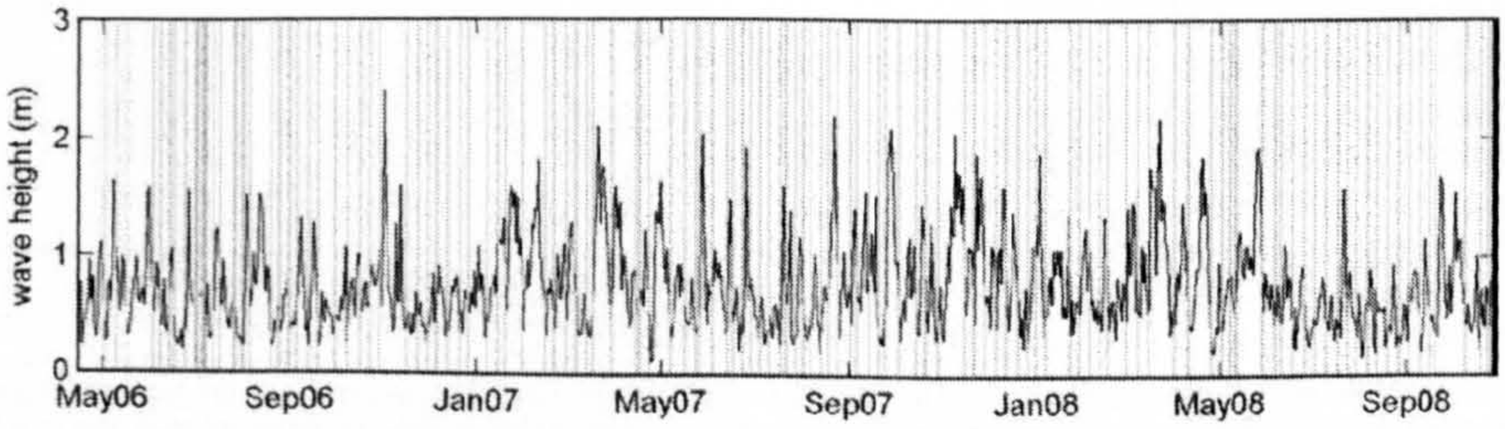

Fig. 5. The incident wave height time series with vertical lines indicating shoreline extraction dates.

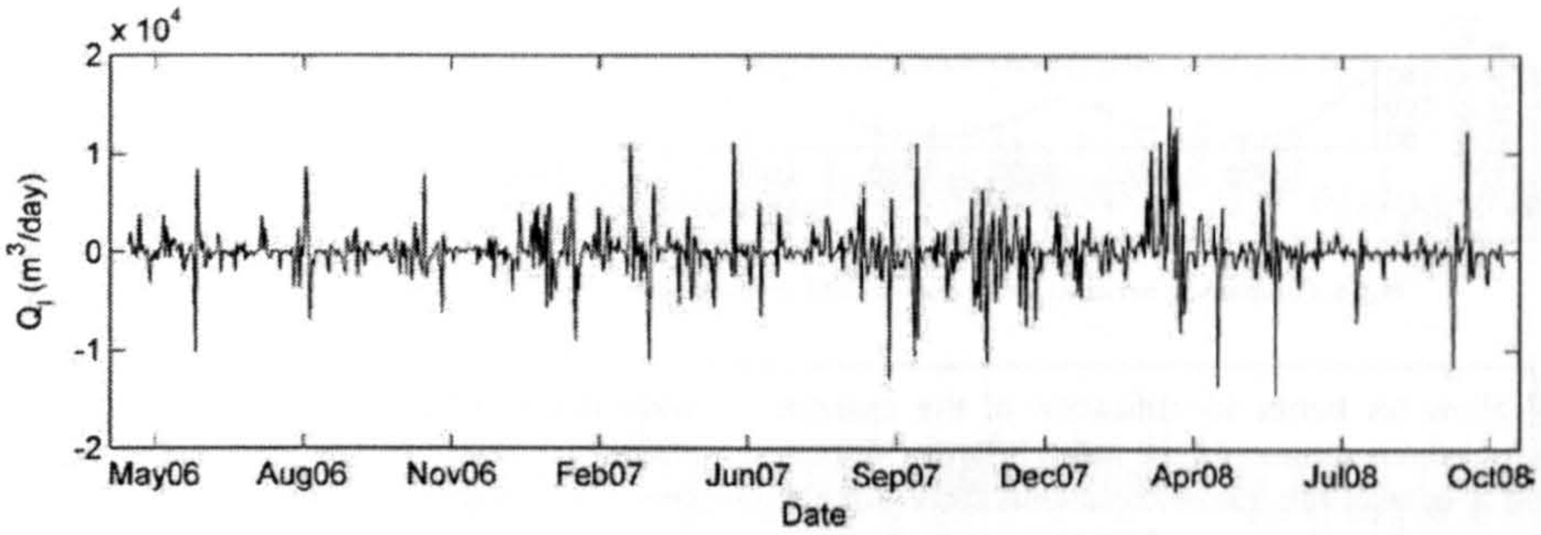

Fig. 6. Estimate of the longshore sediment transport rate with sign indicating direction, negative values indicating transport from the north-west and positive from the south-east.

seasonal trend in wave heights with summers generally showing smaller than mean wave heights (negative gradients) and winters larger than mean wave heights (positive gradients). These general trends are shown by the thick grey lines in Fig. 7. It can be seen that the winter of 2007–2008 exhibited longer periods of larger than mean wave heights than the previous winter. The effect of individual storms is also observable throughout the record in the form of sharp upward shifts in the cumulative integral; for example, the steep upward shift at the start of November 2006 corresponds to a large storm at that time (indicated by an asterisk in Fig. 7).

4. Results

The two schemes show similar responses for the primary and secondary modes but with differing amounts of variance attributed to each mode. The first two modes of scheme one and the first three modes of scheme two will be discussed in detail below.

4.1. Scheme one

The first two modes of response make up 75% of the variance in scheme one. The higher modes each account for <4% of the variance and show similar modes of response to the second mode. Higher modes derived from EOF analysis that show geometric similarities to lower modes can be artificial modes (Dommenget and Latif, 2002) and hence only the first two modes are considered in this analysis. The first mode accounts for 59% of the variance and describes cross-shore changes to the MSL contour position. The first mode is presented in Fig. 8, the upper panel shows the spatial eigenfunction in black and the mean shoreline position in grey, the lower panel shows the temporal co-efficient in black with the cumulative integral of the high tide level in grey. The cumulative integral of the high tide level is shown since it displays the highest correlation with the temporal component (Pearson's product moment correlation co-efficient $r=0.67$). The spatial eigenfunction (Fig. 8A) shows that the primary shoreline change is focussed on the tidal tombolos with lesser magnitude of displacement in the bay centres. The direction of change is opposite for the southern bay compared to the rest of the scheme. A positive temporal component leads to accretion of the majority of the scheme (tombolos and northern bay) and erosion of the southern bay and a negative temporal component gives the reverse effect. There is a slight positive trend through the first mode temporal component, meaning general accretion in the northern bay and tombolos and erosion of the southern bay throughout the period analysed. The correlations against hydrodynamic parameters for temporal components of the discussed modes in both schemes are shown in Table 2. Table 2 gives r values for the different correlation tests with the maximum correlation for each mode in bold type and all values significant at the 99% confidence level shaded grey. The temporal component for the first mode is significantly correlated with the average value of period, the cumulative series for all wave parameters, three of the manifestations of longshore sediment transport, and all the time series including a tidal component. It is important to note that the various time series are not all independent, for example, Q_l is estimated based on the incident wave conditions, and wave steepness is based on wave height and wave length. The highest correlation is with the cumulative high tide level (44% of variance explained). This correlation means that under high tide and surge levels the temporal component is positive and there is a progradation through phase one (except bay C which recedes due to lesser sediment availability). Fig. 8B clearly shows the similarity in trends between the cumulative integral of the de-meaned high tide level and the temporal component.

The second mode accounts for 16% of the dataset variance and describes the longshore translation of the tidal tombolos, this is indicated by the change in sign at the tombolo centres (Fig. 9A) which

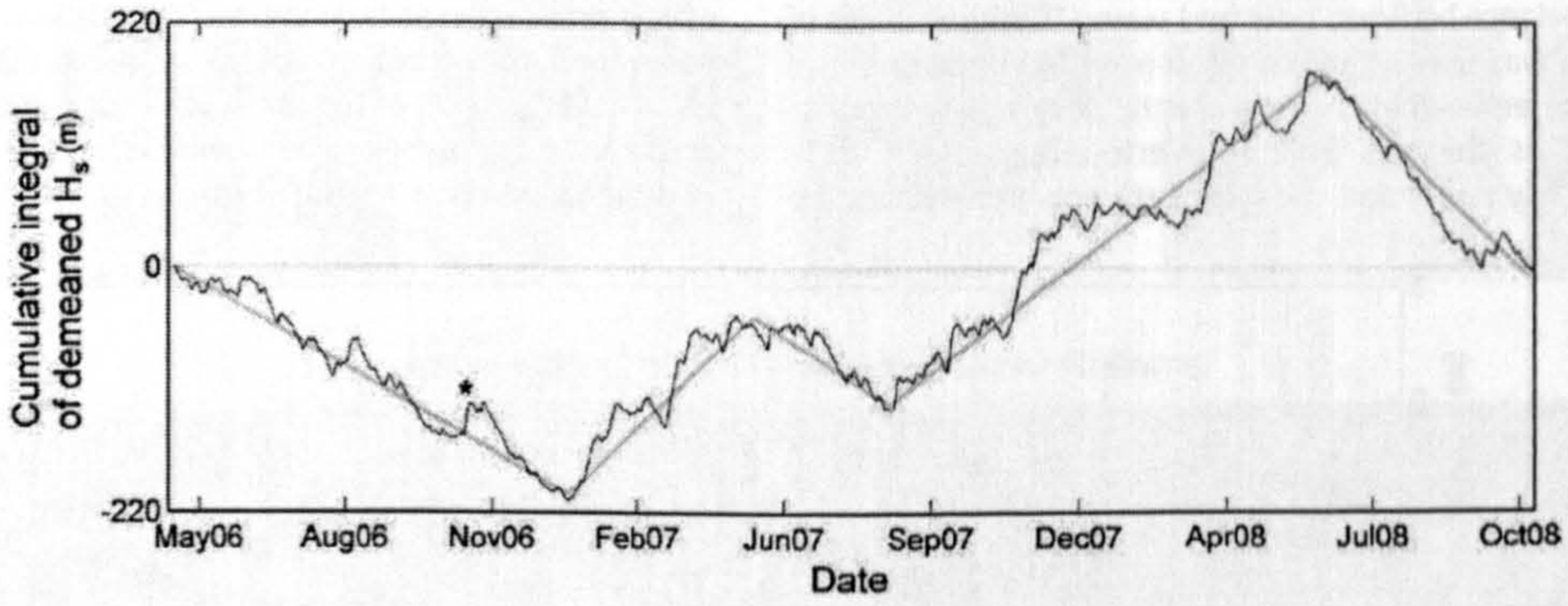

Fig. 7. The cumulative integral of the de-meaned significant wave height; this shows deviation from the mean wave height and has proved useful in comparing hydrodynamic conditions with time series of morphological change. The asterisk indicates a storm induced positive shift in the cumulative integral. The grey lines show general trends in the cumulative integral and make the seasonality in the wave heights more obvious.

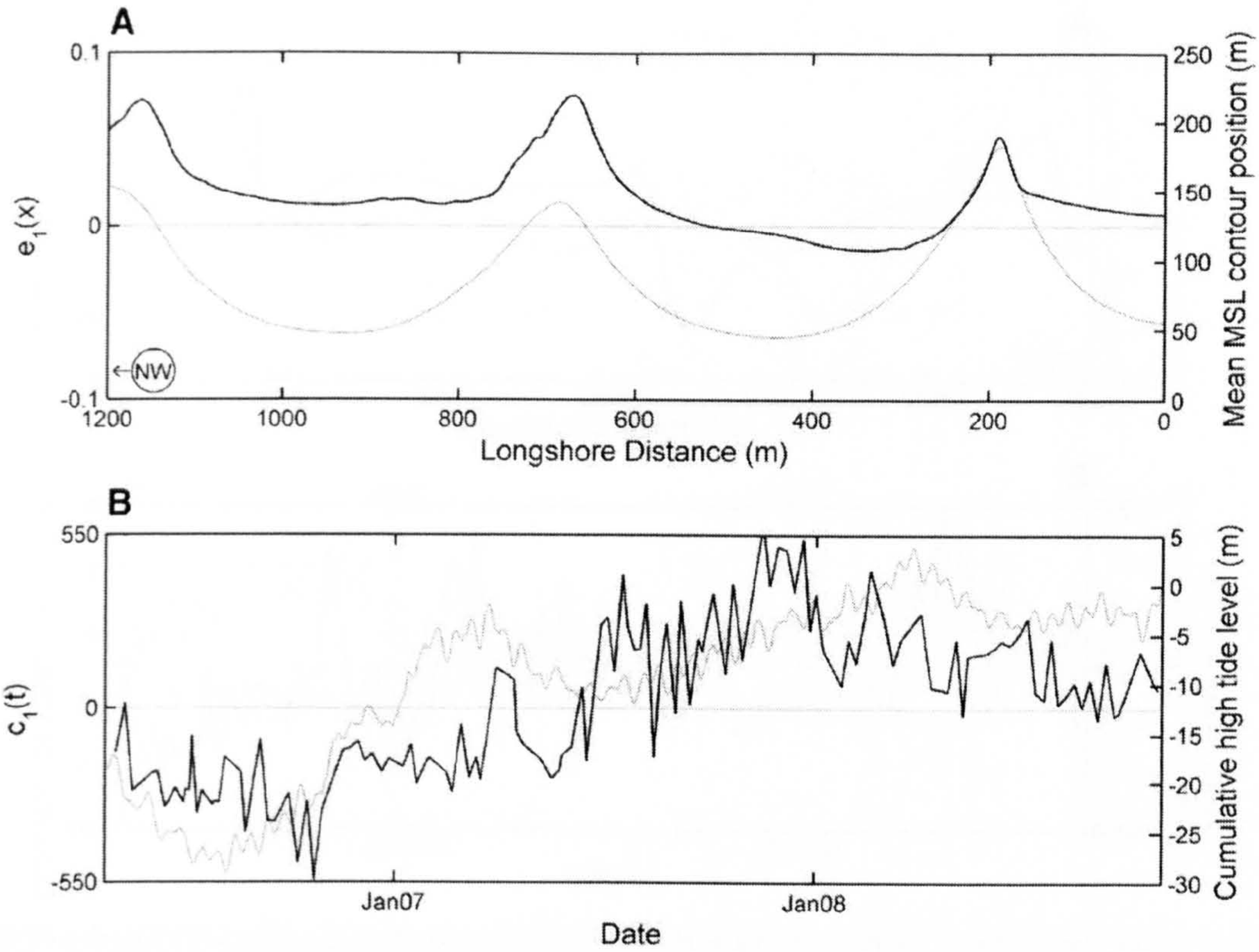

Fig. 8. The first mode of change for scheme one; A) the spatial eigenfunction (black) and the mean shoreline position (grey), north-west is to the left in the figure and south-east to the right; B) The associated temporal component (black) and the cumulative integral of the high tide level (grey).

Table 2
Pearson's product moment correlation co-efficients (r) for the temporal components against tested hydrodynamic parameters.

	Scheme one		Scheme two		
	$c_1(t)$	$c_2(t)$	$c_1(t)$	$c_2(t)$	$c_3(t)$
Significant wave height (H_S)	0.29	0.21	0.06	−0.13	0.24
Mean wave period (T)	0.34	0.06	−0.16	0.04	**0.42**
Wave steepness (H_s/L)	0.16	0.19	0.14	−0.17	0.06
$\int_{t_0}^{t_n}(H_S-\overline{H}_S)dt$	0.52	−0.26	−0.39	−0.75	−0.21
$\int_{t_0}^{t_n}(T-\overline{T})dt$	0.51	−0.38	−0.45	−0.64	−0.14
$\int_{t_0}^{t_n}((H_s/L)-\overline{(H_s/L)})dt$	0.47	−0.16	−0.30	−0.74	−0.22
Longshore sediment transport (Q_1)	0	0.02	−0.13	0.12	0.04
Absolute value of Q_1 ($\lvert Q_1\rvert$)	0.32	0.28	0.10	−0.14	0.27
$\int_{t_0}^{t_n}(Q_1-\overline{Q_1})dt$	−0.38	−0.01	0	−0.06	−0.12
$\int_{t_0}^{t_n}(\lvert Q_1\rvert-\lvert\overline{Q_1}\rvert)dt$	0.54	−0.23	−0.42	−0.76	−0.18
Relative tidal range (RTR)	0.31	−0.34	−0.37	0.61	−0.14
$\int_{t_0}^{t_n}(RTR-\overline{RTR})dt$	−0.56	0.27	−0.37	**−0.77**	0.14
$\int_{t_0}^{t_n}(TR-\overline{TR})dt$	0.62	**−0.57**	−0.49	0.58	0.22
$\int_{t_0}^{t_n}(HT-\overline{HT})dt$	**0.67**	0.51	**−0.51**	0.50	0.40

Correlations significant at the 99% confidence level are shaded grey and maximum correlations for each temporal component are in bold type. All symbols in cumulative integrals are as referred to in table text. Additionally, L stands for wavelength; HT stands for high tide and TR for tidal range.

means that for a given temporal component one side of the tombolo accretes and the other erodes. A positive temporal component corresponds to a south-eastward shift of the tombolos (to the right in the figure) and a negative component corresponds to a shift to the north-west (to the left). The second temporal component (Fig. 9B) regularly changes from positive to negative which means the tombolos are regularly shifting either side of their mean position. The highest correlation is with the cumulative tidal range which accounts for 32% of the variance. This correlation can be seen in the similarity of the two records in Fig. 9B, whilst individual shifts are not visually correlated the trends are opposite throughout the record. The negative correlation means that smaller than mean tidal ranges are linked to movement to the south-east and larger than mean tidal ranges are linked to north-westward transport. The temporal component is also negatively correlated with the cumulative series of period (T) meaning that lower than average values of T lead to a movement to the South-East and higher than average values of T a movement to the north-west.

4.2. Scheme two

There are three clearly distinct modes of change observable for scheme two, representing 82% of the dataset variance. The first mode represents 46% of the variance, the second mode 27% and the third mode 9%. The lower modes each represent just a few percent of the variance. The first mode describes shoreline progradation and recession. The whole scheme shows the same direction of change for a given temporal component with greater changes over the salients (Fig. 10A). The temporal component (Fig. 10B), whilst noisy, shows some seasonality, being largely positive in summer (shoreline progradation) and negative in winter (shoreline recession), although the final summer, whilst increasing from the previous winter is still negative. There is a negative linear trend through the temporal component suggesting an overall

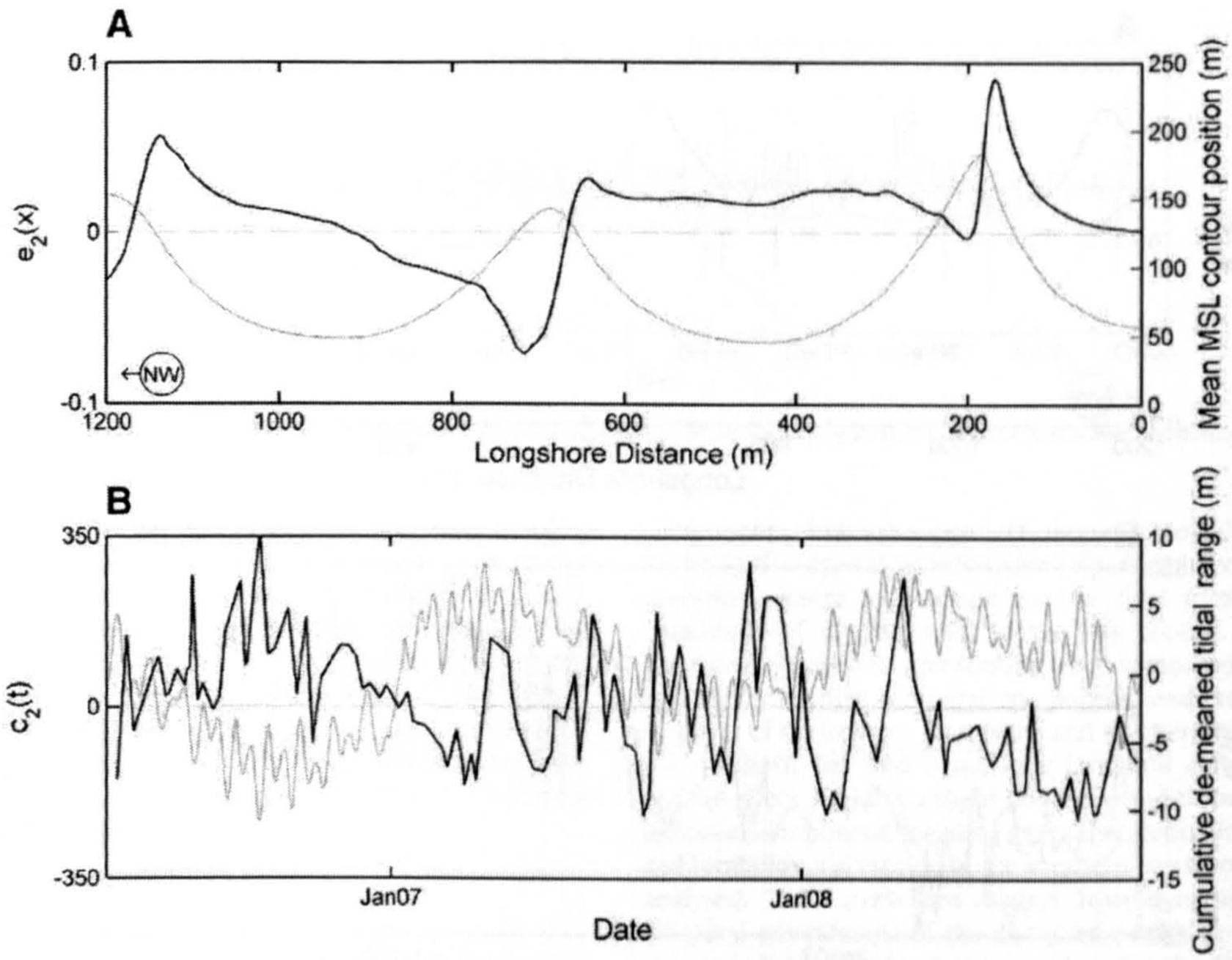

Fig. 9. The second mode of change for scheme one; A) the spatial eigenfunction (black) and the mean shoreline position (grey), north-west is to the left in the figure and south-east to the right; B) the associated temporal component (black) and the cumulative integral of the de-meaned tidal range (grey).

shoreline recession through the measurement period. The temporal component is significantly negatively correlated with the cumulative integrals of the wave parameters (9–19% of the variance described) but most correlated with the cumulative integral of the high tide level. This correlation is negative and represents 26% of the dataset variance, visually the negative correlation is more obvious at the start and end of

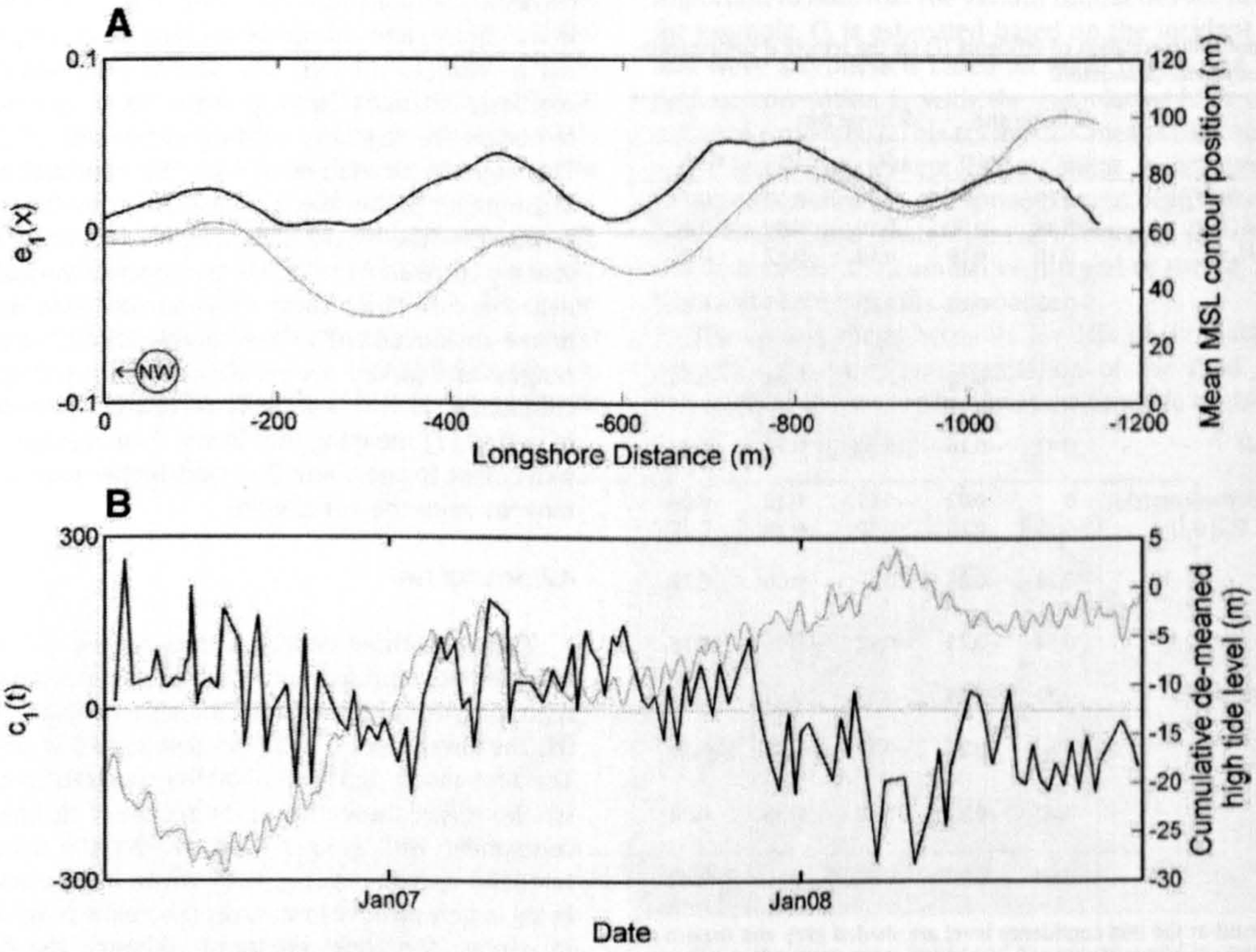

Fig. 10. The first mode of change for scheme two; A) the spatial eigenfunction (black) and the mean shoreline position (grey), north-west is to the left in the figure and south-east to the right; B) the associated temporal component (black) and the cumulative integral of the de-meaned high tide level (grey).

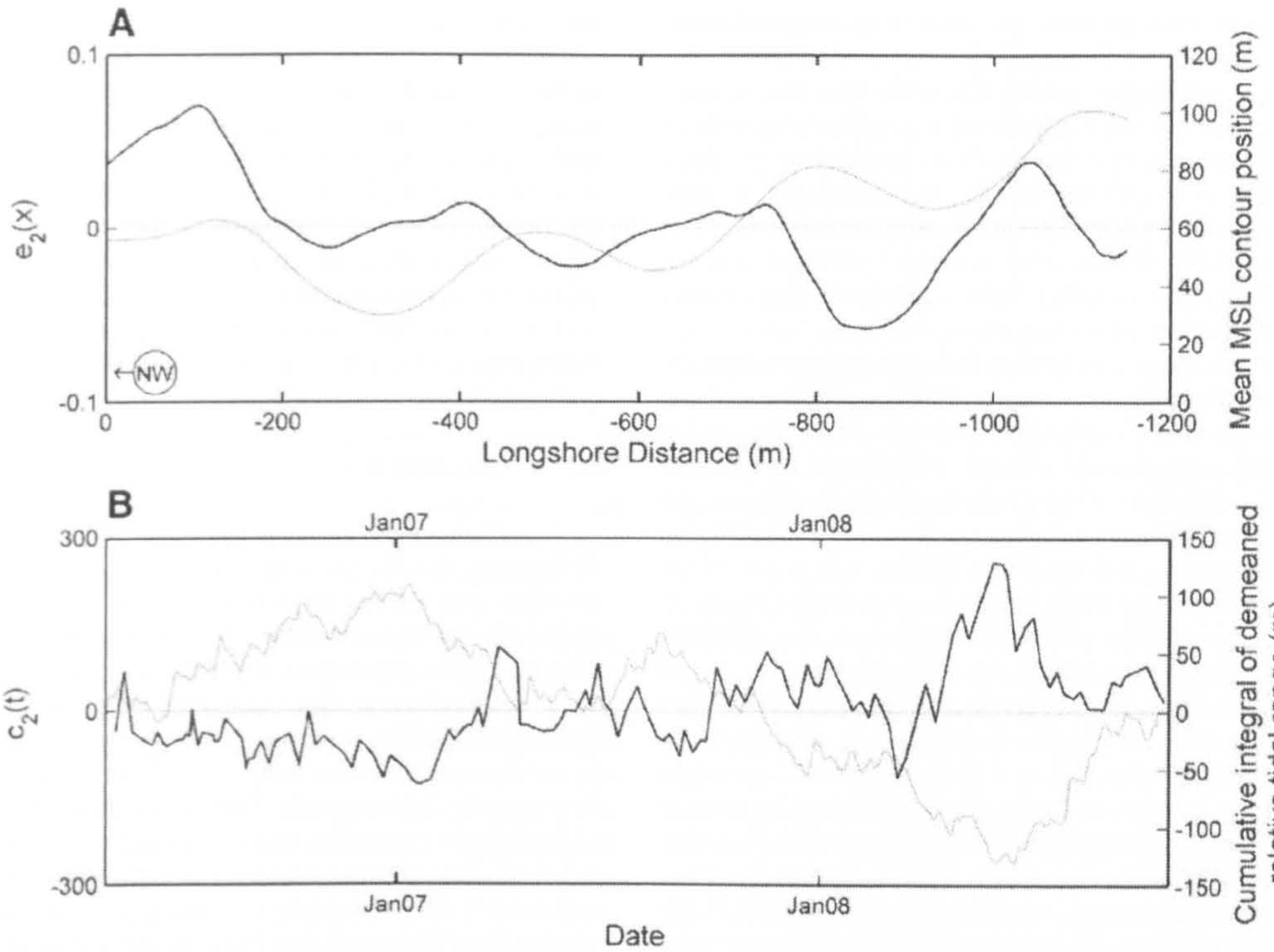

Fig. 11. The second mode of change for scheme two; A) the spatial eigenfunction (black) and the mean shoreline position (grey), north-west is to the left in the figure and south-east to the right; B) the associated temporal component (black) and cumulative integral of the relative tidal range (grey).

the record with a period of seeming positive correlation through second quarter of the study period (Fig. 10B).

The second mode represents the longshore movement of the salients but involves the whole embayments and takes the form of a beach rotation whereby one half of the embayment erodes and the other half accretes. This change is described by the change in sign of the spatial eigenfunction (Fig. 11A) in the bay centres and salient mid-points. A negative component gives a southward shift and a positive

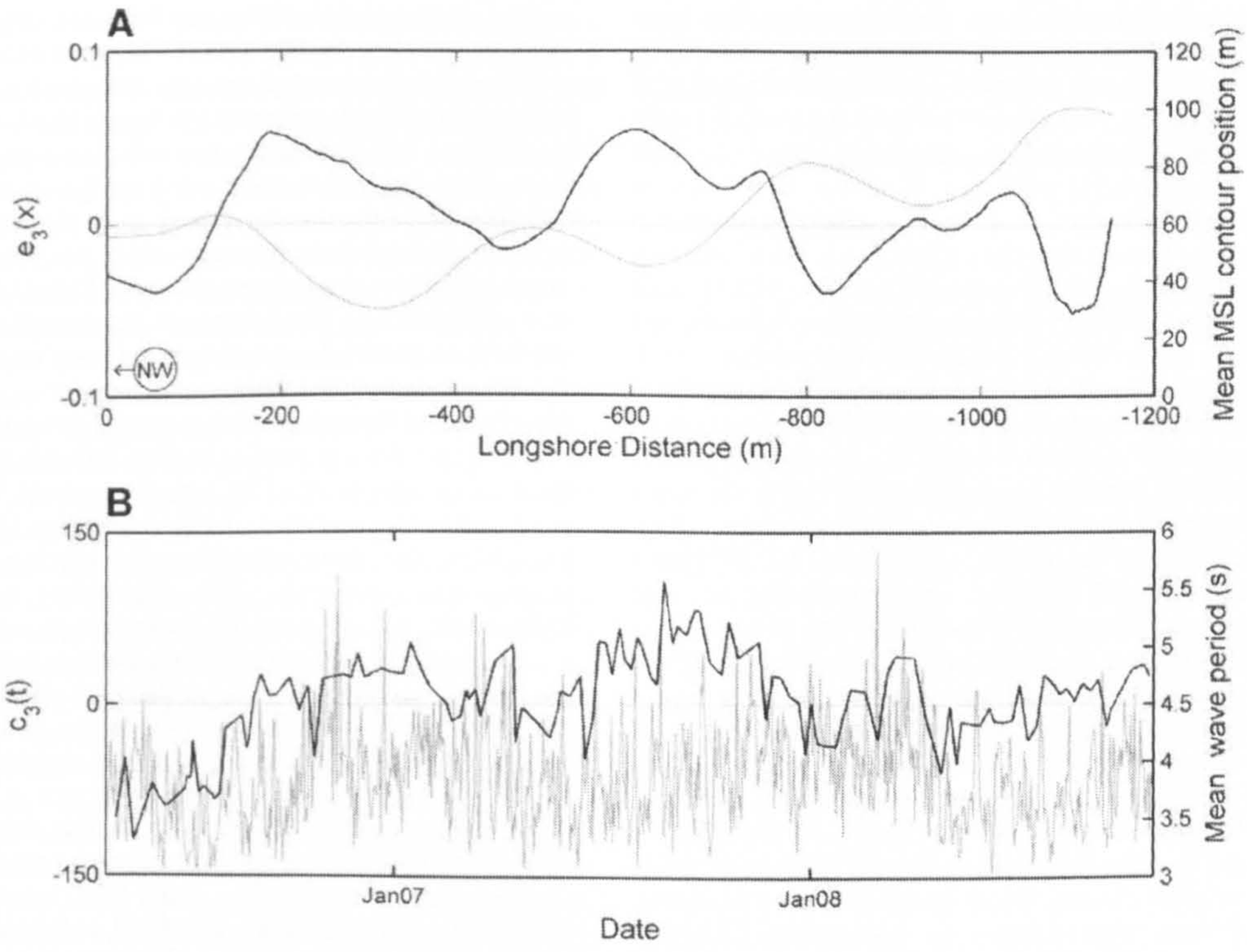

Fig. 12. The third mode of change for scheme two; A) the spatial eigenfunction (black) and the mean shoreline position (grey), north-west is to the left in the figure and south-east to the right; B) the associated temporal component (black) and the mean wave period (grey).

component gives a northward shift. The associated temporal component (Fig. 11B) is significantly negatively correlated with cumulative integrals of H_s, T and steepness (55%, 41% and 54% of the variance explained respectively) but most significantly negatively correlated with the cumulative integral of de-meaned relative tidal range which explains 60% of the variance (Table 2). Negative correlation in both general trends and in short term shifts can be seen in the time series plotted in Fig. 11B. The negative correlation means that large values of *RTR* are linked with the salients being north of mean and small values of *RTR* are linked with the salients being south of mean.

The third mode of change involves an increase or decrease in the sinuosity of the shoreline (Fig. 12A). The salients are either enhanced or subdued depending on the sign of the temporal component and at the same time the embayments eroded or in-filled. A positive temporal component leads to a reduction in salient amplitude and an in-filling of the bay centre, negative temporal components affect an amplification of the salient and erosion of the bay centre shoreline. The temporal component for the third mode of change (Fig. 12B) increases through the winters and reduces through the summers indicating seasonal behaviour with enhanced salients and eroded bays through the summer periods and reduced salients and in-filled bays in the winter periods. The highest correlation is with the wave period which explains 18% of the variance in the temporal component (Table 2). The positive correlation means that for higher than average wave periods the bays are in-filled and salient horns erode, for lower than average wave periods the bays erode and the salients build up. Whilst significant, the correlation is low and this is reflected in the weak visual correlation (Fig. 12B) between the temporal component and wave period. There is also a correlation with wave height (at a lower confidence level of 90%) indicating that larger waves cause decreased sinuosity and smaller waves increased sinuosity.

5. Discussion

5.1. Analysis technique

The method for extracting the mean sea level contour has been shown to be acceptably accurate when compared to DGPS data. Whist there is some deviation (mean difference in cross-shore position of 1.2 m); the variability of the MSL contour position (up to 80 m) is far greater than the error in the shoreline position, allowing for reliable identification of morphological evolution. Moreover, the ability to capture morphological changes at a high temporal and spatial resolution is of greater benefit than the potential increase in accuracy of other methods for a study of this nature. The use of a MSL contour shoreline, rather than cross-shore beach profiles or video derived intertidal surveys, has proved valuable in determining beach behaviour behind a series of detached breakwaters. Cross-shore beach profiles are not applicable to this study for two main reasons: firstly, prohibitively many profile lines would be needed to adequately capture the longshore variability; secondly, definition of the shore normal lines on a coastline of high and varying curvature is non-trivial. 2-dimensional intertidal profiles, whilst useful for short term comparisons, are less useful for longer term monitoring of these beaches where the intertidal region is narrow and the (x, y)-position of the intertidal region varies temporally making comparison difficult. Use of a single shoreline representation does have some shortfalls however, primary being the difficulty of distinguishing between long- and cross-shore drivers of shoreline change.

An EOF analysis was successfully used to decompose the de-meaned shoreline dataset into constituent modes of change. The analysis is a statistical technique which isolates orthogonal modes of change. These modes of change do not necessarily have a physical significance and interpretation must be undertaken with care (Dommenget and Latif, 2002). Miller and Dean (2007) assigned physical meaning based on observation of the patterns in the EOF modes in relation to the shoreline configuration and hard structures and paying particular attention to nodal points. They suggest that when additional observations support the EOF derived modes of change then the physical significance of the EOF modes can be stated with confidence. Other authors have taken a similar approach (Munoz-Perez et al, 2001; Rihouey and Maron, 2003). In this study, the progradation and recession of the shoreline are visible in the images and a previous work has also described the longshore movement of the tombolos and salients (Dolphin et al., 2005; Fairley et al., in press). The observation of similar changes in the data and the EOF results give confidence that the EOF derived modes of change are real and the physical meanings attributed correct.

5.2. Interpretation of results

For all modes of change, the dominant spatial length scales are dictated by the length of the embayments. The first two modes of response are similar in action for the two schemes though the temporal components differ. For both schemes, the first mode of response is the cross-shore translation of the shoreline, however, the variance ascribed to this mode and the details of the changes are different. 67% of the shoreline variance is described by the first mode in scheme one whilst only 46% of the scheme two variance is described by the first mode. There is a greater abundance of sediment in the scheme one region and supra-tidal beach widths seaward of the sea wall are generally greater which allows for freer shoreline movement. The focussing of change on the sheltered regions is greater for scheme one. It is thought that this is due both to the larger size of the tombolos and the greater difference between sheltered and unsheltered regions for the larger breakwaters. For scheme two, the change is all in the same direction for a given temporal component whereas in scheme one the more northern bay shoreline progrades whist the other bay shoreline recedes. The positive trend to the scheme one temporal component shows that the northern bay is generally prograding and the southern bay receding throughout the record. The net sediment transport is from north-west to south-east and the scheme one tombolos are effective in trapping sediment, thus the northern bay in-fills whilst the southern bay is starved of sediment. It is thought that once the northern bay reaches its capacity for storing sediment, sediment will bypass that bay and start in-filling the southern bay. The northernmost bay in scheme one (outside the range of the video analysis) is much shallower and more stable than the other scheme one bays and it is thought that this bay is representative of an embayment which has reached its capacity to store sediment and so allows sediment to pass through to the next most northern bay. The salients in the second scheme do not trap sediment so effectively or constrain sediment transport so extensively and thus the shoreline erodes and accretes as a whole. There is a negative trend through the first temporal component for scheme two which means there is general erosion through scheme two over the duration of the record. This erosion suggests that scheme one is starving scheme two (down drift) of sediment. There is seasonality in the scheme two temporal component which is not present in the scheme one component. This seasonality results in shoreline progradation in summer and recession in winter. The temporal components for both schemes both show maximal correlation with the cumulative integral of high tide level. However for scheme one this correlation is positive (progradation under larger high tide elevations) and for scheme two this is negative (recession under larger high tide elevations). This difference is due to breakwater design and sediment abundance. Higher tide elevations allow greater wave penetration into the embayments, greater mobilisation of sediment and access to the supra-tidal beach. The scheme one breakwaters better trap the mobilised sediment whilst the smaller scheme two structures do not and hence the shoreline recedes and the sediment is lost from the system. The ability of the scheme one

breakwaters to trap sediment means that the down drift scheme two does not receive sufficient sediment to maintain a healthy beach. There is a larger back beach to scheme one which allows for erosion of the supra-tidal region which is deposited in the intertidal region. The high tide line in scheme two is level with the concrete sea wall and thus there is little supra-tidal material available for erosion and subsequent deposition in the intertidal region. Additionally, under surge conditions the most northern tombolo (outside the limits of this analysis) is submerged which opens another sediment transport pathway injecting extra sediment into scheme one.

The second mode of response for both schemes is also similar, representing the longshore movement of the salients and tombolos. A greater amount of variance is attributed to this mode for scheme two than for scheme one, probably because the smaller, lower breakwaters allow for greater longshore movement. The change is focussed on the tombolos for scheme one whilst the longshore movement of the salients is diffused and involves the whole embayment. It is believed that this difference in response is due to the large difference between sheltered and unsheltered regions in scheme one causing more intense and better defined circulation patterns which constrain the longshore changes to the tombolos. The smaller breakwaters in scheme two, which are readily overtopped, provide less variation in shelter and less intense circulation patterns, this means that the salient response is less defined than the tombolo response. The temporal components for both schemes oscillate between positive and negative (tombolos south and north of mean). Curiously, despite previous work demonstrating down drift movement of the salients and tombolos under storm conditions (Dolphin et al, 2005; Fairley et al., in press), neither temporal component demonstrated significant correlation with the directional estimate of longshore sediment transport. This suggests that there are additional, more complex, mechanisms forcing the longshore movement of the features than simple down drift movement of sediment under oblique waves. The breakwater length considerably controls the extent of longshore movement, especially for scheme one, and thus the starting position of the tombolo is of critical importance; if previous forcing has moved the tombolo to the furthest extent of the possible movement continued movement in that direction is impossible. This suggests that the initial morphological conditions exert an important control on subsequent shoreline change. The temporal component for scheme one is best correlated with the cumulative integral of tidal range, smaller than mean tidal ranges lead to south-eastward movement and larger than mean tides lead to north-westward movement. The correlation is weak but significant and describes 32% of the variance. Modelling of storm scale changes has highlighted the importance of tidal currents to morphological change even under substantial wave action (Fairley et al., 2009a). Tidal currents alone are sufficient to entrain sediment over the tombolos (Bacon et al., 2005) and the tidal asymmetry varies over the spring neap cycle (Bacon et al., 2007). It is thought that variation in the current patterns due to changes over the spring neap cycle and interaction with tidally submerged tombolos could force this change in the direction of salient movement. The temporal component also shows significant correlation with the cumulative integral of wave period. Lower than mean wave periods lead to a south-eastward movement and higher than mean periods lead to a north-westward movement of the tombolos. Wave period dictates the way in which the wave rays are turned via refraction and diffraction as they penetrate the embayments, with shorter period waves undergoing lesser turning than longer period waves. Thus short period waves approaching obliquely from the north (the predominant direction for oblique waves) would only act on the southern flank of the embayment whilst longer period waves would refract and diffract to a greater extent thus acting on a greater portion of the embayment.

The temporal component of this mode for scheme two shows higher correlations with the tested parameters, possibly due to the lesser breakwater induced constraints on the movement. The highest correlation, which accounts for 60% of the variance, is with the cumulative integral of relative tidal range. This parameter suggests that the interplay between wave-driven and tide-driven currents is vital. The negative correlation means that large values of *RTR* (large tide ranges, small wave heights) are linked with the salients being north of mean and small values of *RTR* (small tidal ranges, large wave heights) are linked with the salients being south of mean. If a unit wave height is considered (*RTR*=tidal range) the direction of salient movement is the same as tombolo movement. If constant tidal range is considered, the correlation suggests that larger waves (most predominantly incident from the north) lead to southward movement of the salients. The temporal component for the second mode of response in scheme two was also significantly correlated with the cumulative integrals of the basic wave parameters. This indicates the greater importance of waves to the shoreline dynamics of the less sheltered scheme two.

The scheme one dataset only displayed two important modes of change, the higher modes describing very little of the variance individually and the spatial eigenfunctions of the higher modes all closely replicating the second spatial eigenfunction. Scheme two exhibited a third mode of change which accounted for 9% of the dataset variance. The absence of a third mode of change for scheme one shows that the larger breakwaters place greater constraint on the morphodynamics, a previous work by Axe and Chadwick (1997) has also demonstrated a reduction of profile variability behind detached breakwaters compared to an adjacent natural beach. The third mode of change represented an intensification and reduction of the sinuosity of the shoreline. The temporal component indicates seasonality in this change with intensified sinuosity in summer and reduced sinuosity in winter. These changes might be analogous to increased three dimensionality of natural beaches under calmer conditions (Wright and Short, 1984): the temporal component does show some correlation against wave height such that larger waves reduce the sinuosity and smaller waves increase sinuosity. The temporal component is most strongly positively correlated with the wave period; however this correlation is weak with only 18% of variance explained. For higher than average wave periods the bays are in-filled and the salient horns erode, for lower than average wave periods the bays erode and the salients are built up. Previous work (Fairley et al., 2009b) has shown that longer period waves are better transmitted through the phase two breakwaters and this might explain the salient erosion under these conditions.

6. Conclusions

Shoreline changes behind two schemes of detached breakwaters with different dimensions in the same environmental setting have been investigated using EOF analysis. The shorelines were manually extracted from time averaged video images. Comparison with DGPS surveys shows that the technique produced accurate shorelines with the advantage of a higher temporal resolution than traditional surveys. The EOF technique worked well in isolating modes of response in the shoreline dataset, allowed description of the main changes and investigation of their causes via correlation with forcing parameters. Formulation of hydrodynamic data as the cumulative integral of each de-meaned parameter has been shown to improve correlation with forcing and to provide an easily understandable statistic. This lends weight to the theory that change is forced by deviation from mean parameters and suggests the importance of antecedent conditions.

The same two main modes of change were observed for the two different designs of breakwater. The changes were the cross-shore progradation and recession of the shoreline and the longshore movement of the salients and tombolos. Differences in the detail of the changes were noticed. The cross-shore shoreline movement acted in the same direction across the whole scheme for the smaller breakwaters whereas for the larger breakwaters one bay accreted

whilst the other bay eroded. Greater constraint of the longshore tombolo movement was exhibited by scheme one. Change to the cross-shore shoreline location was forced by the high tide elevation, believed to be because higher tides allow for greater wave penetration through the embayments to the intertidal region. However, for scheme one this leads to progradation of the shoreline and for scheme two shoreline recession. The tidal range had a significant effect on the longshore movement of the features and it is believed that this is due to the strength of the tidal currents over these features.

The sizes of the breakwaters play a dominant role in dictating the morphodynamics of the protected beaches. The length scales of the observed changes are determined by the breakwater positions. Scheme one substantially interacts with the natural hydrodynamic regime and traps large quantities of sediment. The ability to trap sediment and the size of the tombolos formed mean that the beaches show little similarity to unprotected beaches. The smaller scheme two breakwaters have a less dramatic effect on the hydrodynamics and thus behaviour is more in common with natural beaches. Two of the three scheme two temporal components show seasonal behaviour similar to unprotected coasts: the MSL contour moves seaward in summer (wider beaches) and shoreward in winter (narrower beaches); and the beaches show greater three dimensionality in summer over winter.

The net direction of longshore sediment transport from north to south is the final key contributor to the morphodynamics of this system. Scheme one traps a large portion of the longshore transported sediment meaning that the down drift scheme two is starved and has been gradually eroding through the studied period. Within scheme one itself the large tombolos hinder trans-embayment sediment exchange and lead to deviation in beach response. The more northern bay in this analysis is trapping sediment gradually in-filling and the MSL contour is exhibiting a slow progradation. This bay traps sufficient quantities of longshore sediment to impinge on the evolution of the southern scheme one bay which is gradually eroding through the timeframe of this work.

Acknowledgements

This work has been conducted as part of a PhD which is tied to the LeaCoastII project and is funded by the UK's Engineering and Physical Sciences Research Council (project reference EP/C010965/1). Thanks must go to all the participants in the LeaCoastII project. Thanks also to Peter Ganderton and Irv Elshoff for their help in the initialisation and maintenance of the Sea Palling system and to Robin Morrelisson for the Argus software assistance.

References

Aarninkhof, S., Morellisen, R., Cohen, A., 2006. The Argus Runtime Environment – Guidelines on Installation and Use. Delft Hydraulics, p. 48.

Ahrens, J.P., Cox, J., 1990. Design and performance of reef breakwaters. Journal of Coastal Research 51 (7), 61–75.

Aubrey, D.G., 1979. Seasonal patterns of onshore/offshore sediment movement. Journal of Geophysical Research 84 (C10), 6347–6354.

Axe, P., Chadwick, A., 1997. Beach variability behind detached breakwaters. In: Thornton, E.B. (Ed.), Coastal Dynamics '97. ASCE, Plymouth, U.K., pp. 744–753.

Bacon, J., Vincent, C.E., Dolphin, T., Taylor, J., Pan, S., O'Connor, B., 2005. The offshore breakwater scheme at sea palling, England; sand transport generated by tidal currents. In: Smith, J.M. (Ed.), Proceedings, 29th International Conference on Coastal Engineering. World Scientific, Lisbon, pp. 1896–1908.

Bacon, J., Vincent, C.E., Dolphin, T., Taylor, J., Pan, S., O'Connor, B., 2007. Shore-parallel breakwaters in meso-tidal conditions: tidal controls on sediment transport and their longer term, regional impacts at Sea Palling, UK. Proceedings of the 9th International Coastal Symposium: Journal of Coastal Research, vol. S.I.50, pp. 369–373.

Bidliot, J.-R., Holt, M.W., 1999. Numerical wave modelling at operational weather centres. Coastal Engineering 37, 409–429.

Boak, E.H., Turner, I.L., 2005. Shoreline definition and detection: a review. Journal of Coastal Research 21 (4), 688–703.

Clayton, K.M., McCave, I.N., Vincent, C.E., 1983. The Establishment of a sand budget for the East Anglian coast and its implications for coastal stability. Shoreline Protection. Thomas Telford, London, pp. 91–96.

Dolphin, T., Taylor, J., Vincent, C., Bacon, J., Pan, S.Q., O'Conner, B., 2005. Storm-scale effects of shore-parallel breakwaters on beaches in a tidal setting (Leacoast). In: Smith, J.M. (Ed.), Proceedings, 29th International Conference on Coastal Engineering. World Scientific, Lisbon, pp. 2849–2861.

Dommenget, D., Latif, M., 2002. A cautionary note on the interpretation of EOFs. Journal of Climate 15, 216–225.

Fairley, I., Davidson, M., Kingston, K., 2009a. The morpho-dynamics of a beach protected by detached breakwaters in a high energy tidal environment. Proceedings of the 10th International Coastal Symposium. Journal of Coastal Research, S.I. 56 (1), 607–611.

Fairley, I., Davidson, M., Kingston, K., 2009b. Video monitoring of overtopping of detached breakwaters in a mesotidal environment. Proceedings, Coastal Structures '07, Venice, pp. 1923–1932.

Fairley, I., Davidson, M., Kingston, K., in press. A video based investigation into the morphological impacts of storms behind a series of detached breakwaters, Poster proceedings, 31st International Conference on Coastal Engineering. BAW, Hamburg.

Golding, B., 1893. A wave prediction system for real-time sea state forecasting. Quarterly Journal Royal Meteorological Society 109, 393–416.

Guza, R.T., Thornton, E.B., 1981. Wave set-up on a natural beach. Journal of Geophysical Research 86 (C5), 4133–4137.

Hamer, B.A., Hayman, S.J., Elsdon, P.A., Fleming, C.A., 1998. Happisburgh to Winterton Sea Defenses: Stage Two, Coastlines, Structures and Breakwaters. Thomas Telford, London.

Holman, R.A., Stanley, J., 2007. The history and technical capabilities of Argus. Coastal Engineering 54 (6–7), 477–491.

Komar, P.D., 1998. Beach Processes and Sedimentation. Prentice Hall, Upper Saddle River, New Jersey. 544 pp.

Masselink, G., Short, A., 1993. The effect of tide range on beach morphodynamics and morphology: a conceptual beach model. Journal of Coastal Research 9 (3), 785–800.

McCormick, M.E., 1993. Equilibrium shoreline response to breakwaters. Journal of Waterway, Port, Coastal and Ocean Engineering 119 (6), 657–670.

Miller, J.K., Dean, R.G., 2007. Shoreline variability via empirical orthogonal function analysis: Part 1 temporal and spatial characteristics. Coastal Engineering 54 (2), 111–131.

Munoz-Perez, J.J., Medina, R., Tejedor, B., 2001. Evolution of longshore beach contour lines determined by the EOF method. Scienta Marina 65 (4), 393–402.

Pilarczyk, K.W., Zeidler, R.B., 1996. Offshore breakwaters and shore evolution control. Balkema, Rotterdam.

Plant, N.G., Aarninkhof, S.G.J., Turner, I.L., Kingston, K.S., 2007. The performance of shoreline detection models applied to video imagery. Journal of Coastal Research 23 (3), 658–670.

Pope, J., Dean, J., 1986. Development of design criteria for segmented. In: Edge, B. (Ed.), Coastal Engineering. ASCE, Taipei, Taiwan, pp. 2144–2158.

Rihouey, D., Maron, P., 2003. Empirical eigenfunction analysis of long-term bathymetric data along the beaches of Anglet. Coastal Engineering VI – Computer Modelling and Experimental Measurements of Seas and Coastal Regions. Wit Press, Cadiz, Spain, pp. 495–504.

Smith, R.K., Bryan, K.R., 2007. Monitoring beach face volume with a combination of intermittent profiling and video imagery. Journal of Coastal Research 23 (4), 892–898.

Sorenson, O.R., Kofoed-Hansen, H., Rugbjerg, M., Sorenson, L.S., 2004. A third-generation spectral wave model using an unstructured finite volume technique. In: Mckee Smith, J. (Ed.), Proceedings of the 29th International Conference on Coastal Engineering. World Scientific, Lisbon, pp. 894–906.

Suh, K., Dalrymple, R., 1987. Offshore Breakwaters in Laboratory and Field. Journal of Waterway, Port, Coastal and Ocean Engineering 113 (2), 105–121.

Thomella, F., Vincent, C.E., Black, K., 2001. The effect of the segmented shore parallel breakwaters at Sea Palling on the longshore transport of sand. Proceedings of the 36th Annual Conference of River and Coastal Engineers. Keele University, pp. 07.2.1–07.2.11.

Turner, I.L., 2006. Discriminating modes of shoreline response to offshore-detached structures. Journal of Waterway, Port, Coastal and Ocean Engineering 132 (3), 180–191.

von Storch, H., Hannostock, G., 1984. Comment on "Empirical orthogonal function analysis of wind vectors over the tropical Pacific region.". Bulletin of the American Meteorological Society 65, 162.

Winant, C.D., Inman, D.L., Nordstrom, C.E., 1975. Description of seasonal beach changes using empirical eigenfunctions. Journal of Geophysical Research 80 (15), 1979–1986.

Wright, L., Short, A., 1984. Morphodynamic variability of surfzones and beaches: A synthesis. Marine Geology 56, 93–118.

Journal of Coastal Research	SI 56	607 - 611	ICS2009 (Proceedings)	Portugal	ISSN 0749-0258

The Morpho-dynamics of a Beach Protected by Detached Breakwaters in a High Energy Tidal Environment

I. Fairley,† M. Davidson† and K. Kingston†
†Coastal Processes Research Group
University of Plymouth, Plymouth
PL4 8AA, U.K.
Iain.fairley@plymouth.ac.uk

ABSTRACT

FAIRLEY, I., DAVIDSON, M., and KINGSTON K., 2009. The morpho-dynamics of a beach protected by detached breakwaters in a high energy tidal environment. Journal of Coastal Research, SI 56 (Proceedings of the 10th International Coastal Symposium), 607 – 611. Lisbon, Portugal, ISSN 0749-0258

This contribution uses a numerical modeling system (MIKE21) to examine the mechanisms causing changes to beach morphology that have been observed in the analysis of video data. In this paper storm scale effects are concentrated upon since such conditions often associated with catastrophic erosion and so are of considerable interest to the coastal manger and engineer. An Argus camera system has been used to evaluate morphological changes under varying wave conditions. A fully coupled hydrodynamic, wave and sediment transport model has been used to investigate the effect of mean wave and tide conditions on the beach morphology. The model produced similar morphological changes to those displayed in the video data. Similar (but opposite) longshore tombolo displacement shown by storms of opposite incidence was shown to be produced by different mechanisms: under northerly incident storms sediment was transported in a down drift direction whereas under easterly wave incidence a gyre formed which moved sediment in an up-drift direction. This emphasizes the influence of tidal currents on wave driven circulation patterns. The importance of tidal currents in modulating near-shore circulation is not often incorporated in design guidelines which may explain the failure of design guidelines in some tidal environments.

ADITIONAL INDEX WORDS: *Video ,Argus, Numerical modeling,MIKE21 Storms, Circulation, Erosion,*

INTRODUCTION

Detached breakwaters are widely implemented as a method of coastal protection; however, beach responses to detached breakwaters vary widely between different case studies. Both erosion (DEAN *et al,* 1997) and accretion, in the form of salients and tombolos (THOMELLA and VINCENT, 2003), have been observed: the nature of the response depending on breakwater design, tidal range, wave climate and sediment type. Design guidelines (POPE, 1986; SUH and DALRYMPLE, 1987; MCCORMICK, 1993) often fail to accurately predict beach response to breakwaters, this is especially the case for tidal environments (PILARCZYK and ZEIDLER, 1996; THOMELLA and VINCENT, 2004). Furthermore, design guidelines only suggest equilibrium response, changes to breakwater influenced beach morphology on shorter, non-equilibrium, timescales is less well researched. The variability of parameters such as shoreline location, tombolo location, beach slope and beach volumes is of great importance to coastal authorities in the management of breakwater protected beaches and when considering complementary strategies like beach re-charge.

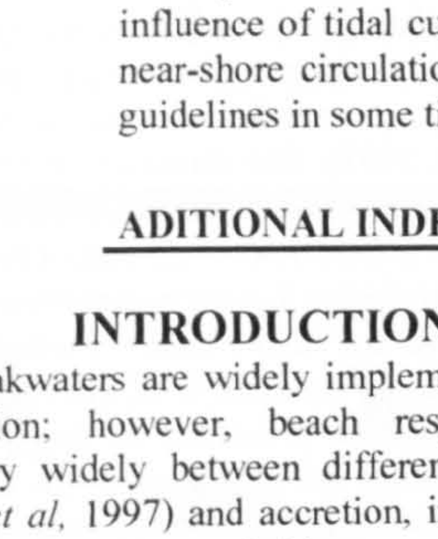

Figure 1. The British Isles with Sea Palling marked with a black dot

Better understanding of breakwater protected beach behavior is needed to fulfill these needs and will help inform future decisions on the implementation of such coastal protection structures.

This work uses MIKE21, a numerical model which includes the influence of waves, tides, and sediment transport processes on the morphodynamic evolution of beaches protected by detached breakwaters at Sea Palling, UK (Figure 1). Morphological changes have been measured with an Argus video system. Two datasets have been extracted from the video images, 3-d intertidal maps pre and post storm (FAIRLEY *et al,* in press) and a weekly times series of mean sea level (MSL) shorelines (FAIRLEY *et al,* in prep.). These datasets show clear, temporally varying, areas of erosion and accretion particularly related to the longshore movement of the tombolos and changes to intertidal beach volumes. Modeling complements video based analysis due to the similarity in spatial extents: comparison of large spatial scale morphological datasets with standard in-situ point measurements is often of limited value. Rather than model real scenarios at this

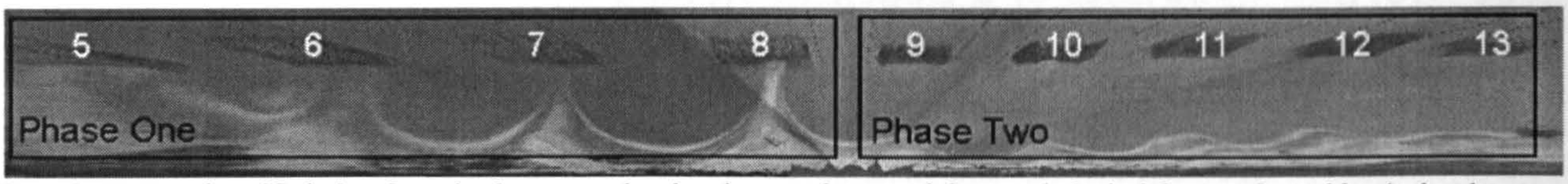

Figure 2. A merged rectified view from the 6 cameras showing the two phases and the morphological features formed by the breakwaters. Breakwater reference numbers are also displayed in white.

scheme a more generic approach was taken. A synthetic mean tidal cycle and characteristic wave conditions were used to look at typical types of morphological change. The rationale for such an approach being that a set of characteristic morphological changes due to differing wave conditions would aid understanding of the longer term morphological development at the site without the prohibitive computational time of simulating real scenarios. These changes were related to the changes observed in the video data and the circulation patterns that effected these changes isolated. This paper will focus on the explanation of storm scale changes. Storms are of particular interest to the coastal manager and engineer due to the possibility of catastrophic beach erosion and coastal flooding under such conditions.

STUDY SITE

This work utilizes a unique site at Sea Palling on the East coast of U.K. (Figure 1) where two designs of breakwaters were built in a meso-tidal environment open to energetic waves. The tidal regime is typical of the North Sea and consists of a progressive tidal wave: peak flood currents are directed towards the SE and are co-incident with high water; peak ebb currents at low water are directed towards the NW. There is a slight tidal asymmetry resulting in stronger flood currents (BACON *et al.*, 2005). The coastline faces NE and typically receives its largest waves from an obliquely incident northerly direction although storm waves can approach the site from all angles, the second most common angle being due east (obliquely incident in the opposing direction). In order to protect the low lying hinterland 9 breakwaters have been built in two phases. Phase one consists of 4 emergent breakwaters and phase two of 5 smaller breakwaters that are submerged at high tide, the last breakwater in phase two is lower than the others and submerged at most tidal levels. Prior to breakwater construction the beach was steep and narrow with a single offshore bar, after breakwater construction tidal tombolos formed behind the phase 1 breakwaters and salients behind the phase two structures (Figure 2). The breakwater reference numbers are also labeled in this figure for ease of future reference. Numbering starts from 5 due to historic reasons as more breakwaters were originally planned.

METHODOLOGY

Video Analysis of Morphology

Information about morphological changes was extracted from a set of Argus video cameras (HOLMAN and STANLEY, 2007). Six high resolution (1392 x 1040 pixel) digital video cameras were placed 27m above MSL on a guyed radio tower situated on the dune crest between the two breakwater phases. Ten minute time averaged images collected every half hour were used in this analysis. Shorelines were extracted manually from the oblique images using a point-and-click interface at known water levels. Only images with good clarity and small incident waves were used in the analysis. These shorelines were converted from image (u,v) to real world (x,y,z) co-ordinate systems using standard routines (HOLLAND *et al*, 1997). The shorelines in real world space were used to produce both intertidal bathymetries, by interpolation of shorelines picked over a half tidal cycle onto a regular grid, and MSL shorelines by interpolation between shorelines picked at the closest water levels above and below MSL. Further details of the extraction process is given in FAIRLEY *et al*, (in Prep.); FAIRLEY *et al*, (in press). For the work presented in this paper intertidal bathymetries were extracted pre and post storm and from these intertidal erosion accretion maps have been produced.

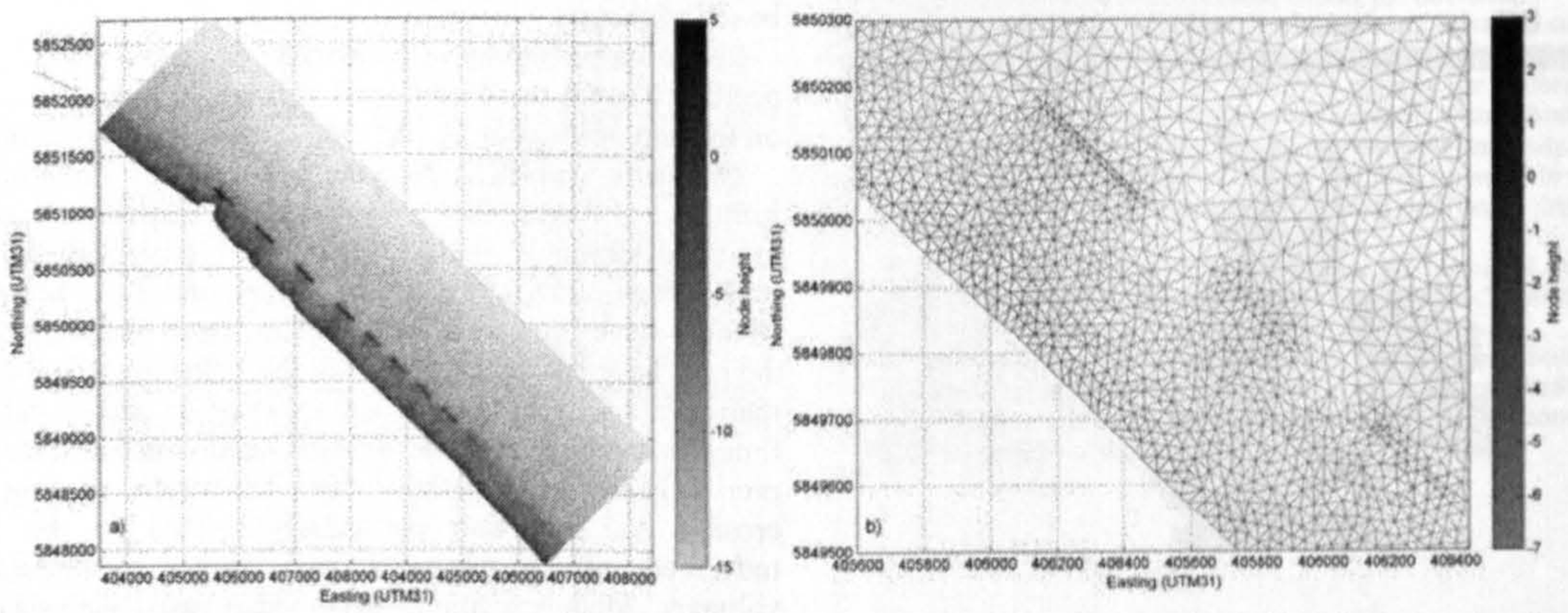

Figure 3. a) the model domain and triangular mesh used; b) a close-up of the domain around the breakwaters showing the depth dependence of element size and the preservation of the breakwater shape

Numerical modeling

Numerical modeling was conducted using DHI's MIKE21 2008 FM model. This is a flexible mesh finite-volume model with triangular elements used in this instance. Three modules were used: hydrodynamic (HD), spectral waves (SW) (SORENSON *et al*, 2004) and non-cohesive sediment transport (ST). These were run in a fully coupled mode whereby the HD module takes wave radiation stress from the SW module, the SW module takes water level and current conditions from the HD module and the ST module takes flow field inputs from the HD module and wave inputs from the SW module and at every time step the morphological change is fed back into the HD and SW modules. The SW module includes diffraction after HOLTHUSIJSEN *et al* (2002), this is process is especially important when considering wave transformations around breakwaters. The model was run with a variety of wave conditions on a synthetic mean tidal cycle.

Model domain

The model domain incorporates both phases and extends far enough away from the scheme such that boundary effects did not impinge on the area of interest (Figure 3a). The actual extent of the domain was confined by the extent of the available offshore bathymetry. The bathymetry used was a combination of DGPS quad bike based beach surveys and bathymetry collected using an RIB with echo-sounder and DGPS. The mesh was made finer in the shallower water around the breakwaters to provide greater detail in the intertidal regions which is the main area of interest of this study. The breakwaters themselves were incorporated by inserting data points representing their dimensions and heights into the bathymetry data. Internal boundaries around the breakwaters were used to preserve the shape of the breakwaters in the elements of the flexible mesh (Figure 3b). No wave transmission through the breakwaters is included in this model and overtopping occurs only when the structures are submerged.

Boundary conditions

Boundary conditions for the HD module were synthesized from current and water level measurements taken either side of the scheme. The measurements were spatially interpolated to give values at the north western and south eastern boundaries. The data was then split into individual tidal cycles, temporally normalized to the mean tidal cycle length and current speeds and water depths averaged to give a mean tidal cycle. In order to force the progressive wave the water level was specified at the northern end and current velocities at the southern end. The offshore boundary was forced with current velocities; the forcing velocities varied along the offshore boundary, being interpolated between current velocities at the northern and southern boundaries.

Characteristic wave parameters (significant wave height, period and direction) for the different storm types were evaluated from 7 years of data from the met office wave model hindcast at a virtual buoy location just offshore and to the north of the Sea Palling scheme. The directional spreading was unknown and so was kept at the MIKE21 default of a directional standard deviation of 23°. The different parameters are shown in Table 1. Since the virtual buoy was in the same water depth as the offshore boundary, no transformation was needed between virtual buoy and model boundary. These wave parameters were input at the offshore boundary, on the north-western and south-eastern boundary the MIKE21 option 'lateral boundary' was used whereby the basic equations are calculated along the boundary line taking the offshore boundary condition at the offshore end and reducing to zero at the inshore end.

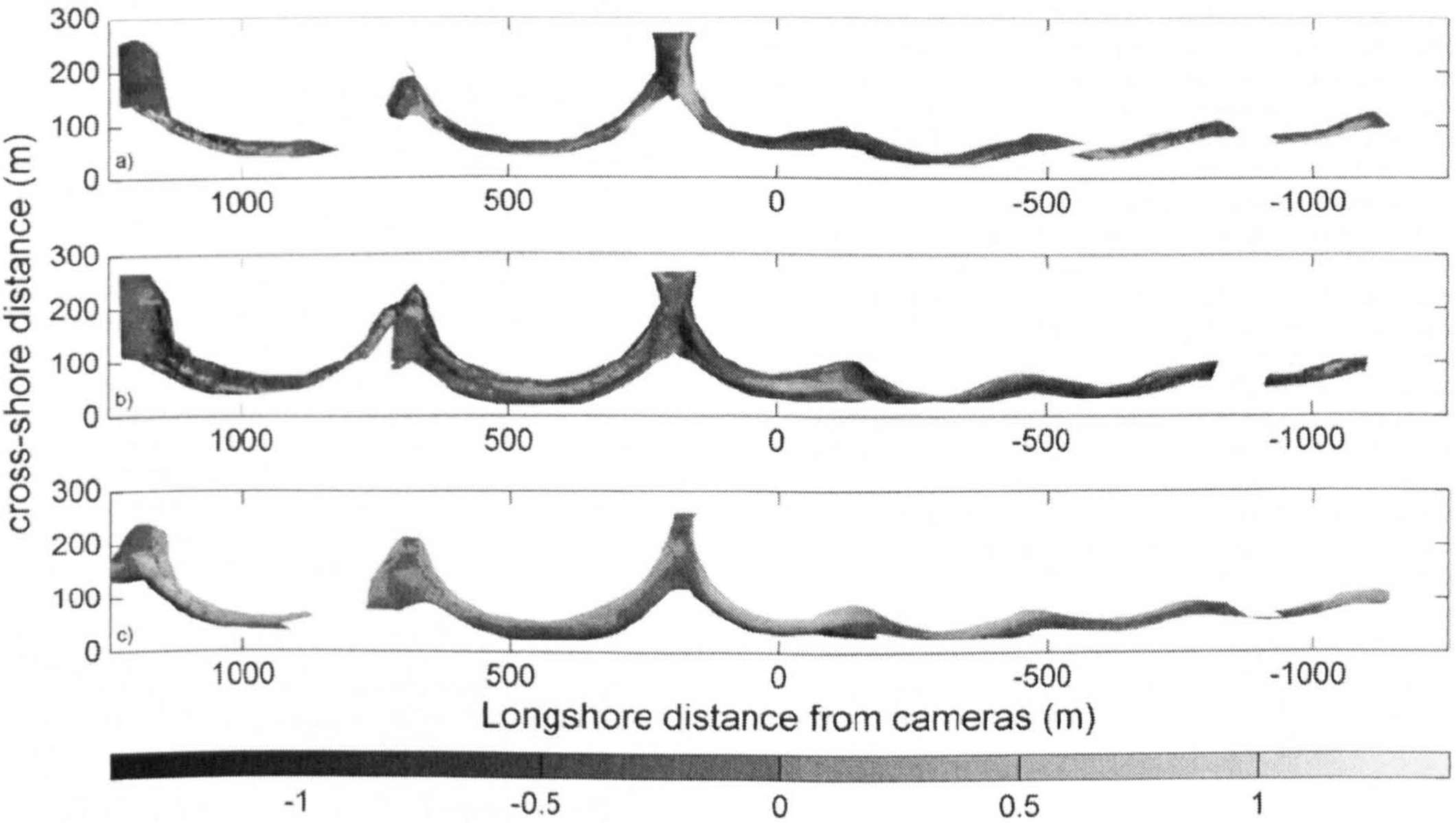

Figure 4.Erosion-Accretion plots for storms from a) northerly, b) easterly and c) shore normal incident directions. Beach level changes are shown by the colour shading: erosion is negative (dark) and accretion positive (light).

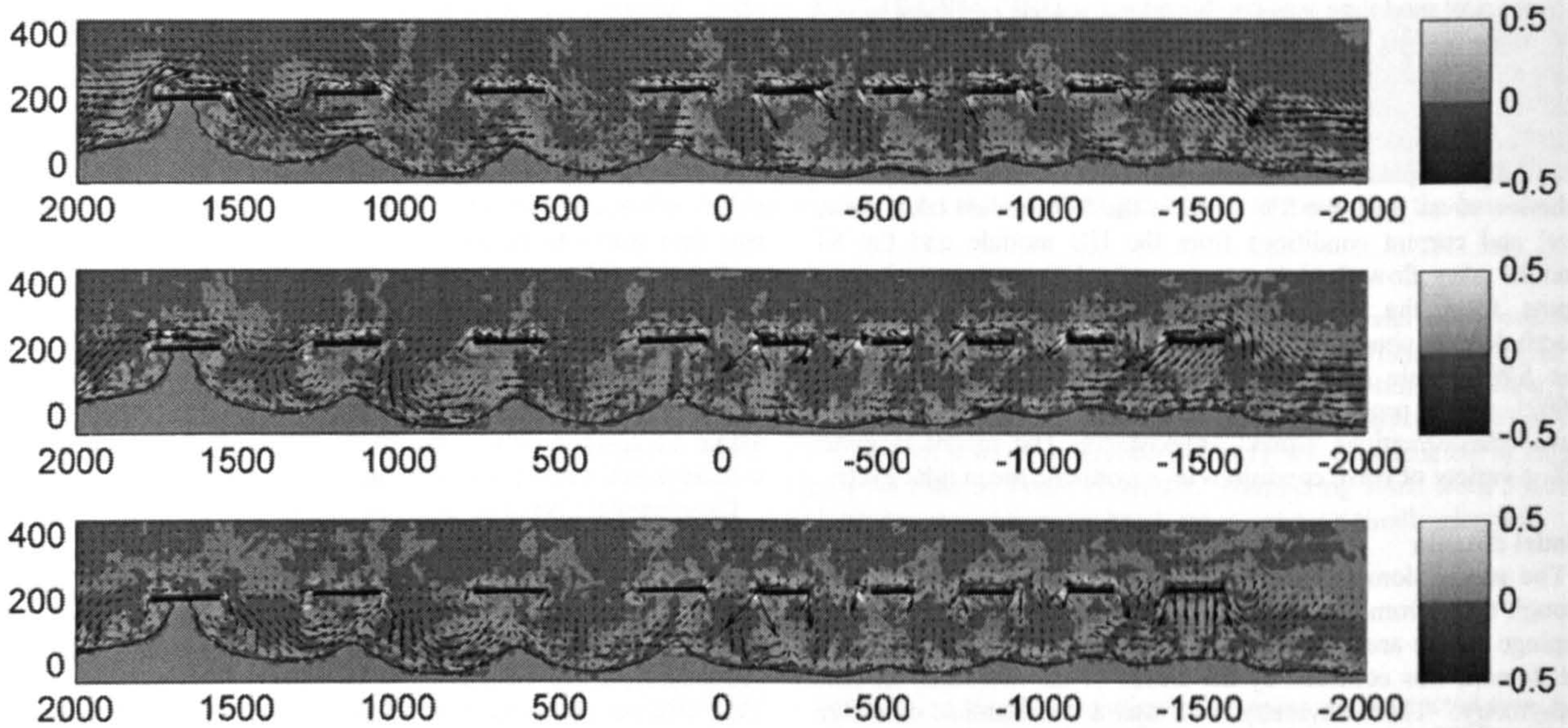

Figure 5. Bed level changes and net sediment transport vectors for a) Northerly, b)Easterly and c) shore normally incident storm waves

RESULTS

Video Analysis of Morphology

A summary of the effects of storms on intertidal beach morphology at this site is presented here, more detailed investigations are presented in (FAIRLEY *el al,* in press).

Figure 4 shows erosion accretion plots from 3 storms, one incident from the north (4a), one from the east (4b) and one with shore normal wave incidence (4c). All plots in the results section are plotted in a right handed co-ordinate system based on camera location such that the camera tower is in the origin, the y axis cross shore, increasing with distance offshore and the x axis, positive in phase one and negative in phase two. The most striking change is the longshore movement of the tombolos in a down drift direction in a) and b) where the storms have oblique incidence. This is shown by erosion on the up-drift side of the tombolos and accretion on the down-drift side. The change is most defined on the tombolo behind breakwater 8. There is a similar movement to the phase two salients but it is much less defined. Accretion is observed in the intertidal regions of the bays of phase one. This is less pronounced in phase two but still observable. The storm of shore normal incidence does not show alongshore movement of the morphological features. Instead general accretion is observed through the intertidal region with some erosion to the upper intertidal zone. Accretion is focused in the sheltered regions behind the breakwaters but erosion is noticeable on the crests of the tombolos behind breakwater 6 and 8.

Table 1: Mean storm parameters from the met office wave data

Storm type	H_s (m)	T_z (s)	Direction
Northerly	2.46	6	10
Easterly	2.43	6	75
Shore Normal (NE)	2.1	6	49

Numerical Modeling results

Plots similar to Figure 4 are shown in Figure 5. These show bed level changes computed over a tidal cycle for mean wave parameters from a northerly, easterly, and a shore normal incident storm. Vectors show net total load sediment transport over the tidal cycle with magnitude indicating amount of sediment transport. All three storm wave parameters show similar erosion and accretion patterns to the video results. Northerly waves lead to net longshore sediment transport through the scheme from NW to SE (left to right in the figure), there are larger rates of transport over the phase one tombolos which leads to erosion on the up-drift flank, transport over the tombolo crest and accretion on the down-drift flank of the tombolos. Similar increase in sediment transport is shown over the phase two salient horns, leading to accretional hotspots down drift of the salients in the lower intertidal regions. Erosion occurs in the upper intertidal and supra tidal regions with milder erosion on the bay floors. Onshore sediment flux is shown through the breakwaters gaps and over the bay floors. Both phases show some deposition of the eroded sediment in the sheltered regions and the intertidal regions of the bays.

The easterly incident storm conditions show similar patterns of erosion and accretion as the northerly incident conditions, with opposite longshore movement of the tombolos. However, the sediment transport pathways that effects this change is not the same. In the phase one embayments, the sediment transport paths take the form of a counterclockwise gyre, although magnitude of total load transport is much greater toward the sheltered region than away from it. This means that sediment is taken from the up-drift side of one tombolo, transported around the embayment and deposited on the down-drift side of tombolo on the other side of the embayment. In phase two the sediment transport pathways are more similar to the reverse of the pathways predicted for northerly wave conditions. For both the obliquely incident wave conditions the longshore movement is most defined behind breakwater 8.

Net sediment transport pathways for the shore normal storm take the form of a double gyre system in phase one, with a larger radius, more intense gyre on the southern (left in figure) half of

the embayment. Again, transport is of greater magnitude towards the sheltered region than away from it. The gyres in phase two are less well defined, net transport vectors being directed onshore in the bay centers, diverging towards the sheltered regions but without any obvious recirculation. The presence of the double gyre in the net sediment transport leads to accretion behind the breakwaters without longshore movement of the features.

DISCUSSION

The modeled bed level changes show similar patterns of erosion and accretion as the video derived changes for the three types of storm. Similar patterns of change has also been shown for a northerly storm using standard DGPS surveys (DOLPHIN *et al.*, 2005). Whilst direct measurements cannot be compared due to the generic nature of the modeling effort, the similarity in patterns of change gives qualitative confidence in the models performance. The model results allow us to look at the sediment transport pathways that effect this change. The most interesting result is that whilst northerly and easterly wave events show opposite longshore tombolo movement, it is not an opposite sediment transport pathway that causes the change. This difference could be forced by the tidal currents, the initial morphology or the influence of currents in adjoining embayments. It is postulated that the primary reason is likely to be the strong tidal currents at the site. This suggests that the importance of the tidal currents at this site should not be neglected, not just due to the background sediment transport pathways (BACON *et al.*, 2005) but also due to the tidal current modulation of the wave generated currents. This is also shown in the asymmetric nature of the double gyre in net sediment transport for the shore normal conditions. This result suggests a reason why previous design guidelines have had less success at predicting beach response in tidal environments: it is not just due to changing parameters (such as breakwater distance offshore) over the tidal cycle as previously postulated (THOMELLA and VINCENT, 2004) but also the presence of tidally driven currents that can be strong enough to alter wave driven currents from their expected shape. Differences in both bed level change and total load transport can be seen between embayments, for example the most defined longshore change is behind breakwater 8, this is due to current interactions between embayments and variations in sediment supply. The end embayments (excluded from the video analysis) are particularly affected by this.

CONCLUSION

A commercially available numerical model, MIKE21, has been used to investigate the sediment transport pathways that cause changes to beach morphology measured by an Argus video system. Characteristic wave and tidal parameters were used. The model performed well, producing similar patterns to the measured changes in bed level. Opposite morphological changes due to waves of opposing oblique incidence was shown not to be produced by opposite sediment transport pathways which highlighted the importance of tidally driven currents in altering wave driven circulation and affected sediment transport.

LITERATURE CITED

BACON, J.C.; VINCENT, C.E.; DOLPHIN, T.; TAYLOR, J.; PAN, S.Q. and O'CONNOR, B., 2005. The offshore breakwater scheme at sea palling, England; Sand transport generated by tidal currents, *Proceedings of the 29th International Conference on Coastal Engineering*. (Lisbon, Portugal, World Scientific), pp. 1896-1908.

DEAN, R.G., CHEN, R.J., BROWDER, A.E., 1997. Full scale monitoring study of a submerged breakwater, Palm Beach, Florida, USA. *Coastal Engineering*, 29(3-4), 291-315.

DOLPHIN, T.; TAYLOR, J.; VINCENT, C.; BACON, J.; PAN, S.Q. and O'CONNER, B., 2004. Storm-scale effects of shore-parallel breakwaters on beaches in a tidal setting (Leacoast). *Proceedings of the 29th International Conference on Coastal Engineering*. (Lisbon, Portugal, World Scientific), pp. 2849-2861.

FAIRLEY, I., DAVIDSON, M., KINGSTON, K., *in press*. A Video Based Investigation into the Morphological Impacts of Storms Behind a Series of Detached Breakwaters. *Proceedings of the 31st International Conference on Coastal Engineering*. (Hamburg, Germany ASCE), Online Poster Proceedings.

FAIRLEY, I., DAVIDSON, M., KINGSTON, K., DOLPHIN, T., PHILLIPS, R., in Prep. Empirical Orthogonal Function Analysis of Shoreline Changes Behind Two Different Designs of Detached Breakwaters. *submitted to Coastal Engineering*.

HOLLAND, K.T., HOLMAN, R.A., LIPPMAN, T.C., STANLEY, J., PLANT, N.,, 1997. Practical use of video imagery in nearshore oceanographic field studies. *IEEE Journal of Oceanic Engineering*, 22(1), 81-92.

HOLMAN, R.A. and STANLEY, J., 2007. The history and technical capabilities of Argus. *Coastal Engineering*, 54(6-7), 477-491.

HOLTHUSIJSEN, L.H., HERMAN, A., BOOIJ, N., CIESLIKIEWICZ, W., 2002. Diffraction in SWAN. *Proceedings of the 28th International Conference on Coastal Engineering*. (Cardiff, UK, World Scientific) pp. 405-412.

MCCORMICK, M.E., 1993. Equilibrium Shoreline Response to Breakwaters. *Journal of Waterway, Port, Coastal and Ocean Engineering*, 119(6), 657-670.

PILARCZYK, K.W., ZEIDLER, R.B.,, 1996. *Offshore breakwaters and shore evolution control*. Rotterdam: Balkema,

POPE. J., D., J. , 1986. Development of Design Criteria for Segmented Breakwaters. *Proceedings of the 20th International Conference on Coastal Engineering*. (Taipei, Taiwan, ASCE), pp. 2144-2158.

SORENSON, O.R., KOFOED-HANSEN, H., RUGBJERG, M., SORENSON, L.S.,, 2004. A third-generation spectral wave model using an unstructured finite volume technique. *Proceedings of the 29th International Conference on Coastal Engineering*. (Lisbon, Portugal, World Scientific), pp. 894-906.

SUH, K., and DALRYMPLE R., 1987. Offshore Breakwaters in Laboratory and Field. *Journal of Waterway, Port, Coastal and Ocean Engineering*, 113(2), 105-121.

THOMELLA, F., and VINCENT, C., 2003. Beach response to shore-parallel breakwaters at Sea Palling, Norfolk, UK. *Estuarine Coastal and Shelf Science*, 56, 203-212.

THOMELLA, F., and VINCENT, C,, 2004. Designing Offshore Breakwaters Using Empirical Relationships: A Case Study from Norfolk, United Kingdom. *Journal of Coastal Research*, 20(4), 1224-1230.

ACKNOWLEDGEMENTS

This work has been conducted as part of a PhD funded by the UK EPSRC LEACOASTII project. All participants in the project must be thanked, in particular, Tony Dolphin and Roger Phillips of the UEA who provided the bathymetry data used in the model. Current and water depth data was provided by Gardline Environment and the UK Environment Agency.

VIDEO MONITORING OF OVERTOPPING OF DETACHED BREAKWATERS IN A MESOTIDAL ENVIRONMENT

Iain Fairley[1], Mark Davidson[1] and Kenneth Kingston[1]

A novel approach has been developed to investigate the overtopping of a detached breakwater via the rapid sampling of specific pixels in an image. A line of pixels across the breakwater in a cross-shore direction were sampled during two storm events. Analysis of these pixel collections allowed the amount of overtopping and type of transmitted waves to be investigated. A critical value of relative freeboard for the onset of overtopping of this type of structure was determined and various regimes in which transmitted waves had differing properties were found. Wave speeds over the breakwater were found to be highly variable and showed little correlation with either linear or non-linear wave theory

INTRODUCTION

Video systems have been used routinely for a number of years to aid oceanographic and engineering research and management of the coastal zone (Davidson 2004). Typically their use focuses on the extraction of intertidal morphology (Aarninkhof 2003), however the power and versatility of video means that hydrodynamic parameters such as surface currents (Chickadel 2003), wave run-up (Stockdon 2006), wave speed and wave direction(Lippmann 1991) have also been measured via rapid sampling of specific pixels. In this paper video based remote sensing has been used to investigate wave overtopping of detached breakwaters. Similar efforts to extract overtopping information from video have been conducted by Archetti who examined wave breaking frequency and surface currents (Archetti 2006).

An Argus video system (Holman and Stanley 2007) situated at Sea Palling on the north Norfolk coast of the U.K is utilized in this work. The system consists of six high resolution (1392 x 1040 pixels) video cameras which capture the entire scheme (Figure 1). The cameras capture a variety of images and have the capability of sampling specific pixels at high frequency.

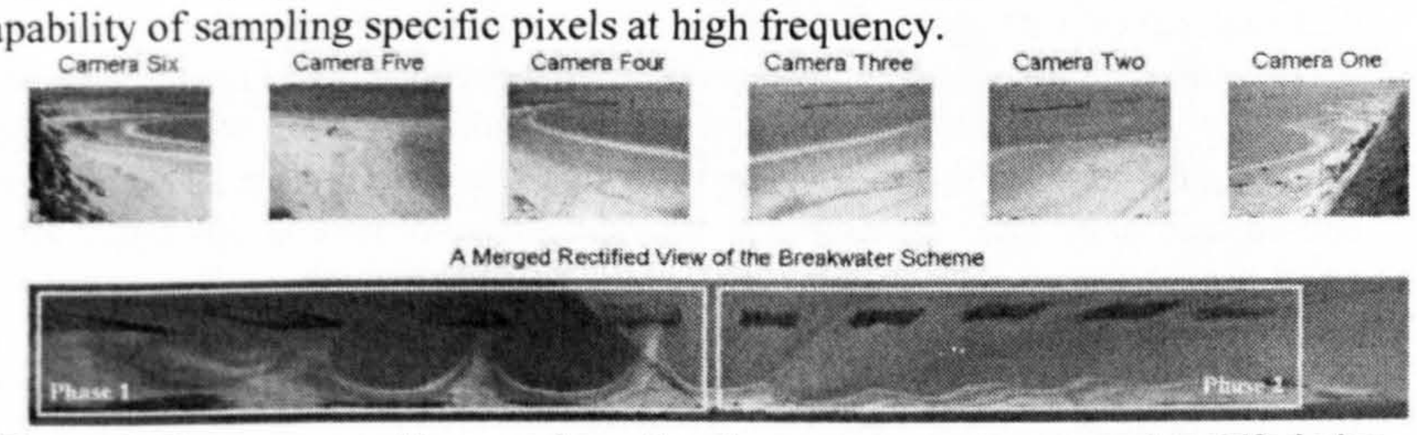

Figure 1: Time averaged images from the six cameras and a merged recitifed plan view of the scheme with the two different phases highlighted.

[1] School of Earth Ocean and Environmental Sciences, University of Plymouth, Drake Circus, Plymouth, Devon, PL4 8AA, United Kingdom

Nine breakwaters have been built at this site in two phases. The first, northern, phase consists of 4 larger breakwaters and the second southern phase consists of 5 smaller structures (Figure 1). Only the second phase is considered in this paper. These breakwaters have a length of 160m and a height of 1.3m ODN meaning they are immersed at spring high tides. The tidal characteristics of the Sea Palling site are meso-tidal with a spring range of ~3m and are typical of the Southern North Sea being a progressive tidal wave. The site is energetic with the majority of storm events approaching from the fetch unlimited north. Storm wave heights can reach in excess of 4m but are typically of order 2.5m.

Significant wave overtopping only occurs at this site under storm conditions. The aim of this experiment was to quantify the nature of this overtopping so that better understanding of the storm condition hydrodynamics could be gained. This would aid understanding of storm scale changes to morphology (Dolphin 2005).

METHODOLOGY

In this experiment two northerly storm events were investigated via the rapid sampling of specific pixels. The first storm had significant wave heights reaching 2.5m and the second 2.9m. A line of pixels at 1m spacing was sampled in a cross shore direction over the left hand breakwater in camera 2 (see Figure 1). These pixels were sampled at 2Hz for 17 minutes every hour. This type of pixel collection has already proved successful in the extraction of other hydrodynamic parameters. A visual representation of a pixel collection is called a time stack (Figure 2a). A time stack is realized by 'stacking' the sequentially sampled pixels from a line perpendicular to the breakwater on top of each other so that sample number (time) increases on the vertical axis and distance from the offshore end of the pixel line on the horizontal axis. Time stacks are a useful way to visualise the data and examine the processes involved. In Figure 2a the dark vertical band centered around 80 on the x-axis is the breakwater. The diagonal bands with positive gradient are the waves propagating towards the breakwater with the white bands representing broken waves. The gradient of the bands is representative of the wave speed with bands of steeper gradients representing waves with lower celerity. Near the top of the time stack two waves can be seen to be overtopping the breakwater. Also of note in this figure are the foam signatures on the lee side of the breakwater throughout the record. It is believed that these are due to transmitted waves exiting the breakwater. The transmitted waves lag behind the overtopping waves which suggest that, for this tidal height, transmitted waves are out of phase with overtopping waves. The right hand panel in Figure 2 displays three de-trended pixel intensity time series; the upper most for the offshore wave, the middle for the center of the breakwater and the bottom for the leeside of the breakwater. The regular incoming waves are visible in the top panel, the middle panel shows

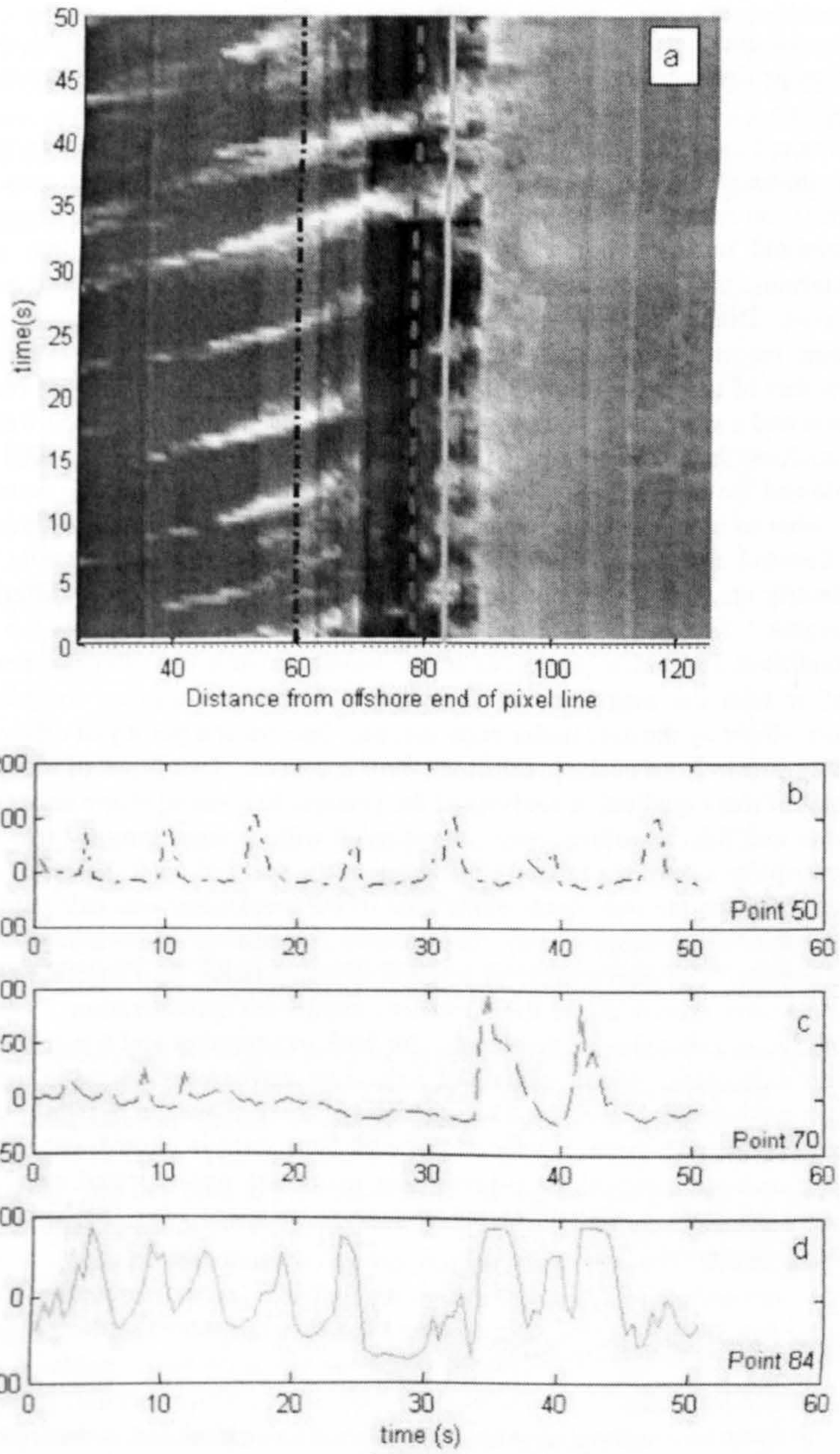

Figure 2: a) An example time stack and b-d) de-trended pixel intensity time series

the two overtopping waves to be clearly visible and the third panel shows an irregular time series with both signatures of transmitted and overtopping waves visible.

Since it is evident that waves overtopping the breakwater are clearly visible in the de-trended pixel intensity time series an up-crossing method was used to count the number of waves overtopping the breakwater in a given sample. A threshold was determined by examining the time stacks and time series to determine the extent of the noise in the signal that did not represent overtopping waves. Difficulties in visualizing the incoming waves in the offshore region in some records meant that a similar method could not be used to determine the number of incoming waves. Instead wave records from an offshore buoy were used and a wave model based on Dally, Dean and Dalrymple (1985) was used to transform the waves to a point just offshore form the breakwater. This analysis allowed the determination of a ratio of the number of overtopping waves to the number of incident waves for differing wave and tidal elevation conditions.

Spectral analysis of the pixel intensity time series was undertaken in order to identify changes in the wave spectra across the breakwater over differing tidal heights. The magnitude of the pixel intensity is dependent on the lighting conditions and visual properties of the waves and still water/breakwater surface rather than the magnitude of the waves. Hence the spectra computed were normalized by the area under each spectra. Spectra at a point just offshore and a point just inshore of the breakwater were analyzed. Two types of analysis were used. Firstly qualitative analysis of the changes to spectral shape under different wave and tidal conditions were investigated with changes grouped into different descriptive categories related to changes to the spectral peak. Secondly, spectral gain between the two points either side of the breakwater was calculated, where the gain was computed as the onshore spectra /offshore spectra at each frequency. The gain represents changes in shape rather than absolute magnitude of the wave spectra due to the previously mentioned normalization.

Wave speeds over the breakwater for both overtopping and transmitted waves were calculated. Visual signals of individual waves were traced in time stacks such as shown in Figure 2a. The gradients of these signals in the time stack were used to calculate the waves speed since the time stack is plotted with distance on the x-axis and time on the y-axis. This procedure was repeated many times in each time stack to determine an average wave speed over the breakwater for each time period.

RESULTS AND DISCUSSION

Overtopping ratio

The ratio of overtopping to incoming waves was calculated as described in the methodology. An overtopping ratio of 1 indicates that all waves approaching the structure overtop the structure and conversely an overtopping ratio of 0 means

that no waves overtop the structure. In this analysis overtopping is considered to be both the breaking of waves over the top of the emerged structure and the case of the submerged structure with waves propagating as bores over its top. This was plotted against the relative freeboard (Figure 3). The relative freeboard (RF) is the breakwater freeboard divided by the incident wave height. The incident wave height was determined from the offshore wave buoy data which had been transformed inshore (see Methodology).

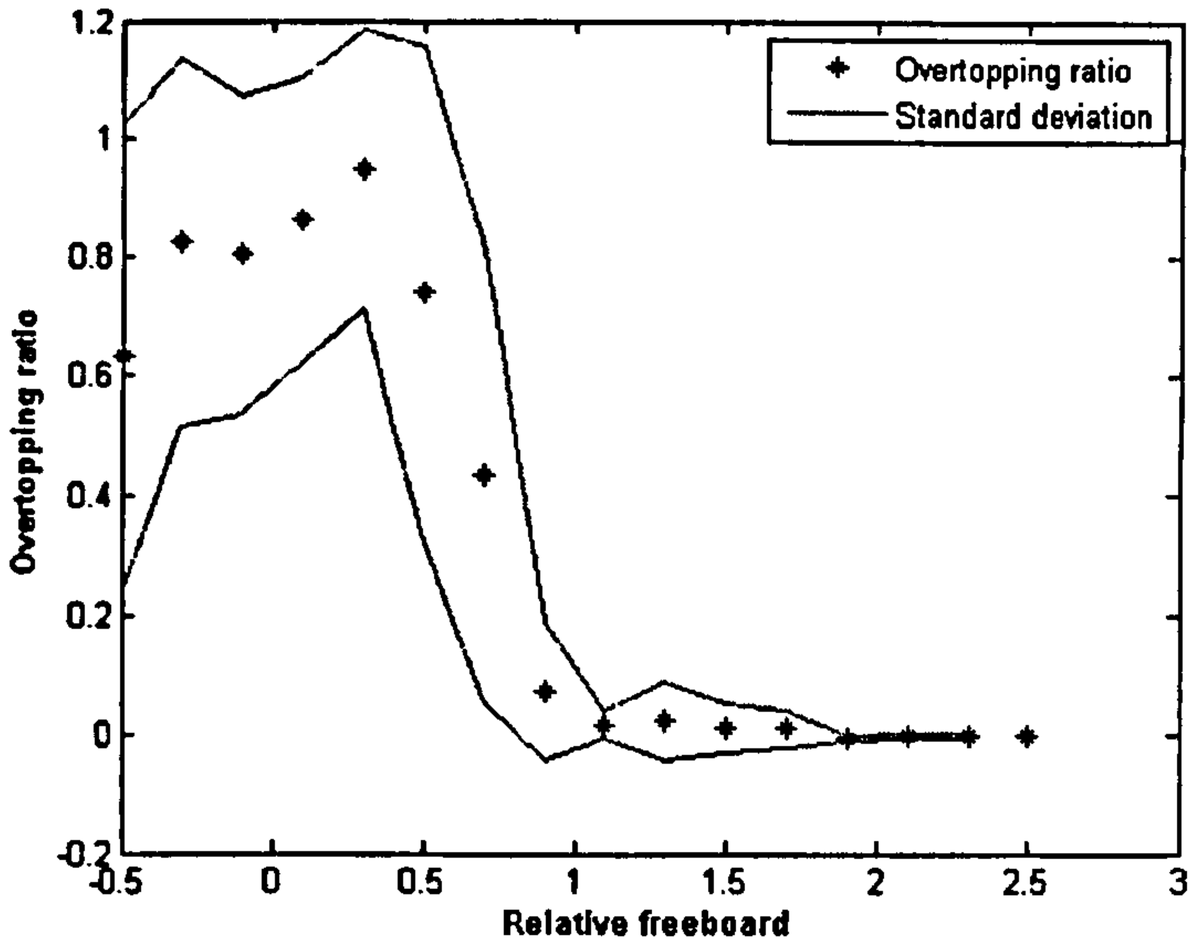

Figure 3: A graph of overtopping ratio against relative freeboard. The values of overtopping are plotted (*) as averages of 0.2 relative freeboard bins with the standard deviations of these bins also plotted

Figure 3 shows that for higher relative freeboard values very little overtopping takes place, at a certain relative freeboard value the overtopping rapidly increases and approaches one. A critical value for the onset of overtopping was determined to be 0.75. The standard deviation increases with the increasing overtopping ratio due both to the non-linearity of the process and the reduction in ease of distinguishing waves as foam from broken waves increases the noise in the signal. It can be seen that the overtopping ratio reduces at the lowest end of the relative freeboard scale. This is a visualization effect since as the tide submerges the breakwater some waves that propagate over the breakwater without breaking do not break the up- crossing threshold. Also present are overtopping ratios greater than one, these values arise due to increased noise caused by foam when the majority of waves are breaking over the structure.

The critical threshold found can be used to determine when overtopping occurs significantly and as such when it should be considered to affect the scheme

hydrodynamics. It is hope that this will allow us to distinguish between morphological effects when overtopping is and is not significant. It is believed that better modeling accuracy may be obtained by utilizing this critical threshold in modeling efforts for the Sea Palling site.

Changes to spectral shape

Seven different types of spectral change were observed. These changes were plotted against breakwater freeboard and wave height (Figure 4). The black line is y=0.75x and represents the critical relative freeboard value for the onset of overtopping.

Out of the seven types of changes, four main types of spectral change were noted that occur in distinct regions in the graph. The four main types were:
1: spectra similar,
2: peak shifted to lower frequency, higher frequencies reduced,
3: peak shifted to higher frequency,
4: energy concentrated in the incident frequency with other frequencies reduced.

The regions populated by the different types of spectral change can be explained by different combinations of breakwater freeboard and wave height. The first region, no spectral change, occurs for all wave heights at tidal heights such that the relative freeboard is below the critical threshold of 0.75RF (the region above the critical relative freeboard line in Figure 4). Since the majority of waves overtop the breakwater the spectral shape will be similar. The similarity of incident and transmitted peak frequency has been previously reported (Van der Meer 2000). It has been suggested that waves breaking over the top of a slightly emerged structure may produce two or more wave in the lee (Van der Meer 2000) and one might expect some spectral changes to occur due to harmonic de-coupling in the submerged case, in both cases leading to an increase in higher frequencies. However, it is believed that the amount of high frequency energy due to wind sea present under storm conditions masks any increase in higher frequencies on the leeside of the breakwater due to these effects.

The second region, spectral peak shifted to a lower frequency, occurs for all wave heights with freeboards such that the relative freeboard is over the critical value of 0.75 (Below the line of critical relative freeboard value on Figure 4). Since very little wave energy is entering the region via overtopping, the only wave energy is due to transmission. For the Sea Palling breakwater design, long waves are preferentially transmitted through the breakwater whilst the short period wind sea is dissipated on or within the breakwater. The dissipation of higher frequencies due to wave transmission through breakwaters has been reported (Ilic 2005; Van der Meer 2005) and the conservation of longer period waves transmitted through detached breakwaters has also been reported (Ilic 2005).

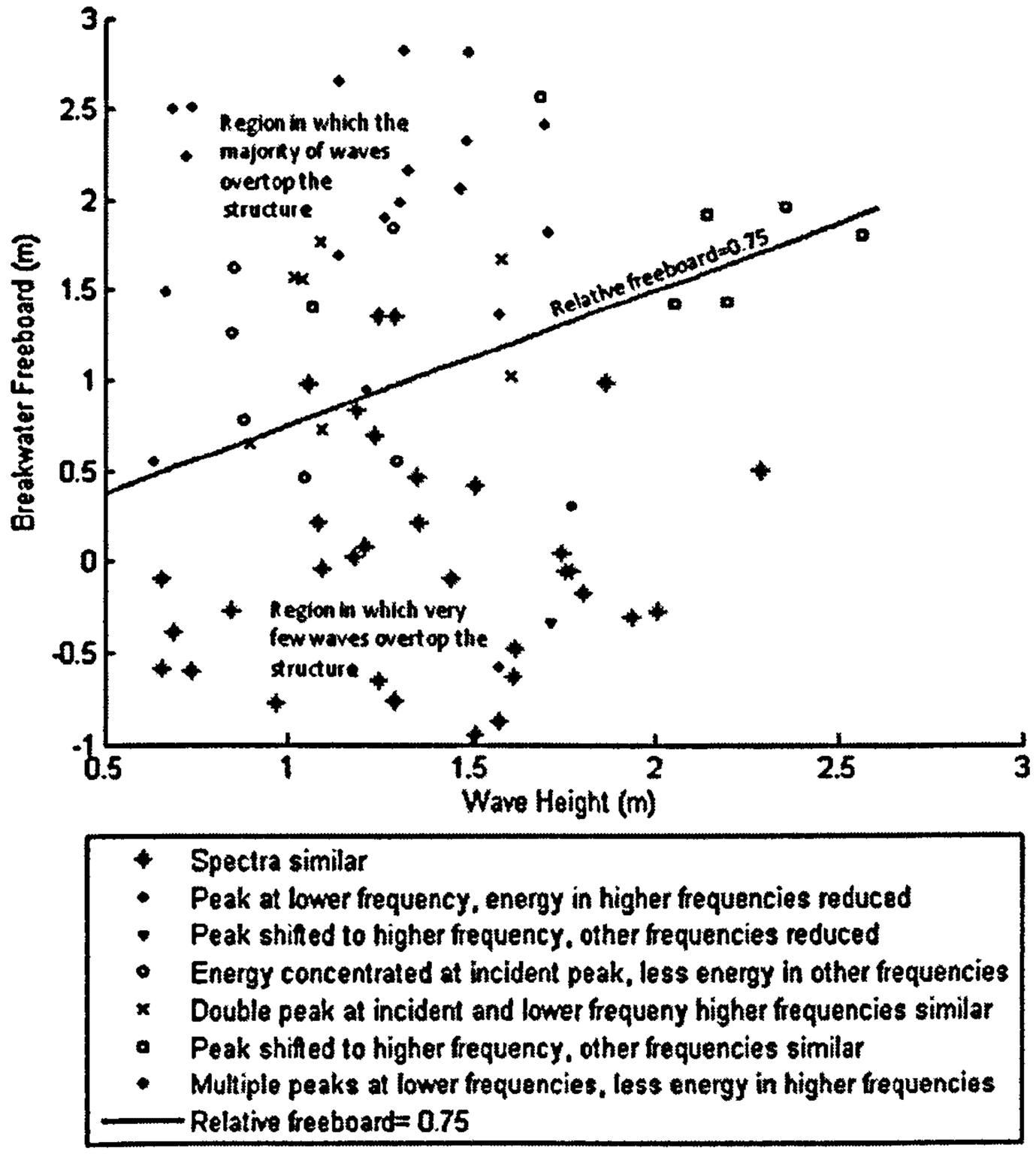

Figure 4: The different types of visually evaluated spectral change plotted against breakwater freeboard and wave height

The third region, in which the spectral peak is shifted to a higher frequency, occurs for higher wave heights and is centered on the RF=0.75 line. This scenario is such as shown in the time stack in figure 2. In this region overtopping is starting to become significant, but due to the larger wave heights the transmitted component is non-negligible compared to the overtopping waves. The transmitted waves are out of phase with the overtopping waves which leads to a spectral peak at a higher frequency.

The fourth region, in which the peak is concentrated at the incident frequency, surrounds the RF=0.75 line but for lower wave heights. In this region the smaller waves mean that the transmitted components are negligible compared to the overtopping components. The smaller waves also mean that only the peak

frequency swell waves have enough energy to overtop the structure leading to energy concentration in the incident peak.

The similarity of the video derived results for the first two types of spectral change with other, laboratory based, experiments give confidence in the acceptance of the video results.

In order to better quantify the changes to spectral shape the gain in spectral shape was plotted against relative freeboard and frequency (Figure 5). For the lower relative freeboard values there is little pattern in the gain, as the relative freeboard increases gain in the lower frequencies becomes evident, especially over the relative freeboard value of 0.75, where there is also a corresponding loss in the higher frequencies. This backs up the qualitative result that above the critical threshold, when transmission rather than overtopping is dominant, the spectral peak is shifted to a lower frequency.

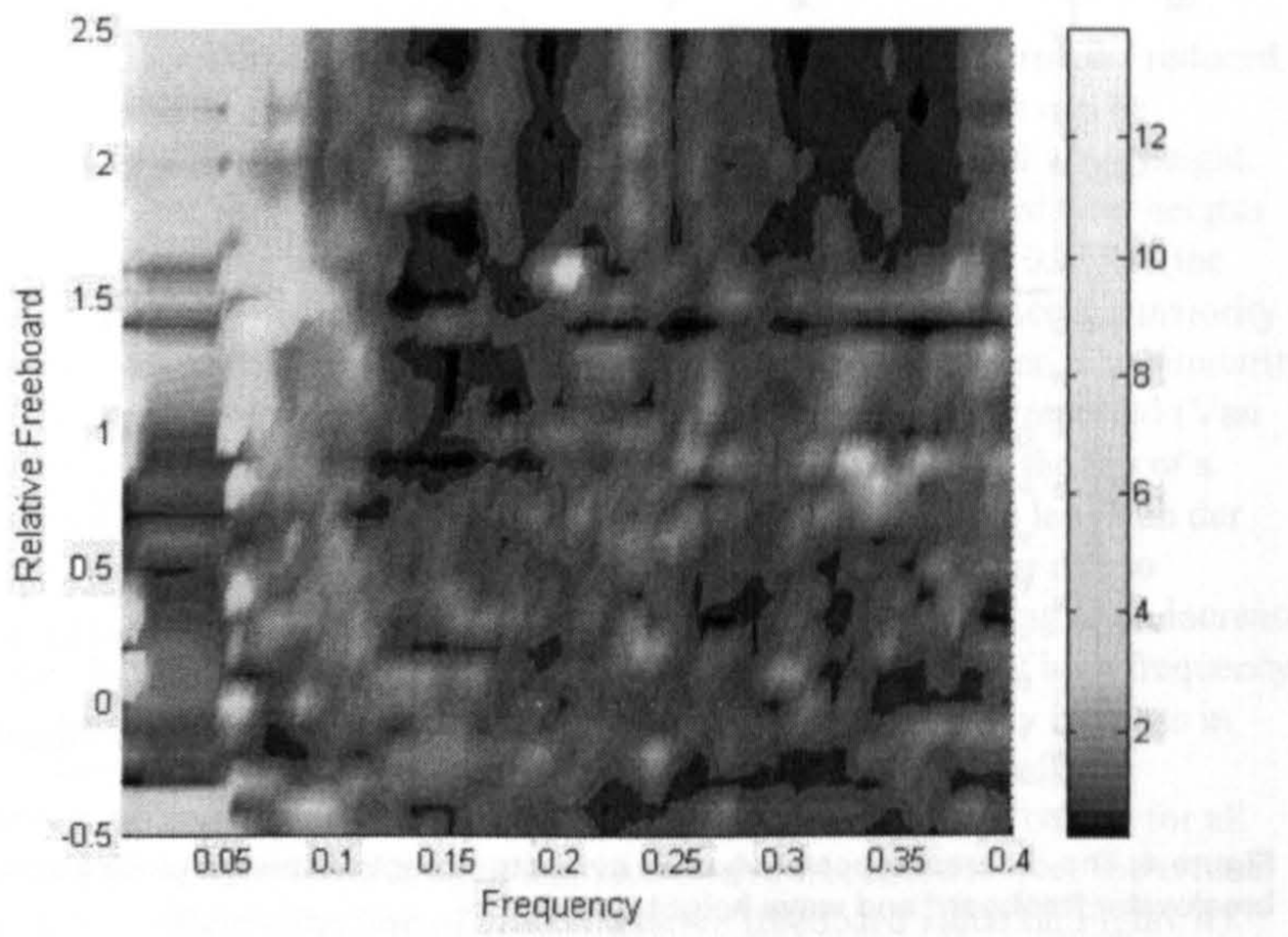

Figure 5: A plot of spectral shape gain against relative freeboard and frequency

These two analyses give information about the spectral shape of the wave climate on the lee side of the breakwater. Such information is important because seas with differing spectra with have differing erosion/accretion characteristics. Small long period waves are more likely produce accretion whilst short period waves are more likely to cause erosion. So in the instance of Sea Palling we may have the scenario that at lower tides the salients are exposed to accretion effects whilst at higher tides the regime is largely one of erosion.

Wave Speeds

A large range of wave speeds were measured over the top of the breakwater both for the emerged case where waves are traveling as bores over exposed breakwater and the submerged case where waves are propagating over the shallow water covering the breakwater. Wave speeds ranged from 4.5ms-1 to 13ms-1.

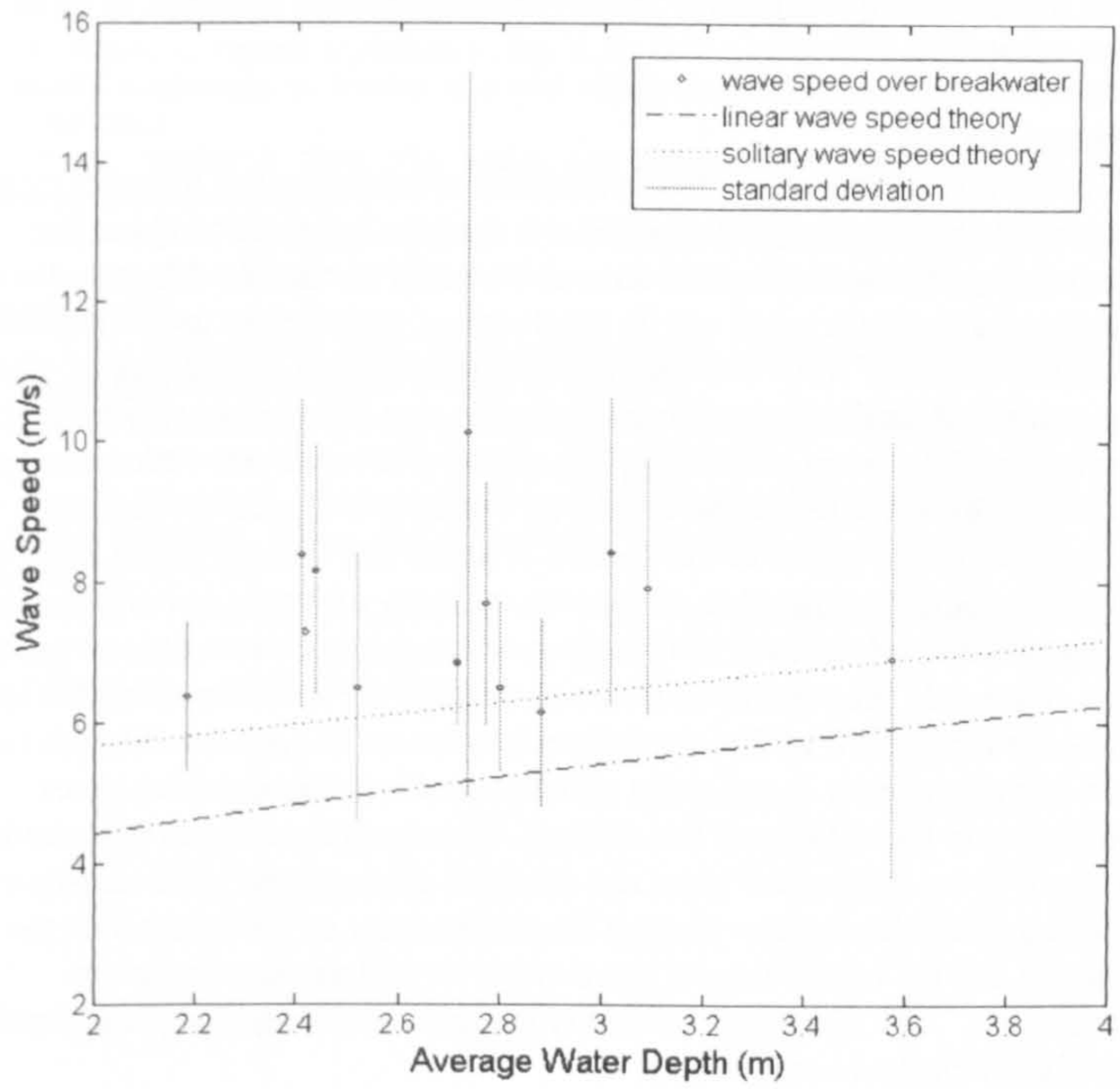

Figure 6: Wave speeds over the submerged breakwater

Figure 6 shows waves speeds plotted against average water depth for the submerged breakwater. It can be seen that there is a large variability in the measured speeds for each water depth(represented by the large standard deviations), the wave speeds were easily measurable in the time stack and this variability is real. The variability in the speeds of submerged waves over the breakwater is put down to the non-linearity of wave-wave and wave structure interactions.

There is no correlation between wave speed and water depth over the breakwater. Generally, the speed of waves over the breakwater is faster than predicted by both solitary and linear wave theory. The steeply sloping

breakwater could mean that there is a delay in the deceleration of the waves, waves are affected not only by the water depth directly beneath them but by the preceding bathymetry (Camfield 1968). It is postulated that for very shallow water depths, the wave speed across the breakwater could be due to the momentum of the wave as it surges across the structure. Wave speeds measured in deeper water offshore of the breakwater did correspond to linear wave theory.

The variability in wave speeds and the lack of conformity to any depth based wave theory pose questions for phase resolving models that seek to incorporate wave overtopping.

CONCLUSIONS

A novel approach using video to measure overtopping has been developed and implemented. This enables full-scale site specific information about the overtopping of detached breakwaters to be easily obtained. Magnitudes of overtopping volumes could not be resolved but nonetheless useful information about the nature of wave overtopping and transmission of this type of structure was gained. A critical value for overtopping was determined which allows prediction of the onset of overtopping, above this value very little overtopping occurred and below this value almost all waves overtopped the structure. Differences in the nature of the spectra offshore and inshore of the breakwater could be related to this value. When the majority of waves overtop the structure the spectra on both sides of the breakwater are similar, when little overtopping takes place only long waves transmitted through the structure reach the leeside which leads to a shift of the spectral peak to lower frequencies. Similar results have been previously found using conventional techniques which gives confidence in the validity of the method. Conclusive results on the speed of waves over the breakwater were not obtained although the wide variation in speeds over the breakwater hints at the nonlinearity of processes over the structure and the importance of wave-wave as well as wave-structure interactions. The observed variability creates a challenge for phase resolving models of detached breakwaters.

ACKNOWLEDGEMENTS

This work has been undertaken as part of a PhD tied to the LEACOASTII project which was funded by the Engineering and Physical Sciences Research Council. Thanks must go to all participants in this project. Particular thanks to John Bacon, Tony Dolphin, Roger Phillips and Estelle Dumont of the University of East Anglia for help with maintenance of the camera system.

REFERENCES

Aarninkhof, S. G. J., Turner, I.L., Dronkers, T.D.T., Caljouw, M., Nipius, L. 2003. A video-based techniqe for mapping intertidal beach bathymetry. *Coastal Engineering* 49: 275-289.

Archetti, R., Lamberti, A. 2006. Study of hydrodynamic induced by low crested structures through image processing. *Proceedings of the 30th international conference on coastal engineering*, World Scientific, 5021-5033

Camfield, F., Street, R., 1968. The effects of bottom configuration on the deformation, breaking and run-up of solitary waves. *Proceedings of the 10th International Conference on Coastal Engineering*, ASCE, 173-189.

Chickadel, C. C., Holman, R.A., Freilich, M.H. 2003. An optical technique for the measurement of longshore currents. *Journal of Geophysical Research* 108(c11): 28-1–28-17.

Dally, W. R., Dean, R.G., Dalrymple, R.A. 1985. Wave Height Variation Across Beaches of Arbitrary Profile. *Journal of Geophysical Research* 90: 11,917-11,927.

Davidson, M. A., Aarninkhof, S.G.J., Van Koningsveld, M., Holman, R.A. 2004. Developing Coastal Video Monitoring Systems in Support of Coastal Zone Management. *Journal of Coastal research* S.I. 39: 463-475.

Dolphin, T., Taylor, J., Vincent, C., Bacon, J., Pan, S. Q., O'Conner, B. 2005. Storm-scale effects of shore-parallel breakwaters on beaches in a tidal setting (Leacoast). *Coastal Engineering 2004*, ASCE, 2849-2861.

Holman, R. A., Stanley J. 2007. The history and technical capabilities of Argus. *Coastal Engineering* 54(6-7): 477-491.

Ilic, S., Chadwick, A., Fleming, C., 2005. Investigation of detached breakwaters. Part 1 - hydrodynamics. *Proceedings of the Institution of Civil Engineers-Maritime Engineering 158*(MA3): 91-102.

Lippmann, T. C., Holman, R.A. 1991. Phase speed and angle of breaking waves measured with video techniques. *Coastal Sediments '91*, ASCE, 542-556.

Stockdon, H. F., Holman, R.A., Howd, P.A., Sallenger Jr., A.H., 2006. Empirical parameterization of setup, swash and runup. *Coastal Engineering* 53(7): 573- 588.

Van der Meer, J., Briganti, R., Zanuttigh, B., Wang, B. 2005. Wave Transmission and Reflection at Low Crested Structures: Design formulae, oblique wave attack and spectral change. *Coastal Engineering* 52: 915-929.

Van der Meer, J. W., Regeling, H.J., de Waal, J.P. 2000. Wave transmission: spectral changes and its effects on run up and overtopping. *Proceedings of the 27th International Conference on Coastal Engineering*, ASCE. 2157-2168

KEYWORDS - CSt07

Abstract number: 28

VIDEO MONITORING OF OVERTOPPING OF DETACHED BREAKWATERS IN A MESOTIDAL ENVIRONMENT

1st Author: Fairley, Iain A
2nd Author: Davidson, Mark A
3rd Author: Kingston, Kenneth

Video
Remote sensing
Detached Breakwaters
Overtopping
Spectral Change

A VIDEO BASED INVESTIGATION INTO THE MORPHOLOGICAL IMPACTS OF STORMS BEHIND A SERIES OF DETACHED BREAKWATERS

Fairley, I.,[1] Davidson, M.[1] and Kingston, K.[1]

A coastal imaging system was used to investigate storm scale changes to beach morphology at a meso-tidal, high energy site where two different designs of detached rubble mound breakwater are present. Intertidal bathymetries were mapped from images pre- and post-storm and thus the protected beaches storm response was measured. Beach responses to the different types of breakwaters were compared. Oblique waves moved the salients/tombolos in a down drift direction; larger breakwaters constrained this response to a greater extent. Beach gradients were largely unchanged over individual storms except for storms combined with large surge events where beach flattening was observed. Greater flattening of beach gradients were observed on the beach protected by the larger breakwaters. It is believed that this is related to sediment abundance as much as breakwater design. General accretion was observed in the intertidal region over storms for both breakwater geometries.

INTRODUCTION

Detached shore parallel breakwaters are a common method of shoreline protection, aiming to increase beach widths via the production of accretionary features in the sheltered lee of the structures. A significant body of work exists as to the hydrodynamic function of such structures (Archetti, 2006; Fairley, 2007; Loveless, 1998; Van Der Meer, 2004) and several design guidelines (Ahrens, 1990; McCormick, 1993; Pope. J., 1986) produced that aim to predict the shape of the resultant morphology. Such work largely assumes the development of equilibrium morphology and produces one line predictions for the response of such structures. A far lesser body of work considers the morphological responses of these protected beaches in detail and in non equilibrium conditions. The responses of detached breakwaters in tidal environments is also poorly understood (Pilarczyk, 1996), with design guidelines commonly failing to predict shoreline response in tidal conditions (Thomella, 2004). The EPSRC funded LeaCoast2 project aims to build upon previous work (LeaCoast) and investigate detached breakwaters in a meso-tidal setting. The site investigated in this work contains two different phases of breakwater design allowing comparison of beach response to two different breakwater geometries undergoing near identical forcing.

Beach responses to storms are of paramount importance in evaluating the success of a coastal protection scheme, as catastrophic erosion is usually

[1] School of Earth, Ocean and Environmental Sciences, University of Plymouth, Drake Circus, Plymouth, Devon, PL4 8AA, UK

synonymous with storm conditions. In addition, previous work on longer term mean water level shoreline response at the system studied here has highlighted the importance of storm scale changes on the longer term shoreline responses of this scheme (Fairley, in Prep.).

Six argus cameras (Holman and Stanley, 2007) have been deployed at this site giving coverage of both phases. Argus systems are superior to traditional survey techniques in the investigation of storm scale responses because they allow the extraction of intertidal bathymetries directly pre and post storm resulting in better isolation of storm scale responses. Standard survey regimes have frequencies between monthly and annual meaning the response to individual storms is not easily distinguishable from other events. Whilst intertidal bathymetries extracted from images suffer some reduction of accuracy compared to DGPS surveys the large magnitude of storm response means the signal to noise ratio is still large and thus the errors do not significantly affect the results.

FIELD SITE

This work focuses on a two phase scheme of rubble mound detached breakwaters situated at Sea Palling, Norfolk, on the East coast of the United Kingdom (Figure 1).

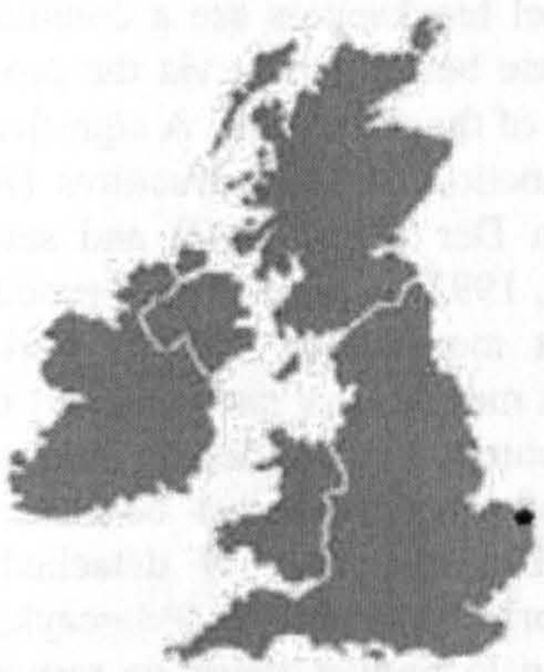

Figure 1: A map of the UK with Sea Palling marked by a black dot.

The site is situated on an eroding coastline that has historically suffered from storm surge induced flooding. The coastline is characterized by a narrow beach with a single offshore bar and backed by a single dune line. D_{50} at the site is 430μm (Bacon et al., 2005), although the beach also has a very sparse armoring of pebbles. The majority of the low lying hinterland is farmland but at Sea Palling, a village is situated directly behind the dune line. The dune line was protected by a concrete sea wall in 1953 and narrowing beach widths lead to the construction of 9 breakwaters between 1994 and 1997 (Hamer, 1998). Two

phases of rubble mound breakwaters were built: phase one consisting of 4 fully emergent breakwaters; phase two, five smaller tidally submerged breakwaters. The dimensions of the breakwaters are displayed in Table 1.

Table 1: Dimensions of the two designs of detached breakwater

	Breakwater length (m)	Gap length (m)	Distance offshore (m)	Spring HW freeboard (m)
Phase one	270	160	270	1.3
Phase two	160	160	270	-0.5

Figure 2 shows a merged rectified view of the breakwaters system at mean low tide with the two phases marked. The different breakwaters have different accretionary features in their lee. The larger phase one breakwaters have produced tidal tombolos (salients at high tide, tombolos at low) in their lee and phase two has produced salients. The large size of the tombolo at the far left of the plot is partially due to the longshore sediment direction and partially due to beach re-charge. The phase one bays are still observed to be infilling suggesting that the scheme is not yet in equilibrium.

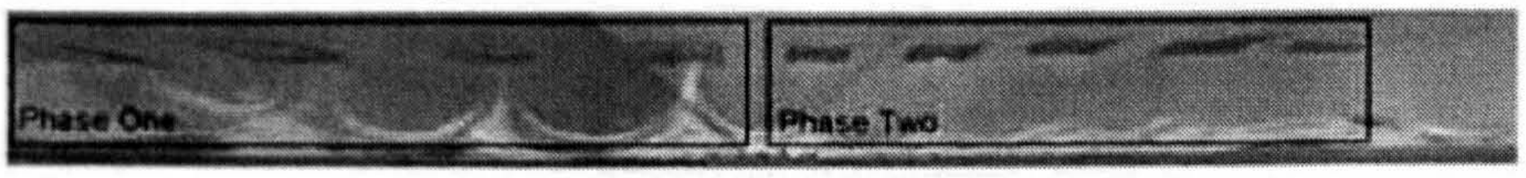

Figure 2: A merged rectified view of the breakwater system, showing the different breakwaters and the different morphological features produced

Hydrodynamic conditions are typical of the southern North Sea. The spring tidal range is ~3.1m and characterized by a progressive tidal wave meaning peak currents occur at high and low tides. Tidal currents alone are sufficient to mobilize sediment (Bacon et al., 2005) and the tide is asymmetric leading to a net current towards the south east. A description of the wave climate is displayed in Figure 3. The plot shows a wave rose of mean wave height against wave period based on 7 years of UK met-office hind cast data. The data has been linearly transformed inshore to just offshore of the breakwaters, only waves incident to the site were transformed hence the lack of waves propagating in an offshore direction. Two peaks in mean wave height can be seen approaching the site from oblique NNE and ENE directions. These represent the two most common storm directions, Northerly events, caused by low pressures tracking eastward from the Atlantic into the North Sea, are the most prevalent storms. The longest period waves approach the site from a shore normal (NE) direction. The prevalence of northerly wave events, along with the asymmetry in the tidal current, lead to a net longshore sediment transport direction to the South East which has been estimated at 100 m^3yr^{-1} (Clayton, 1983).

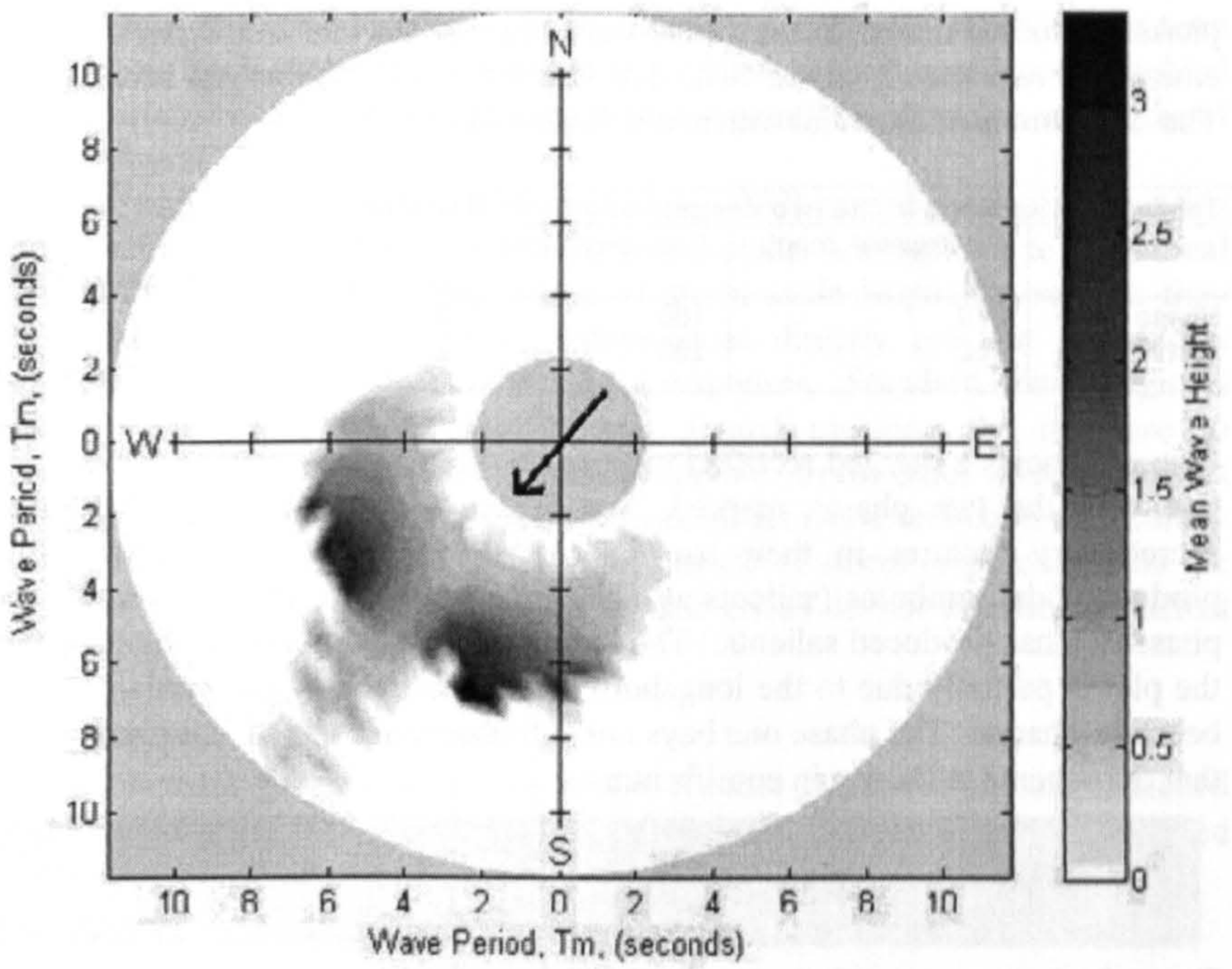

Figure 3: A figure showing mean incident wave height for different wave periods and directions. The wave period increases from 2 at the centre of the rose to 12 on the outside. North is at the top of the plot and the arrow in the centre points to shore normal at Sea Palling.

METHODOLOGY

Six high resolution digital video cameras are positioned on a guyed tower on top of the dune line at an elevation of 27m above mean sea level. A local computer allows for remote access both for image upload and camera control. The cameras are situated in between phase one and phase two and provide coverage of the whole scheme. Accuracy is reduced due to pixel footprint size increasing with distance and hence analysis is restricted to within ~1250m from the camera position. This means that the northernmost and southernmost embayments are excluded.

Three-dimensional intertidal bathymetries are produced by picking shorelines (x, y) at known water elevations (z) from images collected at half hourly intervals over a half tidal cycle. Ten minute time averaged images are used in this analysis. Time averaged images remove short term shoreline variation due to individual swash motions and produce a more stable shoreline feature. Water elevations were measured using a pressure transducer attached to the northern breakwater marker pile. Surface elevation at the shoreline also contains a component due to wave driven set-up, however the sheltering effect of the breakwaters mean that the wave set-up varies around the embayments and

calculation of these differences would have been difficult. Instead the wave set-up component was neglected and images only picked on days with minimal wave heights (sub 0.1m). This leads to maximum set-up based vertical errors of ~0.02m.

Shorelines were extracted manually using a point and click graphical user interface. Manual picking was found to be the most accurate and user efficient method of shoreline extraction: automatic routines routinely frequently failed for the Sea Palling images. Shorelines were picked pre- and post-storm on the closest days to the storm with low waves and good visibility. The *x, y, z* coordinates from the shorelines were interpolated to a regular grid of 1m spacing to create pre- and post-storm intertidal bathymetric maps. From these, erosion accretion maps and cross-shore profiles were produced. Erosion-accretion maps produce valuable descriptions of the spatial distribution of change but some information is lost due to non-overlapping regions, hence it is useful to visualize the morphological change in a variety of ways.

RESULTS

Storms with different angles of incidence, different durations and different surge levels were investigated. An annotated wave power time series for the period evaluated is displayed in Figure 4, and the basic storm parameters are described in Table 2. The directional convention used in the table is 0 being shore normal, positive wave angles represent waves incident from the north and negative angles from the south. Surge level is determined from the NTSLF gauge at Cromer, 15miles from Sea Palling.

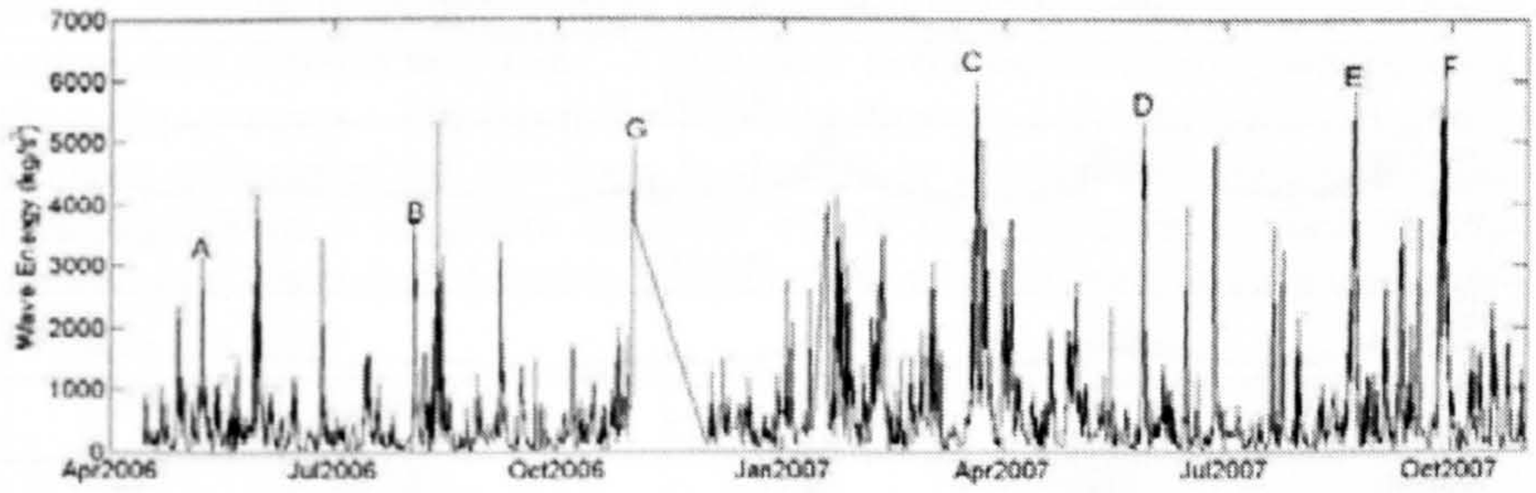

Figure 4: A wave energy time series with the evaluated storms labeled.

Table two: Basic storm parameters for the storms analyzed.				
Storm	Duration	Max. Hsig	Wave Direction	Surge level
A	2	2.6	40	0.5
B	2	2.4	30	0.5
C	6	3	30	1.3
D	1	2.5	-25	0.15
E	4	3	30	0.5
F	4	3	±10	0.4
G	17	3	40	1.3

Erosion-Accretion plots

Erosion accretion plots for the seven storms are shown in Figure 5. The co-ordinate system for this figure is based on the camera location. The *x*-axis is the longshore distance in meters from the camera location. The *y*-axis is cross-shore distance from the camera location in meters. Phase one of the scheme is positive in a longshore direction and phase two negative. Negative *z* values indicate erosion and positive *z* values accretions. The longshore movement of the tombolos and salients is clearly displayed in storm A, with erosion on the updrift and accretion on the down drift side of the tombolos.

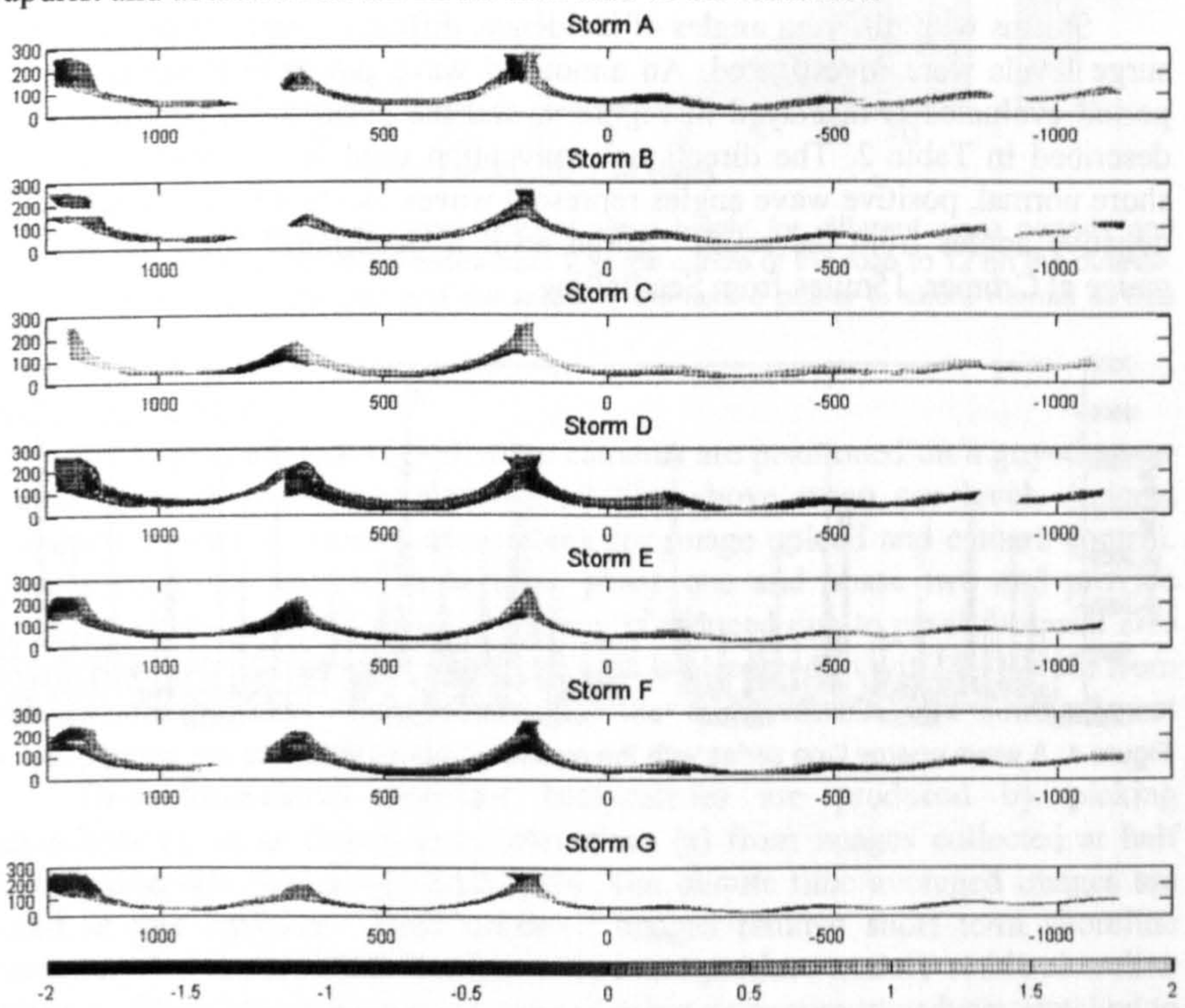

Figure 5: Erosion-Accretion plots for the seven storms analyzed. Erosion is negative and accretion positive.

The salients show less defined displacement although still in the same direction. The same trend is evident, but to a lesser extent in storms B and C. Storm D, where waves are incident from the opposite direction, shows the opposite displacement of the salients and tombolos. Storm F, with shore normal wave incidence shows the tombolos staying at the same longshore location, but flattening, with erosion on the upper horn and accretion either side. The salients show some accretion on their northern flanks corresponding to the waves being incident from south at the tail of the storm and suggesting the salients respond more rapidly to changes in wave direction. Storm E which has waves incident from the same direction as A, B and C and has longer duration and larger wave height does not show the same longshore movement. Both phases show some general accretion over most storms. Phase one shows more accretion in the lower intertidal region and on the tombolos. Phase two shows more uniform accretion over the entire intertidal region. Storm G, with the longer duration shows erosion over the entire phase two and much of phase one. It is only on the tombolo horns that accretion is observable.

Detailed look at changes to a tombolo

Figure 6 shows a tombolo pre- and post-storm for a northerly storm. The movement displayed is characteristic of tombolo movement under such storms and allows elucidation of the changes to the tombolo over the storm. As shown in the erosion accretion plots, the tombolo is moved in a down drift direction, this movement is constrained to the tombolo itself with little movement at the extremes (x>300 and x<100). The movement of the crest centre line is approximately 25m. Also noticeable is an accretion on the horn of the tombolo, this is particularly evident further seaward (200-275m cross-shore) where the salient crest accretes by ~0.5m. A skewness in the tombolo form is induced by the oblique waves. Pre-storm the tombolo displays a symmetrical plan-form, whereas post-storm the plan-form is skewed in a down drift direction. The cross-section in a longshore direction of the tombolo horn is very slightly skewed in a down drift direction pre-storm but this skewness is increased post-storm.

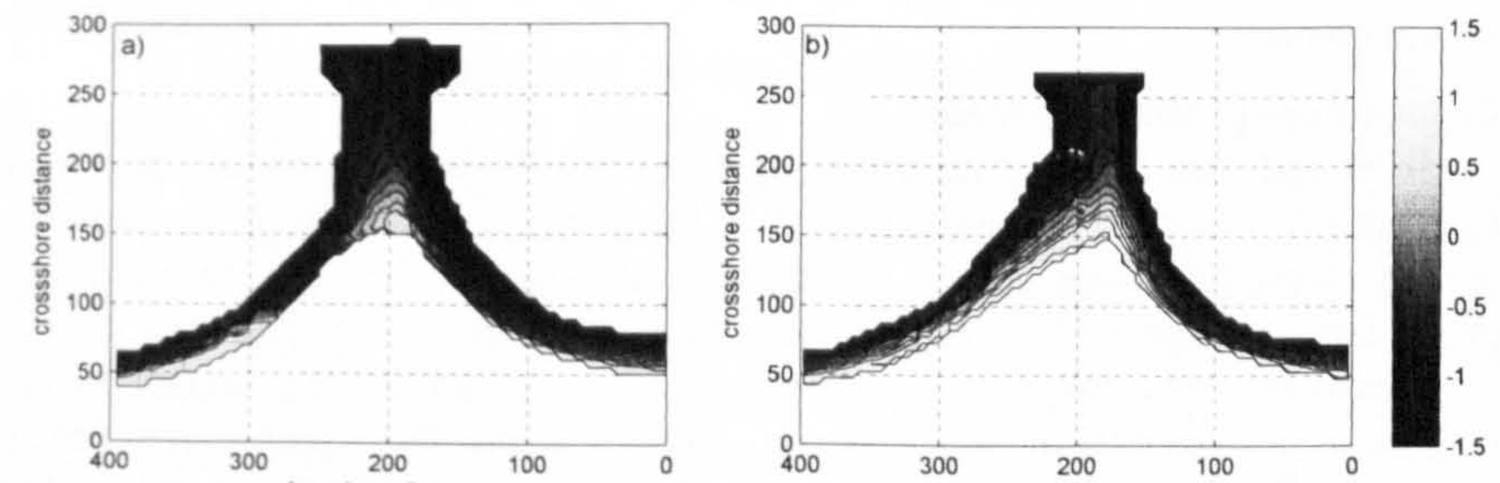

Figure 6: Contour maps of one tombolo a) pre-storm and b) post-storm.

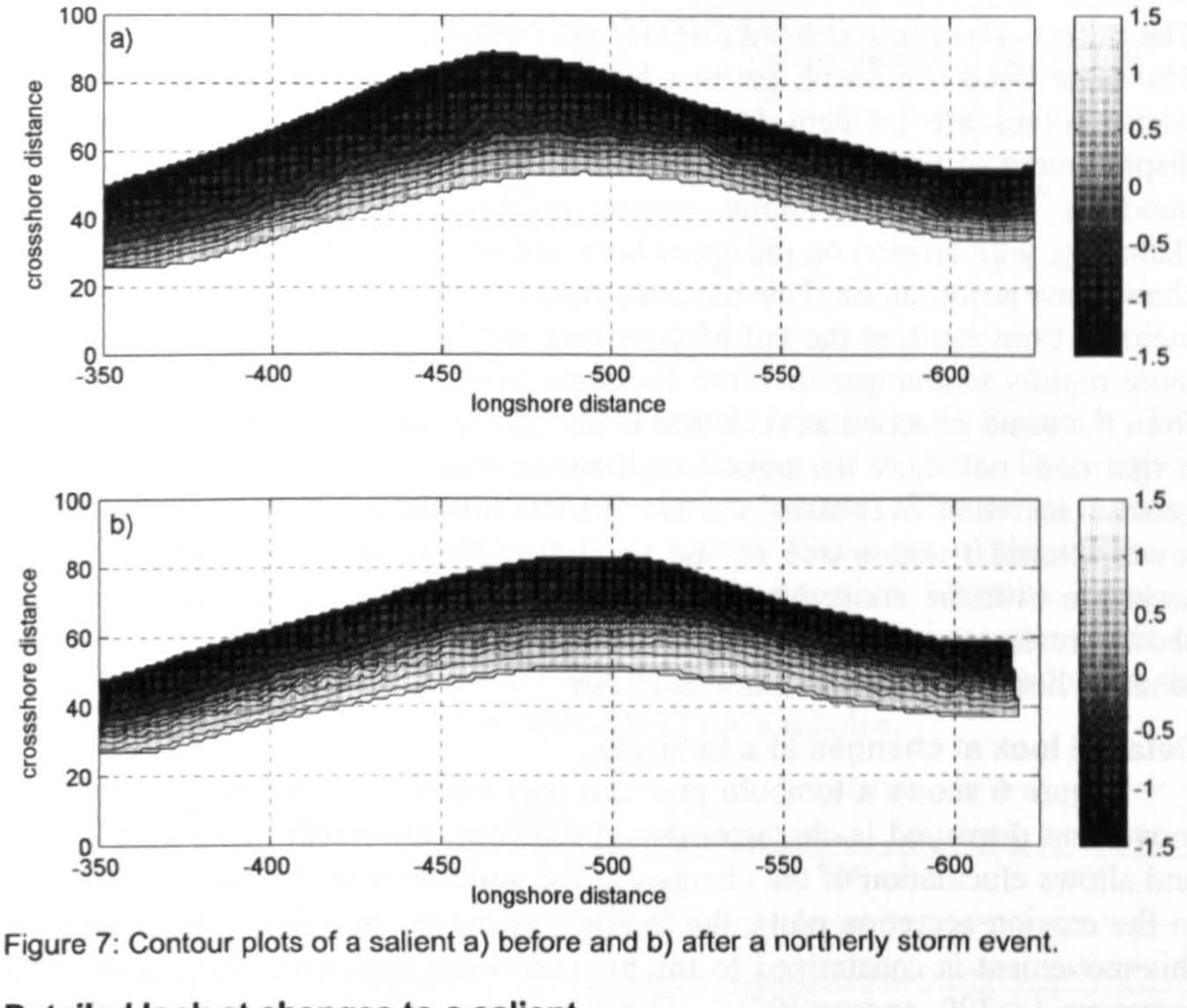

Figure 7: Contour plots of a salient a) before and b) after a northerly storm event.

Detailed look at changes to a salient

Pre- and post-storm contour plots for a phase two salient from the same northerly storm as the previous plots of the tombolo are shown in Figure 7.

It can be seen that there is a similar southward shift of the feature to that displayed in the tombolo (Figure 7), however, the movement is much less defined in the salient. Similar to the tombolo, accretion occurs over the storm but the accretion is over the entire region rather than specifically on the horn of the tombolo. The skewness displayed by the tombolo is not observable in the salient response.

Cross-shore profile changes

Pre and post storm cross-shore profiles from the bay centres are displayed in Figure 8. The profile numbers refer to longshore distance from the cameras; the left hand two columns are phase one embayments, the right two columns phase two and the middle column the transition embayment between phases. Profiles were only taken in the bay centers to minimize the impact of the longshore movement of the salients /tombolos on the cross-shore profile changes. It can be seen that the cross-shore profile gradients in phase two remains similar regardless of wave height or storm duration. Flattening of the beach gradient is more prevalent in phase one. It is only for the storm C with the largest surge level (1.4m) that significant flattening of the beach gradient is

observed, for this storm phase two shows some slight flattening also. The storm with shore normal wave approach (storm F) shows more beach flattening than the other storms with large surges. Storms A, B and C show a general accretion through the intertidal region of both phases, as is shown in the erosion-accretion plots.

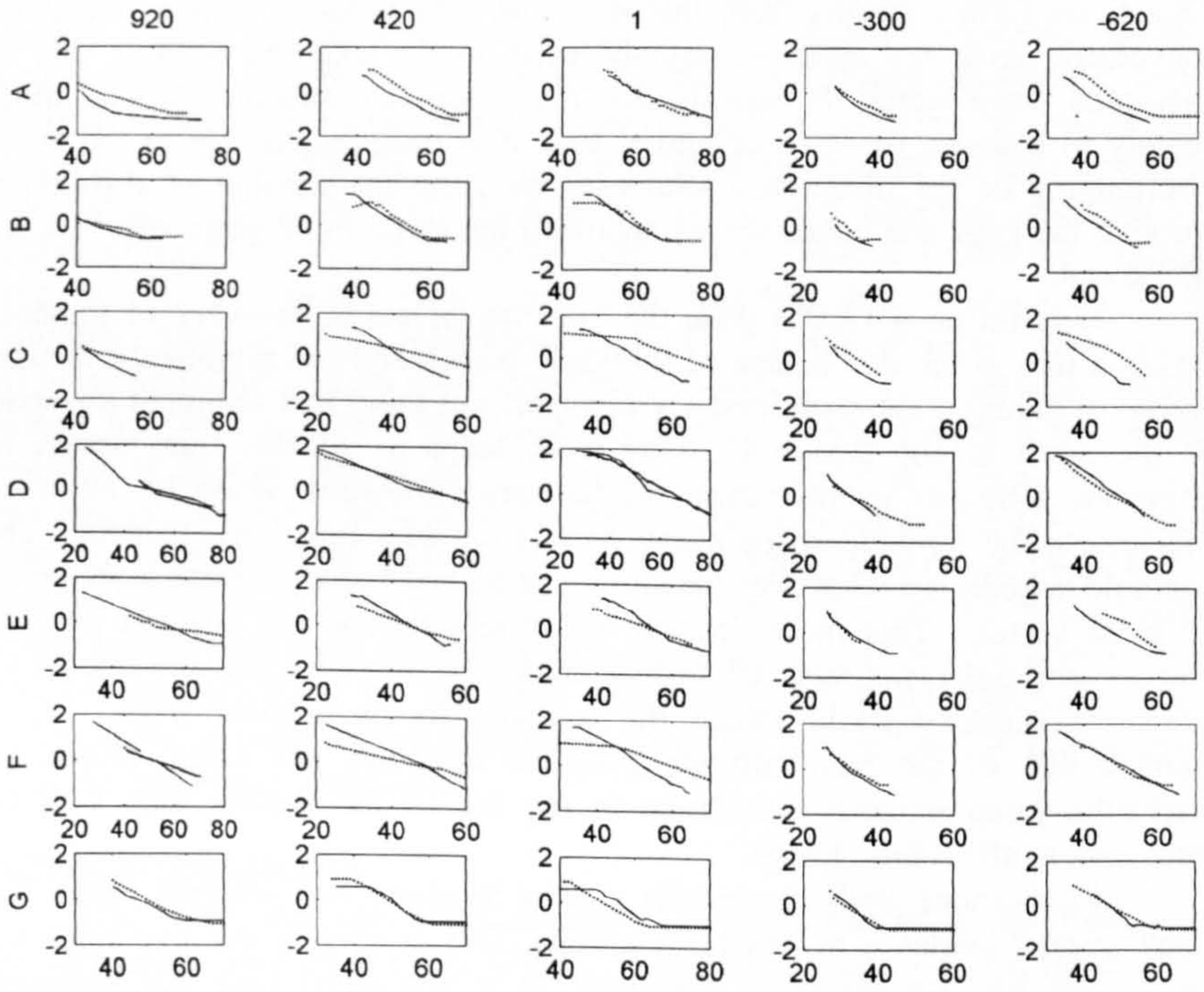

Figure 8: Cross-shore profiles from bay centers, pre- (solid line) and post- (dotted line) storm. Each row is a different storm (A-G) and each column a different profile location (numbered in terms of longshore distance.

DISCUSSION

The southward movement of the tombolos under northerly storm has previously been reported by Dolphin et al (2005) who used GPS surveys to measure morphological changes under two storms in phase one. As expected, the video analysis corroborates these previous findings and shows that for waves from the opposite direction the reverse moment takes place. Whilst such reversal in tombolo movement might seem obvious, the asymmetry in the strong tidal current means such movement cannot be assumed a priori. This work extends the investigation into phase two where the same direction of feature movement is displayed in the salients. The salient movement is more diffuse, this can be explained by the lesser difference between sheltered and unsheltered regions in phase two, cause both by the shorter breakwater lengths and the increased overtopping and wave transmission. The emergent phase one

breakwaters provide much more refined gradients in wave exposure and hence the more defined response in the longshore movement of the features. The nature of features themselves exacerbates this: the tombolo horn positions are more firmly 'tied' to the structure locations. This concept can be used to explain the lack of longshore tombolo movement in storm E: if previous storms from one direction have displaced the tombolos to the limit of the sheltered region, no further storms from that direction will produce further longshore movement since the tombolos cannot exist in the exposed regions due to increased wave attack. It appears that the phase two salients respond more readily to changes to wave direction, this, it is believed, is due to the wave overtopping of the phase two structures reducing the amount of diffraction through the gaps and hence waves approach the shore more obliquely than for phase one.

Dolphin et al (2005) pose the question of storm recovery of tombolo position due to the dominance of northerly waves and the asymmetry in tidal transport giving a net south easterly transport, meaning that sediment transport to the north is not favoured. This work helps to address this: firstly, as expected, southerly events return the features northward; secondly, observed changes to the tombolo shape allow postulation of a return mechanism. The tombolo actually accretes over the storm period and becomes more asymmetric in cross section. This means that in order to return to the original position further accretion is not required, instead erosion of tombolo crest and smoothing of the asymmetry could return the tombolo to its original from. Flow compression of the tidal currents over the tombolos and scour caused by hydraulic jump induced turbulence in the lee of the feature may well be sufficient to affect this change

Cross-shore gradients remain similar in phase two whereas phase one show greater evidence of beach flattening. This is counter-intuitive since the phase one beaches are better protected, it is postulated here that sediment abundance potentially explains this difference. The beaches in phase two are narrower both due to the lesser sheltering of smaller breakwaters and since they are down drift of phase one and suffer from reduced sediment supply. High tide shorelines are constrained by the sea wall, which is reached most high tides, and hence further shoreline recession is impossible. This fact probably restrains the changes to beach gradient. The wider phase one beaches allow for upper-intertidal and supra-tidal erosion and associated flattening of the beach gradient.

It is thought that the sediment deposited for the observed intertidal accretion over the storm could well be taken from the supra-tidal beach, the other likely source is increased longshore sediment transport under storm conditions. Since, as previously stated, there is little supra-tidal sediment in phase two (unless surge levels are high enough to allow erosion of the dune above the sea wall), the general intertidal accretion of phase two is supposed in be due to increased longshore sediment supply. In phase one, larger storm waves intensify circulation patterns and lead to greater deposition on the

tombolo horns where circulation diverges; overtopping of the phase two breakwaters reduces this effect which leads to lesser accretion behind the structures.

CONCLUSIONS

A coastal imaging system has been used to investigate the storm scale responses of beaches protected by detached breakwaters. The use of video remote sensing has allowed for isolation of storm changes from other types of beach response.The beaches protected by the two different designs of rubble mound breakwater show both differences and similarities in storm scale response. This can largely be attributed to differences in breakwater geometry, particularly the presence or absence of overtopping, although abundance of sediment must also be taken into account. Under oblique waves the tombolos and salients are moved in a down drift direction due to alteration of the longshore location of the breakwater induced circulation patterns. Both designs of breakwater produce the same direction of longshore movement under oblique waves but the larger structures constrain this movement giving better defined regions of change. Accretion is observed in the intertidal region over storm periods, but this could well be at the expense of the supra-tidal beach. In phase one this accretion is focussed on the tombolos whilst phase two exhibits a more general accretion over the intertidal area. The beaches protected by the smaller lower breakwaters show little changes to beach gradient over the storm, whereas the beaches protected by the large structures show beach flattening. It is believed that is more related to the presence of the sea wall and lack of sediment than the breakwater geometries.

ACKNOWLEDGMENTS

This work was conducted as part of a PhD attached to the LeaCoastII project and funded by the UK EPSRC. Thanks must go to all members of the LeaCoastII project, especially Tony Dolphin, John Bacon and Roger Phillips of the UEA.

REFERENCES

Ahrens, J.P., Cox, J., 1990. Design and performance of Reef Breakwaters. Journal of Coastal research, 51(7): 61-75.

Archetti, R., Lamberti, A., 2006. Study of hydrodynamic induced by low crested structures through image processing. In: J. Mckee Smith (Editor), Proceedings of the 30th international conference on coastal engineering. World Scientific, San Diego, pp. 5021-5033.

Bacon, J.C. et al., 2005. The offshore breakwater scheme at sea palling, England; Sand transport generated by tidal currents. In: J.M. Smith (Editor), Coastal Engineering 2004, Vols 1-4, pp. 1896-1908.

Clayton, K.M., McCave, I.N., Vincent, C.E., 1983. The Establishment of a sand budget for the East Anglian coast and its implications for coastal stability Shoreline Protection. Thomas Telford, London, pp. 91-96.

Dolphin, T., Taylor, J., Vincent, C., Bacon, J., Pan, S. Q., O'Conner, B., 2005. Storm-scale effects of shore-parallel breakwaters on beaches in a tidal setting (Leacoast). In: J.M. Smith (Editor), Coastal Engineering 2004, , pp. 2849-2861.

Fairley, I., Davidson, M., Kingston, K.,, 2007. Video monitoring of overtopping of detached breakwaters in a mesotidal environment, Coastal Structures '07, Venice.

Fairley, I., Davidson, M., Kingston, K., Dolphin, T., Phillips, R., in Prep. Empirical Orthogonal Function Analysis of Shoreline Changes Behind Two Different Designs of Detached Breakwaters. submitted to Coastal Engineering.

Hamer, B.A., Hayman, S.J., Elsdon, P.A., Fleming, C.A.,, 1998. Happisburgh to Winterton Sea Defenses: Stage Two, Coastlines, Structures and Breakwaters. Thomas Telford, London.

Holman, R.A. and Stanley, J., 2007. The history and technical capabilities of Argus. Coastal Engineering, 54(6-7): 477-491.

Loveless, J., Debski, D., Macleod, B., 1998. Sea level set-up behind detached breakwaters 26th International Conference on Coastal Engineering, Copenhagen, pp. 1665-1678.

McCormick, M.E., 1993. Equilibrium Shoreline Response to Breakwaters. Journal of Waterway, Port, Coastal and Ocean Engineering, 119(6): 657-670.

Pilarczyk, K.W., Zeidler, R.B.,, 1996. Offshore breakwaters and shore evolution control. Balkema, Rotterdam.

Pope. J., D., J. , 1986. Development of Design Criteria for Segmented Breakwaters. In: B. Edge (Editor), Coastal Engineering. ASCE, Taipei, Taiwan, pp. 2144-2158.

Thomella, F., Vincent, C.E.,, 2004. Designing Offshore Breakwaters Using Empirical Relationships: A Case Study from Norfolk, United Kingdom. Journal of Coastal research, 20(4): 1224-1230.

Van Der Meer, J., Briganti, R., Wang, B., Zanuttigh, B., 2004. Wave transmission at low-crested structures, including oblique wave attack, Coastal Engineering 2004, pp. 4152-4164.